

# **A spin-flipper in the vicinity of a superconductor**

By

**SUBHAJIT PAL**

**PHYS11201504018**

**National Institute of Science Education and Research,  
Bhubaneswar**

*A thesis submitted to the  
Board of Studies in Physical Sciences*

*In partial fulfillment of requirements  
for the Degree of*

**DOCTOR OF PHILOSOPHY**

*of*

**HOMI BHABHA NATIONAL INSTITUTE**



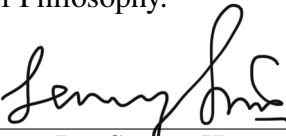
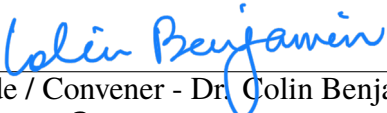

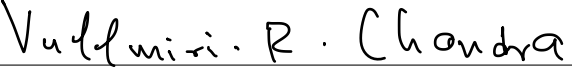


August, 2021



# Homi Bhabha National Institute

## Recommendations of the Viva Voce Committee

As members of the Viva-Voce Committee, we certify that we have read the dissertation prepared by **Subhajit Pal** entitled “**A spin-flipper in the vicinity of a superconductor**” and recommend that it may be accepted as fulfilling the thesis requirement for the award of Degree of Doctor of Philosophy.


<b>Signature:</b> 	20.01.2022
Chairman - Dr. Sanjay Kumar Swain	<b>Date:</b>
<b>Signature:</b> 	20.01.2022
Guide / Convener - Dr. Colin Benjamin	<b>Date:</b>
<b>Signature:</b> 	26/01/2022
Examiner - Prof. Jiannis K. Pachos	<b>Date:</b>
<b>Signature:</b> 	27-01-2022
Member 1 - Dr. V. Ravi Chandra	<b>Date:</b>
<b>Signature:</b> 	28/01/2022
Member 2 - Dr. Kartikeswar Senapati	<b>Date:</b>
<b>Signature:</b> 	29.01.2022
Member 3 - Dr. Niharika Mohapatra	<b>Date:</b>

Final approval and acceptance of this thesis is contingent upon the candidate's submission of the final copies of the thesis to HBNI.

I/We hereby certify that I/We have read this thesis prepared under my/our direction and recommend that it may be accepted as fulfilling the thesis requirement.

**Date** : January 20, 2022

**Place** : Bhubaneswar

  
**Dr. Colin Benjamin**  
 Guide



## **STATEMENT BY AUTHOR**

This dissertation has been submitted in partial fulfillment of requirements for an advanced degree at Homi Bhabha National Institute (HBNI) and is deposited in the library to be made available to borrowers under rules of the HBNI.

Brief quotations from this dissertation are allowable without special permission, provided that accurate acknowledgement of source is made. Requests for permission for extended quotation from or reproduction of this manuscript in whole or in part may be granted by the Competent Authority of HBNI when in his or her judgment the proposed use of the material is in the interests of scholarship. In all other instances, however, permission must be obtained from the author.

*Subhajit Pal*  
(SUBHAJIT PAL)



## DECLARATION

I, Subhajit Pal, hereby declare that the investigation presented in the thesis has been carried out by me. The work is original and has not been submitted earlier as a whole or in part for a degree/diploma at this or any other Institution/University.

*Subhajit Pal*  
(SUBHAJIT PAL)





# List of Publications arising from the thesis

## Journal

### Published

1. “Characterizing a high spin magnetic impurity via Andreev reflection spectroscopy”, Subhajit Pal and Colin Benjamin, *Eur. Phys. J. B*, **2018**, 91, 190.
2. “Tuning the  $0 - \pi$  Josephson junction with a magnetic impurity: Role of tunnel contacts, exchange coupling, electron-electron interactions and high spin states”, Subhajit Pal and Colin Benjamin, *Scientific Reports*, **2018**, 8, 5208.
3. “Yu-Shiba-Rusinov bound states induced by a spin flipper in the vicinity of a  $s$ -wave superconductor”, Subhajit Pal and Colin Benjamin, *Scientific Reports*, **2018**, 8, 11949.
4. “Spin flip scattering engendered quantum spin torque in a Josephson junction”, Subhajit Pal and Colin Benjamin, *Proc. R. Soc. A*, **2019**, 475, 20180775.
5. “Quantized Josephson phase battery”, Subhajit Pal and Colin Benjamin, *Euro Physics Letters*, **2019**, 126, 57002.
6. “Stability of Majorana bound states in the presence of spin-flip scattering”, Subhajit Pal and Colin Benjamin, *Physica E*, **2020**, 126, 114389.
7. “Exciting odd-frequency equal spin-triplet correlations at metal-superconductor interfaces”, Subhajit Pal and Colin Benjamin, *Phys. Rev. B*, **2021**, 104, 054519.

### **Submitted (undergoing peer review)**

8. “Josephson quantum spin thermodynamics”, Subhajit Pal and Colin Benjamin, arXiv:2105.01726.

### **Other publications**

9. “Designing a highly efficient graphene quantum spin heat engine”, Arjun Mani, Subhajit Pal and Colin Benjamin, Scientific Reports, **2019**, 9, 6018.
10. “Probing the helical versus chiral character of topological superconductors via non-local Hanbury-Brown and Twiss correlations.”, Tusaradri Mohapatra, Subhajit Pal and Colin Benjamin, arXiv:2103.14920.

### **Conferences**

1. Presented a poster at “International Conference On Complex and Functional Materials (ICCFM-2018)”, S. N. Bose National Centre for Basic Sciences, Kolkata, India, Dec 2018.
2. Presented a poster at “Annual Condensed Matter Physics Meeting”, NISER, Jatni, India, Feb 2018.
3. Presented a poster at “International Conference On Nanoscience and Nanotechnology (ICONN-2021)”, SRMIST, Kattankulathur, India, Feb 2021.

*Subhajit Pal*  
(SUBHAJIT PAL)

*Dedicated  
to  
My Well Wishers*



## **ACKNOWLEDGEMENTS**

I would first like to express my sincere gratitude to my supervisor Dr. Colin Benjamin for the continuous support of my Ph.D. study and related research, for his patience, motivation, and immense knowledge. His advice helped me in all the time of research and writing of this thesis. I could not have imagined having a better supervisor for my Ph.D. study.

Besides my supervisor, I would like to thank my doctoral committee members Dr. Sanjay Kumar Swain, Dr. V. Ravi Chandra, Dr. Kartikeswar Senapati, and Dr. Niharika Mohapatra, for enthusiastically supporting me.

I am also thankful to the Chairperson of the School of Physical Sciences, Dean of Academics, and all the School of Physical Sciences staff for their immense support throughout my research.

I thank my fellow labmates in the condensed matter theory Group: Tusaradri Mohapatra, Gour Jana, Prabhakar, Subhajyoti Pal, Jyothis V V, and Sujith N S, for the stimulating discussions, for the sleepless nights we were working together before deadlines, and for all the fun we have had in the last six years.

Last but not least, I would like to thank my parents for supporting me spiritually throughout my life.



# Contents

<b>Summary</b>	<b>1</b>
<b>List of Figures</b>	<b>3</b>
<b>List of Tables</b>	<b>15</b>
<b>1 Introduction</b>	<b>17</b>
1.1 Andreev reflection . . . . .	20
1.1.1 Blonder-Tinkham-Klapwijk (BTK) Model . . . . .	21
1.2 Spin flip scattering . . . . .	28
1.3 Andreev reflection mediated transport in Metal-Spin flipper-Superconductor junction . . . . .	39
1.3.1 Andreev Reflection in presence of a spin flipper . . . . .	39
1.3.2 Differential charge conductance . . . . .	46
1.4 DC Josephson effect . . . . .	49
1.4.1 $\pi$ junctions . . . . .	51
1.5 Andreev bound states and Josephson current in SNS junction . . . . .	52
1.5.1 Andreev bound states . . . . .	54
1.5.2 Bound state current . . . . .	55
1.5.3 Continuum current . . . . .	56
1.5.4 Total Josephson current . . . . .	57
1.6 Outline of the thesis . . . . .	58
<b>2 Formation of Yu-Shiba-Rusinov bound states and stability of Majorana bound states in presence of spin flip scattering</b>	<b>61</b>

2.1	Introduction . . . . .	61
2.2	Signature of Yu-Shiba-Rusinov bound states in normal and Andreev reflection probabilities . . . . .	63
2.3	Differential conductance and Probability density . . . . .	69
2.4	Signature of Yu-Shiba-Rusinov bound states in conductance spectra . . . . .	71
2.5	Effect of arbitrary junction length on Yu-Shiba-Rusinov bound states . . . . .	75
2.6	Stability of Majorana zero modes in the presence of a spin flipper . . . . .	77
2.6.1	Spin flipper in vicinity of metal- $p$ -wave superconductor junction . . . . .	78
	Symmetry class of $p$ -wave Hamiltonian: . . . . .	80
2.6.2	Spin flipper in vicinity of metal-spin orbit coupled superconducting wire junction . . . . .	85
	Symmetry class of SOCSW Hamiltonian: . . . . .	87
2.6.3	Comparison of ZBCP between normal metal- $p$ wave and normal metal-SOCSW junction in the vicinity of a spin flipper . . . . .	90
2.6.4	Topological symmetry class in presence of spin flip scattering . . . . .	94
	Symmetry class for pSc in vicinity of a spin flipper . . . . .	95
	Symmetry class for SOCSW in the vicinity of a spin flipper . . . . .	97
2.7	Conclusion . . . . .	101
<b>3</b>	<b>Spin flip scattering induced odd frequency equal spin triplet correlations in metal-superconductor junction</b>	<b>103</b>
3.1	Introduction . . . . .	103
3.2	Spin flip scattering at NS interface . . . . .	106
3.3	Method to calculate induced pairing correlations . . . . .	110
3.3.1	Green's function . . . . .	110
3.3.2	Pairing amplitudes . . . . .	111
3.4	Results . . . . .	112
3.4.1	Zero temperature . . . . .	112
	Odd and even frequency spin-singlet correlations . . . . .	112
	Odd and even frequency equal spin-triplet correlations . . . . .	115
3.4.2	Finite temperature . . . . .	119
	Odd and even frequency spin-singlet correlations . . . . .	119
	Odd and even frequency equal spin triplet correlations . . . . .	121



3.5	Processes at play . . . . .	122
3.5.1	Retarded Green's functions and induced pairing correlations . . . . .	123
	Both spin mixing and spin-flip scattering occur . . . . .	123
	Only spin mixing occurs . . . . .	128
	Only spin-flip scattering occurs . . . . .	128
3.6	Detecting odd frequency correlations . . . . .	129
3.6.1	Spin polarized local density of states (SPLDOS) & local magneti- zation density of states (LMDOS) . . . . .	129
	(i) <u>Both spin mixing and spin flip scattering occur:</u> . . . . .	129
	(ii) <u>Only spin mixing occurs:</u> . . . . .	130
	(iii) <u>Only spin flip scattering occurs:</u> . . . . .	131
3.7	Conclusion . . . . .	137
<b>4</b>	<b>Spin-flip scattering induced tunable <math>0 - \pi</math> Josephson junction and quantized anomalous phase in Ferromagnetic Josephson junction</b>	<b>139</b>
4.1	Introduction . . . . .	139
4.2	SNS junction in presence of a spin flipper . . . . .	142
4.2.1	Josephson current in presence of a spin flipper . . . . .	145
	Total Josephson current . . . . .	145
	Bound state contribution . . . . .	146
	Continuum contribution . . . . .	148
4.2.2	Andreev bound states . . . . .	149
4.2.3	Josephson current: $\pi$ junction behavior . . . . .	151
4.2.4	Josephson current in long junction limit . . . . .	152
4.2.5	Free energy . . . . .	154
4.2.6	Understanding $0 - \pi$ junction transition . . . . .	156
	Effect of tunnel contacts & exchange coupling . . . . .	156
	Effect of electron-electron interaction (phenomenological) . . . . .	158
	Effect of high spin/magnetic moment states . . . . .	159
4.3	Ferromagnetic Josephson junction in the presence of a spin flipper . . . . .	161
4.3.1	Anomalous Josephson current and Andreev bound states . . . . .	164
4.3.2	Quantized anomalous phase . . . . .	168
4.3.3	Reasons for the existence of Anomalous Josephson effect . . . . .	172

	Explaining quantum spin-flip scattering . . . . .	172
	Explaining chiral symmetry breaking . . . . .	173
	Explaining time-reversal symmetry breaking . . . . .	173
4.3.4	How different values of $T/T_c$ affect anomalous Josephson current?	175
4.4	Experimental realization . . . . .	176
4.5	Conclusion . . . . .	177
<b>5</b>	<b>Spin-flip scattering induced quantum spin torque in a Ferromagnetic Josephson junction</b>	<b>179</b>
5.1	Introduction . . . . .	179
5.2	What is quantum spin-torque? . . . . .	181
5.2.1	Difference between equilibrium quantum spin torque and nonequilibrium quantum spin torque . . . . .	182
5.3	Ferromagnetic Josephson junction in the presence of a spin flipper . . . . .	183
5.3.1	Andreev bound states and Josephson charge current . . . . .	187
5.3.2	Equilibrium spin torque . . . . .	188
5.3.3	Analyzing equilibrium quantum spin torque . . . . .	189
5.3.4	Physical picture of equilibrium quantum spin torque . . . . .	195
5.4	Experimental realization . . . . .	196
5.5	Conclusion . . . . .	196
<b>6</b>	<b>Josephson quantum thermodynamics and spin flip scattering</b>	<b>199</b>
6.1	Introduction . . . . .	199
6.2	Theoretical model . . . . .	201
6.2.1	Andreev bound states . . . . .	206
6.2.2	Superconductor-Spin flipper-Superconductor junction as a thermodynamic system . . . . .	207
6.3	Josephson-Stirling Cycle . . . . .	208
6.3.1	Work done and heat exchanged in Josephson-Stirling Cycle . . . . .	210
	Work done . . . . .	211
	Heat exchanged (with right reservoir) . . . . .	211
	Heat exchanged (with left reservoir) . . . . .	212
6.3.2	Josephson-Stirling cycle acting as quantum heat engine . . . . .	213

---

Condition for optimality . . . . .	215
6.3.3 Josephson-Stirling cycle acting as quantum refrigerator . . . . .	216
6.3.4 Phase diagram of Josephson-Stirling cycle . . . . .	216
6.3.5 Why is spin-flip scattering necessary? . . . . .	219
6.3.6 Josephson-Stirling cycle as Joule pump and cold pump . . . . .	220
6.4 Analysis . . . . .	222
6.4.1 Work done ( $W$ ) . . . . .	222
6.4.2 Heat exchanged (with right reservoir) . . . . .	224
6.4.3 Heat exchanged (with left reservoir) . . . . .	225
6.5 Experimental realization . . . . .	227
6.6 Conclusion . . . . .	227
<b>7 Conclusion</b>	<b>231</b>
<b>A Analytical expression for Green's functions</b>	<b>235</b>
A.1 Green's function in normal metal region . . . . .	235
A.2 Green's function in superconducting region . . . . .	237
<b>B Analytical expressions for Andreev bound states and anomalous Josephson current</b>	<b>241</b>
B.1 Explicit form of Matrix $M$ used in chapter 4 . . . . .	242
B.2 Explicit form of Andreev bound states in chapter 4 . . . . .	244
B.3 Table for different values of spin flip probability of spin flipper for different $S$ and $m'$ . . . . .	245
B.4 Explicit form of anomalous Josephson current . . . . .	247
<b>C Analytical expression for equilibrium quantum spin torque</b>	<b>249</b>
C.1 Explicit form of equilibrium quantum spin torque . . . . .	249
<b>D Mathematica code to calculate pairing amplitudes in metallic region</b>	<b>253</b>
<b>E Mathematica code to calculate anomalous Josephson current and anomalous phase</b>	<b>271</b>
E.1 Anomalous Josephson current . . . . .	271
E.2 Anomalous phase . . . . .	275

**Bibliography**

**279**

# Summary

Recent studies that combine superconductivity and spintronics have mainly dwelt on the injection of spin-polarized quasi-particles into superconductors. However, at the interface between metal and Superconductor, new phenomena due to Andreev reflection, like the emergence of odd frequency correlations, formation of Majorana bound states, etc., appear. Further, interfaces between superconductors and ferromagnets have led to many surprising phenomena: Josephson  $\pi$  junction, the anomalous Josephson effect, and novel applications in Josephson qubits.

In this thesis, we study the effects of spin-flip scattering on Andreev reflection-mediated transport. In a Normal metal (N)-Superconductor (S) junction with a spin-flipper at the interface, zero energy Yu-Shiba-Rusinov (YSR) peaks are seen in the conductance. This zero-energy peak is almost quantized at  $2e^2/h$  values. However, it arises due to non-topological reasons in contrast to zero-bias conductance peak (ZBCP) formed due to the presence of Majorana states. Further, Majorana states induced quantized ZBCP remains stable in the presence of spin-flip scattering in a metal- $p$ -wave superconductor junction. At the same time, it loses its stability when the  $p$ -wave Superconductor is replaced by a spin-orbit coupled superconducting wire (SOCSW).

Odd frequency equal spin-triplet pairing at NS interfaces is induced due to spin-flip scattering. The importance of finding these correlations in a  $s$ -wave superconductor implies

that one can effectively tune a  $s$ -wave superconductor into a  $p$ -wave superconductor via doping with a spin-flipper. A hallmark of  $p$ -wave superconductors is the formation of equal spin-triplet pairing of its Cooper pair.  $p$ -wave superconductors are exotic and difficult to work with but are predicted to host Majorana fermions. However, inducing spin-triplet  $p$  wave pairing in a  $s$ -wave superconductor would imply generating and detecting Majorana Fermions could become much more accessible.

In Josephson junction's too, a spin-flipper can induce  $\pi$  junction behavior. Spin flip scattering plays a crucial role in understanding the  $0$  to  $\pi$  junction transition. The free energy of such a system shows bistable behavior, which can play a role in quantum computation applications. Replacing the two normal metals with ferromagnets, one observes anomalous Josephson effect. Our spin-flipper-based junction's main advantage over other proposals involving anomalous Josephson current is that our junction can store quantized amounts of superconducting phase difference in its ground state, implying its use as a quantized Josephson phase battery. Further, a novel quantum spin torque at equilibrium can be seen in such a Josephson junction due to the presence of spin-flip scattering.

Finally, we see that a Josephson junction loop doped with a spin-flipper attached to two thermal reservoirs can act as a quantum heat engine, a quantum refrigerator, or even a Joule pump or a cold pump. This device can be tuned from engine mode to refrigerator mode or any other mode, i.e., Joule pump or cold pump, by either tuning the temperature of reservoirs or via the enclosed flux in the Josephson junction loop. Tuning via externally applied magnetic flux is less prone to errors than tuning temperatures of reservoirs or operating the cycle in reverse, the latter being internal control mechanisms. This makes our proposed Josephson thermodynamic device much more versatile for possible applications.

# List of Figures

1.1	<i>Andreev reflection process: an incident electron from the normal metal is retroreflected as a hole and a Cooper pair is formed inside the s-wave superconductor below the superconducting gap.</i> . . . . .	20
1.2	<i>(a) An electron, with energy <math>E</math> coming from the normal metal (N), interacts at <math>x = 0</math> with a <math>\delta</math>-like potential barrier of strength <math>V</math>. Electron and hole are reflected back to the normal metal (N) and electron-like and hole-like quasiparticles are transmitted into the s-wave superconductor (S). The closed circles denote electrons and electron-like quasiparticles and the open circles denote holes and hole-like quasiparticles. <math>A</math> is Andreev reflection probability, while <math>B</math> denotes probability of normal reflection. <math>C</math> and <math>D</math> are transmission probabilities of electron-like and hole-like quasiparticles respectively, (b) NIS junction where N is connected to voltage <math>V_1</math> and S is connected to voltage <math>V_2</math> and <math>V = V_1 - V_2</math> is the voltage drop across the NIS junction.</i> . . . . .	22
1.3	<i>Plots of reflection (<math>A</math>, <math>B</math>) and transmission (<math>C</math>, <math>D</math>) probabilities at N-S interface.</i> . . . . .	24
1.4	<i>Differential charge conductance normalized by normal state conductance (<math>G_N</math>), as function of voltage for different values of interface transparency <math>Z</math> at zero temperature. Here, <math>G_N = \frac{2N(E_F)e^2v_F\mathcal{A}}{1+Z^2}</math> and <math>\Delta</math> the superconducting gap.</i> . . . . .	28
1.5	<i>(a) A spin up electron with energy <math>E</math> coming from the metallic region <math>N_1</math> interacts at <math>x = 0</math> with a spin flipper (SF) through an exchange potential, leading to finite probability for flipping its own spin and spin of the spin flipper; (b) <math>N_1</math>-SF-<math>N_2</math> junction where <math>N_1</math> is connected to voltage <math>V_1</math> and <math>N_2</math> is connected to voltage <math>V_2</math> and <math>V = V_1 - V_2</math> is the voltage bias applied at the interface. High spin molecules like <math>Fe_{19}</math>-complex can act as a spin flipper.</i> . . . . .	29

LIST OF FIGURES

---

1.6	(a) Reflection probability without flip, (b) Reflection probability with flip, (c) Transmission probability without flip and (d) Transmission probability with flip. Parameter: $m' = -1/2$ . . . . .	36
1.7	(a) Differential charge conductance ( $G_c$ ) normalized by $G_M$ , as function of exchange interaction $J$ for different values of spin $S$ and fixed magnetic moment $m'$ of spin flipper at zero temperature, (b) Differential charge conductance ( $G_c$ ) normalized by $G_M$ , as function of exchange interaction $J$ for different values of magnetic moment $m'$ and fixed spin $S$ of spin flipper at zero temperature. Parameters: (a) $m' = -1/2$ ; (b) $S = 3/2$ and, $G_M = \rho(E_F)e^2v_F\mathcal{W}$ . . . . .	38
1.8	(a) NS junction with spin flipper (SF) at interface ( $x = 0$ ) with spin $S$ and magnetic moment $m'$ . Scattering of an incident spin up electron is shown. Normal reflection, Andreev reflection and quasi-particle transmission into superconductor are depicted, (b) N-SF-S junction where N is connected to voltage $V_1$ and S is connected to voltage $V_2$ and $V = V_1 - V_2$ is the voltage drop across the NS interface. . . . .	39
1.9	(a) Normal reflection probability without flip, (b) normal reflection probability with flip, (c) Andreev reflection probability with flip and (d) Andreev reflection probability without flip. Parameters are: $J = 1$ , $m' = -1/2$ . . . . .	44
1.10	(a) Electron-like quasi-particle transmission without flip, (b) electron-like quasi-particle transmission with flip, (c) hole-like quasi-particle transmission with flip and (d) hole-like quasi-particle transmission without flip. Parameters: $J = 1$ , $m' = -1/2$ . . . . .	45
1.11	(a) Differential charge conductance as function of energy of incident electron in units of $\Delta$ for different values of exchange interaction $J$ at zero temperature, (b) Differential charge conductance as function of exchange interaction $J$ for different values of spin $S$ of spin flipper at zero temperature. Parameters: (a) $S = 1/2$ , $m' = -1/2$ ; (b) $m' = -1/2$ , $E = 1.5\Delta$ and $G_L = \rho(E_F)e^2v_F\mathcal{A}$ . . . . .	47
1.12	An electron $e$ and the Andreev-reflected hole $h$ are shown in weak link, between two $s$ -wave superconductors. A pair of correlated electrons moves from left superconductor to right superconductor, creating a supercurrent flow across the junction. The system is in equilibrium, no voltage bias is applied. . . . .	50
1.13	Josephson junction composed of normal metal sandwiched between two $s$ -wave superconductors. . . . .	53
1.14	Andreev bound states $E^\pm$ in units of $ \Delta $ (the energy gap of $s$ -wave superconductor) as a function of phase difference ( $\varphi$ ) for a short SNS junction. . . . .	56



1.15	<i>The bound, continuum and total Josephson current normalized with respect to <math>I_0 = e\Delta_0/\hbar</math>, as a function of phase difference (<math>\varphi</math>). Parameters: <math>\Delta_0 = 1\text{meV}</math>, <math>T/T_c = 0.01</math>, <math>Z = 0</math>.</i>	58
2.1	<i>(a) A spin flipper with spin <math>S</math> and magnetic moment <math>m'</math> at <math>x = 0</math> in a Normal Metal-Spin flipper-Normal Metal-Insulator-Superconductor junction, (b) The scattering of an up-spin electron incident is shown. Andreev reflection and quasi particle transmission into superconductor are depicted.</i>	63
2.2	<i>(a) Normal reflection probability without flip, (b) Normal reflection probability with flip, (c) Andreev reflection probability with flip, (d) Andreev reflection probability without flip. Parameters are: <math>J = 0.4</math>, <math>Z = 0.85</math>, <math>m' = -1/2</math> and <math>k_F a = 0.8437\pi</math>, are in dimensionless units.</i>	68
2.3	<i>(a) Charge conductance vs energy for no flip case. Parameters are: <math>J = 0.4</math>, <math>S = 19/2</math>, <math>m' = 19/2</math>, <math>k_F a = 0.8437\pi</math>, (b) Charge conductance vs energy for spin flip case. Parameters are: <math>J = 0.4</math>, <math>S = 19/2</math>, <math>m' = -1/2</math>, <math>k_F a = 0.8437\pi</math>, (c) Energy bound states as a function of interface transparency <math>Z</math>. Parameters are: <math>S = 19/2</math>, <math>m' = -1/2</math>, <math>J = 0.4</math>, <math>k_F a = 0.8437\pi</math>. Here charge conductance is in units of <math>e^2/h</math>.</i>	72
2.4	<i>(a) Charge conductance vs energy in transparent regime with <math>S = 7/2</math>, <math>m' = -1/2</math>, (b) Charge conductance vs energy in transparent regime with <math>S = 9/2</math>, <math>m' = -1/2</math>, (c) Charge conductance vs energy in transparent regime with <math>S = 11/2</math>, <math>m' = -1/2</math>. Here charge conductance is in units of <math>e^2/h</math>.</i>	73
2.5	<i>(a) Charge conductance vs energy <math>E</math> for <math>S = 21/2</math>, <math>m' = -1/2</math>, <math>Z = 0.86</math>, <math>J = 0.4</math>, <math>k_F a = 0.8437\pi</math>, (b) Charge conductance vs energy <math>E</math> for <math>S = 23/2</math>, <math>m' = -1/2</math>, <math>Z = 0.92</math>, <math>J = 0.4</math>, <math>k_F a = 0.8492\pi</math>, (c) Probability density vs energy <math>E</math> for <math>S = 21/2</math>, <math>m' = -1/2</math>, <math>Z = 0.86</math>, <math>J = 0.4</math>, <math>k_F a = 0.8437\pi</math>, (d) Probability density vs energy <math>E</math> for <math>S = 23/2</math>, <math>m' = -1/2</math>, <math>Z = 0.92</math>, <math>J = 0.4</math>, <math>k_F a = 0.8492\pi</math>, (e) Energy bound states as a function of interface transparency <math>Z</math>. Parameters are: <math>S = 21/2</math>, <math>m' = -1/2</math>, <math>J = 0.4</math>, <math>k_F a = 0.8437\pi</math>, (f) Energy bound states as a function of interface transparency <math>Z</math>. Parameters are: <math>S = 23/2</math>, <math>m' = -1/2</math>, <math>J = 0.4</math>, <math>k_F a = 0.8492\pi</math>. Here charge conductance is in units of <math>e^2/h</math>.</i>	74
2.6	<i>Charge conductance as a function of energy for different junction lengths ('a'). Parameters are <math>S = 21/2</math>, <math>m' = -1/2</math>, <math>Z = 0.86</math>, <math>J = 0.4</math>, <math>k_F a = 0.8437\pi</math>. Here charge conductance is in units of <math>e^2/h</math>.</i>	77

LIST OF FIGURES

---

2.7	<i>N<sub>1</sub>-N<sub>2</sub>-pSc junction in topological regime (<math>\mu_{pSc} &gt; 0</math>) with a spin flipper (spin <math>S</math>, magnetic moment <math>m'</math>) at <math>x = -a</math> and a <math>\delta</math>-like potential barrier (strength <math>Z</math>) at <math>x = 0</math>. The scattering of an incident spin up electron is shown. Normal reflection, Andreev reflection and quasi-particle transmission into p-wave superconductor are represented.</i>	78
2.8	<i>N<sub>1</sub>-SF-N<sub>2</sub>-SOCSW junction with a spin flipper (spin <math>S</math>, magnetic moment <math>m'</math>) at <math>x = -a</math> and a <math>\delta</math>-like potential barrier (strength <math>Z</math>) at <math>x = 0</math>. The scattering of a incident spin-up electron is shown. Normal reflection, Andreev reflection and quasi particle transmission into SOCSW are shown.</i>	85
2.9	<i>Differential charge conductance in presence of spin flip scattering as a function of energy <math>E</math> for different values of interface barrier strength <math>Z</math> in topological regime, (a) for <math>N_1</math>-SF-N<sub>2</sub>-I-pSc and (b) for <math>N_1</math>-SF-N<sub>2</sub>-I-SOCSW junction. Parameters are: <math>f = f' = \sqrt{3}</math>, <math>S = 3/2</math>, <math>J = 1</math>, <math>\mu_{pSc} = 0.01</math>, <math>\Delta_{pSc} = 0.07</math>, <math>a = \pi</math>, <math>\Delta_0 = 0.001</math>, <math>\beta = 0.5</math>, <math>B_Z = 1.5\Delta_0</math>.</i>	92
2.10	<i>Differential charge conductance in presence of spin flip scattering as a function of energy <math>E</math> for <math>N_1</math>-SF-N<sub>2</sub>-I-SOCSW junction. Parameters are: <math>f = f' = \sqrt{5}</math>, <math>S = 5/2</math>, <math>J = 3</math>, <math>Z = 3</math>, <math>a = \pi</math>, <math>\Delta_0 = 0.001</math>, <math>\beta = 12</math>, <math>B_Z = 1.5\Delta_0</math>.</i>	94
2.11	<i>(a) <math>Q</math> in absence of spin flip scattering as a function of interface transparency <math>Z</math>, (b) <math>Q</math> in absence of spin flip scattering as a function of exchange interaction <math>J</math>, (c) <math>Q</math> in presence of spin flip scattering as a function of interface transparency <math>Z</math>, (d) <math>Q</math> in presence of spin flip scattering as a function of exchange interaction <math>J</math>. Parameters are <math>f = f' = 0</math> (for (a), (b)), <math>f = f' = 1</math> (for (c), (d)), <math>S = 1/2</math>, <math>J = 1</math> (for (a), (c)), <math>Z = 1</math> (for (b), (d)), <math>\mu_{pSc} = 0.01</math>, <math>\Delta_{pSc} = 0.07</math>, <math>a = \pi</math>.</i>	96
2.12	<i>(a) <math>Q'</math> as a function of <math>Z</math> (with <math>J = 1</math>) and (b) <math>Q'</math> as a function of <math>J</math> (with <math>Z = 1</math>) in absence of spin-flip scattering. (c) Absolute value and Argument of complex <math>Q'</math> as a function of <math>Z</math> (with <math>J = 1</math>) and (d) Absolute value and Argument of complex <math>Q'</math> as a function of <math>J</math> (with <math>Z = 1</math>) in presence of spin-flip scattering. Parameters are <math>f = f' = 0</math> (for (a), (b)), <math>f = f' = 1</math> (for (c), (d)), <math>S = 1/2</math>, <math>\Delta_0 = 0.001</math>, <math>\beta = 0.5</math>, <math>a = \pi</math>.</i>	99
3.1	<i>A spin flipper with spin <math>S</math> and magnetic moment <math>m'</math> at <math>x = 0</math> in a NS junction. Scattering of an incident spin up electron is shown. Normal reflection, Andreev reflection and quasi-particle transmission into superconductor are depicted.</i>	107

3.2	<i>Absolute values of even and odd frequency spin-singlet correlation induced in <math>N</math> (<math>x &lt; 0</math>) and <math>S</math> (<math>x &gt; 0</math>) regions as a function of position <math>x</math> for (a) no flip case and (b,c) spin flip case. Parameters are: <math>S = 1/2</math> (for (a) and (b)), <math>S = 5/2</math> (for (c)). Spin-flip probabilities are: <math>f = f' = 0</math> (a), <math>f = f' = 1</math> (b), <math>f = f' = 3</math> (c). Other parameters: <math>J = 1</math>, <math>x' = 0</math>, <math>\omega = 0.1\Delta</math>, <math>E_F = 10\Delta</math>.</i>	114
3.3	<i>Absolute values of even and odd frequency equal spin-triplet correlation induced in <math>N</math> (<math>x &lt; 0</math>) and <math>S</math> (<math>x &gt; 0</math>) regions as function of position <math>x</math> for spin flip case. Parameters are: <math>S = 1/2</math> (for (a)), <math>S = 5/2</math> (for (b)), <math>f = f' = 1</math> (for (a)), <math>f = f' = 3</math> (for (b)), <math>J = 1</math>, <math>x' = 0</math>, <math>\omega = 0.1\Delta</math>, <math>E_F = 10\Delta</math>.</i>	117
3.4	<i>The absolute values of the even and odd frequency spin-singlet correlation induced in the <math>N</math> region (<math>x &lt; 0</math>) and <math>S</math> region (<math>x &gt; 0</math>) as a function of the position <math>x</math> for (a) no flip process and (b) spin flip process. Parameters are: <math>S = 1/2</math> (for (a) and (b)), <math>S = 5/2</math> (for (c)), <math>f = f' = 0</math> (for (a)), <math>f = f' = 1</math> (for (b)), <math>f = f' = 3</math> (for (c)), <math>J = 1</math>, <math>x' = 0</math>, <math>T/T_c = 0.01</math>, <math>E_F = 10\Delta</math>.</i>	120
3.5	<i>Absolute values of even and odd frequency equal spin-triplet correlation induced in <math>N</math> region (<math>x &lt; 0</math>) and <math>S</math> region (<math>x &gt; 0</math>) as a function of position <math>x</math> for spin flip process. Parameters are: <math>S = 1/2</math> (for (a)), <math>S = 5/2</math> (for (b)), <math>f = f' = 1</math> (for (a)), <math>f = f' = 3</math> (for (b)), <math>J = 1</math>, <math>x' = 0</math>, <math>T/T_c = 0.01</math>, <math>E_F = 10\Delta</math>.</i>	121
3.6	<i>Ferromagnet (<math>F_1</math>)-Ferromagnet (<math>F_2</math>)-Superconductor (<math>S</math>) junction with misaligned magnetizations. The scattering of a spin up electron incident is shown. Normal reflection, Andreev reflection and quasi-particle transmission into superconductor are depicted.</i>	123
3.7	<i>Absolute values of even and odd frequency (a) equal spin-triplet correlations and (b) mixed spin-triplet correlations induced in superconducting region for <math>F_1F_2S</math> junction as function of position <math>x</math> when both spin flip scattering and spin mixing occur, (c) Frequency dependence of SPLDOS at <math>x = 0</math> for <math>F_1F_2S</math> junction when both spin flip scattering and spin mixing occur. Parameters are: <math>h_1/E_F = h_2/E_F = 0.8</math>, <math>x' = 0</math>, <math>\omega = 0.1\Delta</math> (for (a) and (b)), <math>E_F = 10\Delta</math>, <math>\theta = \pi/2</math>, <math>k_F a = \pi</math>.</i>	130
3.8	<i>Absolute values of even and odd frequency mixed spin-triplet correlations induced in superconducting region for FS junction as function of position <math>x</math> wherein only spin mixing occurs, (c) Frequency dependence of SPLDOS at <math>x = 0</math> for FS junction. Parameters are: <math>h/E_F = 0.8</math>, <math>x' = 0</math>, <math>\omega = 0.1\Delta</math> (for (a)), <math>E_F = 10\Delta</math>.</i>	131

LIST OF FIGURES

---

3.9	(a) Frequency dependence of SPLDOS at NS interface, (b) spatial dependence of the SPLDOS in $N$ ( $x < 0$ ) and $S$ ( $x > 0$ ) regions. Parameters are: $S = 1/2$ , $f = f' = 1$ , $J = 1$ , $x = 0$ (for (a)), $E_F = 10\Delta$ , $\omega = 0.1\Delta$ (for (b)). . . . .	134
3.10	(a) Frequency dependence of SPLDOS at NS interface, (b) spatial dependence of the SPLDOS in $N$ ( $x < 0$ ) and $S$ ( $x > 0$ ) regions. Parameters are: $S = 5/2$ , $f = f' = 3$ , $J = 1$ , $x = 0$ (for (a)), $E_F = 10\Delta$ , $\omega = 0.1\Delta$ (for (b)). . . . .	134
3.11	Spatial dependence of the (a) local even frequency correlations, (b) local odd frequency correlations and (c) spin-up LDOS in $N$ and $S$ regions. Parameters are: $S = 1/2$ , $f = f' = 1$ , $J = 1$ , $E_F = 10\Delta$ . . . . .	136
4.1	Josephson junction composed of two normal metals and a spin flipper with spin $S$ and magnetic moment $m'$ at $x = 0$ sandwiched between two $s$ -wave superconductors. . .	142
4.2	Andreev bound states as a function of phase difference ( $\varphi$ ). Parameters are $\Delta_0 = 1\text{meV}$ , $S = 1/2$ , $m' = \pm 1/2$ , $J = 1$ , $Z = 0$ , $T/T_c = 0.01$ . . . . .	150
4.3	Andreev bound states as a function of phase difference ( $\varphi$ ). Parameters are $\Delta_0 = 1\text{meV}$ , $S = 9/2$ , $m' = \pm 1/2, \pm 3/2, \pm 9/2$ , $J = 1$ , $Z = 0$ , $T/T_c = 0.01$ . . . . .	150
4.4	The bound, continuum and total Josephson current as a function of phase difference ( $\varphi$ ). Parameters are $\Delta_0 = 1\text{meV}$ , $T/T_c = 0.01$ , $S = 1/2$ , $m' = \pm 1/2$ , $J = 1$ , $Z = 0$ . . .	151
4.5	Josephson supercurrent as a function of phase difference ( $\varphi$ ). Parameters are $\Delta_0 = 1\text{meV}$ , $T/T_c = 0.01$ , $S = 9/2$ , $m' = \pm 9/2, \pm 7/2, \pm 5/2, \pm 3/2, \pm 1/2$ , $J = 1$ , $Z = 0$ . Josephson supercurrent for $m' = 7/2$ and $m' = -9/2$ are same and similarly for $m' = 5/2$ and $m' = -7/2$ , $m' = 3/2$ and $m' = -5/2$ , $m' = 1/2$ and $m' = -3/2$ are same.	152
4.6	(a) Josephson supercurrent as a function of junction length (a) for different values of spin ( $S$ ) of spin flipper. Parameters are $\Delta_0 = 1\text{meV}$ , $T/T_c = 0.01$ , $\varphi = \pi/2$ , $m' = -1/2$ , $J = 1$ , $Z = 0$ , (b) Josephson supercurrent as a function of phase difference ( $\varphi$ ) for different junction length (a). Parameters are $\Delta_0 = 1\text{meV}$ , $T/T_c = 0.01$ , $S = 9/2$ , $m' = -1/2$ , $J = 1$ , $Z = 0$ . . . . .	154
4.7	Free energy as a function of phase difference ( $\varphi$ ). Parameters are $\Delta_0 = 1\text{meV}$ , $T/T_c = 0.01$ , $S = 9/2$ , $m' = \pm 9/2, \pm 7/2, \pm 5/2, \pm 3/2, \pm 1/2$ , $J = 1$ , $Z = 0$ . Free energy for $m' = 7/2$ and $m' = -9/2$ are same and similarly for $m' = 5/2$ and $m' = -7/2$ , $m' = 3/2$ and $m' = -5/2$ , $m' = 1/2$ and $m' = -3/2$ are same. . . . .	155

- 
- 4.8 *Free energy as a function of phase difference ( $\varphi$ ) for different values of interface barrier strength ( $Z$ ). Parameters are  $\Delta_0 = 1\text{meV}$ ,  $T/T_c = 0.01$ ,  $S = 5/2$ ,  $m' = 1/2$ ,  $J = 1$ . . . . . 155*
- 4.9 *Josephson supercurrent as a function of phase difference ( $\varphi$ ) for different values of interface barrier strength ( $Z$ ). Parameters are  $\Delta_0 = 1\text{meV}$ ,  $T/T_c = 0.01$ ,  $J = 1$ ,  $S = 5/2$  and for (a)  $m' = 5/2$ , (b)  $m' = 1/2$  and (c)  $m' = 3/2$ . Josephson supercurrent for  $m' = 3/2$  and  $m' = -5/2$  are same and similarly  $m' = 1/2$  and  $m' = -3/2$  are same. 157*
- 4.10 *Josephson supercurrent as a function of phase difference ( $\varphi$ ) for different values of exchange interaction ( $J$ ). Parameters are  $\Delta_0 = 1\text{meV}$ ,  $T/T_c = 0.01$ ,  $Z = 0$ ,  $S = 5/2$  for (a)  $m' = 5/2$ , (b)  $m' = 3/2$  and (c)  $m' = 1/2$ . Josephson supercurrent for  $m' = 3/2$  and  $m' = -5/2$  are same and similarly  $m' = 1/2$  and  $m' = -3/2$  are same. 157*
- 4.11 *Josephson supercurrent as a function of phase difference ( $\varphi$ ) for different values of electron-electron interaction strength ( $\alpha$ ). Parameters are  $\Delta_0 = 1\text{meV}$ ,  $D_0 = 100\Delta_0$ ,  $T/T_c = 0.01$ ,  $J = 3$ ,  $Z = 0.1$ ,  $S = 5/2$  and for (a)  $m' = 5/2$ , (b)  $m' = 3/2$ , (c)  $m' = 1/2$  and (d)  $m' = -1/2$ . Josephson supercurrent for  $m' = 3/2$  and  $m' = -5/2$  are same and similarly  $m' = 1/2$  and  $m' = -3/2$  are same. . . . . 159*
- 4.12 (a) *Josephson supercurrent vs spin flipper spin ( $S$ ). Parameters are  $\Delta_0 = 1\text{meV}$ ,  $T/T_c = 0.01$ ,  $\varphi = \pi/2$ ,  $J = 1$ ,  $m' = -1/2$ ,  $Z = 0$ , (b) Josephson supercurrent vs spin flipper magnetic moment ( $m'$ ). Parameters are  $\Delta_0 = 1\text{meV}$ ,  $T/T_c = 0.01$ ,  $\varphi = \pi/2$ ,  $J = 1$ ,  $S = 9/2$ ,  $Z = 0$ , (c) Josephson supercurrent vs spin flipper spin ( $S$ ). Parameters are  $\Delta_0 = 1\text{meV}$ ,  $T/T_c = 0.01$ ,  $\varphi = \pi/2$ ,  $J = 1$ ,  $m' = -1/2$ ,  $Z = 1$ , (d) Josephson supercurrent vs spin flipper magnetic moment ( $m'$ ). Parameters are  $\Delta_0 = 1\text{meV}$ ,  $T/T_c = 0.01$ ,  $\varphi = \pi/2$ ,  $J = 1$ ,  $S = 9/2$ ,  $Z = 1$ . . . . . 160*
- 4.13 *Josephson junction with two Ferromagnet's and a spin flipper (spin  $S$ , magnetic moment  $m'$ ) at  $x = 0$  sandwiched between two  $s$ -wave superconductors. . . . . 162*
- 4.14 *Andreev bound state energies as a function of phase difference ( $\varphi$ ) (a) for no flip, (b) for spin flip. (c) Josephson current as a function of phase difference ( $\varphi$ ). Parameters are  $\Delta_0 = 1\text{meV}$ ,  $J = 1$ ,  $h = 0.5E_F$ ,  $I_0 = e\Delta_0/\hbar$ ,  $T/T_c = 0.01$ ,  $Z = 0$ ,  $k_F a = 1.2\pi$ ,  $\theta = \pi/2$ , for flip:  $S = 3/2$ ,  $m' = -1/2$ ,  $f = 2$ , and for no flip:  $S = 3/2$ ,  $m' = 3/2$ ,  $f = 0$ . 166*

4.15	(a) Anomalous Josephson current as a function of exchange interaction $J$ of spin flipper, (b) Anomalous Josephson current as a function of magnetization ( $h$ ) of the Ferromagnet's, (c) Anomalous Josephson current as a function of the interface barrier strength ( $Z$ ), (d) Anomalous Josephson current as a function of misorientation angle ( $\theta$ ) between two Ferromagnets' for different spin flip probabilities of spin flipper. Parameters are $\Delta_0 = 1\text{meV}$ , $I_0 = e\Delta_0/\hbar$ , $T/T_c = 0.01$ , $J = 1$ (for (b), (c) and (d)), $h = 0.5E_F$ (for (a), (d)), $h = 0.8E_F$ (for (c)), $k_F a = \pi$ , $Z = 0$ (for (a), (b) and (d)), $\theta = \pi/2$ (for (a), (b) and (c)). . . . .	167
4.16	Absolute value of anomalous Josephson current as function of the misorientation angle ( $\theta$ ) between two Ferromagnet's for different values of spin and magnetic moment of the spin flipper. Parameters are $\Delta_0 = 1\text{meV}$ , $I_0 = e\Delta_0/\hbar$ , $T/T_c = 0.01$ , $J = 1$ , $h = 0.5E_F$ , $k_F a = \pi$ , $\varphi = 0$ , $Z = 0$ . . . . .	169
4.17	(a) Free energy as a function of exchange interaction $J$ of spin flipper and phase difference $\varphi$ across two superconductors. (b) Free energy as a function of magnetization $h$ of the Ferromagnet's and phase difference $\varphi$ across two superconductors. Parameters are $\Delta_0 = 1\text{meV}$ , $T/T_c = 0.01$ , $S = 1/2$ , $m' = -1/2$ , $h = 0.5E_F$ (for (a)), $k_F a = \pi$ , $\theta = \pi/2$ , $Z = 0$ , $J = 0.5$ (for (b)). . . . .	170
4.18	(a) Phase difference $\varphi_0$ as a function of exchange interaction ( $J$ ) of spin flipper. (b) Phase difference $\varphi_0$ as a function of magnetization ( $h$ ) of Ferromagnet's. (c) Density plot of $\varphi_0$ as function of exchange interaction ( $J$ ) of spin flipper and magnetization ( $h$ ) of Ferromagnet's. Parameters are $\Delta_0 = 1\text{meV}$ , $T/T_c = 0.01$ , $S = 1/2$ , $m' = -1/2$ , $h = 0.5E_F$ (for (a)), $k_F a = \pi$ , $\theta = \pi/2$ , $Z = 0$ , $J = 0.5$ (for (b)). . . . .	171
4.19	(a) Asymmetry of critical current as a function of exchange interaction ( $J$ ) of spin flipper. (b) Asymmetry of critical current as a function of magnetization ( $h$ ) of Ferromagnet's. (c) Asymmetry of the critical current as a function of exchange interaction ( $J$ ) of spin-flipper and magnetization ( $h$ ) of Ferromagnet's. Parameters are $\Delta_0 = 1\text{meV}$ , $T/T_c = 0.01$ , $f = 1$ ( $S = 1/2$ , $m' = -1/2$ ) (for (c)), $h = 0.5E_F$ (for (a)), $k_F a = \pi$ , $\theta = \pi/2$ , $Z = 0$ , $J = 0.5$ (for (b)). . . . .	172

4.20	(a) Anomalous Josephson current as a function of mis-orientation angle ( $\theta$ ) between two Ferromagnets' for different values of temperature. (b) Asymmetry of the critical current for different values of temperature calculated as a function of exchange interaction ( $J$ ) of spin flipper. (c) Phase difference $\varphi_0$ as a function of exchange interaction ( $J$ ) of spin flipper for different values of temperature. Parameters are $\Delta_0 = 1\text{meV}$ , $J = 1$ (for (a)), $h = 0.5E_F$ (for (a), (b) and (c)), $I_0 = e\Delta_0/\hbar$ , $f = 1$ ( $S = 1/2$ , $m' = -1/2$ ), $Z = 0$ , $k_F a = \pi$ , $\theta = \pi/2$ (for (b) and (c)) . . . . .	175
5.1	Conventional mechanism of the equilibrium spin transfer torque in a superconductor-ferromagnet-normal metal-ferromagnet-superconductor junction. (a) Magnetic moments of the ferromagnets are misaligned ( $\theta_1 \neq \theta_2$ ). Equilibrium spin-transfer torque $\tau^{equ} \propto \sin(\theta_1 - \theta_2)$ and points perpendicular to the plane spanned by the two magnetic moments of the ferromagnets, (b) Magnetic moments of the ferromagnets are aligned ( $\theta_1 = \theta_2$ ). $\tau^{equ} = 0$ : equilibrium spin-transfer torque vanishes. . . . .	181
5.2	Josephson junction composed of two ferromagnets and a spin flipper with spin $S$ and magnetic moment $m'$ at $x = 0$ sandwiched between two s-wave superconductors. In our model $\theta_1 = \theta$ and $\theta_2 = 0$ . When ferromagnets are aligned, i.e., $\theta \rightarrow 0$ , equilibrium spin transfer torque vanishes (see Fig. 5.1(b)), however in our setup a new quantum mechanism of spin flip scattering gives rise to a non-zero torque, which we denote as Equilibrium quantum spin torque (EQST). In this chapter, we mainly concentrate on the limit $\theta \rightarrow 0$ . . . . .	184
5.3	Josephson charge current and equilibrium quantum spin torque (EQST) as a function of phase difference ( $\varphi$ ) for different values of interface barrier strength ( $Z$ ). Parameters are $\Delta_0 = 1\text{meV}$ , $I_0 = e\Delta_0/\hbar$ , $T/T_c = 0.01$ , $J = 0.5$ , $h/E_F = 0.5$ , $\theta = 0$ , $S = 5/2$ , $m' = -1/2$ . Both $I_c$ and $\tau^{eq}$ are inhibited by increasing $Z$ and also EQST is zero for $\varphi = 0$ and $\varphi = 2\pi$ . . . . .	190
5.4	EQST as a function of phase difference ( $\varphi$ ) for (a) different values of exchange interaction ( $J$ ) of spin flipper and for (b) different values of magnetization ( $h$ ) of the ferromagnets. Parameters are $\Delta_0 = 1\text{meV}$ , $I_0 = e\Delta_0/\hbar$ , $T/T_c = 0.01$ , $Z = 0$ , $J = 1$ (for (b)), $h/E_F = 0.5$ , $\theta = 0$ , $S = 5/2$ , $m' = -1/2$ . In (a) EQST changes sign with change of exchange interaction $J$ and phase difference $\varphi$ . In (b) EQST increases with increasing magnetization $h$ of the ferromagnets. . . . .	191

5.5	(a) Equilibrium quantum spin torque (EQST) vs spin ( $S$ ) of spin flipper. (b) EQST vs spin flip probability ( $f$ ) of spin flipper for $S = 5/2$ and $m' = 5/2$ ( $f = 0$ ), $m' = 3/2$ and $m' = -5/2$ ( $f = 2.236$ ), $m' = 1/2$ and $m' = -3/2$ ( $f = 2.8284$ ) and $m' = -1/2$ ( $f = 3$ ). Parameters are $\Delta_0 = 1\text{meV}$ , $T/T_c = 0.01$ , $\varphi = \pi/2$ , $J = 1$ , $m' = -1/2$ (for (a)), $Z = 0$ , $\theta = 0$ , $h/E_F = 0.5$ . EQST decreases with increase of spin $S$ of spin flipper. . .	193
5.6	(a) EQST as function of misorientation angle ( $\theta$ ) for $\varphi = \pi/2$ . (b) EQST as function of exchange interaction ( $J$ ) of spin flipper for $\varphi = \pi/2$ and $\theta = 0$ . Parameters are $\Delta_0 = 1\text{meV}$ , $I_0 = e\Delta_0/\hbar$ , $T/T_c = 0.01$ , $Z = 0$ , $h/E_F = 0.5$ , spin flip case: $S = 3/2$ , $m' = -1/2$ , no flip case: $S = 3/2$ , $m' = 3/2$ and for (a) $J = 1$ . In (a) EQST is zero for $J = 0$ and no flip case ( $f = 0$ ), but finite for spin flip case ( $f \neq 0$ ). In (b) EQST changes sign with change in $J$ for antiferromagnetic coupling ( $J < 0$ ) and is also asymmetric with respect to $J$ . . . . .	194
5.7	EQST as a function of interface barrier strength ( $Z$ ). Parameters are $\Delta_0 = 1\text{meV}$ , $I_0 = e\Delta_0/\hbar$ , $T/T_c = 0.01$ , $\theta = 0$ , $h/E_F = 0.5$ , $\varphi = \pi/2$ , $J = 0.5$ , $S = 5/2$ , $m' = -1/2$ . EQST decreases with increase of $Z$ and in the tunneling regime ( $Z \rightarrow \text{large}$ ) EQST vanishes. . . . .	194
6.1	1D Josephson junction (JJ) loop (circumference $L_S$ , in orange) doped with a spin flipper and attached to two thermal reservoirs at temperatures $T_L$ and $T_R$ via two thermal valves $v_L$ and $v_R$ . A magnetic flux $\Phi$ controls phase difference $\varphi$ across spin flipper in JJ loop. $S_L$ and $S_R$ are the left and right superconductors maintained at phase difference $\varphi = \varphi_R - \varphi_L$ . High spin molecules like $\text{Fe}_{19}$ -complex can act as a spin flipper. . . . .	202
6.2	Two superconductors separated by (a) a delta potential magnetic impurity, (b) a rectangular barrier magnetic impurity, (c) a rectangular potential barrier and, (d) a delta potential barrier. . . . .	203
6.3	Josephson-Stirling cycle in $T\Omega$ ( $T$ is temperature and $\Omega$ is entropy) plane. Enclosed area in $T - \Omega$ plane corresponds to total heat exchanged $Q$ , which is equal to total work done $W$ during the cycle. . . . .	209



- 
- 6.4 *Total work done  $W$  and efficiency  $\eta$  of a Josephson-Stirling engine as function of  $\varphi_{fi}$  (for (a,c)) and as function of right reservoir temperature  $T_R$  (for (b,d)). Parameters are: Flip:  $S = -m' = 1/2$ ,  $f = 1$ ; No Flip:  $S = m' = 1/2$ ,  $f = 0$ . Rest of parameters:  $J = 0.1$ ,  $\varphi_{in} = 0$ ,  $\varphi_{fi} = \pi$  (for (b,d)),  $k_B T_R = 0.32\Delta$  (for (a,c)),  $k_B T_L = 0.01\Delta$ ,  $k_B T = 0.01\Delta$ . The black dotted line represents Carnot limit,  $\eta_C = 1 - \frac{T_L}{T_R}$  in (d). . . . . 214*
- 6.5 *Total work done  $W$  and efficiency  $\eta$  of a Josephson-Stirling engine as function of  $\varphi_f$  (for (a,c)) and as function of  $k_B T_R$  (for (b,d)) in presence of spin-flip scattering. Other parameters are:  $J = 0.1$ ,  $\varphi_{in} = 0$ ,  $\varphi_{fi} = \pi$  (for  $f = 1$ ),  $\varphi_{fi} = 0.92\pi$  (for  $f = 3$ ),  $\varphi_{fi} = 0.85\pi$  (for  $f = 5$ ),  $k_B T_L = 0.01\Delta$ ,  $k_B T_R = 0.32\Delta$  (for (a,c)),  $k_B T = 0.01\Delta$ . . . . . 215*
- 6.6 *(a,c) Total work  $W$  absorbed, and (b,d) COP of quantum refrigerator as function of  $\varphi_{fi}$  in presence of spin-flip scattering. Other parameters are:  $J = 0.1$ ,  $k_B T_L = 0.32\Delta$  (for (a,b)),  $k_B T_R = 0.31\Delta$  (for (a,b)),  $S = -m' = 1/2$  (for (c,d)),  $\varphi_{in} = 0$ . . . . . 217*
- 6.7 *(a) Total work  $W$  (b)  $Q_R$  and (c)  $Q_L$ , (d)  $\eta$  or COP as function of  $\varphi_{fi}$  and  $T_R$  in presence of spin flip scattering. Other parameters are:  $S = 1/2$ ,  $m' = -1/2$ ,  $J = 2$ ,  $k_B T_L = 0.01\Delta$ ,  $\varphi_{in} = 0$ . . . . . 218*
- 6.8 *(a) Total work done  $W$  (b)  $Q_R$  and (c)  $Q_L$  (d) efficiency  $\eta$  as function of maximal phase change  $\varphi_{fi}$  during Stirling cycle and right reservoir temperature  $T_R$  in absence of spin-flip scattering. Other parameters are:  $S = m' = 1/2$ ,  $J = 2$ ,  $k_B T_L = 0.01\Delta$ ,  $\varphi_{in} = 0$ . . . . . 219*
- 6.9 *(a) Total work done  $W$ , (b) heat exchanged  $Q_R$  and (c)  $Q_L$  and (d) efficiency  $\eta$  or COP as function of temperatures  $T_R$  and  $T_L$  in presence of spin-flip scattering. Parameters are:  $S = 1/2$ ,  $m' = -1/2$ ,  $J = 1$ ,  $\varphi_{in} = 0$ ,  $\varphi_{fi} = \pi$ . . . . . 221*

## LIST OF FIGURES

---

# List of Tables

2.1	Comparison of differential charge conductance at zero bias ( $E = 0$ ) in the topological regime between $N_1$ -spin flipper- $N_2$ -I-SOCSW and $N_1$ -spin flipper- $N_2$ -I- $p$ -wave junction . . . . .	90
3.1	Comparison of OTE-equal, OTE-mixed, LMDOS and SPLDOS between three cases: both spin mixing and spin flip scattering, only spin mixing and, only spin flip scattering . . . . .	136
4.1	Effect of breaking chiral and/or time reversal symmetry on anomalous Josephson current (spin flip probability is $f$ ; misorientation angle= $\theta$ ) . . . . .	174
6.1	Comparative analysis of Josephson junction based quantum heat engines and refrigerators . . . . .	228
B.1	Spin flip probability ( $f$ ) values of the spin flipper for different $S$ and $m'$ . . . .	245

## LIST OF TABLES

---

# Chapter 1

## Introduction

*“I seem to have been only like a boy playing on the seashore, and diverting myself in now and then finding a smoother pebble or a prettier shell than ordinary, whilst the great ocean of truth lay all undiscovered before me.”*

— Isaac Newton

In 1911, Heike Kamerlingh Onnes discovered a macroscopic quantum phenomenon which is called superconductivity. He first observed that the electrical resistance in certain materials disappeared when they were cooled down below a specific critical temperature  $T_c$ [1]. After that, hundreds of materials were discovered that are superconducting with different critical temperatures. Zero resistance is a fundamental property of a superconductor; however, it is not sufficient to understand the nature of the superconducting state. In 1933, two German physicists Walther Meissner and Robert Ochsenfeld, experimentally discovered another vital property of Superconductor. They observed that inside the Superconductor magnetic field is zero, making the Superconductor a perfect diamagnet. When a superconductor is cooled down from a normal state by applying a magnetic field, then this magnetic field is expelled from the Superconductor. This phenomenon is called the Meissner effect. The two phenomena, one of vanishing electrical resistance and that of the expulsion of

the magnetic field, are observed below the critical temperature, whereas above the critical temperature superconductivity vanishes[2]. Vanishing electrical resistance and expulsion of the magnetic field are two macroscopic quantum phenomena; however, there was no microscopic description of superconductivity for another 20 years. In 1957, Bardeen, Cooper, and Schieffer described the first microscopic theory of superconductivity, which is known as BCS theory[3], for which they got the Nobel Prize in Physics in 1972. They proposed that the supercurrent in a superconductor is carried by pairs of electrons known as Cooper pairs, which are formed due to electron-phonon interaction in the case of conventional superconductors. For temperatures above the critical temperature ( $T > T_c$ ), the lattice vibration energy is larger than the pairing energy of the electrons leading to Cooper pairs breaking and superconductivity being destroyed.

When a superconductor is brought into contact with a non-superconducting material (say, Normal metal), superconducting pair correlations leak into the non-superconducting material. This phenomenon is called the proximity effect. The superconducting pair correlations decay monotonically inside the normal metal[4]. However, when a magnetic material like ferromagnet replaces normal metal, then superconducting correlations show an oscillatory decay[5] inside the ferromagnet, which is superimposed on the exponential decay. This kind of behavior is that for ferromagnet spin-up and spin-down electrons, Fermi surfaces are no longer degenerate. At the superconductor-ferromagnet interface, both superconductivity and spin polarization combine to create a new superconducting state which offers the possibility to reduce heating effects related to spintronic devices[6]. Spintronics is one of the most popular areas of research that offers the control of spin degrees of freedom in solid-state devices. The purpose of combining superconductivity and spintronics is the injection of spin-polarized quasi-particles into superconductors. The interfaces between Superconductor and ferromagnet have led to many surprising

---

phenomena: Josephson  $\pi$  junction, the spin Josephson effect, and novel applications, such as the Josephson qubit. Recently, at superconductor-ferromagnet interfaces, spin-triplet Cooper pairs have been discovered[7] which give a complete synergy between superconductivity and spintronics. Spin triplet supercurrent can have a net spin component which offers the potential to reduce heating effects linked with spintronic devices[6]. Nevertheless, to utilize this supercurrent, one has to generate and manipulate triplet Cooper pairs in devices. Recently, there has been remarkable progress in this area, not only on the experimental side[8] where it has become routine to create triplet Cooper pairs at superconductor-ferromagnet interfaces but on the theoretical side, odd frequency spin-triplet pairing is seen in Metal-Superconductor interfaces due to spin-flip scattering.

This thesis addresses spin transport in normal metals/Ferromagnets junctions with  $s$ -wave superconductors. We make a detailed study of the effects of Andreev reflection mediated transport at metal superconductor junctions in the presence of a spin flipper (magnetic impurity) at the interface. The signature of Yu-Shiba-Rusinov (YSR) bound states are observed for energies in the superconducting gap due to spin-flip scattering at metal-superconductor interfaces. Further, we see that odd frequency equal spin-triplet correlations at metal-superconductor interfaces occur due to spin-flip scattering. We also examine the Josephson effect in the presence of a spin flipper. Theoretically, we show that a tunable  $0 - \pi$  Josephson junction is possible without taking recourse to Ferromagnets or high  $T_c$  superconductors. We also look into the possible applications of this tunable  $0 - \pi$  junction in quantum computation. We study the anomalous Josephson effect in a ferromagnetic Josephson junction in the presence of a spin flipper. We show that this system can act as a phase battery that can store quantized amounts of superconducting phase difference in the ground state of the junction. Further, a novel quantum spin torque at equilibrium is induced in the presence of spin-flip scattering in such a Ferromagnetic

Josephson junction. Finally, we study the application of our spin-flipper doped Josephson junction in quantum thermodynamics. We focus on the theoretical understanding of such new phenomena and their potential significance concerning charge and spin transport. Below we will introduce the three critical phenomena which are needed to understand this thesis: (1) **Andreev reflection**, (2) **Spin flip scattering**, and (3) **Josephson effect**. We start with Andreev reflection.

## 1.1 Andreev reflection

At the interface between Normal metal (N) and Superconductor (S), a particle scattering process occurs known as Andreev reflection. It involves an electron (hole) incident on the interface from the Normal metal side with energy below the superconducting gap. A Cooper pair is formed inside the Superconductor, and there is retroreflection of a hole (electron) of opposite spin and velocity but equal in momentum to the incident electron (hole). Current in Normal metal is converted to a supercurrent in Superconductor by the Andreev reflection process. Each process transfers a charge  $2e$  across the interface, see

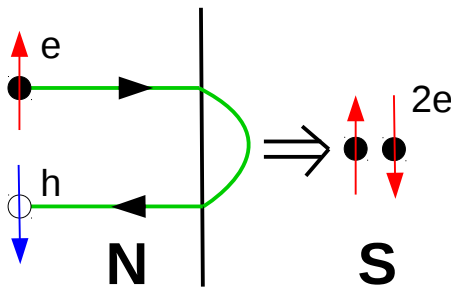


Figure 1.1: *Andreev reflection process: an incident electron from the normal metal is retroreflected as a hole and a Cooper pair is formed inside the s-wave superconductor below the superconducting gap.*



Fig. 1.1(a). An incident electron at the NS interface leads to a hole being retroreflected. The hole is the time-reversed trajectory of an electron. Since the Cooper pair consists of both up and down spin electrons thus, the Andreev process can be thought of as two electrons with opposite spin entering the Superconductor to form a Cooper pair. Similarly, one can also define this Andreev process as breaking up a Cooper pair into two electrons. In this process near the Fermi level, energy and momentum are conserved. However, the spin magnetic moment is not conserved since the incoming electron and Andreev reflected hole occupy opposite spin bands. Andreev reflection is also possible at the Ferromagnet (F)-Superconductor (S) interface but is affected by exchange interaction in a ferromagnet. Since spin-up and spin-down bands in a ferromagnet are different, there is no complete Andreev reflection at an FS interfaces[9, 10].

### 1.1.1 Blonder-Tinkham-Klapwijk (BTK) Model

Blonder, Tinkham, and Klapwijk (BTK) model was developed in 1982. The BTK model[9] describes Andreev and normal reflection at normal metal (N)-superconductor (S) interface, as well as transmission of electron-like and hole-like quasi-particles through the interface above the superconducting gap. In this model, the Normal metal-Superconductor (NS) interface is modeled as a  $\delta$ -shaped potential barrier of strength,  $V$  depicted in Fig. 1.2. If an electron with energy  $E$  is incident at the interface from Normal metal with energy  $E > \Delta$ , this electron can be reflected into the Normal metal. There is also the possibility of Andreev reflection, i.e., a hole can be reflected into Normal metal, while electron-like and hole-like quasi-particles are transmitted into the Superconductor. The model Hamiltonian in Bogoliubov-de Gennes (BdG) formalism for the setup depicted in Fig. 1.2 is given as

$$\begin{pmatrix} H & \Delta\Theta(x) \\ \Delta^*\Theta(x) & -H \end{pmatrix} \Psi(x) = E\Psi(x), \quad (1.1)$$

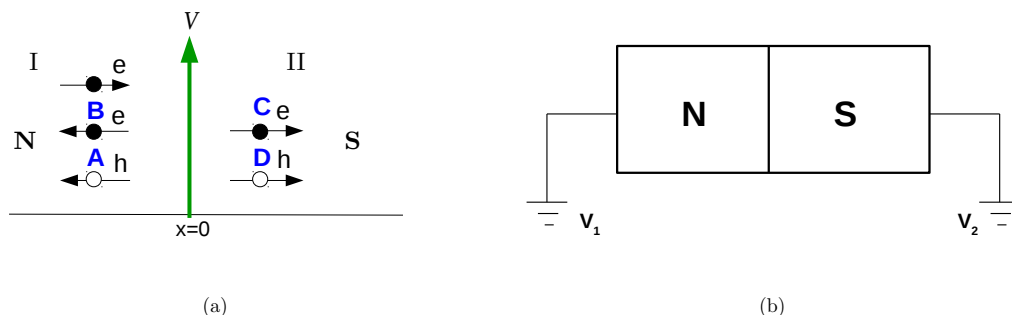


Figure 1.2: (a) An electron, with energy  $E$  coming from the normal metal (N), interacts at  $x = 0$  with a  $\delta$ -like potential barrier of strength  $V$ . Electron and hole are reflected back to the normal metal (N) and electron-like and hole-like quasiparticles are transmitted into the  $s$ -wave superconductor (S). The closed circles denote electrons and electron-like quasiparticles and the open circles denote holes and hole-like quasiparticles.  $A$  is Andreev reflection probability, while  $B$  denotes probability of normal reflection.  $C$  and  $D$  are transmission probabilities of electron-like and hole-like quasiparticles respectively, (b) NIS junction where N is connected to voltage  $V_1$  and S is connected to voltage  $V_2$  and  $V = V_1 - V_2$  is the voltage drop across the NIS junction.

where  $H = \frac{p^2}{2m^*} + V\delta(x) - E_F$ ,  $\Delta$  is the superconducting gap,  $\psi$  is a two component spinor and  $\Theta(x)$  is Heaviside step function. Further, in  $H$  the first term is kinetic energy of incident electron with an effective mass  $m^*$ , second term  $V$  denotes strength of the  $\delta$ -like potential barrier at the NS interface and the third term is Fermi energy.

The wavefunctions in the N and S regions of the system depicted in Fig. 1.2 can be written as

$$\psi_N(x) = \begin{bmatrix} 1 \\ 0 \end{bmatrix} e^{ik_e x} + a \begin{bmatrix} 0 \\ 1 \end{bmatrix} e^{ik_h x} + b \begin{bmatrix} 1 \\ 0 \end{bmatrix} e^{-ik_e x}, \text{ in Normal metal } (x < 0), \quad (1.2)$$

and

$$\psi_S(x) = c \begin{bmatrix} u \\ v \end{bmatrix} e^{iq^+ x} + d \begin{bmatrix} v \\ u \end{bmatrix} e^{-iq^- x}, \text{ in Superconductor } (x > 0). \quad (1.3)$$

$a, b, c, d$  are the corresponding scattering amplitudes for Andreev reflection, normal reflection, transmission of electron-like quasiparticle and transmission of hole-like quasiparticle

respectively.  $u = \sqrt{\frac{1}{2}\left(1 + \frac{\sqrt{E^2 - \Delta^2}}{E}\right)}$ ,  $v = \sqrt{\frac{1}{2}\left(1 - \frac{\sqrt{E^2 - \Delta^2}}{E}\right)}$  are the BCS coherence factors.  $k_{e,h} = \sqrt{\frac{2m^*}{\hbar^2}(E_F \pm E)}$  are wavevectors of electron and hole in the normal metal and  $q_{\pm} = \sqrt{\frac{2m^*}{\hbar^2}(E_F \pm \sqrt{E^2 - \Delta^2})}$  are wavevectors of electron-like and hole-like quasiparticles in superconductor. If we consider Andreev approximation, i.e.,  $E_F \gg E, \Delta$ , then we have  $k_e = k_h = q_+ = q_- = k_F$ , where  $k_F$  is the Fermi wavevector. The boundary conditions at  $x = 0$  are,

$$\psi_S(0) = \psi_N(0), \quad \text{and} \quad \frac{\hbar^2}{2m^*}(\psi'_S(0) - \psi'_N(0)) = V\psi_N(0). \quad (1.4)$$

We impose boundary conditions on the wave functions in Eqs. (1.2), (1.3) and get 4 equations which are,

$$cu + dv = 1 + b, \quad (1.5)$$

$$cv + du = a, \quad (1.6)$$

$$cv - du - a = -i2Za, \quad (1.7)$$

$$cu - dv - 1 + b = -i2Z(1 + b), \quad (1.8)$$

where,  $Z = \frac{m^*V}{\hbar^2 k_F}$  is defined as interface transparency. Solving (1.5)-(1.8) we get the scattering probabilities, for  $E > \Delta$ ,

$$A = |a|^2 = \frac{u^2 v^2}{\gamma^2}, \quad (\gamma^2 = [u^2 + Z^2(u^2 - v^2)]^2), \quad B = |b|^2 = \frac{(u^2 - v^2)^2 Z^2 (1 + Z^2)}{\gamma^2},$$

$$C = (u^2 - v^2) |c|^2 = \frac{(u^2 - v^2) u^2 (1 + Z^2)}{\gamma^2}, \quad D = (u^2 - v^2) |d|^2 = \frac{(u^2 - v^2) v^2 Z^2}{\gamma^2}.$$

and for  $E < \Delta$ ,

$$A = |a|^2 = \frac{\Delta^2}{E^2 + (\Delta^2 - E^2)(1 + 2Z^2)^2}, \quad B = |b|^2 = \frac{4Z^2(1 + Z^2)(\Delta^2 - E^2)}{E^2 + (1 + 2Z^2)^2(\Delta^2 - E^2)}, \quad C = 0, \quad D = 0.$$

$A$  is Andreev reflection probability of an electron reflected back as a hole, while  $B$  denotes probability of normal reflection.  $C$  is transmission probability through interface of an

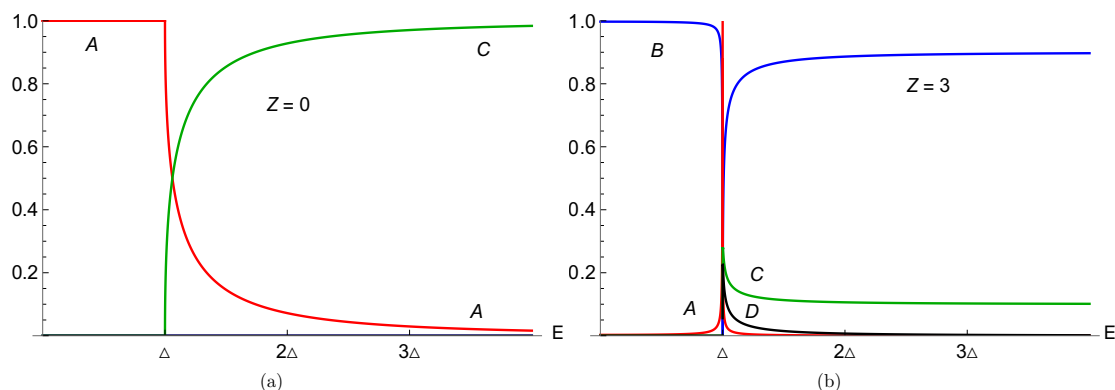


Figure 1.3: Plots of reflection ( $A, B$ ) and transmission ( $C, D$ ) probabilities at N-S interface.

electron-like quasiparticle, while  $D$  is transmission probability through interface of a hole-like quasiparticle. Below the gap, there is no quasiparticle transmission and only a Cooper pair is formed, therefore  $C = D = 0$ . Generally,  $A, B, C,$  and  $D$  depend on the detailed shape of the potential barrier and the incident angle of the trajectory. *For simplicity, in this chapter and much of the thesis, unless mentioned to the contrary, we restrict ourselves to a one-dimensional geometry assuming that the system is translationally invariant along  $y$ - and  $z$ -axis.*

In Fig. 1.3(a) we plot different reflection and transmission probabilities for transparent ( $Z = 0$ ) regime. We see that when there is no barrier at the interface, no normal reflection can occur. Thus normal reflection probability  $B = 0$ , but Andreev reflection probability  $A = 1$ , below the gap for  $Z = 0$ . In Fig. 1.3(b) we plot probabilities in tunneling regime ( $Z = 3$ ). We see here that normal reflection can also occur in contrast to a transparent regime. In the Andreev reflection probability, there is a peak at the gap edge  $E = \Delta$ .

To calculate the current across the interface, we consider the current contribution in the energy  $[E, E + dE]$  interval. This contribution is proportional to several factors. First, electron velocity  $v(E)$ , then the density of states  $N(E)$ , assumed to be energy-dependent.

Next, Fermi distribution function  $f(E)$ , which describes occupancy of electronic states, and finally, electronic charge  $e$ . These factors are taken together and integrated over the interface area  $\mathcal{A}$  (assuming that current density does not vary across the interface), the current contribution due to Andreev reflected electrons could then be written as  $e\mathcal{A}v(E)N(E)A(E)f(E)dE$ . In order to obtain the contribution due to other scattering processes, similar expressions can be obtained by replacing the Andreev reflection probability  $A(E)$  with the respective scattering probability. The product  $N(E)f(E)dE$  equals the density of electrons in the respective energy interval.

Taking into account all the relevant contributions and integrating them over the energy range gives the total current. Since current has to be conserved, one can calculate on either side of the interface. However, it is more convenient to do it on the metal side as current is carried by single particles instead of quasi-particles on the Superconductor side. An incident wave with probability amplitude 1 carries a positive current at any point on the metallic side. The wave corresponding to Andreev reflection probability  $A$  is in the opposite direction. However, it will contribute a positive current since it describes a hole with an opposite charge. The wave corresponding to normal reflection probability  $B$  represents a reflected electron and contributes an opposing current. In addition to this, there will also be a current originating from the Superconductor, which eventually cancels out the current due to the incident and scattered waves. At this moment, we describe the probability of this latter current by the factor  $X$ . No current can pass in the absence of any bias across the NIS junction, and one can equate the several currents moving in either direction. As a result, one can find an expression for the scattering probabilities:  $1 + A = B + X$ , which gives  $X = 1 + A - B$ . We now have a current equation in the absence of bias, which gives a stable situation. Applying a bias  $V$  across the junction means the Fermi level in the metal is raised by  $eV$ . Assuming transport across the interface is ballistic,

which is possible in case it is point contact, with a contact diameter small compared to the electrons mean-free path[9, 11]. The electrons in the biased metal can then be described by an equilibrium Fermi function. The Fermi levels will align when materials are joined, which can be taken as a reference level. Consequently, electrons originating from the metal will have a distribution function  $f(E - eV)$ , and those coming from the Superconductor will have a distribution function  $f(E)$ . Subsequently, the current in one direction will be different from that in the other direction, and a net current will flow through the junction. We consider the linear transport regime, i.e.,  $eV \ll E_F$ , such that transport occurs at or near the Fermi energy. Thus, from BTK theory[9, 12], when a voltage bias  $V$  is applied across the NS interface (see Fig. 1.2(b)), the electrical current at finite temperature in one dimension can be calculated as,

$$I_{NIS} = 2N(E_F)ev_F\mathcal{A} \int_{-\infty}^{\infty} [f(E - eV) - f(E)][1 + A(E) - B(E)]dE, \quad (1.9)$$

where  $f(E)$  is the Fermi Dirac distribution function,  $N(E_F)$  denotes density of states at Fermi level,  $e$  is the electronic charge,  $\mathcal{A}$  is the contact area over which the Normal metal and Superconductor touch, and  $v_F$  is velocity of electrons at the Fermi level. Since Fermi distribution function  $f(E - eV) - f(E)$  is only non-zero in the region  $eV$  around  $E_F$ , for which  $eV \ll E_F$ , and the electron velocity as well as density of states are constant in this interval, one may take them out of the integral.

From Eq. (1.9) its easy to see that normal reflection decreases current, while Andreev reflection increases it. At zero temperature, the Fermi Dirac distribution functions can be written as a Heaviside step function,  $f(E - eV) = \Theta(eV - E)$  and  $f(E) = \Theta(-E)$ . Thus, at zero temperature, Eq. (1.9) reduces to,

$$I_{NIS} = 2N(E_F)ev_F\mathcal{A} \int_0^{eV} [1 + A(E) - B(E)]dE. \quad (1.10)$$

When there is no superconductor, i.e., a NIN junction, for which superconducting gap vanishes ( $\Delta = 0$ ). Then,  $u = 1$  and  $v = 0$ . Thus, we get the scattering probabilities, for  $E > \Delta$ , as

$$A = \frac{u^2 v^2}{[u^2 + Z^2(u^2 - v^2)]^2} = 0, \quad (1.11)$$

$$B = \frac{(u^2 - v^2)^2 Z^2 (1 + Z^2)}{[u^2 + Z^2(u^2 - v^2)]^2} = \frac{Z^2}{1 + Z^2}. \quad (1.12)$$

Eq. (1.10) then gives,

$$I_{NIN} = \frac{2N(E_F)e^2 v_F \mathcal{A} V}{1 + Z^2} = \frac{V}{R_N} = G_N V, \quad (1.13)$$

where  $R_N = \frac{1+Z^2}{2N(E_F)e^2 v_F \mathcal{A}}$  is the normal state resistance and  $G_N = \frac{1}{R_N}$  is the normal state conductance. If we take derivative with respect to  $E$  at  $E = eV$  on both sides of Eq. (1.10), then we will get

$$\frac{dI_{NIS}}{dV} = 2N(E_F)e^2 v_F \mathcal{A} [1 + A(eV) - B(eV)] = \frac{1 + Z^2}{R_N} [1 + A(eV) - B(eV)]. \quad (1.14)$$

$$\text{Thus, } \frac{dI_{NIS}}{dV} = \frac{1 + Z^2}{R_N} [1 + A(eV) - B(eV)] = G_N [1 + Z^2] [1 + A(eV) - B(eV)]. \quad (1.15)$$

The quantity  $\frac{dI_{NIS}}{dV}$  in Eq. (1.15) is defined as the differential charge conductance ( $G_c$ ) at zero temperature and it is proportional to  $(1 + A(E) - B(E))$  at  $E = eV$ . In Fig. 1.4 we plot differential conductance versus voltage for different values of interface transparency  $Z$  at zero temperature. We see that there is a continuous variation of differential conductance from transparent to tunneling limit. For transparent junction,  $G_c/G_N$  is constant at 2, while for tunnel junction  $G_c/G_N$  almost vanishes below the gap.

In this section, we have introduced the Andreev reflection process. We have also discussed BTK formalism and showed how an electron is Andreev reflected as a hole when it is incident with energy  $E$  at NS interface for electron energies below the gap. When

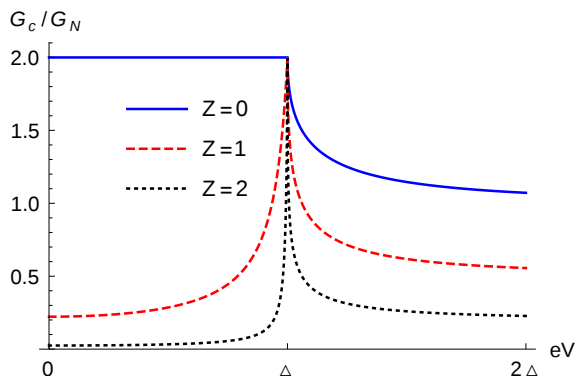


Figure 1.4: Differential charge conductance normalized by normal state conductance ( $G_N$ ), as function of voltage for different values of interface transparency  $Z$  at zero temperature. Here,  $G_N = \frac{2N(E_F)e^2v_F\mathcal{A}}{1+Z^2}$  and  $\Delta$  the superconducting gap.

electron energy is above the gap, there is a possibility of electron-like and hole-like quasi-particle transmission into the Superconductor. The following section will discuss spin-flip scattering, which occurs when an electron interacts with a spin flipper. Following that, we will probe the interplay between Andreev reflection and spin-flip scattering.

## 1.2 Spin flip scattering

Consider a spin-up electron with energy  $E$ , incident from left normal metal ( $N_1$ ) region, as shown in Fig. 1.5(a), onto the interface ( $x = 0$ ). This electron interacts with the spin flipper through an exchange potential which may induce a mutual spin flip. The electron can be reflected (region I,  $x < 0$ ) or transmitted to the right normal metal ( $N_2$ ), region II ( $x > 0$ ), with spin up or down. The model Hamiltonian[13] for the system depicted in Fig. 1.5 is,

$$H = \frac{p^2}{2m^*} - J_0\delta(x)\vec{s}\cdot\vec{S}, \quad (1.16)$$

where the first term is the kinetic energy of electron with effective mass  $m^*$ , in the second term,  $J_0$  is the strength of exchange coupling[13] between electron's spin  $\vec{s}$  and spin flipper's spin  $\vec{S}$ . Explicitly in terms of spin raising and lowering operators for electron as well as a



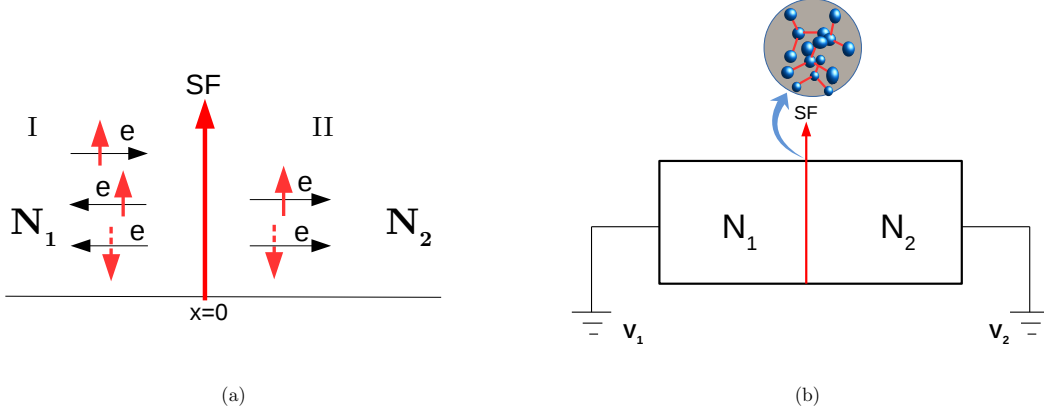


Figure 1.5: (a) A spin up electron with energy  $E$  coming from the metallic region  $N_1$  interacts at  $x = 0$  with a spin flipper (SF) through an exchange potential, leading to finite probability for flipping its own spin and spin of the spin flipper, (b)  $N_1$ -SF- $N_2$  junction where  $N_1$  is connected to voltage  $V_1$  and  $N_2$  is connected to voltage  $V_2$  and  $V = V_1 - V_2$  is the voltage bias applied at the interface. High spin molecules like  $Fe_{19}$ -complex can act as a spin flipper.

spin flipper, we can write,

$$\vec{s} \cdot \vec{S} = s_z S_z + \frac{1}{2}(s^- S^+ + s^+ S^-), \quad (1.17)$$

where  $s_i = \frac{\hbar}{2}\sigma_i$ ,  $\sigma_i$  ( $i = x, y, z$ ) are Pauli spin matrices,  $s^\pm = s_x \pm i s_y$  are spin raising and lowering operators for electron and  $S^\pm = S_x \pm i S_y$  are spin raising and lowering operators for spin flipper. *Spin flipper* is a delta potential magnetic impurity that can be treated similarly to an Anderson impurity. Spin flipper Hamiltonian  $H_{\text{Spin flipper}} = -J_0 \delta(x) \vec{s} \cdot \vec{S}$  is an effective Heisenberg term which reduces the two-electron problem to a one-electron problem[14]. Since our problem is not a time-dependent problem, we solve it using the time-independent Schrödinger equation modified by BdG Hamiltonian. Thus, the spin flipper has no time dependent dynamics of its own, rather it has a spin dependent dynamics which means, if spin-flipper spin is in up state for  $S = 1/2$ ,  $m' = 1/2$  and incident electron's spin is in up state, then it acts as ordinary impurity but if incident electron's spin is in down state, then there is probability of mutual spin flip. The problem is symmetric such that when

spin-flipper's spin is in down state, roles of up and down electron incident are reversed, which differentiates our model spin-flipper from a Kondo-like magnetic impurity[15], which has finite time dynamics, and it leads to a screening of impurity spins by metallic electrons below Kondo temperature[16]. Experimentally, high spin molecules, for example, Fe<sub>19</sub>-complex with a spin of  $S = 33/2$  can to a certain extent be a model for the spin flipper. It is to be noted that the internal dynamics of such a high spin molecule may be quite different from the spin-flipper considered here. Even then, the spin flipper can mimic the half-integer spin states ( $S$ ) up to any arbitrary high value and the associated spin magnetic moment of the high spin molecule and the consequence of an electron interacting with such, to a large extent.

The wavefunctions in the different regions of setup depicted in Fig. 1.5(a) are,

$$\psi_I(x) = \begin{bmatrix} 1 \\ 0 \end{bmatrix} e^{ikx} \phi_{m'}^S + r_{\uparrow\uparrow} \begin{bmatrix} 1 \\ 0 \end{bmatrix} e^{-ikx} \phi_{m'}^S + r_{\uparrow\downarrow} \begin{bmatrix} 0 \\ 1 \end{bmatrix} e^{-ikx} \phi_{m'+1}^S, \text{ for } x < 0, \quad (1.18)$$

$$\psi_{II}(x) = t_{\uparrow\uparrow} \begin{bmatrix} 1 \\ 0 \end{bmatrix} e^{ikx} \phi_{m'}^S + t_{\uparrow\downarrow} \begin{bmatrix} 0 \\ 1 \end{bmatrix} e^{ikx} \phi_{m'+1}^S, \text{ for } x > 0, \quad (1.19)$$

where  $r_{\uparrow\uparrow}$  is the reflection amplitude when an incident spin up electron is reflected as spin up electron, while  $r_{\uparrow\downarrow}$  is the reflection amplitude when an incident spin up electron is reflected as spin down electron. Similarly,  $t_{\uparrow\uparrow}$  is the transmission amplitude, when an incident spin-up electron is transmitted as the spin-up electron, while  $t_{\uparrow\downarrow}$  is the transmission amplitude when an incident spin-up an electron is transmitted as a spin-down electron.  $\phi_{m'}^S$  represents eigen-spinor of spin flipper, wherein  $S$  is spin angular momentum and  $m'$  being spin magnetic moment of spin flipper. The action of  $S_z$  operator of spin flipper on spin flipper eigen spinor is  $S_z \phi_{m'}^S = \hbar m' \phi_{m'}^S$ , and  $k = \sqrt{2m^* E / \hbar^2}$ , with incident electron energy  $E > 0$ . Similarly as mentioned above, if we consider a spin down electron with energy  $E$

incident from  $N_1$ , the wavefunctions in different regions can be written as

$$\psi_I(x) = \begin{bmatrix} 0 \\ 1 \end{bmatrix} e^{ikx} \phi_{m'}^S + r_{\uparrow\downarrow} \begin{bmatrix} 1 \\ 0 \end{bmatrix} e^{-ikx} \phi_{m'-1}^S + r_{\downarrow\downarrow} \begin{bmatrix} 0 \\ 1 \end{bmatrix} e^{-ikx} \phi_{m'}^S, \text{ for } x < 0, \quad (1.20)$$

$$\psi_{II}(x) = t_{\uparrow\uparrow} \begin{bmatrix} 1 \\ 0 \end{bmatrix} e^{ikx} \phi_{m'-1}^S + t_{\downarrow\downarrow} \begin{bmatrix} 0 \\ 1 \end{bmatrix} e^{ikx} \phi_{m'}^S, \text{ for } x > 0, \quad (1.21)$$

where  $r_{\uparrow\downarrow}$  is the reflection amplitude when an incident spin down electron is reflected as spin up electron, while  $r_{\downarrow\downarrow}$  is the reflection amplitude when an incident spin down electron is reflected as spin down electron. Similarly,  $t_{\uparrow\uparrow}$  is the transmission amplitude when an incident spin-down electron is transmitted as a spin-up electron. In contrast,  $t_{\downarrow\downarrow}$  is the transmission amplitude when an incident spin-down electron is transmitted as a spin-down electron. The boundary conditions at interface are,

$$\psi_I(x=0) = \psi_{II}(x=0), \quad \text{and} \quad \left. \frac{d\psi_{II}}{dx} \right|_{x=0} - \left. \frac{d\psi_I}{dx} \right|_{x=0} = -\frac{2m^* J_0 \vec{s} \cdot \vec{S}}{\hbar^2} \psi_I(x=0), \quad (1.22)$$

where  $\vec{s} \cdot \vec{S} = \vec{s} \cdot \vec{S} = s_z S_z + \frac{1}{2}(s^- S^+ + s^+ S^-)$  is exchange operator[13] in Hamiltonian(1.16).  $s^\pm = s_x \pm i s_y$  and  $S^\pm = S_x \pm i S_y$  are spin-raising and spin-lowering operators for electron and spin flipper respectively with  $s_z = \frac{\hbar}{2} \sigma_z$ ,  $s_x = \frac{\hbar}{2} \sigma_x$ ,  $s_y = \frac{\hbar}{2} \sigma_y$ ,  $s^+ = \frac{\hbar}{2}(\sigma_x + i\sigma_y)$  and  $s^- = \frac{\hbar}{2}(\sigma_x - i\sigma_y)$ .

From boundary condition (1.22), when spin up electron is incident, action of  $\vec{s} \cdot \vec{S}$  on  $\psi_I(x=0)$  (see Eq. (1.18)) can be understood as follows:

$$\vec{s} \cdot \vec{S} \psi_I(x=0) = \vec{s} \cdot \vec{S} \begin{bmatrix} 1 \\ 0 \end{bmatrix} \phi_{m'}^S + r_{\uparrow\uparrow} \vec{s} \cdot \vec{S} \begin{bmatrix} 1 \\ 0 \end{bmatrix} \phi_{m'}^S + r_{\downarrow\downarrow} \vec{s} \cdot \vec{S} \begin{bmatrix} 0 \\ 1 \end{bmatrix} \phi_{m'+1}^S. \quad (1.23)$$

In Eq. (1.23) for first term and second term:

$$\begin{aligned} \vec{s} \cdot \vec{S} \begin{bmatrix} 1 \\ 0 \end{bmatrix} \phi_{m'}^S &= [s_z S_z + \frac{1}{2}(s^- S^+ + s^+ S^-)] \begin{bmatrix} 1 \\ 0 \end{bmatrix} \phi_{m'}^S \\ &= s_z S_z \begin{bmatrix} 1 \\ 0 \end{bmatrix} \phi_{m'}^S + \frac{1}{2} s^- S^+ \begin{bmatrix} 1 \\ 0 \end{bmatrix} \phi_{m'}^S + \frac{1}{2} s^+ S^- \begin{bmatrix} 1 \\ 0 \end{bmatrix} \phi_{m'}^S. \end{aligned} \quad (1.24)$$

Herein,  $s_z$  acts on electron spinor  $\begin{bmatrix} 1 \\ 0 \end{bmatrix}$ , while  $S_z$  acts on spin flipper spinor  $\phi_{m'}^S$ . Similarly,

$s^-$ , and  $S^+$  and  $s^+$  and  $S^-$ , they act on their respective spinors. Thus,  $s^+ \begin{bmatrix} 1 \\ 0 \end{bmatrix} = 0$ , since  $s^+$  is the spin raising operator for electron and there are no higher spin states for a spin-1/2 electron than up and so the 3rd term in Eq. (1.24) vanishes, while  $s^- \begin{bmatrix} 1 \\ 0 \end{bmatrix} = \hbar \begin{bmatrix} 0 \\ 1 \end{bmatrix}$ , the spin

lowering operator gives the down spin state  $\begin{bmatrix} 0 \\ 1 \end{bmatrix}$  of electron. Further, for spin-up electron

$s_z \begin{bmatrix} 1 \\ 0 \end{bmatrix} = \frac{\hbar}{2} \begin{bmatrix} 1 \\ 0 \end{bmatrix}$ , and for spin flipper:  $S_z \phi_{m'}^S = \hbar m' \phi_{m'}^S$ . The spin-raising operator acting on spin flipper give:  $S^+ \phi_{m'}^S = C_{sm'}^+ \phi_{m'+1}^S$ . Now, we are going to derive  $C_{sm'}^+$ . Since  $\phi_{m'}^S$  is normalized, we get,

$$(S^+ |\phi_{m'}^S\rangle)^\dagger (S^+ |\phi_{m'}^S\rangle) = |C_{sm'}^+|^2 \langle \phi_{m'+1}^S | \phi_{m'+1}^S \rangle = |C_{sm'}^+|^2. \quad (1.25)$$

$$\text{Thus, } |C_{sm'}^+|^2 = \langle \phi_{m'}^S | S^- S^+ | \phi_{m'}^S \rangle. \quad (1.26)$$

But since  $S^- S^+ = S^2 - S_z^2 - \hbar S_z$ , thus from Eq. (1.26) we get,

$$C_{sm'}^+ = \sqrt{\langle \phi_{m'}^S | S^2 - S_z^2 - \hbar S_z | \phi_{m'}^S \rangle} = \hbar \sqrt{S(S+1) - m'(m'+1)} = \hbar \sqrt{(S-m')(S+m'+1)}. \quad (1.27)$$

## 1.2. Spin flip scattering

Therefore, the spin-raising operator acting on spin flipper give:  $S^+ \phi_{m'}^S = \hbar \sqrt{(S - m')(S + m' + 1)} \phi_{m'+1}^S = \hbar f \phi_{m'+1}^S$ . Similarly, for spin-lowering operator  $S^-$  acting on spin flipper we can derive that  $S^- \phi_{m'+1}^S = \hbar \sqrt{(S - m')(S + m' + 1)} \phi_{m'}^S = \hbar f \phi_{m'}^S$ . Thus, from Eq. (1.24) we get,

$$\vec{s} \cdot \vec{S} \begin{bmatrix} 1 \\ 0 \end{bmatrix} \phi_{m'}^S = \frac{\hbar^2 m'}{2} \begin{bmatrix} 1 \\ 0 \end{bmatrix} \phi_{m'}^S + \frac{\hbar^2 f}{2} \begin{bmatrix} 0 \\ 1 \end{bmatrix} \phi_{m'+1}^S. \quad (1.28)$$

In Eq. (1.23) for third term:

$$\begin{aligned} \vec{s} \cdot \vec{S} \begin{bmatrix} 0 \\ 1 \end{bmatrix} \phi_{m'+1}^S &= [s_z S_z + \frac{1}{2}(s^- S^+ + s^+ S^-)] \begin{bmatrix} 0 \\ 1 \end{bmatrix} \phi_{m'+1}^S \\ &= s_z S_z \begin{bmatrix} 0 \\ 1 \end{bmatrix} \phi_{m'+1}^S + \frac{1}{2} s^- S^+ \begin{bmatrix} 0 \\ 1 \end{bmatrix} \phi_{m'+1}^S + \frac{1}{2} s^+ S^- \begin{bmatrix} 0 \\ 1 \end{bmatrix} \phi_{m'+1}^S. \end{aligned} \quad (1.29)$$

Now,  $s_z = -\frac{\hbar}{2} \begin{bmatrix} 0 \\ 1 \end{bmatrix}$ ,  $s^- \begin{bmatrix} 0 \\ 1 \end{bmatrix} = 0$ ,  $s^+ \begin{bmatrix} 0 \\ 1 \end{bmatrix} = \begin{bmatrix} 1 \\ 0 \end{bmatrix}$ ,  $S_z \phi_{m'+1}^S = \hbar(m' + 1) \phi_{m'+1}^S$  and,

$S^- \phi_{m'+1}^S = \hbar \sqrt{(S - m')(S + m' + 1)} \phi_{m'}^S = \hbar f \phi_{m'}^S$ . Thus, from Eq. (1.29) we get,

$$\vec{s} \cdot \vec{S} \begin{bmatrix} 0 \\ 1 \end{bmatrix} \phi_{m'+1}^S = -\frac{\hbar^2(m' + 1)}{2} \begin{bmatrix} 0 \\ 1 \end{bmatrix} \phi_{m'+1}^S + \frac{\hbar^2 f}{2} \begin{bmatrix} 1 \\ 0 \end{bmatrix} \phi_{m'}^S, \quad (1.30)$$

where  $f = \sqrt{(S - m')(S + m' + 1)}$  is spin flip probability of spin flipper when spin up electron is incident. Similarly, when spin down electron is incident, the action of  $\vec{s} \cdot \vec{S}$  on  $\psi_I$  at interface ( $x = 0$ ) is

$$\vec{s} \cdot \vec{S} \psi_I(x = 0) = \vec{s} \cdot \vec{S} \begin{bmatrix} 0 \\ 1 \end{bmatrix} \phi_{m'}^S + r_{\downarrow\uparrow} \vec{s} \cdot \vec{S} \begin{bmatrix} 1 \\ 0 \end{bmatrix} \phi_{m'-1}^S + r_{\downarrow\downarrow} \vec{s} \cdot \vec{S} \begin{bmatrix} 0 \\ 1 \end{bmatrix} \phi_{m'}^S. \quad (1.31)$$

In Eq. (1.31) for first and third term:

$$\begin{aligned} \vec{s} \cdot \vec{S} \begin{bmatrix} 0 \\ 1 \end{bmatrix} \phi_{m'}^S &= [s_z S_z + \frac{1}{2}(s^- S^+ + s^+ S^-)] \begin{bmatrix} 0 \\ 1 \end{bmatrix} \phi_{m'}^S \\ &= s_z S_z \begin{bmatrix} 0 \\ 1 \end{bmatrix} \phi_{m'}^S + \frac{1}{2} s^- S^+ \begin{bmatrix} 0 \\ 1 \end{bmatrix} \phi_{m'}^S + \frac{1}{2} s^+ S^- \begin{bmatrix} 0 \\ 1 \end{bmatrix} \phi_{m'}^S. \end{aligned} \quad (1.32)$$

Now,  $s_z \begin{bmatrix} 0 \\ 1 \end{bmatrix} = -\frac{\hbar}{2} \begin{bmatrix} 0 \\ 1 \end{bmatrix}$ ,  $s^- \begin{bmatrix} 0 \\ 1 \end{bmatrix} = 0$ ,  $s^+ \begin{bmatrix} 0 \\ 1 \end{bmatrix} = \begin{bmatrix} 1 \\ 0 \end{bmatrix}$  and,  $S^- \phi_{m'}^S = \hbar \sqrt{(S+m')(S-m'+1)} \phi_{m'-1}^S = \hbar f' \phi_{m'-1}^S$ . Thus, from Eq. (1.32) we get,

$$\vec{s} \cdot \vec{S} \begin{bmatrix} 0 \\ 1 \end{bmatrix} \phi_{m'}^S = -\frac{\hbar^2 m'}{2} \begin{bmatrix} 0 \\ 1 \end{bmatrix} \phi_{m'}^S + \frac{\hbar^2 f'}{2} \begin{bmatrix} 1 \\ 0 \end{bmatrix} \phi_{m'-1}^S. \quad (1.33)$$

In Eq. (1.31) for second term:

$$\begin{aligned} \vec{s} \cdot \vec{S} \begin{bmatrix} 1 \\ 0 \end{bmatrix} \phi_{m'-1}^S &= [s_z S_z + \frac{1}{2}(s^- S^+ + s^+ S^-)] \begin{bmatrix} 1 \\ 0 \end{bmatrix} \phi_{m'-1}^S \\ &= s_z S_z \begin{bmatrix} 1 \\ 0 \end{bmatrix} \phi_{m'-1}^S + \frac{1}{2} s^- S^+ \begin{bmatrix} 1 \\ 0 \end{bmatrix} \phi_{m'-1}^S + \frac{1}{2} s^+ S^- \begin{bmatrix} 1 \\ 0 \end{bmatrix} \phi_{m'-1}^S. \end{aligned} \quad (1.34)$$

Now,  $s^+ \begin{bmatrix} 1 \\ 0 \end{bmatrix} = 0$ ,  $s^- \begin{bmatrix} 1 \\ 0 \end{bmatrix} = \hbar \begin{bmatrix} 0 \\ 1 \end{bmatrix}$ ,  $S_z \phi_{m'-1}^S = \hbar(m'-1) \phi_{m'-1}^S$  and,

$S^+ \phi_{m'-1}^S = \hbar \sqrt{(S+m')(S-m'+1)} \phi_{m'}^S = \hbar f' \phi_{m'}^S$ . Thus, from Eq. (1.34) we get,

$$\vec{s} \cdot \vec{S} \begin{bmatrix} 1 \\ 0 \end{bmatrix} \phi_{m'-1}^S = \frac{\hbar^2(m'-1)}{2} \begin{bmatrix} 1 \\ 0 \end{bmatrix} \phi_{m'-1}^S + \frac{\hbar^2 f'}{2} \begin{bmatrix} 0 \\ 1 \end{bmatrix} \phi_{m'}^S, \quad (1.35)$$

where  $f' = \sqrt{(S+m')(S-m'+1)}$  is spin flip probability of spin flipper when spin down electron is incident. We impose boundary conditions (1.22) on wavefunctions for spin up

electron incident in (1.18), (1.19) and get equations which are mentioned below,

$$r_{\uparrow\uparrow} - t_{\uparrow\uparrow} = -1, \quad (1.36)$$

$$r_{\uparrow\downarrow} - t_{\uparrow\downarrow} = 0, \quad (1.37)$$

$$(1 - iJm')r_{\uparrow\uparrow} - iJfr_{\uparrow\downarrow} + t_{\uparrow\uparrow} = 1 + iJm', \quad (1.38)$$

$$-iJfr_{\uparrow\uparrow} + (1 + iJ(m' + 1))r_{\uparrow\downarrow} + t_{\uparrow\downarrow} = iJf, \quad (1.39)$$

where  $J = \frac{m^*J_0}{k}$  is a dimensionless parameter which measures the strength of exchange interaction, as the product  $J_0\delta(x)\vec{s}\cdot\vec{S}$  has dimensions of energy, thus  $\vec{s}$  which represents spin angular momentum of electron is in units of  $\hbar$  and  $\vec{S}$  considered as spin angular momentum of spin-flipper also in units of  $\hbar$ ,  $\delta(x)$  having dimensions of  $1/L$ , therefore  $J_0$  the exchange interaction has dimensions of  $E - L/\hbar^2$ . Similarly, if we impose boundary conditions (1.22) on wavefunctions for spin down electron incident in (1.20), (1.21), we get,

$$r_{\downarrow\uparrow} - t_{\downarrow\uparrow} = 0, \quad (1.40)$$

$$r_{\downarrow\downarrow} - t_{\downarrow\downarrow} = -1, \quad (1.41)$$

$$(1 - iJ(m' - 1))r_{\downarrow\uparrow} - iJf'r_{\downarrow\downarrow} + t_{\downarrow\uparrow} = iJf', \quad (1.42)$$

$$-iJf'r_{\downarrow\uparrow} + (1 + iJm')r_{\downarrow\downarrow} + t_{\downarrow\downarrow} = 1 - iJm'. \quad (1.43)$$

If we solve the equations (1.36)-(1.43) we will get different scattering amplitudes:  $r_{\uparrow\uparrow}, r_{\uparrow\downarrow}, t_{\uparrow\uparrow}, t_{\uparrow\downarrow}$  (for spin up electron incident) from normal metal  $N_1$  and  $r_{\downarrow\uparrow}, r_{\downarrow\downarrow}, t_{\downarrow\uparrow}, t_{\downarrow\downarrow}$  (for spin down electron incident) from normal metal  $N_1$ . Reflection and transmission probabilities for spin up and spin down electron are thus:  $R_{\uparrow\uparrow} = |r_{\uparrow\uparrow}|^2, R_{\uparrow\downarrow} = |r_{\uparrow\downarrow}|^2, T_{\uparrow\uparrow} = |t_{\uparrow\uparrow}|^2, T_{\uparrow\downarrow} = |t_{\uparrow\downarrow}|^2$  (for spin up electron incident) and  $R_{\downarrow\uparrow} = |r_{\downarrow\uparrow}|^2, R_{\downarrow\downarrow} = |r_{\downarrow\downarrow}|^2, T_{\downarrow\uparrow} = |t_{\downarrow\uparrow}|^2, T_{\downarrow\downarrow} = |t_{\downarrow\downarrow}|^2$  (for spin down electron incident). We plot reflection and transmission probabilities with spin-flip and no-flip as a function of exchange interaction  $J$  in Fig. 1.6 for different values of the spin of spin flipper  $S(1/2, 3/2, 5/2)$ . In Fig. 1.6(a), we see reflection probability without flip

increases with an increase in the spin of spin flipper  $S$  independent of exchange interaction  $J$ , while in Fig. 1.6(b) reflection probability with flip increases with an increase in  $S$  only for low values of  $J$  but for high values of  $J$  it decreases with  $S$ . Next, in Fig. 1.6(c), we plot

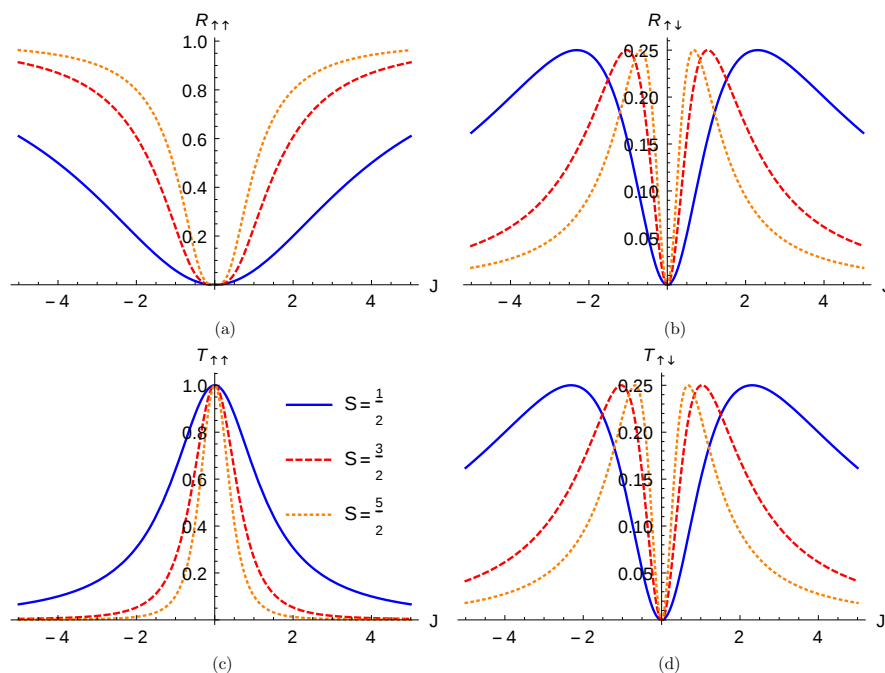


Figure 1.6: (a) Reflection probability without flip, (b) Reflection probability with flip, (c) Transmission probability without flip and (d) Transmission probability with flip. Parameter:  $m' = -1/2$ .

transmission probability without spin-flip. For increasing spin, it continuously decreases independent of  $J$ . Finally, in Fig. 1.6(d), we plot transmission probability with spin-flip; we see transmission probability increases with an increase of  $S$  for low values of  $J$ , while for high values of  $J$ , it decreases with  $S$ .

Similar to how we explained the current calculation in the case of a  $N-I-S$  junction, we consider the contribution of the spin-polarized carriers in the energy interval  $[E, E + dE]$ . This contribution is again proportional to electronic velocity, the density of states, and the Fermi distribution function. The interface area where the two Normal metals touch is now



denoted as  $\mathcal{W}$ . At this interface, the diameters of the metallic contact's are assumed to be much smaller than the electron's mean free path. Further, in the linear response regime, we assume voltage bias applied  $eV \ll E_F$  (the Fermi energy) and the electrons to be moving ballistically across the interface. When a voltage bias  $V(= V_1 - V_2)$  is applied across the  $N_1$ -SF- $N_2$  junction (see Fig. 1.5(b)), the transmitted spin-polarized current through the interface at a finite temperature in one dimension can be calculated as,

$$I_\sigma = \rho(E_F)ev_F\mathcal{W} \int_{-\infty}^{\infty} [f(E - eV) - f(E)][T_{\sigma'\sigma}]dE, \quad (1.44)$$

where  $f(E)$  is the Fermi Dirac distribution function,  $\mathcal{W}$  denotes contact area over which two normal metals touch,  $\rho(E_F)$  is density of states at Fermi energy,  $v_F$  is electron velocity at  $E_F$  and  $T_{\sigma'\sigma}$  is probability for an electron to transmit to  $N_2$  with spin  $\sigma$ , when an electron with spin  $\sigma'$  is incident. Since the function  $[f(E - eV) - f(E)]$  is only finite in the region  $eV$  around Fermi energy  $E_F$ , the density of states as well as the electron velocity are constant in this interval, therefore they are outside the integral. The charge current in  $N_2$  at finite temperature is given as,

$$I_c = I_\uparrow + I_\downarrow = \rho(E_F)ev_F\mathcal{W} \int_{-\infty}^{\infty} [f(E - eV) - f(E)][T_{\uparrow\uparrow} + T_{\uparrow\downarrow}]dE. \quad (1.45)$$

At zero temperature, Fermi Dirac distribution function is defined in terms of Heaviside step function,  $f(E - eV) = \Theta(eV - E)$  and  $f(E) = \Theta(-E)$ . Thus, at zero temperature, Eq. (1.45) reduces to

$$I_c = \rho(E_F)ev_F\mathcal{W} \int_0^{eV} [T_{\uparrow\uparrow} + T_{\uparrow\downarrow}]dE. \quad (1.46)$$

If we take derivative with respect to  $E$  at  $E = eV$  on both sides of Eq. (1.46), then we will get

$$\frac{dI_c}{dV} = \rho(E_F)e^2v_F\mathcal{W}[T_{\uparrow\uparrow} + T_{\uparrow\downarrow}]. \quad (1.47)$$

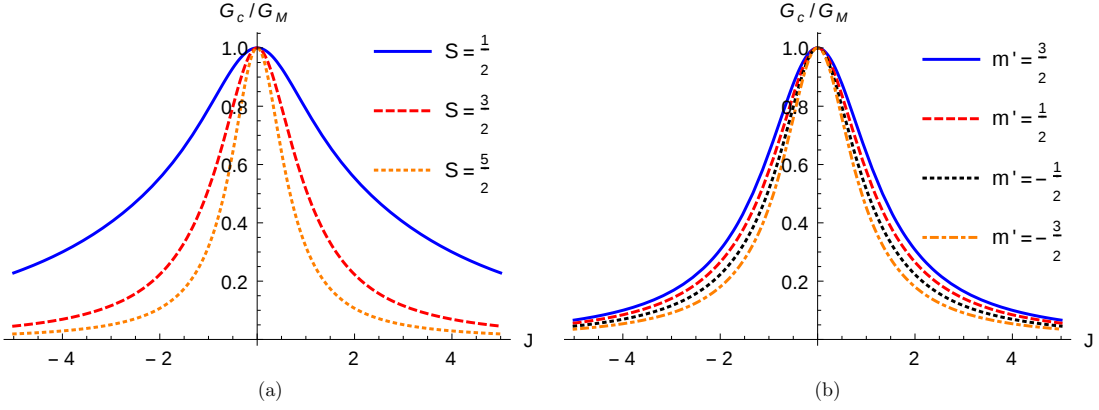


Figure 1.7: (a) Differential charge conductance ( $G_c$ ) normalized by  $G_M$ , as function of exchange interaction  $J$  for different values of spin  $S$  and fixed magnetic moment  $m'$  of spin flipper at zero temperature, (b) Differential charge conductance ( $G_c$ ) normalized by  $G_M$ , as function of exchange interaction  $J$  for different values of magnetic moment  $m'$  and fixed spin  $S$  of spin flipper at zero temperature. Parameters: (a)  $m' = -1/2$ ; (b)  $S = 3/2$  and,  $G_M = \rho(E_F)e^2 v_F \mathcal{W}$ .

The quantity  $\frac{dI_c}{dV}$  in Eq. (1.47) is defined as the differential charge conductance ( $G_c$ ) at zero temperature which is proportional to  $(T_{\uparrow\uparrow} + T_{\uparrow\downarrow})$ . In Fig. 1.7(a), we plot differential charge conductance versus exchange interaction  $J$  for different values of spin  $S$  and fixed magnetic moment  $m'$  of spin flipper at zero temperature. We see that differential charge conductance is symmetric to exchange interaction  $J$ , and with an increase of spin  $S$  of a spin flipper, it decreases for the entire range of  $J$ . In Fig. 1.7(b), we plot differential charge conductance versus  $J$  for different values of magnetic moment  $m'$  and spin  $S$  of the flipper. We see that although the behavior of the differential charge conductance remains the same to  $J$  for different values of  $m'$ , the magnitude of  $G_c$  changes with  $m'$ . For  $S = 3/2$  and for  $m' = 3/2, 1/2, -1/2, -3/2$ , flip probabilities are  $f = 0, \sqrt{3}, 2$  and  $\sqrt{3}$  respectively. Thus, we can also conclude that differential charge conductance decreases with the spin-flip probability of the spin flipper.

## 1.3 Andreev reflection mediated transport in Metal-Spin flipper-Superconductor junction

### 1.3.1 Andreev Reflection in presence of a spin flipper

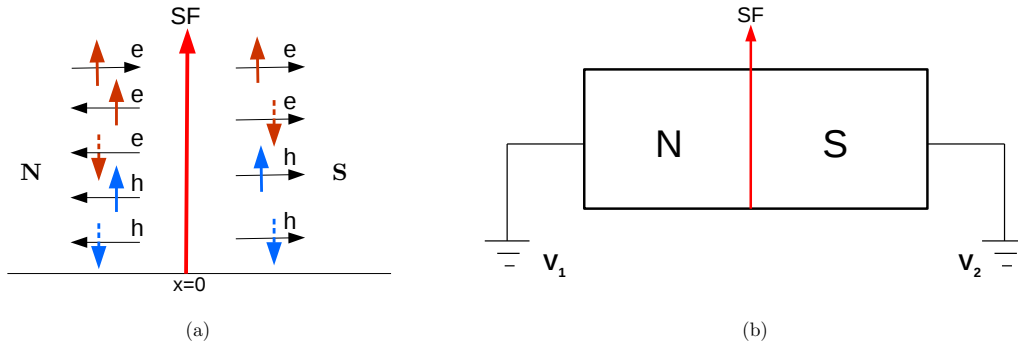


Figure 1.8: (a) NS junction with spin flipper (SF) at interface ( $x = 0$ ) with spin S and magnetic moment  $m'$ . Scattering of an incident spin up electron is shown. Normal reflection, Andreev reflection and quasi-particle transmission into superconductor are depicted, (b) N-SF-S junction where N is connected to voltage  $V_1$  and S is connected to voltage  $V_2$  and  $V = V_1 - V_2$  is the voltage drop across the NS interface.

We consider a metal (N)- $s$ -wave superconductor (S) junction as depicted in Fig. 1.8(a), with a spin flipper at metal superconductor interface ( $x = 0$ ). The Hamiltonian[13, 17] used to describe a spin flipper is again given by,

$$H_{\text{Spin flipper}} = -J_0 \delta(x) \vec{s} \cdot \vec{S}, \quad (1.48)$$

where  $J_0$  is strength of exchange interaction between electron with spin  $\vec{s}$  and spin flipper with spin  $\vec{S}$ .

An electron/hole with spin up/down incident from the metallic (N) region interacts with the spin flipper at the interface, which may result in a mutual spin flip. Electron/hole can be reflected back to N region with spin up or down. Electron-like and hole-like quasi-particles

with spin up or down are transmitted into the superconducting (S) region for energies above the gap. Model Hamiltonian in Bogoliubov-de Gennes (BdG) formalism of our system as shown in Fig. 1.8(a) is given as

$$H_{BdG}(x) = \begin{pmatrix} H\hat{I} & i\Delta\Theta(x)\hat{\sigma}_y \\ -i\Delta^*\Theta(x)\hat{\sigma}_y & -H\hat{I} \end{pmatrix}, \quad (1.49)$$

where  $H = p^2/2m^* - J_0\delta(x)\vec{s}\cdot\vec{S} - E_F$ ,  $\Delta$  is superconducting gap for  $s$ -wave superconductor and  $\Theta(x)$  is Heaviside step function. First term in  $H$  is kinetic energy of an electron with effective mass  $m^*$ , second term describes the exchange interaction  $J_0$  between electron spin ( $\vec{s}$ ) and spin flipper's spin ( $\vec{S}$ ),  $\hat{I}$  is identity matrix,  $\hat{\sigma}$  is the Pauli spin matrix and  $E_F$  is Fermi energy. Strength of exchange coupling[13] can be expressed via dimensionless parameter  $J = \frac{m^*J_0}{k_F}$ , as the product  $J_0\delta(x)\vec{s}\cdot\vec{S}$  has dimensions of energy, thus  $\vec{s}$  which represents spin angular momentum of electron is in units of  $\hbar$  and  $\vec{S}$  considered as spin angular momentum of spin-flipper also in units of  $\hbar$ ,  $\delta(x)$  having dimensions of  $1/L$ , therefore  $J_0$  the exchange interaction has dimensions of  $E - L/\hbar^2$ .

The wave functions of the different regions of our system as shown in Fig. 1.8(a) can be written as, for electron with spin up incident,

$$\begin{aligned} \psi_N(x) &= \varphi_1^N e^{ik_e x} \phi_{m'}^S + r_{ee}^{\uparrow\uparrow} \varphi_1^N e^{-ik_e x} \phi_{m'}^S + r_{ee}^{\uparrow\downarrow} \varphi_2^N e^{-ik_e x} \phi_{m'+1}^S + r_{eh}^{\uparrow\uparrow} \varphi_3^N e^{ik_h x} \phi_{m'+1}^S + r_{eh}^{\uparrow\downarrow} \varphi_4^N e^{ik_h x} \phi_{m'}^S, \text{ for } x < 0, \\ \psi_S(x) &= t_{ee}^{\uparrow\uparrow} \varphi_1^S e^{iq+x} \phi_{m'}^S + t_{ee}^{\uparrow\downarrow} \varphi_2^S e^{iq+x} \phi_{m'+1}^S + t_{eh}^{\uparrow\uparrow} \varphi_3^S e^{-iq-x} \phi_{m'+1}^S + t_{eh}^{\uparrow\downarrow} \varphi_4^S e^{-iq-x} \phi_{m'}^S, \text{ for } x > 0, \end{aligned} \quad (1.50)$$

$$\text{where } \varphi_1^N = \begin{pmatrix} 1 \\ 0 \\ 0 \\ 0 \end{pmatrix}, \varphi_2^N = \begin{pmatrix} 0 \\ 1 \\ 0 \\ 0 \end{pmatrix}, \varphi_3^N = \begin{pmatrix} 0 \\ 0 \\ 1 \\ 0 \end{pmatrix}, \varphi_4^N = \begin{pmatrix} 0 \\ 0 \\ 0 \\ 1 \end{pmatrix}, \varphi_1^S = \begin{pmatrix} u \\ 0 \\ 0 \\ v \end{pmatrix}, \varphi_2^S = \begin{pmatrix} 0 \\ u \\ -v \\ 0 \end{pmatrix}, \varphi_3^S = \begin{pmatrix} 0 \\ -v \\ u \\ 0 \end{pmatrix}$$

### 1.3. Andreev reflection mediated transport in Metal-Spin flipper-Superconductor junction

and,  $\varphi_4^S = \begin{pmatrix} v \\ 0 \\ 0 \\ u \end{pmatrix}$ . In Eq. (1.50),  $\varphi_1^N$  is the spinor for spin-up electron,  $\varphi_2^N$  is the spinor

for spin-down electron,  $\varphi_3^N$  is the spinor for the spin up hole and,  $\varphi_4^N$  is the spinor for a spin-down hole. Similarly,  $\varphi_1^S$  is the spinor for a spin up electron-like quasi-particle,  $\varphi_2^S$  is the spinor for spin-down electron-like quasi-particle,  $\varphi_3^S$  is the spinor for a spin up hole-like quasi-particle and,  $\varphi_4^S$  is the spinor for spin-down hole-like quasi-particle. The amplitudes  $r_{ee}^{\uparrow\uparrow}, r_{ee}^{\uparrow\downarrow}, r_{eh}^{\uparrow\uparrow}, r_{eh}^{\uparrow\downarrow}$  represent normal reflection without flip, normal reflection with spin flip, Andreev reflection with spin flip and Andreev reflection without flip respectively. Similarly  $t_{ee}^{\uparrow\uparrow}, t_{ee}^{\uparrow\downarrow}, t_{eh}^{\uparrow\uparrow}, t_{eh}^{\uparrow\downarrow}$  are the transmission amplitudes corresponding to the reflection process described before.  $\phi_{m'}^S$  is the eigenspinor of the spin flipper, with its  $S_z$  operator acting as:  $S_z \phi_{m'}^S = \hbar m' \phi_{m'}^S$ , with  $m'$  being the spin magnetic moment of the spin flipper. For  $E > \Delta$  (for energies above the gap), the coherence factors are  $u^2 = \frac{1}{2} \left[ 1 + \frac{(E^2 - \Delta^2)^{\frac{1}{2}}}{E} \right]$ ,  $v^2 = \frac{1}{2} \left[ 1 - \frac{(E^2 - \Delta^2)^{\frac{1}{2}}}{E} \right]$ , while wave-vectors in metal are  $k_{e,h} = \sqrt{\frac{2m^*}{\hbar^2} (E_F \pm E)}$  and in superconductor are  $q_{\pm} = \sqrt{\frac{2m^*}{\hbar^2} (E_F \pm \sqrt{E^2 - \Delta^2})}$  and for  $E < \Delta$  (for energies below the gap) the coherence factors are  $u^2 = \frac{1}{2} \left[ \frac{E + i(\Delta^2 - E^2)^{\frac{1}{2}}}{\Delta} \right]$ ,  $v^2 = \frac{1}{2} \left[ \frac{E - i(\Delta^2 - E^2)^{\frac{1}{2}}}{\Delta} \right]$ , while wavevectors in metal are  $k_{e,h} = \sqrt{\frac{2m^*}{\hbar^2} (E_F \pm E)}$  and in superconductor are  $q_{\pm} = \sqrt{\frac{2m^*}{\hbar^2} (E_F \pm i\sqrt{\Delta^2 - E^2})}$  [9], wherein  $E$  is the excitation energy of electron above  $E_F$ . In Andreev approximation, which we will use,  $E_F \gg \Delta, E$  we take  $k_e = k_h = q_+ = q_- = k_F$ .

Similarly as mentioned above, if we consider an electron with spin down incident from normal metal, the wavefunctions for different regions can be written as

$$\begin{aligned} \psi_N(x) &= \varphi_2^N e^{ik_e x} \phi_{m'}^S + r_{ee}^{\uparrow\uparrow} \varphi_1^N e^{-ik_e x} \phi_{m'-1}^S + r_{ee}^{\uparrow\downarrow} \varphi_2^N e^{-ik_e x} \phi_{m'}^S + r_{eh}^{\uparrow\uparrow} \varphi_3^N e^{ik_h x} \phi_{m'}^S + r_{eh}^{\uparrow\downarrow} \varphi_4^N e^{ik_h x} \phi_{m'-1}^S, \text{ for } x < 0, \\ \psi_S(x) &= t_{ee}^{\uparrow\uparrow} \varphi_1^S e^{iq_+ x} \phi_{m'-1}^S + t_{ee}^{\uparrow\downarrow} \varphi_2^S e^{iq_+ x} \phi_{m'}^S + t_{eh}^{\uparrow\uparrow} \varphi_3^S e^{-iq_- x} \phi_{m'}^S + t_{eh}^{\uparrow\downarrow} \varphi_4^S e^{-iq_- x} \phi_{m'-1}^S, \text{ for } x > 0, \end{aligned} \tag{1.51}$$

## 1. INTRODUCTION

---

where  $r_{ee}^{\downarrow\uparrow}, r_{ee}^{\downarrow\downarrow}, r_{eh}^{\downarrow\uparrow}, r_{eh}^{\downarrow\downarrow}$  are the normal reflection amplitude with flip, normal reflection amplitude without flip, Andreev reflection amplitude without flip and Andreev reflection amplitude with flip respectively. Similarly  $t_{ee}^{\downarrow\uparrow}, t_{ee}^{\downarrow\downarrow}, t_{eh}^{\downarrow\uparrow}, t_{eh}^{\downarrow\downarrow}$  are the transmission amplitudes corresponding to the reflection process described before. The wavefunctions (1.50) and (1.51) satisfy the boundary conditions at  $x = 0$ ,

$$\psi_N(x) = \psi_S(x), \quad \text{and} \quad \frac{d\psi_S}{dx} - \frac{d\psi_N}{dx} = -\frac{2m^* J_0 \vec{s} \cdot \vec{S}}{\hbar^2} \psi_N, \quad (1.52)$$

where  $\vec{s} \cdot \vec{S} = s_z S_z + \frac{1}{2}(s^- S^+ + s^+ S^-)$  is the exchange operator in Hamiltonian (1.49),  $s^\pm = s_x \pm i s_y$  are raising and lowering spin operator for electron/hole. As spinors are written in both electron/hole and spin up/down basis the  $\vec{s}$  spin operators for electron/hole are now  $4 \times 4$  matrices instead of  $2 \times 2$  matrices in section 1.2.  $S^\pm = S_x \pm i S_y$  are raising and lowering spin operator for spin flipper with  $s_z = \frac{\hbar}{2} \begin{pmatrix} \sigma_z & 0 \\ 0 & -\sigma_z \end{pmatrix}$ ,  $s_x = \frac{\hbar}{2} \begin{pmatrix} 0 & \sigma_x \\ \sigma_x & 0 \end{pmatrix}$ ,  $s_y = \frac{\hbar}{2} \begin{pmatrix} 0 & \sigma_y \\ \sigma_y & 0 \end{pmatrix}$ ,  $s^+ = s_x + i s_y = \frac{\hbar}{2} \begin{pmatrix} 0 & \sigma_x + i \sigma_y \\ \sigma_x - i \sigma_y & 0 \end{pmatrix}$  and,  $s^- = s_x - i s_y = \frac{\hbar}{2} \begin{pmatrix} 0 & \sigma_x - i \sigma_y \\ \sigma_x + i \sigma_y & 0 \end{pmatrix}$ .  $\sigma_z = \begin{pmatrix} 1 & 0 \\ 0 & -1 \end{pmatrix}$ ,  $\sigma_x = \begin{pmatrix} 0 & 1 \\ 1 & 0 \end{pmatrix}$  and,  $\sigma_y = \begin{pmatrix} 0 & -i \\ i & 0 \end{pmatrix}$  are the usual Pauli spin matrices. Action of exchange operator  $\vec{s} \cdot \vec{S}$  for wave-function involving spin up electron spinor, see (1.50) is,

$$\vec{s} \cdot \vec{S} \varphi_1^N \phi_{m'}^S = s_z S_z \varphi_1^N \phi_{m'}^S + \frac{1}{2} s^- S^+ \varphi_1^N \phi_{m'}^S + \frac{1}{2} s^+ S^- \varphi_1^N \phi_{m'}^S. \quad (1.53)$$

$\vec{s}$  acts on electron spinor, while  $\vec{S}$  acts on spin flipper spinor. Now,  $s^+ \varphi_1^N = 0$ , since  $s^+$  is the spin raising operator for electron and there are no higher spin states for a spin-1/2 electron than up and so the 3rd term in Eq. 1.53 vanishes, while  $s^- \varphi_1^N = \hbar \varphi_2^N$ , the spin lowering operator gives the down spin state  $\varphi_2^N$  of electron. Further, for spin-up electron  $s_z \varphi_1^N = \frac{\hbar}{2} \varphi_1^N$ , and for spin flipper:  $S_z \phi_{m'}^S = \hbar m' \phi_{m'}^S$ . The spin-raising and spin-lowering operators acting on spin flipper give:  $S^+ \phi_{m'}^S = \hbar \sqrt{(S - m')(S + m' + 1)} \phi_{m'+1}^S = \hbar f \phi_{m'+1}^S$

### 1.3. Andreev reflection mediated transport in Metal-Spin flipper-Superconductor junction

and  $S^- \phi_{m'+1}^S = \hbar \sqrt{(S-m')(S+m'+1)} \phi_{m'}^S = \hbar f \phi_{m'}^S$ , see section 1.2 Eqs. (1.25)-(1.27) for derivation of  $S^+ \phi_m^S$  operation.

$$\text{Thus, } \vec{s} \cdot \vec{S} \varphi_1^N \phi_{m'}^S = \frac{\hbar^2 m'}{2} \varphi_1^N \phi_{m'}^S + \frac{\hbar^2 f}{2} \varphi_2^N \phi_{m'+1}^S. \quad (1.54)$$

Similarly, action of  $\vec{s} \cdot \vec{S}$  for wave-function involving spin-down electron spinor, see (1.51) is,

$$\vec{s} \cdot \vec{S} \varphi_2^N \phi_{m'}^S = -\frac{\hbar^2 m'}{2} \varphi_2^N \phi_{m'}^S + \frac{\hbar^2 f'}{2} \varphi_1^N \phi_{m'-1}^S. \quad (1.55)$$

In Eqs. (1.50) and (1.51) we have only given the cases of spin up or spin down electron incident. Similarly, we can write the normal metal wavefunctions in case of either spin up or spin down hole incident. Action of exchange operator for wave-function involving spin up hole is,

$$\vec{s} \cdot \vec{S} \varphi_3^N \phi_{m'}^S = -\frac{\hbar^2 m'}{2} \varphi_3^N \phi_{m'}^S + \frac{\hbar^2 f'}{2} \varphi_4^N \phi_{m'-1}^S, \quad (1.56)$$

and finally action of exchange operator on wavefunction involving spin down hole is,

$$\vec{s} \cdot \vec{S} \varphi_4^N \phi_{m'}^S = \frac{\hbar^2 m'}{2} \varphi_4^N \phi_{m'}^S + \frac{\hbar^2 f}{2} \varphi_3^N \phi_{m'+1}^S. \quad (1.57)$$

In Eqs. (1.54)-(1.57),  $f = \sqrt{(S-m')(S+m'+1)}$  is spin-flip probability of spin flipper when spin up electron or spin down hole is incident, while  $f' = \sqrt{(S+m')(S-m'+1)}$  is the spin-flip probability of spin flipper when spin down electron or spin up hole is incident. We impose the boundary conditions Eq. (1.52) at the interface ( $x = 0$ ) on wave-functions and solve the resulting 8 equations for each spin up and spin down electron incident process and get the different scattering amplitudes:  $r_{ee}^{\uparrow\uparrow}, r_{ee}^{\uparrow\downarrow}, r_{eh}^{\uparrow\uparrow}, r_{eh}^{\uparrow\downarrow}, t_{ee}^{\uparrow\uparrow}, t_{ee}^{\uparrow\downarrow}, t_{eh}^{\uparrow\uparrow}, t_{eh}^{\uparrow\downarrow}$  (for spin up electron incident case) and  $r_{ee}^{\downarrow\uparrow}, r_{ee}^{\downarrow\downarrow}, r_{eh}^{\downarrow\uparrow}, r_{eh}^{\downarrow\downarrow}, t_{ee}^{\downarrow\uparrow}, t_{ee}^{\downarrow\downarrow}, t_{eh}^{\downarrow\uparrow}, t_{eh}^{\downarrow\downarrow}$  (for spin down electron incident case). The reflection and transmission probabilities are thus:  $R_{ee}^{\uparrow\uparrow} = |r_{ee}^{\uparrow\uparrow}|^2, R_{ee}^{\uparrow\downarrow} = |r_{ee}^{\uparrow\downarrow}|^2, R_{eh}^{\uparrow\uparrow} = |r_{eh}^{\uparrow\uparrow}|^2, R_{eh}^{\uparrow\downarrow} = |r_{eh}^{\uparrow\downarrow}|^2, T_{ee}^{\uparrow\uparrow} = (u^2 - v^2) |t_{ee}^{\uparrow\uparrow}|^2, T_{ee}^{\uparrow\downarrow} = (u^2 - v^2) |t_{ee}^{\uparrow\downarrow}|^2, T_{eh}^{\uparrow\uparrow} = (u^2 - v^2) |t_{eh}^{\uparrow\uparrow}|^2, T_{eh}^{\uparrow\downarrow} = (u^2 - v^2) |t_{eh}^{\uparrow\downarrow}|^2$  (for spin up electron incident case) and  $R_{ee}^{\downarrow\uparrow} = |r_{ee}^{\downarrow\uparrow}|^2, R_{ee}^{\downarrow\downarrow} =$

## 1. INTRODUCTION

$|r_{ee}^{\downarrow\downarrow}|^2, R_{eh}^{\downarrow\uparrow} = |r_{eh}^{\downarrow\uparrow}|^2, R_{eh}^{\downarrow\downarrow} = |r_{eh}^{\downarrow\downarrow}|^2, T_{ee}^{\downarrow\uparrow} = (u^2 - v^2)|t_{ee}^{\downarrow\uparrow}|^2, T_{ee}^{\downarrow\downarrow} = (u^2 - v^2)|t_{ee}^{\downarrow\downarrow}|^2, T_{eh}^{\downarrow\uparrow} = (u^2 - v^2)|t_{eh}^{\downarrow\uparrow}|^2, T_{eh}^{\downarrow\downarrow} = (u^2 - v^2)|t_{eh}^{\downarrow\downarrow}|^2$  (for spin down electron incident case).

In Fig. 1.9 we plot normal and Andreev reflection probabilities with spin-flip or no-flip for different values of the spin of spin flipper  $S(1/2, 3/2, 5/2)$ , we fix the magnetic moment of the spin flipper as  $m' = -1/2$ . In Fig. 1.9(a), we see normal reflection probability

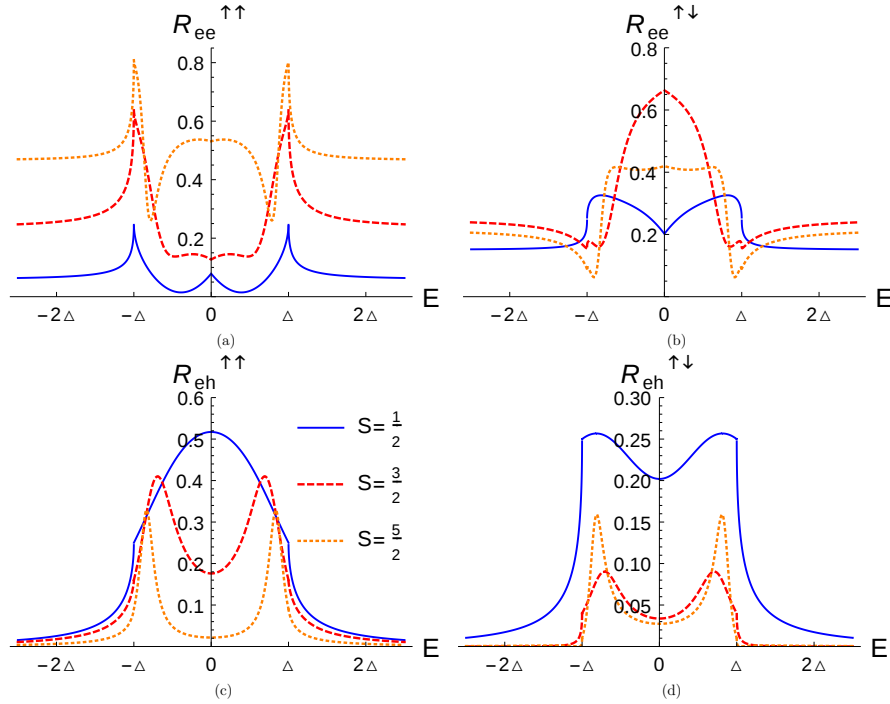


Figure 1.9: (a) Normal reflection probability without flip, (b) normal reflection probability with flip, (c) Andreev reflection probability with flip and (d) Andreev reflection probability without flip. Parameters are:  $J = 1, m' = -1/2$ .

without spin-flip increases with an increase of spin ( $S$ ), while in 1.9(b), normal reflection probability with spin-flip shows a mixed behavior. It first increases then decreases with an increase of  $S$  for the entire range of electron excitation energy. Next, in Fig. 1.9(c), we plot Andreev reflection probability with spin-flip; for increasing spin, it continuously decreases for both above as well as below the gap. Finally, in Fig. 1.9(d), we plot the Andreev



### 1.3. Andreev reflection mediated transport in Metal-Spin flipper-Superconductor junction

reflection probability without spin-flip; we find both above as well as below the gap, the probability decreases as spin increases. Thus, for the high spin values of the flipper, the normal reflection probability is significant, but the Andreev reflection probability is small. The Andreev reflection hence is inhibited by the spin of the flipper.

In Fig. 1.10, we plot the quasi-particle transmission probabilities for spin-flip and without spin-flip for the same parameter values as in Fig. 1.9. There is no single-particle state in the gap, and transport is via Cooper pairs. Thus, there is no quasi-particle transmission below the gap. Since there is no quasi-particle transmission below the gap, we will only focus on the above-the-gap regime. In Fig. 1.10(a), we show that with an increase in the spin

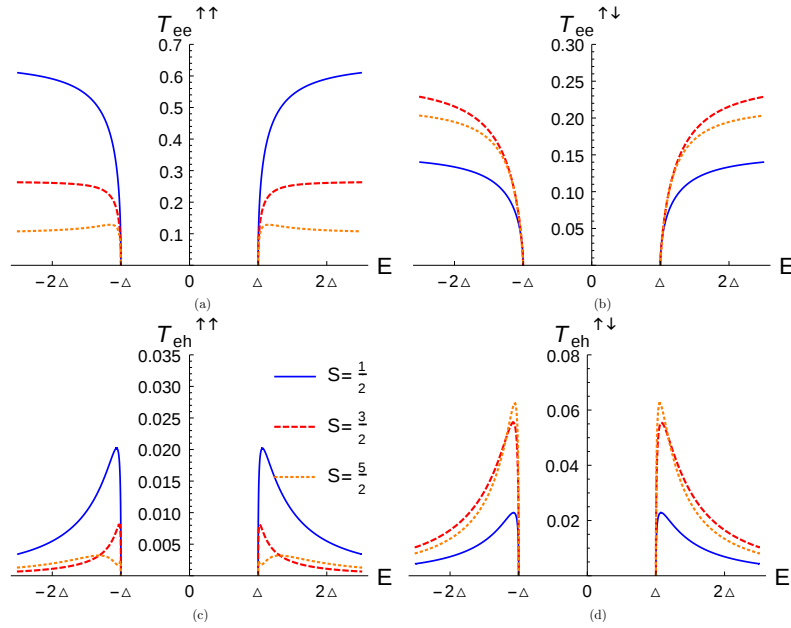


Figure 1.10: (a) *Electron-like quasi-particle transmission without flip*, (b) *electron-like quasi-particle transmission with flip*, (c) *hole-like quasi-particle transmission with flip* and (d) *hole-like quasi-particle transmission without flip*. Parameters:  $J = 1$ ,  $m' = -1/2$ .

of the spin flipper ( $S$ ), the electron-like quasi-particle transmission without flip decreases. On the other hand, in Fig. 1.10(b) with an increase in the spin of the spin flipper ( $S$ ), the electron-like quasi-particle transmission with flip increases. Thus, high spin values of the

flipper inhibit no flip transmission but boost transmission with spin-flip for electron-like quasi-particles. In Fig. 1.10(c) and (d), we plot the probability for hole-like quasi-particle transmission; in (c), we see that with an increase in the spin of the flipper ( $S$ ), the probability for spin-flip transmission decreases while in (d) we see the opposite. Thus high spin values of the flipper show opposite behavior for holes; they inhibit spin-flip transmission while boosting no-flip transmission.

As was seen earlier for  $NIS$  and  $N_1 - SF - N_2$  junctions, we calculate the current in the metallic side also as before we assume ballistic transport. The Metal-Superconductor interface is considered a point contact in which the contact's diameter is small compared to the electron's mean free path. The current as before is proportional to the velocity of charge carriers, the Fermi distribution function, and interface area  $\mathcal{A}$ . Further, the applied bias voltage  $eV \ll E_F$ , implying we are in the linear transport regime. Finally, we consider 1D transport assuming the setup translationally invariant along  $y$  and  $z$  directions.

### 1.3.2 Differential charge conductance

According to the BTK theory[9], when a voltage bias  $V$  is applied at the NS interface (see Fig. 1.8(b)), the charge current through the NS interface at a finite temperature in one dimension is given by,

$$I_c^{NS} = \rho(E_F)ev_F\mathcal{A} \int_{-\infty}^{\infty} [f(E - eV) - f(E)][1 + R_{eh}^{\uparrow\uparrow} + R_{eh}^{\uparrow\downarrow} - R_{ee}^{\uparrow\uparrow} - R_{ee}^{\uparrow\downarrow}]dE, \quad (1.58)$$

where  $\rho(E_F)$  denotes density of states at  $E_F$ ,  $v_F$  is the electron velocity at  $E_F$ ,  $\mathcal{A}$  is the contact area over which the normal metal and superconductor touch and  $f(E)$  is the Fermi Dirac distribution function. Since the function  $[f(E - eV) - f(E)]$  is only finite in the region  $eV$  around  $E_F$ , the density of states as well as the electron velocity are constant in

### 1.3. Andreev reflection mediated transport in Metal-Spin flipper-Superconductor junction

this region, thus they are outside the integral. At zero temperature Eq. (1.58) reduces to,

$$I_c^{NS} = \rho(E_F)ev_F\mathcal{A} \int_0^{eV} [1 + R_{eh}^{\uparrow\uparrow} + R_{eh}^{\uparrow\downarrow} - R_{ee}^{\uparrow\uparrow} - R_{ee}^{\uparrow\downarrow}]dE. \quad (1.59)$$

If we take derivative with respect to  $E$  at  $E = eV$  on both sides of Eq. (1.59), then we will get,

$$\frac{dI_c^{NS}}{dV} = \rho(E_F)e^2v_F\mathcal{A}[1 + R_{eh}^{\uparrow\uparrow} + R_{eh}^{\uparrow\downarrow} - R_{ee}^{\uparrow\uparrow} - R_{ee}^{\uparrow\downarrow}] \quad (1.60)$$

The quantity  $\frac{dI_c^{NS}}{dV}$  in Eq. (1.60) is defined as the differential charge conductance ( $G_c$ ) at

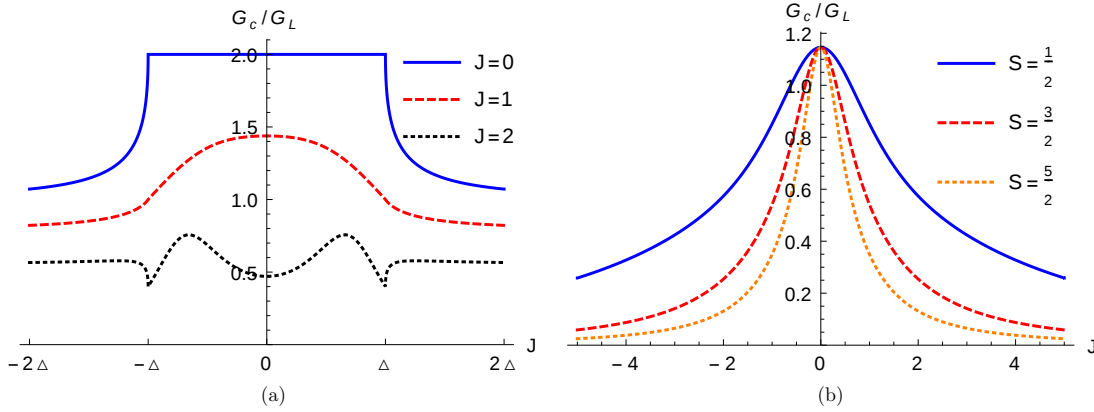


Figure 1.11: (a) Differential charge conductance as function of energy of incident electron in units of  $\Delta$  for different values of exchange interaction  $J$  at zero temperature, (b) Differential charge conductance as function of exchange interaction  $J$  for different values of spin  $S$  of spin flipper at zero temperature. Parameters: (a)  $S = 1/2$ ,  $m' = -1/2$ ; (b)  $m' = -1/2$ ,  $E = 1.5\Delta$  and  $G_L = \rho(E_F)e^2v_F\mathcal{A}$ .

zero temperature which is proportional to  $(1 + R_{eh}^{\uparrow\uparrow} + R_{eh}^{\uparrow\downarrow} - R_{ee}^{\uparrow\uparrow} - R_{ee}^{\uparrow\downarrow})$ . In Fig. 1.11(a), we plot differential charge conductance as a function of the energy of incident electron  $E$  for different values of exchange interaction  $J$  of the spin flipper. We see that with an increase of  $J$ , differential charge conductance decreases. When there is no spin flipper ( $J = 0$ ) at the NS interface ( $x = 0$ ),  $G_c/G_L$  is constant at 2 for below the gap, while above the gap it continuously decreases, where  $G_L = \rho(E_F)e^2v_F\mathcal{A}$  is the normalization constant. However,

in the presence of a spin flipper, differential charge conductance is always less than 2, and for  $J = 1$  beyond a peak at  $E = 0$ ,  $G_c/G_L$  continuously decreases. Further, we notice that for a high value of  $J$  ( $J = 2$ ), there are peaks present symmetrically at both positive and negative energies near the gap edges within the energy gap. In Fig. 1.11(b), we plot differential charge conductance as a function of exchange interaction  $J$  for different values of spin  $S$  of the spin flipper. We see that differential charge conductance is symmetric for  $J$ , and with an increase of spin  $S$  of the spin flipper, it decreases independent of  $J$ . This behavior is similar to what we see in the case of  $N_1$ -SF- $N_2$  junction.

In this section, we have studied the effects of Andreev reflection mediated transport at metal superconductor junction in the presence of a spin flipper at the interface. The reason we study these systems in detail is that in chapter 2 and chapter 3 we explain how this Normal metal-Spin flipper-Superconductor system can reveal Yu-Shiba-Rusinov states (see chapter 2). When the  $s$ -wave Superconductor is replaced by topological  $p$ -wave Superconductor or spin-orbit coupled superconducting wire (SOCSW), one can check the stability of the generated Majorana bound states to spin-flip scattering (see chapter 2). Notably, we see that such a simple system can result in generating odd frequency equal spin-triplet correlations, a fascinating result (see chapter 3).

In the next section, we will discuss the DC Josephson effect. We will then discuss Andreev bound states, the total Josephson current, and its bound and continuum contribution for superconductor-normal metal-superconductor (SNS) junction. In chapter 4 we report on designing a tunable  $0 - \pi$  Josephson junction in the presence of a spin flipper/magnetic impurity without taking recourse to Ferromagnets or high  $T_c$  superconductors, and how a spin flipper in ferromagnetic Josephson junction can result in anomalous Josephson effect.

## 1.4 DC Josephson effect

In 1962, Brian Josephson[18] first predicted that a supercurrent  $I_S$  could exist between two  $s$ -wave superconductors separated by a weak link (which may consist of a thin insulating barrier). The supercurrent is proportional to the sine of the phase difference ( $\phi$ ) between the two superconductors.

$$I_S(\phi) = I_C \sin(\phi) \quad (1.61)$$

This effect is called the DC Josephson effect[18]. AC Josephson effect also exists, but it will not be considered in this thesis. The maximum current  $I_C$  in the current-phase relation is the critical current. The physics behind the DC Josephson effect can be understood in this way, an electron/hole located in the weak link cannot penetrate directly into the superconductor if its energy is below the superconducting gap. However, charge transport via Andreev reflection can occur. An electron incident on, say, the right interface (see Fig. 1.12) is converted to a hole moving in the opposite direction. Thus, a Cooper pair will be generated inside the right superconductor. Consequently, the reflected hole is again Andreev reflected at the left interface and is converted back to an electron, resulting in a Cooper pair being annihilated in the left superconductor (Fig. 1.12). As a result of this cycle, a pair of correlated electrons moves from the left superconductor to the right superconductor, generating a supercurrent flow across the junction.

There are different properties[19] of the Josephson current phase relation, which is independent of the weak link geometry and junction's materials:

(i) If phase of one of the superconducting electrode is rotated by  $2\pi$ , the physical state of the electrodes and the weak link does not change. As a consequence,  $I_S(\phi)$  should not change and is a periodic function of  $2\pi$ ,

$$I_S(\phi) = I_S(\phi + 2\pi). \quad (1.62)$$

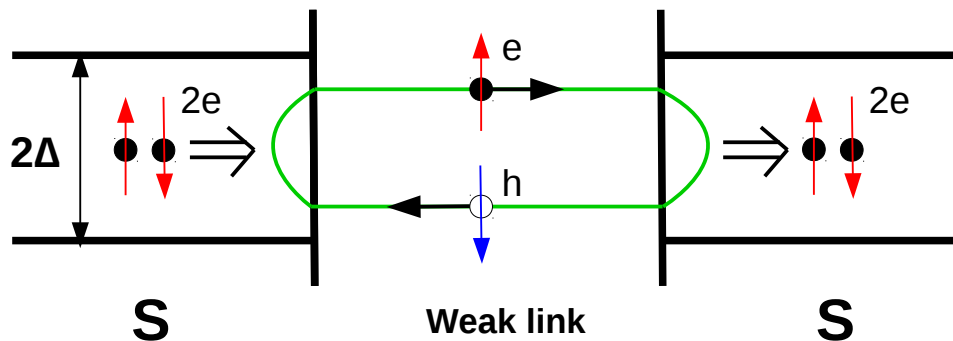


Figure 1.12: An electron  $e$  and the Andreev-reflect hole  $h$  are shown in weak link, between two  $s$ -wave superconductors. A pair of correlated electrons moves from left superconductor to right superconductor, creating a supercurrent flow across the junction. The system is in equilibrium, no voltage bias is applied.

(ii)  $I_S(\phi)$  is an odd function of superconducting phase difference  $\phi$ . In the absence of time-reversal symmetry breaking in the system, a sign change in the phase difference  $\phi$  leads to the change in the direction of the supercurrent,

$$I_S(-\phi) = -I_S(\phi). \quad (1.63)$$

(iii) When phase difference between two superconductors is zero, i.e,  $\phi = 0$ , no supercurrent can flow through the junction,

$$I_S(2\pi n) = 0, \quad n = 0, \pm 1, \pm 2, \dots \quad (1.64)$$

(iv) From (i) and (ii) one can see that the supercurrent is zero at  $\phi = \pi n$ ,

$$I_S(\pi n) = 0, \quad n = 0, \pm 1, \pm 2, \dots, \quad (1.65)$$

thus it is enough to consider the supercurrent  $I_S(\phi)$  only in between  $\phi = 0$  and  $\phi = \pi$ .

From Eqs. (1.62)-(1.65) it follows that,  $I_S(\phi)$  can be described by a Fourier series:

$$I_S(\phi) = \sum_{n=1}^{\infty} I^n \sin(n\phi). \quad (1.66)$$

Eq. (1.66) considers multiple reflections at the interface, and  $I^n$  represents the coefficients of the  $n$ th reflection processes of quasiparticles.

The Josephson Free energy  $E_J$  is determined by  $E_J = \frac{\hbar}{2e} \int_0^\phi I_S(\phi') d\phi'$ . As current phase relation is sinusoidal,  $I_S(\phi) = I_C \sin(\phi)$ , the relation between Josephson Free energy  $E_J$  and phase difference  $\phi$  is

$$E_J(\phi) = \frac{\hbar I_C}{2e} (1 - \cos(\phi)). \quad (1.67)$$

For a standard Josephson junction hence called 0 junction, Josephson Free energy is minimum at  $\phi = 0$  when no current flows through the junction.

### 1.4.1 $\pi$ junctions

An interesting case arises when critical current  $I_C < 0$ , i.e., negative. This type of junction is called  $\pi$  Josephson junction[20, 21] and it follows that,

$$I_S = -I_C \sin(\phi) = |I_C| \sin(\phi + \pi). \quad (1.68)$$

The Josephson Free energy of a  $\pi$ -junction is

$$E_J(\phi) = \left| \frac{\hbar I_C}{2e} \right| (1 + \cos(\phi)) = \left| \frac{\hbar I_C}{2e} \right| (1 - \cos(\phi + \pi)). \quad (1.69)$$

From Eq. (1.69), the minimum of Josephson Free energy occurs at  $\phi = \pi$  and the ground state for such a junction is at  $\phi = \pi$ . It contrasts with a conventional Josephson junction where the Josephson Free energy is minimum at  $\phi = 0$ .

Josephson  $\pi$  junction's can be used as a phase inverter in superconducting quantum interference devices (SQUIDs)[22]. Further,  $\pi$  junctions are preferred as a potential candidate for designing qubits[23].

## 1.5 Andreev bound states and Josephson current in SNS junction

To calculate Andreev bound states and Josephson current, we consider a superconductor (S)-normal metal (N)-superconductor (S) junction where there is a  $\delta$ -function barrier at the interface between normal metal and  $s$ -wave superconductor. Superconducting gap parameters  $\Delta$  for left and right  $s$ -wave superconductors, are assumed to have same magnitude but different phases  $\varphi_L$  and  $\varphi_R$  and are given by  $\Delta = \Delta_0(T)[e^{i\varphi_L}\Theta(-x-a/2) + e^{i\varphi_R}\Theta(x-a/2)]$ ,  $\Theta(x)$  being Heaviside step function,  $\Delta_0(T)$  is temperature dependent gap parameter and it follows  $\Delta_0(T) = \Delta_0 \tanh(1.74\sqrt{(T_c/T - 1)})$ , where  $T_c$  is superconducting critical temperature[24]. The model Hamiltonian in BdG formalism of our system is a  $2 \times 2$  matrix which is given below,

$$\begin{pmatrix} H & \Delta \\ \Delta^* & -H \end{pmatrix} \Psi(x) = E\Psi(x), \quad (1.70)$$

$H = p^2/2m^* + V[\delta(x+a/2) + \delta(x-a/2)] - E_F$ , here  $p^2/2m^*$  is kinetic energy of an electron with effective mass  $m^*$ ,  $V$  is strength of  $\delta$  potential at both interfaces between normal metal and superconductor and  $E_F$  is Fermi energy. If we diagonalize Hamiltonian, Eq. (1.70), we get the wavefunctions in different regions of our system as shown in Fig. 1.13 for electron/hole-like quasiparticle incidence. There are four different types of quasiparticle injection process into the system: an electron-like quasiparticle (ELQ) or a hole-like quasiparticle (HLQ) injected from either the left or from the right superconducting electrode. For a ELQ incident from left superconductor, wave function in left superconductor is,

$$\psi_{SL}(x) = \begin{pmatrix} ue^{i\phi_L/2} \\ ve^{-i\phi_L/2} \end{pmatrix} e^{iq_+x} + a_1 \begin{pmatrix} ve^{i\phi_L/2} \\ ue^{-i\phi_L/2} \end{pmatrix} e^{iq_-x} + b_1 \begin{pmatrix} ue^{i\phi_L/2} \\ ve^{-i\phi_L/2} \end{pmatrix} e^{-iq_+x}, \text{ for } x < -a/2. \quad (1.71)$$



## 1.5. Andreev bound states and Josephson current in SNS junction

---

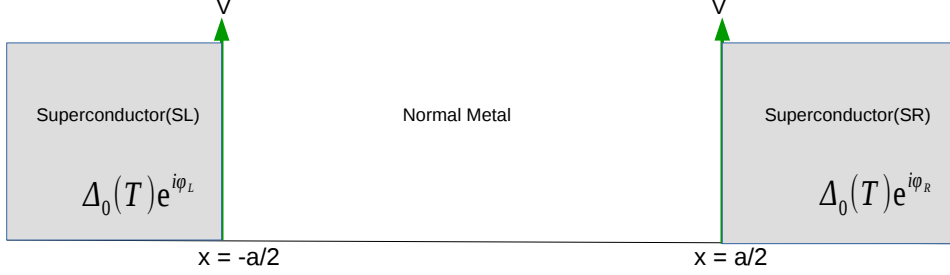


Figure 1.13: Josephson junction composed of normal metal sandwiched between two *s*-wave superconductors.

The corresponding wavefunction in right superconductor is,

$$\psi_{SR}(x) = c_1 \begin{pmatrix} ue^{i\phi_R/2} \\ ve^{-i\phi_R/2} \end{pmatrix} e^{iq_+x} + d_1 \begin{pmatrix} ve^{i\phi_R/2} \\ ue^{-i\phi_R/2} \end{pmatrix} e^{-iq_-x}, \text{ for } x > a/2. \quad (1.72)$$

The wavefunction in the normal metal region is,

$$\psi_N(x) = i_1 \begin{pmatrix} 1 \\ 0 \end{pmatrix} e^{ik_e x} + j_1 \begin{pmatrix} 1 \\ 0 \end{pmatrix} e^{-ik_e x} + k_1 \begin{pmatrix} 0 \\ 1 \end{pmatrix} e^{ik_h x} + l_1 \begin{pmatrix} 0 \\ 1 \end{pmatrix} e^{-ik_h x}, \text{ for } -a/2 < x < a/2. \quad (1.73)$$

The coefficients  $a_1$ ,  $b_1$ ,  $c_1$ , and  $d_1$  correspond to the scattering amplitudes for Andreev reflection, normal reflection, transmission of ELQ, and transmission of HLQ respectively.

$u = \sqrt{\frac{1}{2} \left( 1 + \frac{\sqrt{E^2 - |\Delta|^2}}{E} \right)}$  and  $v = \sqrt{\frac{1}{2} \left( 1 - \frac{\sqrt{E^2 - |\Delta|^2}}{E} \right)}$  are the BCS coherence factors.  $q_{\pm}$  are wavevectors in superconductor and  $k_{e,h}$  are wavevectors in normal metal. We use Andreev approximation [25]  $q_+ = q_- = k_F$  and  $k_{e,h} \approx k_F \pm \frac{k_F E}{2E_F}$ , where  $k_F = \sqrt{2m^* E_F / \hbar^2}$  is the Fermi wavevector, with  $E_F \gg |\Delta|$ . The boundary conditions at  $x = -a/2$ ,

$$\psi_{SL}(x) = \psi_N(x), \text{ (continuity of wavefunctions)} \quad (1.74)$$

$$\frac{d\psi_N}{dx} - \frac{d\psi_{SL}}{dx} = \frac{2m^*V}{\hbar^2}\psi_N, \text{ (discontinuity in first derivative)} \quad (1.75)$$

and at  $x = a/2$ ,

$$\psi_N(x) = \psi_{SR}(x), \quad (1.76)$$

$$\frac{d\psi_{SR}}{dx} - \frac{d\psi_N}{dx} = \frac{2m^*V}{\hbar^2}\psi_N. \quad (1.77)$$

By using the above boundary conditions, one can get the different scattering amplitudes. The wave functions for the other three types of quasiparticle injection processes are formulated in the same way.

### 1.5.1 Andreev bound states

An electron in normal metal is incident at the NS interface with an energy below the superconducting gap and cannot penetrate the superconductor. However, at the NS interface, Andreev reflection occurs, in which a hole with opposite momentum is reflected into normal metal, and a Cooper pair is formed in the superconductor. The same effect is also present at the SN interface with the same coherent electron/hole. Therefore a bound state is generated between the two superconductors, which is called Andreev bound state (ABS)[26].

To calculate Andreev bound states we neglect the contribution from incoming quasiparticle[27], and insert the wavefunctions (Eqs. (1.71)-(1.73)) into boundary conditions (Eqs. (1.74)-(1.77)). We get a homogeneous system of 8 linear equations for the scattering amplitudes. If we express the scattering amplitudes in normal metal region by scattering amplitudes in left and right superconductor we get a homogeneous system of 4 linear equations,

$$Px = 0, \quad (1.78)$$

## 1.5. Andreev bound states and Josephson current in SNS junction

where  $x$  is a  $4 \times 1$  column matrix and is given by  $x = [b_1, a_1, c_1, d_1]^T$  and  $P$  is a  $4 \times 4$  matrix which is given by,

$$P = \begin{pmatrix} -\frac{e^{\frac{ik_F a}{2}} u(y \cos(k_e a) - (i-2Z) \sin(k_e a))}{y} & -\frac{e^{-\frac{i}{2}(k_F a + 2k_e a)} v(-1+y+e^{i2k_e a(1+y-2Z)+i2Z})}{2y} & ul & v/n \\ -\frac{e^{\frac{ik_F a}{2}} v(y_1 \cos(k_h a) - (i-2Z) \sin(k_h a))}{y_1} & -\frac{pu(-1+y_1+e^{i2k_h a(1+y_1-2Z)+i2Z})}{2y_1} & vn & u/l \\ \frac{e^{\frac{ik_F a}{2}} u(y(1+i4Z) \cos(k_e a) - i(y^2+2Z(i-2Z)) \sin(k_e a))}{y} & \frac{ie^{-\frac{ik_F a}{2}} v(y(i+4Z) \cos(k_e a) + (-y^2+2Z(i+2Z)) \sin(k_e a))}{y} & ul & -v/n \\ \frac{e^{\frac{ik_F a}{2}} v(y_1(1+i4Z) \cos(k_h a) - i(y_1^2+2Z(i-2Z)) \sin(k_h a))}{y_1} & \frac{pu(-y_1+y_1^2-e^{i2k_h a(y_1-2iZ)(1+y_1-2iZ)-2iZ+4iy_1Z-4Z^2})}{2y_1} & vn & u/l \end{pmatrix}, \quad (1.79)$$

where  $y = (1 + \frac{E}{2E_F})$ ,  $y_1 = (1 - \frac{E}{2E_F})$ ,  $p = e^{-\frac{i}{2}(k_F a + 2k_h a)}$ ,  $l = e^{\frac{i}{2}(k_F a + \varphi)}$ , and  $n = e^{\frac{i}{2}(k_F a - \varphi)}$ .

For a nontrivial solution of this system of equations to exist,  $\text{Det } P = 0$ , and we get Andreev bound states as a function of phase difference ( $\varphi = \varphi_R - \varphi_L$ ) between two superconductors.

We find that Andreev bound states are given by,

$$-2 \arccos \left( \frac{E_n^\pm}{|\Delta|} \right) \pm \varphi + \left( \frac{E_n^\pm}{\Delta_0} \right) \left( \frac{a}{\xi_0} \right) = 2\pi n, \quad n = 0, \pm 1, \pm 2, \dots \quad (1.80)$$

where  $\xi_0 = \frac{E_F}{k_F \Delta_0}$  is superconducting coherence length. In this thesis we mainly concentrate on short junction limit. In the short junction limit ( $a \ll \xi_0$ ) the third term of the left hand side in Eq. (1.80) is neglected and therefore we get two Andreev bound state energies

$$E^\pm(\varphi) = \pm |\Delta| \cos \left( \frac{\varphi}{2} \right), \quad (1.81)$$

where  $\varphi = \varphi_R - \varphi_L$  is phase difference between right and left superconductor. In Fig. 1.14 we plot ABS's (Eq. (1.81)) as a function of phase difference  $\varphi$  for a short SNS junction.

We see that two degenerate ABS's appear below the superconducting gap.

### 1.5.2 Bound state current

Each Andreev bound state carries a supercurrent in the SNS junction. The Josephson bound state current carried by the discrete Andreev bound states is given by [19] the sum,

$$I_B(\varphi) = \frac{2e}{\hbar} \sum_{n,\pm} f(E_n^\pm(\varphi)) \frac{dE_n^\pm}{d\varphi}, \quad \text{where } n = 0, \pm 1, \pm 2, \dots \quad (1.82)$$

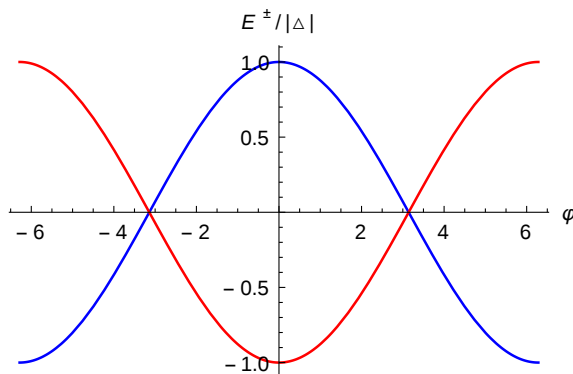


Figure 1.14: Andreev bound states  $E^\pm$  in units of  $|\Delta|$  (the energy gap of  $s$ -wave superconductor) as a function of phase difference ( $\varphi$ ) for a short SNS junction.

In short junction limit ( $a \ll \xi_0$ ) one can derive the Josephson bound state current as[28],

$$I_B(\varphi) = \frac{e\Delta_0(T)}{\hbar} \sin\left(\frac{\varphi}{2}\right) \tanh\left(\frac{\beta\Delta_0(T) \cos(\frac{\varphi}{2})}{2}\right). \quad (1.83)$$

### 1.5.3 Continuum current

Continuum currents can only flow if there is an imbalance in the electrical currents carried by the quasiparticles incident from left and right superconducting contact. The current contribution[29] originating from the imbalance in electrical current per unit energy of the electron-like quasiparticles flowing in the continuum levels is given by,

$$I_C^e(\varphi) = \frac{2e}{\hbar} \left( \int_{-\infty}^{-|\Delta|} + \int_{|\Delta|}^{\infty} \right) \frac{1}{|u^2 - v^2|} \times [T_{L \rightarrow R}^e(E, \varphi) - T_{L \leftarrow R}^e(E, \varphi)] f(E) dE \quad (1.84)$$

Similarly the continuum contribution from hole-like quasiparticles can be calculated by replacing ‘ $e$ ’ in Eq. (1.84) by ‘ $h$ ’. In Eq. (1.84)  $T_{L \rightarrow R}^e = |c_1|^2 - |d_1|^2$  is transmission for the electric currents moving from left to right of the system. We have

$$T_{L \leftarrow R}^e(E, \varphi) = T_{L \rightarrow R}^e(E, -\varphi) \quad (1.85)$$

The continuum contribution from holes is found to be equal to the electronic continuum contribution. Therefore, the total continuum current due to electron-like and hole-like

quasiparticles is given as,

$$I_C(\varphi) = \frac{I_C^e(\varphi) + I_C^h(\varphi)}{2} = I_C^e(\varphi). \quad (1.86)$$

### 1.5.4 Total Josephson current

Total Josephson current ( $I_T$ ) is the sum of bound state and continuum supercurrent, i.e.,  $I_T = I_B + I_C$ . But, it can also be calculated by a different method using detailed balance, first done by Furusaki-Tsukuda in Ref. [30]. Using the generalized version of the Furusaki-Tsukuda formalism[30] the total DC Josephson current is given by,

$$I_T(\varphi) = \frac{e\Delta_0(T)}{2\beta\hbar} \sum_{\omega_n} \frac{q_+(\omega_n) + q_-(\omega_n)}{\Omega_n} \times \left( \frac{a_1(\omega_n)}{q_+(\omega_n)} - \frac{a_2(\omega_n)}{q_-(\omega_n)} \right), \quad (1.87)$$

herein  $\omega_n = (2n + 1)\pi/\beta$  are fermionic Matsubara frequencies with  $n = 0, \pm 1, \pm 2, \dots$  and  $\Omega_n = \sqrt{\omega_n^2 + \Delta_0^2(T)}$ .  $\beta = 1/(k_B T)$ , where  $k_B$  is Boltzmann constant and  $T$  is temperature.  $q_+(\omega_n)$ ,  $q_-(\omega_n)$ , and  $a_i(\omega_n)$  are obtained from  $q_+$ ,  $q_-$  and  $a_i$  by analytically continuing  $E$  to  $i\omega_n$ .  $a_1$  is Andreev reflection amplitude for electron incident from left superconductor, while  $a_2$  is Andreev reflection amplitude for hole incident from left superconductor. We sum over Matsubara frequencies numerically. The detailed balance condition[30, 31] is verified as,

$$\frac{a_1(-\varphi, E)}{q_+} = \frac{a_2(\varphi, E)}{q_-}, \quad (1.88)$$

$$b_i(-\varphi, E) = b_i(\varphi, E), \quad i = 1, 2. \quad (1.89)$$

In Fig. 1.15 we plot bound state, continuum, and total Josephson currents for the transparent regime ( $Z = 0$ ) for an SNS junction. We consider short junction limit ( $a \ll \xi_0$ ). In this limit, the continuum contribution of the total Josephson current is almost zero. Therefore the bound current and total current are almost the same. However, in the case of long junctions ( $a \gg \xi_0$ ), the continuum contribution to the total Josephson current is finite.

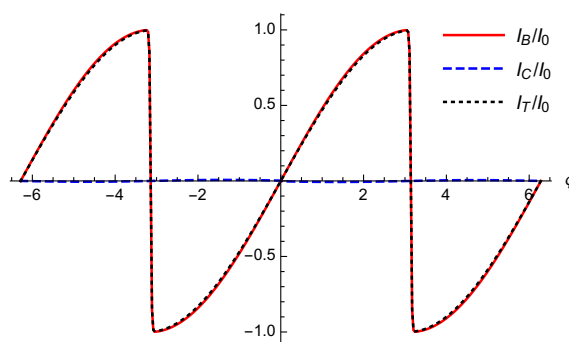


Figure 1.15: *The bound, continuum and total Josephson current normalized with respect to  $I_0 = e\Delta_0/\hbar$ , as a function of phase difference ( $\varphi$ ). Parameters:  $\Delta_0 = 1\text{meV}$ ,  $T/T_c = 0.01$ ,  $Z = 0$ .*

## 1.6 Outline of the thesis

In this thesis, we investigate the effects of spin-flip scattering on Andreev reflection-mediated transport in the vicinity of a superconductor. In chapter 2, we study the formation and characteristics of Yu-Shiba-Rusinov (YSR) bound states below the superconducting gap using the BTK approach in the vicinity of a spin flipper. We analytically calculate the differential conductance for a metal (N)-metal (N)-superconductor (S) junction when there is a spin flipper between the two metals and a  $\delta$ -like potential barrier between metal and superconductor. We concentrate on zero-bias conductance spectra and show the formation of a zero-bias peak due to the merger of two YSR bound states in the presence of spin-flip scattering. However, in the absence of spin-flip scattering, a dip forms at zero bias in conductance spectra. We further examine the stability of Majorana bound states (MBS's) induced zero-bias conductance peak (ZBCP) in a metal-topological superconductor junction in the vicinity of a spin flipper. We show that quantized ZBCP remains stable in the presence of spin-flip scattering for metal- $p$ -wave superconductor junction. However, it loses its stability when the  $p$ -wave superconductor is replaced by a spin-orbit coupled superconducting wire (SOCSW). The work in this chapter is based on the publications

reported in Refs. [32, 33].

In chapter 3, we study the emergence of odd frequency equal spin-triplet correlations in a metal-superconductor junction near a spin flipper. Using Green's function method, we compute the even and odd-frequency spin-singlet and triplet correlations in metallic and superconducting regions. We have done calculations both at zero as well as finite temperatures. We find that in the presence of spin-flip scattering, mixed spin-triplet correlations vanish and only spin-singlet and equal spin-triplet correlations are finite. We also calculate the spin-polarized local density of states (SPLDOS) and find its relationship with odd frequency correlations. The work in this chapter is based on the publication reported in Ref. [34].

In chapter 4, we study the nature of the  $0$  to  $\pi$  Josephson junction transition in the vicinity of a spin flipper. We show that a spin flipper sandwiched between two  $s$ -wave superconductors can transit from a  $0$  to  $\pi$  Josephson junction by tuning system parameters like tunnel contact, spin, and magnetic moment of the spin flipper, or exchange coupling. We also study the anomalous Josephson effect and the direction-dependent critical current in the ferromagnetic Josephson junction wherein a spin flipper is sandwiched between two ferromagnetic layers. We show that when ferromagnets are misaligned in the presence of spin-flip scattering, time reversal and chiral symmetries are broken, and an anomalous Josephson current flows through the junction. Further, this system can act as a phase battery that can store quantized amounts of superconducting phase difference in the ground state of the junction. The work in this chapter is based on the publications reported in Refs. [35, 36].

In chapter 5, we study the origin of quantum spin torque in a ferromagnetic Josephson junction when the magnetic moments of the ferromagnetic layers are aligned parallel or antiparallel, and a spin flipper is embedded between two ferromagnetic layers. An

equilibrium spin-transfer torque is seen in the ferromagnetic Josephson junction when magnetic moments of ferromagnetic layers are misaligned. However, we show that when a spin flipper is sandwiched between two ferromagnets, a novel quantum spin torque is induced, i.e., even when magnetic moments of ferromagnets are aligned parallel or antiparallel due to spin-flip scattering. The work in this chapter is based on the publication reported in Ref. [37].

In chapter 6, we study the application of our spin-flipper doped Josephson junction in quantum thermodynamics. We show that a 1D Josephson junction loop doped with a spin flipper and attached to two thermal reservoirs can operate as a quantum heat engine or quantum refrigerator, or a Joule pump, or even as a cold pump with high efficiency and coefficient of performance. Further, we find that this system can be tuned from engine to refrigerator mode or to any other mode, i.e., Joule pump or cold pump, by either tuning the temperature of reservoirs or via the flux enclosed in the Josephson junction loop. The work in this chapter is based on the publication reported in Ref. [38].

Finally, in chapter 7, this thesis concludes with a summary of our most important results and a perspective on future endeavors.



## Chapter 2

# Formation of Yu-Shiba-Rusinov bound states and stability of Majorana bound states in presence of spin flip scattering

*“The greater is the circle of light, the greater is the boundary of the darkness by which it is confined.”*

— Joseph Priestley

### 2.1 Introduction

In conventional  $s$ -wave superconductors, magnetic impurities induce bound states, whose energy lies within the superconducting gap. It was first discovered by Yu, Shiba, and Rusinov independently in the late 1960s and is now termed as Yu-Shiba-Rusinov[39, 40, 41] (YSR) states. The interaction of the impurity spin with Andreev reflected electrons or holes gives rise to these low-lying YSR excited states. In the past, YSR bound states have been observed experimentally by scanning tunneling spectroscopy[42, 43, 44, 45] on superconducting Pb or Nb surfaces.

## 2. FORMATION OF YU-SHIBA-RUSINOV BOUND STATES AND STABILITY OF MAJORANA BOUND STATES IN PRESENCE OF SPIN FLIP SCATTERING

---

The importance of YSR bound states has been recently enhanced for several reasons. One reason is the prediction of topological superconductivity, and Majorana bound states[46, 47] (MBS's) in chains of magnetic adatoms on superconductors[48]. MBS's are quasiparticle excitations within the superconductor at zero energy which are their anti-particles[49]. Majorana zero modes can be observed at the boundary with a topological superconductor[50]. Another reason is that there has been experimental progress on measuring subgap spectra with much higher resolution than previously possible[51]. It has motivated theoretical and experimental work examining the basic properties of YSR bound states in more detail. Further, YSR bound states carry information on the strength of exchange coupling between impurity spin with the Andreev reflected electrons or holes, which measures the many-body ground state properties of the system[52].

In this chapter, we show the occurrence of YSR states using a simple BTK approach[9] (see Introduction section 1.1.1), in the presence of a spin flipper. The exact setting we will use is shown in Fig. 2.1. It depicts a spin flipper at  $x = 0$  and a  $\delta$ -like potential barrier at  $x = a$ . In regions I ( $x < 0$ ) and II ( $0 < x < a$ ), there are two normal metals, while for  $x > a$ , there is a  $s$ -wave superconductor. We study the signature of YSR bound states through Andreev reflection probabilities and conductance spectra. We focus on zero energy in the conductance spectra and show how a peak is formed at zero energy due to spin-flip scattering, but for no flip, a dip forms at zero energy in the conductance spectra. This zero energy conductance peak is almost quantized at  $2e^2/h$  values. However, it arises due to non-topological reasons in contrast to the zero-energy peak (ZEP) formed due to Majorana states. Technically, YSR bound states are obtained by taking exchange interaction  $J \rightarrow 0$ , impurity spin  $S \rightarrow \infty$ , thus rendering  $JS$ =finite[40, 53]. We also see that YSR states arise for low values of  $J$  and high  $S$  values. Second, we examine the stability of Majorana zero modes in a metal-topological superconductor junction in the vicinity of a spin flipper.

## 2.2. Signature of Yu-Shiba-Rusinov bound states in normal and Andreev reflection probabilities

Using the BTK approach, we analytically calculate the differential charge conductance for metal-spin flipper-topological superconductor junctions with two distinct topological superconductors: (a) spin less  $p$ -wave superconductor and (b) spin-orbit-coupled  $s$ -wave superconducting wire in the presence of a Zeeman field. We find that the quantized ZEP remains stable in the presence of spin-flip scattering for metal- $p$ -wave superconductor junction, while it loses its stability when a SOCSW replaces  $p$ -wave superconductor.

## 2.2 Signature of Yu-Shiba-Rusinov bound states in normal and Andreev reflection probabilities

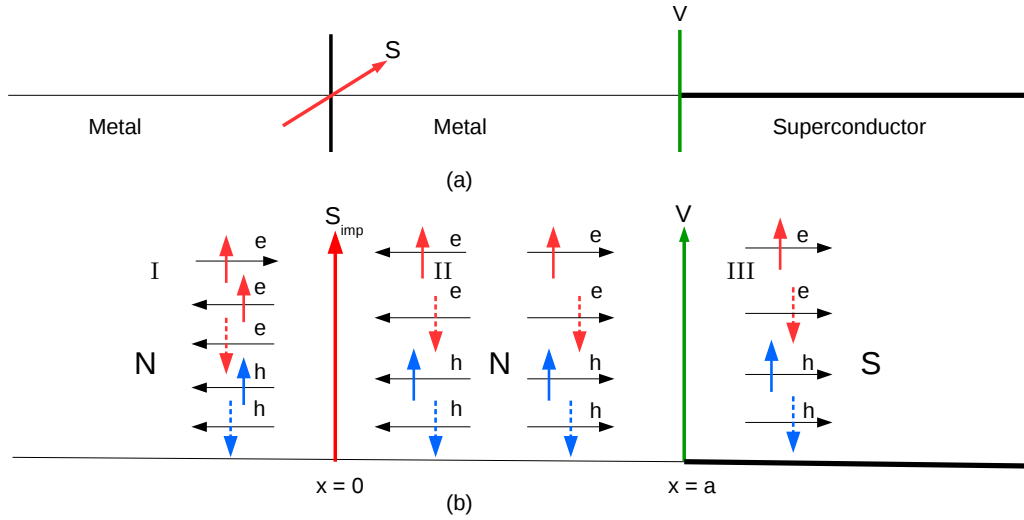


Figure 2.1: (a) A spin flipper with spin  $S$  and magnetic moment  $m'$  at  $x = 0$  in a Normal Metal-Spin flipper-Normal Metal-Insulator-Superconductor junction, (b) The scattering of an up-spin electron incident is shown. Andreev reflection and quasi particle transmission into superconductor are depicted.

We consider a metal (N)-metal (N)-superconductor (S) junction with a spin flipper between two metals at  $x = 0$  and a  $\delta$ -like potential barrier exists at the metal-superconductor

## 2. FORMATION OF YU-SHIBA-RUSINOV BOUND STATES AND STABILITY OF MAJORANA BOUND STATES IN PRESENCE OF SPIN FLIP SCATTERING

---

interface at  $x = a$ . The above model for a spin flipper in an Andreev setting matches quite well with solid-state scenarios such as seen in 1D quantum wires or graphene with an embedded magnetic impurity or quantum dot[14, 54]. When an electron with energy  $E$  and spin up or down is incident from the normal metal, at the  $x = 0$  interface, it interacts with the spin flipper through an exchange potential which may induce a mutual spin flip. The electron can be reflected or transmitted to region II, with spin-up or down. When this transmitted electron is incident at the  $x = a$  interface, it could be reflected from the interface. There is also the possibility of Andreev reflection of a hole with spin-up or down. Electron-like and hole-like quasiparticles with spin-up or down are transmitted into the superconductor for energies above the gap[32, 55]. The model Hamiltonian in BdG formalism of our Normal Metal-Spin flipper-Normal Metal-Insulator-Superconductor system is given below:

$$\begin{bmatrix} H\hat{I} & i\Delta\Theta(x-a)\hat{\sigma}_y \\ -i\Delta^*\Theta(x-a)\hat{\sigma}_y & -H\hat{I} \end{bmatrix} \Psi(x) = E\Psi(x), \quad (2.1)$$

where  $H = p^2/2m^* + V\delta(x-a) - J_0\delta(x)\vec{s}\cdot\vec{S} - E_F$ .  $\Psi$  is a four-component spinor,  $\Delta$  is the gap in  $s$ -wave superconductor, and  $\Theta(x)$  is the Heaviside step function. Further, in  $H$ , the first term is the kinetic energy of an electron with effective mass  $m^*$ , for the second term  $V$  is the strength of the  $\delta$ -like potential at the interface between normal metal and superconductor. The third term describes the exchange interaction of strength  $J_0$  between the electron with spin  $\vec{s}$ , and a spin flipper with spin  $\vec{S}$ ,  $\hat{\sigma}$  is the Pauli spin matrix and  $\hat{I}$  is the identity matrix,  $E_F$  being the Fermi energy. We will later use the dimensionless parameter  $J = \frac{m^*J_0}{k_F}$  as a measure of strength of exchange interaction[13] and  $Z = \frac{m^*V}{\hbar^2k_F}$  as a measure of interface transparency[9].

The wavefunctions in the different regions of the system are as shown in Figs. 2.1(a)

## 2.2. Signature of Yu-Shiba-Rusinov bound states in normal and Andreev reflection probabilities

and 2.1(b) and can be written in spinorial form[27] for an electron with spin up incident from region I (normal metal) as:

$$\psi_N^I(x) = \begin{pmatrix} 1 \\ 0 \\ 0 \\ 0 \end{pmatrix} e^{ik_e x} \phi_{m'}^S + r_{ee}^{\uparrow\uparrow} \begin{pmatrix} 1 \\ 0 \\ 0 \\ 0 \end{pmatrix} e^{-ik_e x} \phi_{m'}^S + r_{ee}^{\uparrow\downarrow} \begin{pmatrix} 0 \\ 1 \\ 0 \\ 0 \end{pmatrix} e^{-ik_e x} \phi_{m'+1}^S + r_{eh}^{\uparrow\uparrow} \begin{pmatrix} 0 \\ 0 \\ 1 \\ 0 \end{pmatrix} e^{ik_h x} \phi_{m'+1}^S + r_{eh}^{\uparrow\downarrow} \begin{pmatrix} 0 \\ 0 \\ 0 \\ 1 \end{pmatrix} e^{ik_h x} \phi_{m'}^S, \text{ for } x < 0, \quad (2.2)$$

$$\begin{aligned} \psi_N^{II}(x) &= t_{ee}^{\prime\uparrow\uparrow} \begin{pmatrix} 1 \\ 0 \\ 0 \\ 0 \end{pmatrix} e^{ik_e x} \phi_{m'}^S + t_{ee}^{\prime\uparrow\downarrow} \begin{pmatrix} 0 \\ 1 \\ 0 \\ 0 \end{pmatrix} e^{ik_e x} \phi_{m'+1}^S + b_{ee}^{\uparrow\uparrow} \begin{pmatrix} 1 \\ 0 \\ 0 \\ 0 \end{pmatrix} e^{-ik_e(x-a)} \phi_{m'}^S + b_{ee}^{\uparrow\downarrow} \begin{pmatrix} 0 \\ 1 \\ 0 \\ 0 \end{pmatrix} e^{-ik_e(x-a)} \phi_{m'+1}^S \\ &+ c_{eh}^{\uparrow\uparrow} \begin{pmatrix} 0 \\ 0 \\ 1 \\ 0 \end{pmatrix} e^{ik_h(x-a)} \phi_{m'+1}^S + c_{eh}^{\uparrow\downarrow} \begin{pmatrix} 0 \\ 0 \\ 0 \\ 1 \end{pmatrix} e^{ik_h(x-a)} \phi_{m'}^S + a_{eh}^{\uparrow\uparrow} \begin{pmatrix} 0 \\ 0 \\ 1 \\ 0 \end{pmatrix} e^{-ik_h x} \phi_{m'+1}^S + a_{eh}^{\uparrow\downarrow} \begin{pmatrix} 0 \\ 0 \\ 0 \\ 1 \end{pmatrix} e^{-ik_h x} \phi_{m'}^S, \text{ for } 0 < x < a, \end{aligned} \quad (2.3)$$

$$\text{and } \psi_S(x) = t_{ee}^{\uparrow\uparrow} \begin{pmatrix} u \\ 0 \\ 0 \\ v \end{pmatrix} e^{iq_+ x} \phi_{m'}^S + t_{ee}^{\uparrow\downarrow} \begin{pmatrix} 0 \\ u \\ -v \\ 0 \end{pmatrix} e^{iq_+ x} \phi_{m'+1}^S + t_{eh}^{\uparrow\uparrow} \begin{pmatrix} 0 \\ -v \\ u \\ 0 \end{pmatrix} e^{-iq_- x} \phi_{m'+1}^S + t_{eh}^{\uparrow\downarrow} \begin{pmatrix} v \\ 0 \\ 0 \\ u \end{pmatrix} e^{-iq_- x} \phi_{m'}^S, \text{ for } x > a. \quad (2.4)$$

$r_{ee}^{\uparrow\uparrow}(r_{ee}^{\uparrow\downarrow})$  and  $r_{eh}^{\uparrow\uparrow}(r_{eh}^{\uparrow\downarrow})$  are the corresponding amplitudes for normal reflection and Andreev reflection with spin up(down).  $t_{ee}^{\uparrow\uparrow}(t_{ee}^{\uparrow\downarrow})$  and  $t_{eh}^{\uparrow\uparrow}(t_{eh}^{\uparrow\downarrow})$  are the corresponding amplitudes for transmission of electron-like quasi-particles and hole-like quasi-particles with spin up(down).  $\phi_{m'}^S$  is the eigenfunction of spin flipper: with its  $S_z$  operator acting as-  $S_z \phi_{m'}^S = \hbar m' \phi_{m'}^S$ , with  $m'$  being the spin magnetic moment of the spin flipper. For  $E > \Delta$  (for energies above the gap), the BCS coherence factors are  $u = \sqrt{\frac{1}{2} \left[ 1 + \frac{(E^2 - \Delta^2)^{\frac{1}{2}}}{E} \right]}$ ,  $v = \sqrt{\frac{1}{2} \left[ 1 - \frac{(E^2 - \Delta^2)^{\frac{1}{2}}}{E} \right]}$ , while the wave-vector in metal is  $k_{e,h} = \sqrt{\frac{2m^*}{\hbar^2} (E_F \pm E)}$  and in su-

2. FORMATION OF YU-SHIBA-RUSINOV BOUND STATES AND STABILITY OF MAJORANA BOUND STATES IN PRESENCE OF SPIN FLIP SCATTERING

perconductor is  $q_{\pm} = \sqrt{\frac{2m^*}{\hbar^2}(E_F \pm \sqrt{E^2 - \Delta^2})}$  and for  $E < \Delta$  (for energies below the gap) the BCS coherence factors are  $u = \sqrt{\frac{1}{2}\left[\frac{E+i(\Delta^2-E^2)^{\frac{1}{2}}}{\Delta}\right]}$ ,  $v = \sqrt{\frac{1}{2}\left[\frac{E-i(\Delta^2-E^2)^{\frac{1}{2}}}{\Delta}\right]}$ , while the wave-vector in metal remains same, and in superconductor is  $q_{\pm} = \sqrt{\frac{2m^*}{\hbar^2}(E_F \pm i\sqrt{\Delta^2 - E^2})}$ [9], wherein  $E$  is the excitation energy of electron above  $E_F$ . In Andreev approximation, which we will use,  $E_F \gg \Delta, E$ , thus we have  $k_e = k_h = q_+ = q_- = k_F$ . The wavefunctions (Eqs. (2.2)-(2.4)) satisfy the boundary conditions at  $x = 0$ ,

$$\psi_N^I(x) = \psi_N^{II}(x) \text{ (continuity of wavefunctions),} \quad (2.5)$$

$$\frac{d\psi_N^{II}}{dx} - \frac{d\psi_N^I}{dx} = -\frac{2m^*J_0\vec{s}\cdot\vec{S}}{\hbar^2}\psi_N^I \text{ (discontinuity in first derivative),} \quad (2.6)$$

and at  $x = a$ ,

$$\psi_N^{II}(x) = \psi_S(x) \text{ (continuity of wavefunctions),} \quad (2.7)$$

$$\frac{d\psi_S}{dx} - \frac{d\psi_N^{II}}{dx} = \frac{2m^*V}{\hbar^2}\psi_N^{II} \text{ (discontinuity in first derivative).} \quad (2.8)$$

When an electron with spin-up is incident from the metallic region, at  $x = 0$  interface, it interacts with the spin flipper via the exchange operator  $\vec{s}\cdot\vec{S}$  in Hamiltonian, which may induce a mutual spin flip. This electron can be reflected with spin up or down. Then from the superconductor, there is also the possibility of Andreev reflection, i.e., a hole with spin up or down is reflected (see Fig. 2.1(b)). Thus the wavefunction of the first metallic region  $\psi_N^I$  (Eq. (2.2)) has four components with (a) spin up electron, (b) spin-down electron, (c) spin-up hole, and (d) spin-down hole. Now when the exchange operator  $\vec{s}\cdot\vec{S}$  acts on the wavefunction  $\psi_N^I$  via Eq. (2.6) we get,

For spin up electron component,

$$\vec{s}\cdot\vec{S} \begin{pmatrix} 1 \\ 0 \\ 0 \\ 0 \end{pmatrix} \phi_{m'}^S = \frac{\hbar^2 m'}{2} \begin{pmatrix} 1 \\ 0 \\ 0 \\ 0 \end{pmatrix} \phi_{m'}^S + \frac{\hbar^2 f}{2} \begin{pmatrix} 0 \\ 1 \\ 0 \\ 0 \end{pmatrix} \phi_{m'+1}^S,$$

## 2.2. Signature of Yu-Shiba-Rusinov bound states in normal and Andreev reflection probabilities

---

while for spin down electron component:

$$\vec{s} \cdot \vec{S} \begin{pmatrix} 0 \\ 1 \\ 0 \\ 0 \\ 0 \end{pmatrix} \phi_{m'+1}^S = -\frac{\hbar^2(m'+1)}{2} \begin{pmatrix} 0 \\ 1 \\ 0 \\ 0 \\ 0 \end{pmatrix} \phi_{m'+1}^S + \frac{\hbar^2 f}{2} \begin{pmatrix} 1 \\ 0 \\ 0 \\ 0 \\ 0 \end{pmatrix} \phi_{m'}^S,$$

for spin up hole component:

$$\vec{s} \cdot \vec{S} \begin{pmatrix} 0 \\ 0 \\ 1 \\ 0 \\ 0 \end{pmatrix} \phi_{m'+1}^S = -\frac{\hbar^2(m'+1)}{2} \begin{pmatrix} 0 \\ 0 \\ 1 \\ 0 \\ 0 \end{pmatrix} \phi_{m'+1}^S + \frac{\hbar^2 f}{2} \begin{pmatrix} 0 \\ 0 \\ 0 \\ 0 \\ 1 \end{pmatrix} \phi_{m'}^S,$$

and finally for spin down hole component:

$$\vec{s} \cdot \vec{S} \begin{pmatrix} 0 \\ 0 \\ 0 \\ 0 \\ 1 \end{pmatrix} \phi_{m'}^S = \frac{\hbar^2 m'}{2} \begin{pmatrix} 0 \\ 0 \\ 0 \\ 0 \\ 1 \end{pmatrix} \phi_{m'}^S + \frac{\hbar^2 f}{2} \begin{pmatrix} 0 \\ 0 \\ 1 \\ 0 \\ 0 \end{pmatrix} \phi_{m'+1}^S.$$

Here  $f = \sqrt{(S - m')(S + m' + 1)}$  is the spin-flip probability[13] for spin flipper. Using the above equations and from boundary conditions (Eqs. (2.5)-(2.8)) we get 16 equations. We solve the 16 equations to calculate the different normal and Andreev reflection probabilities:

$$R_{ee}^{\uparrow\uparrow} = |r_{ee}^{\uparrow\uparrow}|^2, R_{ee}^{\uparrow\downarrow} = |r_{ee}^{\uparrow\downarrow}|^2, R_{eh}^{\uparrow\uparrow} = |r_{eh}^{\uparrow\uparrow}|^2, R_{eh}^{\uparrow\downarrow} = |r_{eh}^{\uparrow\downarrow}|^2.$$

In Fig. 2.2 we plot the normal and Andreev reflection probabilities with a spin-flip or no flip for different values of the spin  $S$  (19/2, 21/2, 23/2) of the spin flipper. We fix magnetic moment of the spin flipper-  $m' = -1/2$  and take  $Z = 0.85$ , i.e., non transparent regime. In Fig. 2.2(a), we plot normal reflection probability without spin-flip at both below as well as above the gap. We see that at zero energy, i.e.,  $E = 0$ , there is a dip related to the band

## 2. FORMATION OF YU-SHIBA-RUSINOV BOUND STATES AND STABILITY OF MAJORANA BOUND STATES IN PRESENCE OF SPIN FLIP SCATTERING

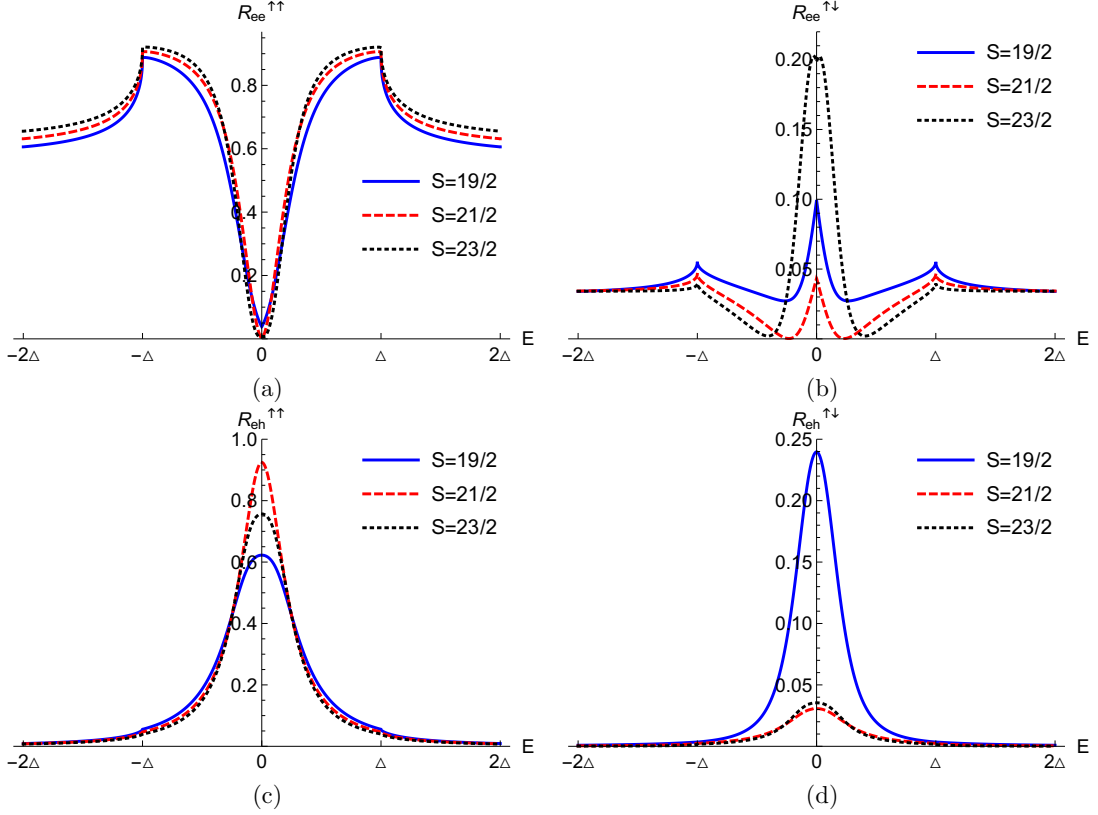


Figure 2.2: (a) Normal reflection probability without flip, (b) Normal reflection probability with flip, (c) Andreev reflection probability with flip, (d) Andreev reflection probability without flip. Parameters are:  $J = 0.4$ ,  $Z = 0.85$ ,  $m' = -1/2$  and  $k_F a = 0.8437\pi$ , are in dimensionless units.

of YSR states, and it is robust for high spin  $S = 23/2$  of the spin flipper. In Fig. 2.2(b), we plot normal reflection probability with spin-flip for both below and above the gap. We see a peak related to YSR bound states at zero energy  $E = 0$  within the energy gap. The explanation of why we address the zero energy peaks as related to YSR states is given in the next section, where we show how they arise by plotting the real part of complex poles of the conductance. Next, in Fig. 2.2(c), we plot the Andreev reflection probability with a spin-flip at both below and above the gap. We also see a peak at zero energy  $E = 0$  due to YSR bound states within the superconducting gap. Finally, in Fig. 2.2(d), we plot Andreev



reflection probability for no spin-flip at both below as well as above the gap. We see that there is zero energy peak related to YSR bound states.

## 2.3 Differential conductance and Probability density

The differential charge conductance at zero temperature is defined as[56, 57]-

$$G_c = 1 + R_{eh}^{\uparrow\uparrow} + R_{eh}^{\uparrow\downarrow} - R_{ee}^{\uparrow\uparrow} - R_{ee}^{\uparrow\downarrow}. \quad (2.9)$$

After deriving the amplitudes of normal and Andreev reflection by solving the scattering problem, we get an expression for the differential charge conductance at  $k_F a = 0$  as

$$G_c = \frac{R}{Q}, \quad (2.10)$$

where  $R = 8\Delta^2(4E^2 + (2 + J^2((1 + m')^2 - f^2) + 4J(1 + m')Z + 4Z^2)^2(\Delta^2 - E^2) + f^2 J^2((4 + (J + 2Jm')^2)\Delta^2 - J(1 + 2m')E(J(E + 2m'E) + 4\sqrt{\Delta^2 - E^2})))$ ,

(2.11)

and  $Q = 4E^2(4 + J^2(1 + 2f^2 + 2m' + 2m'^2) + 4JZ + 8Z^2)^2(\Delta^2 - E^2) + (E^2(J^4(f^2 + m' + m'^2)^2 - 4J^3(f^2 + m' + m'^2)Z + 8J(Z + 2Z^3) + 8(1 + 2Z^2 + 2Z^4) + J^2(2 + 4Z^2 + f^2(4 - 8Z^2) + m'(4 - 8Z^2) + m'^2(4 - 8Z^2))) - (J^4(f^2 + m' + m'^2)^2 - 4J^3(f^2 + m' + m'^2)Z + 4(1 + 2Z^2)^2 + 8J(Z + 2Z^3) + J^2(2 + (4 - 8f^2)Z^2 + m'(4 - 8Z^2) + m'^2(4 - 8Z^2)))\Delta^2)^2$

(2.12)

The differential charge conductance at zero bias or zero energy from Eq. (2.10) is then,

$$G_c = \frac{8(f^2 J^2(4 + (J + 2Jm')^2) + (2 + J^2(-f^2 + (1 + m')^2) + 4J(1 + m')Z + 4Z^2)^2)}{(J^4(f^2 + m' + m'^2)^2 - 4J^3(f^2 + m' + m'^2)Z + 4(1 + 2Z^2)^2 + 8J(Z + 2Z^3) + J^2(2 + (4 - 8f^2)Z^2 + m'(4 - 8Z^2) + m'^2(4 - 8Z^2)))^2} \quad (2.13)$$

From complex poles of the conductance  $G_c$  in Eqs. (2.9), (2.10) one can get the YSR bound states  $E^\pm$ . Real part of the poles gives the energy where YSR peaks occur, while the imaginary part gives the width of the peak. For  $k_F a = 0$  we get,

$$\frac{E^\pm}{\Delta} = \pm \sqrt{\frac{X_0}{Y_0}}, \quad \text{where} \quad (2.14)$$

2. FORMATION OF YU-SHIBA-RUSINOV BOUND STATES AND STABILITY OF MAJORANA BOUND STATES IN PRESENCE OF SPIN FLIP SCATTERING

---

$$\begin{aligned}
X_0 = & (J^2(f^2 + m' + m'^2) - 2JZ - 4Z^2)((J^2(f^2 + m' + m'^2) - 2JZ - 4Z^2)^2 + 2(2 + J^2(1 + 2m'(1 + m'))) \\
& + 4JZ + 8Z^2))\sqrt{(J^2(f^2 + m' + m'^2) - 2JZ - 4Z^2)^2 + 4(4 + J^2(1 + 2f^2 + 2m'(1 + m'))) + 4JZ + 8Z^2)} \\
& + J^8(f^2 + m' + m'^2)^4 - 8J^7(f^2 + m' + m'^2)^3Z + 64(1 + Z^2)(Z + 2Z^3)^2 + 32J(Z + 10Z^3 + 24Z^5 + 16Z^7) \\
& - 4J^6(f^2 + m' + m'^2)^2(-1 - 6Z^2 + (m' + m'^2)(-2 + 4Z^2)) + f^2(-1 + 4Z^2) + 16J^5(f^2 + m' + m'^2)Z \\
& (-1 + (-2 + 6f^2)Z^2 + (m' + m'^2)(-1 + 6Z^2)) - 16J^3Z(-1 - 8Z^2 - 8Z^4 + 3f^2(1 + 4Z^2 + 8Z^4) + (m' \\
& + m'^2)(1 + 8Z^2 + 24Z^4)) - 8J^2(-1 - 14Z^2 - 56Z^4 - 48Z^6 + 2m'(1 + m')(-1 + 2Z^2 + 8Z^4 + 16Z^6) + \\
& 2f^2(1 + 6Z^2 + 12Z^4 + 16Z^6)) + 2J^4(1 + 8Z^2 + 8Z^4 + (4m'^3 + 2m'^4)(5 - 8Z^2 + 24Z^4) - 4m'(-1 + 8Z^2 \\
& + 24Z^4) - 2m'^2(-7 + 24Z^2 + 24Z^4) + f^4(2 + 48Z^4) + 4f^2(-2Z^2(5 + 12Z^2) + (m' + m'^2)(3 - 4Z^2 + 24Z^4))),
\end{aligned} \tag{2.15}$$

$$\begin{aligned}
\text{and } Y_0 = & 2(J^2(f^2 + m' + m'^2) - 2JZ - 4Z^2)^2((J^2(f^2 + m' + m'^2) - 2JZ - 4Z^2)^2 + 4(4 + J^2(1 + 2f^2 + 2m'(1 + m'))) \\
& + 4JZ + 8Z^2)).
\end{aligned} \tag{2.16}$$

The condition when two YSR bound state energies merge at zero energy, i.e.,  $E^\pm = 0$ , is then from Eq. (2.14),-

$$\begin{aligned}
Z = & \frac{1}{4f}(-fJ + \sqrt{(2 + 4f^4J^2 + 8m' + 8m'^2 + f^2(J + 2Jm')^2 \pm 2\sqrt{(4f^8J^2(-1 + J^2) + 8f^6J^2(-1 + J^2)m'(1 + m') + (1 + 2m')^4} \\
& + (f + 2fm')^2(1 + 4J^2m'(1 + m')) + 4f^4(J^4m'^2(1 + m')^2 - (1 + 2m')^2 + J^2(1 + 4m' + 3m'^2 - 2m'^3 - m'^4))})))
\end{aligned} \tag{2.17}$$

The above condition leads to the formation of the peaks at zero energy in conductance spectra. The zero-energy YSR states are the fingerprint of quantum phase transitions in the ground state of the junction[58]. These zero-energy YSR conductance peaks are non-topological in contrast to the zero-energy  $2e^2/h$  quantized conductance Majorana peaks, therefore it helps to distinguish between trivial and non-trivial zero energy conductance peaks. There are some important differences between YSR bound states and Andreev bound states.

(i) Andreev bound states arise due to ordinary (non-magnetic) impurity, but YSR bound states arise due to magnetic impurity.

(ii) Andreev bound state can also arise at the gap edges ( $E = \pm\Delta$ ), however YSR bound state can only arise below the superconducting gap ( $-\Delta < E < \Delta$ ).

In our work in presence of spin-flip scattering Andreev bound states and YSR bound states merge, thus we can not differentiate Andreev bound states from YSR bound states. In absence of spin flipper ( $J = 0$  case) and for no flip ( $f = 0$ ) there are no YSR states within gap  $[-\Delta, \Delta]$ . The signature of YSR bound states can also be seen in probability density. To evaluate this, we integrate the squared absolute value of wavefunction amplitude in normal metal region II.

$$\int_0^a |\psi_N^{II}(x)|^2 dx = P = |t_{ee}^{\uparrow\uparrow}|^2 + |t_{ee}^{\uparrow\downarrow}|^2 + |b_{ee}^{\uparrow\uparrow}|^2 + |b_{ee}^{\uparrow\downarrow}|^2 + |c_{eh}^{\uparrow\uparrow}|^2 + |c_{eh}^{\uparrow\downarrow}|^2 + |a_{eh}^{\uparrow\uparrow}|^2 + |a_{eh}^{\uparrow\downarrow}|^2 \quad (2.18)$$

where  $t_{ee}^{\uparrow\uparrow}$ ,  $t_{ee}^{\uparrow\downarrow}$ ,  $b_{ee}^{\uparrow\uparrow}$ ,  $b_{ee}^{\uparrow\downarrow}$ ,  $c_{eh}^{\uparrow\uparrow}$ ,  $c_{eh}^{\uparrow\downarrow}$ ,  $a_{eh}^{\uparrow\uparrow}$ ,  $a_{eh}^{\uparrow\downarrow}$  are the reflection amplitudes of electrons and holes with spin up and down in region II (normal metal).

## 2.4 Signature of Yu-Shiba-Rusinov bound states in conductance spectra

We focus on the zero energy YSR peak. In Fig. 2.3 we plot conductance spectra for both no flip as well as the spin-flip case. We see that for no flip case ( $f = 0$ ), there is a dip at zero energy for all values of interface transparency  $Z$  ( $Z = 0.5, 0.78, 1$ ). But in contrast to no flip case for the spin-flip case, we see that for  $Z = 0.78$ , a peak occurs at  $E = 0$  due to two YSR states merging. But for  $Z = 0.5$  and  $Z = 1$ , there are dips at  $E = 0$ , same as no flip case. In Fig. 2.3(b), we also see there are peaks, due to YSR bound states, present symmetrically at both positive and negative energies for  $Z = 0.5$  and  $Z = 1$ . The calculated real part of poles of conductance for spin-flip case in Fig. 2.3(b) are:  $\pm 0.46\Delta$  (for  $Z = 0.5$ ),  $\pm 0.00028\Delta$  (for  $Z = 0.78$ ),  $\pm 0.22\Delta$  (for  $Z = 1$ ) and they clearly match with the conductance peaks shown in Fig. 2.3(b). In Fig. 2.3(c), we plot the energy bound state

## 2. FORMATION OF YU-SHIBA-RUSINOV BOUND STATES AND STABILITY OF MAJORANA BOUND STATES IN PRESENCE OF SPIN FLIP SCATTERING

as a function of interface transparency  $Z$  for the same parameters as shown in Fig. 2.3(b). We see two energy-bound states merge at  $Z = 0.78$  and  $1.62$ , where zero energy peaks are observed in conductance spectra due to YSR states.

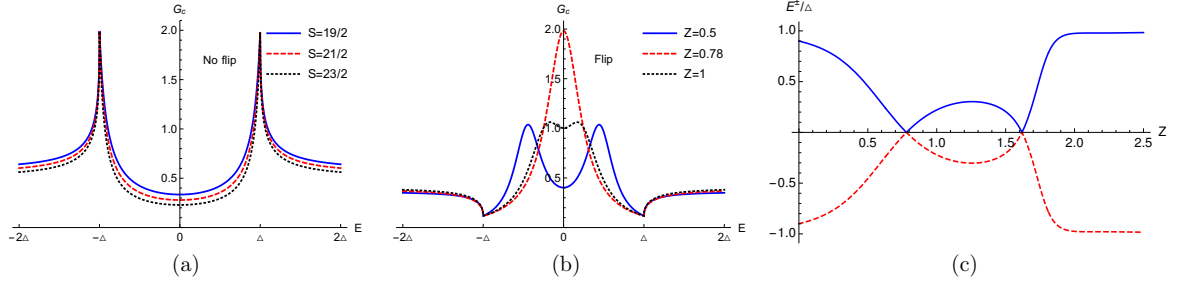


Figure 2.3: (a) Charge conductance vs energy for no flip case. Parameters are:  $J = 0.4$ ,  $S = 19/2$ ,  $m' = 19/2$ ,  $k_F a = 0.8437\pi$ , (b) Charge conductance vs energy for spin flip case. Parameters are:  $J = 0.4$ ,  $S = 19/2$ ,  $m' = -1/2$ ,  $k_F a = 0.8437\pi$ , (c) Energy bound states as a function of interface transparency  $Z$ . Parameters are:  $S = 19/2$ ,  $m' = -1/2$ ,  $J = 0.4$ ,  $k_F a = 0.8437\pi$ . Here charge conductance is in units of  $e^2/h$ .

In Fig. 2.4(a) we plot charge conductance as function of energy  $E$  for  $S = 7/2$  and different values of  $J$  ( $J = 0.3, 0.4$ ). We see a peak, related to YSR states, present symmetrically at both positive and negative energies for  $J = 0.3$  and  $J = 0.4$ . The energies where YSR peaks occur, i.e., values of the real part of pole of conductance calculated from Eq. (2.14), i.e.,  $\pm 0.63\Delta$  (for  $J = 0.3$ ) and  $\pm 0.69\Delta$  (for  $J = 0.4$ ) match quite well with conductance peaks shown in Fig. 2.4(a). In Fig. 2.4(b) we plot charge conductance spectra for spin flipper spin  $S = 9/2$ . We also find peaks due to YSR bound states near the gap edge within the energy gap for both  $J = 0.3$  and  $J = 0.4$ . Energies where YSR peaks occur, i.e., values of the real part of the pole of conductance calculated from Eq. (2.14),  $\pm 0.68\Delta$  (for  $J = 0.3$ ) and  $\pm 0.75\Delta$  (for  $J = 0.4$ ) match quite well with the conductance peak shown in Fig. 2.4(b). In Fig. 2.4(c), we plot charge conductance spectra for spin  $S = 11/2$  of the spin flipper. For  $J = 0.3$  and  $J = 0.4$ , we note that there are peaks due to YSR states near

## 2.4. Signature of Yu-Shiba-Rusinov bound states in conductance spectra

the gap edges within the energy gap. In Figs. 2.4(a), (b), and (c), we give a comparison

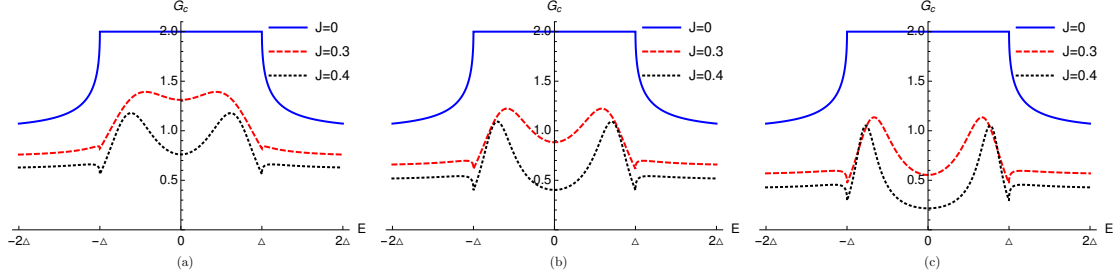


Figure 2.4: (a) Charge conductance vs energy in transparent regime with  $S = 7/2, m' = -1/2$ , (b) Charge conductance vs energy in transparent regime with  $S = 9/2, m' = -1/2$ , (c) Charge conductance vs energy in transparent regime with  $S = 11/2, m' = -1/2$ . Here charge conductance is in units of  $e^2/h$ .

with the  $J = 0$  case (absence of spin flipper) wherein there is no YSR bound state peaks in conductance spectra. The energies where YSR peaks occur, i.e., values of the real part of the pole of conductance calculated from Eq. (2.14) are  $\pm 0.72\Delta$  (for  $J = 0.3$ ) and  $\pm 0.79\Delta$  (for  $J = 0.4$ ) match quite well with the conductance peaks shown in Fig. 2.4(c). Thus we can conclude that it is spin-flip scattering enabled by the spin flipper, which is the reason behind the occurrence of YSR bound states near the gap edges.

Next in Fig. 2.5 we plot charge conductance and probability density as a function of energy  $E$ . We see there is a peak at zero energy in conductance spectra due to YSR bound states. We take large spin flipper/impurity spin for (a)  $S = 21/2$ , (b)  $S = 23/2$  and exchange interaction  $J = 0.4$ . In Figs. 2.5(c), (d) zero energy peak is also observed in probability density. In Figs. 2.5(c), (d) we take same parameters as in Figs. 2.5(a), (b) respectively. The calculated real part of poles of conductance in Figs. 2.5(a) and 2.5(b) are:  $\pm 0.00013\Delta$  and  $\pm 0.00018\Delta$  respectively and they match with the peak shown in Figs. 2.5(a) and 2.5(b). In Figs. 2.5(e) and (f) we plot energy bound states as a function of interface transparency ( $Z$ ) for same parameters as in Figs. 2.5(a) and (b) respectively. In Fig. 2.5(e) for  $S = 21/2$ , we

## 2. FORMATION OF YU-SHIBA-RUSINOV BOUND STATES AND STABILITY OF MAJORANA BOUND STATES IN PRESENCE OF SPIN FLIP SCATTERING

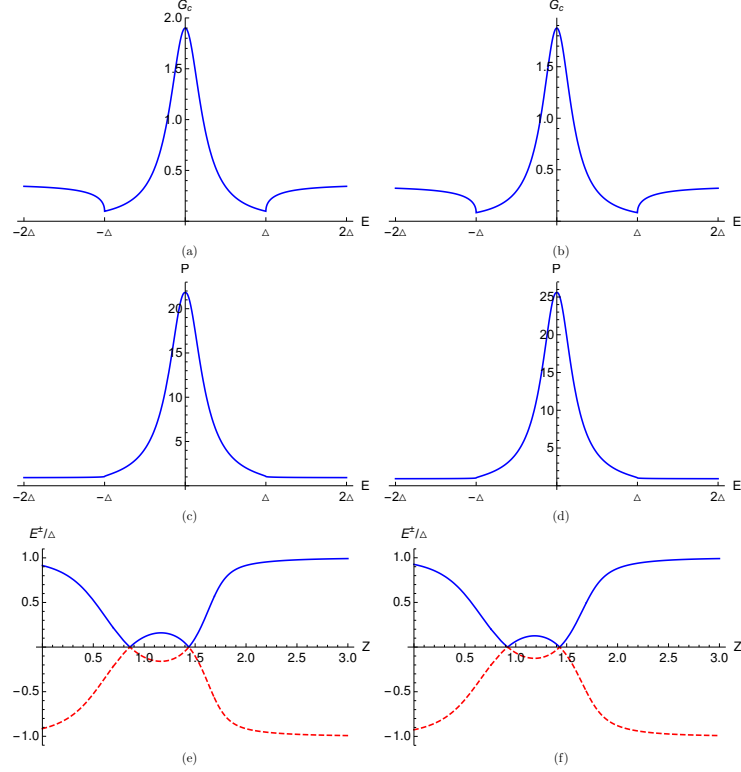


Figure 2.5: (a) Charge conductance vs energy  $E$  for  $S = 21/2, m' = -1/2, Z = 0.86, J = 0.4, k_F a = 0.8437\pi$ , (b) Charge conductance vs energy  $E$  for  $S = 23/2, m' = -1/2, Z = 0.92, J = 0.4, k_F a = 0.8492\pi$ , (c) Probability density vs energy  $E$  for  $S = 21/2, m' = -1/2, Z = 0.86, J = 0.4, k_F a = 0.8437\pi$ , (d) Probability density vs energy  $E$  for  $S = 23/2, m' = -1/2, Z = 0.92, J = 0.4, k_F a = 0.8492\pi$ , (e) Energy bound states as a function of interface transparency  $Z$ . Parameters are:  $S = 21/2, m' = -1/2, J = 0.4, k_F a = 0.8437\pi$ , (f) Energy bound states as a function of interface transparency  $Z$ . Parameters are:  $S = 23/2, m' = -1/2, J = 0.4, k_F a = 0.8492\pi$ . Here charge conductance is in units of  $e^2/h$ .

see that two bound state energies merge at  $Z = 0.86$  and  $1.44$ , where we see the zero energy peaks in the conductance spectra due to YSR bound states. In Fig. 2.5(f) for  $S = 23/2$ , we also note that energy bound states merge at  $Z = 0.92$  and  $1.43$ , where zero energy peaks due to YSR states are seen in conductance spectra.

In Ref. [59], a NS junction is considered, where magnetic impurities are distributed homogeneously on the NS interface, however in this thesis there is a spin-flipper or single

magnetic impurity placed between two normal metals in N-SF-N-I-S junction. Thus, Ref. [59] deals with a different system and in Ref. [59] it is also seen that YSR bound state energies don't merge and these YSR peaks appear only near the gap edge.

## 2.5 Effect of arbitrary junction length on Yu-Shiba-Rusinov bound states

In previous sections, we mainly concentrate on the short junction limit. In this limit, we see YSR bound states occur at zero energy in conductance spectra for low values of  $J$  and high  $S$  values. In this section, we study the effect of junction length on YSR bound states. We provide a comparison of YSR bound states for short and long junctions.

For an electron with spin up incident, the wavefunction in the normal metal region I is given in long junction limit, following Ref. [60] as

$$\psi_N^I(x) = \begin{pmatrix} u \\ 0 \\ 0 \\ 0 \end{pmatrix} e^{ik_e x} \phi_{m'}^S + r_{ee}^{\uparrow\uparrow} \begin{pmatrix} v \\ 0 \\ 0 \\ 0 \end{pmatrix} e^{-ik_e x} \phi_{m'}^S + r_{ee}^{\uparrow\downarrow} \begin{pmatrix} 0 \\ -v \\ 0 \\ 0 \end{pmatrix} e^{-ik_e x} \phi_{m'+1}^S + r_{eh}^{\uparrow\uparrow} \begin{pmatrix} 0 \\ 0 \\ -v \\ 0 \end{pmatrix} e^{ik_h x} \phi_{m'+1}^S + r_{eh}^{\uparrow\downarrow} \begin{pmatrix} 0 \\ 0 \\ 0 \\ v \end{pmatrix} e^{ik_h x} \phi_{m'}^S, \text{ for } x < 0. \quad (2.19)$$

Similarly wavefunction in normal metal region II is given by-

$$\begin{aligned} \psi_N^{II}(x) = & t_{ee}^{\uparrow\uparrow} \begin{pmatrix} u \\ 0 \\ 0 \\ 0 \end{pmatrix} e^{ik_e x} \phi_{m'}^S + t_{ee}^{\uparrow\downarrow} \begin{pmatrix} 0 \\ u \\ 0 \\ 0 \end{pmatrix} e^{ik_e x} \phi_{m'+1}^S + b_{ee}^{\uparrow\uparrow} \begin{pmatrix} v \\ 0 \\ 0 \\ 0 \end{pmatrix} e^{-ik_e(x-a)} \phi_{m'}^S + b_{ee}^{\uparrow\downarrow} \begin{pmatrix} 0 \\ -v \\ 0 \\ 0 \end{pmatrix} e^{-ik_e(x-a)} \phi_{m'+1}^S \\ & + c_{eh}^{\uparrow\uparrow} \begin{pmatrix} 0 \\ 0 \\ -v \\ 0 \end{pmatrix} e^{ik_h(x-a)} \phi_{m'+1}^S + c_{eh}^{\uparrow\downarrow} \begin{pmatrix} 0 \\ 0 \\ 0 \\ v \end{pmatrix} e^{ik_h(x-a)} \phi_{m'}^S + a_{eh}^{\uparrow\uparrow} \begin{pmatrix} 0 \\ 0 \\ u \\ 0 \end{pmatrix} e^{-ik_h x} \phi_{m'+1}^S + a_{eh}^{\uparrow\downarrow} \begin{pmatrix} 0 \\ 0 \\ 0 \\ u \end{pmatrix} e^{-ik_h x} \phi_{m'}^S, \text{ for } 0 < x < a. \end{aligned} \quad (2.20)$$

## 2. FORMATION OF YU-SHIBA-RUSINOV BOUND STATES AND STABILITY OF MAJORANA BOUND STATES IN PRESENCE OF SPIN FLIP SCATTERING

---

The corresponding wavefunction in superconductor is,

$$\psi_S(x) = t_{ee}^{\uparrow\uparrow} \begin{pmatrix} u \\ 0 \\ 0 \\ v \end{pmatrix} e^{iq_+x} \phi_{m'}^S + t_{ee}^{\uparrow\downarrow} \begin{pmatrix} 0 \\ u \\ -v \\ 0 \end{pmatrix} e^{iq_+x} \phi_{m'+1}^S + t_{eh}^{\uparrow\uparrow} \begin{pmatrix} 0 \\ -v \\ u \\ 0 \end{pmatrix} e^{-iq_-x} \phi_{m'+1}^S + t_{eh}^{\uparrow\downarrow} \begin{pmatrix} 0 \\ 0 \\ 0 \\ u \end{pmatrix} e^{-iq_-x} \phi_{m'}^S, \text{ for } x > a. \quad (2.21)$$

For  $|E| \ll E_F$ , we can write  $k_{e,h} \approx k_F \pm \frac{E}{2\Delta\xi}$ , where  $\xi = E_F/(k_F\Delta)$  is Cooper pair coherence length[25]. Boundary conditions at the different interfaces of our system are mentioned before in Eqs. (2.5)-(2.8). By imposing boundary conditions on wavefunctions mentioned in Eqs. (2.19)-(2.21) one can get different scattering amplitudes. After getting scattering amplitudes, using Eq. (2.9) we can calculate charge conductance for arbitrary junction length. In Fig. 2.6 we plot charge conductance as a function of energy  $E$  for different junction lengths ‘ $a$ ’. In Fig. 2.6(a) we concentrate on short junction limit ( $a < \xi$ ). In this limit we take three different values of  $a$  ( $a = 0$ ,  $a = 0.1\xi$ ,  $a = 0.4\xi$ ). We see that a peak appears at zero energy in conductance spectra due to YSR states. We also see that peaks in conductance formed due to merger of YSR bound states at zero energy are robust to change in length  $a$  of the junction. We take large spin flipper spin  $S = 21/2$ , and small exchange interaction  $J = 0.4$ . However, these YSR peaks at zero energy are unfortunately not as robust to changes in other parameters, e.g.,  $Z$ ,  $J$ ,  $S$ ,  $m'$ . Next, in Fig. 2.6(b) we concentrate on intermediate junction limit ( $a \sim \xi$ ). This limit also shows a peak at zero energy in conductance spectra due to YSR bound states. Further, we see peaks due to YSR bound states present asymmetrically at both positive and negative energies near the gap edge in the subgap regime. Finally, in Fig. 2.6(c) we focus on long junction limit ( $a > \xi$ ). In this limit we take two different values of  $a$  ( $a = 2\xi$ ,  $a = 5\xi$ ). We see that there is a peak at zero energy in conductance spectra. Further, many YSR peaks appear in the subgap regime of conductance spectra. Similar features have also been seen in Ref. [52], where the magnetic



## 2.6. Stability of Majorana zero modes in the presence of a spin flipper

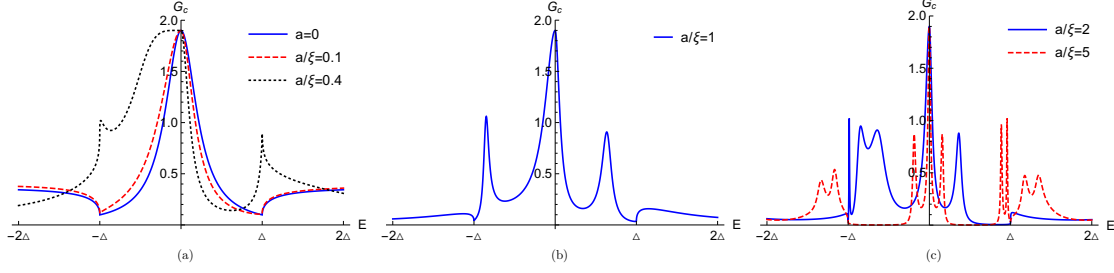


Figure 2.6: Charge conductance as a function of energy for different junction lengths ( $a$ ). Parameters are  $S = 21/2$ ,  $m' = -1/2$ ,  $Z = 0.86$ ,  $J = 0.4$ ,  $k_F a = 0.8437\pi$ . Here charge conductance is in units of  $e^2/h$ .

impurity is outside the superconductor. Many YSR peaks appear in the subgap regime of conductance spectra with an increase in temperature (see Figs. 4(b), (c) of Ref. [52]). When the temperature is increased, superconducting coherence length decreases, and the junction behaves like a long junction ( $a > \xi$ ). Thus, many YSR peaks are seen in the subgap regime of conductance spectra in the long junction limit. If the spin flipper is put at the right junction, then the distance between spin-flipper and superconductor is zero. In that case we still see a peak appearing at zero energy in the conductance spectra due to YSR bound states, see Fig. 2.6(a).

## 2.6 Stability of Majorana zero modes in the presence of a spin flipper

In previous sections, we have shown the formation and characteristics of YSR bound states in the subgap regime of a Metal-Spin flipper-Metal-Insulator- $s$ -wave superconductor junction. This section examines the stability of Majorana bound states (MBS's) induced, zero bias (zero energy) conductance peak in metal-topological superconductor junction in the vicinity of a spin flipper. Zero energy  $2e^2/h$  quantized conductance Majorana peaks are topological in contrast to the zero-energy YSR conductance peaks which arise

## 2. FORMATION OF YU-SHIBA-RUSINOV BOUND STATES AND STABILITY OF MAJORANA BOUND STATES IN PRESENCE OF SPIN FLIP SCATTERING

due to non-topological reasons. YSR bound states are induced by the spin-flipper or a magnetic impurity, while Majorana bound states can be induced without any magnetic impurity. Majorana peaks do not change or they are robust to spin-flip scattering and therefore are topological while YSR peaks are not. We contrast Majorana states arising at metal- $p$ -wave superconductor interfaces with those appearing at metal-spin orbit coupled superconducting wire (SOCSW) interfaces.

### 2.6.1 Spin flipper in vicinity of metal- $p$ -wave superconductor junction

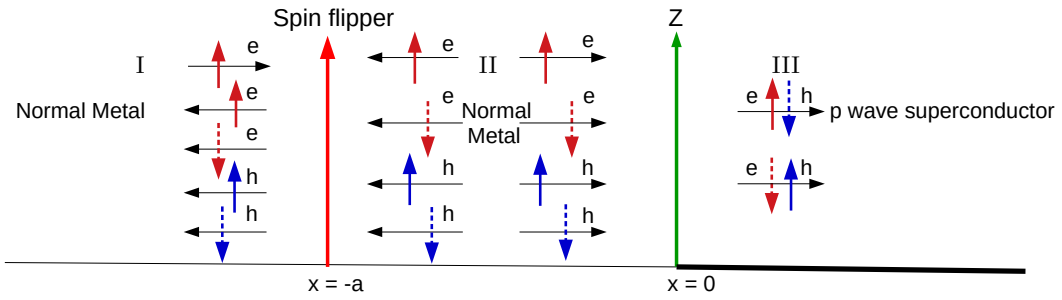


Figure 2.7:  $N_1$ - $N_2$ - $p$ Sc junction in topological regime ( $\mu_{pSc} > 0$ ) with a spin flipper (spin  $S$ , magnetic moment  $m'$ ) at  $x = -a$  and a  $\delta$ -like potential barrier (strength  $Z$ ) at  $x = 0$ . The scattering of an incident spin up electron is shown. Normal reflection, Andreev reflection and quasi-particle transmission into  $p$ -wave superconductor are represented.

We consider a 1D normal metal ( $N_1$ )-normal metal ( $N_2$ )- $p$ -wave superconductor (pSc) junction wherein a spin flipper is embedded between the two metallic regions at  $x = -a$ . The interface at  $x = 0$  is modeled by a  $\delta$ -like potential barrier (strength  $Z$ ) as shown in Fig. 2.7 and the problem is solved using BTK[9] approach, see section 1.1.1. Normal metals  $N_1$  and  $N_2$  are spinful. When a spin up/down electron with energy  $E$  is incident from the metallic region, at  $x = -a$  interface, it interacts with spin flipper through an exchange

## 2.6. Stability of Majorana zero modes in the presence of a spin flipper

---

interaction which may cause a mutual spin flip. The incident electron is either reflected or transmitted to  $N_2$ , with spin-up or down. When this transmitted electron with spin-up is incident at  $x = 0$  interface, it can be normally reflected as an electron with spin-up from the interface or could be Andreev reflected, as spin-down hole back to  $N_2$ . In  $p$ -wave superconductor, the spin-up electron and spin-down hole form one channel of transport, while spin-down electron and spin-up hole form another transport channel for energies above the superconducting gap. There is no spin mixing in the  $p$ -wave superconductor.

Spin flipper is a point-like magnetic impurity, see also Ref. [13]. When an electron interacts with a spin flipper, there are two possible processes. In the first process, an electron (with spin  $s$  and magnetic moment  $m$ ) can scatter from the spin flipper (with spin  $S$  and magnetic moment  $m'$ ) while flipping its spin and flipping the spin of the spin flipper with a finite probability. In the second process, an electron (with spin  $s$  and magnetic moment  $m$ ) scatters from the spin flipper (with spin  $S$  and magnetic moment  $m'$ ) without flipping either its spin or the spin of the spin flipper, and there is no possibility of spin-flip scattering.

The BdG Hamiltonians for NM and pSc, from Ref. [61] are-

$$H_{NM} = (-\hbar^2 \partial_x^2 / 2m^* - \mu_{NM}) \tau_z, \quad (2.22a)$$

$$H_{pSc} = (-\hbar^2 \partial_x^2 / 2m^* - \mu_{pSc}) \tau_z - i \Delta_{pSc} \partial_x \tau_x, \quad (2.22b)$$

where  $\mu_{NM}$  and  $\mu_{pSc}$  are respective chemical potentials,  $m^*$  mass of electron,  $\Delta_{pSc} \geq 0$  is  $p$ -wave pairing potential,  $\tau_\mu = \sigma_\mu \otimes I$ , with  $I$  being  $2 \times 2$  identity matrix and  $\sigma_\mu$  ( $\mu = x, y, z$ ) are Pauli matrices. For simplicity, we consider  $\hbar = \mu_{NM} = 2m^* = 1$ . The energy spectrum are then for Normal metals:  $\varepsilon_{NM,\pm}(k) = \pm(k^2 - 1)$  and for  $p$ -wave superconductor:  $\varepsilon_{pSc,\pm}(k) = \pm \sqrt{(k^2 - \mu_{pSc})^2 + (\Delta_{pSc} k)^2}$ , respectively. The energy spectra of pSc for different values of  $\mu_{pSc}$  is plotted in Fig. 1 of Ref. [61]. It is seen that energy spectrum

## 2. FORMATION OF YU-SHIBA-RUSINOV BOUND STATES AND STABILITY OF MAJORANA BOUND STATES IN PRESENCE OF SPIN FLIP SCATTERING

becomes gapless at  $\mu_{pSc} = 0$ . But for nontopological regime, there is a energy gap  $|\mu_{pSc}|$  in energy spectrum. Here we only concentrate on topological regime[61], i.e.,  $\mu_{pSc} > 0$ . For  $\mu_{pSc} > \Delta_{pSc}^2/2$ , positive energy spectrum for pSc shows characteristic “double-well” BCS structure with minima at  $\epsilon_1 = \Delta_{pSc}\sqrt{\mu_{pSc} - \Delta_{pSc}^2/4}$  for  $k = \pm\sqrt{\mu_{pSc} - \Delta_{pSc}^2/2}$  and a local maximum at  $\epsilon_2 = \mu_{pSc}$  for  $k = 0$ , as also seen in Fig. 1 of Ref. [61].

### Symmetry class of $p$ -wave Hamiltonian:

If a Hamiltonian possesses particle-hole symmetry then  $\mathcal{H}(k) = -\tau_x\mathcal{H}^*(-k)\tau_x$  (or,  $\tau_y\sigma_y\mathcal{H}^*(-k)\tau_y\sigma_y = -\mathcal{H}(k)$ , or  $\mathcal{H}(k) = -\mathcal{H}^*(-k)$ , or  $\mathcal{H}(k) = -\tau_z\sigma_y\mathcal{H}^*(-k)\sigma_y\tau_z$ , or  $\mathcal{H}(k) = -\sigma_y\mathcal{H}^*(-k)\sigma_y$ , or  $\mathcal{H}(k) = -\tau_y\mathcal{H}^*(-k)\tau_y$ ), where  $k$  is the wavevector

$$\text{and } \tau_x = \begin{pmatrix} 0 & 0 & 1 & 0 \\ 0 & 0 & 0 & 1 \\ 1 & 0 & 0 & 0 \\ 0 & 1 & 0 & 0 \end{pmatrix}, \tau_y = \begin{pmatrix} 0 & 0 & -i & 0 \\ 0 & 0 & 0 & -i \\ i & 0 & 0 & 0 \\ 0 & i & 0 & 0 \end{pmatrix} \text{ and } \tau_z = \begin{pmatrix} 1 & 0 & 0 & 0 \\ 0 & 1 & 0 & 0 \\ 0 & 0 & -1 & 0 \\ 0 & 0 & 0 & -1 \end{pmatrix} \text{ are Pauli}$$

$$\text{matrices in particle-hole space, while } \sigma_x = \begin{pmatrix} 0 & 1 & 0 & 0 \\ 1 & 0 & 0 & 0 \\ 0 & 0 & 0 & 1 \\ 0 & 0 & 1 & 0 \end{pmatrix}, \sigma_y = \begin{pmatrix} 0 & -i & 0 & 0 \\ i & 0 & 0 & 0 \\ 0 & 0 & 0 & -i \\ 0 & 0 & i & 0 \end{pmatrix} \text{ and}$$

$$\sigma_z = \begin{pmatrix} 1 & 0 & 0 & 0 \\ 0 & -1 & 0 & 0 \\ 0 & 0 & 1 & 0 \\ 0 & 0 & 0 & -1 \end{pmatrix} \text{ are Pauli matrices in spin space.}$$

Similarly, if Hamiltonian possesses time reversal symmetry then  $\mathcal{H}(k) = \tau_z\mathcal{H}^*(-k)\tau_z$  (or,  $\mathcal{H}(k) = \tau_y\mathcal{H}^*(-k)\tau_y$ , or  $\mathcal{H}(k) = \tau_x\mathcal{H}^*(-k)\tau_x$ , or  $\mathcal{H}(k) = \sigma_y\mathcal{H}^*(-k)\sigma_y$ , or  $\mathcal{H}(k) = \mathcal{H}^*(-k)$ ) and finally if Hamiltonian possesses chiral symmetry then  $\mathcal{H}(k) = -\tau_x\mathcal{H}(-k)\tau_x$ ,

## 2.6. Stability of Majorana zero modes in the presence of a spin flipper

or  $\mathcal{H}(k) = -\tau_z \mathcal{H}(k) \tau_z$ .

In 1D,  $p$ -wave Hamiltonian preserves all three symmetries- particle-hole, time reversal and chiral. The 1D  $p$ -wave Hamiltonian in Eq. (2.22b) can be written as,

$$H_{pSc}(k) = \begin{pmatrix} k^2 - \mu_{pSc} & 0 & \Delta_{pSc}k & 0 \\ 0 & k^2 - \mu_{pSc} & 0 & \Delta_{pSc}k \\ \Delta_{pSc}k & 0 & -k^2 + \mu_{pSc} & 0 \\ 0 & \Delta_{pSc}k & 0 & -k^2 + \mu_{pSc} \end{pmatrix} \quad (2.23)$$

Using Eq. (2.23) we get-

$$\tau_x H_{pSc}^*(-k) \tau_x = \begin{pmatrix} -k^2 + \mu_{pSc} & 0 & -\Delta_{pSc}k & 0 \\ 0 & -k^2 + \mu_{pSc} & 0 & -\Delta_{pSc}k \\ -\Delta_{pSc}k & 0 & k^2 - \mu_{pSc} & 0 \\ 0 & -\Delta_{pSc}k & 0 & k^2 - \mu_{pSc} \end{pmatrix} \quad (2.24)$$

From Eqs. (2.23) and (2.24), we see  $H_{pSc}(k) = -\tau_x H_{pSc}^*(-k) \tau_x$ . Similarly we can show that  $H_{pSc}(k) = \tau_z H_{pSc}^*(-k) \tau_z$  and  $H_{pSc}(k) = -\tau_x H_{pSc}(-k) \tau_x$ . Thus,  $p$ -wave Hamiltonian in Eq. (2.22b) satisfies particle-hole, time reversal and chiral symmetries and therefore belongs to symmetry class BDI.

The wave functions for different regions of our system as in Fig. 2.7 can be written for a spin-up electron incident at  $x = -a$  interface as

$$\psi_{NM}^I(x) = \begin{pmatrix} 1 \\ 0 \\ 0 \\ 0 \end{pmatrix} e^{i(x+a)} \phi_{m'+r}^{S_{ee}\uparrow\uparrow} \begin{pmatrix} 1 \\ 0 \\ 0 \\ 0 \end{pmatrix} e^{-i(x+a)} \phi_{m'+r}^{S_{ee}\uparrow\downarrow} \begin{pmatrix} 0 \\ 1 \\ 0 \\ 0 \end{pmatrix} e^{-i(x+a)} \phi_{m'+1+r}^{S_{eh}\uparrow\uparrow} \begin{pmatrix} 0 \\ 0 \\ 0 \\ 1 \end{pmatrix} e^{i(x+a)} \phi_{m'+r}^{S_{eh}\uparrow\downarrow} \begin{pmatrix} 0 \\ 0 \\ 1 \\ 0 \end{pmatrix} e^{i(x+a)} \phi_{m'+1}^S, \quad \text{for } x < -a, \quad (2.25)$$

2. FORMATION OF YU-SHIBA-RUSINOV BOUND STATES AND STABILITY OF MAJORANA BOUND STATES IN PRESENCE OF SPIN FLIP SCATTERING

---

$$\begin{aligned} \psi_{NM}^{II}(x) = & t_{ee}^{\uparrow\uparrow} \begin{pmatrix} 1 \\ 0 \\ 0 \\ 0 \end{pmatrix} e^{i(x+a)} \phi_{m'}^S + t_{ee}^{\uparrow\downarrow} \begin{pmatrix} 0 \\ 1 \\ 0 \\ 0 \end{pmatrix} e^{i(x+a)} \phi_{m'+1}^S + b_{ee}^{\uparrow\uparrow} \begin{pmatrix} 1 \\ 0 \\ 0 \\ 0 \end{pmatrix} e^{-ix} \phi_{m'}^S + b_{ee}^{\uparrow\downarrow} \begin{pmatrix} 0 \\ 1 \\ 0 \\ 0 \end{pmatrix} e^{-ix} \phi_{m'+1}^S \\ & + c_{eh}^{\uparrow\uparrow} \begin{pmatrix} 0 \\ 0 \\ 0 \\ 1 \end{pmatrix} e^{ix} \phi_{m'}^S + c_{eh}^{\uparrow\downarrow} \begin{pmatrix} 0 \\ 0 \\ 1 \\ 0 \end{pmatrix} e^{ix} \phi_{m'+1}^S + a_{eh}^{\uparrow\uparrow} \begin{pmatrix} 0 \\ 0 \\ 0 \\ 1 \end{pmatrix} e^{-i(x+a)} \phi_{m'}^S + a_{eh}^{\uparrow\downarrow} \begin{pmatrix} 0 \\ 0 \\ 1 \\ 0 \end{pmatrix} e^{-i(x+a)} \phi_{m'+1}^S, \text{ for } -a < x < 0, \end{aligned} \quad (2.26)$$

$$\psi_{pSc}(x) = t_{ee}^{\uparrow\uparrow} \begin{pmatrix} \eta_- \\ 0 \\ 0 \\ 1 \end{pmatrix} e^{ik_-x} \phi_{m'}^S + t_{ee}^{\uparrow\downarrow} \begin{pmatrix} 0 \\ \eta_- \\ 1 \\ 0 \end{pmatrix} e^{ik_-x} \phi_{m'+1}^S + t_{eh}^{\uparrow\uparrow} \begin{pmatrix} \eta_+ \\ 0 \\ 0 \\ 1 \end{pmatrix} e^{ik_+x} \phi_{m'}^S + t_{eh}^{\uparrow\downarrow} \begin{pmatrix} 0 \\ \eta_+ \\ 1 \\ 0 \end{pmatrix} e^{ik_+x} \phi_{m'+1}^S, \text{ for } x > 0, \quad (2.27)$$

where  $\eta_{\pm} = \frac{E+k_{\pm}^2-\mu_{pSc}}{\Delta_{pSc}k_{\pm}}$ .  $r_{ee}^{\uparrow\uparrow}$  and  $r_{ee}^{\uparrow\downarrow}$  are normal reflection amplitudes for an incoming electron with spin up ( $\uparrow$ ) reflected as an electron with either spin up ( $\uparrow$ ) or spin down ( $\downarrow$ ) respectively, while  $r_{eh}^{\uparrow\uparrow}$  and  $r_{eh}^{\uparrow\downarrow}$  are Andreev reflection amplitudes for an incoming electron with spin up ( $\uparrow$ ) reflected as a hole with either spin up ( $\uparrow$ ) or spin down ( $\downarrow$ ) respectively. Similarly,  $t_{ee}^{\uparrow\uparrow}$ ,  $t_{ee}^{\uparrow\downarrow}$ ,  $t_{eh}^{\uparrow\uparrow}$ ,  $t_{eh}^{\uparrow\downarrow}$  are transmission amplitudes into pSc. In Eqs. (2.25), and (2.26) we approximate wave vector in normal metal by Fermi wave vector  $k_F = \sqrt{2m^* \mu_{NM}/\hbar} = 1$  (since  $\hbar = \mu_{NM} = 2m^* = 1$ ) with  $E \ll E_F$ . Wave vector's  $k_{\pm}$  in  $p$ -wave superconductor are solutions of-

$$E^2 = (k^2 - \mu_{pSc})^2 + (\Delta_{pSc}k)^2. \quad (2.28)$$

Solutions of Eq. (2.28) for various values of chemical potential  $\mu_{pSc} > 0$  (in topological regime) with energy  $E$  are mentioned in Table I of Ref. [61].

Similarly, if we consider a spin down electron incident from metallic region I, the

## 2.6. Stability of Majorana zero modes in the presence of a spin flipper

wavefunctions for different regions can be written as

$$\psi_{NM}^I(x) = \begin{pmatrix} 0 \\ 1 \\ 0 \\ 0 \end{pmatrix} e^{i(x+a)} \phi_{m'}^S + r_{ee}^{\downarrow\uparrow} \begin{pmatrix} 1 \\ 0 \\ 0 \\ 0 \end{pmatrix} e^{-i(x+a)} \phi_{m'-1}^S + r_{ee}^{\downarrow\downarrow} \begin{pmatrix} 0 \\ 1 \\ 0 \\ 0 \end{pmatrix} e^{-i(x+a)} \phi_{m'}^S + r_{eh}^{\downarrow\uparrow} \begin{pmatrix} 0 \\ 0 \\ 0 \\ 1 \end{pmatrix} e^{i(x+a)} \phi_{m'-1}^S + r_{eh}^{\downarrow\downarrow} \begin{pmatrix} 0 \\ 0 \\ 1 \\ 0 \end{pmatrix} e^{i(x+a)} \phi_{m'}^S, \quad \text{for } x < -a, \quad (2.29)$$

$$\begin{aligned} \psi_{NM}^{II}(x) &= t_{ee}^{\downarrow\uparrow} \begin{pmatrix} 1 \\ 0 \\ 0 \\ 0 \end{pmatrix} e^{i(x+a)} \phi_{m'-1}^S + t_{ee}^{\downarrow\downarrow} \begin{pmatrix} 0 \\ 1 \\ 0 \\ 0 \end{pmatrix} e^{i(x+a)} \phi_{m'}^S + b_{ee}^{\downarrow\uparrow} \begin{pmatrix} 1 \\ 0 \\ 0 \\ 0 \end{pmatrix} e^{-ix} \phi_{m'-1}^S + b_{ee}^{\downarrow\downarrow} \begin{pmatrix} 0 \\ 1 \\ 0 \\ 0 \end{pmatrix} e^{-ix} \phi_{m'}^S, \\ +c_{eh}^{\downarrow\uparrow} \begin{pmatrix} 0 \\ 0 \\ 0 \\ 1 \end{pmatrix} e^{ix} \phi_{m'-1}^S + c_{eh}^{\downarrow\downarrow} \begin{pmatrix} 0 \\ 0 \\ 1 \\ 0 \end{pmatrix} e^{ix} \phi_{m'}^S + a_{eh}^{\downarrow\uparrow} \begin{pmatrix} 0 \\ 0 \\ 0 \\ 1 \end{pmatrix} e^{-i(x+a)} \phi_{m'-1}^S + a_{eh}^{\downarrow\downarrow} \begin{pmatrix} 0 \\ 0 \\ 1 \\ 0 \end{pmatrix} e^{-i(x+a)} \phi_{m'}^S, \quad \text{for } -a < x < 0, \quad (2.30) \end{aligned}$$

$$\psi_{pSc}(x) = t_{ee}^{\downarrow\uparrow} \begin{pmatrix} \eta_- \\ 0 \\ 0 \\ 1 \end{pmatrix} e^{ik_-x} \phi_{m'-1}^S + t_{ee}^{\downarrow\downarrow} \begin{pmatrix} 0 \\ \eta_- \\ 1 \\ 0 \end{pmatrix} e^{ik_-x} \phi_{m'}^S + t_{eh}^{\downarrow\uparrow} \begin{pmatrix} \eta_+ \\ 0 \\ 0 \\ 1 \end{pmatrix} e^{ik_+x} \phi_{m'-1}^S + t_{eh}^{\downarrow\downarrow} \begin{pmatrix} 0 \\ \eta_+ \\ 1 \\ 0 \end{pmatrix} e^{ik_+x} \phi_{m'}^S, \quad \text{for } x > 0, \quad (2.31)$$

$r_{ee}^{\downarrow\uparrow}$  and  $r_{ee}^{\downarrow\downarrow}$  are normal reflection amplitudes for an incoming electron with spin down ( $\downarrow$ ) reflected as an electron with either spin up ( $\uparrow$ ) or spin down ( $\downarrow$ ) respectively, while  $r_{eh}^{\downarrow\uparrow}$  and  $r_{eh}^{\downarrow\downarrow}$  are Andreev reflection amplitudes for an incoming electron with spin down ( $\downarrow$ ) reflected as a hole with either spin up ( $\uparrow$ ) or spin down ( $\downarrow$ ) respectively. Similarly,  $t_{ee}^{\downarrow\uparrow}$ ,  $t_{ee}^{\downarrow\downarrow}$ ,  $t_{eh}^{\downarrow\uparrow}$ ,  $t_{eh}^{\downarrow\downarrow}$  are corresponding transmission amplitudes into pSc.

Boundary conditions at  $x = -a$  are:  $\psi_{NM}^I(x) = \psi_{NM}^{II}(x)$  and,  $2i\partial_x\tau_z\psi_{NM}^I(x) - 2i\partial_x\tau_z\psi_{NM}^{II}(x) = 2iJ\vec{s}\cdot\vec{S}\tau_z\psi_{NM}^I(x)$ . Boundary conditions at  $x = 0$  are:  $\psi_{NM}^{II}(x) = \psi_{pSc}(x)$  and,  $(-2i\partial_x\tau_z + \Delta_{pSc}\tau_x)\psi_{pSc}(x) + 2i\partial_x\tau_z\psi_{NM}^{II}(x) = -2iZ\tau_z\psi_{NM}^{II}(x)$ .

2. FORMATION OF YU-SHIBA-RUSINOV BOUND STATES AND STABILITY OF MAJORANA BOUND STATES IN PRESENCE OF SPIN FLIP SCATTERING

---

The action of spin-flipper Hamiltonian  $\vec{s} \cdot \vec{S}$ , from boundary condition at  $x = -a$ , gives for wave-function involving spin up electron spinor,

$$\vec{s} \cdot \vec{S} \tau_z \begin{pmatrix} 1 \\ 0 \\ 0 \\ 0 \end{pmatrix} \phi_{m'}^S = \frac{m'}{2} \begin{pmatrix} 1 \\ 0 \\ 0 \\ 0 \end{pmatrix} \phi_{m'}^S + \frac{f}{2} \begin{pmatrix} 0 \\ 1 \\ 0 \\ 0 \end{pmatrix} \phi_{m'+1}^S. \quad (2.32)$$

Similarly, the action of exchange operator for wave-function involving spin-down electron spinor gives-

$$\vec{s} \cdot \vec{S} \tau_z \begin{pmatrix} 0 \\ 1 \\ 0 \\ 0 \end{pmatrix} \phi_{m'}^S = -\frac{m'}{2} \begin{pmatrix} 0 \\ 1 \\ 0 \\ 0 \end{pmatrix} \phi_{m'}^S + \frac{f'}{2} \begin{pmatrix} 1 \\ 0 \\ 0 \\ 0 \end{pmatrix} \phi_{m'-1}^S. \quad (2.33)$$

Further, the action of exchange operator for wave-function involving spin down hole gives-

$$\vec{s} \cdot \vec{S} \tau_z \begin{pmatrix} 0 \\ 0 \\ 1 \\ 0 \end{pmatrix} \phi_{m'}^S = \frac{m'}{2} \begin{pmatrix} 0 \\ 0 \\ 1 \\ 0 \end{pmatrix} \phi_{m'}^S - \frac{f'}{2} \begin{pmatrix} 0 \\ 0 \\ 0 \\ 1 \end{pmatrix} \phi_{m'}^S, \quad (2.34)$$

and finally the action of exchange operator on spin up holes gives-

$$\vec{s} \cdot \vec{S} \tau_z \begin{pmatrix} 0 \\ 0 \\ 0 \\ 1 \end{pmatrix} \phi_{m'}^S = -\frac{m'}{2} \begin{pmatrix} 0 \\ 0 \\ 0 \\ 1 \end{pmatrix} \phi_{m'}^S - \frac{f}{2} \begin{pmatrix} 0 \\ 0 \\ 1 \\ 0 \end{pmatrix} \phi_{m'+1}^S. \quad (2.35)$$

Using the above equations and solving boundary conditions we obtain 16 equations for each spin up and spin down electron incident process. From these 16 equations we can compute



## 2.6. Stability of Majorana zero modes in the presence of a spin flipper

the different scattering probabilities:  $R_{ee}^{\uparrow\uparrow} = |r_{ee}^{\uparrow\uparrow}|^2$ ,  $R_{ee}^{\uparrow\downarrow} = |r_{ee}^{\uparrow\downarrow}|^2$ ,  $R_{eh}^{\uparrow\uparrow} = |r_{eh}^{\uparrow\uparrow}|^2$ ,  $R_{eh}^{\uparrow\downarrow} = |r_{eh}^{\uparrow\downarrow}|^2$  (for spin up electron incident) and  $R_{ee}^{\downarrow\uparrow} = |r_{ee}^{\downarrow\uparrow}|^2$ ,  $R_{ee}^{\downarrow\downarrow} = |r_{ee}^{\downarrow\downarrow}|^2$ ,  $R_{eh}^{\downarrow\uparrow} = |r_{eh}^{\downarrow\uparrow}|^2$ ,  $R_{eh}^{\downarrow\downarrow} = |r_{eh}^{\downarrow\downarrow}|^2$  (for spin down electron incident). Next we will look at spin flip scattering in vicinity of Normal metal-SOCSW junction, since in this junction too MBS's have been predicted.

### 2.6.2 Spin flipper in vicinity of metal-spin orbit coupled superconducting wire junction

In this subsection we consider a spinful normal metal ( $N_1$ )-spin flipper-normal metal ( $N_2$ )-insulator (I)-spin orbit coupled superconducting wire (SOCSW) junction as shown in Fig. 2.8. Similar to previous subsection, we model metal superconductor interface

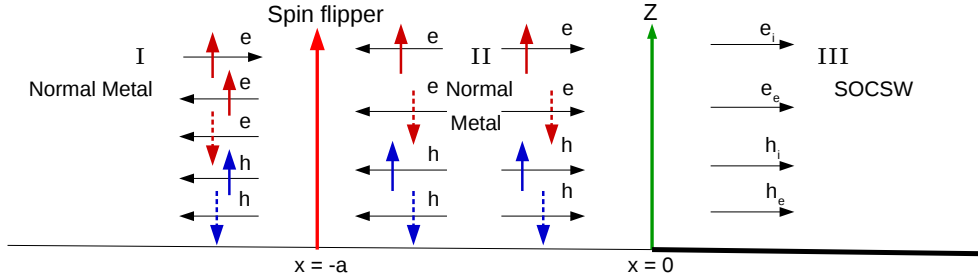


Figure 2.8:  $N_1$ -SF- $N_2$ -SOCSW junction with a spin flipper (spin  $S$ , magnetic moment  $m'$ ) at  $x = -a$  and a  $\delta$ -like potential barrier (strength  $Z$ ) at  $x = 0$ . The scattering of a incident spin-up electron is shown. Normal reflection, Andreev reflection and quasi particle transmission into SOCSW are shown.

as a  $\delta$ -like potential barrier with strength  $Z$ . Using the same convention as before, i.e.,  $\hbar = 2m^* = \mu_{NM} = 1$ , the BdG Hamiltonians for  $N_1$ ,  $N_2$  and SOCSW can be written as[61]-

2. FORMATION OF YU-SHIBA-RUSINOV BOUND STATES AND STABILITY OF MAJORANA BOUND STATES IN PRESENCE OF SPIN FLIP SCATTERING

---

$$H_{N_1} = H_{N_2} = (-\partial_x^2 - 1)\tau_z, \quad (2.36a)$$

$$H_{SOCSW} = -\partial_x^2\tau_z - i\beta\partial_x\tau_z\sigma_z + B_Z\sigma_x + \Delta_0\tau_x, \quad (2.36b)$$

with  $\beta$  being strength of spin orbit interaction,  $B_Z$  is Zeeman field, and  $\Delta_0 \geq 0$ - the proximity induced  $s$ -wave pairing potential. We also consider uniform electron masses throughout the system and fix chemical potential of SOCSW and Zeeman interaction in the lead to be zero[61]. The positive branches of energy spectrum[61] of SOCSW are given as  $\varepsilon_{SOCSW,\pm}(k) = (k^4 + \beta^2k^2 + \Delta_0^2 + B_Z^2 \pm 2\sqrt{k^4(\beta^2k^2 + B_Z^2) + \Delta_0^2B_Z^2})^{1/2}$ . The energy spectrum for SOCSW is shown in Fig. 4(b,c,d) of Ref. [61] for nontopological ( $B_Z < \Delta_0$ ), topological ( $B_Z > \Delta_0$ ) and transition regimes ( $B_Z = \Delta_0$ ). There is a gap in energy spectrum except for  $B_Z = \Delta_0$ . We focus only on topological regime  $B_Z > \Delta_0$ [61, 62]. In the limit of strong spin orbit interaction (SOC) ( $\beta \gg B_Z, \Delta_0$ ), the energy spectrum of the SOCSW has two branches[61]-(i) interior branch, and (ii) exterior branch. In Fig. 5(b) of Ref. [61] the energy spectrum for SOCSW is plotted in the limit of strong SOC. The energy spectrum about the minima at  $k = 0$  form the interior branches, while the energy spectrum about the minima at  $k = \pm\beta$  constitute the exterior branches. For low energies, SOCSW Hamiltonian, Eq. (2.36b) can be linearized about these minima ( $k = 0$  and  $k = \pm\beta$ ) by introducing the ansatz for the wavefunction:

$$\psi_{SOCSW\uparrow}(x) \approx R_\uparrow(x) + L_\uparrow(x)e^{-i\beta x}, \quad (2.37a)$$

$$\psi_{SOCSW\downarrow}(x) \approx R_\downarrow(x)e^{i\beta x} + L_\downarrow(x), \quad (2.37b)$$

where  $R_\sigma(x)$  and  $L_\sigma(x)$  (with  $\sigma = \uparrow, \downarrow$ ) denote the slowly varying right moving and left moving waves respectively. By inserting this ansatz for the superconducting wavefunction in SOCSW Hamiltonian, Eq. (2.36b), and neglecting terms involving  $e^{\pm i\beta x}$  (fast oscillating

---

## 2.6. Stability of Majorana zero modes in the presence of a spin flipper

terms), we get effective Hamiltonian corresponding to interior and exterior branches[61],

$$\mathcal{H}_{SOCSW}^{(L)} = \frac{1}{2} \int dx \Psi_{SOCSW}^{(L)}(x)^\dagger H_{SOCSW}^{(L)} \Psi_{SOCSW}^{(L)}(x), \quad (2.38)$$

where  $L = i, e$  represents interior and exterior branches respectively. BdG Hamiltonians for interior and exterior branches are written as,

$$H_{SOCSW}^{(i)} = -i\beta\tau_z\sigma_z\partial_x + B_Z\sigma_x + \Delta_0\tau_x, \quad (2.39a)$$

$$H_{SOCSW}^{(e)} = -i\beta\tau_z\sigma_z\partial_x + \Delta_0\tau_x. \quad (2.39b)$$

### Symmetry class of SOCSW Hamiltonian:

In 1D, SOCSW Hamiltonian only satisfies particle-hole symmetry. The 1D SOCSW Hamiltonian in Eq. (2.36b) can be written as,

$$H_{SOCSW}(k) = \begin{pmatrix} k^2 + \beta k & B_Z & \Delta_0 & 0 \\ B_Z & k^2 - \beta k & 0 & \Delta_0 \\ \Delta_0 & 0 & -k^2 - \beta k & B_Z \\ 0 & \Delta_0 & B_Z & -k^2 + \beta k \end{pmatrix}. \quad (2.40)$$

Using Eq. (2.40) we get-

$$\tau_y\sigma_y H_{SOCSW}^*(-k)\tau_y\sigma_y = \begin{pmatrix} -k^2 - \beta k & -B_Z & -\Delta_0 & 0 \\ -B_Z & -k^2 + \beta k & 0 & -\Delta_0 \\ -\Delta_0 & 0 & k^2 + \beta k & -B_Z \\ 0 & -\Delta_0 & -B_Z & k^2 - \beta k \end{pmatrix} \quad (2.41)$$

From Eqs. (2.40), (2.41), we see  $\tau_y\sigma_y H_{SOCSW}^*(-k)\tau_y\sigma_y = -H_{SOCSW}(k)$ . Similarly, we can show that time reversal symmetry does not hold as,  $H_{SOCSW}(k) \neq \tau_z H_{SOCSW}^*(-k)\tau_z$ ,

## 2. FORMATION OF YU-SHIBA-RUSINOV BOUND STATES AND STABILITY OF MAJORANA BOUND STATES IN PRESENCE OF SPIN FLIP SCATTERING

---

or  $H_{SOCSW}(k) \neq \tau_y H_{SOCSW}^*(-k) \tau_y$ , or  $H_{SOCSW}(k) \neq \tau_x H_{SOCSW}^*(-k) \tau_x$ , or  $H_{SOCSW}(k) \neq \sigma_y H_{SOCSW}^*(-k) \sigma_y$ , or  $H_{SOCSW}(k) \neq H_{SOCSW}^*(-k)$ . Finally, chiral symmetry also does not hold as,  $H_{SOCSW}(k) \neq -\tau_x H_{SOCSW}(-k) \tau_x$ , or  $H_{SOCSW}(k) \neq -\tau_z H_{SOCSW}(k) \tau_z$ . Thus, SOCSW Hamiltonian in Eq. (2.36b) only satisfies particle-hole symmetry relation and therefore belongs to symmetry class D. The exterior branches of Hamiltonian Eq. (2.39b) in Ref. [61] also satisfy particle-hole symmetry relation  $\tau_y \sigma_y H_{SOCSW}^{(e)*}(-k) \tau_y \sigma_y = -H_{SOCSW}^{(e)}(k)$ , and therefore belong to D class[63]. The interior branch Hamiltonian Eq. (2.39a) in Ref. [61] also satisfies only particle-hole symmetry and therefore belongs to same symmetry class D.

The wavefunction in metallic regions I and II for spin-up electron incident with energy  $E$  is as mentioned in Eqs. (2.25), (2.26). For SOCSW, the spinors for interior and exterior branches are described in terms of slowly varying left and right moving waves as

$$\Psi_{SOCSW}^{(i)} = \begin{pmatrix} R_{\uparrow}(x) \\ L_{\downarrow}(x) \\ L_{\downarrow}^{\dagger}(x) \\ -R_{\uparrow}^{\dagger}(x) \end{pmatrix} \text{ and } \Psi_{SOCSW}^{(e)} = \begin{pmatrix} L_{\uparrow}(x) \\ R_{\downarrow}(x) \\ R_{\downarrow}^{\dagger}(x) \\ -L_{\uparrow}^{\dagger}(x) \end{pmatrix}. \text{ After diagonalizing the Hamiltonians in}$$

Eqs. (2.39a), (2.39b), we will get eigenfunctions for both interior and exterior branches. The wavefunction in SOCSW is sum of solutions for exterior as well as an interior branch (Eq. (2.39)) and in the topological regime for spin up electron incident can be written as[61],

$$\psi_{SOCSW}(x) = t_1^{(i)} \begin{pmatrix} -u_- \phi_{m'}^S \\ -v_- \phi_{m'+1}^S \\ v_- \phi_{m'+1}^S \\ u_- \phi_{m'}^S \end{pmatrix} e^{ik_-^{(i)}x} + t_2^{(i)} \begin{pmatrix} u_+ \phi_{m'}^S \\ v_+ \phi_{m'+1}^S \\ v_+ \phi_{m'+1}^S \\ u_+ \phi_{m'}^S \end{pmatrix} e^{ik_+^{(i)}x} + t_1^{(e)} \begin{pmatrix} v_0 \phi_{m'}^S \\ 0 \\ u_0 \phi_{m'+1}^S \\ 0 \end{pmatrix} e^{i(k_0^{(e)} - \beta)x} + t_2^{(e)} \begin{pmatrix} 0 \\ u_0 \phi_{m'+1}^S \\ 0 \\ v_0 \phi_{m'}^S \end{pmatrix} e^{i(k_0^{(e)} + \beta)x}, \quad (2.42)$$

where the first two terms on right-hand side denote contributions from interior branches,

## 2.6. Stability of Majorana zero modes in the presence of a spin flipper

while other two terms give contributions from exterior branches.  $t_{(1,2)}^{(i)}$  and  $t_{(1,2)}^{(e)}$  are transmission amplitudes into SOCSW. In Eq. (2.42), for  $E \geq |\Delta_\lambda|$ ,  $u_\lambda^2 = \frac{E+(E^2-\Delta_\lambda^2)^{1/2}}{2E}$  and  $u_\lambda^2 + v_\lambda^2 = 1$ , while for  $0 \leq E < |\Delta_\lambda|$ ,  $u_\lambda^2 = \frac{E+i(\Delta_\lambda^2-E^2)^{1/2}}{2|\Delta_\lambda|}$  and  $u_\lambda^2 + v_\lambda^2 = \frac{E}{|\Delta_\lambda|}$ , where  $\lambda = \pm, 0$ , and  $\Delta_\pm = \Delta_0 \pm B_Z$ . The wave vectors in Eq. (2.42) are  $k_\pm^{(i)} = \frac{(E^2-\Delta_\pm^2)^{1/2}}{\beta}$  for the interior branch, and  $k_0^{(e)} = \frac{(E^2-\Delta_0^2)^{1/2}}{\beta}$  for the exterior branch. In strong SOC limit ( $\beta \gg B_Z, \Delta_0$ ), we neglect terms proportional to  $k_+^{(i)}, k_-^{(i)}, k_0^{(e)} \ll 1$  in our calculation.

Boundary conditions at  $x = -a$  are:  $\psi_{NM}^I(x) = \psi_{NM}^{II}(x)$  and,  $2i\partial_x\tau_z\psi_{NM}^I(x) - 2i\partial_x\tau_z\psi_{NM}^{II}(x) = 2iJ\vec{s}\cdot\vec{S}\tau_z\psi_{NM}^I(x)$ , while boundary conditions at  $x = 0$  are:  $\psi_{NM}^{II}(x) = \psi_{SOCSW}(x)$  and,  $(-2i\partial_x\tau_z + \beta\tau_z\sigma_z)\psi_{SOCSW}(x) + 2i\partial_x\tau_z\psi_{NM}^{II}(x) = -2iZ\tau_z\psi_{NM}^{II}(x)$ . Substituting wavefunctions (Eqs. (2.25), (2.26), (2.42)) in these boundary conditions we get 16 equations. Solving these 16 equations we get the normal and Andreev reflection probabilities:  $R_{ee}^{\uparrow\uparrow} = |r_{ee}^{\uparrow\uparrow}|^2$ ,  $R_{ee}^{\uparrow\downarrow} = |r_{ee}^{\uparrow\downarrow}|^2$ ,  $R_{eh}^{\uparrow\uparrow} = |r_{eh}^{\uparrow\uparrow}|^2$ ,  $R_{eh}^{\uparrow\downarrow} = |r_{eh}^{\uparrow\downarrow}|^2$ . Similarly, if we consider a spin down electron incident from normal metal (region I), as shown in previous subsection we can easily write wavefunctions, solve for the afore mentioned boundary conditions and get reflection probabilities as:  $R_{ee}^{\downarrow\uparrow} = |r_{ee}^{\downarrow\uparrow}|^2$ ,  $R_{ee}^{\downarrow\downarrow} = |r_{ee}^{\downarrow\downarrow}|^2$ ,  $R_{eh}^{\downarrow\uparrow} = |r_{eh}^{\downarrow\uparrow}|^2$ ,  $R_{eh}^{\downarrow\downarrow} = |r_{eh}^{\downarrow\downarrow}|^2$ .

Using the well established definitions as in Refs. [56, 57], we calculate net differential charge conductance as,

$$G_c = G_c^\uparrow + G_c^\downarrow, \text{ with } G_c^\uparrow = G_0(1 + R_{eh}^{\uparrow\uparrow} + R_{eh}^{\uparrow\downarrow} - R_{ee}^{\uparrow\uparrow} - R_{ee}^{\uparrow\downarrow})$$

$$\text{and } G_c^\downarrow = G_0(1 + R_{eh}^{\downarrow\uparrow} + R_{eh}^{\downarrow\downarrow} - R_{ee}^{\downarrow\uparrow} - R_{ee}^{\downarrow\downarrow}) \quad (2.43)$$

with,  $G_0 = e^2/h$  and  $G_c^\uparrow$  being differential charge conductance when spin up electron is incident from region I, while  $G_c^\downarrow$  being differential charge conductance when spin down electron is incident from region I.

### 2.6.3 Comparison of ZBCP between normal metal- $p$ wave and normal metal-SOCSW junction in the vicinity of a spin flipper

In Table 2.1, we compare the zero-bias conductance of a  $N_1$ -spin flipper- $N_2$ -I-SOCSW junction and  $N_1$ -spin flipper- $N_2$ -I- $p$ Sc junction for both transparent ( $Z = 0$ ) and tunnel ( $Z = 3$ ) regimes. For spin flip case,  $f \neq 0$  and  $f' \neq 0$ , see Eqs. (2.32)-(2.34), implying there is finite possibility for spin-flipper to flip its own spin while interacting with an electron/hole incident from metallic region. On the other hand, for no flip case,  $f = f' = 0$ . We take two different values of spin orbit coupling strength  $\beta$  ( $\beta = 1$  and  $\beta = 2$ ) for SOCSW in second and third column of Table 2.1. We also take two different values of  $\mu_{pSc} = 0.01, 0.001$ , for  $p$ Sc in fourth and fifth column of Table 2.1.

Table 2.1: Comparison of differential charge conductance at zero bias ( $E = 0$ ) in the topological regime between  $N_1$ -spin flipper- $N_2$ -I-SOCSW and  $N_1$ -spin flipper- $N_2$ -I- $p$ -wave junction

Parameters $\downarrow \rightarrow$	$N_1$ -SF- $N_2$ -I-SOCSW		$N_1$ -SF- $N_2$ -I- $p$ -wave	
	$Z = 0, E = 0, a = \pi, \Delta_0 = 0.001, B_Z = 1.5\Delta_0$		$Z = 0, E = 0, a = \pi, \Delta_{pSc} = 0.07$	
	$G_c/G_0$ for $\beta = 1$	$G_c/G_0$ for $\beta = 2$	$G_c/G_0$ ( $\mu_{pSc}=0.001$ )	$G_c/G_0$ ( $\mu_{pSc}=0.01$ )
No flip ( $f = f' = 0$ )	2	2	4	4
Flip ( $f = f' = 1$ )	$\frac{800+272J^2+50J^4}{400+200J^2+29J^4}$	$\frac{2048+128J^2+50J^4}{1024+320J^2+41J^4}$	4	4
Flip ( $f = f' = \sqrt{3}$ )	$\frac{800+976J^2+578J^4}{400+680J^2+301J^4}$	$\frac{2048+640J^2+578J^4}{1024+1088J^2+337J^4}$	4	4
Flip ( $f = f' = 3$ )	$\frac{800+6928J^2+20402J^4}{400+4040J^2+10237J^4}$	$\frac{2048+8320J^2+20402J^4}{1024+6464J^2+10345J^4}$	4	4
Parameters $\downarrow \rightarrow$	$Z = 3, E = 0, a = \pi, \Delta_0 = 0.001, B_Z = 1.5\Delta_0$		$Z = 3, E = 0, a = \pi, \Delta_{pSc} = 0.07$	
	$G_c/G_0$ ( $\beta = 1$ )	$G_c/G_0$ ( $\beta = 2$ )	$G_c/G_0$ ( $\mu_{pSc}=0.001$ )	$G_c/G_0$ ( $\mu_{pSc}=0.01$ )
No flip ( $f = f' = 0$ )	2	2	4	4
Flip ( $f = f' = 1$ )	$\frac{53792+15744J+4304J^2+480J^3+50J^4}{26896+7872J+2792J^2+336J^3+29J^4}$	$\frac{61952+16896J+4160J^2+480J^3+50J^4}{30976+8448J+4640J^2+624J^3+41J^4}$	4	4
Flip ( $f = f' = 3$ )	$\frac{53792+15744J+66256J^2+9696J^3+20402J^4}{26896+7872J+38888J^2+5712J^3+10237J^4}$	$\frac{61952+16896J+67648J^2+9696J^3+20402J^4}{30976+8448J+56864J^2+8304J^3+10345J^4}$	4	4

## 2.6. Stability of Majorana zero modes in the presence of a spin flipper

---

For no flip case we see that normalized zero bias conductance  $G_c/G_0$  is quantized at 2 for  $N_1$ -SF- $N_2$ -I-SOCSW junction, while for  $N_1$ -SF- $N_2$ -I-pSc junction it is quantized at 4 regardless of other parameters like  $S, m', J, Z, \beta, \mu_{pSc}$ , etc. The reason for this is that the Andreev and normal reflection probabilities exactly cancel at zero bias in Eq. (2.43) for  $N_1$ -SF- $N_2$ -I-SOCSW junction while for  $N_1$ -SF- $N_2$ -I-pSc junction there is perfect Andreev reflection (i.e., normal reflection probabilities vanish) at zero bias and thus from Eq. (2.43),  $G_c/G_0$  is quantized at 4. In Table 2.1, we notice that for  $N_1$ -SF- $N_2$ -I-SOCSW junction,  $G_c/G_0$  is no longer quantized and depends on the parameters  $S, m', J, Z, \beta$ , etc. However, this is not the case for  $N_1$ -SF- $N_2$ -I-pSc junction, wherein  $G_c/G_0$  is robustly quantized and is independent of spin-flip scattering. For  $N_1$ -SF- $N_2$ -I-pSc junction, there is perfect Andreev reflection at zero bias even in the presence of spin-flip scattering. Thus, from Eq. (2.43), zero-bias conductance is quantized at  $4e^2/h$  and does not depend on parameters  $S, m', J, Z, \mu_{pSc}$ , etc. For no flip case  $G_c/G_0$  is robustly quantized in topological regime for both cases, see Table 2.1. Thus, in a metal-pSc junction, the ‘‘Majorana states’’ are not affected by the presence of spin flipper. In contrast, for metal-SOCSW junction, the ‘‘Majorana states’’ are affected by the presence of the spin flipper. In Fig. 2.9 we plot differential charge conductance as a function of incident electron energy  $E$  for different values of interface barrier strength  $Z$  in topological regime. In Fig. 2.9(a) for a  $N_1$ -SF- $N_2$ -I-pSc junction we see that  $G_c/G_0$  at  $E = 0$  is quantized and independent of  $Z$  and spin flip probability of spin-flipper. Thus topological character of zero-bias conductance peak is evident, implying the stability of Majorana state in  $N_1$ -SF- $N_2$ -I-pSc junction. The differential conductance for  $N_1$ -SF- $N_2$ -I-pSc junction decreases with increase of  $Z$  (transparency of junction). Furthermore, the width of the ZBCP also decreases with increasing  $Z$ . A discontinuity appears in the differential conductance curve at the gap edge  $\epsilon_1 = \Delta_{pSc} \sqrt{\mu_{pSc} - \Delta_{pSc}^2/4} = 0.007$ , where  $\Delta_{pSc} = 0.07$ ,  $\mu_{pSc} = 0.01$  (topological regime)

## 2. FORMATION OF YU-SHIBA-RUSINOV BOUND STATES AND STABILITY OF MAJORANA BOUND STATES IN PRESENCE OF SPIN FLIP SCATTERING

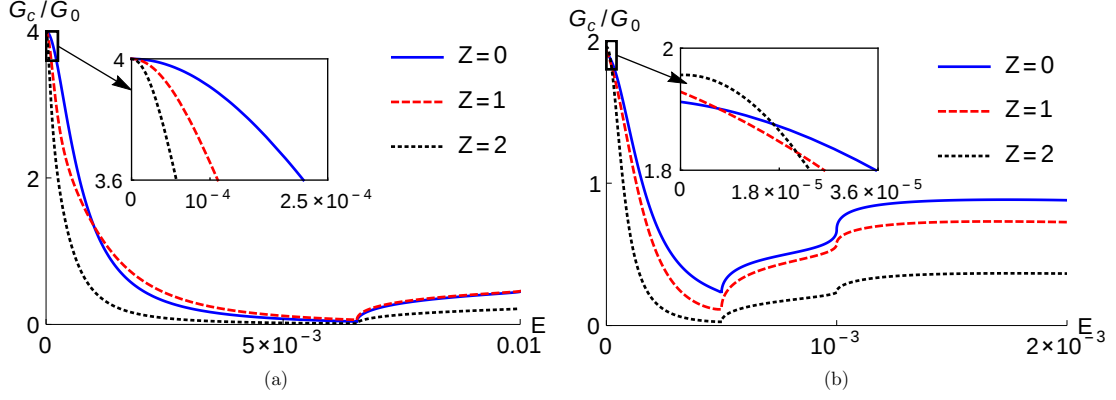


Figure 2.9: Differential charge conductance in presence of spin flip scattering as a function of energy  $E$  for different values of interface barrier strength  $Z$  in topological regime, (a) for  $N_1$ -SF- $N_2$ -I- $p$ Sc and (b) for  $N_1$ -SF- $N_2$ -I-SOCSW junction. Parameters are:  $f = f' = \sqrt{3}$ ,  $S = 3/2$ ,  $J = 1$ ,  $\mu_{pSc} = 0.01$ ,  $\Delta_{pSc} = 0.07$ ,  $a = \pi$ ,  $\Delta_0 = 0.001$ ,  $\beta = 0.5$ ,  $B_Z = 1.5\Delta_0$ .

and  $\mu_{pSc} > \Delta_{pSc}^2/2$  regardless of  $Z$ . The reason for this discontinuity is that the wave vectors  $k_{\pm}$  in  $p$ -wave superconductor are different for below ( $E < \epsilon_1$ ) and above ( $E > \epsilon_1$ ) the gap (see Table I of Ref. [61]).

In Fig. 2.9(b) we do the same for  $N_1$ -SF- $N_2$ -I-SOCSW junction. We see that  $G_c/G_0$  at zero energy is not quantized and depends on interface transparency  $Z$ . The zero-bias differential conductance ( $G_c/G_0$  at  $E = 0$ ) increases with increase in  $Z$  (junction transparency). The differential charge conductance in  $N_1$ -SF- $N_2$ -I-SOCSW case exhibits much more complex structure than that for a junction with  $p$ -wave superconductor. Further, we observe a discontinuity in differential conductance for SOCSW case at energy corresponding to energy gaps  $|\Delta_-| (= 0.5\Delta_0)$  and  $\Delta_0$ . The reason for this behavior is that  $u_{\lambda}$  and  $v_{\lambda}$  are different for below ( $0 \leq E < |\Delta_{\lambda}|$ ) and above ( $E \geq |\Delta_{\lambda}|$ ) the energy gap, where  $\lambda = \pm, 0$ . Thus, in the presence of spin-flip scattering, the topological character of ZBCP seen in the case of  $N_1$ -SF- $N_2$ -I-SOCSW junction is dubious, suggesting that Majorana states seen in such junctions aren't stable and vanish in the presence of spin-flip scattering, begging



## 2.6. Stability of Majorana zero modes in the presence of a spin flipper

the question, whether the states seen in  $N_1$ -SF- $N_2$ -I-SOCSW junction are Majoranas in the first place?

The reason for quantized zero bias conductance for  $N_1$ -SF- $N_2$ -I-SOCSW junction in absence of spin-flip scattering is exact cancellation between normal and Andreev reflection probabilities in the conductance formula (Eq. (2.43)). Differential charge conductance is given as,  $G_c = e^2/h(2 + (R_{ee}^{\uparrow\uparrow} + R_{ee}^{\uparrow\downarrow} + R_{ee}^{\downarrow\uparrow} + R_{ee}^{\downarrow\downarrow}) - (R_{eh}^{\uparrow\uparrow} + R_{eh}^{\uparrow\downarrow} + R_{eh}^{\downarrow\uparrow} + R_{eh}^{\downarrow\downarrow}))$ . For no flip process and at zero energy ( $E = 0$ ),  $R_{ee}^{\uparrow\uparrow} + R_{ee}^{\uparrow\downarrow} + R_{ee}^{\downarrow\uparrow} + R_{ee}^{\downarrow\downarrow} = R_{eh}^{\uparrow\uparrow} + R_{eh}^{\uparrow\downarrow} + R_{eh}^{\downarrow\uparrow} + R_{eh}^{\downarrow\downarrow} = 1$ . Thus, normal reflection probabilities and Andreev reflection probabilities exactly cancel in conductance formula and this leads to quantized conductance ( $G_c = 2e^2/h$ ) at zero bias. But, in presence of spin-flip scattering ( $f = f' = 1$ ) and for parameters  $E = 0$ ,  $\beta = 1$  and  $B_Z = 1.5\Delta_0$  from Eq. (2.43) we get-

$$R_{ee}^{\uparrow\uparrow} + R_{ee}^{\uparrow\downarrow} + R_{ee}^{\downarrow\uparrow} + R_{ee}^{\downarrow\downarrow} = \frac{400+264J^2+33J^4+320JZ+144J^3Z+640Z^2+352J^2Z^2+256JZ^3+256Z^4}{400+200J^2+29J^4+320JZ+112J^3Z+640Z^2+288J^2Z^2+256JZ^3+256Z^4}, \quad (2.44)$$

$$R_{eh}^{\uparrow\uparrow} + R_{eh}^{\uparrow\downarrow} + R_{eh}^{\downarrow\uparrow} + R_{eh}^{\downarrow\downarrow} = \frac{400+136J^2+25J^4+320JZ+80J^3Z+640Z^2+224J^2Z^2+256JZ^3+256Z^4}{400+200J^2+29J^4+320JZ+112J^3Z+640Z^2+288J^2Z^2+256JZ^3+256Z^4}. \quad (2.45)$$

From Eqs. (2.44), (2.45), it is evident that,  $R_{ee}^{\uparrow\uparrow} + R_{ee}^{\uparrow\downarrow} + R_{ee}^{\downarrow\uparrow} + R_{ee}^{\downarrow\downarrow} \neq R_{eh}^{\uparrow\uparrow} + R_{eh}^{\uparrow\downarrow} + R_{eh}^{\downarrow\uparrow} + R_{eh}^{\downarrow\downarrow}$ . Thus, at zero bias normal and Andreev reflection probabilities do not cancel in presence of spin flip scattering and as a consequence ZBCP isn't quantized at  $2e^2/h$  and depends on parameters like  $J$ ,  $Z$ , etc. Remarkably, by tuning parameters we can get a far greater deviation from charge conduction quantization at 2 in case of  $N_1$ -SF- $N_2$ -I-SOCSW junction in presence of spin flip scattering. For  $f = f' = \sqrt{5}$ ,  $S = 5/2$ ,  $J = 3$ ,  $Z = 3$ ,  $\beta = 12$ ,  $a = \pi$ ,  $\Delta_0 = 0.001$ ,  $B_Z = 1.5\Delta_0$  we get  $G_c/G_0 = 0.25$  at  $E = 0$ , which is much smaller than quantized value of 2. We have plotted the normalized conductance as a function of energy  $E$  for above mentioned parameters in Fig. 2.10. We see that there is a dip at zero energy in the conductance spectra. Further, charge conductance deviates largely from its

## 2. FORMATION OF YU-SHIBA-RUSINOV BOUND STATES AND STABILITY OF MAJORANA BOUND STATES IN PRESENCE OF SPIN FLIP SCATTERING

quantized value  $2e^2/h$ .

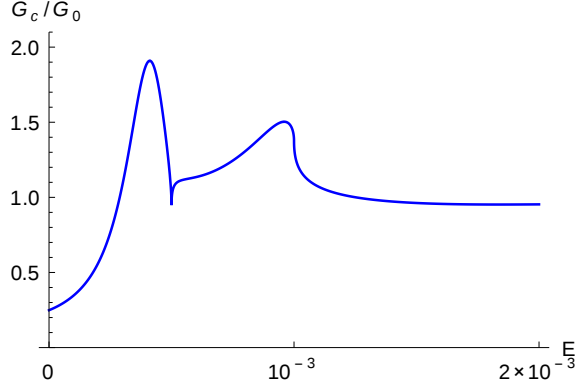


Figure 2.10: *Differential charge conductance in presence of spin flip scattering as a function of energy  $E$  for  $N_1$ -SF- $N_2$ -I-SOCSW junction. Parameters are:  $f = f' = \sqrt{5}$ ,  $S = 5/2$ ,  $J = 3$ ,  $Z = 3$ ,  $a = \pi$ ,  $\Delta_0 = 0.001$ ,  $\beta = 12$ ,  $B_Z = 1.5\Delta_0$ .*

In the next subsection we try to find out possible reasons for this behavior by looking at the symmetries of scattering matrix and the associated topological quantum number.

### 2.6.4 Topological symmetry class in presence of spin flip scattering

To understand the deviation from topological character due to spin flip scattering in case of  $N_1$ -SF- $N_2$ -I-SOCSW junction, we analyze the scattering matrix of our system, which is a  $4 \times 4$  matrix in the subgap regime, given by,

$$\mathcal{S}_{NS} = \begin{pmatrix} s_{ee} & s_{eh} \\ s_{he} & s_{hh} \end{pmatrix}, \quad (2.46)$$

where  $s_{ee} = \begin{pmatrix} r_{ee}^{\uparrow\uparrow} & r_{ee}^{\uparrow\downarrow} \\ r_{ee}^{\downarrow\uparrow} & r_{ee}^{\downarrow\downarrow} \end{pmatrix}$ ,  $s_{eh} = \begin{pmatrix} r_{eh}^{\uparrow\downarrow} & r_{eh}^{\uparrow\uparrow} \\ r_{eh}^{\downarrow\downarrow} & r_{eh}^{\downarrow\uparrow} \end{pmatrix}$ ,  $s_{he} = \begin{pmatrix} r_{he}^{\downarrow\uparrow} & r_{he}^{\downarrow\downarrow} \\ r_{he}^{\uparrow\uparrow} & r_{he}^{\uparrow\downarrow} \end{pmatrix}$ ,  $s_{hh} = \begin{pmatrix} r_{hh}^{\downarrow\downarrow} & r_{hh}^{\downarrow\uparrow} \\ r_{hh}^{\uparrow\downarrow} & r_{hh}^{\uparrow\uparrow} \end{pmatrix}$  being  $2 \times 2$  block matrix.  $r_{e(h)e(h)}^{\sigma\sigma'}$  is normal reflection amplitude for an incoming electron (hole) with spin  $\sigma$  reflected as a electron (hole) with spin  $\sigma'$ . Similarly,  $r_{e(h)h(e)}^{\sigma\sigma'}$  is Andreev reflection amplitude of an incoming electron (hole) with spin  $\sigma$  reflected as a hole (electron) with spin

$\sigma', \sigma = \uparrow, \downarrow$  and  $\sigma' = \uparrow, \downarrow$ . Following a similar procedure as mentioned before in subsections 2.6.1 and 2.6.2, if we consider a spin up (down) hole incident from normal metal region I, we will get different reflection amplitudes as,  $r_{hh}^{\uparrow\uparrow} (r_{hh}^{\downarrow\downarrow}), r_{hh}^{\uparrow\downarrow} (r_{hh}^{\downarrow\uparrow}), r_{he}^{\uparrow\uparrow} (r_{he}^{\downarrow\downarrow}), r_{he}^{\uparrow\downarrow} (r_{he}^{\downarrow\uparrow})$ .

### Symmetry class for pSc in vicinity of a spin flipper

The scattering matrix for pSc for no flip process ( $f = f' = 0$ ), and parameters  $J = 1$ ,  $a = \pi$ ,  $Z = 1$ ,  $E = 0$ ,  $\mu_{pSc} = 0.01$  and  $\Delta_{pSc} = 0.07$  is given as,

$$\mathcal{S}_{NS} = \begin{pmatrix} s_{ee} & s_{eh} \\ s_{he} & s_{hh} \end{pmatrix} = \begin{pmatrix} 0 & 0 & 0 & -i \\ 0 & 0 & -i & 0 \\ 0 & i & 0 & 0 \\ i & 0 & 0 & 0 \end{pmatrix}. \quad (2.47)$$

$s_{\alpha\beta}$  being  $2 \times 2$  matrices, with  $\{\alpha, \beta\} \in \{e, h\}$ .  $\mathcal{S}_{NS}$  is an unitary matrix with  $\mathcal{S}_{NS} \cdot \mathcal{S}_{NS}^\dagger = 1$  and  $\text{Det } \mathcal{S}_{NS} = 1$ . The scattering matrix  $\mathcal{S}_{NS}$  and its determinant,  $\text{Det } \mathcal{S}_{NS}$  ( $\text{Det } \mathcal{S}_{NS} = 1$ ) do not change with change of parameters like  $J$ ,  $Z$ ,  $a$ . In Eq. (2.47) block scattering matrices satisfy particle-hole symmetry,  $s_{ee} = s_{hh}^*$  and  $s_{eh} = s_{he}^*$ . Using this particle-hole symmetry we can choose a basis where all  $s_{\alpha\beta}$  matrices have purely real elements. This is called Majorana basis[64, 65] in which scattering matrix  $\mathcal{S}_{NS}$  is a real orthogonal matrix. Majorana character of Bogoliubov quasiparticles is hidden in particle-hole basis, but becomes evident in Majorana basis. Thus, to transform particle-hole basis into Majorana basis of scattering matrix  $\mathcal{S}_{NS}$ , we do a unitary transformation on scattering matrix  $\mathcal{S}_{NS}$  such that the transformed scattering matrix is,

$$\mathcal{S} = \Omega \mathcal{S}_{NS} \Omega^\dagger = \begin{pmatrix} 0 & 0 & 0 & -1 \\ 0 & 0 & -1 & 0 \\ 0 & -1 & 0 & 0 \\ -1 & 0 & 0 & 0 \end{pmatrix}, \quad \text{where } \Omega = \frac{1}{\sqrt{2}} \begin{pmatrix} 1 & 0 & 1 & 0 \\ 0 & 1 & 0 & 1 \\ -i & 0 & i & 0 \\ 0 & -i & 0 & i \end{pmatrix}, \quad (2.48)$$

## 2. FORMATION OF YU-SHIBA-RUSINOV BOUND STATES AND STABILITY OF MAJORANA BOUND STATES IN PRESENCE OF SPIN FLIP SCATTERING

see Ref. [64] for details of  $\Omega$ . The matrix  $\mathcal{S}$  is also unitary with  $\text{Det } \mathcal{S} = \text{Det } \mathcal{S}_{NS} = 1$ . The transformed scattering matrix  $\mathcal{S}$  and its determinant  $\text{Det } \mathcal{S}$  remain unchanged with change of different junction parameters like  $J$ ,  $Z$ ,  $a$ . Since,  $\mathcal{S}$  satisfies  $\mathcal{S} = \mathcal{S}^*$  (particle-hole symmetry),  $\mathcal{S} = \mathcal{S}^T$  (time-reversal symmetry) and  $\mathcal{S}^2 = 1$  (chiral symmetry), thus according to classification of symmetries of scattering matrix for 1D  $N_1$ -SF- $N_2$ -I- $p$ -wave superconductor junction is in symmetry class BDI[64]. In 1D, BDI class is topological with topological quantum number  $Q$ , defined as number of negative eigenvalues of scattering matrix[63, 64], i.e.,

$$Q = \nu(r) \quad (2.49)$$

where  $\nu(r)$  is number of negative eigenvalues of scattering matrix  $\mathcal{S}$ . Eigenvalues of  $\mathcal{S}$

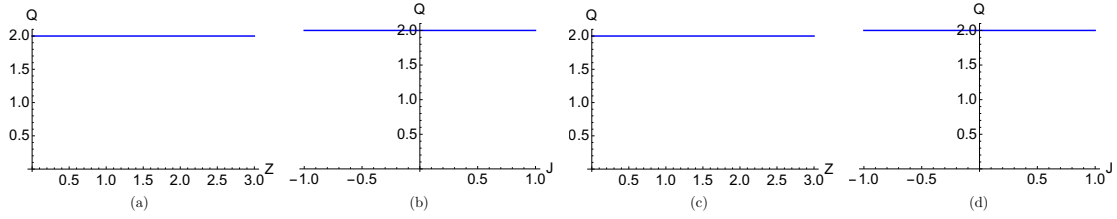


Figure 2.11: (a)  $Q$  in absence of spin flip scattering as a function of interface transparency  $Z$ , (b)  $Q$  in absence of spin flip scattering as a function of exchange interaction  $J$ , (c)  $Q$  in presence of spin flip scattering as a function of interface transparency  $Z$ , (d)  $Q$  in presence of spin flip scattering as a function of exchange interaction  $J$ . Parameters are  $f = f' = 0$  (for (a), (b)),  $f = f' = 1$  (for (c), (d)),  $S = 1/2$ ,  $J = 1$  (for (a), (c)),  $Z = 1$  (for (b), (d)),  $\mu_{pSc} = 0.01$ ,  $\Delta_{pSc} = 0.07$ ,  $a = \pi$ .

are-  $-1$ ,  $-1$ ,  $1$ ,  $1$ . Thus, in no flip process topological quantum number for class BDI is 2. In Figs. 2.11(a) and 2.11(b) we plot topological quantum number  $Q$  as a function of  $Z$  and  $J$  respectively. Figs. 2.11(a) and (b) shows that  $Q$  is constant ( $= 2$ ), independent of  $J$  and  $Z$ . Thus, topological quantum number  $Q$  for BDI remains robust against any change of parameters in absence of spin-flip scattering.

Now in presence of spin-flip scattering, scattering matrix  $\mathcal{S}_{NS}$  (Eq. (2.47)) for  $N_1$ -SF- $N_2$ -I- $p$ Sc junction remains identical. Similar to the preceding case of no spin-flip

scattering, the scattering matrix and its determinant do not change with the change of different parameters for spin-flip scattering. Thus, in the presence of spin-flip scattering, 1D  $N_1$ -SF- $N_2$ -I-pSc junction also belongs to the same symmetry class BDI with topological quantum number  $Q = 2$ . In Figs. 2.11(c) and 2.11(d) we plot topological quantum number  $Q$  as a function of  $Z$  and  $J$  respectively in presence of spin-flip scattering. We see that  $Q$  remains constant ( $= 2$ ) and does not change with change in  $Z$  and  $J$ , similar to no flip process. The topological quantum number determines the number of Majorana fermions at the edge of a topological superconductor. For  $p$ -wave junction, the topological quantum number for class BDI is the number of negative eigenvalues of scattering matrix for pSc, which is 2 irrespective of spin-flip scattering. Thus, the number of Majorana fermions is two at the edge of  $p$ -wave superconductor.

### Symmetry class for SOCSW in the vicinity of a spin flipper

Next, we do a similar analysis as was done for  $N_1$ -SF- $N_2$ -I-pSc junction for  $N_1$ -SF- $N_2$ -I-SOCSW junction. Our aim is to understand the loss of ZBCP in presence of spin flip scattering in a NM-spin flipper-NM-I-SOCSW junction. We first analyze the case where there is no spin flip scattering. The scattering matrix, for no flip process ( $f = f' = 0$ ,  $S = 1/2$ ), and for parameters  $J = 1$ ,  $Z = 1$ ,  $E = 0$ ,  $\beta = 0.5$ ,  $a = \pi$ , and  $B_Z = 1.5\Delta_0$  is-

$$\mathcal{S}_{NS} = \begin{pmatrix} 0.065 - 0.261i & -0.543 - 0.043i & -0.130 + 0.326i & 0.696 + 0.152i \\ 0.326 - 0.130i & -0.369 - 0.609i & 0.261 - 0.065i & -0.217 - 0.5i \\ 0.217 - 0.5i & 0.261 + 0.065i & -0.369 + 0.609i & -0.326 - 0.130i \\ 0.696 - 0.152i & 0.130 + 0.326i & 0.543 - 0.043i & 0.065 + 0.261i \end{pmatrix} \quad (2.50)$$

where  $\mathcal{S}_{NS}$  is an unitary matrix with  $\mathcal{S}_{NS} \cdot \mathcal{S}_{NS}^\dagger = 1$  and  $\text{Det } \mathcal{S}_{NS} = -1$ . The scattering matrix  $\mathcal{S}_{NS}$  however changes with change of parameters unlike scattering matrix for  $N_1$ -

2. FORMATION OF YU-SHIBA-RUSINOV BOUND STATES AND STABILITY OF MAJORANA BOUND STATES IN PRESENCE OF SPIN FLIP SCATTERING

---

SF-N<sub>2</sub>-I-pSc junction. For  $a = \pi/2$  it is-

$$\mathcal{S}_{NS} = \begin{pmatrix} -0.133 + 0.668i & 0.594 - 0.096i & -0.214 + 0.228i & 0.255 + 0.107i \\ -0.214 + 0.228i & 0.255 + 0.107i & 0.659 - 0.173i & -0.346 - 0.492i \\ 0.346 - 0.492i & 0.659 + 0.173i & 0.255 - 0.107i & 0.214 + 0.228i \\ 0.255 - 0.107i & 0.214 + 0.228i & -0.594 - 0.096i & -0.133 - 0.668i \end{pmatrix} \quad (2.51)$$

with the other parameters being same as for Eq. (2.50). As shown in Eqs. (2.50), (2.51), the scattering matrix for a 1D N<sub>1</sub>-SF-N<sub>2</sub>-I-SOCSW junction in absence of spin-flip scattering changes with change in junction length  $a$ , while its determinant ( $\text{Det } \mathcal{S}_{NS} = -1$ ) does not depend on  $a$ . In both cases, for  $a = \pi$  and  $a = \pi/2$ ,  $\text{Det } \mathcal{S}_{NS} = -1$ . We have checked that scattering matrix  $\mathcal{S}_{NS}$  changes with other parameters like  $J$ ,  $Z$ , although its determinant remains constant at  $-1$ , i.e.,  $\text{Det } \mathcal{S}_{NS} = -1$ . Similarly, as mentioned before, when we transform the particle-hole basis of the scattering matrix into Majorana basis by doing an unitary transformation on  $\mathcal{S}_{NS}$ , the transformed scattering matrix is,

$$\text{for } a = \pi: \mathcal{S} = \begin{pmatrix} -0.109 + 0.087i & 0.043 + 0.022i & 0.848 + 0.391i & -0.326i \\ 0.913 - 0.196i & -0.196 - 0.261i & 0.087 + 0.109i & 0.022 - 0.043i \\ -0.022 - 0.043i & 0.087 - 0.109i & -0.196 + 0.261i & -0.913 - 0.196i \\ 0.326i & -0.848 + 0.391i & -0.043 + 0.022i & -0.109 - 0.087i \end{pmatrix} \quad (2.52)$$

$$\text{and for } a = \pi/2 \text{ is: } \mathcal{S} = \begin{pmatrix} 0.127 + 0.148i & 0.861 + 0.206i & -0.028 + 0.087i & 0.129 + 0.392i \\ 0.053 - 0.074i & -0.005 - 0.412i & -0.195 - 0.012i & -0.747 + 0.474i \\ 0.747 + 0.474i & -0.195 + 0.012i & -0.005 + 0.412i & -0.053 - 0.074i \\ 0.129 - 0.392i & 0.028 + 0.087i & -0.861 + 0.206i & 0.127 - 0.148i \end{pmatrix} \quad (2.53)$$

$\mathcal{S}$  is again an unitary matrix with  $\text{Det } \mathcal{S} = \text{Det } \mathcal{S}_{NS} = -1$ . Similar to  $\mathcal{S}_{NS}$ , the transformed scattering matrix  $\mathcal{S}$  changes with change of parameters like  $J$ ,  $Z$ ,  $a$ , but its determinant remains unchanged. We verify that  $\mathcal{S}$  only satisfies particle-hole symmetry relation  $\tau_y \sigma_y \mathcal{S}^* \tau_y \sigma_y = \mathcal{S}$ , thus scattering matrix for no spin-flip scattering in case of a 1D N<sub>1</sub>-SF-N<sub>2</sub>-I-SOCSW junction belongs to symmetry class D. In 1D, symmetry class D is

## 2.6. Stability of Majorana zero modes in the presence of a spin flipper

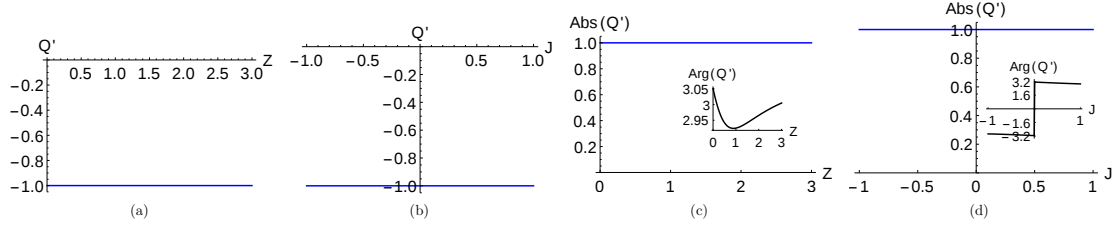


Figure 2.12: (a)  $Q'$  as a function of  $Z$  (with  $J = 1$ ) and (b)  $Q'$  as a function of  $J$  (with  $Z = 1$ ) in absence of spin-flip scattering. (c) Absolute value and Argument of complex  $Q'$  as a function of  $Z$  (with  $J = 1$ ) and (d) Absolute value and Argument of complex  $Q'$  as a function of  $J$  (with  $Z = 1$ ) in presence of spin-flip scattering. Parameters are  $f = f' = 0$  (for (a), (b)),  $f = f' = 1$  (for (c), (d)),  $S = 1/2$ ,  $\Delta_0 = 0.001$ ,  $\beta = 0.5$ ,  $a = \pi$ .

topological with topological quantum number for class D defined as determinant of the scattering matrix[63, 64],

$$Q' = \text{Det}(S) \quad (2.54)$$

In Figs. 2.12(a) and (b), topological quantum number  $Q'$  is plotted as a function of  $Z$  and  $J$  respectively. We see that  $Q'$  is constant ( $= -1$ ) and does not change with  $Z$  and  $J$ . Thus, the topological quantum number  $Q'$  for class D remains robust against any change of parameters in the absence of spin-flip scattering.

In presence of spin-flip scattering ( $f = f' = 1$ ,  $S = 1/2$ ), and parameters  $J = 1$ ,  $Z = 1$ ,  $E = 0$ ,  $\beta = 0.5$  and  $B_Z = 1.5\Delta_0$ , the scattering matrix for a 1D  $N_1$ -SF- $N_2$ -I-SOCSW junction is given as-

$$a = \frac{\pi}{2}: S_{NS} = \begin{pmatrix} -0.055 + 0.435i & 0.428 + 0.199i & -0.109 + 0.207i & 0.698 + 0.207i \\ -0.436 + 0.492i & -0.055 + 0.435i & 0.184 - 0.039i & -0.232 - 0.536i \\ -0.232 - 0.536i & 0.698 + 0.207i & 0.151 - 0.301i & -0.022 - 0.123i \\ 0.184 - 0.039i & -0.109 + 0.207i & -0.767 - 0.456i & 0.151 - 0.301i \end{pmatrix}, \quad (2.55)$$

$$\text{while for } a = \pi: S_{NS} = \begin{pmatrix} -0.166 - 0.525i & -0.313 + 0.121i & 0.249 + 0.299i & 0.656 + 0.037i \\ 0.546 + 0.028i & -0.166 - 0.525i & 0.289 - 0.140i & 0.161 - 0.518i \\ 0.161 - 0.518i & 0.656 + 0.037i & -0.158 + 0.343i & -0.145 - 0.332i \\ 0.289 - 0.140i & 0.249 + 0.299i & 0.733 - 0.254i & -0.158 + 0.343i \end{pmatrix}, \quad (2.56)$$

## 2. FORMATION OF YU-SHIBA-RUSINOV BOUND STATES AND STABILITY OF MAJORANA BOUND STATES IN PRESENCE OF SPIN FLIP SCATTERING

where  $\mathcal{S}_{NS}$  is an unitary matrix with  $\mathcal{S}_{NS} \cdot \mathcal{S}_{NS}^\dagger = 1$ . The determinant of  $\mathcal{S}_{NS}$  for  $a = \pi/2$  and  $a = \pi$  are  $e^{-i2.76667}$  and  $e^{i2.92505}$  respectively with absolute value 1. In contrast to no flip case, both  $\mathcal{S}_{NS}$  and its determinant  $\text{Det } \mathcal{S}_{NS}$  change with change of parameters like  $J$ ,  $Z$ . Similarly, as discussed before, when we do a unitary transformation on  $\mathcal{S}_{NS}$  to transform its basis from particle-hole to Majorana, we have,

$$\text{for } a = \frac{\pi}{2}, \mathcal{S} = \begin{pmatrix} -0.123 - 0.098i & 0.901 + 0.245i & 0.003 - 0.164i & -0.161 + 0.225i \\ -0.418 - 0.021i & -0.123 - 0.098i & -0.474 + 0.166i & -0.73 - 0.041i \\ 0.739 + 0.041i & 0.161 - 0.225i & 0.219 + 0.231i & -0.495 - 0.168i \\ 0.474 - 0.166i & -0.003 + 0.164i & -0.785 + 0.057i & 0.219 + 0.231i \end{pmatrix}, \quad (2.57)$$

$$\text{while for } a = \pi, \mathcal{S} = \begin{pmatrix} 0.043 - 0.200i & 0.427 - 0.068i & 0.843 - 0.048i & -0.227 - 0.084i \\ 0.929 - 0.253i & 0.043 - 0.200i & -0.141 - 0.093i & 0.026 + 0.041i \\ -0.026 - 0.041i & 0.227 + 0.084i & -0.368 + 0.018i & -0.885 - 0.143i \\ 0.141 + 0.093i & -0.843 + 0.048i & 0.351 + 0.027i & -0.368 + 0.018i \end{pmatrix}, \quad (2.58)$$

where  $\mathcal{S}$  is an unitary matrix with  $\text{Det } \mathcal{S} = \text{Det } \mathcal{S}_{NS}$ . Similar to  $\mathcal{S}_{NS}$ , its determinant  $\text{Det } \mathcal{S}$  depends on various junction parameters. We find that  $\tau_y \sigma_y \mathcal{S}^* \tau_y \sigma_y \neq \mathcal{S}$ , i.e.,  $\mathcal{S}$  does not satisfy particle-hole symmetry relations in presence of spin flip scattering. Thus, spin flip scattering leads to breaking of particle-hole symmetry. We have also checked that scattering matrix  $\mathcal{S}$  does not satisfy any symmetry relation and therefore belongs to class A in presence of spin flip scattering.

In Figs. 2.12(c) and 2.12(d) we plot both absolute value and argument of the complex  $Q'$  (determinant of  $\mathcal{S}$ ) as a function of  $Z$  and  $J$  respectively for a 1D  $N_1$ -SF- $N_2$ -I-SOCSW junction (Fig. 2.8). We notice that  $\text{Abs}(Q')$  remains constant at 1, while the argument of  $Q'$  ( $\text{Arg}(\text{Det } \mathcal{S})$ ) changes with  $J$  and  $Z$ .



## 2.7 Conclusion

In this chapter, we have analytically studied YSR bound states in the vicinity of a  $s$ -wave superconductor in the presence of a spin flipper using a BTK approach. We focus on zero energy in the conductance spectra. We see that when the spin flipper does not flip, there is a dip at zero energy in conductance spectra; however, a zero-energy peak is observed due to the occurrence of YSR bound states. We plot the real part of the complex poles of conductance as a function of interface transparency  $Z$  and see that two YSR bound states merge at particular values of  $Z$ . Where the bound states merge gives a zero-energy peak in conductance spectra. We also study the effect of arbitrary junction length on YSR bound states. We see that YSR peaks appear at zero energy in conductance spectra for any arbitrary length of the junction. Further, for long junctions, multiple YSR peaks are seen in the subgap regime of the conductance spectra. This zero-energy peak is robust against change in junction length  $a$ , but not against any other parameter values like exchange interaction  $J$ , interface transparency  $Z$ , etc.

Moving on to the effect of spin-flip scattering on MBS's, we have shown that zero bias quantized conductance Majorana peaks remain unaffected in the presence of spin-flip scattering for  $N_1$ -SF- $N_2$ -I-pSc junction while the zero bias quantized conductance Majorana peak at  $N_1$ -SF- $N_2$ -I-SOCSW junction loses its quantization in the presence of spin-flip scattering. We find that in the presence of spin-flip scattering, a 1D  $N_1$ -SF- $N_2$ -I-pSc junction Hamiltonian and scattering matrix belong to symmetry class BDI and topological quantum number for class BDI does not change with a change of parameters. The scattering matrix for a 1D  $N_1$ -SF- $N_2$ -I-SOCSW junction satisfies only particle-hole symmetry relation. It belongs to topological symmetry class D in the absence of spin-flip scattering. In contrast, in the presence of spin-flip scattering, the scattering matrix does not satisfy any symmetry

## 2. FORMATION OF YU-SHIBA-RUSINOV BOUND STATES AND STABILITY OF MAJORANA BOUND STATES IN PRESENCE OF SPIN FLIP SCATTERING

---

relation and belongs to the non-topological class A. The reason for ZBCP in a 1D  $N_1$ -SF- $N_2$ -I-SOCSW junction, in the absence of spin-flip scattering, is the exact cancellation at zero bias of normal and Andreev reflection probabilities. However, in the presence of spin-flip scattering in a 1D  $N_1$ -SF- $N_2$ -I-SOCSW junction, the exact cancellation of normal and Andreev reflection probabilities doesn't occur. As a consequence, ZBCP loses its quantization.

# Chapter 3

## Spin flip scattering induced odd frequency equal spin triplet correlations in metal-superconductor junction

*“A theorist can explain any correlation, and its inverse”*

— Thomas Gold

### 3.1 Introduction

The symmetry of the Cooper pair defines the characteristics of a superconductor. Fermi-Dirac statistics imply that the Cooper pair wave function or pairing amplitude must be anti-symmetric under the exchange of all quantum numbers: time (or frequency), spin, and orbital coordinates. In general, pairing occurs between electrons at equal times. It leads to either even frequency, spin-singlet, and even parity (ESE) state or even frequency, spin-triplet, and odd parity (ETO) state where even or odd denotes the orbital part of the Cooper pair wave-function.  $s$  and  $d$  wave pairing are examples of ESE pairing, while  $p$  wave pairing is an example of ETO symmetry[66]. However, pairing, surprisingly, may

### 3. SPIN FLIP SCATTERING INDUCED ODD FREQUENCY EQUAL SPIN TRIPLET CORRELATIONS IN METAL-SUPERCONDUCTOR JUNCTION

---

also occur at different times or finite frequency, first noticed in Ref. [67] in  ${}^3\text{He}$  and then predicted to occur in disordered superconductors[68, 69] also. This finite frequency pairing implies an odd frequency superconductor with either odd frequency, spin-singlet, and odd parity (OSO) or odd frequency, spin-triplet, and even parity (OTE) pairing. Odd-frequency superconductivity implies that the Cooper pair's two electrons are odd in the relative time coordinate or frequency. OSO pairing state has been predicted to occur in a conventional spin-singlet superconductor[70]. Recently, odd frequency superconductivity has also been expected to occur in a host of different systems[71, 72, 73, 74, 75], in addition to driven systems[76, 77].

Odd-frequency superconducting pairing can also be induced in hybrid systems such as normal metal-superconductor (NS) junction[78, 79, 80], ferromagnet-superconductor (FS) junctions[7, 81, 82, 83, 84], as well as topological insulator-superconductor junctions[85, 86, 87, 88]. In NS junctions odd frequency pairing arises because spatial parity may be broken at the interface leading to transition from even s-wave to odd p-wave symmetry[89]. Further, odd frequency pairing has been seen in systems with Rashba spin-orbit coupling[89, 90, 91]. Odd frequency pairing enables long range superconducting correlations, as seen in FS junctions[92, 93, 94]. Moreover, there is a deep relationship between odd frequency correlation and topological superconductors which might host Majorana fermions (MF's)[95, 96, 97, 98]. For a MF, the normal propagator ( $G_{ee}^r$ ) which describes the propagation of free electrons and the anomalous propagator ( $G_{eh}^r$ ) which describes dynamics of Cooper pairs are same,  $G_{ee}^r(\omega_m) = G_{eh}^r(\omega_m)$ [99], where  $\omega_m$  is Matsubara frequency. Further, since  $G_{eh}^r(\omega_m) = 1/(i\omega_m)$  for a MF, the pair amplitude ( $G_{eh}^r$ ) for an isolated MF is necessarily odd in frequency[100, 101, 102].

This chapter shows that odd frequency equal spin-triplet pairing can be induced in an NS junction due to interface spin-flip scattering. To date, most predictions of odd

frequency pairing in NS junctions have either been spin-singlet or mixed spin-triplet type[103, 104]. Odd frequency mixed spin-triplet correlations have been predicted to occur in various hybrid superconducting junctions due to a magnetic interface at an NS junction[103], a thin ferromagnetic layer in an NS junction[104], a Kondo-type impurity embedded in a  $s$ -wave superconductor[15] or randomly embedded magnetic impurities in a  $s$ -wave superconductor[105]. A recent experimental paper on a single embedded magnetic impurity in a  $s$ -wave superconductor also sees odd frequency mixed spin-triplet correlations[106]. Odd frequency mixed spin-triplet correlations can also be induced by the spin mixing process[103, 104]. Spin mixing and spin-flip scattering are two different processes. In spin mixing, an electron experiences spin-dependent phase shifts[107], while via spin-flip scattering an electron/hole flips its spin[13]. A thin ferromagnetic layer at the NS interface can only generate spin mixing, and it can not generate any spin-flip scattering[104]. However, a spin flipper at the NS interface generates spin-flip scattering and does not generate any spin mixing. We will discuss this in more detail in section 3.5. Further, in Refs. [15, 105] odd frequency mixed spin-triplet correlations arise due to magnetic impurity similar to what happens in NFS junction wherein only spin mixing occurs, however in this chapter, we will show that spin-flip scattering at NS interface induces both even and odd frequency equal spin-triplet correlations. What differentiates our work in this chapter from the examples above is equal spin-triplet correlations, which are not seen in any of these works.

Now, why are odd frequency equal spin-triplet correlations important? The importance of seeing these correlations in a  $s$ -wave superconductor implies that we have effectively turned a  $s$ -wave superconductor to a  $p$ -wave superconductor via interface spin-flip scattering in an NS junction. A hallmark of  $p$ -wave superconductor is equal spin-triplet pairing of its Cooper pair. Examples of  $p$ -wave superconductors are  $Sr_2RuO_4$ , which are exotic

and difficult to work with but are predicted to host Majorana fermions. However, inducing spin-triplet  $p$ -wave pairing in a  $s$ -wave superconductor would imply generating and detecting Majorana Fermions could become much more accessible. Further, equal spin-triplet correlations support dissipationless pure spin currents, which are generally long-range and are of great interest in superconducting spintronics[107, 108]. Dissipationless pure spin current reduces power consumption by several orders of magnitude in ultralow-power computers[109].

Using a scattering Green's function approach, we calculate the even and odd frequency spin-singlet and triplet pairing correlations induced in normal metal and superconducting regions. We see that locally, only even frequency, spin-singlet even parity correlations, and odd frequency equal spin-triplet, even parity correlations are finite. Non locally, however, both even and odd frequency, spin-singlet, and equal spin-triplet correlations are non-zero. We further determine the local magnetization density of states (LMDOS) and the spin-polarized local density of states (SPLDOS), which can help detect these odd-frequency equal spin-triplet correlations.

## 3.2 Spin flip scattering at NS interface

A NS junction is shown in Fig. 3.1, with a spin flipper at the interface ( $x = 0$ ). The BdG Hamiltonian of this system is given as

$$H_{BdG}(x) = \begin{pmatrix} H\hat{I} & i\Delta\Theta(x)\hat{\sigma}_y \\ -i\Delta^*\Theta(x)\hat{\sigma}_y & -H\hat{I} \end{pmatrix}, \quad (3.1)$$

where  $H = p^2/2m^* - J_0\delta(x)\vec{s}\cdot\vec{S} - E_F$ ,  $\Delta$  is superconducting gap for  $s$ -wave superconductor and  $\Theta(x)$  is Heaviside step function. First term in  $H$  is kinetic energy of an electron/hole with effective mass  $m^*$  and momentum  $p$ , second term describes the exchange interaction

### 3.2. Spin flip scattering at NS interface

$J_0$  between electron/hole spin ( $\vec{s}$ ) and spin flipper's spin ( $\vec{S}$ ),  $\hat{I}$  is identity matrix,  $\hat{\sigma}$  is the Pauli spin matrix and  $E_F$  is Fermi energy. We will later use the dimensionless parameter  $J = \frac{m^* J_0}{k_F}$  as a measure of strength of exchange coupling[13].

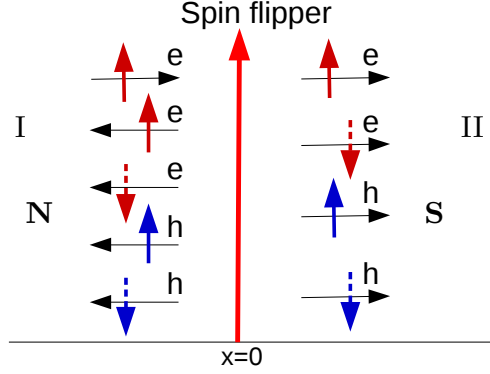


Figure 3.1: A spin flipper with spin  $S$  and magnetic moment  $m'$  at  $x = 0$  in a NS junction. Scattering of an incident spin up electron is shown. Normal reflection, Andreev reflection and quasi-particle transmission into superconductor are depicted.

If we diagonalize BdG Hamiltonian (Eq. (3.1)) we get wavefunctions in different regions of the NS junction, for various types of scattering processes, which are given as,

$$\Psi_1(x) = \begin{cases} \varphi_1^N e^{ik_e x} \phi_{m'}^S + b_{11} \varphi_1^N e^{-ik_e x} \phi_{m'}^S + b_{12} \varphi_2^N e^{-ik_e x} \phi_{m'+1}^S + a_{11} \varphi_3^N e^{ik_h x} \phi_{m'+1}^S + a_{12} \varphi_4^N e^{ik_h x} \phi_{m'}^S, & x < 0, \\ c_{11} \varphi_1^S e^{ik_e^S x} \phi_{m'}^S + c_{12} \varphi_2^S e^{ik_e^S x} \phi_{m'+1}^S + d_{11} \varphi_3^S e^{-ik_h^S x} \phi_{m'+1}^S + d_{12} \varphi_4^S e^{-ik_h^S x} \phi_{m'}^S, & x > 0. \end{cases}$$

$$\Psi_2(x) = \begin{cases} \varphi_2^N e^{ik_e x} \phi_{m'}^S + b_{21} \varphi_1^N e^{-ik_e x} \phi_{m'-1}^S + b_{22} \varphi_2^N e^{-ik_e x} \phi_{m'}^S + a_{21} \varphi_3^N e^{ik_h x} \phi_{m'}^S + a_{22} \varphi_4^N e^{ik_h x} \phi_{m'-1}^S, & x < 0, \\ c_{21} \varphi_1^S e^{ik_e^S x} \phi_{m'-1}^S + c_{22} \varphi_2^S e^{ik_e^S x} \phi_{m'}^S + d_{21} \varphi_3^S e^{-ik_h^S x} \phi_{m'}^S + d_{22} \varphi_4^S e^{-ik_h^S x} \phi_{m'-1}^S, & x > 0. \end{cases}$$

$$\Psi_3(x) = \begin{cases} \varphi_3^N e^{-ik_h x} \phi_{m'}^S + a_{31} \varphi_1^N e^{-ik_e x} \phi_{m'-1}^S + a_{32} \varphi_2^N e^{-ik_e x} \phi_{m'}^S + b_{31} \varphi_3^N e^{ik_h x} \phi_{m'}^S + b_{32} \varphi_4^N e^{ik_h x} \phi_{m'-1}^S, & x < 0, \\ c_{31} \varphi_1^S e^{ik_e^S x} \phi_{m'-1}^S + c_{32} \varphi_2^S e^{ik_e^S x} \phi_{m'}^S + d_{31} \varphi_3^S e^{-ik_h^S x} \phi_{m'}^S + d_{32} \varphi_4^S e^{-ik_h^S x} \phi_{m'-1}^S, & x > 0. \end{cases}$$

$$\Psi_4(x) = \begin{cases} \varphi_4^N e^{-ik_h x} \phi_{m'}^S + a_{41} \varphi_1^N e^{-ik_e x} \phi_{m'}^S + a_{42} \varphi_2^N e^{-ik_e x} \phi_{m'+1}^S + b_{41} \varphi_3^N e^{ik_h x} \phi_{m'+1}^S + b_{42} \varphi_4^N e^{ik_h x} \phi_{m'}^S, & x < 0, \\ c_{41} \varphi_1^S e^{ik_e^S x} \phi_{m'}^S + c_{42} \varphi_2^S e^{ik_e^S x} \phi_{m'+1}^S + d_{41} \varphi_3^S e^{-ik_h^S x} \phi_{m'+1}^S + d_{42} \varphi_4^S e^{-ik_h^S x} \phi_{m'}^S, & x > 0. \end{cases}$$

### 3. SPIN FLIP SCATTERING INDUCED ODD FREQUENCY EQUAL SPIN TRIPLET CORRELATIONS IN METAL-SUPERCONDUCTOR JUNCTION

$$\begin{aligned}
\Psi_5(x) &= \begin{cases} c_{51}\varphi_1^N e^{-ik_e x} \phi_{m'}^S + c_{52}\varphi_2^N e^{-ik_e x} \phi_{m'+1}^S + d_{51}\varphi_3^N e^{ik_h x} \phi_{m'+1}^S + d_{52}\varphi_4^N e^{ik_h x} \phi_{m'}^S, & x < 0, \\ \varphi_1^S e^{-ik_e^S x} \phi_{m'}^S + b_{51}\varphi_1^S e^{ik_e^S x} \phi_{m'}^S + b_{52}\varphi_2^S e^{ik_e^S x} \phi_{m'+1}^S + a_{51}\varphi_3^S e^{-ik_h^S x} \phi_{m'+1}^S + a_{52}\varphi_4^S e^{-ik_h^S x} \phi_{m'}^S, & x > 0. \end{cases} \\
\Psi_6(x) &= \begin{cases} c_{61}\varphi_1^N e^{-ik_e x} \phi_{m'-1}^S + c_{62}\varphi_2^N e^{-ik_e x} \phi_{m'}^S + d_{61}\varphi_3^N e^{ik_h x} \phi_{m'}^S + d_{62}\varphi_4^N e^{ik_h x} \phi_{m'-1}^S, & x < 0, \\ \varphi_2^S e^{-ik_e^S x} \phi_{m'}^S + b_{61}\varphi_1^S e^{ik_e^S x} \phi_{m'-1}^S + b_{62}\varphi_2^S e^{ik_e^S x} \phi_{m'}^S + a_{61}\varphi_3^S e^{-ik_h^S x} \phi_{m'}^S + a_{62}\varphi_4^S e^{-ik_h^S x} \phi_{m'-1}^S, & x > 0. \end{cases} \\
\Psi_7(x) &= \begin{cases} c_{71}\varphi_1^N e^{-ik_e x} \phi_{m'-1}^S + c_{72}\varphi_2^N e^{-ik_e x} \phi_{m'}^S + d_{71}\varphi_3^N e^{ik_h x} \phi_{m'}^S + d_{72}\varphi_4^N e^{ik_h x} \phi_{m'-1}^S, & x < 0, \\ \varphi_3^S e^{ik_h^S x} \phi_{m'}^S + a_{71}\varphi_1^S e^{ik_e^S x} \phi_{m'-1}^S + a_{72}\varphi_2^S e^{ik_e^S x} \phi_{m'}^S + b_{71}\varphi_3^S e^{-ik_h^S x} \phi_{m'}^S + b_{72}\varphi_4^S e^{-ik_h^S x} \phi_{m'-1}^S, & x > 0. \end{cases} \\
\Psi_8(x) &= \begin{cases} c_{81}\varphi_1^N e^{-ik_e x} \phi_{m'}^S + c_{82}\varphi_2^N e^{-ik_e x} \phi_{m'+1}^S + d_{81}\varphi_3^N e^{ik_h x} \phi_{m'+1}^S + d_{82}\varphi_4^N e^{ik_h x} \phi_{m'}^S, & x < 0, \\ \varphi_4^S e^{ik_h^S x} \phi_{m'}^S + a_{81}\varphi_1^S e^{ik_e^S x} \phi_{m'}^S + a_{82}\varphi_2^S e^{ik_e^S x} \phi_{m'+1}^S + b_{81}\varphi_3^S e^{-ik_h^S x} \phi_{m'+1}^S + b_{82}\varphi_4^S e^{-ik_h^S x} \phi_{m'}^S, & x > 0. \end{cases}
\end{aligned} \tag{3.2}$$

$$\text{where } \varphi_1^N = \begin{pmatrix} 1 \\ 0 \\ 0 \\ 0 \end{pmatrix}, \varphi_2^N = \begin{pmatrix} 0 \\ 1 \\ 0 \\ 0 \end{pmatrix}, \varphi_3^N = \begin{pmatrix} 0 \\ 0 \\ 1 \\ 0 \end{pmatrix}, \varphi_4^N = \begin{pmatrix} 0 \\ 0 \\ 0 \\ 1 \end{pmatrix}, \varphi_1^S = \begin{pmatrix} u \\ 0 \\ 0 \\ v \end{pmatrix}, \varphi_2^S = \begin{pmatrix} 0 \\ u \\ -v \\ 0 \end{pmatrix}, \varphi_3^S = \begin{pmatrix} 0 \\ -v \\ u \\ 0 \end{pmatrix} \text{ and}$$

$$\varphi_4^S = \begin{pmatrix} v \\ 0 \\ 0 \\ u \end{pmatrix}. \Psi_1, \Psi_2, \Psi_3 \text{ and } \Psi_4 \text{ represent scattering processes when spin up electron, spin}$$

down electron, spin up hole and spin down hole are incident from N region, while  $\Psi_5, \Psi_6, \Psi_7$  and  $\Psi_8$  represent scattering processes when spin up electron-like quasiparticle (ELQ), spin down ELQ, spin up hole-like quasiparticle (HLQ) and spin down HLQ are incident from S region respectively.  $b_{ij}$  and  $a_{ij}$  are normal and Andreev reflection amplitudes, while  $c_{ij}$  and  $d_{ij}$  are transmission amplitudes for ELQ's and HLQ's.  $\phi_{m'}^S$  represents eigenspinor for spin flipper with its  $S_z$  operator acting as:  $S_z \phi_{m'}^S = \hbar m' \phi_{m'}^S$ , with  $m'$  being spin magnetic moment of spin flipper.  $u = \sqrt{\frac{1}{2}(1 + \frac{\sqrt{\omega^2 - \Delta^2}}{\omega})}$  and  $v = \sqrt{\frac{1}{2}(1 - \frac{\sqrt{\omega^2 - \Delta^2}}{\omega})}$  are



BCS coherence factors.  $k_{e,h} = \sqrt{\frac{2m^*}{\hbar^2}(E_F \pm \omega)}$  are electron/hole wave-vectors in normal metal, while  $k_{e,h}^S = \sqrt{\frac{2m^*}{\hbar^2}(E_F \pm \sqrt{\omega^2 - \Delta^2})}$  are ELQ/HLQ wave-vectors in superconductor. Conjugated processes  $\tilde{\Psi}_i$  required to construct Green's functions in next section are obtained by diagonalizing Hamiltonian  $H_{BdG}^*(-k)$  instead of  $H_{BdG}(k)$ . In case of Normal metal-spin flipper-Superconductor junction (Fig. 3.1) we find that  $\tilde{\varphi}_i^{N(S)} = \varphi_i^{N(S)}$ , hence  $\tilde{\Psi}_i = \Psi_i$ , resulting in identical scattering amplitude, e.g.,  $\tilde{b}_{i1} = b_{i1}$  and so on. In the limit  $E_F \gg \Delta, \omega$  one can approximate  $k_{e,h} \approx k_F(1 \pm \frac{\omega}{2E_F})$  with  $k_F = \sqrt{2m^*E_F/\hbar^2}$  and  $k_{e,h}^S \approx k_F \pm i\kappa$  with  $\kappa = \sqrt{\Delta^2 - \omega^2}[k_F/(2E_F)]$ . Further, superconducting coherence length [110] is given by  $\xi = \hbar/(m^*\Delta)$ .

Scattering amplitudes are determined from boundary conditions, which at  $x = 0$  are,

$$\Psi_i(x < 0) = \Psi_i(x > 0), \text{ and, } \frac{d\Psi_i(x > 0)}{dx} - \frac{d\Psi_i(x < 0)}{dx} = -\frac{2m^*J_0\vec{s}\cdot\vec{S}}{\hbar^2}\Psi_i(x = 0), \quad (3.3)$$

where  $\vec{s}\cdot\vec{S} = s_zS_z + \frac{1}{2}(s^-S^+ + s^+S^-)$  is exchange operator in Hamiltonian Eq. (3.1).  $s^\pm = s_x \pm is_y$  are raising and lowering spin operator for electron/hole, while  $S^\pm = S_x \pm iS_y$  are raising and lowering spin operator for spin-flipper.  $s^\pm$  are  $4 \times 4$  matrix defined in section 1.3 of chapter 1. From boundary conditions (3.3) we get 8 equations for each scattering process, see Eq. (3.2). From each set of these 8 equations we can calculate different scattering amplitudes:  $b_{ij}, a_{ij}, c_{ij}, d_{ij}$ . In the next section we will use these scattering amplitudes to compute retarded Green's function in each region of our system. From retarded Green's function we can calculate the induced pairing correlations, e.g., ESE, ETO, OSO, OTE, and SPLDOS in each region of the junction. Further, we also calculate the LMDOS & SPLDOS which will help in detecting these pairing correlations.

### 3.3 Method to calculate induced pairing correlations

#### 3.3.1 Green's function

Our motivation in this chapter is to see if via spin flip scattering one can induce odd frequency spin triplet pairing in our setup. For this purpose, we use the approach of Refs. [88, 89] and set up retarded Green's function  $G^r(x, x', \omega)$  with incoming and outgoing waves in both N and S regions due to interface[111] scattering. Retarded Green's function then are,

$$G^r(x, x', \omega) = \begin{cases} \Psi_1(x)[\alpha_{11}\tilde{\Psi}_5^T(x') + \alpha_{12}\tilde{\Psi}_6^T(x') + \alpha_{13}\tilde{\Psi}_7^T(x') + \alpha_{14}\tilde{\Psi}_8^T(x')] \\ + \Psi_2(x)[\alpha_{21}\tilde{\Psi}_5^T(x') + \alpha_{22}\tilde{\Psi}_6^T(x') + \alpha_{23}\tilde{\Psi}_7^T(x') + \alpha_{24}\tilde{\Psi}_8^T(x')] \\ + \Psi_3(x)[\alpha_{31}\tilde{\Psi}_5^T(x') + \alpha_{32}\tilde{\Psi}_6^T(x') + \alpha_{33}\tilde{\Psi}_7^T(x') + \alpha_{34}\tilde{\Psi}_8^T(x')] \\ + \Psi_4(x)[\alpha_{41}\tilde{\Psi}_5^T(x') + \alpha_{42}\tilde{\Psi}_6^T(x') + \alpha_{43}\tilde{\Psi}_7^T(x') + \alpha_{44}\tilde{\Psi}_8^T(x')], & x > x' \\ \Psi_5(x)[\beta_{11}\tilde{\Psi}_1^T(x') + \beta_{12}\tilde{\Psi}_2^T(x') + \beta_{13}\tilde{\Psi}_3^T(x') + \beta_{14}\tilde{\Psi}_4^T(x')] \\ + \Psi_6(x)[\beta_{21}\tilde{\Psi}_1^T(x') + \beta_{22}\tilde{\Psi}_2^T(x') + \beta_{23}\tilde{\Psi}_3^T(x') + \beta_{24}\tilde{\Psi}_4^T(x')] \\ + \Psi_7(x)[\beta_{31}\tilde{\Psi}_1^T(x') + \beta_{32}\tilde{\Psi}_2^T(x') + \beta_{33}\tilde{\Psi}_3^T(x') + \beta_{34}\tilde{\Psi}_4^T(x')] \\ + \Psi_8(x)[\beta_{41}\tilde{\Psi}_1^T(x') + \beta_{42}\tilde{\Psi}_2^T(x') + \beta_{43}\tilde{\Psi}_3^T(x') + \beta_{44}\tilde{\Psi}_4^T(x')], & x < x' \end{cases} \quad (3.4)$$

Coefficients  $\alpha_{ij}$  and  $\beta_{mn}$  in Eq. (3.4) are calculated from

$$[\omega - H_{BdG}(x)]G^r(x, x', \omega) = \delta(x - x'), \quad (3.5)$$

Eq. (3.5) on integration at  $x = x'$  yields,

$$[G^r(x > x')]_{x=x'} = [G^r(x < x')]_{x=x'}, \quad \text{and} \quad \left[\frac{d}{dx}G^r(x > x')\right]_{x=x'} - \left[\frac{d}{dx}G^r(x < x')\right]_{x=x'} = \eta\tau_z\sigma_0, \quad (3.6)$$

wherein  $\eta = 2m^*/\hbar^2$  and  $\tau_i, \sigma_i$  are Pauli matrices in particle-hole and spin spaces. Green's functions are  $2 \times 2$  matrix in particle-hole space,

$$G^r(x, x', \omega) = \begin{bmatrix} G_{ee}^r & G_{eh}^r \\ G_{he}^r & G_{hh}^r \end{bmatrix}, \quad (3.7)$$

where each element is a matrix, which in presence of spin flip scattering, can be written as

$$G_{\alpha\beta}^r(x, x', \omega) = \begin{pmatrix} [G_{\alpha\beta}^r]_{\uparrow\uparrow} & [G_{\alpha\beta}^r]_{\uparrow\downarrow} \\ [G_{\alpha\beta}^r]_{\downarrow\uparrow} & [G_{\alpha\beta}^r]_{\downarrow\downarrow} \end{pmatrix}, \text{ with } \alpha, \beta \in \{e, h\}. \quad (3.8)$$

Analytical expressions of all Green's functions are provided in Appendix A.

### 3.3.2 Pairing amplitudes

The anomalous Green's function propagator  $G_{eh}^r$  (off diagonal element in Eq. (3.7)) can be expressed in terms of pairing amplitude ' $f_\lambda^r$ ' as

$$G_{eh}^r(x, x', \omega) = i \sum_{\lambda=0}^3 f_\lambda^r \sigma_\lambda \sigma_2, \quad (3.9)$$

where  $\sigma_0$  is identity matrix,  $\sigma_\lambda$  ( $\lambda = 1, 2, 3$ ) are Pauli matrices. In Eq. (3.9),  $f_0^r$  is spin-singlet ( $\uparrow\downarrow - \downarrow\uparrow$ ),  $f_{1,2}^r$  are equal spin-triplet ( $\downarrow\downarrow \pm \uparrow\uparrow$ ) and  $f_3^r$  is mixed spin triplet ( $\uparrow\downarrow + \downarrow\uparrow$ ) component. Equal spin triplet components  $\uparrow\uparrow$  and  $\downarrow\downarrow$  are given by  $f_{\uparrow\uparrow} = if_2^r - f_1^r$  and  $f_{\downarrow\downarrow} = if_2^r + f_1^r$ , respectively. Herein,  $f_\lambda^r$  denotes pairing amplitude or correlation, while  $|f_\lambda^r| = \sqrt{(f_\lambda^r)(f_\lambda^r)^*}$  refers to pairing magnitude. Using Eqs. (3.7)-(3.9), we get pairing amplitudes or correlations as,

$$\begin{aligned} f_0^r(x, x', \omega) &= \frac{[G_{eh}^r]_{\uparrow\downarrow} - [G_{eh}^r]_{\downarrow\uparrow}}{2}, & f_1^r(x, x', \omega) &= \frac{[G_{eh}^r]_{\downarrow\downarrow} - [G_{eh}^r]_{\uparrow\uparrow}}{2}, \\ f_2^r(x, x', \omega) &= \frac{[G_{eh}^r]_{\downarrow\downarrow} + [G_{eh}^r]_{\uparrow\uparrow}}{2i}, & \text{and } f_3^r(x, x', \omega) &= \frac{[G_{eh}^r]_{\uparrow\downarrow} + [G_{eh}^r]_{\downarrow\uparrow}}{2}. \end{aligned} \quad (3.10)$$

The even and odd frequency components can be extracted from (3.10) as,

$$f_\lambda^E(x, x', \omega) = \frac{f_\lambda^r(x, x', \omega) + f_\lambda^a(x, x', -\omega)}{2}, \quad \text{and } f_\lambda^O(x, x', \omega) = \frac{f_\lambda^r(x, x', \omega) - f_\lambda^a(x, x', -\omega)}{2}, \quad (3.11)$$

### 3. SPIN FLIP SCATTERING INDUCED ODD FREQUENCY EQUAL SPIN TRIPLET CORRELATIONS IN METAL-SUPERCONDUCTOR JUNCTION

---

where  $f_\lambda^a$  is related to advanced Green's function, which can be determined from retarded Green's functions, via  $G^a(x, x', \omega) = [G^r(x', x, \omega)]^\dagger$  [88]. Even and odd frequency components of equal spin triplet correlations can be obtained from Eq. (3.11) as,

$$f_{\uparrow\uparrow}^E = if_2^E - f_1^E, \quad f_{\downarrow\downarrow}^E = if_2^E + f_1^E, \quad f_{\uparrow\uparrow}^O = if_2^O - f_1^O, \quad \text{and} \quad f_{\downarrow\downarrow}^O = if_2^O + f_1^O. \quad (3.12)$$

At finite temperature we go to the Matsubara representation and replace  $\omega$  with  $i\omega_n$ . In this case Eq. (3.9) can be written [112] as,

$$\sum_{\omega_n > 0} G_{eh}^r(x, x', i\omega_n) = i \sum_{\lambda=0}^3 f_\lambda^r \sigma_\lambda \sigma_2, \quad (3.13)$$

$\omega_n = \pi k_B T (2n + 1)$  are Matsubara frequencies and  $n = 0, \pm 1, \pm 2, \dots$

## 3.4 Results

Following the procedure mentioned in section 3.3, herein we analyze the induced odd/even frequency spin-singlet and spin-triplet correlations in N ( $x < 0$ ) and S ( $x > 0$ ) regions at zero as well as at finite temperatures.

### 3.4.1 Zero temperature

#### Odd and even frequency spin-singlet correlations

Induced odd/even frequency pairing amplitudes or correlations are directly calculated from anomalous particle-hole component of retarded Green's function using Eqs. (3.10)-(3.12). Detailed derivation is provided in Appendix A and the Mathematica code used to calculate pairing correlations are mentioned in Appendix D. For even and odd frequency spin singlet

correlations we get,

$$f_0^E(x, x', \omega) = \begin{cases} -\frac{i\eta a_{12}}{2k_e} e^{-ik^M(x+x')} \cos[k_F(x-x')], & \text{for } x < 0 \text{ (N region)} \\ \frac{\eta uv}{2i(u^2-v^2)} e^{-\kappa|x-x'|} \left[ \frac{e^{ik_F|x-x'|}}{k_e^S} + \frac{e^{-ik_F|x-x'|}}{k_h^S} \right] + \frac{\eta uv}{2i(u^2-v^2)} e^{-\kappa(x+x')} \left[ \frac{b_{51} e^{ik_F(x+x')}}{k_e^S} + \frac{b_{82} e^{-ik_F(x+x')}}{k_h^S} \right] + \frac{\eta}{2i(u^2-v^2)} e^{-\kappa(x+x')} \frac{a_{81} \cos[k_F(x-x')](k_F + i\kappa(u^2-v^2))}{(k_F^2 + \kappa^2)}, & \text{for } x > 0 \text{ (S region)} \end{cases} \quad (3.14)$$

$$f_0^O(x, x', \omega) = \begin{cases} -\frac{\eta a_{12}}{2k_e} e^{-ik^M(x+x')} \sin[k_F(x-x')], & \text{for } x < 0 \text{ (N region)} \\ \frac{\eta a_{81}(k_F(u^2-v^2) + i\kappa)}{2(u^2-v^2)(k_F^2 + \kappa^2)} \sin[k_F(x-x')] e^{-\kappa(x+x')}, & \text{for } x > 0 \text{ (S region)} \end{cases} \quad (3.15)$$

where  $k^M = \omega k_F / (2E_F)$ . Both even frequency spin singlet (ESE) and odd frequency spin singlet (OSO) correlations are interface contributions in normal metal(N) region ( $x < 0$ ) as is evident, being proportional to Andreev reflection amplitude  $a_{12}$ . In S region ( $x > 0$ ), ESE correlations have a bulk contribution (first term of Eq. (3.14) for  $x > 0$ ), in addition to interface contribution while OSO correlations have only an interface contribution. Bulk contribution to ESE correlations in S region ( $x > 0$ ), from Eq. (3.14) (independent of interface scattering amplitudes) is

$$f_{0,B}^E = \frac{\eta uv}{2i(u^2-v^2)} e^{-\kappa|x-x'|} \left[ \frac{e^{ik_F|x-x'|}}{k_e^S} + \frac{e^{-ik_F|x-x'|}}{k_h^S} \right], \quad (3.16)$$

while interface contributions from Eq. (3.14) which depend on interface scattering amplitudes, are

$$f_{0,I}^E = \frac{\eta uv}{2i(u^2-v^2)} e^{-\kappa(x+x')} \left[ \frac{b_{51} e^{ik_F(x+x')}}{k_e^S} + \frac{b_{82} e^{-ik_F(x+x')}}{k_h^S} \right] + \frac{\eta}{2i(u^2-v^2)} e^{-\kappa(x+x')} \frac{a_{81} \cos[k_F(x-x')](k_F + i\kappa(u^2-v^2))}{(k_F^2 + \kappa^2)}. \quad (3.17)$$

Bulk contributions do not exhibit any local space dependence, as substituting  $x = x'$  in Eq. (3.16), makes them independent of  $x$ . In contrast interface contributions Eq. (3.17), are  $x$  dependent. Thus, for  $x \rightarrow \infty$  bulk contribution Eq. (3.16), is finite, while interface contribution Eq. (3.17), vanishes. Therefore, local even frequency spin singlet correlations are finite in bulk. From Eq. (3.14) we see that ESE correlation in S region depends on both

### 3. SPIN FLIP SCATTERING INDUCED ODD FREQUENCY EQUAL SPIN TRIPLET CORRELATIONS IN METAL-SUPERCONDUCTOR JUNCTION

normal reflection ( $b_{51}$ ,  $b_{82}$ ) and Andreev reflection amplitude ( $a_{81}$ ), while in Eq. (3.15) OSO correlation in S region is proportional to Andreev reflection amplitude  $a_{81}$ . At  $x = x'$ , OSO vanishes, while ESE is finite and becomes maximum.

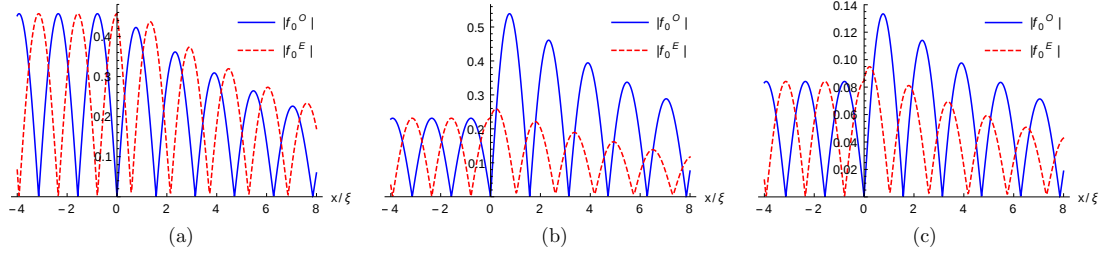


Figure 3.2: Absolute values of even and odd frequency spin-singlet correlation induced in N ( $x < 0$ ) and S ( $x > 0$ ) regions as a function of position  $x$  for (a) no flip case and (b,c) spin flip case. Parameters are:  $S = 1/2$  (for (a) and (b)),  $S = 5/2$  (for (c)). Spin-flip probabilities are:  $f = f' = 0$  (a),  $f = f' = 1$  (b),  $f = f' = 3$  (c). Other parameters:  $J = 1$ ,  $x' = 0$ ,  $\omega = 0.1\Delta$ ,  $E_F = 10\Delta$ .

We plot spin-singlet pairing correlation induced in N and S regions in Fig. 3.2. In Fig. 3.2(a) OSO (blue, solid) and ESE (red, dashed) correlations are finite and show nice periodic oscillations as function of position  $x$  in N ( $x < 0$ ) region, while in S ( $x > 0$ ) region both OSO and ESE correlations exhibit an oscillatory decay in absence of spin-flip scattering, i.e., flip probability:  $f = f' = 0$ . The decay length  $1/\kappa$  with  $\kappa = \sqrt{\Delta^2 - \omega^2}[k_F/(2E_F)]$ , and oscillatory nature of correlations is determined from Fermi energy  $E_F$  (through  $k_F$ , see Eqs. (3.14), (3.15) for  $x > 0$ ). In Fig. 3.2(b) for finite spin-flip scattering, i.e., flip probability  $f = f' = 1$ , we see similar oscillatory behavior, albeit with a lower magnitude than no-flip case. The more interesting thing is what is shown in Fig. 3.2(b) in the S region, wherein we see OSO correlations dominating over ESE correlations. For high values of spin-flip scattering, i.e.,  $f = f' = 3$ , both OSO and ESE correlations are suppressed, but their nature does not change as shown in Fig. 3.2(c). Further, we also note that non-local ( $x \neq x'$ ) spin-singlet correlations are finite regardless of

odd or even frequency. In contrast, local ( $x = x'$ ) OSO correlations vanish, and local ESE correlations are finite. In all figures,  $x$  has been normalized by superconducting coherence length  $\xi$  to make it dimensionless.

### Odd and even frequency equal spin-triplet correlations

Even and odd frequency, spin-triplet correlations are of two distinct types, mixed spin-triplet or equal spin triplet. To distinguish between these, we denote odd frequency equal spin-triplet correlation as OTE-equal, while odd frequency mixed spin-triplet correlation as OTE-mixed. Similarly, in the case of even frequency, we have ETO-equal and ETO-mixed correlations. Uniquely, we find that mixed spin-triplet correlation for both odd and even frequency vanishes ( $f_3^E = f_3^O = 0$ ) in our set-up, while equal spin-triplet correlation for both odd and even frequency is finite ( $f_{\uparrow\uparrow}^{E,O} = -f_{\downarrow\downarrow}^{E,O} \neq 0$ ).

The reason why mixed spin triplet correlations (both even and odd frequency) vanish, can be traced back to the scattering amplitudes, and Green's functions derived from them in sections 3.2 and 3.3. If one looks at the Andreev reflection amplitudes, they satisfy the relations:  $a_{31} = -a_{42}$  and  $a_{32} = -a_{41}$ . Thus, anomalous electron-hole components of Green's functions in N region are related as:  $[G_{eh}^r]_{\uparrow\uparrow} = -[G_{eh}^r]_{\downarrow\downarrow}$  and  $[G_{eh}^r]_{\uparrow\downarrow} = -[G_{eh}^r]_{\downarrow\uparrow}$  (see Appendix A for detailed calculation). This same relation, for anomalous electron-hole components of Green's functions also holds true in S ( $x > 0$ ) region as well. Therefore, from Eq. (3.10),  $f_2^r = 0$  and  $f_3^r = 0$ , with  $f_{\uparrow\uparrow} = -f_{\downarrow\downarrow}$ . Spin flip scattering at junction interfaces, induces equal spin triplet correlations only. Interestingly, we find odd frequency equal spin-triplet correlation (OTE-equal) dominating over even frequency equal spin-triplet correlation (ETO-equal) in the S region, which can have significant applications in superconducting spintronics.

### 3. SPIN FLIP SCATTERING INDUCED ODD FREQUENCY EQUAL SPIN TRIPLET CORRELATIONS IN METAL-SUPERCONDUCTOR JUNCTION

For the even/odd frequency equal spin triplet correlations, using Eq. (3.12) we obtain

$$f_{\uparrow\uparrow}^E(x, x', \omega) = -f_{\downarrow\downarrow}^E(x, x', \omega) = \begin{cases} -\frac{\eta a_{11}}{2k_e} e^{-ik^M(x+x')} \sin[k_F(x-x')], & \text{for } x < 0 \text{ (N region)} \\ -\frac{\eta a_{62}(k_F(u^2-v^2)+i\kappa)}{2(u^2-v^2)(k_F^2+\kappa^2)} \sin[k_F(x-x')]e^{-\kappa(x+x')}, & \text{for } x > 0 \text{ (S region)} \end{cases} \quad (3.18)$$

$$f_{\uparrow\uparrow}^O(x, x', \omega) = -f_{\downarrow\downarrow}^O(x, x', \omega) = \begin{cases} -\frac{i\eta a_{11}}{2k_e} e^{-ik^M(x+x')} \cos[k_F(x-x')], & \text{for } x < 0 \text{ (N region)} \\ \frac{\eta uv}{2i(u^2-v^2)} e^{-\kappa(x+x')} \left[ \frac{b_{72} e^{-ik_F(x+x')}}{k_h^S} - \frac{b_{61} e^{ik_F(x+x')}}{k_e^S} \right] \\ -\frac{\eta}{2i(u^2-v^2)} e^{-\kappa(x+x')} \frac{a_{62} \cos[k_F(x-x')](k_F+i\kappa(u^2-v^2))}{(k_F^2+\kappa^2)}, & \text{for } x > 0 \text{ (S region)} \end{cases} \quad (3.19)$$

in presence of spin flip scattering, while in absence of spin flip scattering they vanish. In absence of spin flip scattering, both incident quasi particle spin and spin flipper's spin are in same direction (either up or down) and they do not flip their spins after interaction. For  $S = 1/2$ ,  $m'$  can be  $1/2$  (when spin flipper's spin is in up direction) or  $-1/2$  (when spin flipper's spin is in down direction). When spin up quasiparticle is incident, no-flip process implies  $S = m'$  (i.e.,  $f = 0$ ) while when spin down quasiparticle is incident  $S = -m'$  (i.e.,  $f' = 0$ ). When spin up quasiparticle is incident and  $m' = 1/2$ , then there won't be any spin flip scattering ( $f = 0$ ) and from Eq. (1.54) we get

$$\vec{s} \cdot \vec{S} \varphi_1^N \phi_{\frac{1}{2}}^{\frac{1}{2}} = \frac{1}{4} \varphi_1^N \phi_{\frac{1}{2}}^{\frac{1}{2}}. \quad (3.20)$$

Similarly, when spin down quasiparticle is incident and  $m' = -1/2$ , then there will not be any spin flip scattering ( $f' = 0$ ) and from Eq. (1.55) we get

$$\vec{s} \cdot \vec{S} \varphi_2^N \phi_{-\frac{1}{2}}^{\frac{1}{2}} = \frac{1}{4} \varphi_2^N \phi_{-\frac{1}{2}}^{\frac{1}{2}}. \quad (3.21)$$

From Eqs. (3.20), (3.21) we see that in absence of spin-flip scattering  $\vec{s} \cdot \vec{S}$  operates similarly on spin up and spin down quasiparticle spinors, and therefore the system becomes spin-inactive. Thus, at NS interface when spin flipper does not flip its spin, spin-singlet to spin-triplet conversion can not take place, and spin triplet correlations do not arise in such a situation (see Appendix A for detailed calculation of how spin triplet correlations



vanish in absence of spin flip scattering). From Eqs. (3.18), (3.19), we see that both even and odd frequency, equal spin triplet correlations are interface contributions. We further notice that in S ( $x > 0$ ) region ETO-equal correlation is proportional to Andreev reflection amplitude  $a_{62}$ , while OTE-equal correlation depends on both normal and Andreev reflection amplitudes. In N ( $x < 0$ ) region both even and odd frequency equal spin triplet correlations are proportional to Andreev reflection amplitude  $a_{11}$ . At  $x = x'$ , local ETO-equal correlations vanish, i.e.,  $f_{\uparrow\uparrow}^E = -f_{\downarrow\downarrow}^E = 0$ , but local OTE-equal correlation is finite, i.e.,  $f_{\uparrow\uparrow}^O = -f_{\downarrow\downarrow}^O \neq 0$ .

In Fig. 3.3 ETO-equal and OTE-equal correlations are plotted as function of position  $x$  for low ( $f = f' = 1$ , Fig. 3.3(a)) and high ( $f = f' = 3$ , Fig. 3.3(b)) values of spin flip scattering. We see that in the metallic region  $f_{\uparrow\uparrow}^{E,O}$  or  $f_{\downarrow\downarrow}^{E,O}$  is finite and exhibits an oscillatory behavior as function of position  $x$  and survives infinitely far away in presence of spin flip scattering. The reason for this kind of behavior can be understood from Eqs. (3.18), (3.19)

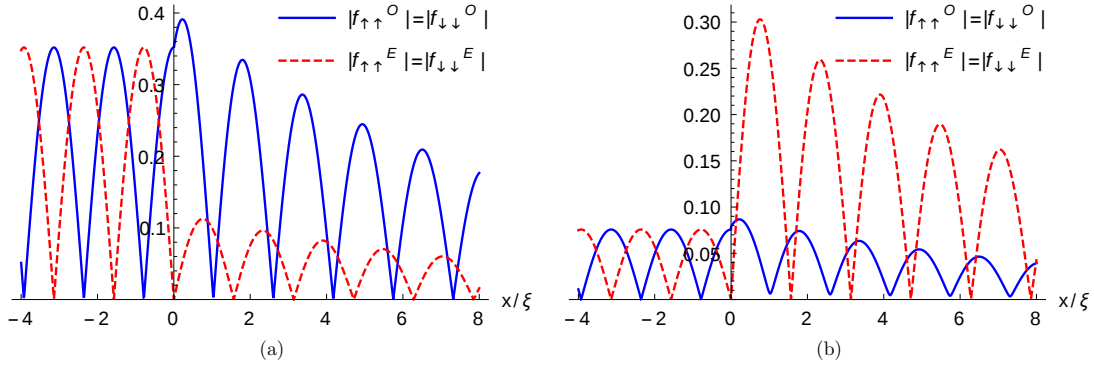


Figure 3.3: Absolute values of even and odd frequency equal spin-triplet correlation induced in N ( $x < 0$ ) and S ( $x > 0$ ) regions as function of position  $x$  for spin flip case. Parameters are:  $S = 1/2$  (for (a)),  $S = 5/2$  (for (b)),  $f = f' = 1$  (for (a)),  $f = f' = 3$  (for (b)),  $J = 1$ ,  $x' = 0$ ,  $\omega = 0.1\Delta$ ,  $E_F = 10\Delta$ .

for  $x < 0$ , where we see that the equal spin-triplet pairings are proportional to  $\sin[k_F(x - x')]$  for even frequency and  $\cos[k_F(x - x')]$  for odd frequency respectively. However, in the

### 3. SPIN FLIP SCATTERING INDUCED ODD FREQUENCY EQUAL SPIN TRIPLET CORRELATIONS IN METAL-SUPERCONDUCTOR JUNCTION

---

S region, we find that both ETO-equal and OTE-equal correlations exhibit an oscillatory decay in the presence of spin-flip scattering. It contrasts with what we see for spin-triplet correlations in the normal metal region ( $x < 0$ ). The reason one obtains different results for equal spin-triplet correlations in N and S regions can be understood from Eq. (3.18) for  $x > 0$ , where we see that equal spin-triplet correlation in the S region is proportional to  $\sin[k_F(x - x')]e^{-\kappa(x+x')}$  and therefore shows an oscillatory decay with decay length  $1/\kappa$ . In contrast, in the N region, correlations don't decay. Another interesting thing to note from Fig. 3.3 is that in a ballistic NS junction, non-local even and odd frequency equal spin-triplet correlations are finite only in the presence of spin-flip scattering, which is an exceptional result since other papers in NS junctions report odd frequency mixed spin-triplet correlations with vanishing odd frequency equal spin-triplet correlations[88, 89]. Further, locally at  $x = x'$ , we notice that ETO-equal correlations vanish, but OTE-equal correlations are non-zero. In addition, we notice that in the S region, the OTE-equal correlation is larger than the ETO-equal correlation for low values of spin-flip scattering. In contrast, for high values of spin-flip scattering, ETO-equal correlation dominates over OTE-equal correlation. Finally, we reiterate that both ETO-mixed and OTE-mixed correlations vanish regardless of spin-flip scattering, i.e.,  $f_3^E = f_3^O = 0$  in our setup.

As an aside, for an NS junction based on 1D nanowires with Rashba spin-orbit coupling[89] and proximity-induced  $s$ -wave spin-singlet superconductivity, although even/odd frequency mixed spin-triplet correlations are induced, the even/odd frequency equal spin-triplet correlations vanish. Spin-orbit coupling does not generate equal spin-triplet correlations in NS junctions.

### 3.4.2 Finite temperature

In the previous section we have discussed spin singlet and triplet correlations at zero temperature. In this section we will study effect of finite temperature on spin singlet and triplet correlations. To calculate correlations at finite temperature we use Matsubara representation, replacing  $\omega$  with  $i\omega_n$  in anomalous electron-hole propagator (see Eqs. (3.9), (3.13)). In electron-hole propagator at finite temperature (Eq. (3.13)), summation is taken over positive frequencies only because all pairing correlations become odd functions of frequency. From electron-hole propagator at finite temperature (Eq. (3.13)), we can compute even/odd frequency spin singlet and spin triplet correlations, see Eqs (3.14), (3.15), (3.18), (3.19).

#### Odd and even frequency spin-singlet correlations

At zero temperature, both even and odd frequency spin-singlet correlations in the N region exhibit an oscillatory behavior and survive infinitely far away. But, at finite temperature ESE and OSO correlations show an oscillatory decay in the N region since decay length ( $\xi_N$ ) in the N region goes as  $\frac{1}{T}$  [113, 114].

Even and odd frequency spin singlet correlations at finite temperature are given as,

$$f_0^E(x, x', T) = \sum_{\omega_n > 0} f_0^E(x, x', \omega \rightarrow i\omega_n), \quad \text{and} \quad f_0^O(x, x', T) = \sum_{\omega_n > 0} f_0^O(x, x', \omega \rightarrow i\omega_n) \quad (3.22)$$

where  $f_0^E(x, x', \omega)$  and  $f_0^O(x, x', \omega)$  are given in Eqs. (3.14), (3.15). In Fig. 3.4 we plot spin singlet correlation induced in N( $x < 0$ ) and S( $x > 0$ ) regions as function of position  $x$  at finite temperature for both no flip (Fig. 3.4(a)) and spin flip (Figs. 3.4(b,c)) processes. Even and odd frequency spin singlet pairings are finite and show a nice oscillatory decay as function of position  $x$  in normal region. The reason for this kind of behavior can be understood by substituting  $\omega$  with  $i\omega_n$  in Eqs. (3.14), (3.15) where ESE correlation is proportional to

### 3. SPIN FLIP SCATTERING INDUCED ODD FREQUENCY EQUAL SPIN TRIPLET CORRELATIONS IN METAL-SUPERCONDUCTOR JUNCTION

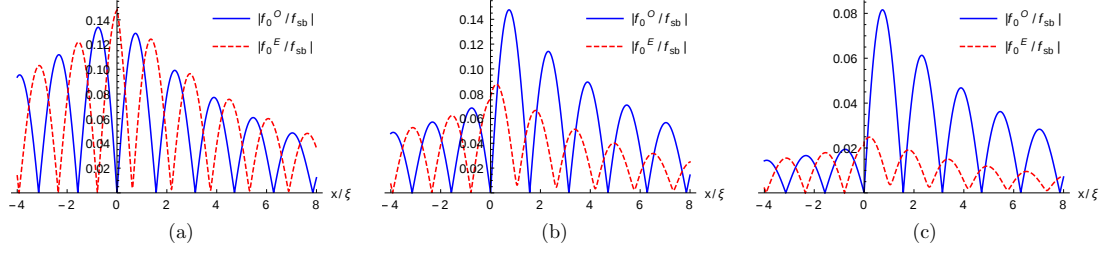


Figure 3.4: The absolute values of the even and odd frequency spin-singlet correlation induced in the N region ( $x < 0$ ) and S region ( $x > 0$ ) as a function of the position  $x$  for (a) no flip process and (b) spin flip process. Parameters are:  $S = 1/2$  (for (a) and (b)),  $S = 5/2$  (for (c)),  $f = f' = 0$  (for (a)),  $f = f' = 1$  (for (b)),  $f = f' = 3$  (for (c)),  $J = 1$ ,  $x' = 0$ ,  $T/T_c = 0.01$ ,  $E_F = 10\Delta$ .

$e^{k^{M'}(x+x')} \cos[k_F(x-x')]$  and OSO correlation is proportional to  $e^{k^{M'}(x+x')} \sin[k_F(x-x')]$  in N region ( $x < 0$ ), with  $k^{M'} = \omega_n k_F / (2E_F)$ . This is in contrast to what we observe at zero temperature where ESE and OSO correlations exhibit a nice oscillation instead of oscillatory decay at zero temperature. In S region, we see a nice oscillatory decay similar to zero temperature, only the magnitudes of pairing correlations may change but qualitatively there is no change when  $\omega \rightarrow i\omega_n$  since the factor  $\kappa (= \sqrt{(\Delta^2 - \omega^2)} [k_F / (2E_F)])$  occurring in the superconducting wavefunctions is function of  $\omega^2$ .

In our figures we normalize the pairing amplitudes to the value of spin singlet pairing amplitude in the bulk superconductors[115],

$$f_{sb} = 2 \sum_{\omega_n} \frac{\Delta}{\sqrt{\omega_n^2 + \Delta^2}}. \quad (3.23)$$

The temperature dependence of the bulk pair potential  $\Delta$  is given as

$$\Delta(T) = \Delta(0) \tanh(1.74\sqrt{T_c/T - 1}),$$

where  $T_c$  is the critical temperature[24].

### Odd and even frequency equal spin triplet correlations

Finite temperature, even and odd frequency equal spin triplet correlations ( $f_{\uparrow\uparrow}^E(x, x', T)$ ,  $f_{\uparrow\uparrow}^O(x, x', T)$ ) are derived by substituting  $i\omega_n$  for  $\omega$  in Eqs. (3.18), (3.19). Thus

$$f_{\uparrow\uparrow}^E(x, x', T) = -f_{\downarrow\downarrow}^E(x, x', T) = \sum_{\omega_n > 0} f_{\uparrow\uparrow}^E(x, x', \omega \rightarrow i\omega_n) = - \sum_{\omega_n > 0} f_{\downarrow\downarrow}^E(x, x', \omega \rightarrow i\omega_n), \quad (3.24)$$

$$f_{\uparrow\uparrow}^O(x, x', T) = -f_{\downarrow\downarrow}^O(x, x', T) = \sum_{\omega_n > 0} f_{\uparrow\uparrow}^O(x, x', \omega \rightarrow i\omega_n) = - \sum_{\omega_n > 0} f_{\downarrow\downarrow}^O(x, x', \omega \rightarrow i\omega_n), \quad (3.25)$$

in presence of spin flip scattering. Similar to zero temperature case, in absence of spin flip scattering equal spin triplet correlations (Eq. (3.24), (3.25)) vanish.

In Fig. 3.5 we plot ETO-equal ( $f_{\uparrow\uparrow}^E$ ,  $f_{\downarrow\downarrow}^E$ ) and OTE-equal ( $f_{\uparrow\uparrow}^O$ ,  $f_{\downarrow\downarrow}^O$ ) correlations as a function of position  $x$  for small ( $f = f' = 1$ , Fig. 3.5(a)) and large ( $f = f' = 3$ , Fig. 3.5(b)) values of spin flip scattering. We see that equal spin triplet correlations are finite and exhibit an oscillatory decay in N region. This is in contrast to what we see for equal spin triplet correlations at zero temperature, see Figs. 3.3(a), 3.3(b). The reason for this behavior can be

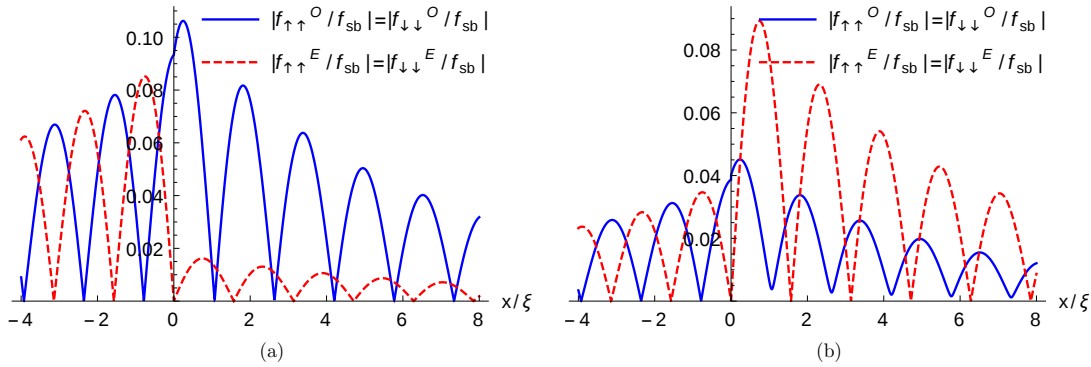


Figure 3.5: Absolute values of even and odd frequency equal spin-triplet correlation induced in N region ( $x < 0$ ) and S region ( $x > 0$ ) as a function of position  $x$  for spin flip process. Parameters are:  $S = 1/2$  (for (a)),  $S = 5/2$  (for (b)),  $f = f' = 1$  (for (a)),  $f = f' = 3$  (for (b)),  $J = 1$ ,  $x' = 0$ ,  $T/T_c = 0.01$ ,  $E_F = 10\Delta$ .

understood by substituting  $\omega$  with  $i\omega_n$  in Eqs. (3.18), (3.19) where ETO-equal correlation is proportional to  $e^{k^{M'}(x+x')} \sin[k_F(x - x')]$  and OTE-equal correlation is proportional

### 3. SPIN FLIP SCATTERING INDUCED ODD FREQUENCY EQUAL SPIN TRIPLET CORRELATIONS IN METAL-SUPERCONDUCTOR JUNCTION

---

to  $e^{kM'(x+x')} \cos[k_F(x-x')]$  in the N region ( $x < 0$ ). In S region we see the similar behavior for both ETO-equal ( $f_{\uparrow\uparrow}^E, f_{\downarrow\downarrow}^E$ ) and OTE-equal ( $f_{\uparrow\uparrow}^O, f_{\downarrow\downarrow}^O$ ) correlations as seen at zero temperature. Finally, we note that both even as well as odd frequency mixed spin triplet correlations vanish regardless of spin flip scattering, i.e.,  $f_3^E(x, x', T) = f_3^O(x, x', T) = 0$ .

## 3.5 Processes at play

In section 3.4 we see finite odd frequency equal spin-triplet correlations with vanishing odd frequency mixed spin-triplet correlations when only spin-flip scattering is present in the system. In this section, we explain the reasons behind our results. We examine three different situations: (a) when both spin-flip scattering and spin mixing are present in the system, (b) when only spin mixing is present in the system, and (c) when only spin-flip scattering is present in the system (sections 3.3 & 3.4). Spin mixing and spin-flip scattering are two separate processes. In the spin mixing process, an electron experiences spin-dependent phase shifts[107], while in the spin-flip scattering process, an electron flips its spin[9]. Thus, when an electron propagates through a ferromagnetic layer, only spin mixing occurs[116], while when an electron propagates through two ferromagnetic layers with misaligned magnetizations, both spin mixing and spin-flip scattering occur[117]. However, only spin-flip scattering occurs when an electron interacts with the spin flipper in an NS junction. We will discuss below the spin structure of the retarded Green's functions and induced pairing correlations and SPLDOS for each of these three cases.

### 3.5.1 Retarded Green's functions and induced pairing correlations

#### Both spin mixing and spin-flip scattering occur

In the case of Superconductor-Ferromagnet-Ferromagnet-Superconductor (S-F<sub>1</sub>-F<sub>2</sub>-S) junction or Ferromagnet-Ferromagnet-Superconductor (F<sub>1</sub>-F<sub>2</sub>-S) junction with misaligned magnetizations both spin mixing and spin-flip scattering occur when an electron/hole propagates through two ferromagnetic layers. The S-F<sub>1</sub>-F<sub>2</sub>-S junction case has been dealt with elaborately in Ref. [117]. Hereinbelow, we show the calculations for F<sub>1</sub>F<sub>2</sub>S junction.

A F<sub>1</sub>F<sub>2</sub>S junction is shown in Fig. 3.6, wherein magnetization vectors of the two Ferromagnets make an angle  $\theta$  with each other. In Fig. 3.6, the scattering of an up spin electron incident is shown and normal reflection, Andreev reflection and quasi-particle transmission into superconductor are represented. The model Hamiltonian in BdG formalism of

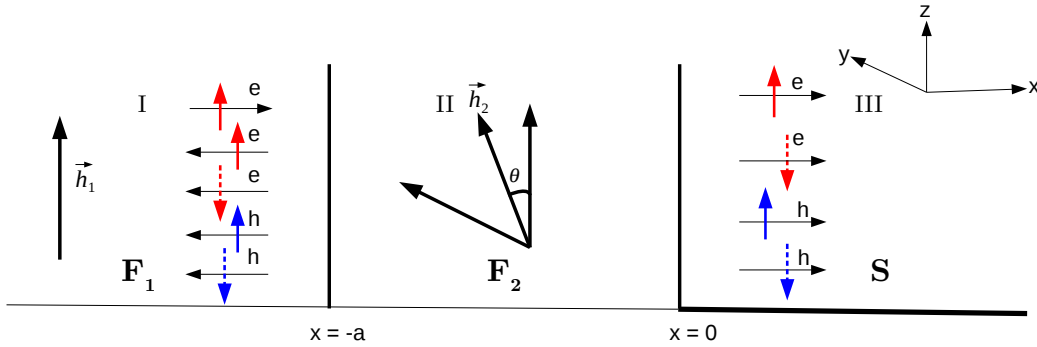


Figure 3.6: Ferromagnet (F<sub>1</sub>)-Ferromagnet (F<sub>2</sub>)-Superconductor (S) junction with misaligned magnetizations. The scattering of a spin up electron incident is shown. Normal reflection, Andreev reflection and quasi-particle transmission into superconductor are depicted.

the system as depicted in Fig. 3.6 is given as:

$$H_{F,BdG}(x) = \begin{pmatrix} H_F \hat{I} & i\Delta \Theta(x) \hat{\sigma}_y \\ -i\Delta^* \Theta(x) \hat{\sigma}_y & -H_F \hat{I} \end{pmatrix}, \quad (3.26)$$

### 3. SPIN FLIP SCATTERING INDUCED ODD FREQUENCY EQUAL SPIN TRIPLET CORRELATIONS IN METAL-SUPERCONDUCTOR JUNCTION

where  $H_F = p^2/2m^* - \vec{h}_1 \cdot \hat{\sigma} \Theta(-x-a) - \vec{h}_2 \cdot \hat{\sigma} \Theta(x+a) \Theta(-x) - E_F$ . The magnetization vector ( $\vec{h}_2$ ) of right ferromagnetic layer ( $F_2$ ) is at an angle  $\theta$  with  $z$  axis in the  $y - z$  plane, while that of left ferromagnetic layer ( $F_1$ ) is fixed along the  $z$  axis. Thus,  $\vec{h}_2 \cdot \hat{\sigma} = h_2 \sin \theta \hat{\sigma}_y + h_2 \cos \theta \hat{\sigma}_z$ . If we diagonalize BdG Hamiltonian  $H_{F,BdG}(x)$  we will get wavefunctions in different regions of our system for various types of scattering processes. Wavefunctions for different types of scattering processes are given as

$$\Psi_1(x) = \begin{cases} \varphi_1^N e^{iq_1^+(x+a)} + a'_{11} \varphi_3^N e^{iq_1^-(x+a)} + a'_{12} \varphi_4^N e^{iq_1^-(x+a)} + b'_{11} \varphi_1^N e^{-iq_1^+(x+a)} + b'_{12} \varphi_2^N e^{-iq_1^+(x+a)}, & x < -a \\ c'_{11} \varphi_1^F e^{iq_1^+(x+a)} + c'_{12} \varphi_2^F e^{iq_1^+(x+a)} + d'_{11} \varphi_1^F e^{-iq_1^+x} + d'_{12} \varphi_2^F e^{-iq_1^+x} + e'_{11} \varphi_3^F e^{iq_1^-x} + e'_{12} \varphi_4^F e^{iq_1^-x} \\ + f'_{11} \varphi_3^F e^{-iq_1^-(x+a)} + f'_{12} \varphi_4^F e^{-iq_1^-(x+a)}, & -a < x < 0 \\ g'_{11} \varphi_1^S e^{ik_e^S x} + g'_{12} \varphi_2^S e^{ik_e^S x} + h'_{11} \varphi_3^S e^{-ik_h^S x} + h'_{12} \varphi_4^S e^{-ik_h^S x}, & x > 0 \end{cases}$$

$$\Psi_2(x) = \begin{cases} \varphi_2^N e^{iq_1^+(x+a)} + a'_{21} \varphi_3^N e^{iq_1^-(x+a)} + a'_{22} \varphi_4^N e^{iq_1^-(x+a)} + b'_{21} \varphi_1^N e^{-iq_1^+(x+a)} + b'_{22} \varphi_2^N e^{-iq_1^+(x+a)}, & x < -a \\ c'_{21} \varphi_1^F e^{iq_1^+(x+a)} + c'_{22} \varphi_2^F e^{iq_1^+(x+a)} + d'_{21} \varphi_1^F e^{-iq_1^+x} + d'_{22} \varphi_2^F e^{-iq_1^+x} + e'_{21} \varphi_3^F e^{iq_1^-x} + e'_{22} \varphi_4^F e^{iq_1^-x} \\ + f'_{21} \varphi_3^F e^{-iq_1^-(x+a)} + f'_{22} \varphi_4^F e^{-iq_1^-(x+a)}, & -a < x < 0 \\ g'_{21} \varphi_1^S e^{ik_e^S x} + g'_{22} \varphi_2^S e^{ik_e^S x} + h'_{21} \varphi_3^S e^{-ik_h^S x} + h'_{22} \varphi_4^S e^{-ik_h^S x}, & x > 0 \end{cases}$$

$$\Psi_3(x) = \begin{cases} \varphi_3^N e^{-iq_1^-(x+a)} + a'_{31} \varphi_1^N e^{-iq_1^+(x+a)} + a'_{32} \varphi_2^N e^{-iq_1^+(x+a)} + b'_{31} \varphi_3^N e^{iq_1^-(x+a)} + b'_{32} \varphi_4^N e^{iq_1^-(x+a)}, & x < -a \\ c'_{31} \varphi_1^F e^{iq_1^+(x+a)} + c'_{32} \varphi_2^F e^{iq_1^+(x+a)} + d'_{31} \varphi_1^F e^{-iq_1^+x} + d'_{32} \varphi_2^F e^{-iq_1^+x} + e'_{31} \varphi_3^F e^{iq_1^-x} + e'_{32} \varphi_4^F e^{iq_1^-x} \\ + f'_{31} \varphi_3^F e^{-iq_1^-(x+a)} + f'_{32} \varphi_4^F e^{-iq_1^-(x+a)}, & -a < x < 0 \\ g'_{31} \varphi_1^S e^{ik_e^S x} + g'_{32} \varphi_2^S e^{ik_e^S x} + h'_{31} \varphi_3^S e^{-ik_h^S x} + h'_{32} \varphi_4^S e^{-ik_h^S x}, & x > 0 \end{cases}$$

$$\Psi_4(x) = \begin{cases} \varphi_4^N e^{-iq_1^-(x+a)} + a'_{41} \varphi_1^N e^{-iq_1^+(x+a)} + a'_{42} \varphi_2^N e^{-iq_1^+(x+a)} + b'_{41} \varphi_3^N e^{iq_1^-(x+a)} + b'_{42} \varphi_4^N e^{iq_1^-(x+a)}, & x < -a \\ c'_{41} \varphi_1^F e^{iq_1^+(x+a)} + c'_{42} \varphi_2^F e^{iq_1^+(x+a)} + d'_{41} \varphi_1^F e^{-iq_1^+x} + d'_{42} \varphi_2^F e^{-iq_1^+x} + e'_{41} \varphi_3^F e^{iq_1^-x} + e'_{42} \varphi_4^F e^{iq_1^-x} \\ + f'_{41} \varphi_3^F e^{-iq_1^-(x+a)} + f'_{42} \varphi_4^F e^{-iq_1^-(x+a)}, & -a < x < 0 \\ g'_{41} \varphi_1^S e^{ik_e^S x} + g'_{42} \varphi_2^S e^{ik_e^S x} + h'_{41} \varphi_3^S e^{-ik_h^S x} + h'_{42} \varphi_4^S e^{-ik_h^S x}, & x > 0 \end{cases}$$



$$\begin{aligned}
 \Psi_5(x) &= \begin{cases} g'_{51}\varphi_1^N e^{-iq_1^+(x+a)} + g'_{52}\varphi_2^N e^{-iq_1^-(x+a)} + h'_{51}\varphi_3^N e^{iq_1^-(x+a)} + h'_{52}\varphi_4^N e^{iq_1^-(x+a)}, & x < -a \\ c'_{51}\varphi_1^F e^{iq_1^+(x+a)} + c'_{52}\varphi_2^F e^{iq_1^-(x+a)} + d'_{51}\varphi_1^F e^{-iq_1^+x} + d'_{52}\varphi_2^F e^{-iq_1^+x} + e'_{51}\varphi_3^F e^{iq_1^-x} + e'_{52}\varphi_4^F e^{iq_1^-x} \\ + f'_{51}\varphi_3^F e^{-iq_1^-(x+a)} + f'_{52}\varphi_4^F e^{-iq_1^-(x+a)}, & -a < x < 0 \\ \varphi_1^S e^{-ik_e^S x} + a'_{51}\varphi_3^S e^{-ik_h^S x} + a'_{52}\varphi_4^S e^{-ik_h^S x} + b'_{51}\varphi_1^S e^{ik_e^S x} + b'_{52}\varphi_2^S e^{ik_e^S x}, & x > 0 \end{cases} \\
 \Psi_6(x) &= \begin{cases} g'_{61}\varphi_1^N e^{-iq_1^+(x+a)} + g'_{62}\varphi_2^N e^{-iq_1^-(x+a)} + h'_{61}\varphi_3^N e^{iq_1^-(x+a)} + h'_{62}\varphi_4^N e^{iq_1^-(x+a)}, & x < -a \\ c'_{61}\varphi_1^F e^{iq_1^+(x+a)} + c'_{62}\varphi_2^F e^{iq_1^-(x+a)} + d'_{61}\varphi_1^F e^{-iq_1^+x} + d'_{62}\varphi_2^F e^{-iq_1^+x} + e'_{61}\varphi_3^F e^{iq_1^-x} + e'_{62}\varphi_4^F e^{iq_1^-x} \\ + f'_{61}\varphi_3^F e^{-iq_1^-(x+a)} + f'_{62}\varphi_4^F e^{-iq_1^-(x+a)}, & -a < x < 0 \\ \varphi_2^S e^{-ik_e^S x} + a'_{61}\varphi_3^S e^{-ik_h^S x} + a'_{62}\varphi_4^S e^{-ik_h^S x} + b'_{61}\varphi_1^S e^{ik_e^S x} + b'_{62}\varphi_2^S e^{ik_e^S x}, & x > 0 \end{cases} \\
 \Psi_7(x) &= \begin{cases} g'_{71}\varphi_1^N e^{-iq_1^+(x+a)} + g'_{72}\varphi_2^N e^{-iq_1^-(x+a)} + h'_{71}\varphi_3^N e^{iq_1^-(x+a)} + h'_{72}\varphi_4^N e^{iq_1^-(x+a)}, & x < -a \\ c'_{71}\varphi_1^F e^{iq_1^+(x+a)} + c'_{72}\varphi_2^F e^{iq_1^-(x+a)} + d'_{71}\varphi_1^F e^{-iq_1^+x} + d'_{72}\varphi_2^F e^{-iq_1^+x} + e'_{71}\varphi_3^F e^{iq_1^-x} + e'_{72}\varphi_4^F e^{iq_1^-x} \\ + f'_{71}\varphi_3^F e^{-iq_1^-(x+a)} + f'_{72}\varphi_4^F e^{-iq_1^-(x+a)}, & -a < x < 0 \\ \varphi_3^S e^{ik_h^S x} + a'_{71}\varphi_1^S e^{ik_e^S x} + a'_{72}\varphi_2^S e^{ik_e^S x} + b'_{71}\varphi_3^S e^{-ik_h^S x} + b'_{72}\varphi_4^S e^{-ik_h^S x}, & x > 0 \end{cases} \\
 \Psi_8(x) &= \begin{cases} g'_{81}\varphi_1^N e^{-iq_1^+(x+a)} + g'_{82}\varphi_2^N e^{-iq_1^-(x+a)} + h'_{81}\varphi_3^N e^{iq_1^-(x+a)} + h'_{82}\varphi_4^N e^{iq_1^-(x+a)}, & x < -a \\ c'_{81}\varphi_1^F e^{iq_1^+(x+a)} + c'_{82}\varphi_2^F e^{iq_1^-(x+a)} + d'_{81}\varphi_1^F e^{-iq_1^+x} + d'_{82}\varphi_2^F e^{-iq_1^+x} + e'_{81}\varphi_3^F e^{iq_1^-x} + e'_{82}\varphi_4^F e^{iq_1^-x} \\ + f'_{81}\varphi_3^F e^{-iq_1^-(x+a)} + f'_{82}\varphi_4^F e^{-iq_1^-(x+a)}, & -a < x < 0 \\ \varphi_4^S e^{ik_h^S x} + a'_{81}\varphi_1^S e^{ik_e^S x} + a'_{82}\varphi_2^S e^{ik_e^S x} + b'_{81}\varphi_3^S e^{-ik_h^S x} + b'_{82}\varphi_4^S e^{-ik_h^S x}, & x > 0 \end{cases}
 \end{aligned} \tag{3.27}$$

$$\text{where } \varphi_1^F = \begin{pmatrix} \cos \frac{\theta}{2} \\ i \sin \frac{\theta}{2} \\ 0 \\ 0 \end{pmatrix}, \varphi_2^F = \begin{pmatrix} i \sin \frac{\theta}{2} \\ \cos \frac{\theta}{2} \\ 0 \\ 0 \end{pmatrix}, \varphi_3^F = \begin{pmatrix} 0 \\ 0 \\ \cos \frac{\theta}{2} \\ -i \sin \frac{\theta}{2} \end{pmatrix}, \varphi_4^F = \begin{pmatrix} 0 \\ 0 \\ -i \sin \frac{\theta}{2} \\ \cos \frac{\theta}{2} \end{pmatrix}. \Psi_1, \Psi_2, \Psi_3 \text{ and } \Psi_4$$

represents the scattering processes when spin up electron, spin down electron, spin up hole and spin down hole are incident from ferromagnetic region I respectively, while  $\Psi_5$ ,  $\Psi_6$ ,  $\Psi_7$  and  $\Psi_8$  represents the scattering processes when spin up electron, spin down electron, spin

### 3. SPIN FLIP SCATTERING INDUCED ODD FREQUENCY EQUAL SPIN TRIPLET CORRELATIONS IN METAL-SUPERCONDUCTOR JUNCTION

up hole and spin down hole are incident from superconducting region respectively.  $b'_{ij}$  and  $a'_{ij}$  are normal reflection amplitudes and Andreev reflection amplitudes respectively, while  $g'_{ij}$  and  $h'_{ij}$  are transmission amplitudes for electron-like quasi-particles and hole-like quasi-particles respectively.  $q_{\sigma}^{\pm} = \sqrt{\frac{2m^*}{\hbar^2}(E_F \pm \omega + \rho_{\sigma}h)}$  are the wave-vectors for electron ( $q_{\sigma}^+$ ) and hole ( $q_{\sigma}^-$ ) in the Ferromagnet, with  $\rho_{\sigma} = +1(-1)$ ,  $\sigma = \uparrow(\downarrow)$ . Conjugated processes  $\tilde{\psi}_i$  needed to construct the Green's functions are determined by diagonalizing the Hamiltonian  $H_{F,BdG}^*(-k)$  instead of  $H_{F,BdG}(k)$ . In case of F<sub>1</sub>F<sub>2</sub>S junction we find that  $\tilde{\varphi}_i^{N(S)} = \varphi_i^{N(S)}$  and  $\tilde{\varphi}_i^F = (\varphi_i^F)^*$ . In the limit of  $E_F \gg \Delta, \omega$  we approximate  $q_{\sigma}^{\pm} \approx k_F(1 \pm \frac{\omega}{2E_F} + \rho_{\sigma} \frac{h}{2E_F})$  with  $k_F = \sqrt{2m^*E_F/\hbar^2}$ . Scattering amplitudes are obtained from the boundary conditions, at  $x = -a$ :

$$\psi_i(x < -a) = \psi_i(-a < x < 0), \quad \text{and,} \quad \frac{d\psi_i(-a < x < 0)}{dx} - \frac{d\psi_i(x < -a)}{dx} = 0, \quad (3.28)$$

at  $x = 0$ :

$$\psi_i(-a < x < 0) = \psi_i(x > 0), \quad \text{and,} \quad \frac{d\psi_i(x > 0)}{dx} - \frac{d\psi_i(-a < x < 0)}{dx} = 0. \quad (3.29)$$

Solving the above boundary conditions, we get 16 equations for each type of scattering process as discussed in Eq. (3.27). From each set of these 16 equations we can determine the different scattering amplitudes. Using these scattering amplitudes and following the similar procedure as discussed in section 3.3, we can compute retarded Green's function and induced pairing correlations in each region of junction. In the left ferromagnetic region for electron-electron and electron-hole components of Green's function we get,

$$\begin{aligned} [G_{ee}^r]_{\uparrow\uparrow} &= -\frac{i\eta}{2q_{\uparrow}^+} [b'_{11} e^{-iq_{\uparrow}^+(x+x')} + e^{iq_{\uparrow}^+|x-x'|}], & [G_{ee}^r]_{\downarrow\downarrow} &= -\frac{i\eta}{2q_{\downarrow}^+} [b'_{22} e^{-iq_{\downarrow}^+(x+x')} + e^{iq_{\downarrow}^+|x-x'|}], \\ [G_{ee}^r]_{\uparrow\downarrow} &= -\frac{i\eta}{2q_{\downarrow}^+} b'_{21} e^{-i(q_{\uparrow}^+x+q_{\downarrow}^+x')}, & [G_{ee}^r]_{\downarrow\uparrow} &= -\frac{i\eta}{2q_{\uparrow}^+} b'_{12} e^{-i(q_{\downarrow}^+x+q_{\uparrow}^+x')}, \\ [G_{eh}^r]_{\uparrow\uparrow} &= -\frac{i\eta}{2q_{\uparrow}^+} a'_{31} e^{-i(q_{\uparrow}^+x-q_{\uparrow}^-x')}, & [G_{eh}^r]_{\downarrow\downarrow} &= -\frac{i\eta}{2q_{\downarrow}^+} a'_{42} e^{-i(q_{\downarrow}^+x-q_{\downarrow}^-x')}, \\ [G_{eh}^r]_{\uparrow\downarrow} &= -\frac{i\eta}{2q_{\downarrow}^+} a'_{41} e^{-i(q_{\uparrow}^+x-q_{\downarrow}^-x')}, & \text{and } [G_{eh}^r]_{\downarrow\uparrow} &= -\frac{i\eta}{2q_{\uparrow}^+} a'_{32} e^{-i(q_{\downarrow}^+x-q_{\uparrow}^-x')}. \end{aligned} \quad (3.30)$$

Substituting Eq. (3.30) in Eq. (3.10) we get,

$$\begin{aligned} f_0^r(x, x', \omega) &= -\frac{i\eta}{4} \left( \frac{a'_{41} e^{-i(q_1^+ x - q_1^- x')}}{q_-} - \frac{a'_{32} e^{-i(q_1^+ x - q_1^- x')}}{q_+} \right), \quad f_1^r(x, x', \omega) = -\frac{i\eta}{4} \left( \frac{a'_{42} e^{-i(q_1^+ x - q_1^- x')}}{q_-} - \frac{a'_{31} e^{-i(q_1^+ x - q_1^- x')}}{q_+} \right), \\ f_2^r(x, x', \omega) &= -\frac{\eta}{4} \left( \frac{a'_{31} e^{-i(q_1^+ x - q_1^- x')}}{q_+} + \frac{a'_{42} e^{-i(q_1^+ x - q_1^- x')}}{q_-} \right), \quad \text{and } f_3^r(x, x', \omega) = -\frac{i\eta}{4} \left( \frac{a'_{41} e^{-i(q_1^+ x - q_1^- x')}}{q_-} + \frac{a'_{32} e^{-i(q_1^+ x - q_1^- x')}}{q_+} \right). \end{aligned} \quad (3.31)$$

Thus, equal spin triplet correlations  $f_{\uparrow\uparrow}$  and  $f_{\downarrow\downarrow}$  are finite,  $f_{\uparrow\uparrow} = i f_2^r - f_1^r = -\frac{i\eta}{2q_+} a'_{31} e^{-i(q_1^+ x - q_1^- x')}$ , and  $f_{\downarrow\downarrow} = i f_2^r + f_1^r = -\frac{i\eta}{2q_-} a'_{42} e^{-i(q_1^+ x - q_1^- x')}$  and mixed spin triplet correlations  $f_3^r$  are also finite. For even and odd frequency spin singlet correlations, using Eq. (3.11) we get,

$$\begin{aligned} f_0^E(x, x', \omega) &= \frac{i\eta}{4} \left[ \frac{a'_{32} e^{-ik^N(x+x')}}{q_+} - \frac{a'_{41} e^{-ik^{N'}(x+x')}}{q_-} \right] \cos[k_F(x-x')], \quad \text{and} \\ f_0^O(x, x', \omega) &= \frac{\eta}{4} \left[ \frac{a'_{32} e^{-ik^N(x+x')}}{q_+} - \frac{a'_{41} e^{-ik^{N'}(x+x')}}{q_-} \right] \sin[k_F(x-x')], \end{aligned} \quad (3.32)$$

where  $k^N = \frac{(\omega-h_1)k_F}{2E_F}$  and  $k^{N'} = \frac{(\omega+h_1)k_F}{2E_F}$ . Similarly, for even and odd frequency equal spin triplet correlations, using Eqs. (3.11) and (3.12) we obtain,

$$\begin{aligned} f_{\uparrow\uparrow}^E(x, x', \omega) &= -\frac{\eta a'_{31}}{2q_+} e^{-ik^M(x+x')} \sin[k^L(x-x')], \quad f_{\uparrow\uparrow}^O(x, x', \omega) = -\frac{i\eta a'_{31}}{2q_+} e^{-ik^M(x+x')} \cos[k^L(x-x')], \\ f_{\downarrow\downarrow}^E(x, x', \omega) &= -\frac{\eta a'_{42}}{2q_-} e^{-ik^M(x+x')} \sin[k^{L'}(x-x')], \quad \text{and } f_{\downarrow\downarrow}^O(x, x', \omega) = -\frac{i\eta a'_{42}}{2q_-} e^{-ik^M(x+x')} \cos[k^{L'}(x-x')], \end{aligned} \quad (3.33)$$

where  $k^M = \frac{\omega k_F}{2E_F}$ ,  $k^L = k_F(1 + \frac{h}{2E_F})$  and  $k^{L'} = k_F(1 - \frac{h}{2E_F})$ . Finally, even and odd frequency mixed spin triplet correlations, using Eq. (3.11) we get,

$$\begin{aligned} f_3^E(x, x', \omega) &= -\frac{\eta}{4} \left[ \frac{a'_{32} e^{-ik^N(x+x')}}{q_+} - \frac{a'_{41} e^{-ik^{N'}(x+x')}}{q_-} \right] \sin[k_F(x-x')], \quad \text{and} \\ f_3^O(x, x', \omega) &= -\frac{i\eta}{4} \left[ \frac{a'_{32} e^{-ik^N(x+x')}}{q_+} - \frac{a'_{41} e^{-ik^{N'}(x+x')}}{q_-} \right] \cos[k_F(x-x')]. \end{aligned} \quad (3.34)$$

From Eqs. (3.33), (3.34) we see that both even and odd frequency equal and mixed spin-triplet correlations are finite when spin mixing and spin-flip scattering both are present in the system.

### Only spin mixing occurs

In Fig. 3.6, when magnetization vectors of the two Ferromagnets are parallel to each other, i.e.,  $\theta = 0$ , then spin flip scattering does not occur and only spin mixing occurs in the system due to the exchange field of the Ferromagnets. Spin mixing also arises in NS junction with Rashba spin-orbit coupling, see Ref. [89]. In case of spin mixing process occurring in a FS junction (this is same as a F<sub>1</sub>F<sub>2</sub>S junction with aligned magnetization, and with vanishing length of F<sub>2</sub> layer, see Fig. 3.6), normal and Andreev reflection amplitudes with flip are zero, i.e.,  $b'_{12} = b'_{21} = a'_{31} = a'_{42} = 0$ . Thus, from Eq. (3.30) we get  $[G'_{ee}]_{\uparrow\downarrow} = [G'_{ee}]_{\downarrow\uparrow} = [G'_{eh}]_{\uparrow\uparrow} = [G'_{eh}]_{\downarrow\downarrow} = 0$  and from Eq. (3.33) we get  $f_{\uparrow\uparrow}^E = f_{\uparrow\uparrow}^O = f_{\downarrow\downarrow}^E = f_{\downarrow\downarrow}^O = 0$ . Therefore, when only spin mixing occurs, even and odd frequency equal spin-triplet correlations vanish, but mixed spin-triplet correlations ( $f_3^r$ ) are finite (see Eq. (3.34)).

### Only spin-flip scattering occurs

In the case of Normal metal (N)-Spin flipper (SF)-Superconductor (S) junction, our chosen system depicted in Fig. 3.1, only spin-flip scattering occurs. In section 3.4.1 we have already shown that when only spin-flip scattering occurs, even and odd frequency equal spin-triplet correlations are finite, but mixed spin-triplet correlations vanish.

In our system, there is a spin flipper at the N-S interface. When an electron/hole with spin up/down is incident from the metallic region at N-S interface, it interacts with the spin flipper through an exchange potential ( $J_0\vec{s}\cdot\vec{S}$ ), which may induce a mutual spin flip. Electron/hole can be reflected with spin-up or down. Spin-up or down electron-like and hole-like quasiparticles are transmitted into the S region for energies above the gap. Electron/hole does not experience any spin-dependent phase shifts when interacting with the spin flipper. Thus, there is no spin mixing, and only spin-flip scattering occurs. Spin flip scattering induces only equal spin-triplet correlations as shown in Fig. 3.3.

## 3.6 Detecting odd frequency correlations

To detect experimentally odd frequency pairing correlations, one makes use of LDOS  $\nu(x, \omega)$  and local magnetization density of state (LMDOS)  $\mathbf{m}(x, \omega)$  which can be calculated[15] from retarded Green's function as,

$$\nu(x, \omega) = -\frac{1}{\pi} \lim_{\epsilon \rightarrow 0} \text{Im}(\text{Tr}\{G_{ee}^r(x, x, \omega + i\epsilon)\}), \quad \text{and} \quad \mathbf{m}(x, \omega) = -\frac{1}{\pi} \lim_{\epsilon \rightarrow 0} \text{Im}(\text{Tr}\{\vec{\sigma}_\lambda \cdot G_{ee}^r(x, x, \omega + i\epsilon)\}). \quad (3.35)$$

From Eq. (3.35), spin up ( $\sigma = +1$ ) and spin-down ( $\sigma = -1$ ) components of SPLDOS are given as  $\nu_\sigma = (\nu + \sigma|\mathbf{m}|)/2$ .

### 3.6.1 Spin polarized local density of states (SPLDOS) & local magnetization density of states (LMDOS)

From section 3.5, we have three cases:

#### (i) Both spin mixing and spin flip scattering occur:

In case of  $F_1F_2S$  junction with misaligned magnetizations as shown in Fig. 3.6, both spin mixing and spin flip scattering are present in the system. LMDOS for  $F_1F_2S$  junction, using Eq. (3.35) is given by,

$$\mathbf{m}(x, \omega) = -\frac{1}{\pi} \lim_{\epsilon \rightarrow 0} \text{Im}[( [G_{ee}^r]_{\uparrow\downarrow} + [G_{ee}^r]_{\downarrow\uparrow} )\hat{x} + i([G_{ee}^r]_{\uparrow\downarrow} - [G_{ee}^r]_{\downarrow\uparrow})\hat{y} + ([G_{ee}^r]_{\uparrow\uparrow} - [G_{ee}^r]_{\downarrow\downarrow})\hat{z}], \quad (3.36)$$

and SPLDOS is given by,

$$\begin{aligned} \nu_\sigma = & -\frac{1}{2\pi} \lim_{\epsilon \rightarrow 0} \text{Im}([G_{ee}^r]_{\uparrow\uparrow} + [G_{ee}^r]_{\downarrow\downarrow}) \\ & + \frac{\sigma}{2\pi} \lim_{\epsilon \rightarrow 0} \sqrt{\text{Im}([G_{ee}^r]_{\uparrow\downarrow} + [G_{ee}^r]_{\downarrow\uparrow})^2 + \text{Im}(i([G_{ee}^r]_{\uparrow\downarrow} - [G_{ee}^r]_{\downarrow\uparrow}))^2 + \text{Im}([G_{ee}^r]_{\uparrow\uparrow} - [G_{ee}^r]_{\downarrow\downarrow})^2}, \end{aligned} \quad (3.37)$$

### 3. SPIN FLIP SCATTERING INDUCED ODD FREQUENCY EQUAL SPIN TRIPLET CORRELATIONS IN METAL-SUPERCONDUCTOR JUNCTION

where  $[G_{ee}^r]_{\uparrow\uparrow}$ ,  $[G_{ee}^r]_{\uparrow\downarrow}$ ,  $[G_{ee}^r]_{\downarrow\uparrow}$ , and  $[G_{ee}^r]_{\downarrow\downarrow}$  are mentioned in Eq. (3.30) for left ferromagnetic region. Thus, both equal ( $\uparrow\uparrow$  or  $\downarrow\downarrow$ ) and mixed ( $\uparrow\downarrow$  or  $\downarrow\uparrow$ ) spin components of Green's function are finite and contribute to LMDOS and SPLDOS.

In Figs. 3.7(a) and 3.7(b) we plot even and odd frequency equal and mixed spin-triplet correlations respectively as a function of position  $x$  in the superconducting region ( $x > 0$ ) for  $F_1F_2S$  junction when magnetization vectors of the two ferromagnetic layers are misaligned ( $\theta \neq 0$ ). We see that along with odd frequency correlations dominating over

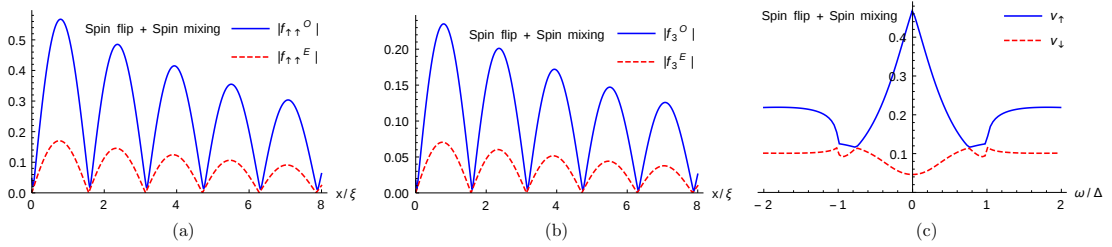


Figure 3.7: Absolute values of even and odd frequency (a) equal spin-triplet correlations and (b) mixed spin-triplet correlations induced in superconducting region for  $F_1F_2S$  junction as function of position  $x$  when both spin flip scattering and spin mixing occur, (c) Frequency dependence of SPLDOS at  $x = 0$  for  $F_1F_2S$  junction when both spin flip scattering and spin mixing occur. Parameters are:  $h_1/E_F = h_2/E_F = 0.8$ ,  $x' = 0$ ,  $\omega = 0.1\Delta$  (for (a) and (b)),  $E_F = 10\Delta$ ,  $\theta = \pi/2$ ,  $k_F a = \pi$ .

even frequency correlations, there is also a peak at  $\omega = 0$  for spin-up LDOS ( $v_{\uparrow}$ ), while there is a dip at  $\omega = 0$  for spin-down LDOS ( $v_{\downarrow}$ ), see Fig. 3.7(c).

#### (ii) Only spin mixing occurs:

In case of a NS junction with Rashba spin-orbit coupling or a NFS junction or for a FS junction, spin flip scattering is absent and only spin mixing occurs. In absence of spin flip scattering,  $[G_{ee}^r]_{\uparrow\downarrow} = [G_{ee}^r]_{\downarrow\uparrow} = 0$ . From the definition of LMDOS and SPLDOS, see Eq. (3.35), one can calculate LMDOS and SPLDOS for a NFS junction or FS junction as,

$$\mathbf{m}(x, \omega) = -\frac{1}{\pi} \lim_{\epsilon \rightarrow 0} \text{Im}([G_{ee}^r]_{\uparrow\uparrow} - [G_{ee}^r]_{\downarrow\downarrow}) \hat{z}, \quad (3.38)$$

and SPLDOS is given by,

$$\nu_{\sigma} = -\frac{1}{2\pi} \lim_{\epsilon \rightarrow 0} \text{Im}([G_{ee}^r]_{\uparrow\uparrow} + [G_{ee}^r]_{\downarrow\downarrow}) + \frac{\sigma}{2\pi} \lim_{\epsilon \rightarrow 0} \sqrt{\text{Im}([G_{ee}^r]_{\uparrow\uparrow} - [G_{ee}^r]_{\downarrow\downarrow})^2}. \quad (3.39)$$

Thus, only equal ( $\uparrow\uparrow$  or  $\downarrow\downarrow$ ) spin components of Green's function are finite and contribute to the LMDOS and SPLDOS.

Since, there is no spin flip scattering, even and odd frequency equal spin-triplet correlations vanish and therefore in Fig. 3.8 we plot even and odd frequency mixed spin-triplet correlations and SPLDOS. We see that when odd frequency mixed spin-triplet correlations

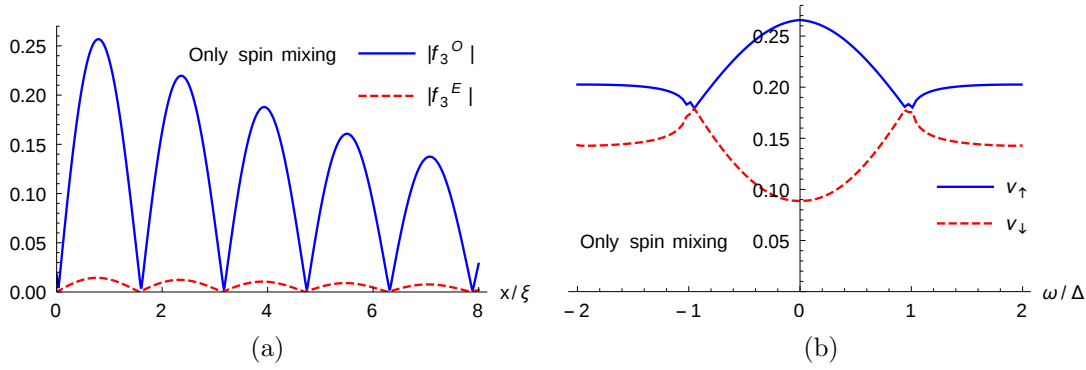


Figure 3.8: Absolute values of even and odd frequency mixed spin-triplet correlations induced in superconducting region for FS junction as function of position  $x$  wherein only spin mixing occurs, (c) Frequency dependence of SPLDOS at  $x = 0$  for FS junction. Parameters are:  $\hbar/E_F = 0.8$ ,  $x' = 0$ ,  $\omega = 0.1\Delta$  (for (a)),  $E_F = 10\Delta$ .

dominate over even frequency mixed spin-triplet correlations, a peak is seen at  $\omega = 0$  for spin-up LDOS ( $\nu_{\uparrow}$ ), while a dip is seen at  $\omega = 0$  for spin-down LDOS ( $\nu_{\downarrow}$ ) at FS interface, while LMDOS is polarized in  $z$ -direction.

### (iii) Only spin flip scattering occurs:

In case of a Normal metal-Spin flipper-Superconductor junction we find that,  $[G_{ee}^r]_{\uparrow\uparrow} = [G_{ee}^r]_{\downarrow\downarrow}$  and  $[G_{ee}^r]_{\uparrow\downarrow} = [G_{ee}^r]_{\downarrow\uparrow}$  both in normal metal and superconducting region. Thus,

### 3. SPIN FLIP SCATTERING INDUCED ODD FREQUENCY EQUAL SPIN TRIPLET CORRELATIONS IN METAL-SUPERCONDUCTOR JUNCTION

---

from Eq. 3.35, we get,

$$\mathbf{m}(x, \omega) = -\frac{2}{\pi} \text{Im}([G_{ee}^r]_{\uparrow\downarrow})\hat{x}, \quad \text{and} \quad \nu_\sigma = -\frac{1}{\pi} \lim_{\epsilon \rightarrow 0} \text{Im}([G_{ee}^r]_{\uparrow\uparrow}) + \frac{\sigma}{\pi} \lim_{\epsilon \rightarrow 0} \text{Im}([G_{ee}^r]_{\uparrow\downarrow}). \quad (3.40)$$

From Eq. (3.40) we see that only mixed ( $\uparrow\downarrow$ ) spin component of the Green's function contributes to the LMDOS, while both equal ( $\uparrow\uparrow$ ) and mixed ( $\uparrow\downarrow$ ) spin components of the Green's function contribute to the SPLDOS. The mixed spin component of the Green's function, i.e.,  $[G_{ee}^r]_{\uparrow\downarrow}$  is finite only in presence of spin flip scattering. Thus,  $[G_{ee}^r]_{\uparrow\downarrow}$  is responsible for the modification of the predicted SPLDOS at NS interface. In both N ( $x < 0$ ) and S ( $x > 0$ ) regions for SPLDOS we find,

$$\nu_\sigma(x, \omega) = \begin{cases} \frac{1}{2\pi} \text{Im}\left(\frac{i\eta(1+b_{11}e^{-i2k_e x})}{k_e}\right) + \frac{\sigma}{2\pi} \sqrt{\text{Im}\left(\frac{i\eta b_{12}e^{-i2k_e x}}{k_e}\right)^2}, & \text{for } x < 0 \text{ (N region)} \\ e^{-2\kappa x} \times \left(\frac{1}{2\pi} \text{Im}(\rho_1) + \frac{\sigma}{2\pi} \sqrt{\text{Im}(\rho_2)^2}\right), & \text{for } x > 0 \text{ (S region)} \end{cases} \quad (3.41)$$

where,

$$\rho_1 = \frac{i\eta(2a_{81}k_F uv + b_{51}e^{i2k_F x} u^2(k_F - i\kappa) + b_{82}e^{-i2k_F x} v^2(k_F + i\kappa) + e^{2\kappa x}(k_F - i(u^2 - v^2)\kappa))}{(u^2 - v^2)(k_F^2 + \kappa^2)},$$

$$\rho_2 = \frac{i\eta(b_{72}v^2(k_F + i\kappa)e^{-i2k_F x} - 2a_{62}k_F uv - b_{61}u^2(k_F - i\kappa)e^{i2k_F x})}{(u^2 - v^2)(k_F^2 + \kappa^2)}.$$

From Eq. (3.41) we see that SPLDOS has a bulk as well as interface contribution. Further, there is a decay term  $e^{-2\kappa x}$  in Eq. (3.41) for  $x > 0$ . The first term in Eq. (3.41) represents LDOS, while the second term represents LMDOS. For LMDOS, from Eq. (3.35) we get

$$\mathbf{m}(x, \omega) = \begin{cases} \frac{1}{\pi} \text{Im}\left(\frac{i\eta b_{12}e^{-i2k_e x}}{k_e}\right)\hat{x}, & \text{for } x < 0 \text{ (N region)} \\ \frac{1}{\pi} \text{Im}(\rho_2)\hat{x}, & \text{for } x > 0 \text{ (S region)} \end{cases} \quad (3.42)$$

From Eq. (3.42) we see that LMDOS is parallel to  $x$  axis. The reason why LMDOS is parallel to  $x$  direction, can be found from the scattering amplitudes and Green's functions obtained for them in sections 3.2 and 3.3. If one looks at the normal reflection amplitudes,



they satisfy the relations:  $b_{11} = b_{22}$  and  $b_{12} = b_{21}$ . Thus, normal electron-electron components of Green's functions in N region are related as:  $[G'_{ee}]_{\uparrow\uparrow} = [G'_{ee}]_{\downarrow\downarrow}$  and  $[G'_{ee}]_{\uparrow\downarrow} = [G'_{ee}]_{\downarrow\uparrow}$  (see Appendix A for detailed calculation). This same relation, for normal electron-electron components of Green's functions holds true in S region as well. Therefore, from Eq. (3.35),  $y$  and  $z$  components of LMDOS vanish and LMDOS is parallel to  $x$  axis. In presence of spin-flip scattering, scattering amplitude  $b_{12}$  (normal metal region) and  $\rho_2$  (in superconducting region) are finite in Eq. (3.41). Thus, spin up and spin down components of SPLDOS are unequal, i.e.,  $\nu_{\uparrow} \neq \nu_{\downarrow}$ , therefore LDOS is spin-polarized, although  $f_{\uparrow\uparrow} = -f_{\downarrow\downarrow}$ . However, in absence of spin-flip scattering both  $b_{12}$  and  $\rho_2$  are zero in Eq. (3.41), which implies LDOS is unpolarized, i.e.,  $\nu_{\uparrow} = \nu_{\downarrow} = \nu$ . While, in Ref. [89], the presence of Rashba spin-orbit coupling leads to mixed spin-triplet correlations and spin-polarized LDOS. In our setup, spin-flip scattering leads to equal spin-triplet correlations and spin-polarized LDOS. However, in Ref. [89], in the absence of spin-orbit coupling, as also in our setup in the absence of spin-flip scattering, LDOS is not spin-polarized. To conclude, while in Ref. [89] spin orbit coupling is responsible for spin polarization of LDOS, in our setup spin flip scattering is responsible for spin polarization of LDOS.

In Figs. 3.9(a) and 3.10(a) we plot spin-up and spin-down LDOS as a function of  $\omega$  at the NS interface ( $x = 0$ ). We see that for low values of spin flip scattering ( $f = f' = 1$ ) when  $f_{\uparrow\uparrow}^O$  dominates over  $f_{\uparrow\uparrow}^E$ , there is a peak at  $\omega = 0$ . But, for increasing values of spin flip scattering ( $f = f' = 3$ ) when even frequency-equal spin triplet correlation (ETO-equal), i.e.,  $f_{\uparrow\uparrow}^E$  is greater than odd frequency equal spin triplet correlation (OTE-equal), i.e.,  $f_{\uparrow\uparrow}^O$ , there is a dip at  $\omega = 0$  in Fig. 3.10(a). In Figs. 3.9(b) and 3.10(b) we plot spin polarized LDOS as function of position  $x$  in both N ( $x < 0$ ) and S ( $x > 0$ ) regions. We notice that SPLDOS in N region shows nice periodic oscillations, while SPLDOS in S region ( $x > 0$ ) exhibits an oscillatory decay due to normal reflection. Next we analyze, possible relation

### 3. SPIN FLIP SCATTERING INDUCED ODD FREQUENCY EQUAL SPIN TRIPLET CORRELATIONS IN METAL-SUPERCONDUCTOR JUNCTION

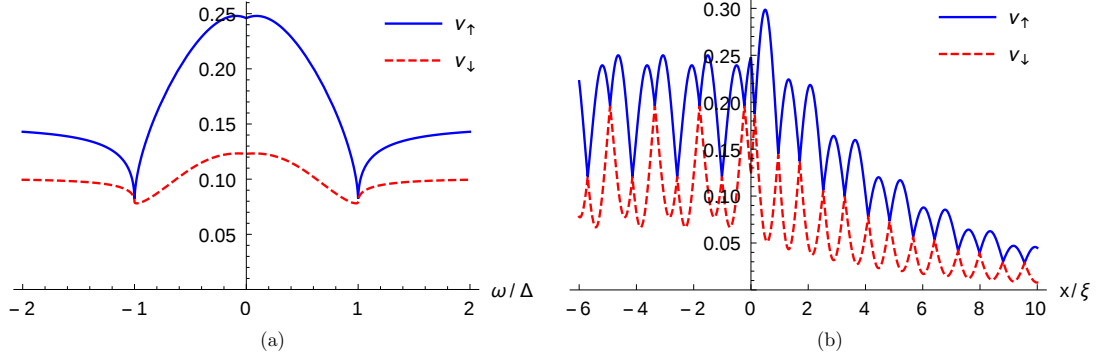


Figure 3.9: (a) Frequency dependence of SPLDOS at NS interface, (b) spatial dependence of the SPLDOS in N ( $x < 0$ ) and S ( $x > 0$ ) regions. Parameters are:  $S = 1/2$ ,  $f = f' = 1$ ,  $J = 1$ ,  $x = 0$  (for (a)),  $E_F = 10\Delta$ ,  $\omega = 0.1\Delta$  (for (b)).

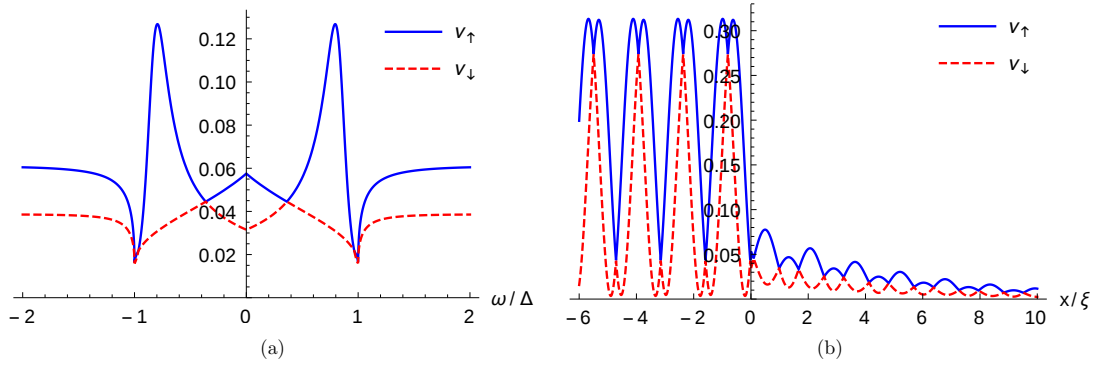


Figure 3.10: (a) Frequency dependence of SPLDOS at NS interface, (b) spatial dependence of the SPLDOS in N ( $x < 0$ ) and S ( $x > 0$ ) regions. Parameters are:  $S = 5/2$ ,  $f = f' = 3$ ,  $J = 1$ ,  $x = 0$  (for (a)),  $E_F = 10\Delta$ ,  $\omega = 0.1\Delta$  (for (b)).

between odd and even frequency pairing amplitudes with SPLDOS. SPLDOS in N region depends on normal reflection (see Eq. (3.41) for  $x < 0$ ), while even and odd frequency spin singlet as well as spin triplet correlations in N region depend only on Andreev reflection (see Eqs. (3.14), (3.15), (3.18), (3.19) for  $x < 0$ ). In S region, SPLDOS depends on both normal and Andreev reflection (see Eq. (3.41) for  $x > 0$ ), while only even frequency spin singlet correlations and odd frequency equal spin triplet correlations in S region depend on both normal and Andreev reflection (see Eqs. (3.14), (3.19) for  $x > 0$ ). In addition, since

SPLDOS is a local measurement, it is quite natural to analyze only local ( $x = x'$ ) odd and even frequency correlations. We see that only ESE and OTE-equal correlations survive at  $x = x'$ , see Eqs. (3.43) and (3.44) below,

$$f_0^{E,L}(x, \omega) = \begin{cases} -\frac{i\eta a_{12}}{2k_e} e^{-2ik^M x}, & \text{for } x < 0 \text{ (N region)} \\ \frac{\eta uv}{2i(u^2-v^2)} \left[ \frac{1}{k_e^S} + \frac{1}{k_h^S} \right] + \frac{\eta uv}{2i(u^2-v^2)} e^{-2\kappa x} \left[ \frac{b_{51} e^{2ik_F x}}{k_e^S} + \frac{b_{82} e^{-2ik_F x}}{k_h^S} \right] \\ + \frac{\eta}{2i(u^2-v^2)} e^{-2\kappa x} \frac{a_{81}(k_F + i\kappa(u^2-v^2))}{(k_F^2 + \kappa^2)}, & \text{for } x > 0 \text{ (S region)} \end{cases} \quad (3.43)$$

$$f_{\uparrow\uparrow}^{O,L}(x, \omega) = -f_{\downarrow\downarrow}^{O,L}(x, \omega) = \begin{cases} -\frac{i\eta a_{11}}{2k_e} e^{-2ik^M x}, & \text{for } x < 0 \text{ (N region)} \\ e^{-2\kappa x} \times \left[ \frac{\eta uv}{2i(u^2-v^2)} \left( \frac{b_{72} e^{-i2k_F x}}{k_h^S} - \frac{b_{61} e^{i2k_F x}}{k_e^S} \right) \right. \\ \left. - \frac{\eta}{2i(u^2-v^2)} \frac{a_{62}(k_F + i\kappa(u^2-v^2))}{(k_F^2 + \kappa^2)} \right], & \text{for } x > 0 \text{ (S region)}. \end{cases} \quad (3.44)$$

Since OSO and ETO-equal correlations are proportional to  $\sin[k_F(x - x')]$  as shown in Eqs. (3.15), (3.18), they vanish at  $x = x'$ . In Fig. 3.11 we present spatial dependence of local odd and even frequency correlations and spin-up LDOS in the N( $x < 0$ ) and S( $x > 0$ ) regions. In S region ( $x > 0$ ) both local odd frequency equal spin triplet correlation and spin-up LDOS show an exponential decay and a nice oscillatory behavior. But, in N region,  $x < 0$ , local odd and even frequency correlations are independent of position  $x$ , while spin-up LDOS exhibits a nice periodic oscillation. From Figs. 3.11(a) and 3.11(b), we also see that only local OTE-equal correlations show a nice oscillatory decay in the S region similar to spin-up LDOS. In contrast, local ESE correlations exhibit an oscillatory behavior without decay. Therefore, one is justified in associating only local odd frequency equal spin-triplet correlation with SPLDOS. By computing SPLDOS, we can extract the associated coefficients and calculate odd frequency equal spin-triplet correlations in the superconducting region of our junction. Consequently, a large SPLDOS indicates significant odd frequency equal spin-triplet pairing whose signature can be seen

### 3. SPIN FLIP SCATTERING INDUCED ODD FREQUENCY EQUAL SPIN TRIPLET CORRELATIONS IN METAL-SUPERCONDUCTOR JUNCTION

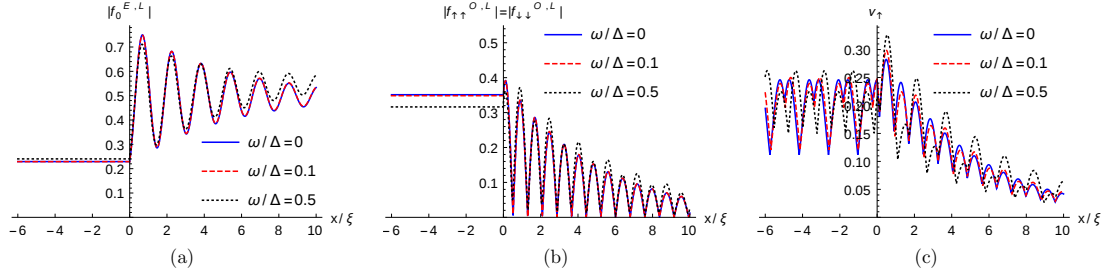


Figure 3.11: Spatial dependence of the (a) local even frequency correlations, (b) local odd frequency correlations and (c) spin-up LDOS in  $N$  and  $S$  regions. Parameters are:  $S = 1/2$ ,  $f = f' = 1$ ,  $J = 1$ ,  $E_F = 10\Delta$ .

experimentally.

Thus, in all three cases, LDOS is spin-polarized, or LMDOS is finite. In Table 3.1, we compare OTE-equal and OTE-mixed correlations along with LMDOS and SPLDOS seen in these three cases. We find that both OTE-equal and OTE-mixed correlations are finite,

Table 3.1: Comparison of OTE-equal, OTE-mixed, LMDOS and SPLDOS between three cases: both spin mixing and spin flip scattering, only spin mixing and, only spin flip scattering

	OTE-equal	OTE-mixed	LMDOS	SPLDOS	
				$\omega = 0$	$\omega \approx \pm\Delta$
Both spin mixing and spin flip scattering ( $F_1F_2S$ junction with misaligned magnetizations, Fig. 3.6)	Finite	Finite	Polarized in arbitrary direction with $\hat{x}$ , $\hat{y}$ , $\hat{z}$ components	Peak in spin-up LDOS and dip in spin-down LDOS (Fig. 3.7(c))	Dip in spin-up LDOS and peak in spin-down LDOS (Fig. 3.7(c))
Only spin mixing (NS junction with Rashba spin-orbit coupling (Ref. [89]) or FS junction)	Zero	Finite	Polarized in $z$ -direction	Peak in spin-up LDOS and dip in spin-down LDOS (Fig. 3.8(b))	Dip in spin-up LDOS and peak in spin-down LDOS (Fig. 3.8(b))
Only spin flip scattering (NS junction with spin flipper, Fig. 3.1)	Finite	Zero	Polarized in $x$ -direction	Peak in <b>both</b> spin-up LDOS and spin-down LDOS for low values of spin flip scattering (Fig. 3.9(a))	Dip in <b>both</b> spin-up LDOS and spin-down LDOS for low values of spin flip scattering (Fig. 3.9(a))

and LMDOS is polarized in an arbitrary direction when both spin mixing and spin-flip

scattering occur. When only spin mixing occurs, OTE-equal correlations vanish, but OTE-mixed correlations are finite with LMDOS polarized in  $z$ -direction. Finally, when only spin-flip scattering occurs, OTE-equal correlations are finite, but OTE-mixed correlations vanish with LMDOS polarized in  $x$ -direction.

### 3.7 Conclusion

In this chapter, we have studied the emergence of odd frequency equal spin-triplet correlations at the interface of an NS junction with a spin flipper. We have analytically calculated even and odd frequency spin-singlet and equal spin-triplet correlations using scattering Green's function approach. Interestingly, we have found that in the presence of spin-flip scattering, mixed spin-triplet pairing vanishes, and only spin-singlet and equal spin-triplet pairings exist in our setup. In our normal metal-spin flipper-superconductor junction, we have observed that pairing correlations in the normal metal region show a nice oscillatory behavior at zero temperature. In contrast, at finite temperature, they show an oscillatory decay. In superconducting region pairing correlations exhibit an oscillatory decay at both zero and finite temperatures. At low frequency and small values of spin-flip scattering, odd frequency equal spin-triplet correlations dominate over even frequency equal spin-triplet correlations in the superconducting region. It tallies with large values of the spin-polarized local density of states found for the same parameters. We have also compared our obtained results for normal metal-spin flipper-superconductor junction with results from other hybrid junctions wherein either only spin mixing or both spin mixing and spin-flip scattering occur. When only spin mixing occurs, odd frequency equal spin-triplet correlations vanish but odd frequency mixed spin-triplet correlations are finite with local magnetization density of state polarized in  $z$ -direction. When both spin mixing and spin-flip scattering occur, both

### 3. SPIN FLIP SCATTERING INDUCED ODD FREQUENCY EQUAL SPIN TRIPLET CORRELATIONS IN METAL-SUPERCONDUCTOR JUNCTION

---

odd frequency equal spin-triplet correlations and odd frequency mixed spin-triplet correlations are finite, and the local magnetization density of the state is polarized in an arbitrary direction. However, in the  $N - SF - S$  system, only spin-flip scattering is present, leading to finite odd frequency equal spin-triplet correlations with vanishing odd frequency mixed spin-triplet correlations and local magnetization density of state polarized in  $x$ -direction. Odd frequency equal and odd frequency mixed spin-triplet correlations can be effectively distinguished via the spin-polarized local density of states or local magnetization density of states.

# Chapter 4

## Spin-flip scattering induced tunable

## $0 - \pi$ Josephson junction and quantized

## anomalous phase in Ferromagnetic

## Josephson junction

*“In order to describe a particular subculture, you might want to portray people who are typical or representative of that subculture; but to dramatize it, to make it an interesting setting for a story, you want to bring someone anomalous into that setting, to see how she conforms to it, and it to her.”*

— Jonathan Dee

### 4.1 Introduction

Josephson junctions were introduced in chapter 1. They are generally of two types:  $0$  junction (when Free energy is minimum at zero phase difference across the left and right superconductors) and  $\pi$  junction (when Free energy is minimum at  $\pi$  phase difference

#### 4. SPIN-FLIP SCATTERING INDUCED TUNABLE $0 - \pi$ JOSEPHSON JUNCTION AND QUANTIZED ANOMALOUS PHASE IN FERROMAGNETIC JOSEPHSON JUNCTION

---

across the two superconductors).  $\pi$  junctions are in high demand as the basic building blocks of a quantum computer[118]. Tunable  $0 - \pi$  Josephson junctions have inherent potential applications as a cryogenic memory element[119], which is an essential component of a superconducting computer that would be much more energy-efficient than supercomputers[119, 120, 121] based on current semiconductor technology.

Interestingly, Josephson Free energy can sometimes be minimum at a phase difference  $\varphi_0$  ( $\neq 0$  or  $\pi$ ). The current-phase relation in such  $\varphi_0$ - Josephson junction's[122, 123, 124] satisfies  $I(\varphi) = I_c \sin(\varphi + \varphi_0)$ , i.e., there is a phase shift  $\varphi_0$  in the conventional current-phase relation. This suggests that Josephson current can flow even at zero phase difference ( $\varphi = 0$ ) between two superconducting electrodes[125, 126, 127, 128, 129]. This effect is known as anomalous Josephson effect (AJE), and the junction which shows this effect is called anomalous Josephson junction.  $I_{an} = I(0) = I_c \sin(\varphi_0)$  is referred to as anomalous Josephson current.

The physics behind the anomalous Josephson effect is naturally linked with the breaking of some symmetries of the system[130, 131]. One of them is time-reversal symmetry (TRS) and it implies  $I(-\varphi) = -I(\varphi)$ , which results in  $I(\varphi = 0)$  being zero. So, when the system preserves TRS, there is no anomalous current in the junction. However, breaking TRS is necessary but insufficient to produce anomalous Josephson current at  $\varphi = 0$ . For junctions with ferromagnetic coupling, TRS is broken, but there is no anomalous Josephson current[5, 82]. It implies some other symmetry is present in the system, which prevents the appearance of anomalous Josephson current at  $\varphi = 0$ . This symmetry is called chiral symmetry[132] which ensures that at  $\varphi = 0$  the tunneling amplitude relating electron tunneling from left superconductor to right superconductor is the same as the one related to tunneling in reverse, i.e., from right to the left superconductor. These leftward and rightward tunneling processes cancel each other, leading to vanishing current flow at  $\varphi = 0$ . Thus, to have



anomalous Josephson current at  $\varphi = 0$ , one needs to break both symmetries. Different ways have been suggested earlier to break these symmetries and generate anomalous Josephson current. These include Josephson junctions with conventional *s*-wave superconductors in the presence of both spin-orbit interaction and Zeeman field[133, 134], ferromagnetic Josephson junctions with non-coplanar magnetizations[127], SNS junctions with *s*-wave superconductors where N region is a normal magnetic metal[135, 136, 137], a quantum dot[138, 139] or a quantum point contact[140, 141]. Further, anomalous Josephson effect can also be found in systems with unconventional superconductors[142, 143, 144, 145, 146]. Experimentally,  $\varphi_0$  phase shift has been recently predicted in a Josephson junction-based nanowire quantum dot[147]. More interestingly, some Josephson junctions reveal the remarkable feature that the phase shift  $\varphi_0$  is accompanied by a direction-dependent critical current ( $I_{c+} \neq I_{c-}$ ), where  $I_{c+}$  and  $I_{c-}$  are the absolute values of maximum and minimum Josephson current respectively[148].

In this chapter, first, we show that a spin flipper sandwiched between two *s*-wave superconductors can transit from a 0 to  $\pi$  Josephson junction via tuning any one of the system parameters like interface transparency  $Z$ , the spin  $S$  or magnetic moment of the spin flipper or the exchange coupling  $J$ . Our motivation for looking at this setup stems from the fact that most of the  $\pi$  junction proposals depend on either ferromagnet or *d*-wave superconductor[149, 150] for their functioning. Integrating Ferromagnets into current superconductor circuit technology has not been easy. Controlling Ferromagnets is an onerous task. Further *d*-wave superconductors, in effect high  $T_c$  superconductors, also have a poor record of being integrated into current superconductor technology. This chapter obviates the need for any Ferromagnets or *d*-wave superconductors by implementing a Josephson  $\pi$  junction with a spin flipper. Second, we study the anomalous Josephson effect and the direction-dependent critical current in a junction consisting of two Ferromagnets with

#### 4. SPIN-FLIP SCATTERING INDUCED TUNABLE $0 - \pi$ JOSEPHSON JUNCTION AND QUANTIZED ANOMALOUS PHASE IN FERROMAGNETIC JOSEPHSON JUNCTION

misaligned magnetizations and a spin flipper sandwiched between two  $s$ -wave superconductors. This system acts as a quantized phase battery that can supply anomalous current even at zero phase difference. The main advantage of our system over other proposals involving anomalous Josephson current is that our system can store quantized amounts of phase  $\varphi_0$  in the ground state of junction. The reason we are interested in  $\varphi_0$  Josephson junction is because of the various applications of such junctions in phase qubits[151], superconducting computer memory components[152], superconducting phase batteries[153] and in rectifiers[140].

### 4.2 SNS junction in presence of a spin flipper

We consider a junction of two normal metals with a spin flipper sandwiched between two conventional  $s$ -wave singlet superconductors, as shown in Fig. 4.1. There are normal metal regions in  $-a/2 < x < 0$  and  $0 < x < a/2$  and a spin flipper at  $x = 0$  and two superconductors at  $x < -a/2$  and  $x > a/2$ . The above model for a spin flipper in

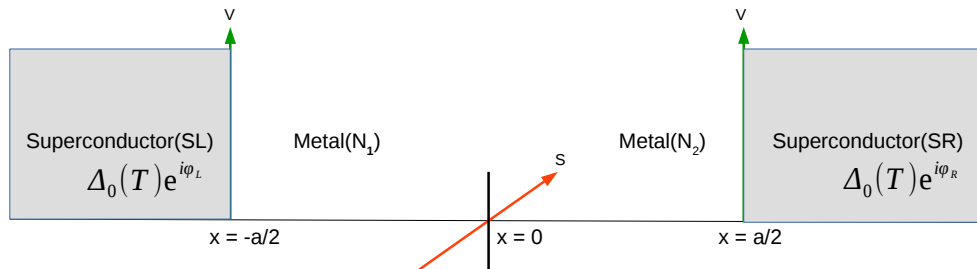


Figure 4.1: Josephson junction composed of two normal metals and a spin flipper with spin  $S$  and magnetic moment  $m'$  at  $x = 0$  sandwiched between two  $s$ -wave superconductors.

a Josephson junction matches quite well with solid-state scenarios such as seen in 1D

quantum wires or graphene with an embedded magnetic impurity or quantum dot[14, 54]. The model Hamiltonian in BdG formalism of our system is a  $4 \times 4$  matrix which is given below:

$$\begin{pmatrix} H\hat{I} & i\Delta\hat{\sigma}_y \\ -i\Delta^*\hat{\sigma}_y & -H\hat{I} \end{pmatrix}\Psi(x) = E\Psi(x), \quad (4.1)$$

$H = p^2/2m^* + V[\delta(x + a/2) + \delta(x - a/2)] - J_0\delta(x)\vec{s}\cdot\vec{S} - E_F$ , here  $p^2/2m^*$  is the kinetic energy of an electron with effective mass  $m^*$ ,  $V$  is the strength of the  $\delta$  potential at the interfaces between normal metal and superconductor,  $J_0$  is the strength of exchange interaction between the electron/hole with spin  $\vec{s}$  and a spin flipper with spin  $\vec{S}$ . Further,  $\Psi$  is a four-component spinor,  $\hat{\sigma}$  is Pauli spin matrix and  $\hat{I}$  is  $2 \times 2$  unit matrix,  $E_F$  being Fermi energy. The superconducting gap parameters  $\Delta$  for left and right superconductor, are assumed to have the same magnitude but different phases  $\varphi_L$  and  $\varphi_R$  and are given by  $\Delta = \Delta_0(T)[e^{i\varphi_L}\Theta(-x - a/2) + e^{i\varphi_R}\Theta(x - a/2)]$ ,  $\Theta(x)$  is the Heaviside step function,  $\Delta_0(T)$  is temperature dependent gap parameter and it follows  $\Delta_0(T) = \Delta_0 \tanh(1.74\sqrt{(T_c/T) - 1})$ , where  $T_c$ - the superconducting critical temperature[24] for a widely used  $s$ -wave superconductor like lead is 7.2K. If we diagonalize BdG Hamiltonian (Eq. (4.1)), we get the wavefunctions in different regions of our system for electron/hole-like quasiparticle incidence. There can be eight different types of quasiparticle injection into our system: an electron-like quasiparticle (ELQ) with spin up or down or a hole-like quasiparticle (HLQ) with spin up or down injected from either the left or from the right superconducting electrode. For injection of spin up ELQ from left superconductor, the wave function is given by[27]-

$$\psi_{SL}(x) = \varphi_1^{SL} e^{iq_+x} \phi_{m'+r}^S \uparrow \uparrow \varphi_1^{SL} e^{-iq_+x} \phi_{m'+r}^S \downarrow \downarrow \varphi_2^{SL} e^{-iq_+x} \phi_{m'+1}^S \uparrow \uparrow \varphi_3^{SL} e^{iq_-x} \phi_{m'+1}^S \downarrow \downarrow \varphi_4^{SL} e^{iq_-x} \phi_{m'}^S, \text{ for } x < -\frac{a}{2}, \quad (4.2)$$

#### 4. SPIN-FLIP SCATTERING INDUCED TUNABLE $0 - \pi$ JOSEPHSON JUNCTION AND QUANTIZED ANOMALOUS PHASE IN FERROMAGNETIC JOSEPHSON JUNCTION

where  $\varphi_1^{SL} = \begin{pmatrix} u \\ 0 \\ 0 \\ v \end{pmatrix}$ ,  $\varphi_2^{SL} = \begin{pmatrix} 0 \\ u \\ -v \\ 0 \end{pmatrix}$ ,  $\varphi_3^{SL} = \begin{pmatrix} 0 \\ -v \\ u \\ 0 \end{pmatrix}$  and,  $\varphi_4^{SL} = \begin{pmatrix} v \\ 0 \\ 0 \\ u \end{pmatrix}$ . The amplitudes  $r_{ee}^{\uparrow\uparrow}, r_{ee}^{\uparrow\downarrow}, r_{eh}^{\uparrow\uparrow}, r_{eh}^{\uparrow\downarrow}$

represent normal reflection without flip, normal reflection with spin flip, Andreev reflection with spin flip and Andreev reflection without flip respectively.

The corresponding wave function in the right superconductor is-

$$\psi_{SR}(x) = t_{ee}^{\uparrow\uparrow} \varphi_1^{SR} e^{iq_+x} \phi_{m'}^S + t_{ee}^{\uparrow\downarrow} \varphi_2^{SR} e^{iq_+x} \phi_{m'+1}^S + t_{eh}^{\uparrow\uparrow} \varphi_3^{SR} e^{-iq_-x} \phi_{m'+1}^S + t_{eh}^{\uparrow\downarrow} \varphi_4^{SR} e^{-iq_-x} \phi_{m'}^S, \text{ for } x > \frac{a}{2}, \quad (4.3)$$

where  $\varphi_1^{SR} = \begin{pmatrix} ue^{i\varphi} \\ 0 \\ 0 \\ v \end{pmatrix}$ ,  $\varphi_2^{SR} = \begin{pmatrix} 0 \\ ue^{i\varphi} \\ -v \\ 0 \end{pmatrix}$ ,  $\varphi_3^{SR} = \begin{pmatrix} 0 \\ -ve^{i\varphi} \\ u \\ 0 \end{pmatrix}$ ,  $\varphi_4^{SR} = \begin{pmatrix} ve^{i\varphi} \\ 0 \\ 0 \\ u \end{pmatrix}$  and,  $t_{ee}^{\uparrow\uparrow}, t_{ee}^{\uparrow\downarrow}, t_{eh}^{\uparrow\uparrow}, t_{eh}^{\uparrow\downarrow}$

are the transmission amplitudes, corresponding to the reflection process described above and  $\varphi = \varphi_R - \varphi_L$  is the phase difference between right side and left side superconductor.

The BCS coherence factors are defined as  $u = \sqrt{\frac{1}{2} \left( 1 + \frac{\sqrt{E^2 - |\Delta|^2}}{E} \right)}$ ,  $v = \sqrt{\frac{1}{2} \left( 1 - \frac{\sqrt{E^2 - |\Delta|^2}}{E} \right)}$ .

$q_{\pm} = \sqrt{\frac{2m^*}{\hbar^2} (E_F \pm \sqrt{E^2 - |\Delta|^2})}$  is the wavevector for electron-like quasiparticle ( $q_+$ ) and hole-like quasiparticle ( $q_-$ ) in the left and right superconducting wavefunctions,  $\psi_{SL}$  and  $\psi_{SR}$ . The wavefunction in the normal metal region ( $N_1$ ) is given by-

$$\begin{aligned} \psi_{N_1}(x) = & (e_N e^{ik_e(x+a/2)} + f_N e^{-ik_e x}) \varphi_1^N \phi_{m'}^S + (e'_N e^{ik_e(x+a/2)} + f'_N e^{-ik_e x}) \varphi_2^N \phi_{m'+1}^S \\ & + (g_N e^{-ik_h(x+a/2)} + h_N e^{ik_h x}) \varphi_3^N \phi_{m'+1}^S + (g'_N e^{-ik_h(x+a/2)} + h'_N e^{ik_h x}) \varphi_4^N \phi_{m'}^S, \text{ for } -\frac{a}{2} < x < 0. \end{aligned} \quad (4.4)$$

Similarly the wavefunction in the normal metal region ( $N_2$ ) is given by-

$$\begin{aligned} \psi_{N_2}(x) = & (a_N e^{ik_e x} + b_N e^{-ik_e(x-a/2)}) \varphi_1^N \phi_{m'}^S + (a'_N e^{ik_e x} + b'_N e^{-ik_e(x-a/2)}) \varphi_2^N \phi_{m'+1}^S \\ & + (c_N e^{-ik_h x} + d_N e^{ik_h(x-a/2)}) \varphi_3^N \phi_{m'+1}^S + (c'_N e^{-ik_h x} + d'_N e^{ik_h(x-a/2)}) \varphi_4^N \phi_{m'}^S, \text{ for } 0 < x < \frac{a}{2}, \end{aligned} \quad (4.5)$$

## 4.2. SNS junction in presence of a spin flipper

where  $\varphi_i^N$ ,  $i = 1, 2, 3, 4$  are as defined in section 1.3 of chapter 1.  $k_{e,h} = \sqrt{\frac{2m^*}{\hbar^2}(E_F \pm E)}$  are the wave vector in normal metals. We use Andreev approximation[25]  $q_+ = q_- = k_F$  and  $k_{e,h} \approx k_F \pm \frac{k_F E}{2E_F}$ , where  $k_F$  is Fermi wavevector, with  $E_F \gg |\Delta|$ .

The boundary conditions at  $x = -a/2$  are,

$$\psi_{SL}(x) = \psi_{N_1}(x), \quad \frac{d\psi_{N_1}}{dx} - \frac{d\psi_{SL}}{dx} = \frac{2m^*V}{\hbar^2}\psi_{N_1}, \quad (4.6)$$

and at  $x = 0$  are,

$$\psi_{N_1}(x) = \psi_{N_2}(x), \quad \frac{d\psi_{N_2}}{dx} - \frac{d\psi_{N_1}}{dx} = -\frac{2m^*J_0\vec{s}\cdot\vec{S}}{\hbar^2}\psi_{N_1}. \quad (4.7)$$

Finally, at  $x = a/2$  are,

$$\psi_{N_2}(x) = \psi_{SR}(x), \quad \frac{d\psi_{SR}}{dx} - \frac{d\psi_{N_2}}{dx} = \frac{2m^*V}{\hbar^2}\psi_{N_2}. \quad (4.8)$$

We will later use the dimensionless parameter  $J = \frac{m^*J_0}{k_F}$  as a measure of strength of exchange interaction and  $Z = \frac{m^*V}{\hbar^2k_F}$  as a measure of interface transparency. By imposing boundary conditions on the wavefunctions, one can get the different scattering amplitudes. The wave functions for the other seven types of quasiparticle injection processes are formulated in the same way.

### 4.2.1 Josephson current in presence of a spin flipper

#### Total Josephson current

Using the generalized version of Furusaki-Tsukuda formalism[30] we can calculate the total DC Josephson current-

$$I_T(\varphi) = \frac{e\Delta_0(T)}{2\beta\hbar} \frac{1}{2\pi} \int_0^{2\pi} \sum_{\omega_n} \frac{q_+(\omega_n) + q_-(\omega_n)}{\Omega_n} \times \left[ \frac{a_1(\omega_n) - a_2(\omega_n)}{q_+(\omega_n)} + \frac{a_3(\omega_n) - a_4(\omega_n)}{q_-(\omega_n)} \right] d(k_F a), \quad (4.9)$$

#### 4. SPIN-FLIP SCATTERING INDUCED TUNABLE $0 - \pi$ JOSEPHSON JUNCTION AND QUANTIZED ANOMALOUS PHASE IN FERROMAGNETIC JOSEPHSON JUNCTION

---

herein  $\omega_n = (2n + 1)\pi/\beta$  are fermionic Matsubara frequencies with  $n = 0, \pm 1, \pm 2, \dots$  and  $\Omega_n = \sqrt{\omega_n^2 + \Delta_0^2(T)}$ .  $k_F a$  is the phase accumulated in normal metal region.  $\beta = 1/(k_B T)$ ,  $k_B$  is Boltzmann constant, and  $T$  is temperature.  $q_+(\omega_n)$ ,  $q_-(\omega_n)$ , and  $a_i(\omega_n)$  are obtained from  $q_+$ ,  $q_-$  and  $a_i$  by analytically continuing  $E$  to  $i\omega_n$ . Here  $a_i$  ( $i = 1, 2, 3, 4$ ) with  $a_1 = r_{eh}^{\uparrow\downarrow}$  is Andreev reflection amplitude without flip for spin-up ELQ, incident from left superconductor, similarly  $a_2 = r_{eh}^{\downarrow\uparrow}$  is Andreev reflection amplitude without flip for spin-down ELQ, incident from left superconductor,  $a_3 = r_{he}^{\uparrow\downarrow}$  and  $a_4 = r_{he}^{\downarrow\uparrow}$  are Andreev reflection amplitudes without flip for spin-up HLQ and spin-down HLQ incident from left superconductor respectively. There are other ways of writing Josephson supercurrent formula in Furusaki-Tsukuda approach[27, 154], all such ways give identical total Josephson current. These different ways involve different scattering amplitudes, as due to the fact that Furusaki-Tsukuda procedure obeys both detailed balance as well as probability conservation, allowing for the possibility of different representations of the same formula. We sum over the Matsubara frequencies numerically. The detailed balance conditions[30] are verified as follows:

$$\frac{a_1(-\varphi, E)}{q_+} = \frac{a_4(\varphi, E)}{q_-}, \quad \frac{a_2(-\varphi, E)}{q_+} = \frac{a_3(\varphi, E)}{q_-} \quad \text{and} \quad b_i(-\varphi, E) = b_i(\varphi, E),$$

where  $b_i$  ( $i = 1, 2, 3, 4$ ) with  $b_1 = r_{ee}^{\uparrow\uparrow}$  is normal reflection amplitude without flip for spin-up ELQ, incident from left superconductor, similarly  $b_2 = r_{ee}^{\downarrow\downarrow}$  is normal reflection amplitude without flip for spin-down ELQ, incident from left superconductor,  $b_3 = r_{hh}^{\uparrow\uparrow}$  and  $b_4 = r_{hh}^{\downarrow\downarrow}$  are normal reflection amplitudes without flip for spin-up HLQ and spin-down HLQ incident from left superconductor respectively.

#### **Bound state contribution**

Neglecting the contribution from incoming quasiparticle[27] and inserting the wave function into the boundary conditions, we get a homogeneous system of 24 linear equations

## 4.2. SNS junction in presence of a spin flipper

for the scattering amplitudes. If we express the scattering amplitudes in the two normal metal regions by the scattering amplitudes in the left and right superconductor we get a homogeneous system of 8 linear equations[24],

$$Mx = 0, \quad (4.10)$$

where  $x$  is a  $8 \times 1$  column matrix, given by  $x = [r_{ee}^{\uparrow\uparrow}, r_{ee}^{\uparrow\downarrow}, r_{eh}^{\uparrow\uparrow}, r_{eh}^{\uparrow\downarrow}, t_{ee}^{\uparrow\uparrow}, t_{ee}^{\uparrow\downarrow}, t_{eh}^{\uparrow\uparrow}, t_{eh}^{\uparrow\downarrow}]^T$  and  $M$  is a  $8 \times 8$  matrix which is explicitly written in Appendix B. For a nontrivial solution of this system of equations,  $\det M = 0$ , we can get a relation between the Andreev bound state energy and phase difference, i.e., Andreev levels with dispersion  $E_i, i = \{1, \dots, 4\}$ [155]. We find that  $E_i(\varphi) = E_{\sigma}^{\pm}(\varphi) = \pm E_{\sigma}(\varphi)$ , ( $\sigma = \uparrow, \downarrow$ ) and

$$E_{\sigma}^{\pm}(\varphi) = \pm \Delta_0(T) \sqrt{\frac{|A(\varphi)| + \rho_{\sigma} \sqrt{|B(\varphi)|}}{2|C|}}, \quad (4.11)$$

wherein  $\rho_{\uparrow(\downarrow)} = +1(-1)$  and  $A(\varphi), B(\varphi), C$  depend on all junction parameters. Their explicit form is given in Appendix B. For simplicity we have taken all wavevectors equal to the Fermi wavevector (Andreev approximation). For transparent regime ( $Z = 0$ ) we find-

$$\begin{aligned} E_{\sigma}^{\pm}(\varphi) = \pm \frac{\Delta_0(T)}{\sqrt{2}} & (\sqrt{((2(8 + J^4(f^2 + m' + m'^2)^2 + J^2(3 + 2f^2 + 6m'(1 + m')) + (8 + J^2(1 - 2f^2 + 2m'(1 + m')))) \cos(\varphi))} \\ & + \rho_{\sigma} \sqrt{(2J^2(64f^4J^2 + 3(J + 2Jm')^2 + 4f^2(16 + J^2(5 + 4m'(1 + m')))) + 4J^2(-4f^2 + 16f^4 - (1 + 2m')^2) \cos(\varphi) \\ & + ((J + 2Jm')^2 - 4f^2(16 + (J + 2Jm')^2)) \cos(2\varphi))}) / (16 + J^4(f^2 + m' + m'^2)^2 + J^2(4 + 8f^2 + 8m'(1 + m')))) \end{aligned} \quad (4.12)$$

For  $Z = 0$ , interestingly the bound states are independent of any phase ( $k_F a$ ) accumulated in normal metal region. For tunneling regime ( $Z \rightarrow Large$ ) we get-

$$E_{\sigma}^{\pm}(\varphi) = \pm \Delta_0(T) \left[ 1 + \frac{(8 + J^2(1 - 2f^2 + 2m'(1 + m')) + (8 + J^2(-1 + 2f^2 - 2m'(1 + m')))) \cos(k_F a) \cos(\varphi)}{16Z^4 \sin(\frac{k_F a}{2})^2 (4 - J^2(f^2 + m' + m'^2) + (4 + J^2(f^2 + m' + m'^2)) \cos(k_F a) + 2J \sin(k_F a))^2} \right]. \quad (4.13)$$

#### 4. SPIN-FLIP SCATTERING INDUCED TUNABLE $0 - \pi$ JOSEPHSON JUNCTION AND QUANTIZED ANOMALOUS PHASE IN FERROMAGNETIC JOSEPHSON JUNCTION

For  $Z \rightarrow \text{Large}$ , we can clearly say that bound states are phase ( $k_F a$ ) dependent. From Andreev bound states energies Eq. (4.11) we can derive the Josephson bound state current[19]-

$$I_B(\varphi) = \frac{2e}{\hbar} \frac{1}{2\pi} \int_0^{2\pi} \sum_i f(E_i) \frac{dE_i}{d\varphi} d(k_F a) = -\frac{2e}{\hbar} \frac{1}{2\pi} \int_0^{2\pi} \sum_{\sigma} \tanh\left(\frac{\beta E_{\sigma}}{2}\right) \frac{dE_{\sigma}}{d\varphi} d(k_F a), \quad (4.14)$$

wherein  $e$  is electronic charge and  $f(E_i)$  denotes Fermi-Dirac distribution function. For transparent regime ( $Z = 0$ ) we obtain the current-phase relation,

$$\frac{I_B(\varphi)}{I_0} = \frac{\Delta_0(T) \sin(\varphi) ((C_1 + C_2) \frac{1}{E_{\downarrow}} \tanh\left(\frac{\beta E_{\downarrow}}{2}\right) - (C_1 - C_2) \frac{1}{E_{\uparrow}} \tanh\left(\frac{\beta E_{\uparrow}}{2}\right))}{C_3}, \quad (4.15)$$

$$\begin{aligned} \text{where, } C_1 &= ((\sqrt{2}J^4(4f^2 - 16f^4 + (1 + 2m')^2) + \sqrt{2}J^2(4f^2(16 + (J + 2Jm')^2) - (J + 2Jm')^2) \cos(\varphi)), \\ C_2 &= (8 + J^2 - 2J^2f^2 + 2J^2m'(1 + m'))\sqrt{(J^2(64f^4J^2 + 3(J + 2Jm')^2 + 4f^2(16 + J^2(5 + 4m'(1 + m'))))} \\ &\quad + 4J^2(-4f^2 + 16f^4 - (1 + 2m')^2) \cos(\varphi) + ((J + 2Jm')^2 - 4f^2(16 + (J + 2Jm')^2)) \cos(2\varphi)), \\ C_3 &= ((16 + J^4(f^2 + m' + m'^2)^2 + J^2(4 + 8f^2 + 8m'(1 + m')))\sqrt{(J^2(64f^4J^2 + 3(J + 2Jm')^2 + 4f^2(16 \\ &\quad + J^2(5 + 4m'(1 + m')))) + 4J^2(-4f^2 + 16f^4 - (1 + 2m')^2) \cos(\varphi) + ((J + 2Jm')^2 - 4f^2(16 + (J \\ &\quad + 2Jm')^2)) \cos(2\varphi)))). \end{aligned}$$

In Eq. (4.15),  $I_0 = e\Delta_0/\hbar$  and  $E_{\uparrow(\downarrow)}$  are given in Eq. (4.11). For tunneling regime ( $Z \rightarrow \text{Large}$ ) and at zero temperature, we find,

$$\frac{I_B(\varphi)}{I_0} = \frac{1}{2\pi} \int_0^{2\pi} \left[ \frac{(8 + J^2(1 - 2f^2 + 2m'(1 + m')) + (8 + J^2(-1 + 2f^2 - 2m'(1 + m')) \cos(k_F a)) \sin(\varphi)) \sin(\varphi)}{4Z^4 \sin(\frac{k_F a}{2})^2 (4 - J^2(f^2 + m' + m'^2) + (4 + J^2(f^2 + m' + m'^2)) \cos(k_F a) + 2J \sin(k_F a))^2} \right] d(k_F a). \quad (4.16)$$

#### Continuum contribution

The continuum contribution to Josephson current is a sum of currents carried by ELQ and HLQ outside the gap. Using formalism, developed earlier in Refs. [29, 156] the continuum contribution from ELQ is given below[29]

$$I_C^e(\varphi) = \frac{2e}{\hbar} \frac{1}{2\pi} \int_0^{2\pi} \left\{ \left( \int_{-\infty}^{-|\Delta|} + \int_{|\Delta|}^{\infty} \right) \frac{1}{|u^2 - v^2|} \times [T_{L \rightarrow R}^{e\uparrow\uparrow}(E, \varphi) + T_{L \rightarrow R}^{e\uparrow\downarrow}(E, \varphi) - T_{L \leftarrow R}^{e\uparrow\uparrow}(E, \varphi) - T_{L \leftarrow R}^{e\uparrow\downarrow}(E, \varphi)] f(E) dE \right\} d(k_F a). \quad (4.17)$$



Similarly continuum contribution from HLQ can be calculated by replacing ' $e$ ' in Eq. (4.17) with ' $h$ '. In Eq. (4.17)  $T_{L \rightarrow R}^{e \uparrow \uparrow} = |t_{ee}^{\uparrow \uparrow}|^2 - |t_{eh}^{\uparrow \uparrow}|^2$ , is transmission without flip for ELQ currents moving from left to right of the system as depicted in Fig. 4.1.  $T_{L \rightarrow R}^{e \uparrow \downarrow} = |t_{ee}^{\uparrow \downarrow}|^2 - |t_{eh}^{\uparrow \downarrow}|^2$  is transmission with flip for ELQ currents moving from left to right of the system and similarly  $T_{L \leftarrow R}^{e \uparrow \uparrow}$  and  $T_{L \leftarrow R}^{e \uparrow \downarrow}$  are transmission without flip and with flip for ELQ currents moving from right to left of the system respectively. Here we have,

$$T_{L \leftarrow R}^{e \uparrow \uparrow}(E, \varphi) = T_{L \rightarrow R}^{e \uparrow \uparrow}(E, -\varphi), \quad T_{L \leftarrow R}^{e \uparrow \downarrow}(E, \varphi) = T_{L \rightarrow R}^{e \uparrow \downarrow}(E, -\varphi).$$

The continuum contribution from HLQ is found to be equal to the ELQ continuum contribution. Therefore, the total continuum current due to ELQ and HLQ is given as,

$$I_C(\varphi) = \frac{I_C^e(\varphi) + I_C^h(\varphi)}{2} = I_C^e(\varphi). \quad (4.18)$$

We have verified the total current conservation:  $I_T(\varphi) = I_B(\varphi) + I_C(\varphi)$ .

## 4.2.2 Andreev bound states

The Andreev bound states (ABS) as obtained in Eq. (4.11) are analyzed in this subsection. We focus on the role of spin  $S$  and magnetic moment  $m'$  of the spin flipper on ABS. In Fig. 4.2(a), we plot ABS for  $S = 1/2$  and  $m' = 1/2$ , as here the spin flip probability  $f = \sqrt{(S - m')(S + m' + 1)} = 0$  which corresponds to no flip, we get only two bound states, but in Fig. 4.2(b) with  $S = 1/2$  and  $m' = -1/2$ ,  $f \neq 0$  thus due to spin flip processes we get four bound states. In Fig. 4.2(b) we see that two bound state energies touch at phase difference  $\varphi = 0.72\pi$  and  $\varphi = 1.29\pi$ . Andreev bound states do not cross but they are degenerate at those  $\varphi$  values. In Josephson junctions where either spin-flip scattering (S-N<sub>1</sub>-SF-N<sub>2</sub>-S junction) or spin mixing (S-F-S junction) is present two bound state energies can touch, however in case of SNS junction where neither spin-flip scattering

#### 4. SPIN-FLIP SCATTERING INDUCED TUNABLE $0 - \pi$ JOSEPHSON JUNCTION AND QUANTIZED ANOMALOUS PHASE IN FERROMAGNETIC JOSEPHSON JUNCTION

nor spin mixing is present, two bound state energies cross, see Fig. 1.14. To address the situation of large spin  $S$  in spin flipper in Fig. 4.3 we plot ABS for  $S = 9/2$  and all allowed  $m'$  values. For particular  $S$ , as  $m'$  changes, the separation between the electron (positive)

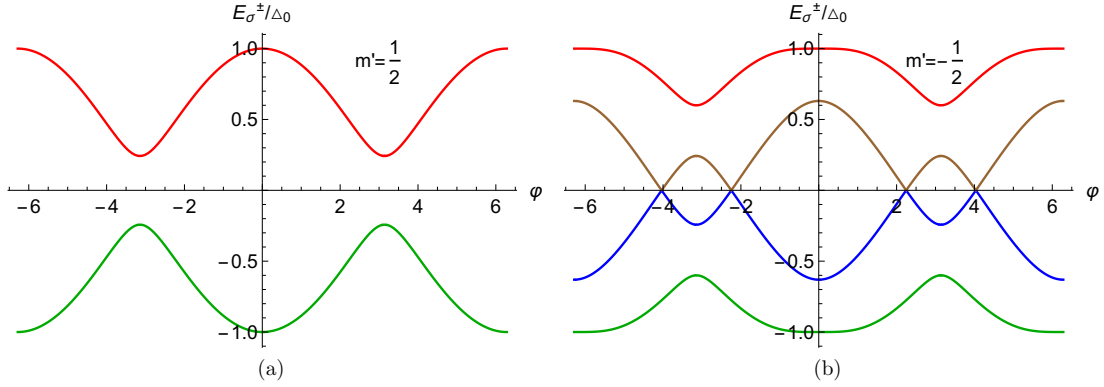


Figure 4.2: Andreev bound states as a function of phase difference ( $\varphi$ ). Parameters are  $\Delta_0 = 1\text{meV}$ ,  $S = 1/2$ ,  $m' = \pm 1/2$ ,  $J = 1$ ,  $Z = 0$ ,  $T/T_c = 0.01$ .

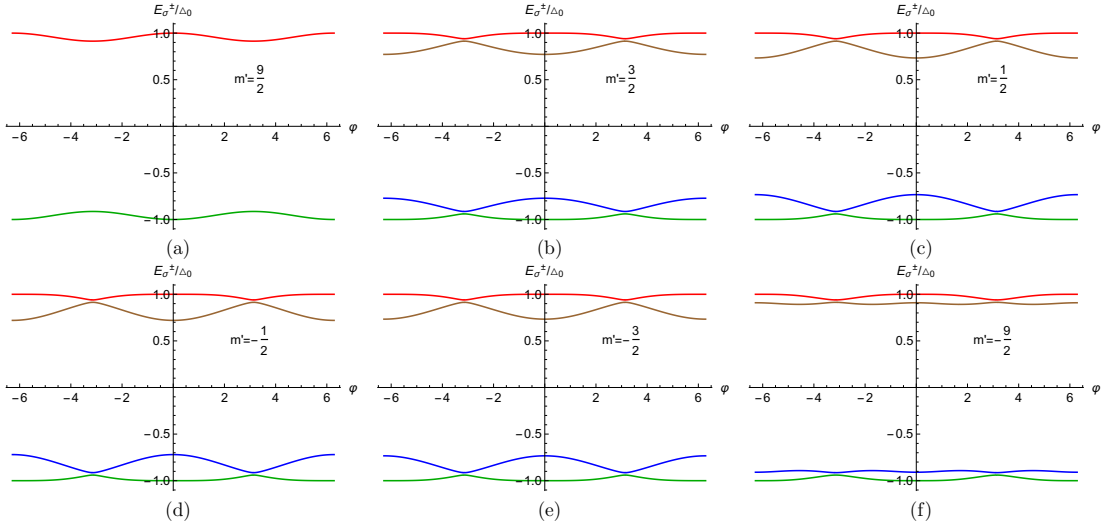


Figure 4.3: Andreev bound states as a function of phase difference ( $\varphi$ ). Parameters are  $\Delta_0 = 1\text{meV}$ ,  $S = 9/2$ ,  $m' = \pm 1/2, \pm 3/2, \pm 9/2$ ,  $J = 1$ ,  $Z = 0$ ,  $T/T_c = 0.01$ .

bound states and hole (negative) bound states increases. Similarly, for particular  $m'$ , as we

change  $S$ , this separation increases. For large  $S$ , ABS lie at the gap edge. It is seen for large  $m'$  as well. This behavior is also seen as one changes  $J$ ,  $Z$  as well. We only plot ABS for  $m' = \pm 1/2, \pm 3/2, \pm 9/2$ , but we do not plot for  $m' = \pm 5/2, \pm 7/2$  because the separation between electron bound states and hole bound states increases from  $m' = 3/2$  to  $m' = 9/2$  and these  $m'$  values lie between  $m' = 3/2$  and  $m' = 9/2$ . Large  $S$ ,  $m'$ ,  $Z$ ,  $J$  lead to ABS shifting to gap edge.

### 4.2.3 Josephson current: $\pi$ junction behavior

The considered model (Fig. 4.1) shows  $\pi$  junction behavior. To see this, we plot the bound state, continuum, and total Josephson currents for spin-flipper spin  $S = 1/2$  (Fig. 4.4) and  $S = 9/2$  (Fig. 4.5). We choose the transparent regime ( $Z = 0$ ) case. A separate subsection will be devoted to the effect of tunnel contacts. One can conclude that continuum contribution to the total current is negligible. Therefore bound state current and total current are almost the same. In Fig. 4.4(a), as there is no flip, we have a 0 junction. The Josephson current changes sign in the  $0 < \varphi < \pi$  regime for the spin-flip case. In Fig. 4.5 we

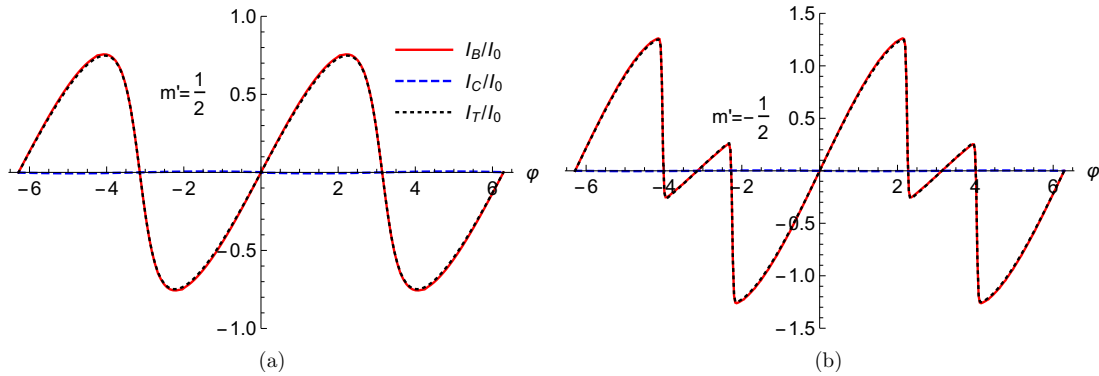


Figure 4.4: The bound, continuum and total Josephson current as a function of phase difference ( $\varphi$ ). Parameters are  $\Delta_0 = 1\text{meV}$ ,  $T/T_c = 0.01$ ,  $S = 1/2$ ,  $m' = \pm 1/2$ ,  $J = 1$ ,  $Z = 0$ .

deal with the high spin ( $S = 9/2$ ) value of the spin flipper. Here, also we see that for

#### 4. SPIN-FLIP SCATTERING INDUCED TUNABLE $0 - \pi$ JOSEPHSON JUNCTION AND QUANTIZED ANOMALOUS PHASE IN FERROMAGNETIC JOSEPHSON JUNCTION

$m' = 5/2, 3/2, 1/2, -1/2, -3/2, -5/2, -7/2$  we get  $\pi$  junction. But for  $m' = 9/2, 7/2, -9/2$  we get  $0$  junction. So, here too, there is a switching from  $0$  to  $\pi$  and again from  $\pi$  to  $0$  with the change of  $m'$  from  $9/2$  to  $-9/2$ . **One can safely conclude that all  $\pi$  shifts are due to spin-flip scattering ( $\mathbf{f} \neq 0$ ), but the reverse is not necessarily true.** This  $\pi$ -junction state has been studied earlier in Ref. [157] with spin-active normal metal superconductor (NS) interfaces, but they did not consider any high spin magnetic impurity. Their system shows a  $0 - \pi$  transition as a function of the kinematic phase, misorientation angle, and temperature.

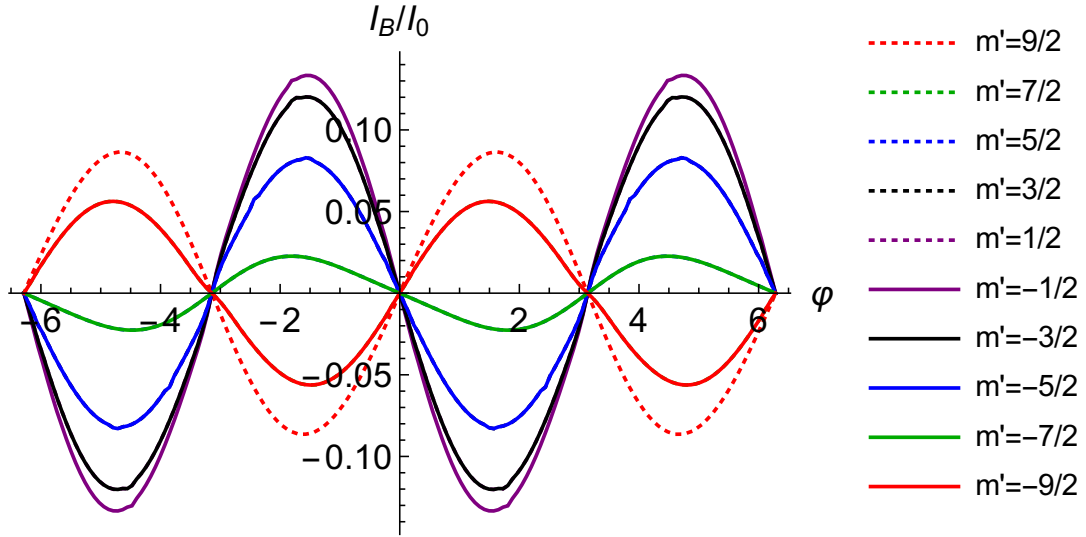


Figure 4.5: *Josephson supercurrent as a function of phase difference ( $\varphi$ ). Parameters are  $\Delta_0 = 1\text{meV}$ ,  $T/T_c = 0.01$ ,  $S = 9/2$ ,  $m' = \pm 9/2, \pm 7/2, \pm 5/2, \pm 3/2, \pm 1/2$ ,  $J = 1$ ,  $Z = 0$ . Josephson supercurrent for  $m' = 7/2$  and  $m' = -9/2$  are same and similarly for  $m' = 5/2$  and  $m' = -7/2$ ,  $m' = 3/2$  and  $m' = -5/2$ ,  $m' = 1/2$  and  $m' = -3/2$  are same.*

#### 4.2.4 Josephson current in long junction limit

There are eight different types of quasiparticle injection into our system: an electron-like quasiparticle (ELQ) with spin up or down or a hole-like quasiparticle (HLQ) with spin up or down injected from either the left or from the right superconducting electrode. Following

## 4.2. SNS junction in presence of a spin flipper

the procedure established in section 4.2, we write the wavefunction for the injection of spin up ELQ in left side superconductor as-

$$\psi_{SL}(x) = \varphi_1^{SL} e^{iq+x} \phi_{m'}^S + r_{ee}^{\uparrow\uparrow} \varphi_1^{SL} e^{-iq+x} \phi_{m'}^S + r_{ee}^{\uparrow\downarrow} \varphi_2^{SL} e^{-iq+x} \phi_{m'+1}^S + r_{eh}^{\uparrow\uparrow} \varphi_3^{SL} e^{iq-x} \phi_{m'+1}^S + r_{eh}^{\uparrow\downarrow} \varphi_4^{SL} e^{iq-x} \phi_{m'}^S, \text{ for } x < -\frac{a}{2}. \quad (4.19)$$

Similarly the corresponding wave function for right side superconductor is-

$$\psi_{SR}(x) = t_{ee}^{\uparrow\uparrow} \varphi_1^{SR} e^{iq+x} \phi_{m'}^S + t_{ee}^{\uparrow\downarrow} \varphi_2^{SR} e^{iq+x} \phi_{m'+1}^S + t_{eh}^{\uparrow\uparrow} \varphi_3^{SR} e^{-iq-x} \phi_{m'+1}^S + t_{eh}^{\uparrow\downarrow} \varphi_4^{SR} e^{-iq-x} \phi_{m'}^S, \text{ for } x > \frac{a}{2}. \quad (4.20)$$

The wavefunction in the normal metal region ( $N_1$ ) is given by for the long junction limit following Ref. [60],

$$\begin{aligned} \psi_{N_1}(x) = & e_N e^{ike(x+a/2)} v \varphi_1^N \phi_{m'}^S + f_N e^{-ike x} u \varphi_1^N \phi_{m'}^S + e'_N e^{ike(x+a/2)} (-v) \varphi_2^N \phi_{m'+1}^S + f'_N e^{-ike x} u \varphi_2^N \phi_{m'+1}^S \\ & + g_N e^{-ikh(x+a/2)} (-v) \varphi_3^N \phi_{m'+1}^S + h_N e^{ikh x} u \varphi_3^N \phi_{m'+1}^S + g'_N e^{-ikh(x+a/2)} v \varphi_4^N \phi_{m'}^S + h'_N e^{ikh x} u \varphi_4^N \phi_{m'}^S, \text{ for } -\frac{a}{2} < x < 0. \end{aligned} \quad (4.21)$$

Similarly the wavefunction in the normal metal region ( $N_2$ ) is given by-

$$\begin{aligned} \psi_{N_2}(x) = & a_N e^{ike x} v \varphi_1^N \phi_{m'}^S + b_N e^{-ike(x-a/2)} u \varphi_1^N \phi_{m'}^S + a'_N e^{ike x} (-v) \varphi_2^N \phi_{m'+1}^S + b'_N e^{-ike(x-a/2)} u \varphi_2^N \phi_{m'+1}^S \\ & + c_N (-v) \varphi_3^N e^{-ikh x} \phi_{m'+1}^S + d_N e^{ikh(x-a/2)} u \varphi_3^N \phi_{m'+1}^S + c'_N e^{-ikh x} v \varphi_4^N \phi_{m'}^S + d'_N e^{ikh(x-a/2)} u \varphi_4^N \phi_{m'}^S, \text{ for } 0 < x < \frac{a}{2}. \end{aligned} \quad (4.22)$$

For  $|E| \ll E_F$ , we can write  $k_{e,h} \approx k_F \pm \frac{E}{2\Delta_0 \xi_0}$ , where  $\xi_0 = E_F / (k_F \Delta_0)$  is the BCS coherence length[25]. By using boundary conditions as mentioned in section 4.2 one can get the different scattering amplitudes. The wavefunction for the other seven types of quasiparticle injection process are formulated in the same way. Using the generalized version of Furusaki-Tsukuda Josephson current formula mentioned in subsection 4.2.1 we can calculate the total DC Josephson current in long junction limit. In Fig. 4.6 we plot the Josephson current for a long junction. In Fig. 4.6(a) we plot Josephson supercurrent as a function of junction length  $a$  for  $\varphi = \pi/2$  and different values of spin ( $S$ ) of spin flipper from  $S = 1/2$  to  $S = 11/2$ . We see that Josephson supercurrent dies monotonically with an increase in the junction's length ( $a$ ). For large  $a$ , the Josephson supercurrent goes to zero.

#### 4. SPIN-FLIP SCATTERING INDUCED TUNABLE $0 - \pi$ JOSEPHSON JUNCTION AND QUANTIZED ANOMALOUS PHASE IN FERROMAGNETIC JOSEPHSON JUNCTION

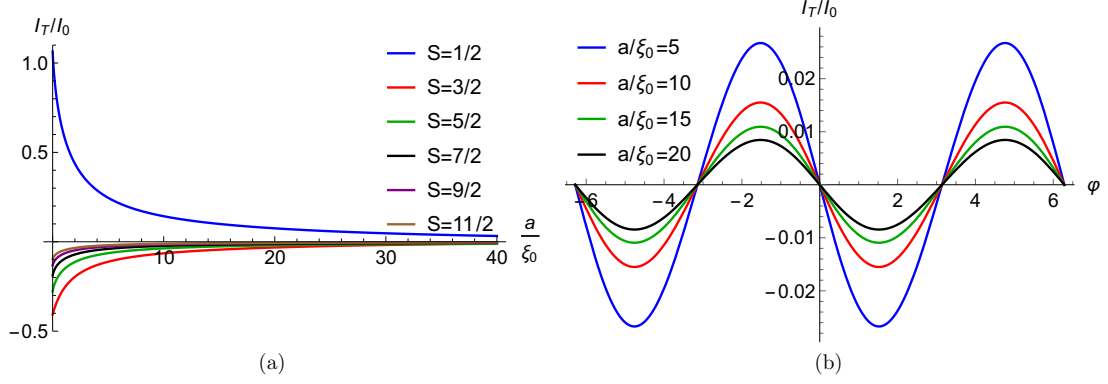


Figure 4.6: (a) Josephson supercurrent as a function of junction length ( $a$ ) for different values of spin ( $S$ ) of spin flipper. Parameters are  $\Delta_0 = 1\text{meV}$ ,  $T/T_c = 0.01$ ,  $\varphi = \pi/2$ ,  $m' = -1/2$ ,  $J = 1$ ,  $Z = 0$ , (b) Josephson supercurrent as a function of phase difference ( $\varphi$ ) for different junction length ( $a$ ). Parameters are  $\Delta_0 = 1\text{meV}$ ,  $T/T_c = 0.01$ ,  $S = 9/2$ ,  $m' = -1/2$ ,  $J = 1$ ,  $Z = 0$ .

In Fig. 4.6(b), we have plotted Josephson supercurrent as a function of phase difference ( $\varphi$ ) for different junction lengths  $a$  and high spin of the spin flipper ( $S = 9/2$ ). We see that Josephson supercurrent decreases with an increase of junction length  $a$ . In Fig. 4.6(a) and 4.6(b) the magnetic moment of spin flipper  $m' = -1/2$  and the junction transparency  $Z = 0$ . However, change in length does not affect the sign of the Josephson current, signifying that the  $\pi$  junction is robust to change in normal metal length.

#### 4.2.5 Free energy

We can also determine the nature of the junction, i.e.,  $0$  or  $\pi$  by the minimum of the Free energy, which is given by

$$F(\varphi) = -\frac{1}{\beta} \frac{1}{2\pi} \int_0^{2\pi} \ln \left[ \prod_i (1 + e^{-\beta E_i(\varphi)}) \right] d(k_F a) = -\frac{2}{\beta} \frac{1}{2\pi} \int_0^{2\pi} \sum_{\sigma} \ln \left[ 2 \cosh \left( \frac{\beta E_{\sigma}(\varphi)}{2} \right) \right] d(k_F a) \quad (4.23)$$

In Fig. 4.7 we have plotted  $F/\Delta_0$  as a function of phase difference for spin  $S = 9/2$  and different values of  $m'$ , we have considered a transparent junction ( $Z = 0$ ). In the same

figure we see that the Free energy for  $m' = 9/2$  is almost half than that of the other cases ( $m' \neq 9/2$ ). A plausible reason for why these occurs could be that for  $m' = 9/2$  there is

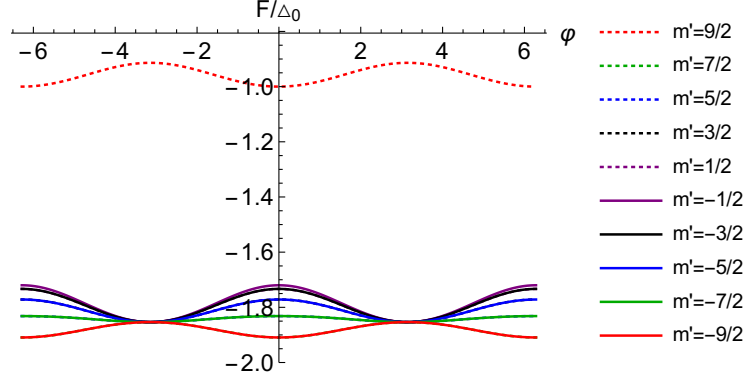


Figure 4.7: Free energy as a function of phase difference ( $\varphi$ ). Parameters are  $\Delta_0 = 1\text{meV}$ ,  $T/T_c = 0.01$ ,  $S = 9/2$ ,  $m' = \pm 9/2, \pm 7/2, \pm 5/2, \pm 3/2, \pm 1/2$ ,  $J = 1$ ,  $Z = 0$ . Free energy for  $m' = 7/2$  and  $m' = -9/2$  are same and similarly for  $m' = 5/2$  and  $m' = -7/2$ ,  $m' = 3/2$  and  $m' = -5/2$ ,  $m' = 1/2$  and  $m' = -3/2$  are same.

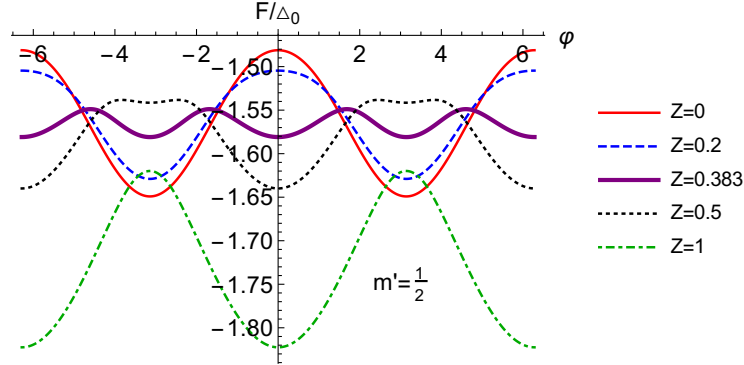


Figure 4.8: Free energy as a function of phase difference ( $\varphi$ ) for different values of interface barrier strength ( $Z$ ). Parameters are  $\Delta_0 = 1\text{meV}$ ,  $T/T_c = 0.01$ ,  $S = 5/2$ ,  $m' = 1/2$ ,  $J = 1$ .

no spin-flip process ( $f = 0$ ) while for the other cases  $f$  ranges from 3 to 5. In Fig. 4.8 we plot the Free energy for  $S = 5/2$  and  $m' = 1/2$  for different values of interface transparency  $Z$ . At a particular value of  $Z = 0.383$ , the Free energy shows a bistable behavior, i.e., the Free energy minima occur at both  $0$  and  $\pi$ , meaning that the system's ground state does

not occur at either  $0$  or  $\pi$  exclusively but is shared by both. These bistable junctions have a major role to play in quantum computation applications[158, 159, 160].

## 4.2.6 Understanding $0 - \pi$ junction transition

### Effect of tunnel contacts & exchange coupling

In Fig. 4.9 we plot Josephson supercurrent as a function of phase difference for different values of interface barrier strength. From Fig. 4.9(a) where  $m' = 5/2$  we see that there is no  $\pi$  shift from transparent to tunnel regime, and the ground state of the system always stays at  $\varphi = 0$ . The reason that ground state stays at  $\varphi = 0$  in Fig. 4.9(a) is due to absence of spin-flip processes as  $S = m' = 5/2$  and  $f = 0$ . In Fig. 4.9(b) the ground state of the system shifts from  $\varphi = \pi$  to  $\varphi = 0$  as function of  $Z$ . In fact, for a transparent junction ( $Z = 0$ ), the ground state is at  $\varphi = \pi$ , and as we increase  $Z$ , we see the ground state shift from  $\pi$  to  $0$  state. Of course, in this case, as  $S = 5/2$  and  $m' = 1/2$ , therefore the probability for the spin flipper to flip ( $f \neq 0$ ) is nonzero. **Thus, spin-flip processes aid in the transition from  $0$  to  $\pi$  junction.** Notably, this transition can be tunned by the transparency ( $Z$ ) of the junction, as is evident from Fig. 4.9(b). Of course, not all cases wherein the spin flipper flips its spin leads to a transition from  $0$  to  $\pi$  state, as is evident in Fig. 4.9(c). In Fig. 4.9(c) the ground state stays at  $\varphi = 0$ , but here as  $S = 5/2$ ,  $m' = 3/2$  and  $f \neq 0$ , so spin-flip processes occur in contrast to Fig. 4.9(a). In Fig. 4.9 the strength of exchange interaction  $J$  is taken as 1. It has to be pointed out that  $J$  has a nontrivial role in the  $0$  to  $\pi$  state transition, evident in the next subsection. Thus our conclusions regarding Fig. 4.9(c) has to be qualified by the fact that we have not focused on the issue of exchange interaction so far.

In Hamiltonian  $H$ , in Eq. (4.1) the term  $J_0\delta(x)\vec{s}\cdot\vec{S}$  represents the exchange coupling of strength  $J_0$  between the electron/hole with spin  $\vec{s}$  and a spin flipper with spin  $\vec{S}$ . In Fig. 4.10



## 4.2. SNS junction in presence of a spin flipper

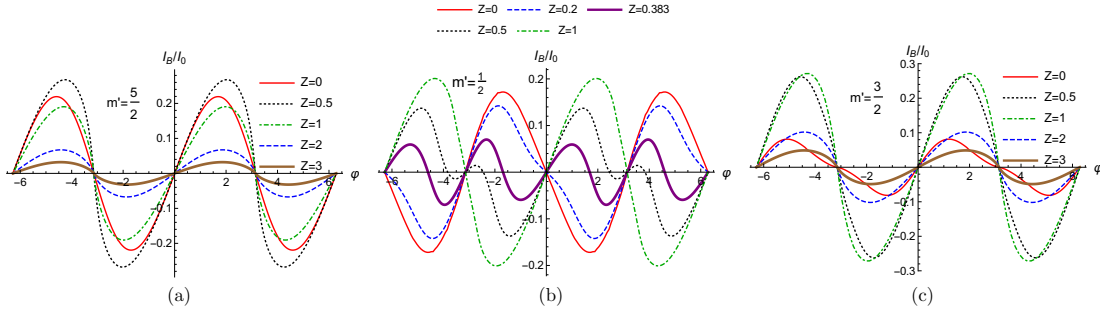


Figure 4.9: Josephson supercurrent as a function of phase difference ( $\varphi$ ) for different values of interface barrier strength ( $Z$ ). Parameters are  $\Delta_0 = 1\text{meV}$ ,  $T/T_c = 0.01$ ,  $J = 1$ ,  $S = 5/2$  and for (a)  $m' = 5/2$ , (b)  $m' = 1/2$  and (c)  $m' = 3/2$ . Josephson supercurrent for  $m' = 3/2$  and  $m' = -5/2$  are same and similarly  $m' = 1/2$  and  $m' = -3/2$  are same.

the Josephson supercurrent is plotted as a function of phase difference for different values of strength of exchange interaction in the transparent regime. We choose  $S = 5/2$  and

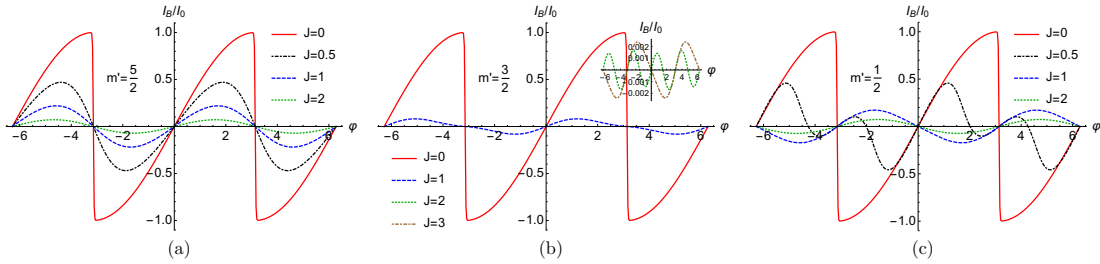


Figure 4.10: Josephson supercurrent as a function of phase difference ( $\varphi$ ) for different values of exchange interaction ( $J$ ). Parameters are  $\Delta_0 = 1\text{meV}$ ,  $T/T_c = 0.01$ ,  $Z = 0$ ,  $S = 5/2$  for (a)  $m' = 5/2$ , (b)  $m' = 3/2$  and (c)  $m' = 1/2$ . Josephson supercurrent for  $m' = 3/2$  and  $m' = -5/2$  are same and similarly  $m' = 1/2$  and  $m' = -3/2$  are same.

allowed values of  $m'$ . For the no spin-flip case, one sees there is no transition from 0 to  $\pi$  junction, while for cases with spin-flip, one can see a 0 to  $\pi$  state transition. Thus all spin-flip process i.e.,  $f \neq 0$  and with  $J > 2$  show  $\pi$  junction behavior.

### Effect of electron-electron interaction (phenomenological)

We have considered a phenomenological[161, 162] approach to electron-electron interactions. The effect of such interactions are included through an energy-dependent transmission probability which is given as-

$$T(E) = \frac{T_0 \left| \frac{E}{D_0} \right|^\alpha}{1 - T_0 \left( 1 - \left| \frac{E}{D_0} \right|^\alpha \right)} \quad (4.24)$$

with  $T_0$  being the transparency of the metal superconductor interface in the absence of electron-electron interactions.  $\alpha$  ( $0 < \alpha < 1$ ) represents the electron-electron interaction strength ( $\alpha = 0$  corresponds to no interactions while  $\alpha = 1$  corresponds to a maximally interacting system),  $D_0$  is a high energy cutoff obtained by the energy bandwidth of the electronic states. Now for non-interacting case the parameter  $Z$  is a constant and is related to the transmission probability  $T_0$  as

$$Z^2 = \frac{1 - T_0}{T_0}. \quad (4.25)$$

Now in the presence of electron-electron interaction,  $T_0$  is replaced by  $T(E)$  in the above equation. Thus, the interface transparency  $Z$ , which is considered identical at both interfaces, will be energy-dependent and will change from  $Z$  to  $Z_{ee}$ :

$$Z_{ee}^2 = \left| \frac{E}{D_0} \right|^{-\alpha} \frac{1 - T_0}{T_0} = \left| \frac{E}{D_0} \right|^{-\alpha} Z^2. \quad (4.26)$$

For  $Z = 0$  ( $T_0 = 1$ ),  $Z_{ee} = 0$  which implies that for a transparent interface electron-electron interaction have no effect on electronic transport. In Fig. 4.11 we plot the Josephson supercurrent as a function of phase difference for different values of electron-electron interaction parameter  $\alpha$ . We see that for  $m' = 5/2, 1/2, -3/2$  there is no  $0-\pi$  transition with increase of electron-electron interaction strength. But for  $m' = 3/2, -1/2, -5/2$  there is a change from  $\pi$  to  $0$  junction with increase of electron-electron interaction strength ( $\alpha$ ).

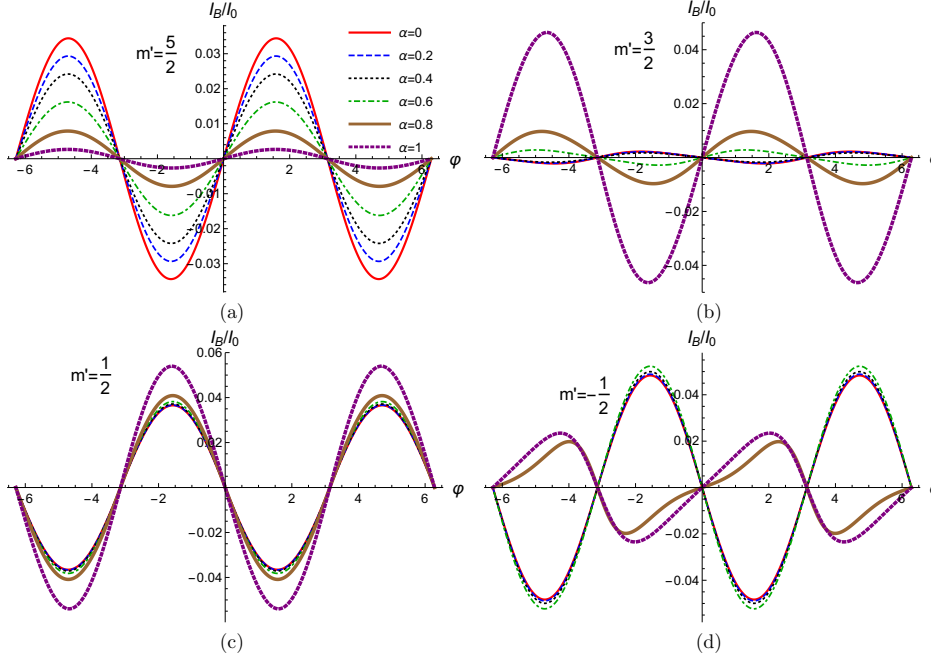


Figure 4.11: Josephson supercurrent as a function of phase difference ( $\varphi$ ) for different values of electron-electron interaction strength ( $\alpha$ ). Parameters are  $\Delta_0 = 1\text{meV}$ ,  $D_0 = 100\Delta_0$ ,  $T/T_c = 0.01$ ,  $J = 3$ ,  $Z = 0.1$ ,  $S = 5/2$  and for (a)  $m' = 5/2$ , (b)  $m' = 3/2$ , (c)  $m' = 1/2$  and (d)  $m' = -1/2$ . Josephson supercurrent for  $m' = 3/2$  and  $m' = -5/2$  are same and similarly  $m' = 1/2$  and  $m' = -3/2$  are same.

### Effect of high spin/magnetic moment states

In Fig. 4.12(a) we see that Josephson supercurrent at  $\varphi = \pi/2$  is positive for  $S = 1/2$ , but as we increase spin ( $S$ ) of spin flipper it changes to negative from  $S = 3/2$  to  $S = 9/2$ . We choose phase difference  $\varphi = \pi/2$  to see the sign change of the Josephson supercurrent. In the inset of Fig. 4.12(a), we plot the Josephson supercurrent for still higher spin states of the spin flipper ( $S = 11/2$  to  $19/2$  in steps of 1). In Fig. 4.12(a) for different values of  $S$ , the magnetic moment of spin flipper is  $m' = -1/2$  and junction transparency  $Z = 0$ . The reason for the change in sign of the Josephson supercurrent can be guessed from the fact that spin-flip probability ( $f$ ) of spin flipper for negative Josephson supercurrent is greater

#### 4. SPIN-FLIP SCATTERING INDUCED TUNABLE $0 - \pi$ JOSEPHSON JUNCTION AND QUANTIZED ANOMALOUS PHASE IN FERROMAGNETIC JOSEPHSON JUNCTION

than 1. However, this previous statement is subject to qualification: negative supercurrent for low spin states of spin flipper requires smaller values of spin-flip probability  $f$  than do high spin states of the spin flipper. In Fig. 4.12(b), we look at the effect of spin magnetic

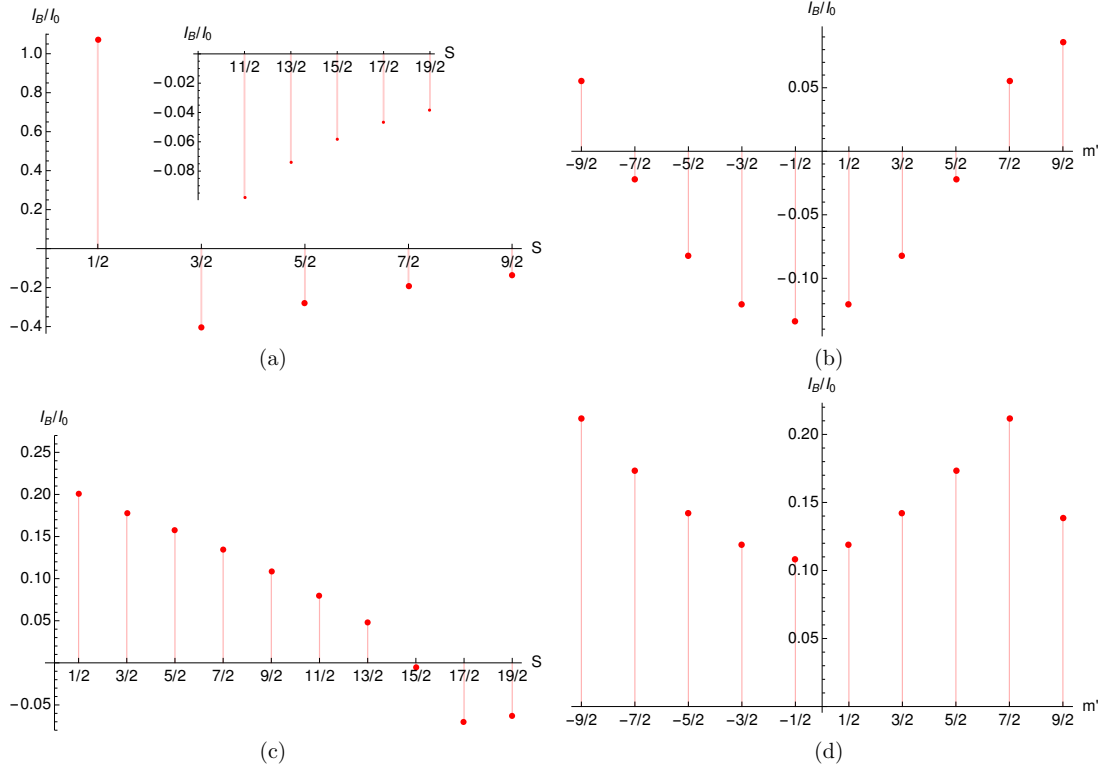


Figure 4.12: (a) Josephson supercurrent vs spin flipper spin ( $S$ ). Parameters are  $\Delta_0 = 1\text{meV}$ ,  $T/T_c = 0.01$ ,  $\varphi = \pi/2$ ,  $J = 1$ ,  $m' = -1/2$ ,  $Z = 0$ , (b) Josephson supercurrent vs spin flipper magnetic moment ( $m'$ ). Parameters are  $\Delta_0 = 1\text{meV}$ ,  $T/T_c = 0.01$ ,  $\varphi = \pi/2$ ,  $J = 1$ ,  $S = 9/2$ ,  $Z = 0$ , (c) Josephson supercurrent vs spin flipper spin ( $S$ ). Parameters are  $\Delta_0 = 1\text{meV}$ ,  $T/T_c = 0.01$ ,  $\varphi = \pi/2$ ,  $J = 1$ ,  $m' = -1/2$ ,  $Z = 1$ , (d) Josephson supercurrent vs spin flipper magnetic moment ( $m'$ ). Parameters are  $\Delta_0 = 1\text{meV}$ ,  $T/T_c = 0.01$ ,  $\varphi = \pi/2$ ,  $J = 1$ ,  $S = 9/2$ ,  $Z = 1$ .

moment states on Josephson supercurrent. We consider the spin  $S$  of the spin flipper to be  $9/2$ . The Josephson supercurrent changes sign with  $m'$ . One can see when the spin-flip probability of spin flipper ( $f$ )  $> 3$ , Josephson supercurrent is negative, but for flip probability  $f < 3$ , Josephson supercurrent is positive for transparent junction,  $Z = 0$ . We

see in Fig. 4.12(c) the possibility of a  $\pi$  junction also at  $Z = 1$  (intermediate transparency). In Fig. 4.12(c), we plot the Josephson supercurrent, including still higher spin states of the spin flipper ( $S = 1/2$  to  $19/2$  in steps of 1). In Appendix B we juxtapose the spin state  $S$ , magnetic moment  $m'$ , and spin-flip probability  $f$  of the spin flipper in a tabular format. Finally in Fig. 4.12(d) we plot Josephson supercurrent at  $Z = 1$  (non-transparent junction) as a function of spin magnetic moment  $m'$  for  $S = 9/2$ . We see non-transparent junctions inhibits a  $0 - \pi$  junction transition for  $S = 9/2$ . However, one has to qualify the statement above by looking at Fig. 4.12(c). In Fig. 4.12(c), we see that finite  $Z$  ( $= 1$ ) can act as a barrier to the  $0 - \pi$  junction transition. To overcome this barrier, one needs to go to higher spin states like  $S = 15/2, 17/2, 19/2$ . Thus in Fig. 4.12(d) instead of plotting for  $S = 9/2$  if we had plotted  $S = 15/2, 17/2, 19/2$  we would have seen a  $0 - \pi$  junction transition for some value of  $m'$ . So to conclude this subsection for transparent interfaces, spin-flip processes lead to a  $0$  to  $\pi$  junction transition. However, when junction transparency reduces, one has to go to higher spin states to see a  $0 - \pi$  junction transition. The moral of the story is that a finite  $Z$  inhibits  $0 - \pi$  transition, but a large  $S$  can overcome the  $Z$  barrier. The  $\pi$ -shift seen due to change in  $S$  can be experimentally implemented. One can control the impurity spin  $S$  optically as shown in Refs. [163, 164].

## 4.3 Ferromagnetic Josephson junction in the presence of a spin flipper

We designed a tunable  $0 - \pi$  Josephson junction with a spin flipper and two normal metals sandwiched between two conventional  $s$ -wave superconductors in the previous section. We also studied the role of tunnel contacts, exchange coupling, electron-electron interactions, and high spin states on  $0 - \pi$  junction transition. In this section, we replace the two normal

#### 4. SPIN-FLIP SCATTERING INDUCED TUNABLE $0 - \pi$ JOSEPHSON JUNCTION AND QUANTIZED ANOMALOUS PHASE IN FERROMAGNETIC JOSEPHSON JUNCTION

metals on either side of spin-flipper with Ferromagnets, see Fig. 4.13, which shows a spin flipper at  $x = 0$  and two superconductors: one at left,  $x < -a/2$  and another at right,  $x > a/2$ . The magnetization vectors of the two Ferromagnet's make an angle  $\theta$  with each other. The BdG equation for our junction is[27],

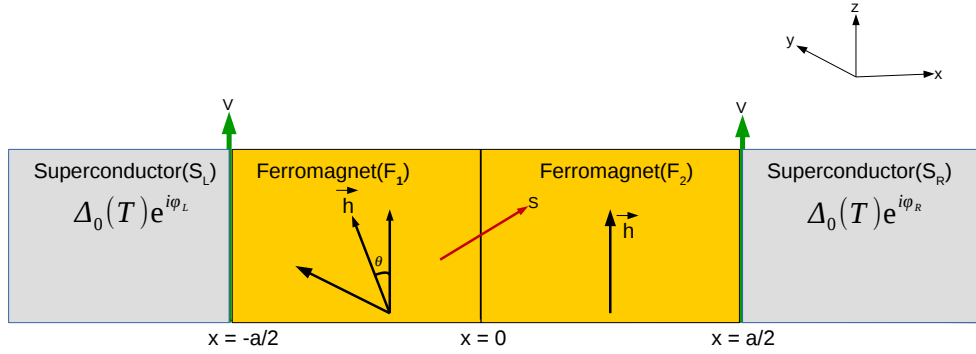


Figure 4.13: Josephson junction with two Ferromagnet's and a spin flipper (spin  $S$ , magnetic moment  $m'$ ) at  $x = 0$  sandwiched between two  $s$ -wave superconductors.

$$\begin{pmatrix} H\hat{I} & i\Delta\hat{\sigma}_y \\ -i\Delta^*\hat{\sigma}_y & -H^*\hat{I} \end{pmatrix} \psi(x) = E\psi(x), \quad (4.27)$$

where  $H = p^2/2m^* + V[\delta(x + a/2) + \delta(x - a/2)] - J_0\delta(x)\vec{s}\cdot\vec{S} - \vec{h}\cdot\hat{\sigma}[\Theta(x + a/2) + \Theta(a/2 - x)] - E_F$ , with  $p^2/2m^*$  being the kinetic energy of an electron/hole with effective mass  $m^*$ ,  $V$  denotes the strength of  $\delta$  potentials at the interfaces between Ferromagnet's and Superconductor,  $J_0$  denotes strength of exchange coupling between electron/hole with spin  $\vec{s}$  and spin flipper with spin  $\vec{S}$ .  $\psi(x)$  defines a four-component spinor, while  $E_F$  is Fermi energy,  $\hat{\sigma}$ 's are Pauli spin matrices and  $\hat{I}$  is  $2 \times 2$  identity matrix. The magnetization vector ( $\vec{h}$ ) of left ferromagnetic layer ( $F_1$ ) is at an angle  $\theta$  with  $z$  axis in  $y - z$  plane, while that of right ferromagnetic layer ( $F_2$ ) is fixed along  $z$  axis. Thus,  $\vec{h}\cdot\hat{\sigma} = h \sin \theta \hat{\sigma}_y + h \cos \theta \hat{\sigma}_z$ [165].

### 4.3. Ferromagnetic Josephson junction in the presence of a spin flipper

If we diagonalize BdG Hamiltonian, Eq. (4.27), we get wavefunctions in different regions of our junction for ELQ/HLQ incidence. If a spin up ELQ is incident at  $x = -a/2$  interface from left superconductor, then wave function[27] in left superconductor ( $S_L$ ) is,

$$\psi_{S_L}(x) = \varphi_1^{S_L} e^{ik_+x} \phi_{m'}^S + r_{ee}^{\uparrow\uparrow} \varphi_1^{S_L} e^{-ik_+x} \phi_{m'}^S + r_{ee}^{\uparrow\downarrow} \varphi_2^{S_L} e^{-ik_+x} \phi_{m'+1}^S + r_{eh}^{\uparrow\uparrow} \varphi_3^{S_L} e^{ik_-x} \phi_{m'+1}^S + r_{eh}^{\uparrow\downarrow} \varphi_4^{S_L} e^{ik_-x} \phi_{m'}^S, \quad (4.28)$$

where  $r_{ee}^{\uparrow\uparrow}, r_{ee}^{\uparrow\downarrow}, r_{eh}^{\uparrow\uparrow}, r_{eh}^{\uparrow\downarrow}$  are amplitudes for normal reflection without flip, normal reflection with spin flip, Andreev reflection with spin flip and Andreev reflection without flip respectively. The corresponding wave-function in right superconductor ( $S_R$ ) is,

$$\psi_{S_R}(x) = t_{ee}^{\uparrow\uparrow} \varphi_1^{S_R} e^{ik_+x} \phi_{m'}^S + t_{ee}^{\uparrow\downarrow} \varphi_2^{S_R} e^{ik_+x} \phi_{m'+1}^S + t_{eh}^{\uparrow\uparrow} \varphi_3^{S_R} e^{-ik_-x} \phi_{m'+1}^S + t_{eh}^{\uparrow\downarrow} \varphi_4^{S_R} e^{-ik_-x} \phi_{m'}^S, \quad (4.29)$$

where  $t_{ee}^{\uparrow\uparrow}, t_{ee}^{\uparrow\downarrow}, t_{eh}^{\uparrow\uparrow}, t_{eh}^{\uparrow\downarrow}$  are transmission amplitudes, corresponding to reflection processes described above. The wave-function in left Ferromagnet ( $F_1$ ) is,

$$\begin{aligned} \psi_{F_1}(x) = & (e_F e^{iq_1^+(x+a/2)} + f_F e^{-iq_1^+x}) \varphi_1^F \phi_{m'}^S + (e'_F e^{iq_1^+(x+a/2)} + f'_F e^{-iq_1^+x}) \varphi_2^F \phi_{m'+1}^S \\ & + (g_F e^{-iq_1^-(x+a/2)} + h_F e^{iq_1^-x}) \varphi_3^F \phi_{m'+1}^S + (g'_F e^{-iq_1^-(x+a/2)} + h'_F e^{iq_1^-x}) \varphi_4^F \phi_{m'}^S, \end{aligned} \quad (4.30)$$

where  $\varphi_i^F, i = 1, 2, 3, 4$  are defined in section 3.5 of chapter 3. Similarly wave-function in right Ferromagnet ( $F_2$ ) is,

$$\begin{aligned} \psi_{F_2}(x) = & (a_F e^{iq_1^+x} + b_F e^{-iq_1^+(x-a/2)}) \varphi_1^N \phi_{m'}^S + (a'_F e^{iq_1^+x} + b'_F e^{-iq_1^+(x-a/2)}) \varphi_2^N \phi_{m'+1}^S \\ & + (c_F e^{-iq_1^-x} + d_F e^{iq_1^-(x-a/2)}) \varphi_3^N \phi_{m'+1}^S + (c'_F e^{-iq_1^-x} + d'_F e^{iq_1^-(x-a/2)}) \varphi_4^N \phi_{m'}^S, \end{aligned} \quad (4.31)$$

and  $q_\sigma^\pm = \sqrt{\frac{2m^*}{\hbar^2}(E_F + \rho_\sigma h \pm E)}$  is wave-vector for electron ( $q_\sigma^+$ ) and hole ( $q_\sigma^-$ ) in Ferromagnet, wherein  $\rho_\sigma = +1(-1)$  with  $\sigma = \uparrow(\downarrow)$ . We use Andreev approximation, i.e.,  $k_+ = k_- = \sqrt{\frac{2m^*E_F}{\hbar^2}} = k_F$  and  $q_{\uparrow,\downarrow} = k_F \sqrt{1 \pm \frac{h}{E_F}}$ , with  $k_F$  being the Fermi wave-vector, and  $E_F \gg |\Delta|, E$ .

The boundary conditions at  $x = -a/2$  are,

$$\psi_{S_L}(x) = \psi_{F_1}(x), \quad \frac{d\psi_{F_1}}{dx} - \frac{d\psi_{S_L}}{dx} = \frac{2m^*V}{\hbar^2} \psi_{F_1}, \quad (4.32)$$

#### 4. SPIN-FLIP SCATTERING INDUCED TUNABLE $0 - \pi$ JOSEPHSON JUNCTION AND QUANTIZED ANOMALOUS PHASE IN FERROMAGNETIC JOSEPHSON JUNCTION

---

and at  $x = 0$  are,

$$\psi_{F_1}(x) = \psi_{F_2}(x), \quad \frac{d\psi_{F_2}}{dx} - \frac{d\psi_{F_1}}{dx} = -\frac{2m^* J_0 \vec{s} \cdot \vec{S}}{\hbar^2} \psi_{F_1}. \quad (4.33)$$

Finally, at  $x = a/2$  are,

$$\psi_{F_2}(x) = \psi_{S_R}(x), \quad \frac{d\psi_{S_R}}{dx} - \frac{d\psi_{F_2}}{dx} = \frac{2m^* V}{\hbar^2} \psi_{F_2}. \quad (4.34)$$

We use dimensionless parameters  $J = \frac{m^* J_0}{k_F}$  as a measure of strength of exchange interaction[13] and  $Z = \frac{m^* V}{\hbar^2 k_F}$  is a measure of interface transparency[9].

##### 4.3.1 Anomalous Josephson current and Andreev bound states

To calculate bound state contribution to Josephson current we follow the procedure established in section 4.2 and Ref. [24]. We neglect contribution from incoming quasi-particle, i.e., first term  $\varphi_1^{S_L} e^{ik_+ x} \phi_m^S$ , of Eq. (4.28) and insert wavefunctions into boundary conditions. We get a homogeneous system of linear equations for the scattering amplitudes,

$$Rx = 0, \quad (4.35)$$

where  $x$  is a  $8 \times 1$  column vector, given by  $x = \left( r_{ee}^{\uparrow\uparrow} \ r_{ee}^{\uparrow\downarrow} \ r_{eh}^{\uparrow\uparrow} \ r_{eh}^{\uparrow\downarrow} \ t_{ee}^{\uparrow\uparrow} \ t_{ee}^{\uparrow\downarrow} \ t_{eh}^{\uparrow\uparrow} \ t_{eh}^{\uparrow\downarrow} \right)^T$ ,  $R$  is a  $8 \times 8$  matrix obtained by eliminating the scattering amplitudes for the two Ferromagnet's via the scattering amplitudes of the left and right superconductor. For a nontrivial solution of this system, the determinant of  $R = 0$ . If we solve  $\det R = 0$  for energy  $E$ , we get the Andreev bound state energy spectrum  $E = E_i$ ,  $i = \{1, \dots, 8\}$ [155]. We find that Andreev energy bound states  $E_i$  ( $i = 1, \dots, 8$ ) can be written as  $\varepsilon_l^\pm = \pm \varepsilon_l$  ( $l = 1, \dots, 4$ ). From Andreev bound state energies we get Free energy[24] of our system as,

$$F = -\frac{1}{\beta} \ln \left[ \prod_i (1 + e^{-\beta E_i}) \right] = -\frac{2}{\beta} \sum_{l=1}^4 \ln \left[ 2 \cosh \left( \frac{\beta \varepsilon_l}{2} \right) \right]. \quad (4.36)$$



### 4.3. Ferromagnetic Josephson junction in the presence of a spin flipper

We consider the short junction limit, such that the total Josephson current can be determined by considering bound state contribution only. The Josephson current at finite temperature is defined as the derivative of the Free energy  $F$  of our system to the phase difference  $\varphi$  between left and right superconductors[166],

$$I = \frac{2e}{\hbar} \frac{\partial F}{\partial \varphi} = -\frac{2e}{\hbar} \sum_{l=1}^4 \tanh\left(\frac{\beta \varepsilon_l}{2}\right) \frac{\partial \varepsilon_l}{\partial \varphi}. \quad (4.37)$$

Using Eq. (4.37) we can calculate the anomalous Josephson current, which is given as-  $I_{an} = I(\varphi = 0)$ , absolute value of maximum Josephson current, as-  $I_{c+} = |\max I(\varphi)|$  and absolute value of minimum Josephson current, as-  $I_{c-} = |\min I(\varphi)|$ . In case interfaces are completely transparent, i.e.,  $Z = 0$ , we have,

$$I_{an} = \frac{2e\Delta_0^2(T)}{\hbar} \left( \tanh\left(\frac{\beta A_1}{2}\right) A'_1 + \tanh\left(\frac{\beta A_2}{2}\right) A'_2 + \tanh\left(\frac{\beta A_3}{2}\right) A'_3 + \tanh\left(\frac{\beta A_4}{2}\right) A'_4 \right) \quad (4.38)$$

wherein  $A_1, A_2, A_3, A_4, A'_1, A'_2, A'_3$  and  $A'_4$  are expressions that depend on exchange interaction ( $J$ ), magnetization of Ferromagnet's, spin ( $S$ ) and magnetic moment ( $m'$ ) of spin-flipper, phase ( $k_F a$ ) accumulated in Ferromagnet's and spin-flip probability ( $f$ ). The explicit forms for  $A_k$ 's and  $A'_k$ 's ( $k = 1, 2, 3, 4$ ) are given in Appendix B.4. In Appendix B.4 we show that for no flip ( $f = 0$ ) or absence of spin-flipper ( $J = 0$ ) or  $\theta = 0$  (magnetizations of Ferromagnet's are aligned), the anomalous Josephson current ( $I_{an}$ ) vanishes.

In Fig. 4.14 we plot Andreev bound states and Josephson current as a function of phase difference  $\varphi$  between two superconductors for both no flip and spin-flip cases. In Fig. 4.14(a) we deal with the no flip case, i.e.,  $f = 0$ , and  $S = m'$ , i.e.,  $S = 3/2, m' = 3/2$ . A spin flipper cannot flip its spin while interacting with an electron/hole if  $S = m'$ . However, there is a finite probability for the spin of an electron or hole to flip due to the misalignment in the magnetization of the Ferromagnets. We see that there are four positive and four negative Andreev levels. In junction where time reversal symmetry is not broken,

#### 4. SPIN-FLIP SCATTERING INDUCED TUNABLE $0 - \pi$ JOSEPHSON JUNCTION AND QUANTIZED ANOMALOUS PHASE IN FERROMAGNETIC JOSEPHSON JUNCTION

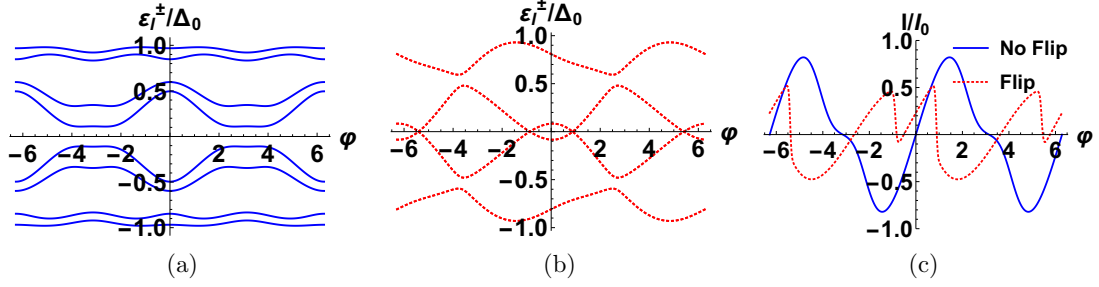


Figure 4.14: Andreev bound state energies as a function of phase difference ( $\varphi$ ) (a) for no flip, (b) for spin flip. (c) Josephson current as a function of phase difference ( $\varphi$ ). Parameters are  $\Delta_0 = 1\text{meV}$ ,  $J = 1$ ,  $h = 0.5E_F$ ,  $I_0 = e\Delta_0/\hbar$ ,  $T/T_c = 0.01$ ,  $Z = 0$ ,  $k_F a = 1.2\pi$ ,  $\theta = \pi/2$ , for flip:  $S = 3/2$ ,  $m' = -1/2$ ,  $f = 2$ , and for no flip:  $S = 3/2$ ,  $m' = 3/2$ ,  $f = 0$ .

Andreev bound states  $\varepsilon_l(\varphi)$  are invariant with respect to inversion of phase difference  $\varphi$ , i.e.,  $\varepsilon_l(-\varphi) = \varepsilon_l(\varphi)$ . As a result, in Fig. 4.14(c), for no flip case Josephson current satisfies  $I(-\varphi) = -I(\varphi)$  and there is no current flowing through the junction when phase difference  $\varphi$  between two superconductors is zero. Thus, absolute value of maximum Josephson current,  $I_{c+}$  is identical to absolute value of minimum Josephson current,  $I_{c-}$ . In Fig. 4.14(b) we deal with spin flip case, i.e.,  $f \neq 0$ , for this case  $S \neq m'$ , i.e.,  $S = 3/2$ ,  $m' = -1/2$ , for spin flipper. Thus, there is finite probability for spin flipper to flip its own spin when interacting with electron/hole. We see that for  $m' = -1/2$ , Andreev levels are doubly degenerate and phase inversion symmetry, i.e.,  $\varepsilon_l(-\varphi) = \varepsilon_l(\varphi)$  is broken. As a result, anomalous Josephson current flows, i.e.,  $I(-\varphi) \neq -I(\varphi)$  for spin-flip process in Fig. 4.14(c), where not only the anomalous current  $I(\varphi = 0) \neq 0$ , but also difference between the absolute value of maximum and absolute value of minimum Josephson currents,  $I_{c+} \neq I_{c-}$  is finite.

In Fig. 4.15 we show the effects of exchange interaction ( $J$ ) of the spin flipper, the magnetization of Ferromagnet's ( $h$ ), interface transparency ( $Z$ ), and misorientation angle ( $\theta$ ) between two ferromagnetic layers on the anomalous Josephson current. In Fig. 4.15(a),

### 4.3. Ferromagnetic Josephson junction in the presence of a spin flipper

we plot anomalous Josephson current as a function of exchange interaction  $J$  of spin flipper for different spin-flip probabilities. We see no change in the direction of anomalous

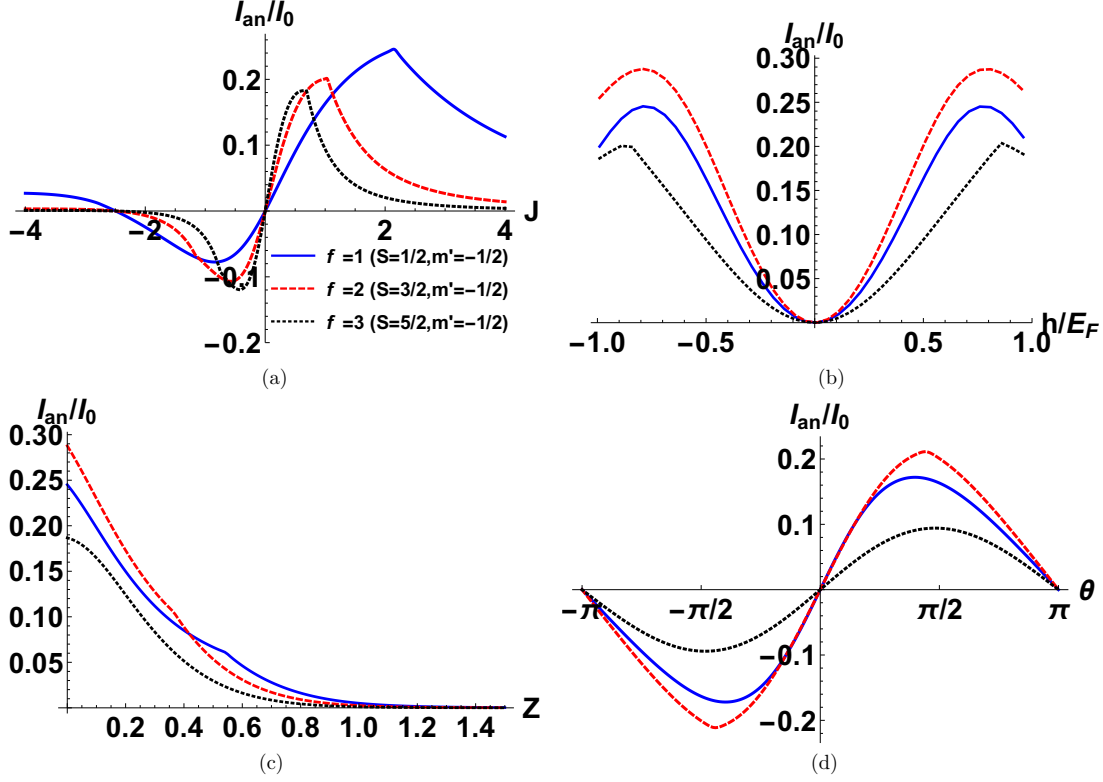


Figure 4.15: (a) Anomalous Josephson current as a function of exchange interaction  $J$  of spin flipper, (b) Anomalous Josephson current as a function of magnetization ( $h$ ) of the Ferromagnets, (c) Anomalous Josephson current as a function of the interface barrier strength ( $Z$ ), (d) Anomalous Josephson current as a function of misorientation angle ( $\theta$ ) between two Ferromagnets' for different spin flip probabilities of spin flipper. Parameters are  $\Delta_0 = 1 \text{ meV}$ ,  $I_0 = e\Delta_0/\hbar$ ,  $T/T_c = 0.01$ ,  $J = 1$  (for (b), (c) and (d)),  $h = 0.5E_F$  (for (a), (d)),  $h = 0.8E_F$  (for (c)),  $k_F a = \pi$ ,  $Z = 0$  (for (a), (b) and (d)),  $\theta = \pi/2$  (for (a), (b) and (c)).

Josephson current for ferromagnetic coupling ( $J > 0$ ) with a change in  $J$ . However, for anti-ferromagnetic coupling ( $J < 0$ ), there is a change in the direction of  $I_{an}$  as  $J$  changes from  $J = 0$  to  $J = -4$ , implying tun-ability of the sign of anomalous Josephson current via exchange interaction of spin flipper. We also see that anomalous Josephson current

is asymmetric to  $J$ . Further, the maximum value of  $I_{an}$  decreases with an increase of spin-flip probability of spin flipper. The Mathematica code used to calculate anomalous Josephson current  $I_{an}$  is mentioned in Appendix E. In Fig. 4.15(b), we plot anomalous Josephson current as a function of magnetization ( $h$ ) of the ferromagnetic layers. In contrast to Fig. 4.15(a), anomalous Josephson current is symmetric to magnetization  $h$  of Ferromagnets. In Fig. 4.15(c) we plot  $I_{an}$  as a function of interface barrier strength ( $Z$ ). We see that there is no change in the direction of  $I_{an}$  with an increase of interface barrier strength  $Z$ . Further, the anomalous Josephson current is almost zero in the tunneling regime. It is also evident from Fig. 4.15(b) and Fig. 4.15(c) that maximum of  $I_{an}$  decreases for large values of spin-flip probability. In Fig. 4.15(d)  $I_{an}$  is plotted as function of misorientation angle ( $\theta$ ) between two ferromagnetic layers. We see that magnitude of anomalous current decreases with increasing spin-flip probability. Further, one can see that sign of anomalous Josephson current can be tuned via misorientation angle  $\theta$  between magnetization direction of two Ferromagnets. Anomalous current is periodic as a function of misorientation angle with period  $2\pi$ . From Fig. 4.15(d), we also see that when the magnetic moments of the Ferromagnet's are aligned parallel or anti-parallel ( $\theta = 0$  or  $\theta = \pi$ ), anomalous Josephson current vanishes even when the spin flipper flips its spin.

In Fig. 4.16 we plot the absolute value of the anomalous Josephson currents as a function of the misorientation angle  $\theta$  for the same parameter values as in Fig. 4.15(d). We see that the anomalous current, regardless of flip probability, is symmetric about  $y$ -axis but asymmetric to  $z$ -axis.

### 4.3.2 Quantized anomalous phase

In the previous subsection, we have shown the results of Andreev bound states and Anomalous Josephson current. In this subsection we discuss the results of anomalous phase  $\varphi_0$  and

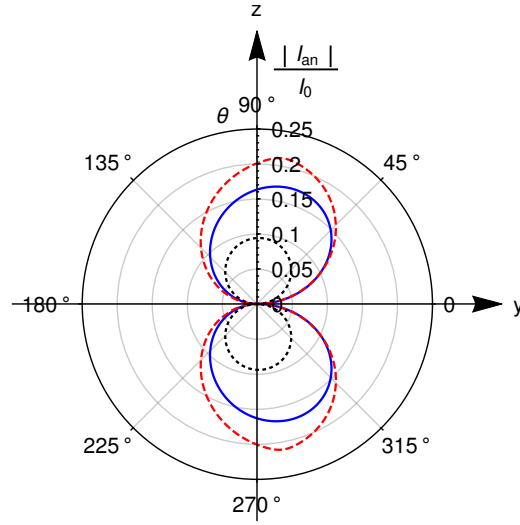


Figure 4.16: Absolute value of anomalous Josephson current as function of the misorientation angle ( $\theta$ ) between two Ferromagnet's for different values of spin and magnetic moment of the spin flipper. Parameters are  $\Delta_0 = 1\text{meV}$ ,  $I_0 = e\Delta_0/\hbar$ ,  $T/T_c = 0.01$ ,  $J = 1$ ,  $h = 0.5E_F$ ,  $k_F a = \pi$ ,  $\varphi = 0$ ,  $Z = 0$ .

asymmetry of the critical current  $\aleph = (I_{c+} - I_{c-})/(I_{c+} + I_{c-})$ . In Fig. 4.17(a), we plot Free energy as a function of exchange interaction  $J$  and phase difference  $\varphi$ . When  $J \neq 0$ , for particular values of  $J$ , the minimum Free energy is at  $\varphi = \varphi_0 (\neq 0, \pm\pi)$  and a  $\varphi_0$ -Josephson junction is realized[122, 123, 124]. Thus, for each value of  $J$ , we get the anomalous phase  $\varphi_0$  numerically, where the Free energy of the junction becomes minimum. In Fig. 4.17(b) we plot Free energy as function of magnetization  $h$  and phase difference  $\varphi$ . When  $h \neq 0$ , for each value of  $h$ , the minimum Free energy is at  $\varphi = \varphi_0 (\neq 0, \pm\pi)$ . Thus, again for each value of  $h$ , we get an anomalous phase  $\varphi_0$  numerically, where the Free energy of the junction is minimum. This procedure of calculating  $\varphi_0$  is well known and is also done in Refs. [133, 148].

In Fig. 4.18 we plot anomalous phase  $\varphi_0$  as function of exchange interaction  $J$  of spin flipper and magnetization  $h$  of the Ferromagnet's. In Fig. 4.18(a), we see “**quantized**” steps in the anomalous phase  $\varphi_0$  which are of the same magnitude ( $\pi/100$  radians) although the

#### 4. SPIN-FLIP SCATTERING INDUCED TUNABLE $0 - \pi$ JOSEPHSON JUNCTION AND QUANTIZED ANOMALOUS PHASE IN FERROMAGNETIC JOSEPHSON JUNCTION

---

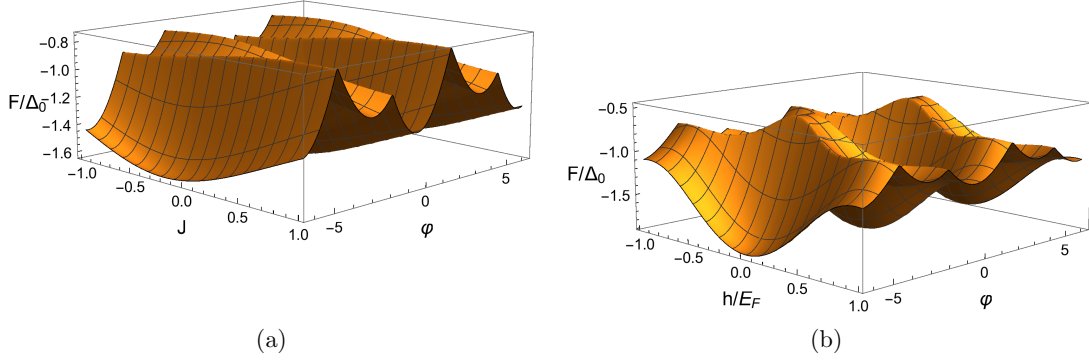


Figure 4.17: (a) Free energy as a function of exchange interaction  $J$  of spin flipper and phase difference  $\varphi$  across two superconductors. (b) Free energy as a function of magnetization  $h$  of the Ferromagnet's and phase difference  $\varphi$  across two superconductors. Parameters are  $\Delta_0 = 1\text{meV}$ ,  $T/T_c = 0.01$ ,  $S = 1/2$ ,  $m' = -1/2$ ,  $h = 0.5E_F$  (for (a)),  $k_F a = \pi$ ,  $\theta = \pi/2$ ,  $Z = 0$ ,  $J = 0.5$  (for (b)).

width linearly decreases as one goes from anti-ferromagnetic to ferromagnetic coupling. In our work, an anomalous current is always accompanied by a quantized anomalous phase. We never see anomalous current with nonquantized anomalous phase. In Fig. 4.18(b) anomalous phase  $\varphi_0$  is shown as a function of the normalized magnetization  $h/E_F$  of Ferromagnet's. Similar to Fig. 4.18(a), we also see quantized steps in anomalous phase  $\varphi_0$  which are again exactly of the same magnitude ( $\pi/100$  radians). However, the width initially decreases and then increases as one changes  $h/E_F$  from  $-0.99$  to  $0$  and then from  $0$  to  $0.99$ . The quantized step magnitude or height remains the same for different spin values, magnetic moment, and different spin-flip probability of spin flipper. Quantized behavior of  $\varphi_0$  is also shown in Fig. 4.18(c), where we show density plot of  $\varphi_0$  as a function of  $J$  and  $h$ . It is also evident from Fig. 4.18(c) larger values of exchange interaction and magnetization correspond to increasing magnitudes of anomalous phase  $\varphi_0$ . The Mathematica code used to calculate anomalous phase  $\varphi_0$  is mentioned in Appendix E. In Ref. [133], anomalous

### 4.3. Ferromagnetic Josephson junction in the presence of a spin flipper

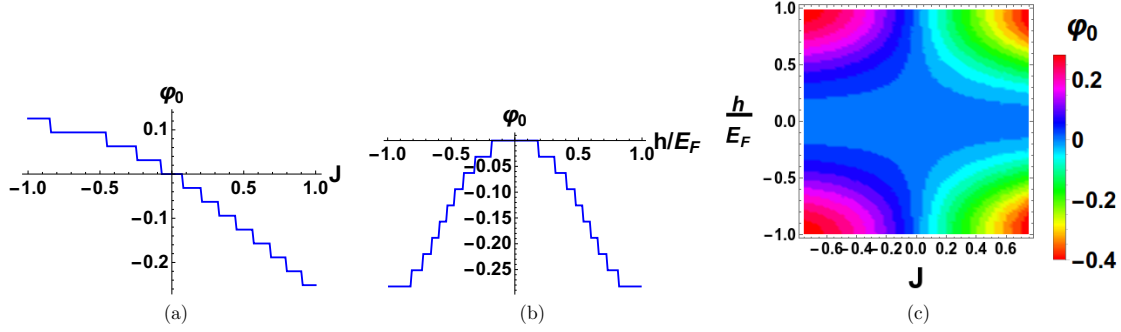


Figure 4.18: (a) Phase difference  $\varphi_0$  as a function of exchange interaction ( $J$ ) of spin flipper. (b) Phase difference  $\varphi_0$  as a function of magnetization ( $h$ ) of Ferromagnet's. (c) Density plot of  $\varphi_0$  as function of exchange interaction ( $J$ ) of spin flipper and magnetization ( $h$ ) of Ferromagnet's. Parameters are  $\Delta_0 = 1\text{meV}$ ,  $T/T_c = 0.01$ ,  $S = 1/2$ ,  $m' = -1/2$ ,  $h = 0.5E_F$  (for (a)),  $k_F a = \pi$ ,  $\theta = \pi/2$ ,  $Z = 0$ ,  $J = 0.5$  (for (b)).

Josephson current is seen in a semiconducting nanowire-based junction in the presence of both spin-orbit interaction (SO) and Zeeman field, which is equivalent to what we see for finite spin-flip probability in our system without any need for spin-orbit scattering or Zeeman fields. However, in Ref. [133] anomalous phase  $\varphi_0$  changes continuously with change in a magnetic field and is not quantized in contrast to what is shown in this chapter.

Finally, in Fig. 4.19 we perform a similar analysis for the asymmetry of the critical current, defined as [148]  $\aleph = (I_{c+} - I_{c-}) / (I_{c+} + I_{c-})$ . In Fig. 4.19(a), we plot  $\aleph$  as a function of the exchange interaction  $J$  and see that the maximum value of  $\aleph$  almost remains the same for different spin-flip probabilities. Further, it is also evident from Fig. 4.19(a), the sign of  $\aleph$  can be tuned via  $J$ , and  $\aleph$  is asymmetric to  $J$ . Figure 4.19(b) shows the asymmetry  $\aleph$  as a function of magnetization  $h$  of Ferromagnet's. We see that in contrast to Fig. 4.19(a), the maximum in  $\aleph$  is different for different spin-flip probabilities. Further,  $\aleph$  is symmetric with respect to  $h/E_F$ . In Fig. 4.19(c), we show a density plot for asymmetry in critical current ( $\aleph$ ) as a function of exchange interaction  $J$  of the spin flipper and magnetization  $h$

#### 4. SPIN-FLIP SCATTERING INDUCED TUNABLE $0 - \pi$ JOSEPHSON JUNCTION AND QUANTIZED ANOMALOUS PHASE IN FERROMAGNETIC JOSEPHSON JUNCTION

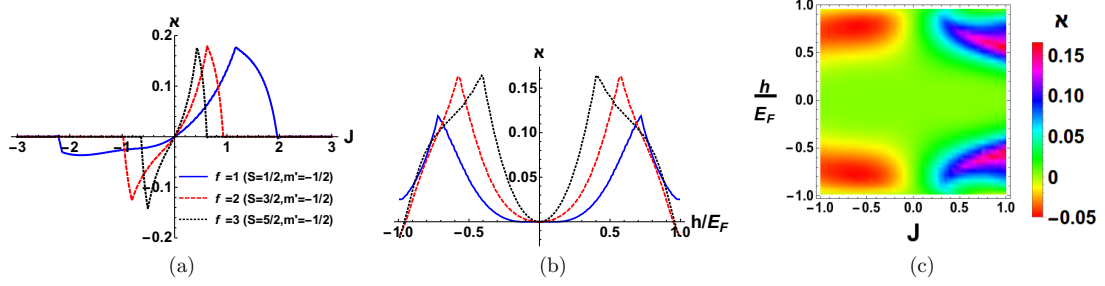


Figure 4.19: (a) Asymmetry of critical current as a function of exchange interaction ( $J$ ) of spin flipper. (b) Asymmetry of critical current as a function of magnetization ( $h$ ) of Ferromagnet's. (c) Asymmetry of the critical current as a function of exchange interaction ( $J$ ) of spin-flipper and magnetization ( $h$ ) of Ferromagnet's. Parameters are  $\Delta_0 = 1\text{meV}$ ,  $T/T_c = 0.01$ ,  $f = 1$  ( $S = 1/2$ ,  $m' = -1/2$ ) (for (c)),  $h = 0.5E_F$  (for (a)),  $k_F a = \pi$ ,  $\theta = \pi/2$ ,  $Z = 0$ ,  $J = 0.5$  (for (b)).

of Ferromagnets. We find a maximum value of  $\mathcal{N} \approx 0.16$  with  $\mathcal{N}$  changing sign from anti-ferromagnetic to ferromagnetic coupling. Asymmetry of critical current is also calculated in Ref. [148] as a function of spin-orbit interaction and magnetization. Nevertheless, in contrast to our case,  $\mathcal{N}$  is larger for larger spin-orbit interaction and magnetization values.

### 4.3.3 Reasons for the existence of Anomalous Josephson effect

#### Explaining quantum spin-flip scattering

The significant role played by the spin flipper entails a detailed analysis of this process. The Josephson current flowing through either ferromagnetic layer ( $F_1$  or  $F_2$ ) is spin-polarized in the direction of magnetization of that ferromagnetic layer. Subsequently when this spin-polarized Josephson current state, denoted by a macroscopic wave-function  $\sim |\Psi_{S_K}\rangle e^{i\varphi_K} \approx (u\ 0\ 0\ v)^T e^{i\varphi_K}$  (where  $K = L$  or  $R$ , i.e., left or right superconductor), interacts with the spin flipper, there is finite probability for mutual spin flip. It is, of course, a probability, not a certainty, since the interaction of spin-polarized Josephson current with spin flipper is quantum in nature. Thus, the combined state of spin-polarized



Josephson current and spin flipper after the interaction is in a superposition of mutual spin-flip and no flip state given by the joint wavefunction of spin-polarized Josephson current and spin flipper. Quantum spin-flip scattering plays an integral role in observing the anomalous Josephson effect, as we discuss later. In the absence of spin-flip scattering probability ( $f = 0$ ), anomalous Josephson current vanishes since time-reversal symmetry is not broken, which we will explain later.

### Explaining chiral symmetry breaking

All standard Josephson junctions have a symmetry, called chiral symmetry. Due to this symmetry, at  $\varphi = 0$  one cannot distinguish between electron tunneling from left to right superconductor and vice-versa. Thus, electron tunneling amplitude from left to right superconductor equals that from right to left superconductor when there is no phase difference between two superconductors ( $\varphi = 0$ ). Thus for our system, as in Fig. 4.13, when Ferromagnet's are aligned ( $\theta = 0$ ),  $t_{ee}^{\uparrow\uparrow}(\varphi = 0) |_{L \rightarrow R} = t_{ee}^{\uparrow\uparrow}(\varphi = 0) |_{L \leftarrow R}$ , where  $t_{ee}^{\uparrow\uparrow} |_{L \rightarrow R}$  and  $t_{ee}^{\uparrow\uparrow} |_{L \leftarrow R}$  are the transmission amplitudes for electron tunneling from left to right superconductor and vice-versa. This implies chiral symmetry is not broken and as a result,  $I(\varphi = 0)$  is strictly zero. But, when Ferromagnet's are misaligned ( $\theta \neq 0$ ), then  $t_{ee}^{\uparrow\uparrow}(\varphi = 0) |_{L \rightarrow R} \neq t_{ee}^{\uparrow\uparrow}(\varphi = 0) |_{L \leftarrow R}$ , i.e., chiral symmetry is broken.

### Explaining time-reversal symmetry breaking

Hamiltonian matrix, in Eq. (4.27) is denoted as  $H_{BdG}(\varphi)$ , such that  $H_{BdG}(\varphi)\psi(x) = E\psi(x)$ . When spin flip probability  $f = 0$  or Ferromagnet's are aligned  $\theta = 0$ ,  $H_{BdG}(\varphi)$  preserves time reversal symmetry ( $T$ ), thus  $TH_{BdG}(\varphi)T^\dagger = H_{BdG}(-\varphi)$ , which implies that if  $H_{BdG}(\varphi)$  possess an energy eigenvalue  $\varepsilon_l(\varphi)$ , then  $H_{BdG}(-\varphi)$  must have the same energy eigenvalue. The Andreev bound states then satisfy:  $\varepsilon_l(\varphi) = \varepsilon_l(-\varphi)$ , and as a result for Josephson

#### 4. SPIN-FLIP SCATTERING INDUCED TUNABLE $0 - \pi$ JOSEPHSON JUNCTION AND QUANTIZED ANOMALOUS PHASE IN FERROMAGNETIC JOSEPHSON JUNCTION

current  $I(\varphi) = -I(-\varphi)$  and there is no anomalous Josephson effect. In presence of spin flip scattering ( $f \neq 0$ ) and when Ferromagnet's are misaligned ( $\theta \neq 0$ ), time reversal symmetry is broken, as a result,  $\varepsilon_I(\varphi) \neq \varepsilon_I(-\varphi)$ , i.e., Andreev bound state symmetry is also broken and thus Josephson current obeys  $I(-\varphi) \neq -I(\varphi)$ , which implies  $I(\varphi = 0) \neq 0$ . Thus, when both  $f \neq 0$  and  $\theta \neq 0$ , i.e., both time reversal symmetry and chiral symmetry are broken, an anomalous Josephson current flows across the junction. In contrast, when  $f = 0$  and  $\theta \neq 0$ , i.e., only chiral symmetry is broken, but time reversal symmetry is not broken then anomalous Josephson current vanishes.

In Table 4.1 we discuss time reversal symmetry, chiral symmetry, anomalous Josephson current and Josephson current for three distinct cases: (a) finite spin flip scattering but Ferromagnets are aligned, i.e.,  $f \neq 0$  but  $\theta = 0$ , (b) no spin flip scattering but Ferromagnets are misaligned, i.e.,  $f = 0$  but  $\theta \neq 0$  and (c) when spin flip scattering is finite and Ferromagnets are misaligned, i.e.,  $f \neq 0$  and  $\theta \neq 0$ . We see that when  $f \neq 0$  and

Table 4.1: Effect of breaking chiral and/or time reversal symmetry on anomalous Josephson current (spin flip probability is  $f$ ; misorientation angle= $\theta$ )

Parameters→ Properties↓	$f \neq 0$ and $\theta = 0$	$f = 0$ and $\theta \neq 0$	$f \neq 0$ and $\theta \neq 0$
Time reversal symmetry	Preserved, $\varepsilon_I(\varphi) = \varepsilon_I(-\varphi)$	Preserved, $\varepsilon_I(\varphi) = \varepsilon_I(-\varphi)$	Broken, $\varepsilon_I(\varphi) \neq \varepsilon_I(-\varphi)$
Chiral symmetry	Preserved, $t_{ee}^{\uparrow\uparrow}(\varphi = 0)  _{L \rightarrow R} = t_{ee}^{\uparrow\uparrow}(\varphi = 0)  _{L \leftarrow R}$	Broken, $t_{ee}^{\uparrow\uparrow}(\varphi = 0)  _{L \rightarrow R} \neq t_{ee}^{\uparrow\uparrow}(\varphi = 0)  _{L \leftarrow R}$	Broken, $t_{ee}^{\uparrow\uparrow}(\varphi = 0)  _{L \rightarrow R} \neq t_{ee}^{\uparrow\uparrow}(\varphi = 0)  _{L \leftarrow R}$
Anomalous Josephson current	Zero	Zero	Finite
Josephson current	$I(-\varphi) = -I(\varphi)$	$I(-\varphi) = -I(\varphi)$	$I(-\varphi) \neq -I(\varphi)$

$\theta = 0$ , both time-reversal symmetry and chiral symmetry are preserved. As a result, anomalous Josephson current vanishes, and Josephson current satisfies the relation  $I(\varphi) = -I(-\varphi)$ . For  $f = 0$  and  $\theta \neq 0$ , chiral symmetry is broken, but time-reversal symmetry is

preserved. As a result, anomalous Josephson current is zero, and Josephson current follows  $I(\varphi) = -I(-\varphi)$ . In contrast, when  $f \neq 0$  and  $\theta \neq 0$ , both time-reversal symmetry and chiral symmetry are broken. As a result, anomalous Josephson current flows through the junction, and Josephson current obeys  $I(\varphi) \neq -I(-\varphi)$ .

#### 4.3.4 How different values of $T/T_c$ affect anomalous Josephson current?

In Fig. 4.20, we show the effect of finite temperature on anomalous Josephson current, anomalous phase, and asymmetry of the critical current in the presence of scattering with  $f = 1$ , i.e.,  $S = 1/2$  and  $m' = -1/2$ , while  $J = 1$  for a transparent junction. In Fig. 4.20(a) of our manuscript, we plot anomalous Josephson current as a function of misorientation angle ( $\theta$ ) between two ferromagnetic layers for different values of  $T/T_c$ . We see that magnitude of anomalous current increases with increasing  $T/T_c$ . Further, the sign of anomalous current does not change with  $T/T_c$ . In Fig. 4.20(b) we plot asymmetry of the

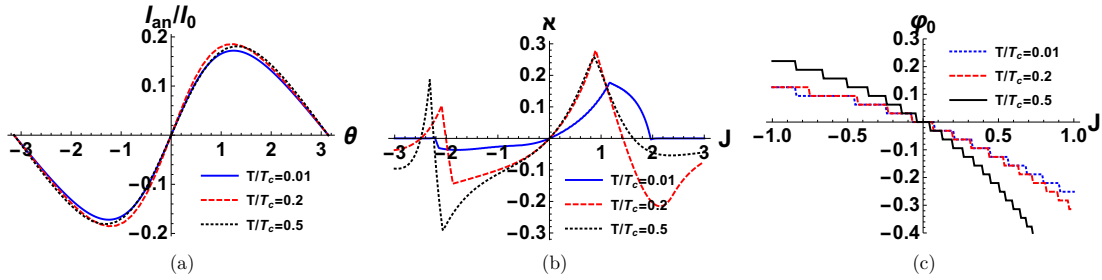


Figure 4.20: (a) Anomalous Josephson current as a function of mis-orientation angle ( $\theta$ ) between two Ferromagnets' for different values of temperature. (b) Asymmetry of the critical current for different values of temperature calculated as a function of exchange interaction ( $J$ ) of spin flipper. (c) Phase difference  $\varphi_0$  as a function of exchange interaction ( $J$ ) of spin flipper for different values of temperature. Parameters are  $\Delta_0 = 1\text{meV}$ ,  $J = 1$  (for (a)),  $h = 0.5E_F$  (for (a), (b) and (c)),  $I_0 = e\Delta_0/\hbar$ ,  $f = 1$  ( $S = 1/2$ ,  $m' = -1/2$ ),  $Z = 0$ ,  $k_F a = \pi$ ,  $\theta = \pi/2$  (for (b) and (c))

critical current  $\kappa$  as a function of exchange interaction  $J$  for different values of  $T/T_c$ . We

see that the maximum value of  $\aleph$  increases with increasing temperature. In Fig. 4.20(c) we plot anomalous phase  $\varphi_0$  as a function of exchange interaction  $J$  of spin flipper for different values of  $T/T_c$ . We see that magnitude of anomalous phase  $\varphi_0$  increases with increasing  $T/T_c$  although magnitude of the “**quantized**” steps in the anomalous phase  $\varphi_0$  remain unchanged, i.e.,  $\pi/100$  radians regardless of  $T/T_c$ , meaning the quantization of steps at the value  $\pi/100$  radians is independent of  $T/T_c$ . Further this quantization at  $\pi/100$  radians is independent of  $J, Z, h, \theta, S, m'$  and  $k_{Fa}$  suggesting this is an “**universal**” feature of our device.

## 4.4 Experimental realization

The set-up as envisaged in Figs. 4.1 and 4.13 can be realized in a experimental lab. Superconductor-Normal metal-Superconductor Josephson junctions have been experimentally realized since long [167]. Superconductor-Ferromagnet-Ferromagnet-Superconductor (S-F-F-S) Josephson junctions have also been designed experimentally for quite some time now [168]. The amalgamation of a Superconductor-Normal metal-Superconductor (SNS) junction with a spin flipper or embedding an S-F-F-S junction with a spin flipper at the interface between two ferromagnets should not be difficult, especially with a  $s$ -wave superconductor like Aluminum or Lead, it should be perfectly possible.  $\pi$  Josephson junction with a quantum dot sandwiched between two superconductors has been demonstrated experimentally in Ref. [169]. They observe a gate-controlled transition from the 0 to the  $\pi$  state. Further, in Ref. [170] they look at the Josephson effect in a quantum spin Hall system coupled with a localized magnetic impurity. Our work in this chapter will help experimentalists in designing tunable  $\pi$  junctions without taking recourse to Ferromagnets or high  $T_c$  superconductors or any applied magnetic fields and also designing anomalous Josephson

junction without applying any external magnetic field but with only a spin flipper.

## 4.5 Conclusion

In this chapter, we have provided an exhaustive study of the nature of the  $0$  to  $\pi$  Josephson junction transition in the presence of a spin flipper. We have studied various aspects of the problem like the strength of the exchange interaction ( $J$ ) between the spin flipper and charge carriers, the effect of electron-electron interactions ( $\alpha$ ) albeit phenomenologically, the effect of junction transparencies ( $Z$ ), and of course the high spin states  $S$ , spin magnetic moment  $m'$  of the spin flipper itself. We identify the spin-flip probability of the spin flipper as the key to understand the  $0$  to  $\pi$  junction transition. We also focused on applications of our junction in quantum computation proposals.

Further, we have studied the anomalous Josephson effect and the direction-dependent critical current in  $S$ - $F_1$ -spin flipper- $F_2$ - $S$  junction where  $F_1$ ,  $F_2$  are the two ferromagnetic layers with misaligned magnetization. In absence of spin-flip scattering, Andreev bound states are time-reversal symmetric, i.e.,  $\varepsilon_l(\varphi) = \varepsilon_l(-\varphi)$ . As a result, Josephson current is sinusoidal with  $I(\varphi) = -I(-\varphi)$ , and there is no anomalous Josephson supercurrent at  $\varphi = 0$ . However, in the presence of spin-flip scattering, an anomalous Josephson effect is seen. Andreev bound states break time-reversal symmetry, i.e.,  $\varepsilon_l(\varphi) \neq \varepsilon_l(-\varphi)$  as well as chiral symmetry, as a result, Josephson current breaks phase inversion symmetry  $I(\varphi) \neq -I(-\varphi)$ , and an anomalous Josephson current can flow at phase difference  $\varphi = 0$ . More importantly, the ferromagnetic Josephson junction with spin-flipper acts as a phase battery that can store quantized amounts of anomalous phase  $\varphi_0$  in the ground state of the junction.



# Chapter 5

## Spin-flip scattering induced quantum spin torque in a Ferromagnetic Josephson junction

*“To be successful, you’ve got to get the kind of torque that’s created by a push and a pull”*

— Roger Ailes

### 5.1 Introduction

When a spin-polarized current enters a ferromagnetic layer, there is generally a transfer of spin angular momentum between the conduction electrons and the magnetization of the ferromagnet. It was first proposed by Slonczewski[171] and Berger[172] in 1996 as a novel mechanism for switching the magnetization of a ferromagnet by a spin-polarized current. It was experimentally realized in spin-valve trilayers in 2000[173]. Since then, spin-transfer torque has been investigated in various magnetic nanostructures[174, 175]. In a spin valve, when an electric current passes through a fixed magnetic layer, it becomes

## 5. SPIN-FLIP SCATTERING INDUCED QUANTUM SPIN TORQUE IN A FERROMAGNETIC JOSEPHSON JUNCTION

---

spin polarized along the direction of the magnetic moment of the fixed magnetic layer. After passing through a nonmagnetic metal layer, the current enters into the free magnetic layer and polarizes along the magnetization direction of the free magnetic layer. When the magnetic moments of the two magnetic layers are not parallel or antiparallel, the free magnetic layer can absorb the spin-polarized current[176]. Due to this absorption, some angular momentum can be transferred to the free layer. Thus, a torque arises on the magnetic moment of the free layer, which can cause the switching of the free layer's magnetization. The torque above is generally described as nonequilibrium spin-transfer torque since it needs a voltage bias to operationalize it. The spin-transfer torque can also arise in an equilibrium situation without a voltage bias as in a Josephson junction.

In ferromagnetic Josephson junction's[177, 178], Josephson current at equilibrium generates an equilibrium spin transfer torque on the magnetic moments of the ferromagnetic layers[179] which is proportional to the sine of the difference in magnetization direction of the two ferromagnets. If  $\mathcal{F}$  is the free energy of the superconductor-ferromagnet-normal metal-ferromagnet-superconductor ( $SF_1NF_2S$ ) junction and  $\theta$  is the angle between the magnetic moments of the ferromagnets, then equilibrium spin transfer torque is defined as[179]  $\tau^{eq} = \frac{\partial \mathcal{F}}{\partial \theta}$ , with Josephson supercurrent[166],  $I = \frac{2e}{\hbar} \frac{\partial \mathcal{F}}{\partial \varphi}$ , and  $\varphi$  being the phase difference between the two superconductors. Thus,  $\frac{\partial I}{\partial \theta} = \frac{2e}{\hbar} \frac{\partial \tau^{eq}}{\partial \varphi}$ , relates Josephson supercurrent to equilibrium spin-transfer torque. The Josephson supercurrent, as shown in Fig. 5.1, depends on the sine of phase difference across superconductors ( $\varphi_L - \varphi_R$ ). This Josephson supercurrent induces an equilibrium spin-transfer torque due to the misaligned magnetic moments of the ferromagnetic layers. Equilibrium spin-transfer torque points perpendicular to the plane spanned by the two magnetic moments of the ferromagnetic layers[179] and its magnitude is sinusoidal in the difference of magnetization directions of the two ferromagnets. Sign and magnitude of the equilibrium spin transfer torque can be



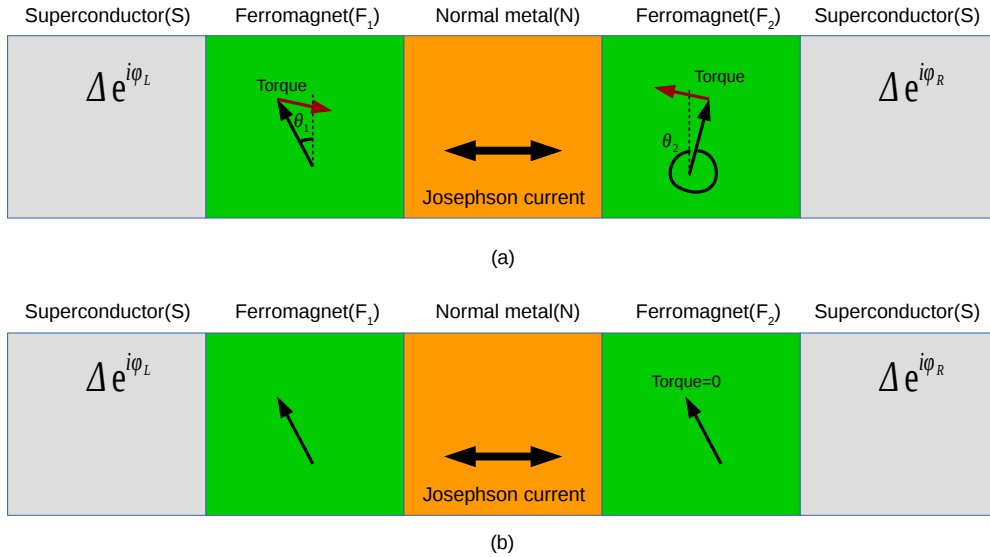


Figure 5.1: *Conventional mechanism of the equilibrium spin transfer torque in a superconductor-ferromagnet-normal metal-ferromagnet-superconductor junction. (a) Magnetic moments of the ferromagnets are misaligned ( $\theta_1 \neq \theta_2$ ). Equilibrium spin-transfer torque  $\tau^{equ} \propto \sin(\theta_1 - \theta_2)$  and points perpendicular to the plane spanned by the two magnetic moments of the ferromagnets, (b) Magnetic moments of the ferromagnets are aligned ( $\theta_1 = \theta_2$ ).  $\tau^{equ} = 0$ : equilibrium spin-transfer torque vanishes.*

controlled by the phase difference between the two superconductors[179].

## 5.2 What is quantum spin-torque?

Spin torque seen previously in SFFS junction[179] or SFFFS junction[165] or SFSFS junction[180] is due to misalignments of ferromagnets leading to equilibrium spin-transfer torque. The origin of equilibrium spin-transfer torque is “classical”. It can be easily understood via a “classical mechanism”. But, this conventional view of the origin of spin-transfer torque may not always be applicable. The quantum origins of spin torque, as opposed to the “classical” spin-transfer torque, have been speculated recently in Refs. [181, 182].

This chapter gives an example where the spin torque mechanism is quantum in nature and due to spin-flip scattering alone. Classically, when the electron's magnetic moment is parallel or antiparallel to the magnetic field, there is no torque exerted on the electron. Similarly, when the two magnetic moments of the ferromagnetic layers are parallel or antiparallel, equilibrium spin-transfer torque vanishes, see Fig. 5.1(b). In Ref. [179], the equilibrium spin-transfer torque also follows the same behavior. But in this chapter, our primary motivation is to show that in Ref. [179] if we replace normal metal with a spin flipper between two ferromagnetic layers, we will see a new effect- the existence of a finite equilibrium spin-torque even when magnetic moments of the ferromagnets are aligned parallel or antiparallel. We show that a spin flipper can engender torque in such a junction. We call this effect "equilibrium quantum spin torque". Thus spin-flip scattering can lead to finite equilibrium spin-torque, which has no classical analog.

We are interested in spin-transfer torque because of possible applications in switching the magnetization of ferromagnets for sufficiently large current without any external magnetic field. This switching provides a mechanism to create fast magnetic random access memories[183]. Further spin-transfer torque can also be used for excitation of spin waves[184]. The equilibrium spin-transfer torque first shown in Ref. [179] with *s*-wave superconductor has been extended to *d*-wave in Ref. [185].

### 5.2.1 Difference between equilibrium quantum spin torque and nonequilibrium quantum spin torque

Quantum spin-torque discussed in this chapter arises in equilibrium when Josephson current flows through the Superconductor-Ferromagnet-Spin flipper-Ferromagnet-Superconductor (S-F-SF-F-S) junction with aligned magnetizations. It is called equilibrium quantum spin torque. However, quantum spin torque can also arise in a nonequilibrium situation,

i.e., in the presence of a voltage bias, when a current flows perpendicular to the layers in Ferromagnet-Spin flipper-Ferromagnet (F-SF-F) junction with aligned magnetizations. There are some crucial differences between equilibrium and nonequilibrium quantum spin torque.

(i) Equilibrium quantum spin-torque points perpendicular to the plane spanned by the magnetization vectors of the two ferromagnetic layers. On the other hand, nonequilibrium quantum spin-torque mainly lies in the plane spanned by the magnetization vectors of the ferromagnets.

(ii) Equilibrium quantum spin torques on the magnetic moments of both ferromagnets are equal in magnitude but opposite in sign. However, no such relationship exists for nonequilibrium quantum spin torque.

(iii) Equilibrium quantum spin torque can be tuned via phase difference across the superconductors. But, nonequilibrium quantum spin torque can be tuned by the direction of the current flow through the junction.

## 5.3 Ferromagnetic Josephson junction in the presence of a spin flipper

To show the existence of an equilibrium quantum spin torque even when magnetizations in ferromagnets are aligned, we consider a Josephson junction consisting of two ferromagnets with a spin flipper sandwiched between two conventional  $s$ -wave superconductors. The superconductors are isotropic and our model is shown in Fig. 5.2, with a spin flipper at  $x = 0$ , two  $s$ -wave superconductors on either side at  $x < -a/2$  and  $x > a/2$  and two ferromagnetic layers in regions:  $-a/2 < x < 0$  and  $0 < x < a/2$ . In general,  $\theta$  the magnetization vectors of the two ferromagnetic layers are misaligned by an angle

## 5. SPIN-FLIP SCATTERING INDUCED QUANTUM SPIN TORQUE IN A FERROMAGNETIC JOSEPHSON JUNCTION

$\theta$ . However, in our calculation  $\theta \rightarrow 0$ , i.e., magnetization vectors are aligned parallelly. We take the superconducting pair potential of the form  $\Delta = \Delta_0(T)[e^{i\varphi_L}\Theta(-x - a/2) + e^{i\varphi_R}\Theta(x - a/2)]$ , where  $\Delta_0(T)$  is temperature dependent gap parameter,  $\varphi_L$  and  $\varphi_R$  are the superconducting phases for left and right superconductor respectively. The temperature dependence of  $\Delta_0(T)$  is given by  $\Delta_0(T) = \Delta_0 \tanh(1.74\sqrt{(T_c/T - 1)})$ , where  $T_c$  is the superconducting critical temperature[24].

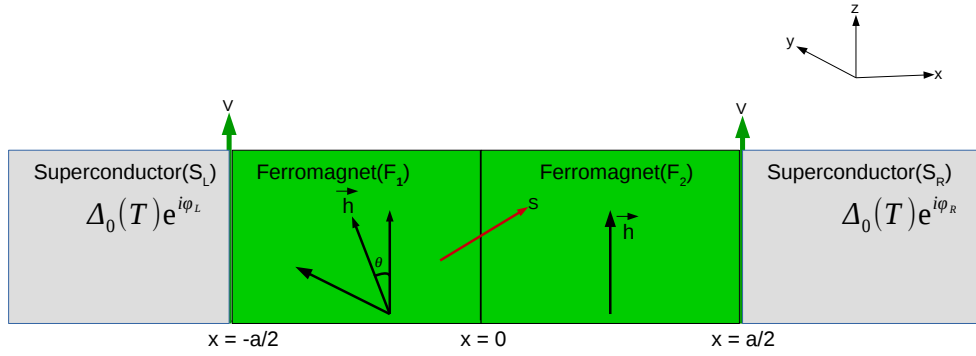


Figure 5.2: Josephson junction composed of two ferromagnets and a spin flipper with spin  $S$  and magnetic moment  $m'$  at  $x = 0$  sandwiched between two  $s$ -wave superconductors. In our model  $\theta_1 = \theta$  and  $\theta_2 = 0$ . When ferromagnets are aligned, i.e.,  $\theta \rightarrow 0$ , equilibrium spin transfer torque vanishes (see Fig. 5.1(b)), however in our setup a new quantum mechanism of spin flip scattering gives rise to a non-zero torque, which we denote as Equilibrium quantum spin torque (EQST). In this chapter, we mainly concentrate on the limit  $\theta \rightarrow 0$ .

The BdG equation of our system is given below[27]:

$$\begin{pmatrix} H_0 \hat{I} & i\Delta \hat{\sigma}_y \\ -i\Delta^* \hat{\sigma}_y & -H_0^* \hat{I} \end{pmatrix} \psi(x) = E\psi(x), \quad (5.1)$$

where  $H_0 = p^2/2m^* + V[\delta(x + a/2) + \delta(x - a/2)] - J_0\delta(x)\vec{s}\cdot\vec{S} - \vec{h}\cdot\hat{\sigma}[\Theta(x + a/2) + \Theta(a/2 - x)] - E_F$ . In the Hamiltonian “ $H_0$ ”, the first term describes kinetic energy of an electron with mass  $m^*$ , the second term depicts interfaces:  $V$  is the strength of the  $\delta$ -like potential at the two interfaces between ferromagnet and superconductor, the third term describes

### 5.3. Ferromagnetic Josephson junction in the presence of a spin flipper

spin flipper with  $J_0$  being the strength of exchange interaction between electron with spin  $\vec{s}$  and spin flipper with spin  $\vec{S}$ [13], the fourth term describes ferromagnets with  $\vec{h}$  being the magnetization vectors of the two ferromagnets and  $\Theta$  is the Heaviside step function. Further,  $\psi(x)$  is a four-component spinor,  $E_F$  is Fermi energy,  $\hat{\sigma}$  is Pauli spin matrix and  $\hat{I}$  is a  $2 \times 2$  identity matrix. In general, magnetization vector ( $\vec{h}$ ) of left ferromagnet ( $F_1$ ) is assumed to be at an angle of  $\theta$  with  $z$  axis in the  $y-z$  plane, while that of right ferromagnet ( $F_2$ ) is fixed along the  $z$  axis. Thus,  $\vec{h} \cdot \hat{\sigma} = h \sin \theta \hat{\sigma}_y + h \cos \theta \hat{\sigma}_z$ [165]. However, in our study we only concentrate on the case where  $\theta \rightarrow 0$ , i.e., Ferromagnets are aligned. In the subsequent analysis we take the dimensionless version of  $J_0$  and  $V$  given as  $J = \frac{m^* J_0}{k_F}$  and  $Z = \frac{m^* V}{\hbar^2 k_F}$ [9].

If we solve the BdG equation for superconductors, see Eq. (5.1), we will get wavefunctions for left and right superconductors. Let us consider a spin up electron incident at  $x = -a/2$  interface from left superconductor. The wave function[27] in left superconductor (for  $x < -\frac{a}{2}$ ) is,

$$\psi_{S_L}(x) = \varphi_1^{S_L} e^{ik_+x} \phi_{m'}^S + r_{ee}^{\uparrow\uparrow} \varphi_1^{S_L} e^{-ik_+x} \phi_{m'}^S + r_{ee}^{\uparrow\downarrow} \varphi_2^{S_L} e^{-ik_+x} \phi_{m'+1}^S + r_{eh}^{\uparrow\uparrow} \varphi_3^{S_L} e^{ik_-x} \phi_{m'+1}^S + r_{eh}^{\uparrow\downarrow} \varphi_4^{S_L} e^{ik_-x} \phi_{m'}^S, \quad (5.2)$$

where  $\varphi_i^{S_L}$ ,  $i = 1, 2, 3, 4$  are as defined in section 4.2 of chapter 4 and amplitudes  $r_{ee}^{\uparrow\uparrow}, r_{ee}^{\uparrow\downarrow}, r_{eh}^{\uparrow\uparrow}, r_{eh}^{\uparrow\downarrow}$  are the normal reflection without spin flip, normal reflection with spin flip, Andreev reflection with spin flip and Andreev reflection without spin flip respectively.

The corresponding wave function in right superconductor (for  $x > \frac{a}{2}$ ) is given by,

$$\psi_{S_R}(x) = t_{ee}^{\uparrow\uparrow} \varphi_1^{S_R} e^{ik_+x} \phi_{m'}^S + t_{ee}^{\uparrow\downarrow} \varphi_2^{S_R} e^{ik_+x} \phi_{m'+1}^S + t_{eh}^{\uparrow\uparrow} \varphi_3^{S_R} e^{-ik_-x} \phi_{m'+1}^S + t_{eh}^{\uparrow\downarrow} \varphi_4^{S_R} e^{-ik_-x} \phi_{m'}^S, \quad (5.3)$$

where  $\varphi_i^{S_R}$ ,  $i = 1, 2, 3, 4$  are as defined in section 4.2 of chapter 4 and  $t_{ee}^{\uparrow\uparrow}, t_{ee}^{\uparrow\downarrow}, t_{eh}^{\uparrow\uparrow}, t_{eh}^{\uparrow\downarrow}$  represent transmission amplitudes, corresponding to the reflection process described above and  $\varphi = \varphi_R - \varphi_L$  represents phase difference between right and left superconductors.

Similarly solving the BdG equation for ferromagnets, we get the wavefunction in

## 5. SPIN-FLIP SCATTERING INDUCED QUANTUM SPIN TORQUE IN A FERROMAGNETIC JOSEPHSON JUNCTION

---

ferromagnets. The wavefunction in the left ferromagnet ( $F_1$ ) is given by,

$$\begin{aligned} \psi_{F_1}(x) = & (e_F e^{iq_1^+(x+a/2)} + f_F e^{-iq_1^+x}) \varphi_1^F \phi_{m'}^S + (e'_F e^{iq_1^+(x+a/2)} + f'_F e^{-iq_1^+x}) \varphi_2^F \phi_{m'+1}^S \\ & + (g_F e^{-iq_1^-(x+a/2)} + h_F e^{iq_1^-x}) \varphi_3^F \phi_{m'+1}^S + (g'_F e^{-iq_1^-(x+a/2)} + h'_F e^{iq_1^-x}) \varphi_4^F \phi_{m'}^S, \text{ for } -\frac{a}{2} < x < 0, \end{aligned} \quad (5.4)$$

where  $\varphi_i^F$ ,  $i = 1, 2, 3, 4$  are defined in section 3.5 of chapter 3. Similarly, the wavefunction in the right ferromagnet ( $F_2$ ) is given by,

$$\begin{aligned} \psi_{F_2}(x) = & (a_F e^{iq_1^+x} + b_F e^{-iq_1^+(x-a/2)}) \varphi_1^N \phi_{m'}^S + (a'_F e^{iq_1^+x} + b'_F e^{-iq_1^+(x-a/2)}) \varphi_2^N \phi_{m'+1}^S \\ & + (c_F e^{-iq_1^-x} + d_F e^{iq_1^-(x-a/2)}) \varphi_3^N \phi_{m'+1}^S + (c'_F e^{-iq_1^-x} + d'_F e^{iq_1^-(x-a/2)}) \varphi_4^N \phi_{m'}^S, \text{ for } 0 < x < \frac{a}{2}. \end{aligned} \quad (5.5)$$

where  $\varphi_i^N$ ,  $i = 1, 2, 3, 4$  are defined in section 1.3 of chapter 1.  $q_\sigma^\pm = \sqrt{\frac{2m^*}{\hbar^2}(E_F + \rho_\sigma h \pm E)}$  is the wavevector for electron ( $q_\sigma^+$ ) and hole ( $q_\sigma^-$ ) in the ferromagnetic layers, wherein  $\rho_\sigma = +1(-1)$  is related to  $\sigma = \uparrow(\downarrow)$ . We have used the Andreev approximation  $k_+ = k_- = \sqrt{\frac{2m^*E_F}{\hbar^2}} = k_F$  and  $q_{\uparrow,\downarrow} = k_F \sqrt{1 \pm \frac{\hbar}{E_F}}$ , where  $k_F$  is the Fermi wavevector, with  $E_F \gg \Delta, E$ .

The boundary conditions[27] can be written as follows: at  $x = -a/2$ ,  $\psi_{S_L}(x) = \psi_{F_1}(x)$  and,  $\frac{d\psi_{F_1}}{dx} - \frac{d\psi_{S_L}}{dx} = \frac{2m^*V}{\hbar^2}\psi_{F_1}$ , while at  $x = 0$  (see Fig. 5.2),  $\psi_{F_1}(x) = \psi_{F_2}(x)$ , and  $\frac{d\psi_{F_2}}{dx} - \frac{d\psi_{F_1}}{dx} = -\frac{2m^*J_0\vec{s}\cdot\vec{S}}{\hbar^2}\psi_{F_1}$ . Finally, at  $x = a/2$ , the boundary conditions are-  $\psi_{F_2}(x) = \psi_{S_R}(x)$ ,  $\frac{d\psi_{S_R}}{dx} - \frac{d\psi_{F_2}}{dx} = \frac{2m^*V}{\hbar^2}\psi_{F_2}$ .  $\vec{s}\cdot\vec{S} = s_z S_z + \frac{1}{2}(s^- S^+ + s^+ S^-)$  is exchange coupling due to spin flipper in the Hamiltonian.  $\vec{s}$  represents electron spin operator acting on electron/hole states  $\phi_m^s$ , while  $\vec{S}$  represents the spin operator acting on spin flipper states  $\phi_{m'}^S$ .  $\phi_m^s$  is eigenspinor of electron/hole while  $\phi_{m'}^S$  is eigenspinor of spin flipper with  $m$  and  $m'$  being spin magnetic moment of electron/hole and spin flipper respectively.  $s$  is spin of electron, while  $S$  is spin of spin flipper, with  $s^\pm = s_x \pm i s_y$ ,  $s_z = \frac{\hbar}{2} \begin{pmatrix} \sigma_z & 0 \\ 0 & -\sigma_z \end{pmatrix}$ ,  $s_x = \frac{\hbar}{2} \begin{pmatrix} 0 & \sigma_x \\ \sigma_x & 0 \end{pmatrix}$ ,  $s_y = \frac{\hbar}{2} \begin{pmatrix} 0 & \sigma_y \\ \sigma_y & 0 \end{pmatrix}$ , where  $\sigma_z = \begin{pmatrix} 1 & 0 \\ 0 & -1 \end{pmatrix}$ ,  $\sigma_x = \begin{pmatrix} 0 & 1 \\ 1 & 0 \end{pmatrix}$ ,  $\sigma_y = \begin{pmatrix} 0 & -i \\ i & 0 \end{pmatrix}$ . The action of spin raising and spin lowering operators for spin flipper are discussed below.

### 5.3. Ferromagnetic Josephson junction in the presence of a spin flipper

For spin up electron incident  $\phi_m^s = \varphi_1^N$ , with  $s = 1/2$ ,  $m = 1/2$ . Now, when spin flip term of our Hamiltonian acts on spin up electron  $\varphi_1^N$ , and the spin flipper state  $\phi_{m'}^S$ , we have-

$$\vec{s} \cdot \vec{S} \varphi_1^N \phi_{m'}^S = s_z S_z \varphi_1^N \phi_{m'}^S + \frac{1}{2} s^- S^+ \varphi_1^N \phi_{m'}^S + \frac{1}{2} s^+ S^- \varphi_1^N \phi_{m'}^S. \quad (5.6)$$

Now,  $s^+ \varphi_1^N = 0$ , since  $s^+$  is the spin raising operator and there are no higher spin states for a spin-1/2 electron than up and so the 3rd term in Eq. (5.6) vanishes, while  $s^- \varphi_1^N = \hbar \varphi_2^N$ , the spin lowering operator gives the down spin state  $\varphi_2^N$  of electron. Further, for spin-up electron  $s_z \varphi_1^N = \frac{\hbar}{2} \varphi_1^N$ , and for spin flipper-  $S_z \phi_{m'}^S = \hbar m' \phi_{m'}^S$ . Further, the spin-raising and spin-lowering operators acting on spin flipper give:  $S^+ \phi_{m'}^S = \hbar f \phi_{m'+1}^S = \hbar \sqrt{(S - m')(S + m' + 1)} \phi_{m'+1}^S$  and  $S^- \phi_{m'+1}^S = \hbar \sqrt{(S - m')(S + m' + 1)} \phi_{m'}^S$ .

$$\text{Thus, } \vec{s} \cdot \vec{S} \varphi_1^N \phi_{m'}^S = \frac{\hbar^2}{2} m' \varphi_1^N \phi_{m'}^S + \frac{\hbar^2}{2} \sqrt{(S - m')(S + m' + 1)} \varphi_2^N \phi_{m'+1}^S \quad (5.7)$$

From Eqs. (5.6), (5.7) we thus have-

$$\vec{s} \cdot \vec{S} \varphi_1^N \phi_{m'}^S = \frac{\hbar^2}{2} m' \varphi_1^N \phi_{m'}^S + \frac{\hbar^2}{2} f \varphi_2^N \phi_{m'+1}^S \quad (\text{for both no flip and spin flip processes})$$

#### 5.3.1 Andreev bound states and Josephson charge current

Following the procedure enunciated in Ref. [24] to calculate bound state contribution to Josephson supercurrent we neglect the contribution from incoming quasiparticle, i.e., first term  $\varphi_1^{S_L} e^{ik+x} \phi_{m'}^S$ , of Eq. (5.2) and insert the wave functions in the boundary conditions, we get a homogeneous system of linear equations for the scattering amplitudes,  $Qx = 0$ , where  $x$  is a  $8 \times 1$  column matrix and is given by  $x = [r_{ee}^{\uparrow\uparrow}, r_{ee}^{\uparrow\downarrow}, r_{eh}^{\uparrow\uparrow}, r_{eh}^{\uparrow\downarrow}, t_{ee}^{\uparrow\uparrow}, t_{ee}^{\uparrow\downarrow}, t_{eh}^{\uparrow\uparrow}, t_{eh}^{\uparrow\downarrow}]^T$  and  $Q$  is a  $8 \times 8$  matrix obtained by expressing the scattering amplitudes in the two ferromagnetic layers by the scattering amplitudes in the left and right superconductor. For a nontrivial solution of this system, Determinant of  $Q = 0$ , we get the Andreev bound state energy spectrum  $E_i$ ,  $i = \{1, \dots, 8\}$ [155]. This is the usual procedure for calculating the bound state spectra in

## 5. SPIN-FLIP SCATTERING INDUCED QUANTUM SPIN TORQUE IN A FERROMAGNETIC JOSEPHSON JUNCTION

---

Josephson junctions, see Refs. [24, 27]. We find that  $E_i (i = 1, \dots, 8) = \pm \varepsilon_p (p = 1, \dots, 4)$ . From Andreev bound states energies[155] we get the Free energy of our system, which is given by[24]:

$$\mathcal{F} = -\frac{1}{\beta} \frac{1}{2\pi} \int_0^{2\pi} \ln \left[ \prod_i (1 + e^{-\beta E_i}) \right] d(k_F a) = -\frac{2}{\beta} \frac{1}{2\pi} \int_0^{2\pi} \sum_{p=1}^4 \ln \left[ 2 \cosh \left( \frac{\beta \varepsilon_p}{2} \right) \right] d(k_F a). \quad (5.8)$$

We consider only the short junction limit, i.e.,  $a \ll \xi$ , where  $\xi$  is the superconducting coherence length and  $a$  the width of the intervening ferromagnetic layers between superconductors, such that only the bound state contribution determines the total Josephson current, the continuum contribution is negligible and so neglected[24, 27]. The charge Josephson current at finite temperature is the derivative of the Free energy  $\mathcal{F}$  of our system to the phase difference  $\varphi$  between left and right superconductors[27, 166],

$$I_c = \frac{2e}{\hbar} \frac{\partial \mathcal{F}}{\partial \varphi} = -\frac{2e}{\hbar} \frac{1}{2\pi} \int_0^{2\pi} \sum_{p=1}^4 \tanh \left( \frac{\beta \varepsilon_p}{2} \right) \frac{\partial \varepsilon_p}{\partial \varphi} d(k_F a). \quad (5.9)$$

### 5.3.2 Equilibrium spin torque

From the Free energy of our system, Eq. (5.8) we calculate the equilibrium spin torque[179] by taking derivative of the Free energy with respect to misorientation angle ' $\theta$ ' (the angle between magnetic moments of the two ferromagnets),

$$\tau^{eq} = \frac{\partial \mathcal{F}}{\partial \theta} = -\frac{1}{2\pi} \int_0^{2\pi} \sum_{p=1}^4 \tanh \left( \frac{\beta \varepsilon_p}{2} \right) \frac{\partial \varepsilon_p}{\partial \theta} d(k_F a). \quad (5.10)$$

The equilibrium spin torque is also referred as equilibrium spin current in some papers[6, 180]. In our calculation as previously mentioned we focus on the case where magnetization in two ferromagnets is aligned, i.e.,  $\theta \rightarrow 0$ . In this limit we surprisingly see a finite equilibrium quantum spin torque (EQST) due to spin flip scattering upending, the classical



reason behind spin torque being due to nonaligned magnetization. For transparent regime ( $Z = 0$ ) we find,

$$\tau^{eq} |_{\theta \rightarrow 0} = \frac{\Delta_0^2(T)}{2\pi} \int_0^{2\pi} \left( \tanh\left(\frac{\beta M_1}{2}\right) M_1' + \tanh\left(\frac{\beta M_2}{2}\right) M_2' + \tanh\left(\frac{\beta M_3}{2}\right) M_3' + \tanh\left(\frac{\beta M_4}{2}\right) M_4' \right) d(k_F a) \quad (5.11)$$

where  $M_1, M_2, M_3, M_4, M_1', M_2', M_3'$  and  $M_4'$  are functions of exchange interaction ( $J$ ), magnetization of ferromagnets, spin ( $S$ ) and magnetic moment ( $m'$ ) of spin flipper, the phase ( $k_F a$ ) accumulated in ferromagnetic region and spin flip probability of spin flipper ( $f$ ). Their explicit forms are given in Appendix C. In Appendix C we show that for no flip case, the EQST ( $\tau^{eq} |_{\theta \rightarrow 0}$ ) vanishes. In the next subsection from figures we will show that the EQST is zero in the limit  $J \rightarrow 0$  and  $Z \rightarrow \infty$ .

### 5.3.3 Analyzing equilibrium quantum spin torque

In this subsection we analyze via various plots this unique quantum spin torque due to spin flip scattering alone. In Fig. 5.3 we plot both Josephson charge supercurrent as well as the EQST for different interface transparencies  $Z$  as function of the phase difference  $\varphi$ . We consider magnetic moments of the ferromagnetic layers to be parallel ( $\theta \rightarrow 0$ ) and deal with the spin-flip case, i.e.,  $f \neq 0$ . For this case,  $S \neq m'$ , for the spin flipper. Thus there is a finite probability for the spin flipper to flip its spin while interacting with an electron/hole. We see both Josephson charge current and EQST is inhibited by increasing interface barrier strength ( $Z$ ). Further, similar to the charge Josephson current, the EQST vanishes at  $\varphi = 0$  and  $\varphi = 2\pi$ . Usually, the spin-transfer torque opposes the Josephson current (see Ref. [179]), however the equilibrium quantum spin torque (EQST), as shown here, can flow in the same direction as the Josephson current, see Fig. 5.3(a),  $-0.7 < \varphi < 0.7$ . This behavior is also seen in Ref. [182] for the quantum spin-transfer torque in a different context.

## 5. SPIN-FLIP SCATTERING INDUCED QUANTUM SPIN TORQUE IN A FERROMAGNETIC JOSEPHSON JUNCTION

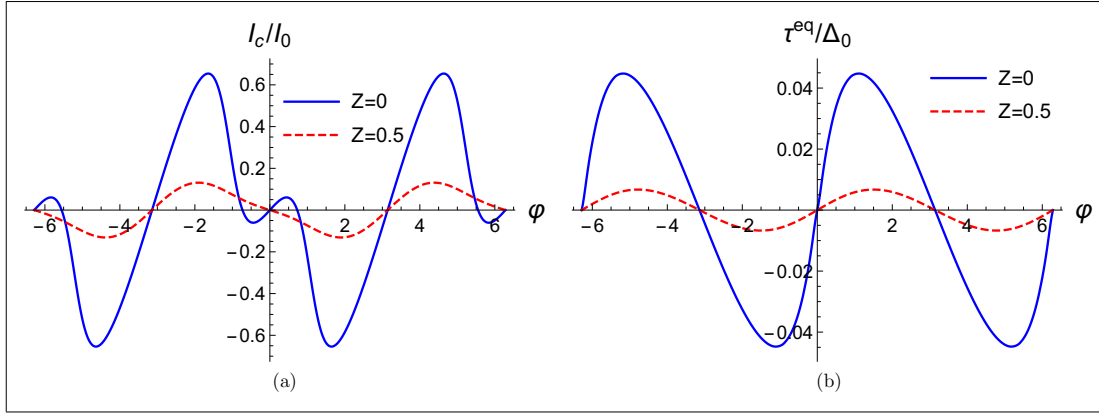


Figure 5.3: Josephson charge current and equilibrium quantum spin torque (EQST) as a function of phase difference ( $\varphi$ ) for different values of interface barrier strength ( $Z$ ). Parameters are  $\Delta_0 = 1\text{meV}$ ,  $I_0 = e\Delta_0/\hbar$ ,  $T/T_c = 0.01$ ,  $J = 0.5$ ,  $\hbar/E_F = 0.5$ ,  $\theta = 0$ ,  $S = 5/2$ ,  $m' = -1/2$ . Both  $I_c$  and  $\tau^{eq}$  are inhibited by increasing  $Z$  and also EQST is zero for  $\varphi = 0$  and  $\varphi = 2\pi$ .

In Fig. 5.4(a) we plot EQST as a function of phase difference ( $\varphi$ ) for different values of exchange interaction  $J$  again for  $\theta \rightarrow 0$ . We see that with change of exchange interaction  $J$  there is a sign change in EQST. The change in sign of  $\tau^{eq}$  via a change in ‘ $J$ ’ implies that the EQST seen in our system can be tuned via ‘ $J$ ’ and the sign of  $\tau^{eq}$  can be controlled by the phase difference as shown in Figs. 5.3(b), 5.4(a) & 5.4(b). In Fig. 5.4(b) we plot EQST as function of phase difference ( $\varphi$ ) for different values of magnetization ( $h$ ) of the ferromagnets. We see that the EQST increases with increasing ‘ $h$ ’.

In Fig. 5.5 we study EQST from low to high spin states of spin-flipper and for different values of spin-flip probability of spin flipper again at  $\theta \rightarrow 0$  for a transparent junction, i.e.,  $Z = 0$ . In Fig. 5.5(a),  $J = 1$  and we see that EQST monotonically decreases with increasing ‘ $S$ ’, for particular value of  $m' = -\frac{1}{2}$ , implying high spin states inhibit EQST. In Fig. 5.5(b), we plot EQST for a particular spin  $S = 5/2$  and all possible values of spin-flip probability of spin flipper. We see that EQST is enhanced for  $f > S$ , but for  $f < S$ , EQST is suppressed.

### 5.3. Ferromagnetic Josephson junction in the presence of a spin flipper

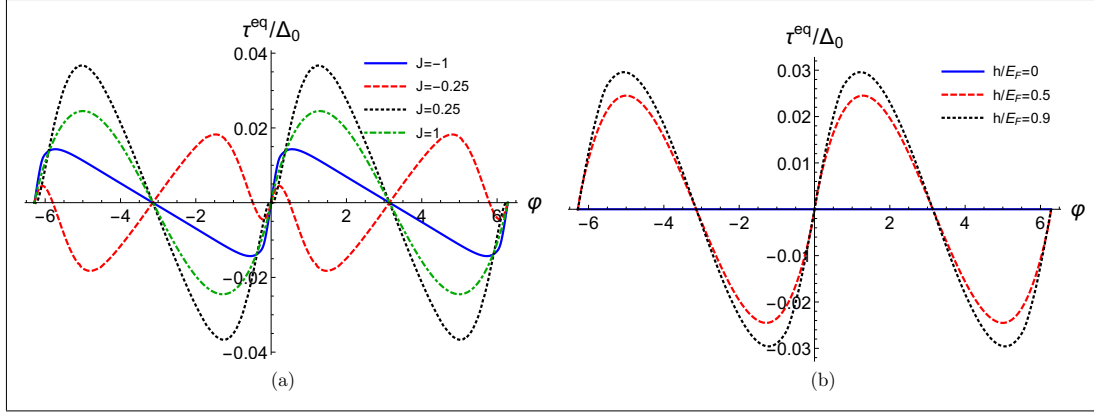


Figure 5.4: EQST as a function of phase difference ( $\varphi$ ) for (a) different values of exchange interaction ( $J$ ) of spin flipper and for (b) different values of magnetization ( $h$ ) of the ferromagnets. Parameters are  $\Delta_0 = 1\text{meV}$ ,  $I_0 = e\Delta_0/\hbar$ ,  $T/T_c = 0.01$ ,  $Z = 0$ ,  $J = 1$  (for (b)),  $h/E_F = 0.5$ ,  $\theta = 0$ ,  $S = 5/2$ ,  $m' = -1/2$ . In (a) EQST changes sign with change of exchange interaction  $J$  and phase difference  $\varphi$ . In (b) EQST increases with increasing magnetization  $h$  of the ferromagnets.

In Fig. 5.6(a) we plot the EQST for flip ( $S = 3/2, m' = -1/2, f \neq 0$ ) case as well as no flip ( $S = 3/2, m' = 3/2, f = 0$ ) case and also for a superconductor-ferromagnet-ferromagnet-superconductor ( $S$ - $F_1$ - $F_2$ - $S$ ) junction without spin flipper ( $J = 0$ ) in the same figure as a function of misorientation angle ( $\theta$ ) between ferromagnets. We see that in contrast to  $S$ - $F_1$ - $F_2$ - $S$  junction ( $J = 0$  case) and no flip case, EQST is finite at  $\theta \rightarrow 0$  and  $\theta = \pi$  when spin flipper flips its spin. Thus the reason for finite EQST at  $\theta \rightarrow 0$  is a finite probability for flipping. It can be explained as follows- after passing through the first ferromagnetic layer, the supercurrent becomes polarized in the magnetization direction of the first ferromagnetic layer. When spin-polarized supercurrent interacts with the spin flipper through the exchange interaction, there is a finite probability for a mutual spin flip. The equation below depicts the interaction process:

$$|s.c\rangle \otimes |\phi_{m'}^S\rangle = \sqrt{\frac{m'}{2}}|\text{No flip}\rangle + \sqrt{\frac{f}{2}}|\text{Mutual-flip}\rangle \quad (5.12)$$

where  $|s.c\rangle$  is the state of spin-polarized supercurrent, see paragraphs above and below

Eq. (5.7) on how this equation described above comes into being. Due to this spin-flip scattering, the direction of the spin of supercurrent will be in a superposition too and thus will differ from the direction of the magnetization vector of the ferromagnetic layer. Thus, when the supercurrent enters the second ferromagnetic layer, the magnetization vector of the second ferromagnetic layer will exert a torque on the spin flipped component of the supercurrent wave function to rotate the supercurrent's spin along the direction of magnetization while leaving the non-spin flipped component as it is. From the conservation of spin angular momentum, the supercurrent will also exert an equal and opposite torque on the magnetic moment of the second ferromagnetic layer leading to a finite EQST even at  $\theta \rightarrow 0$ . However, in the absence of a spin flipper ( $J = 0$  case) and for no flip case, the spin-polarized supercurrent state does not flip its spin. Thus, in the absence of spin flipper or the case of no-flip scattering, the spin-polarized supercurrent's spin and the magnetization vector of the ferromagnetic layers will be in the same direction. Therefore, EQST vanishes in the case of  $J = 0$  and the no-flip process, but for the spin-flip process, it is finite. This finite  $\tau^{eq}$  can be a check also on whether *SFFS* junctions are clean or contaminated with magnetic adatoms. In Fig. 5.6(b) we plot EQST as a function of exchange interaction  $J$  from antiferromagnetic coupling ( $J < 0$ ) to ferromagnetic coupling ( $J > 0$ ) at phase difference  $\varphi = \pi/2$ . For  $\theta \rightarrow 0$ , ferromagnets have no role in flipping the electron's/hole's spin[186] and spin-flip is only due to the spin flipper. We see that for ferromagnetic coupling, there is no change in the direction of the EQST with a change in  $J$ . However, for antiferromagnetic coupling ( $J < 0$ ), there is a change in the direction of  $\tau^{eq}$  as  $J$  changes from  $J = 0$  to  $J = -2$ , implying tunability of the sign of EQST via the exchange interaction of spin flipper.

Finally, in Fig. 5.7 we plot EQST as a function of interface barrier strength ( $Z$ ). We see no change in the direction of EQST with the increase of interface barrier strength  $Z$ .

### 5.3. Ferromagnetic Josephson junction in the presence of a spin flipper

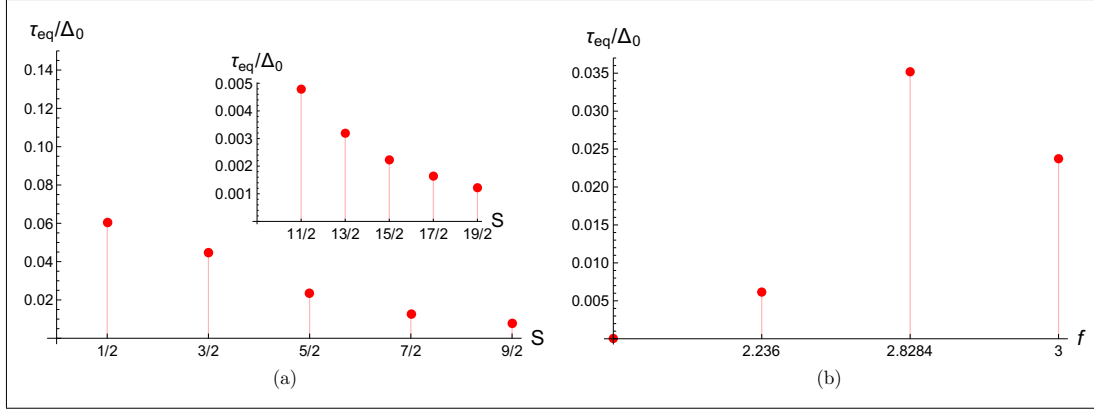


Figure 5.5: (a) Equilibrium quantum spin torque (EQST) vs spin ( $S$ ) of spin flipper. (b) EQST vs spin flip probability ( $f$ ) of spin flipper for  $S = 5/2$  and  $m' = 5/2$  ( $f = 0$ ),  $m' = 3/2$  and  $m' = -5/2$  ( $f = 2.236$ ),  $m' = 1/2$  and  $m' = -3/2$  ( $f = 2.8284$ ) and  $m' = -1/2$  ( $f = 3$ ). Parameters are  $\Delta_0 = 1\text{meV}$ ,  $T/T_c = 0.01$ ,  $\varphi = \pi/2$ ,  $J = 1$ ,  $m' = -1/2$  (for (a)),  $Z = 0$ ,  $\theta = 0$ ,  $h/E_F = 0.5$ . EQST decreases with increase of spin  $S$  of spin flipper.

Further, EQST is almost zero in the tunneling regime.

The theoretically predicted numerical value of equilibrium spin-transfer torque (ESTT) is  $\sim 10^{-2}$  meV in Ref. [179]. On the other hand, for the parameter values  $Z = 0$ ,  $J = 0.5$ ,  $\varphi = \pi/2$ ,  $S = 5/2$  and  $m' = -1/2$ , the numerical value of equilibrium quantum spin torque (EQST) is 0.04 meV. Thus, the value of equilibrium quantum spin torque (EQST) is almost the same as the value of equilibrium spin-transfer torque as predicted in Ref. [179].

Equilibrium spin current/torque in superconductor-ferromagnet-superconductor junctions with inhomogeneous magnetization is studied in Ref. [187]. They pointed out discontinuous jumps in the equilibrium spin current or torque whenever the junction undergoes a  $0 - \pi$  transition. They find numerically that the spin current or torque is symmetric to the phase difference between two superconductors. They also show that for specific values of the thickness of the ferromagnetic layer, a pure spin current can flow through the junction without any charge current. Similar to their work, we see quantum spin torque is finite even when charge current vanishes. This finite quantum spin torque is antisymmetric to phase

## 5. SPIN-FLIP SCATTERING INDUCED QUANTUM SPIN TORQUE IN A FERROMAGNETIC JOSEPHSON JUNCTION

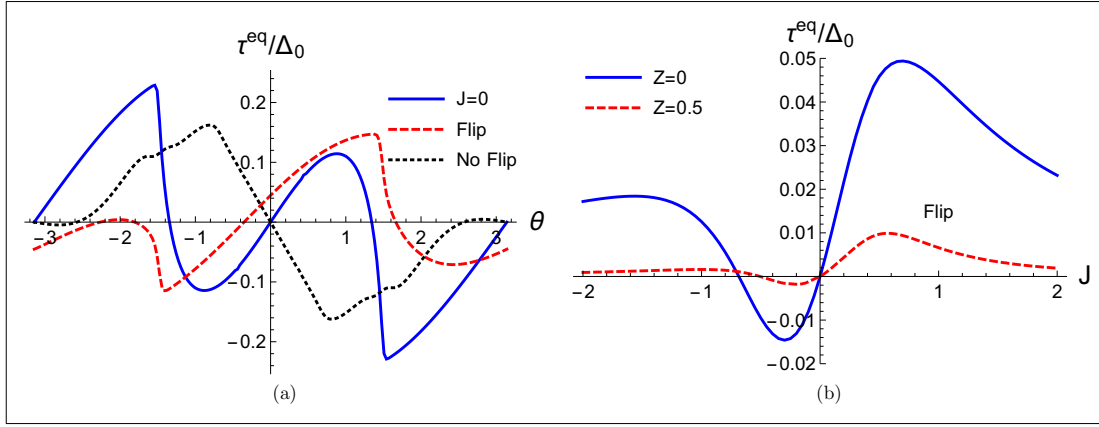


Figure 5.6: (a) EQST as function of misorientation angle ( $\theta$ ) for  $\varphi = \pi/2$ . (b) EQST as function of exchange interaction ( $J$ ) of spin flipper for  $\varphi = \pi/2$  and  $\theta = 0$ . Parameters are  $\Delta_0 = 1\text{meV}$ ,  $I_0 = e\Delta_0/\hbar$ ,  $T/T_c = 0.01$ ,  $Z = 0$ ,  $h/E_F = 0.5$ , spin flip case:  $S = 3/2, m' = -1/2$ , no flip case:  $S = 3/2, m' = 3/2$  and for (a)  $J = 1$ . In (a) EQST is zero for  $J = 0$  and no flip case ( $f = 0$ ), but finite for spin flip case ( $f \neq 0$ ). In (b) EQST changes sign with change in  $J$  for antiferromagnetic coupling ( $J < 0$ ) and is also asymmetric with respect to  $J$ .

difference between two superconductors in contrast to their work.

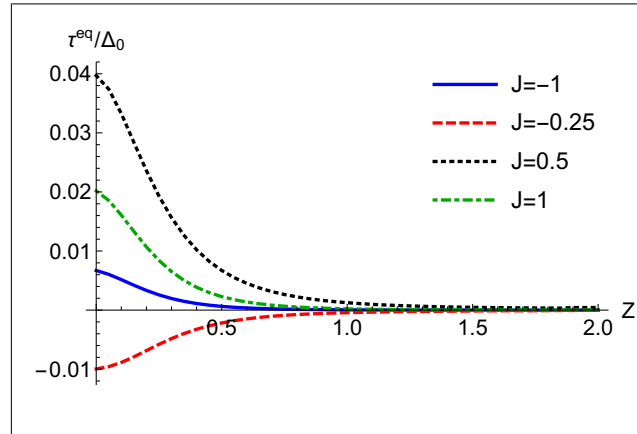


Figure 5.7: EQST as a function of interface barrier strength ( $Z$ ). Parameters are  $\Delta_0 = 1\text{meV}$ ,  $I_0 = e\Delta_0/\hbar$ ,  $T/T_c = 0.01$ ,  $\theta = 0$ ,  $h/E_F = 0.5$ ,  $\varphi = \pi/2$ ,  $J = 0.5$ ,  $S = 5/2$ ,  $m' = -1/2$ . EQST decreases with increase of  $Z$  and in the tunneling regime ( $Z \rightarrow \text{large}$ ) EQST vanishes.

### 5.3.4 Physical picture of equilibrium quantum spin torque

To understand the physical basis of the equilibrium quantum spin torque, we go back to Fig. 5.2. When the Josephson supercurrent enters the first ferromagnetic layer, it becomes spin-polarized along the magnetization direction of the first ferromagnetic layer. This spin-polarized supercurrent then interacts with the spin flipper through the exchange coupling, and there is a finite probability for a mutual spin flip. One should note that this is a probability, not a certainty, since the interaction of spin-polarized supercurrents is quantum in nature. Thus while before interaction the supercurrent wavefunction and spin flipper wavefunction are completely independent after interaction both are in a entangled and in a superposed state of:  $\sqrt{\frac{m'}{2}}|No - flip\rangle + \sqrt{\frac{f}{2}}|Mutual - flip\rangle$ .

This finite probability of spin-flip scattering implies the direction of the supercurrent's spin polarization is now in a superposition of either polarized in the direction of the magnetization of ferromagnetic layers or not. Thus, since the direction of the magnetization vector in both ferromagnetic layers is the same, this implies the magnetization direction of the second ferromagnetic layer will now differ from that of the supercurrent's spin polarization state, which is in a superposition. Thus, when this supercurrent enters the second ferromagnetic layer, the magnetic moment of the second ferromagnetic layer will exert a torque on that part of the supercurrent wave-function, which is not in the same direction as the ferromagnets. This results in rotation of the spin state of the spin flipped component of supercurrent's wave-function along the direction of magnetization while leaving the non-spin flipped part of the supercurrent's wave-function as it is. From the conservation of spin angular momentum, the spin flipped component of the supercurrent's wave function will also exert an equal and opposite torque on the magnetic moment of the second ferromagnetic layer. In this way, a torque arises although ferromagnets are aligned.

However, for the no flip process, wave-function is not in a superposition, and in that case, there is only a single no flip component. The spin-polarized state of the supercurrent does not flip its spin when interacting with the spin flipper. Thus, in case of no flip scattering, the direction of spin-polarized supercurrent and direction of magnetization of the ferromagnets will remain the same. Thus, equilibrium quantum spin-torque vanishes in case of no flip process, but it is finite for the spin-flip process.

## 5.4 Experimental realization

The experimental detection of the novel phenomena pointed out in this chapter shouldn't be difficult. Superconductor-Ferromagnet-Ferromagnet-Superconductor (S-F-F-S) junctions have been fabricated experimentally for quite some time now[168]. Doping a magnetic adatom or spin flipper in S-F-F-S junctions with identical magnetization for ferromagnets will experimentally implement our setup as shown in Fig. 5.2.

## 5.5 Conclusion

This chapter presents an exhaustive study of the nature of equilibrium spin torque in the presence of a spin flipper in a hybrid Ferromagnet-Superconductor junction. We focus on the situation when the magnetic moments of the ferromagnetic layers are parallel. We identify spin-flip scattering to be critical in inducing a quantum spin torque in such an equilibrium configuration. Further, we see that one can control the sign of this spin-flip scattering induced equilibrium quantum spin-torque via the exchange interaction of spin flipper and the phase difference across the two superconductors. Tuning the direction of the equilibrium quantum spin-torque leads to control over the magnetization of the ferromagnets. It has critical applications in various spintronic devices as by changing



the direction of magnetization, designing faster magnetic random access memories[183] becomes easier.



# Chapter 6

## Josephson quantum thermodynamics and spin flip scattering

*“Weather systems are natural heat engines, and like all other heat engines, both natural and artificial, they are driven not by temperature per se, but by differences in temperature between one location and another.”*

— Robert Zubrin

### 6.1 Introduction

Recently, superconducting hybrid systems have drawn attention due to their possible device applications as sensitive detectors[188, 189, 190], low-temperature sensitive thermometers[191, 192, 193], heat valves[194, 195, 196], solid-state quantum machines[197, 198, 199], solid-state micro-refrigerators[200, 201, 202] and thermoelectric generators[203, 204, 205]. Quantum thermodynamics implies the study of thermodynamic processes from the principle of quantum mechanics[206]. Refrigeration means the transfer of heat from low to high-temperature region[207] aided by work done on the system. Thermodynamic[208, 209, 210, 211] properties of a Josephson Stirling engine have been discussed in Ref. [212],

wherein a quantum spin Hall insulator based Josephson junction is shown to act as a quantum heat engine. Josephson Stirling engines are not the only game in town. Diffusive SNS junctions have been shown to operate as Josephson-Otto or as Josephson-Stirling engines in Ref. [213].

In this chapter, by doping a spin flipper in a 1D Josephson junction (JJ) loop, which is in turn attached to two thermal reservoirs at unequal temperatures via thermal valves, we show that the device can be employed both as a quantum heat engine as well as a refrigerator and can also work as a Joule pump or cold pump. When operating as a quantum heat engine, the efficiency of this device exceeds that of some recent Josephson heat engine proposals. Further, as a quantum refrigerator, the coefficient of performance of this device is much higher than previously proposed Josephson junction-based refrigerators. In addition, this device can be tuned from engine mode to refrigerator mode or any other mode, i.e., Joule pump or cold pump, by either tuning the temperature of reservoirs or via the enclosed magnetic flux in the Josephson junction loop. It makes the proposed device much more versatile as regards possible applications.

Our proposed device's main advantage over other proposals is its tunability by the magnetic flux that threads the JJ loop. Tuning our device via magnetic flux means external control. However, tuning via temperatures or by controlling thermal valves means internal control. External control is always better than internal control since external control does not lead to any decoherence. Internal control implies tuning system parameters which at small length scales is always tricky and prone to errors.

## 6.2 Theoretical model

The model device, depicted in Fig. 6.1, is formed from a 1D superconducting loop[214] interrupted by a spin flipper. An external magnetic flux  $\Phi$  controls the superconducting phase difference across the spin-flipper. The JJ loop is attached, via two thermal valves  $v_L$  and  $v_R$ , to reservoirs at either end, which in turn are at temperatures  $T_L$  and  $T_R$ . The two reservoirs can exchange heat  $Q_L$  and  $Q_R$  with the JJ loop. The scattering problem is solved using BTK approach[9] for superconductor-spin flipper-superconductor junction as shown in the dashed line box of Fig. 6.1. The two reservoirs control the temperature of the JJ loop via thermal valves  $v_L$  and  $v_R$ . When valve  $v_R$  is opened and  $v_L$  is closed, the JJ loop is in thermal contact with the right reservoir at temperature  $T_R$ . Similarly, when valve  $v_L$  is opened and  $v_R$  is closed, the JJ loop is in thermal contact with the left reservoir at temperature  $T_L$ . On the other hand, phase difference across the JJ loop is controlled via magnetic flux  $\Phi$  enclosed by the loop. Thus, the JJ device can be driven from one state to another by controlling both temperature and phase difference. We discuss this in more detail for a Stirling cycle in the next section.

In our proposed set-up, a spin-flipper is embedded in the JJ loop of circumference  $L_S$ , see Fig. 6.1. We used BTK approach[9] to solve the scattering problem. In our work spin-flipper is a delta potential magnetic impurity[13] fixed between two superconductors. For proper understanding of our system we compare our delta potential magnetic impurity with a rectangular potential barrier magnetic impurity in Fig. 6.2. In Fig. 6.2(a), a single magnetic impurity is lying along the solid black color line at  $x = 0$ . The magnetic impurity is designed as a delta potential along the  $x$ -direction but is uniform along the  $y$ -direction. We assume magnetic impurity to have a finite width with a translational invariance along the  $y$ -direction. To understand it properly we can compare with a rectangular potential barrier

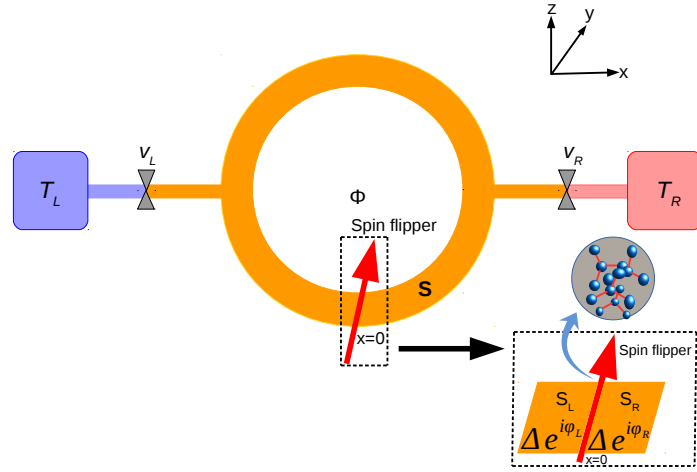


Figure 6.1: 1D Josephson junction (JJ) loop (circumference  $L_S$ , in orange) doped with a spin flipper and attached to two thermal reservoirs at temperatures  $T_L$  and  $T_R$  via two thermal valves  $v_L$  and  $v_R$ . A magnetic flux  $\Phi$  controls phase difference  $\varphi$  across spin flipper in JJ loop.  $S_L$  and  $S_R$  are the left and right superconductors maintained at phase difference  $\varphi = \varphi_R - \varphi_L$ . High spin molecules like  $Fe_{19}$ -complex can act as a spin flipper.

placed between two superconductors as shown in Fig. 6.2(c). In Fig. 6.2(c), we show the setup which has a rectangular potential barrier between  $x = 0$  and  $x = L$  with translational invariance along  $y$  direction. The rectangular potential barrier influences the transmission of incident particles along the  $x$  direction but doesn't influence the transmission along the  $y$  direction because the transmitting particle cannot experience the potential change along the  $y$  direction. When one decreases the length  $L$  of the rectangular potential barrier, it becomes equivalent to a delta potential barrier located at  $x = 0$ , see Refs. [14, 215]. Similarly, in Fig. 6.2(b) we show that a magnetic impurity can have a finite width between  $x = 0$  and  $x = L$  with a translational invariance along the  $y$  direction. If we reduce the width  $L$  of the impurity, it becomes a delta function like profile influencing the transmission along the  $x$  direction but not along the  $y$  direction, as shown in Fig. 6.2(a). In Fig. 6.2(d) we show that a rectangular potential barrier in Fig. 6.2(c) can be approximated as a delta

potential barrier. Similar concepts have been used to model magnetic impurity in similar junctions, for e.g., graphene-magnetic impurity-graphene junction, see Refs. [14, 215].

BdG Hamiltonian for JJ loop is given as,

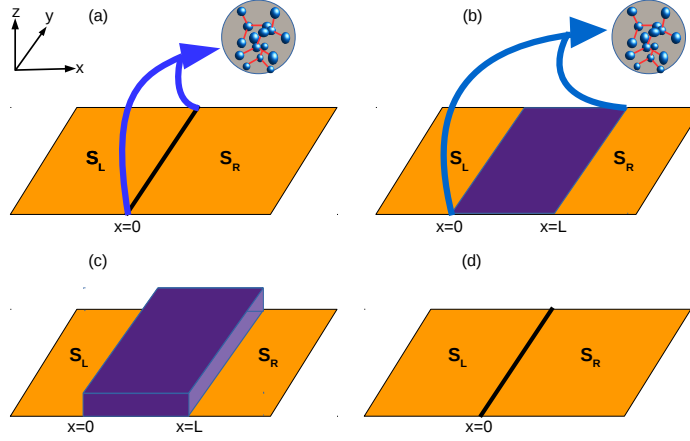


Figure 6.2: Two superconductors separated by (a) a delta potential magnetic impurity, (b) a rectangular barrier magnetic impurity, (c) a rectangular potential barrier and, (d) a delta potential barrier.

$$H_{BdG}(x) = \begin{pmatrix} H\hat{I} & i\Delta(x)\hat{\sigma}_y \\ -i\Delta^*(x)\hat{\sigma}_y & -H\hat{I} \end{pmatrix}, \quad (6.1)$$

where  $H = p^2/2m^* - J_0\delta(x)\vec{s}\cdot\vec{S} - E_F$ , with  $p^2/2m^*$  representing kinetic energy of electron-like or hole-like quasiparticle of mass  $m^*$ , and  $E_F$  is Fermi energy. Superconducting gap  $\Delta(x) = \Delta[e^{i\varphi_L}\Theta(-x) + e^{i\varphi_R}\Theta(x)]$ . For simplicity, we consider superconducting gap to be independent of temperature, i.e.,  $\Delta(T) \approx \Delta(T=0)$  with  $\frac{\partial\Delta}{\partial T} \approx 0$ , which is valid if  $T \ll T_c$ ,  $T_c$  being superconducting critical temperature.  $\varphi_L$  and  $\varphi_R$  are superconducting phases for left and right superconductors respectively as shown in dashed line box of Fig. 6.1. We use dimensionless parameter  $J = \frac{m^*J_0}{k_F}$  as a measure of strength of exchange interaction[13] between quasi-particles and spin-flipper. The product  $J_0\delta(x)\vec{s}\cdot\vec{S}$  has dimensions of energy, thus  $\vec{s}$  which represents spin angular momentum of electron is in units of  $\hbar$  and  $\vec{S}$  considered

as spin angular momentum of spin-flipper also in units of  $\hbar$ ,  $\delta(x)$  having dimensions of  $1/L$ , therefore  $J_0$  the exchange interaction has dimensions of  $E - L/\hbar^2$ .

Diagonalizing BdG Hamiltonian, Eq. (6.1) one gets the wavefunctions in superconducting regions of our system for electron/hole-like quasiparticle incidence. For electronlike quasiparticle (ELQ) with spin up incident from left superconductor, wave function[27] in left superconductor is,

$$\psi_{S_L}(x) = \varphi_1^{S_L} e^{iq_+x} \phi_{m'}^S + r_{ee}^{\uparrow\uparrow} \varphi_1^{S_L} e^{-iq_+x} \phi_{m'}^S + r_{ee}^{\uparrow\downarrow} \varphi_2^{S_L} e^{-iq_+x} \phi_{m'+1}^S + r_{eh}^{\uparrow\uparrow} \varphi_3^{S_L} e^{iq_-x} \phi_{m'+1}^S + r_{eh}^{\uparrow\downarrow} \varphi_4^{S_L} e^{iq_-x} \phi_{m'}^S, \text{ for } x < 0, \quad (6.2)$$

where  $\varphi_i^{S_L}$ ,  $i = 1, 2, 3, 4$  are defined in section 4.2 of chapter 4 and  $r_{ee}^{\uparrow\uparrow}, r_{ee}^{\uparrow\downarrow}, r_{eh}^{\uparrow\uparrow}, r_{eh}^{\uparrow\downarrow}$  are normal reflection amplitude without flip, normal reflection amplitude with flip, Andreev reflection amplitude with flip and Andreev reflection amplitude without flip respectively. The corresponding wave function in right superconductor is,

$$\psi_{S_R}(x) = t_{ee}^{\uparrow\uparrow} \varphi_1^{S_R} e^{iq_+x} \phi_{m'}^S + t_{ee}^{\uparrow\downarrow} \varphi_2^{S_R} e^{iq_+x} \phi_{m'+1}^S + t_{eh}^{\uparrow\uparrow} \varphi_3^{S_R} e^{-iq_-x} \phi_{m'+1}^S + t_{eh}^{\uparrow\downarrow} \varphi_4^{S_R} e^{-iq_-x} \phi_{m'}^S, \text{ for } x > 0, \quad (6.3)$$

where  $\varphi_i^{S_R}$ ,  $i = 1, 2, 3, 4$  are defined in section 4.2 of chapter 4 and  $t_{ee}^{\uparrow\uparrow}, t_{ee}^{\uparrow\downarrow}, t_{eh}^{\uparrow\uparrow}, t_{eh}^{\uparrow\downarrow}$  being transmission amplitudes, corresponding to reflection processes described above and  $\varphi = \varphi_R - \varphi_L$  is phase difference between right and left superconductors. Wavevectors for electron-like quasiparticles ( $q_+$ ) and hole-like quasiparticles ( $q_-$ ) are  $q_{\pm} = \sqrt{\frac{2m^*}{\hbar^2} (E_F \pm \sqrt{E^2 - \Delta^2})}$ . Andreev approximation[25] gives  $q_+ = q_- = k_F$ , with  $k_F$  being Fermi wavevector, and  $E_F \gg \Delta$ . Imposing boundary conditions on Eqs. (6.2), (6.3) at  $x = 0$ , gives

$$\psi_{S_L}(x) = \psi_{S_R}(x) \quad \text{and} \quad \frac{d\psi_{S_R}}{dx} - \frac{d\psi_{S_L}}{dx} = -\frac{2m^* J_0 \vec{s} \cdot \vec{S}}{\hbar^2} \psi_{S_L}, \quad (6.4)$$

where  $\vec{s} \cdot \vec{S} = s_z S_z + \frac{1}{2}(s^- S^+ + s^+ S^-)$  represents exchange operator of spin flipper, with

$$\vec{s} \cdot \vec{S} \psi_{S_L}(x=0) = \vec{s} \cdot \vec{S} \varphi_1^{S_L} \phi_{m'}^S + r_{ee}^{\uparrow\uparrow} \vec{s} \cdot \vec{S} \varphi_1^{S_L} \phi_{m'}^S + r_{ee}^{\uparrow\downarrow} \vec{s} \cdot \vec{S} \varphi_2^{S_L} \phi_{m'+1}^S + r_{eh}^{\uparrow\uparrow} \vec{s} \cdot \vec{S} \varphi_3^{S_L} \phi_{m'+1}^S + r_{eh}^{\uparrow\downarrow} \vec{s} \cdot \vec{S} \varphi_4^{S_L} \phi_{m'}^S. \quad (6.5)$$



$s^\pm = s_x \pm i s_y$  and  $S^\pm = S_x \pm i S_y$  are spin raising and spin lowering operators for electron-like quasiparticle/holelike quasiparticle and spin-flipper respectively. In our theoretical treatment, we solve the scattering problem using BTK approach for superconductor-spin flipper-superconductor junction as shown in dashed line box of Fig. 1. As depicted in Fig. 1, spin-flipper is placed at  $x = 0$  and there is a phase difference  $\varphi$  across the spin flipper. This phase difference is generated by magnetic flux  $\Phi$  in Josephson junction loop, which can control it. We solve the scattering problem at  $x = 0$ , thus our results do not depend on  $x$  or loop circumference  $L_S$ . Action of exchange operator  $\vec{s} \cdot \vec{S}$  on spin up electron-like quasi-particle spinor is shown below,

$$\vec{s} \cdot \vec{S} \varphi_1^{S_L} \phi_{m'}^S = \frac{\hbar^2 m'}{2} \varphi_1^{S_L} \phi_{m'}^S + \frac{\hbar^2 f}{2} \varphi_2^{S_L} \phi_{m'+1}^S, \quad (6.6)$$

where,  $f = \sqrt{(S - m')(S + m' + 1)}$  denotes flip probability[13] for spin-flipper. Similarly, action of  $\vec{s} \cdot \vec{S}$  on the spin down electron-like quasi-particle spinor is

$$\vec{s} \cdot \vec{S} \varphi_2^{S_L} \phi_{m'+1}^S = -\frac{\hbar^2 (m' + 1)}{2} \varphi_2^{S_L} \phi_{m'+1}^S + \frac{\hbar^2 f}{2} \varphi_1^{S_L} \phi_{m'}^S. \quad (6.7)$$

Further, action of exchange operator  $\vec{s} \cdot \vec{S}$  on spin-up hole-like quasi-particle spinor is

$$\vec{s} \cdot \vec{S} \varphi_3^{S_L} \phi_{m'+1}^S = -\frac{\hbar^2 (m' + 1)}{2} \varphi_3^{S_L} \phi_{m'+1}^S + \frac{\hbar^2 f}{2} \varphi_4^{S_L} \phi_{m'}^S, \quad (6.8)$$

action of exchange operator  $\vec{s} \cdot \vec{S}$  on spin down hole-like quasi-particle spinor is

$$\vec{s} \cdot \vec{S} \varphi_4^{S_L} \phi_{m'}^S = \frac{\hbar^2 m'}{2} \varphi_4^{S_L} \phi_{m'}^S + \frac{\hbar^2 f}{2} \varphi_3^{S_L} \phi_{m'+1}^S. \quad (6.9)$$

In quantum spin flip scattering process, wherein Josephson supercurrent (state of Josephson supercurrent is given as  $|s.c\rangle$ ) is denoted by a macroscopic wavefunction  $\sim |\Psi_{S_N}| e^{i\varphi_N} \approx (u 0 0 v)^T e^{i\varphi_N}$  (where  $N$  can be  $L$  or  $R$ ) interacts with the spin flipper, the spin flipper can flip its spin with finite probability, but there is no certainty for flipping its spin. In addition

to the spin flip process, there is the other process of no flip. Thus, while before interaction, the supercurrent wavefunction and spin-flipper wavefunction are completely independent after interaction both are in a entangled and in a superposed state of:

$$\underbrace{|s.c\rangle \otimes |\phi_{m'}^S\rangle}_{\text{Before interaction}} = \underbrace{\frac{m'}{2} \overbrace{|\text{No-flip}\rangle}^{\text{Product state}} + \frac{p}{2} \overbrace{|\text{Mutual-flip}\rangle}^{\text{Entangled state}}}_{\text{After interaction}}.$$

The interaction of unpolarized Josephson current with spin-flipper leads to with finite flip probability an entangled state of spin up Josephson current and spin down spin-flipper & spin down Josephson current and spin up spin-flipper and may also lead to with a product state of spin down Josephson current and spin down spin-flipper for no flip case,

$$\begin{array}{l} \text{Spin flip:} \\ \text{No flip:} \end{array} \begin{array}{l} \underbrace{|\uparrow\rangle_{s.c}}_{\text{Josephson current state}} \otimes \underbrace{|\downarrow\rangle_{\phi_{m'}^S}}_{\text{Spin-flipper state}} \\ \underbrace{|\downarrow\rangle_{s.c}}_{\text{Josephson current state}} \times \underbrace{|\downarrow\rangle_{\phi_{m'}^S}}_{\text{Spin-flipper state}} \end{array} \xrightarrow{\text{interaction}} \begin{array}{l} \overbrace{|\downarrow\rangle_{s.c} \otimes |\uparrow\rangle_{\phi_{m'}^S} + |\uparrow\rangle_{s.c} \otimes |\downarrow\rangle_{\phi_{m'}^S}}^{\text{Entangled state}} \\ \underbrace{|\downarrow\rangle_{s.c} \times |\downarrow\rangle_{\phi_{m'}^S}}_{\text{Product state}} \end{array}.$$

In our case spin-flipper interacts with Josephson current state. The whole macroscopic wavefunction of supercurrent is entangled with spin flipper wavefunction.

### 6.2.1 Andreev bound states

To calculate Andreev bound states we neglect contribution from incoming quasiparticle and insert wavefunctions, Eqs. (6.2), (6.3) into boundary conditions (Eq. (6.4)). We get a homogeneous system of 8 linear equations for the scattering amplitudes,

$$Ny = 0 \tag{6.10}$$

where  $y$  is a  $8 \times 1$  column matrix and given as  $y = [r_{ee}^{\uparrow\uparrow}, r_{ee}^{\uparrow\downarrow}, r_{eh}^{\uparrow\uparrow}, r_{eh}^{\uparrow\downarrow}, t_{ee}^{\uparrow\uparrow}, t_{ee}^{\uparrow\downarrow}, t_{eh}^{\uparrow\uparrow}, t_{eh}^{\uparrow\downarrow}]^T$ ,  $N$  being a  $8 \times 8$  matrix. For nontrivial solution of this system, the determinant of  $N = 0$  and we get Andreev bound states as a function of phase difference  $\varphi$  between two superconductors,

i.e., Andreev bound state energy spectrum  $E_j$ ,  $j = \{1, \dots, 4\}$ [155]. We find that  $E_j(\varphi) = E_\sigma^\pm(\varphi) = \pm E_\sigma(\varphi)$ , ( $\sigma = \uparrow, \downarrow$ ),

$$E_\sigma^\pm(\varphi) = \pm \Delta \sqrt{1 + \frac{A_0(\varphi)}{C_0} + \rho_\sigma \frac{\sqrt{B_0(\varphi)}}{C_0}}, \quad (6.11)$$

where,  $A_0(\varphi) = J^2(2 + f^4 J^2 + 2f^2(-2 + J^2 m'(1 + m')) + m'(1 + m')(4 + J^2 m'(1 + m')))$   
 $+ 2(8 + J^2(1 - 2f^2 + 2m'(1 + m')))\cos(\varphi)$ ,

$B_0(\varphi) = 2J^2(64f^4 J^2 + 3(J + 2Jm')^2 + 4f^2(16 + J^2(5 + 4m'(1 + m')))) + 4J^2(-4f^2 + 16f^4 -$   
 $(1 + 2m')^2)\cos(\varphi) + ((J + 2Jm')^2 - 4f^2(16 + (J + 2Jm')^2))\cos(2\varphi)$ ,

$C_0 = (16 + J^4(f^2 + m' + m'^2)^2 + J^2(4 + 8f^2 + 8m'(1 + m')))$ ,

and  $\rho_{\uparrow(\downarrow)} = +1(-1)$ . In absence of spin flip scattering ( $f = 0$ ), Eq. (6.11) reduces to,

$$E(\varphi) = \pm \Delta \sqrt{\frac{4 \cos^2(\varphi/2) + J^2 m'^2}{4 + J^2 m'^2}}. \quad (6.12)$$

### 6.2.2 Superconductor-Spin flipper-Superconductor junction as a thermodynamic system

Before analyzing the thermodynamic behavior of setup, Fig. 6.1, we introduce the different thermodynamic quantities. From Andreev bound state energies we can determine phase-dependent part of Free energy of JJ[19] (inset of Fig. 6.1) as,

$$F(\varphi, T) = -\frac{1}{\beta} \ln \left[ \prod_j (1 + e^{-\frac{E_j(\varphi)}{k_B T}}) \right] = -\frac{2}{\beta} \sum_\sigma \ln \left[ 2 \cosh \left( \frac{E_\sigma(\varphi)}{2k_B T} \right) \right], \quad (6.13)$$

where  $k_B$  is Boltzmann constant. In Eq. (6.13), we neglect contribution from the quasi-particle states in continuum with energies above the superconducting gap, whose density of states is  $\rho_c$ . In the case of short Josephson junction (length of the weak link much

smaller than superconducting coherence length),  $\rho_c$  is the same as in a bulk superconductor and therefore is phase independent. For Superconductor-Spin flipper-Superconductor junction, across the spin flipper, the junction length is infinitesimally small, and thus  $\rho_c$  is phase independent. Eq. (6.13) is only the phase-dependent part of the Free energy. Since Josephson current is the derivative of the Free energy to phase difference across the superconductors, thus phase-independent part of the Free energy does not contribute to Josephson current in our Superconductor-Spin flipper-Superconductor junction. Further, in work done and the heat exchanged calculation phase-independent part of the Free energy cancels out and therefore does not contribute. From Free energy, we can calculate total Josephson current[166] as

$$I(\varphi, T) = \frac{2e}{\hbar} \frac{\partial F(\varphi, T)}{\partial \varphi}, \quad (6.14)$$

where  $e$  is charge of electron. Entropy of our device can then be calculated from Free energy as,

$$\Omega(\varphi, T) = -\frac{\partial F(\varphi, T)}{\partial T}. \quad (6.15)$$

From entropy  $\Omega$  one determines heat capacity of JJ as,

$$C(\varphi, T) = T \frac{\partial \Omega(\varphi, T)}{\partial T}. \quad (6.16)$$

### 6.3 Josephson-Stirling Cycle

The Josephson-Stirling cycle[212, 213] represented in Fig. 6.3, involves two isothermal and two isophasic processes. States **1,2** involve right reservoir, while states **3,4** involve left reservoir. Below we summarize these different processes,

- **Isothermal process (1 → 2):** Thermal valve  $v_R$  is open while  $v_L$  is closed, thus system is in thermal contact with right reservoir at temperature  $T_R$ . The device or system goes from state **1**  $\equiv (\varphi = 0, T_R)$  to state **2**  $\equiv (\varphi = \varphi_{fi}, T_R)$ .

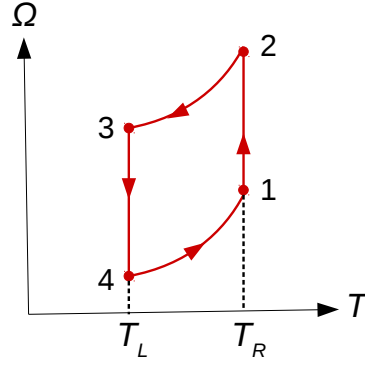


Figure 6.3: *Josephson-Stirling cycle in  $T\Omega$  ( $T$  is temperature and  $\Omega$  is entropy) plane. Enclosed area in  $T - \Omega$  plane corresponds to total heat exchanged  $Q$ , which is equal to total work done  $W$  during the cycle.*

- **Isophasic process (2 → 3):** Thermal valve  $v_L$  is open while  $v_R$  is closed and system is driven from state  $\mathbf{2} \equiv (\varphi = \varphi_{fi}, T_R)$  to state  $\mathbf{3} \equiv (\varphi = \varphi_{fi}, T_L)$ .
- **Isothermal process (3 → 4):** In this stage valve  $v_R$  is closed and  $v_L$  is open. System is transferred from state  $\mathbf{3} \equiv (\varphi = \varphi_{fi}, T_L)$  to state  $\mathbf{4} \equiv (\varphi = 0, T_L)$ .
- **Isophasic process (4 → 1):** Final stage of cycle involves closing valve  $v_L$  and opening valve  $v_R$ , with system being driven from state  $\mathbf{4} \equiv (\varphi = 0, T_L)$  to state  $\mathbf{1} \equiv (\varphi = 0, T_R)$ .

When the device or system is driven from state ‘ $in$ ’ to state ‘ $fi$ ’ ( $in \rightarrow fi$ ) during a quasi-static process, work done and heat released during the process are given as  $W_{infi} = -\frac{\hbar}{2e} \int_{\varphi_{in}}^{\varphi_{fi}} I(\varphi, T) d\varphi$  and  $Q_{infi} = \int_{\Omega(\varphi_{in}, T)}^{\Omega(\varphi_{fi}, T)} T d\Omega$  respectively, where  $I(\varphi, T)$  is Josephson current and  $\Omega$  is entropy of setup depicted in Fig. 6.1. In expressions for work done and heat released below, we have taken sign convention such that  $W_{infi}$  is positive when work is released to the universe while  $Q_{infi}$  is positive when heat is absorbed from the

universe. Work done and heat released for an isothermal process, where phase difference  $\varphi$  changes from  $\varphi_{in} \rightarrow \varphi_{fi}$  at constant temperature  $T$  is given as  $W_{infi} = -[F(\varphi_{fi}, T) - F(\varphi_{in}, T)]$  and  $Q_{infi} = T[\Omega(\varphi_{fi}, T) - \Omega(\varphi_{in}, T)]$  respectively. For an isophasic process, temperature changes from  $T_{in} \rightarrow T_{fi}$  at constant phase difference  $\varphi$ ,  $W_{infi} = 0$  and  $Q_{infi} = \int_{T_{in}}^{T_{fi}} C(\varphi, T) dT$ .

### 6.3.1 Work done and heat exchanged in Josephson-Stirling Cycle

We can now explicitly calculate total work done and heat exchanged during each stage of the Josephson-Stirling cycle, shown in Fig. 6.3. We also distinguish between four distinct modes of operation of the Josephson-Stirling cycle. In heat engine mode:  $W > 0$ ,  $Q_R > 0$  and  $Q_L < 0$ , where  $W$  is the work done,  $Q_R$  and  $Q_L$  are heat exchanged with right and left reservoirs respectively. It implies that when the Josephson-Stirling cycle operates as an engine, work is done by the system on the universe, the cycle absorbs heat  $Q_R$  from the hot reservoir at temperature  $T_R$  and releases heat  $|Q_L|$  ( $< Q_R$ ) to cold reservoir at temperature  $T_L$ . Thus, for quantum heat engine  $T_R > T_L$ . In refrigerator mode:  $W < 0$ ,  $Q_R > 0$  and  $Q_L < 0$ . Thus, when the Stirling cycle acts as a refrigerator, work is done on the system by the universe, the cycle absorbs heat  $Q_R$  from a cold reservoir at temperature  $T_R$  and releases heat  $|Q_L|$  ( $> Q_R$ ) to a hot reservoir at temperature  $T_L$ . Thus, for refrigerator  $T_L > T_R$ . Further in Joule pump mode:  $W < 0$ ,  $Q_R < 0$  and  $Q_L < 0$ , with  $T_L > T_R$ . Thus, when the cycle acts as a Joule pump, it completely converts work into heat released to reservoirs. Finally, in cold pump mode:  $W < 0$ ,  $Q_R < 0$  and  $Q_L > 0$ , with  $T_L > T_R$ . It implies that when the cycle operates as a cold pump, it absorbs heat  $Q_L$  from a hot reservoir at temperature  $T_L$  and releases heat  $|Q_R|$  to the cold reservoir at temperature  $T_R$ . We have taken sign convention such that  $W$  is positive ( $W > 0$ ) when the system releases work to the universe, while heat  $Q$  is positive ( $Q > 0$ ) when the system absorbs heat from the universe.

### Work done

The total work done per cycle is  $W = W_{12} + W_{34}$ , where  $W_{12} = -[F(\varphi_{fi}, T_R) - F(0, T_R)]$  and  $W_{34} = -[F(0, T_L) - F(\varphi_{fi}, T_L)]$ ,  $F(\varphi, T)$  being defined in Eq. (6.13). Since  $2 \rightarrow 3$  and  $4 \rightarrow 1$  are isophasic processes and in isophasic process phase difference  $\varphi$  is constant, therefore  $W_{23} = W_{41} = 0$ . Thus, work done  $W$ , can be calculated as,

$$W = \Delta \left\{ \left( y_R \ln \left[ 4 \cosh \left( \frac{x_R E_{\uparrow}(\varphi_{fi})}{\Delta} \right) \right] + y_R \ln \left[ \cosh \left( \frac{x_R E_{\downarrow}(\varphi_{fi})}{\Delta} \right) \right] - y_L \ln \left[ 4 \cosh \left( \frac{x_L E_{\uparrow}(\varphi_{fi})}{\Delta} \right) \right] - y_L \ln \left[ \cosh \left( \frac{x_L E_{\downarrow}(\varphi_{fi})}{\Delta} \right) \right] \right) - \left( y_R \ln \left[ \cosh(x_R) \right] + y_R \ln \left[ 4 \cosh(x_R C') \right] - y_L \ln \left[ \cosh(x_L) \right] - y_L \ln \left[ 4 \cosh(x_L C') \right] \right) \right\},$$

$$\text{where, } x_L = \frac{\Delta}{2k_B T_L}, \quad x_R = \frac{\Delta}{2k_B T_R}, \quad y_L = \frac{1}{x_L}, \quad y_R = \frac{1}{x_R},$$

$$C_{1(2)} = \sqrt{16 + J^4(p^2 + m' + m'^2)^2 + J^2(4 \mp 8p^2 + 8m'(1 + m'))}, \quad \text{and } C' = \frac{C_1}{C_2}.$$

(6.17)

In absence of spin flip scattering ( $f = 0$ ), work done, 'W' in Eq. (6.17), reduces to,

$$W = \Delta \left\{ \left( y_L \ln \left[ \cosh(x_L) \right] - y_R \ln \left[ \cosh(x_R) \right] \right) - \left( y_L \ln \left[ \cosh \left( \frac{x_L E(\varphi_{fi})}{\Delta} \right) \right] - y_R \ln \left[ \cosh \left( \frac{x_R E(\varphi_{fi})}{\Delta} \right) \right] \right) \right\},$$

(6.18)

where,  $E(\varphi) = \Delta \sqrt{\frac{4 \cos^2(\varphi/2) + J^2 m'^2}{4 + J^2 m'^2}}$  is Andreev bound state energy for no flip case.

### Heat exchanged (with right reservoir)

The heat exchanged with right reservoir at temperature  $T_R$ ,  $Q_R = Q_{12} + Q_{41}$ , where  $Q_{12} = T_R[\Omega(\varphi_{fi}, T_R) - \Omega(0, T_R)]$  and  $Q_{41} = \int_{T_L}^{T_R} C(0, T) dT$ , is,

$$Q_R = \Delta \left( \ln \left[ \cosh \left( \frac{x_R E_{\uparrow}(\varphi_{fi})}{\Delta} \right) \right] + \ln \left[ 4 \cosh \left( \frac{x_R E_{\downarrow}(\varphi_{fi})}{\Delta} \right) \right] \right) y_R - E_{\uparrow}(\varphi_{fi}) \tanh \left( \frac{x_R E_{\uparrow}(\varphi_{fi})}{\Delta} \right) - E_{\downarrow}(\varphi_{fi}) \tanh \left( \frac{x_R E_{\downarrow}(\varphi_{fi})}{\Delta} \right) + \Delta C' \tanh(x_L C') + \Delta \tanh(x_L) - \Delta \left( \ln \left[ \cosh(x_R) \right] + \ln \left[ 4 \cosh(x_R C') \right] \right) y_R.$$

(6.19)

For no flip process ( $f = 0$ ), Eq. (6.19) reduces to,

$$Q_R = \Delta \left( -\ln \left[ \cosh(x_R) \right] + \ln \left[ \cosh \left( \frac{x_R E(\varphi_{fi})}{\Delta} \right) \right] \right) y_R + \Delta \tanh(x_L) - E(\varphi_{fi}) \tanh \left( \frac{x_R E(\varphi_{fi})}{\Delta} \right). \quad (6.20)$$

### Heat exchanged (with left reservoir)

Finally, heat exchanged with left reservoir at temperature  $T_L$ ,  $Q_L = Q_{23} + Q_{34}$ , where  $Q_{23} = \int_{T_R}^{T_L} C(\varphi_{fi}, T) dT$  and  $Q_{34} = T_L[\Omega(0, T_L) - \Omega(\varphi_{fi}, T_L)]$ , is,

$$Q_L = E_{\uparrow}(\varphi_{fi}) \tanh\left(\frac{x_R E_{\uparrow}(\varphi_{fi})}{\Delta}\right) + E_{\downarrow}(\varphi_{fi}) \tanh\left(\frac{x_R E_{\downarrow}(\varphi_{fi})}{\Delta}\right) + \Delta \left( \ln \left[ \cosh(x_L C') \right] + \ln \left[ 4 \cosh(x_L) \right] \right) y_L \\ - \Delta C' \tanh(x_L C') - \Delta \tanh(x_L) - \Delta \left( \ln \left[ 4 \cosh\left(\frac{x_L E_{\uparrow}(\varphi_{fi})}{\Delta}\right) \right] + \ln \left[ \cosh\left(\frac{x_L E_{\downarrow}(\varphi_{fi})}{\Delta}\right) \right] \right) y_L. \quad (6.21)$$

For no flip process ( $f = 0$ ), Eq. (6.21), reduces to,

$$Q_L = \Delta \left( \ln \left[ \cosh(x_L) \right] - \ln \left[ \cosh\left(\frac{x_L E(\varphi_{fi})}{\Delta}\right) \right] \right) y_L - \Delta \tanh(x_L) + E(\varphi_{fi}) \tanh\left(\frac{x_R E(\varphi_{fi})}{\Delta}\right). \quad (6.22)$$

Upper limit for  $T_L$  and  $T_R$  is much smaller than the superconducting transition temperature  $T_c$ . In this chapter, we consider lead (*Pb*) superconductor; thus upper limit for  $T_R$ ,  $T_L$  is fixed at 3.7K. From the conservation of energy  $W = Q$ , with  $Q = Q_R + Q_L$  being total heat exchanged during the cycle. When the Josephson-Stirling cycle acts as a heat engine, work done is  $W$ , and the efficiency of the heat engine is  $\eta = W/Q_R$ . In refrigerator mode, the work done is  $W$ , and the coefficient of performance[213] of the refrigerator is given as  $COP = Q_R/|W|$ . Finally, in Joule pump mode[216]  $COP$  is  $(|Q_L| + |Q_R|)/|W|$  with  $Q_R < 0$  and  $Q_L < 0$ , as Joule pump converts the work to heat and transfers it to both reservoirs. A cold pump[216], on the other hand, has  $COP = |Q_R|/|W|$ , as in a cold pump,  $Q_R$  is negative, implying heat energy is released to the right reservoir, which is a cold reservoir because of  $T_L > T_R$ . A cold pump is used to heat the colder reservoir by transferring heat from the hotter reservoir, cooling the hotter reservoir. Please also note that the expressions for COP in case of Joule pump differ slightly from that in Ref. [216] as we have taken the sign convention of work done or heat energy such that work done is positive when the system releases work to the universe, while heat energy is positive when the system absorbs heat from the universe.



### 6.3.2 Josephson-Stirling cycle acting as quantum heat engine

In Fig. 6.4 we plot work done  $W$  (Eq. (6.17)) and efficiency  $\eta$  of Josephson quantum heat engine and compare no flip with the spin-flip process. In Figs. 6.4(a) and 6.4(c),  $W$  and  $\eta$  are plotted as function of maximal phase change  $\varphi_{fi}$  during the cycle. The reason we plot work done, efficiency, and COP as a function of phase are because phase lends itself to external control via magnetic flux enclosed in Josephson junction loop, see Fig. 6.1. We consider here the right reservoir to be hot and the left reservoir to be cold, i.e.,  $T_R > T_L$ . In the inset of Fig. 6.4(a), we show Free energy as function of  $\varphi_{fi}$ . In Fig. 6.4(a), we see that  $W$  is maximum at  $\varphi_{fi} = \pi$ , irrespective of spin-flip scattering. However, the magnitude of  $W_{max}$  for no flip process is much smaller than the spin-flip process. In the presence of spin-flip scattering magnitude of  $W$  at  $\varphi_{fi} = \pi$ , i.e.,  $W = 0.735\Delta$  is maximum work done by our system. From the inset of Fig. 6.4(a), we notice that Free energy is minimum at  $\varphi_{fi} = 0$ , i.e., when the system shows 0-junction behavior. From Fig. 6.4(c), we notice that at  $\varphi_{fi} = \pi$ , efficiency  $\eta$  for no flip case is a little bit larger than spin-flip case. Thus, spin flip process is better for work done, but no flip process is better for efficiency. In Figs. 6.4(b) and 6.4(d) we show dependence of work done and efficiency on  $k_B T_R$  (in units of  $\Delta$ ) for fixed  $k_B T_L = 0.01\Delta$  and compare the cycle's performance for no flip and spin flip scattering. In addition we plot Carnot efficiency in Fig. 6.4(d). Three important take home messages from Fig. 6.4 are (i) work done is maximum at  $\varphi_{fi} = \pi$  (see Fig. 6.4(a)), (ii) spin-flip scattering enhances work done (see Fig. 6.4(a)) and (iii) at  $k_B T_R = 0.32\Delta$ , work done is maximum (see Fig. 6.4(b)).

From Fig. 6.4(d), we notice that for small values of  $k_B T_R$  (in units of  $\Delta$ ), the efficiency of a Josephson-Stirling engine is equal to Carnot efficiency  $\eta_C$  regardless of spin-flip scattering. In contrast, at large values of  $k_B T_R$ , in the absence of spin-flip scattering, the

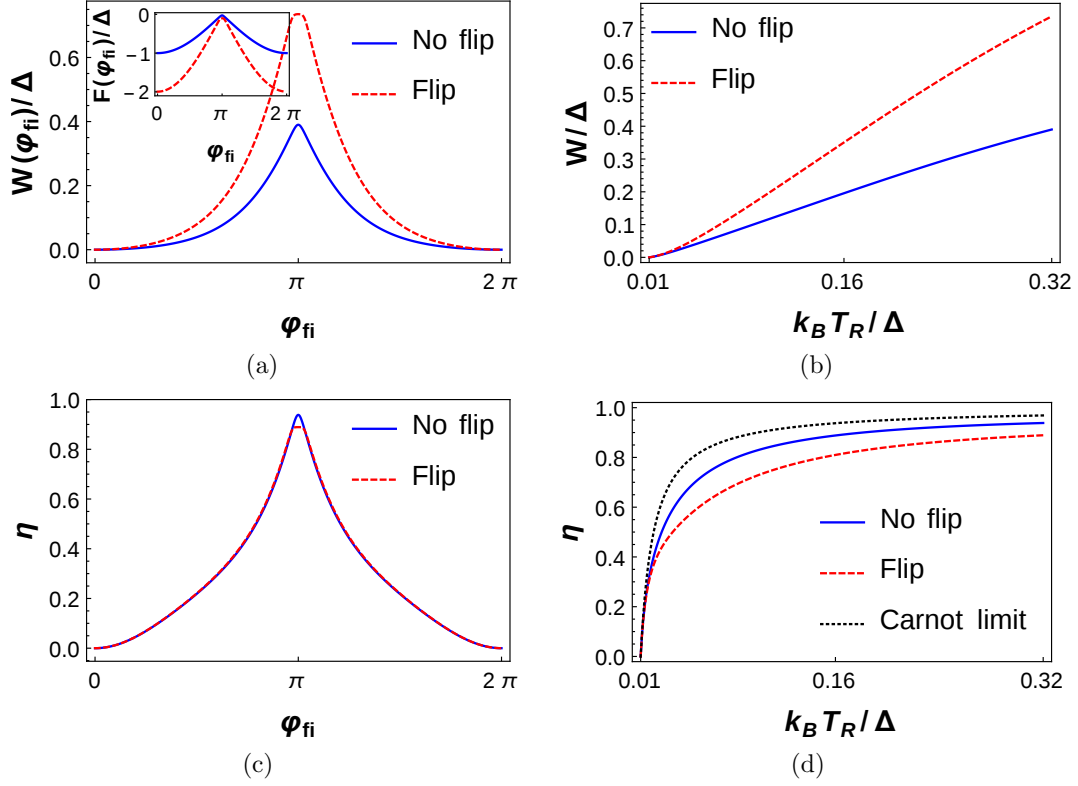


Figure 6.4: Total work done  $W$  and efficiency  $\eta$  of a Josephson-Stirling engine as function of  $\varphi_{fi}$  (for (a,c)) and as function of right reservoir temperature  $T_R$  (for (b,d)). Parameters are: Flip:  $S = -m' = 1/2$ ,  $f = 1$ ; No Flip:  $S = m' = 1/2$ ,  $f = 0$ . Rest of parameters:  $J = 0.1$ ,  $\varphi_{in} = 0$ ,  $\varphi_{fi} = \pi$  (for (b,d)),  $k_B T_R = 0.32\Delta$  (for (a,c)),  $k_B T_L = 0.01\Delta$ ,  $k_B T = 0.01\Delta$ . The black dotted line represents Carnot limit,  $\eta_C = 1 - \frac{T_L}{T_R}$  in (d).

engine is more efficient, and efficiency is close to the Carnot limit. The reason we take low values of exchange coupling  $J$  ( $= 0.1$ ) is because for these values of  $J$  we get maximum work output ' $W$ ' and efficiency ' $\eta$ '.

Next, in Fig. 6.5 we plot total work done  $W$  and efficiency  $\eta$  of a Josephson-Stirling engine for different values of spin-flip scattering. In Figs. 6.5(a) and 6.5(c) we plot  $W$  and  $\eta$  as function of  $\varphi_{fi}$ . We see that at  $\varphi_{fi} = \pi$  and for low values of spin-flip scattering, work done and efficiency attain their maximum. In the inset of Fig. 6.5(a), we notice that

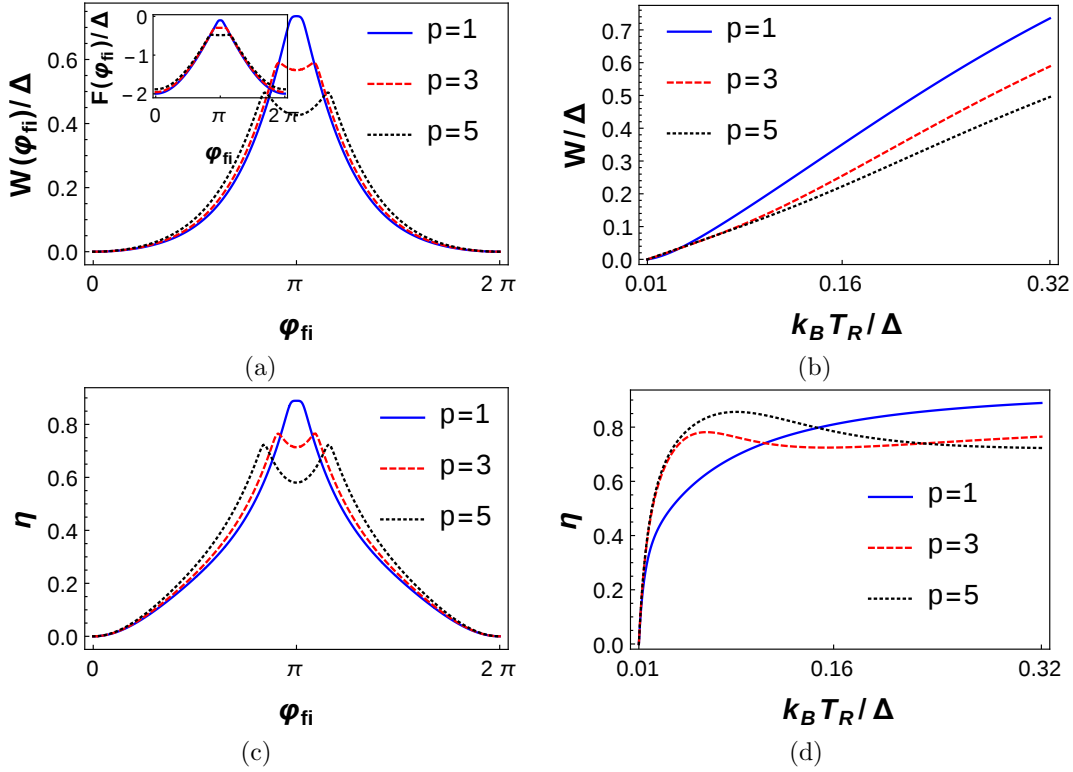


Figure 6.5: Total work done  $W$  and efficiency  $\eta$  of a Josephson-Stirling engine as function of  $\varphi_f$  (for (a,c)) and as function of  $k_B T_R$  (for (b,d)) in presence of spin-flip scattering. Other parameters are:  $J = 0.1$ ,  $\varphi_{in} = 0$ ,  $\varphi_{fi} = \pi$  (for  $f = 1$ ),  $\varphi_{fi} = 0.92\pi$  (for  $f = 3$ ),  $\varphi_{fi} = 0.85\pi$  (for  $f = 5$ ),  $k_B T_L = 0.01\Delta$ ,  $k_B T_R = 0.32\Delta$  (for (a,c)),  $k_B T = 0.01\Delta$ .

the minimum of Free energy occurs at  $\varphi_{fi} = 0$ , i.e., the system shows 0-junction behavior when it operates as a Josephson quantum heat engine. In Figs. 6.5(b) and 6.5(d) we plot  $W$  and  $\eta$  as function of  $k_B T_R$  for different values of spin-flip scattering at fixed  $k_B T_L = 0.01\Delta$ . We choose  $\varphi_{fi}$  in such a way that  $W$  becomes maximum. We see that for low values of spin-flip scattering, work done and efficiency are larger than for high values.

### Condition for optimality

Further, we find in Fig. 6.5 that, at  $k_B T_R = 0.32\Delta$ , both  $W$  and  $\eta$  are maximum. Thus, for spin-flip probability,  $f = 1$ ,  $J = 0.1$ ,  $\varphi_{fi} = \pi$ ,  $k_B T_L = 0.01\Delta$  and  $k_B T_R = 0.32\Delta$

work done and efficiency of our Josephson quantum heat engine are larger and therefore this regime is an optimal operating range of our Josephson quantum heat engine. This condition of optimality for our case is contrasted with that in Ref. [212]. In Ref. [212], parity-conserving heat engine operates in an optimal operating range at  $\varphi_{fi} = 2\pi$ , while non-parity-conserving heat engine works in an optimal operating range at  $\varphi_{fi} = \pi$ .

### 6.3.3 Josephson-Stirling cycle acting as quantum refrigerator

In the previous subsection we have discussed work done and efficiency when Josephson-Stirling cycle acts as a quantum heat engine. In Fig. 6.6 we show action of Stirling cycle as a Josephson quantum refrigerator and calculate work done and coefficient of performance (COP). In Figs. 6.6(a) and 6.6(b), total work absorbed by refrigerator and COP are plotted as function of  $\varphi_{fi}$ , for  $T_R < T_L$  ( $k_B T_L = 0.32\Delta$  and  $k_B T_R = 0.31\Delta$ ). We see that for low values of spin-flip scattering both  $|W|$  and COP are larger and the product of COP and  $|W|$  is maximum at  $\varphi_{fi} = \pi$ . Thus, Josephson quantum refrigerator works in an optimal operating range for parameters in Fig. 6.6. For optimal parameters,  $|W| = 0.02\Delta$  and  $\text{COP} = 30.61$ . Although, our system exhibits maximum  $|W|$  of  $0.62\Delta$  at  $k_B(T_L - T_R) = 0.25\Delta$ , however maximum COP is same with the optimal value as shown in Figs. 6.6(c) and 6.6(d) respectively.

### 6.3.4 Phase diagram of Josephson-Stirling cycle

In Figs. 6.4, 6.5, 6.6 we depict the performance of this device as a quantum heat engine or quantum refrigerator depending on relative temperatures of reservoirs. In this subsection we will discuss phase diagram of a Josephson-Stirling cycle as function of phase difference  $\varphi_{fi}$  during the cycle. In Fig. 6.7, we plot  $W$ ,  $Q_R$ ,  $Q_L$ ,  $\eta$  and COP as functions of  $\varphi_{fi}$  and  $T_R$  for low values of spin-flip scattering ( $S = 1/2$ ,  $m' = -1/2$ ,  $f = 1$ ) and high values of

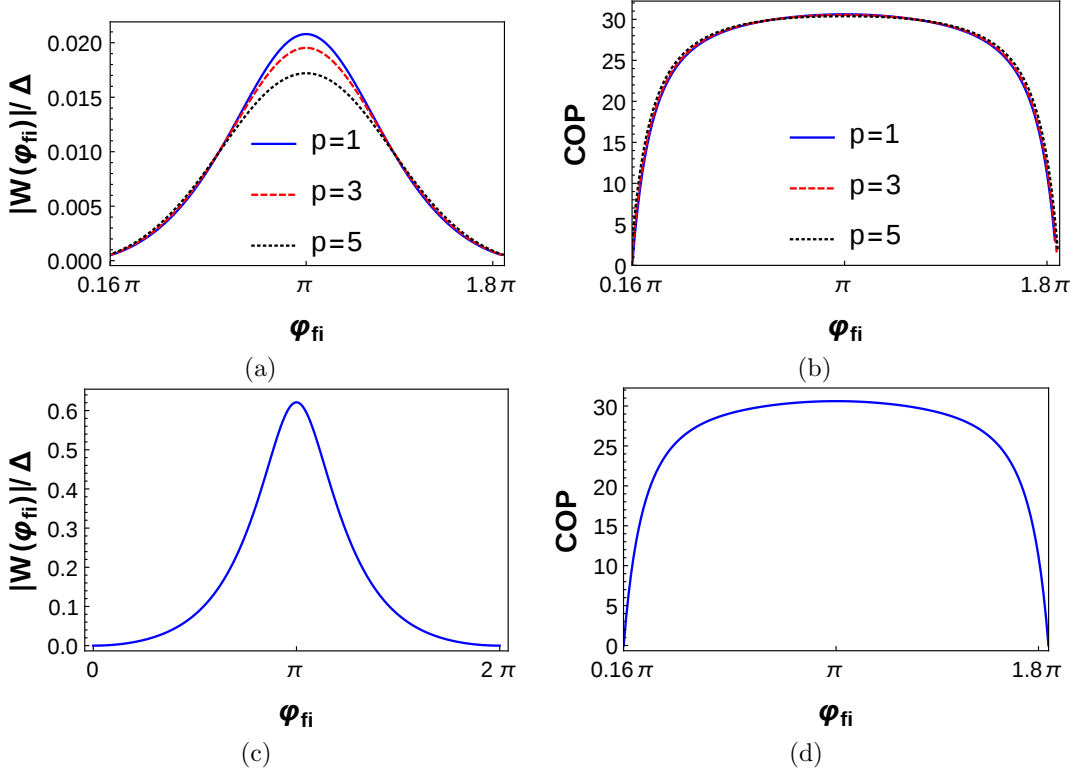


Figure 6.6: (a,c) Total work  $W$  absorbed, and (b,d) COP of quantum refrigerator as function of  $\varphi_{fi}$  in presence of spin-flip scattering. Other parameters are:  $J = 0.1$ ,  $k_B T_L = 0.32\Delta$  (for (a,b)),  $k_B T_R = 0.31\Delta$  (for (a,b)),  $S = -m' = 1/2$  (for (c,d)),  $\varphi_{in} = 0$ .

exchange coupling ( $J = 2$ ) of spin flipper. We fix  $k_B T_L = 0.01\Delta$  and consider  $T_R > T_L$ . From Fig. 6.7(a) we notice that with change of  $\varphi_{fi}$  there is a sign change in  $W$ .  $W$  changes sign from  $W > 0$  to  $W < 0$  between  $\varphi_{fi} = 0$  and  $\varphi_{fi} = \pi$  and again changes sign from  $W < 0$  to  $W > 0$  between  $\varphi_{fi} = \pi$  and  $\varphi_{fi} = 2\pi$ . The regime where  $W$  is positive ( $W > 0$ ) in Fig. 6.7(a),  $Q_R$  is positive (Fig. 6.7(b)) but  $Q_L$  is negative (Fig. 6.7(c)), in these regimes Josephson-Stirling cycle acts as an engine. Similarly, in a regime, wherein both  $W$  and  $Q_L$  are negative, the cycle acts as a refrigerator if  $Q_R$  is positive while the cycle acts as a Joule pump if  $Q_R$  is negative. A Joule pump transforms work into heat released to the reservoirs. Thus, there is a transition from engine mode to refrigerator or Joule pump mode

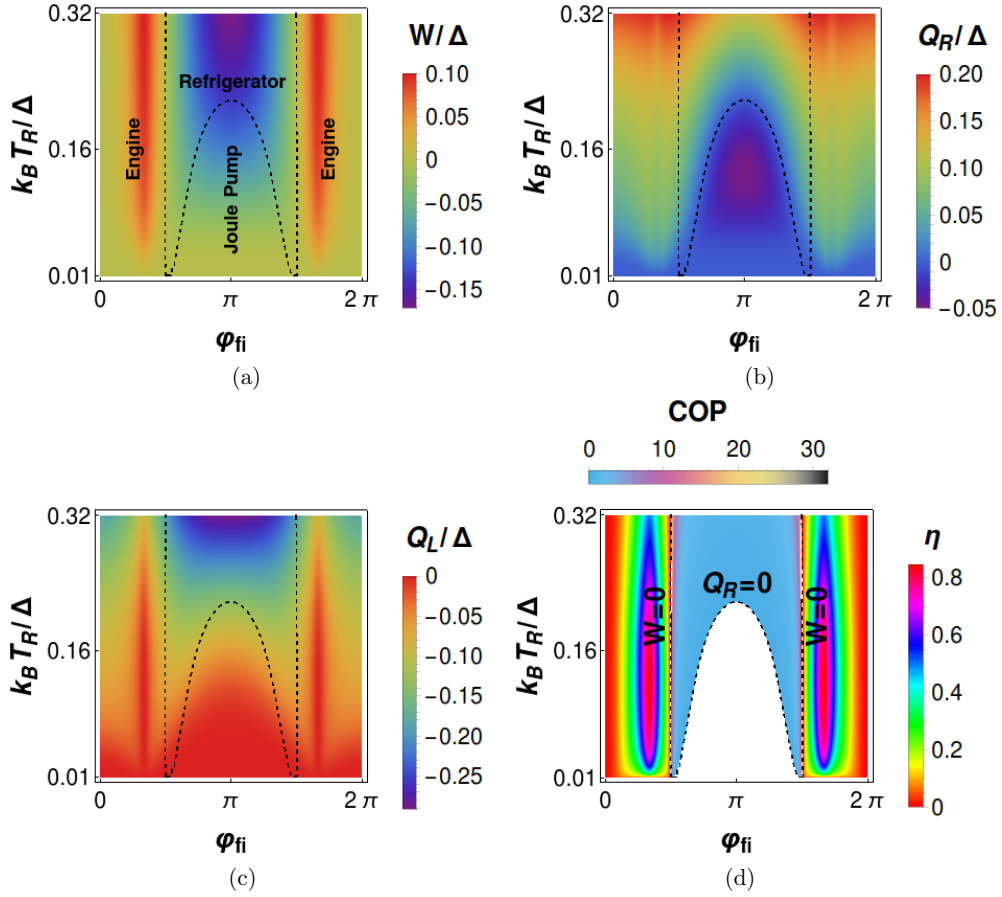


Figure 6.7: (a) Total work  $W$  (b)  $Q_R$  and (c)  $Q_L$ , (d)  $\eta$  or COP as function of  $\varphi_{fi}$  and  $T_R$  in presence of spin flip scattering. Other parameters are:  $S = 1/2$ ,  $m' = -1/2$ ,  $J = 2$ ,  $k_B T_L = 0.01\Delta$ ,  $\varphi_{in} = 0$ .

with the change of  $\varphi_{fi}$ . Since,  $\varphi_{fi}$  is controlled by magnetic flux  $\Phi$ , therefore by changing the enclosed flux  $\Phi$  in the Josephson junction loop, we can tune our system from engine mode to refrigerator/Joule pump mode, which is an attractive feature of our device.

### 6.3.5 Why is spin-flip scattering necessary?

In absence of spin-flip scattering ( $f = 0$ ), we find work done (see Eq. (6.18))  $W > 0$ ,

$$(Y_L \ln[\cosh(X_L)] - Y_R \ln[\cosh(X_R)]) > (Y_L \ln[\cosh(X_L E(\varphi_{fi})/\Delta)] - Y_R \ln[\cosh(X_R E(\varphi_{fi})/\Delta)]), \quad (6.23)$$

for  $T_R > T_L$  and regardless of  $\varphi_{fi}$ . Thus,  $W$  is always positive ( $W > 0$ ) in absence of

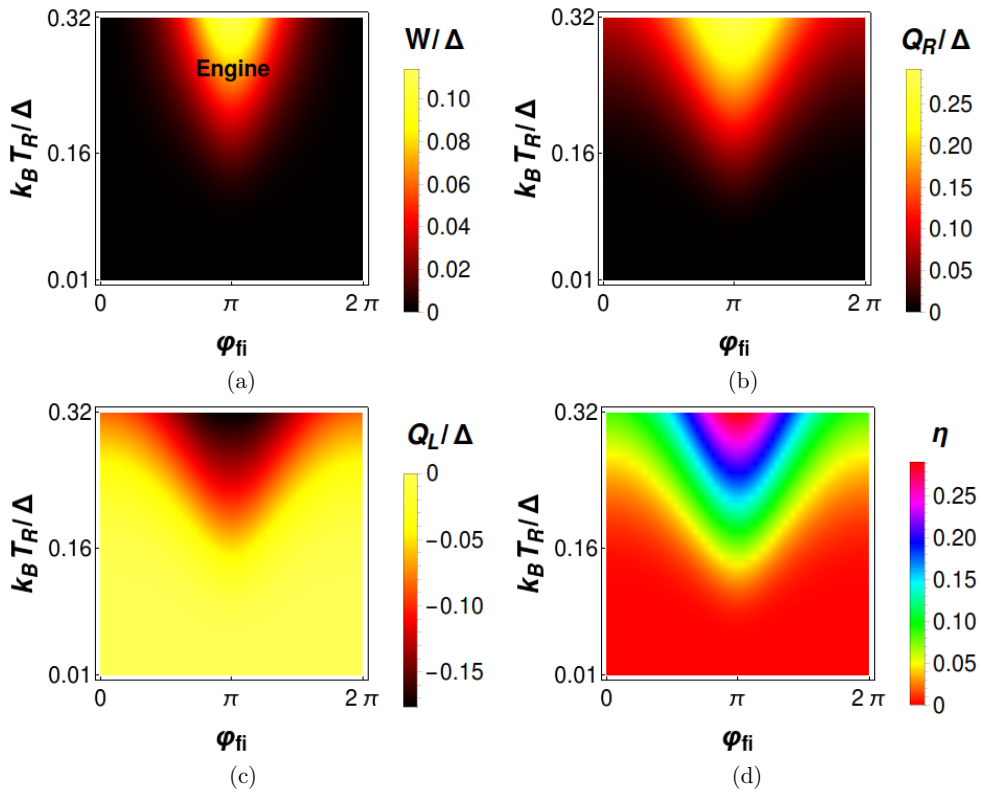


Figure 6.8: (a) Total work done  $W$  (b)  $Q_R$  and (c)  $Q_L$  (d) efficiency  $\eta$  as function of maximal phase change  $\varphi_{fi}$  during Stirling cycle and right reservoir temperature  $T_R$  in absence of spin-flip scattering. Other parameters are:  $S = m' = 1/2$ ,  $J = 2$ ,  $k_B T_L = 0.01\Delta$ ,  $\varphi_{in} = 0$ .

spin-flip scattering irrespective of  $\varphi_{fi}$  and the Josephson-Stirling cycle operates solely as a quantum heat engine. However, in presence of spin-flip scattering ( $f \neq 0$ ) and with  $T_R > T_L$ , we find  $W$  (see Eq. (6.17)) is not always positive and depending on other parameter values,

$W$  can be negative ( $W < 0$ ) in certain range of  $\varphi_{fi}$ . In the parameter regime wherein  $W$  is negative and  $Q_L$  is negative with  $Q_R$  being positive, the Josephson-Stirling cycle operates as a refrigerator. Similarly, in parameter regime wherein  $W$ ,  $Q_R$  and  $Q_L$  are all negative, Josephson-Stirling cycle acts as a Joule pump. Thus, in presence of spin-flip scattering when  $W$  is negative, the Josephson-Stirling cycle can act as a refrigerator or Joule pump even when  $T_R > T_L$ . This is unique to this proposal since in other proposals[212, 213],  $W$  is always positive and Josephson-Stirling cycle only acts as a heat engine when  $T_R > T_L$ . In Fig. 6.8,  $W$ ,  $Q_R$ ,  $Q_L$  and  $\eta$  are plotted as function of  $\varphi_{fi}$  and  $T_R$  in absence of spin-flip scattering ( $S = m' = 1/2$ ,  $f = 0$ ). We see that  $W$  does not change nature with  $\varphi_{fi}$ , and thus there is no transition from engine mode to refrigerator or Joule pump mode. Therefore, we can conclude that spin-flip scattering is responsible for tuning our system from engine mode to refrigerator/Joule pump mode via magnetic flux  $\Phi$ .

### 6.3.6 Josephson-Stirling cycle as Joule pump and cold pump

Finally, our device does not only exhibit the engine, refrigerator, and Joule pump phases. It also exhibits a cold pump phase again in the presence of spin-flip scattering only. The thin sliver in Fig. 6.9(a) at the bottom right corner shows the cold pump phase. In Fig. 6.9, we plot  $W$ ,  $Q_R$ ,  $Q_L$ , efficiency of engine and COP of refrigerator as functions of  $T_R$  and  $T_L$  for low values of spin-flip scattering ( $S = 1/2$ ,  $m' = -1/2$ ,  $f = 1$ ) and high values of exchange coupling ( $J = 1$ ) of spin flipper. We choose  $\varphi_{fi}$  such that  $|W|$  will be maximized. We see that for  $T_R > T_L$ , the Josephson-Stirling cycle acts as an engine. We take high values of  $J$  ( $J = 1$ ) to see all phases in the phase diagram, however for low values of  $J$  ( $J = 0.1$ ), at  $k_B T_L = 0.01\Delta$  and  $k_B T_R = 0.32\Delta$ , the work done and efficiency in the engine mode attain their maximum values which are  $W_{max} = 0.735\Delta$  and  $\eta_{max} = 0.89$ . For  $T_R < T_L$ , we notice that the machine acts as a refrigerator or as Joule pump or cold pump



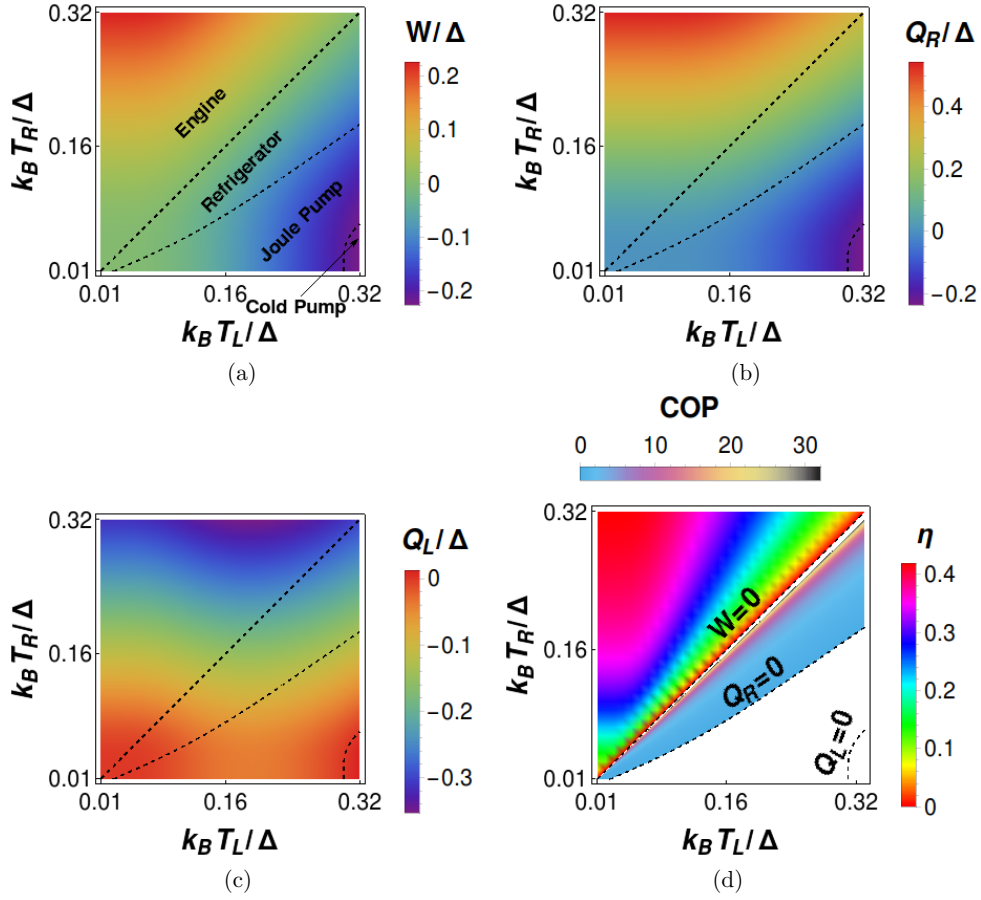


Figure 6.9: (a) Total work done  $W$ , (b) heat exchanged  $Q_R$  and (c)  $Q_L$  and (d) efficiency  $\eta$  or COP as function of temperatures  $T_R$  and  $T_L$  in presence of spin-flip scattering. Parameters are:  $S = 1/2$ ,  $m' = -1/2$ ,  $J = 1$ ,  $\varphi_{in} = 0$ ,  $\varphi_{fi} = \pi$ .

depending on the sign of  $Q_R$  and  $Q_L$ . The work done in the refrigerator mode is maximum at  $k_B T_L = 0.32\Delta$  and  $k_B T_R = 0.07\Delta$  and the maximum value is  $|W|_{max} = 0.62\Delta$ , while the COP of the refrigerator is maximum at  $k_B T_L = 0.32\Delta$  and  $k_B T_R = 0.31\Delta$  and the maximum value is  $COP_{max} = 30.61$ . Further, in the Joule pump mode the work done is maximum at  $k_B T_L = 0.32\Delta$  and  $k_B T_R = 0.01\Delta$  and the maximum value is  $|W|_{max} = 0.735\Delta$ , while the maximum COP of the Joule pump is  $COP_{max} = 1$ . If  $Q_R < 0$ ,  $W < 0$  and  $Q_L > 0$ , the cycle acts as a cold pump which transfers heat from the hot reservoir to the cold reservoir.

The work done in the cold pump mode is maximum at  $k_B T_L = 0.32\Delta$  and  $k_B T_R = 0.01\Delta$  and the maximum value is  $|W|_{max} = 0.23\Delta$ , while the COP of the cold pump is maximum at  $k_B T_L = 0.32\Delta$  and  $k_B T_R = 0.01\Delta$  and the maximum value is  $COP_{max} = 1.05$ . Thus, by tuning the temperature of the reservoirs our system can be tuned from engine mode to refrigerator or Joule pump or cold pump mode.

## 6.4 Analysis

In this section, we analyze in detail the expressions for work done (Eqs. (6.17), (6.18)) and heat exchanged with left and right reservoirs (Eqs. (6.19)-(6.22)).

### 6.4.1 Work done ( $W$ )

In presence of spin flip scattering, from Eq. (6.17) we find that

$$\text{for work done } (W) > 0: X^{\frac{T_R}{T_L}} > X', \text{ and for } W < 0: X^{\frac{T_R}{T_L}} < X', \quad (6.24)$$

where  $X = \frac{e^{-\frac{F(\varphi_{fi}, T_R)}}{2k_B T_R}}{D_R}$ ,  $X' = \frac{e^{-\frac{F(\varphi_{fi}, T_L)}}{2k_B T_L}}{D_L}$ ,  $D_R = 4 \cosh(x_R) \cosh(x_R C')$ , and  $D_L = 4 \cosh(x_L) \cosh(x_L C')$ .

From Eq. (6.24), after some algebraic calculations we get,

$$\text{for } W > 0: F(\varphi_{fi}, T_L) - F(\varphi_{fi}, T_R) > 2k_B(T_R \ln[D_R] - T_L \ln[D_L]), \text{ and} \quad (6.25)$$

$$\text{for } W < 0: F(\varphi_{fi}, T_L) - F(\varphi_{fi}, T_R) < 2k_B(T_R \ln[D_R] - T_L \ln[D_L]).$$

In our figures, the range of  $2k_B(T_R \ln[D_R] - T_L \ln[D_L])$  for heat engine, refrigerator, Joule pump and cold pump modes are 0 to  $0.36\Delta$ ,  $-0.096\Delta$  to 0,  $-0.11\Delta$  to 0, and  $-0.11\Delta$  to  $-0.10\Delta$  respectively, i.e., it always positive for heat engine mode, while it always negative for refrigerator, Joule pump and cold pump modes. Thus, when  $W > 0$ ,  $F(\varphi_{fi}, T_L) > F(\varphi_{fi}, T_R)$  and when  $W < 0$ ,  $F(\varphi_{fi}, T_L) < F(\varphi_{fi}, T_R)$ . When work done is positive ( $W > 0$ ), the cycle operates as a heat engine, while when work done is negative

( $W < 0$ ), the cycle operates as a refrigerator or a Joule pump or a cold pump depending on the sign of  $Q_R$  and  $Q_L$  (see section 6.3.1). Thus, Eqs. (6.24), (6.25) help us to understand the operating modes of our device. From Eqs. (6.24), (6.25), we also see that by changing the reservoir temperatures  $T_R$  and  $T_L$  or phase  $\varphi_{fi}$  one can control the sign of  $W$ . Since  $\varphi_{fi}$  can be controlled via magnetic flux  $\Phi$  enclosed in the Josephson junction loop, thus by controlling the temperature of reservoirs or magnetic flux  $\Phi$ , we can experimentally implement the condition for  $W > 0$  or  $W < 0$  in the presence of spin-flip scattering.

Herein, we prove that if spin flip scattering is absent, then there is only phase, the heat engine phase in our device, if temperatures  $T_R, T_L$  are fixed and only flux changes. In absence of spin flip scattering from Eq. (6.18) we get

$$\text{for } W > 0: Y^{\frac{T_R}{T_L}} > Y', \text{ and for } W < 0: Y^{\frac{T_R}{T_L}} < Y', \quad (6.26)$$

where  $Y = \frac{e^{-\frac{F(\varphi_{fi}, T_R)}{2k_B T_R}}}{2 \cosh(x_R)}$ , and  $Y' = \frac{e^{-\frac{F(\varphi_{fi}, T_L)}{2k_B T_L}}}{2 \cosh(x_L)}$ . From Eq. (6.26), after some algebraic calculations we get,

$$\begin{aligned} \text{for } W > 0: & F(\varphi_{fi}, T_L) - F(\varphi_{fi}, T_R) > 2k_B(T_R \ln[2 \cosh(x_R)] - T_L \ln[2 \cosh(x_L)]), \text{ and} \\ \text{for } W < 0: & F(\varphi_{fi}, T_L) - F(\varphi_{fi}, T_R) < 2k_B(T_R \ln[\cosh(x_R)] - T_L \ln[2 \cosh(x_L)]). \end{aligned} \quad (6.27)$$

In our figures, the range of  $2k_B(T_R \ln[2 \cosh(x_R)] - T_L \ln[2 \cosh(x_L)])$  for engine mode is  $0 - 0.03\Delta$ .

$$\text{If } G = Y^{\frac{T_R}{T_L}} - Y' = \left( \cosh\left(\frac{x_R E(\varphi_{fi})}{\Delta}\right) \text{sech}(x_R) \right)^{\frac{T_R}{T_L}} - \left( \cosh\left(\frac{x_L E(\varphi_{fi})}{\Delta}\right) \text{sech}(x_L) \right), \text{ then} \quad (6.28)$$

$$\frac{dG}{d\varphi_{fi}} = \frac{x_L \sin(\varphi_{fi}) \left( \text{sech}(x_L) \sinh\left(\frac{x_L E(\varphi_{fi})}{\Delta}\right) - \left( \cosh\left(\frac{x_R E(\varphi_{fi})}{\Delta}\right) \text{sech}(x_R) \right)^{\frac{T_R}{T_L}} \tanh\left(\frac{x_R E(\varphi_{fi})}{\Delta}\right) \right)}{\sqrt{4 + J^2 m'^2} \sqrt{2 + J^2 m'^2 + 2 \cos(\varphi_{fi})}} \quad (6.29)$$

When  $G$  is maximum or minimum with respect to  $\varphi_{fi}$ , then  $\frac{dG}{d\varphi_{fi}} = 0$ . Thus, from Eq. (6.29) we get  $\sin(\varphi_{fi}) = 0$  or  $\varphi_{fi} = 0, \pi$ , and  $2\pi$ . For,  $\varphi_{fi} = 0$  or  $\varphi_{fi} = 2\pi$ , we find that

$$\frac{d^2G}{d\varphi_{fi}^2} = \frac{x_L(\tanh(x_L) - \tanh(x_R))}{4 + J^2m'^2} = \frac{\Delta \left( \tanh\left(\frac{\Delta}{2k_B T_L}\right) - \tanh\left(\frac{\Delta}{2k_B T_R}\right) \right)}{2k_B T_L(4 + J^2m'^2)}. \quad (6.30)$$

In Eq. (6.30), when  $T_R > T_L$ ,  $\tanh\left(\frac{\Delta}{2k_B T_L}\right) > \tanh\left(\frac{\Delta}{2k_B T_R}\right)$ , thus  $\frac{d^2G}{d\varphi_{fi}^2} > 0$  at  $\varphi_{fi} = 0$  or  $\varphi_{fi} = 2\pi$ . Therefore, at  $\varphi_{fi} = 0$  or  $\varphi_{fi} = 2\pi$ ,  $G$  is minimum and from Eq. (6.28) the minimum value of  $G$  is  $G_{min} = 0$ . Since, the minimum value of  $G$  is zero for  $T_R > T_L$ , thus  $G$  is positive or  $Y^{\frac{T_R}{T_L}} > Y'$  irrespective of  $\varphi_{fi}$  for  $T_R > T_L$ . Thus, we can conclude that for no flip process, although the magnitude of  $W$  depends on both reservoir temperatures and phase  $\varphi_{fi}$ , but the sign of  $W$  depends only on temperature of the reservoirs in contrast to spin flip case where the sign of  $W$  depends on both reservoir temperatures and  $\varphi_{fi}$ . Similarly, for  $T_R < T_L$ ,  $\frac{d^2G}{d\varphi_{fi}^2} < 0$  at  $\varphi_{fi} = 0$  or  $\varphi_{fi} = 2\pi$ . Thus, at  $\varphi_{fi} = 0$  or  $\varphi_{fi} = 2\pi$ ,  $G$  is maximum when  $T_R < T_L$  and from Eq. (6.28) the maximum value of  $G$  is  $G_{max} = 0$ . Since, the maximum value of  $G$  is zero for  $T_R < T_L$ , thus  $G$  is negative or  $Y^{\frac{T_R}{T_L}} < Y'$  irrespective of  $\varphi_{fi}$  for  $T_R < T_L$ . In the absence of spin-flip scattering, the sign of  $W$  can not be tuned via magnetic flux. Thus, our device can not be tuned from heat engine mode to other operating modes like refrigerator, Joule pump, or cold pump by changing magnetic flux.

### 6.4.2 Heat exchanged (with right reservoir)

Similarly, in presence of spin flip scattering from Eq. (6.19) we find that

$$\begin{aligned} \text{for } Q_R > 0: X e^{\frac{F(\varphi_{fi}, T_R)}{2k_B T_R} + \frac{\Omega(\varphi_{fi}, T_R)}{2k_B} + x_R C' \tanh(x_L C') + x_R \tanh(x_L)} &> 1, \text{ and} \\ \text{for } Q_R < 0: X e^{\frac{F(\varphi_{fi}, T_R)}{2k_B T_R} + \frac{\Omega(\varphi_{fi}, T_R)}{2k_B} + x_R C' \tanh(x_L C') + x_R \tanh(x_L)} &< 1, \end{aligned} \quad (6.31)$$

From Eq. (6.31), after some algebraic calculations we get,

$$\begin{aligned} \text{for } Q_R > 0: \Omega(\varphi_{fi}, T_R) &> 2k_B(\ln[D_R] - G_R), \text{ and} \\ \text{for } Q_R < 0: \Omega(\varphi_{fi}, T_R) &< 2k_B(\ln[D_R] - G_R), \end{aligned} \quad (6.32)$$

where  $G_R = x_R C' \tanh(x_L C') + x_R \tanh(x_L)$ . In our figures, the range of  $2k_B(\ln[D_R] - G_R)$  for heat engine, refrigerator, Joule pump and cold pump modes are  $0 - 1.49k_B$ ,  $0 - 1.34k_B$ ,  $0 - 20.62k_B$ , and  $3.97k_B - 23.84k_B$  respectively, i.e., it always positive. Thus, when  $Q_R > 0$ ,  $\Omega(\varphi_{fi}, T_R) > 0$ . In Eqs. (6.31), (6.32), the sign of  $Q_R$  depends on both reservoir temperatures  $T_R$ ,  $T_L$  and phase  $\varphi_{fi}$ . When  $Q_R$  is positive ( $Q_R > 0$ ) the cycle operates as a heat engine or refrigerator depending on the sign of  $W$ , while when  $Q_R$  is negative ( $Q_R < 0$ ) the cycle operates as a Joule pump or cold pump depending on the sign of  $Q_L$  (see section 6.3.1). Thus, the sign of  $Q_R$  helps to understand the different operating modes of our device.

In absence of spin flip scattering from Eq. (6.20) we get,

$$\begin{aligned} \text{for } Q_R > 0: Y e^{\frac{F(\varphi_{fi}, T_R)}{2k_B T_R} + \frac{\Omega(\varphi_{fi}, T_R)}{2k_B} + x_R \tanh(x_L)} &> 1, \text{ and} \\ \text{for } Q_R < 0: Y e^{\frac{F(\varphi_{fi}, T_R)}{2k_B T_R} + \frac{\Omega(\varphi_{fi}, T_R)}{2k_B} + x_R \tanh(x_L)} &< 1. \end{aligned} \quad (6.33)$$

From Eq. (6.33), after some algebraic calculations we get,

$$\begin{aligned} \text{for } Q_R > 0: \Omega(\varphi_{fi}, T_R) &> 2k_B(\ln[2 \cosh(x_R)] - x_R \tanh(x_L)), \text{ and} \\ \text{for } Q_R < 0: \Omega(\varphi_{fi}, T_R) &< 2k_B(\ln[2 \cosh(x_R)] - x_R \tanh(x_L)). \end{aligned} \quad (6.34)$$

In our figures, the range of  $2k_B(\ln[2 \cosh(x_R)] - x_R \tanh(x_L))$  for heat engine mode is  $0 - 0.32k_B$ . Since, in no flip process there is no transition from heat engine mode to other operating mode like refrigerator or Joule pump or cold pump with change of  $\varphi_{fi}$ , thus the sign of  $Q_R$  does not change with  $\varphi_{fi}$ .

### 6.4.3 Heat exchanged (with left reservoir)

Finally, in presence of spin flip scattering from Eq. (6.21) we get,

$$\begin{aligned} \text{for } Q_L > 0: X' e^{\frac{F(\varphi_{fi}, T_R)}{2k_B T_L} + \frac{\Omega(\varphi_{fi}, T_R) T_R}{2k_B T_L} + x_L C' \tanh(x_L C') + x_L \tanh(x_L)} &< 1, \text{ and} \\ \text{for } Q_L < 0: X' e^{\frac{F(\varphi_{fi}, T_R)}{2k_B T_L} + \frac{\Omega(\varphi_{fi}, T_R) T_R}{2k_B T_L} + x_L C' \tanh(x_L C') + x_L \tanh(x_L)} &> 1, \end{aligned} \quad (6.35)$$

From Eq. (6.35), after some algebraic calculations we get,

$$\begin{aligned} \text{for } Q_L > 0: & (F(\varphi_{fi}, T_R) - F(\varphi_{fi}, T_L)) + \Omega(\varphi_{fi}, T_R)T_R < 2k_B T_L (\ln[D_L] - G_L), \text{ and} \\ \text{for } Q_L < 0: & (F(\varphi_{fi}, T_R) - F(\varphi_{fi}, T_L)) + \Omega(\varphi_{fi}, T_R)T_R > 2k_B T_L (\ln[D_L] - G_L), \end{aligned} \quad (6.36)$$

where  $G_L = x_L C' \tanh(x_L C') + x_L \tanh(x_L)$ . In our work, the range of  $2k_B T_L (\ln[D_L] - G_L)$  for heat engine, refrigerator, Joule pump and cold pump modes are  $0 - 3.87k_B$ ,  $0 - 4.05k_B$ ,  $0 - 4.05k_B$ , and  $3.74k_B - 4.05k_B$  respectively, it always positive. Thus, when  $Q_L < 0$ ,  $(F(\varphi_{fi}, T_L) - F(\varphi_{fi}, T_R)) < \Omega(\varphi_{fi}, T_R)T_R$ . In Eqs. (6.35), (6.36), the sign of  $Q_L$  depends on both reservoir temperatures  $T_R, T_L$  and phase  $\varphi_{fi}$ . When  $Q_L$  is positive ( $Q_L > 0$ ) the cycle operates as a cold pump, while when  $Q_L$  is negative ( $Q_L < 0$ ) the cycle operates as a heat engine or refrigerator or Joule pump depending on the sign of  $W$  and  $Q_R$  (see section 6.3.1). Thus, similar to  $Q_R$ , the sign of  $Q_L$  also helps to understand the different operating modes of our device.

In absence of spin flip scattering from Eq. (6.22) we find that

$$\begin{aligned} \text{for } Q_L > 0: & Y' e^{\frac{F(\varphi_{fi}, T_R)}{2k_B T_L} + \frac{\Omega(\varphi_{fi}, T_R)T_R}{2k_B T_L} + x_L \tanh(x_L)} < 1, \text{ and} \\ \text{for } Q_L < 0: & Y' e^{\frac{F(\varphi_{fi}, T_R)}{2k_B T_L} + \frac{\Omega(\varphi_{fi}, T_R)T_R}{2k_B T_L} + x_L \tanh(x_L)} > 1, \end{aligned} \quad (6.37)$$

From Eq. (6.37), after some algebraic calculations we get,

$$\begin{aligned} \text{for } Q_L > 0: & (F(\varphi_{fi}, T_R) - F(\varphi_{fi}, T_L)) + \Omega(\varphi_{fi}, T_R)T_R < 2k_B T_L (\ln[2 \cosh(x_L)] - x_L \tanh(x_L)), \text{ and} \\ \text{for } Q_L < 0: & (F(\varphi_{fi}, T_R) - F(\varphi_{fi}, T_L)) + \Omega(\varphi_{fi}, T_R)T_R > 2k_B T_L (\ln[2 \cosh(x_L)] - x_L \tanh(x_L)). \end{aligned} \quad (6.38)$$

In our work, the range of  $2k_B T_L (\ln[2 \cosh(x_L)] - x_L \tanh(x_L))$  for heat engine mode is  $0 - 1.17k_B$ . Since, in no flip process there is no transition between different operating modes of the Josephson-Stirling cycle with change of  $\varphi_{fi}$ , thus the sign of  $Q_L$  does not change with  $\varphi_{fi}$ .

## 6.5 Experimental realization

Our proposed Josephson quantum spin thermodynamic device acts as a heat engine or refrigerator or Joule pump, or as a cold pump via spin-flip scattering and is experimentally realizable. Doping a magnetic adatom or spin-flipper in a one-dimensional superconducting loop should not be difficult, especially with a  $s$ -wave superconductor like Lead or Aluminum. It should be perfectly possible. Our proposed experimental scheme is suitable for measuring the work done and exchanged heat in a single realization of the thermodynamic cycle. Work done per cycle during each isothermal process can be experimentally determined via the current-phase relation. For a Josephson Stirling cycle, work done during each isothermal process is given as  $W_{infi} = -\frac{\hbar}{2e} \int_{\varphi_{in}}^{\varphi_{fi}} I(\varphi, T) d\varphi$ , where  $\varphi_{in}$  and  $\varphi_{fi}$  are initial and final phases respectively. In the isophasic process, since phase difference  $\varphi$  is constant, no work is done. Thus, to experimentally measure work done, one needs to control phase difference  $\varphi$  across the junction, regulated by flux  $\Phi$ , and know about the Josephson current  $I$  flowing through the loop. It can be done using a scanning superconducting quantum interference device (SQUID) microscope to perform the measurements of the current-phase relation of the junction[212, 217, 218]. By applying a current through the field coil of the SQUID sensor, the magnetic flux through the Josephson junction loop can be tuned. This magnetic flux controls the phase difference across JJ and induces a supercurrent in the Josephson junction loop. The supercurrent leads to a signal which is measured by pickup loop of SQUID sensor[217, 219].

## 6.6 Conclusion

This chapter shows that a 1D Josephson junction loop doped with a spin flipper attached to two thermal reservoirs at unequal temperatures via thermal valves can act as a Josephson

quantum heat engine, quantum refrigerator, or Joule pump, or even as a cold pump. The proposed device can be tuned from engine mode to other operating modes like refrigerator or Joule pump/cold pump not only via changing the temperatures of the reservoirs but also via the enclosed flux in the Josephson junction loop, which is the most lucrative aspect of work since this fact alone implies a much greater possibility of our proposal is experimentally realized.

We have compared our proposal with other Josephson quantum heat engines and refrigerators in Table 6.1. While, Refs. [212], [213] are significant works that laid down the principle of Josephson quantum heat engine and refrigerator, efficiency and coefficient of performance (COP) of these can none-the-less be still enhanced, and the tunability of the device improved as we show in this chapter. In both Refs. [212] and [213], the Josephson

Table 6.1: Comparative analysis of Josephson junction based quantum heat engines and refrigerators

	Heat engine mode		Refrigerator mode	
	$W_{max}$	$\eta_{max}$	$ W_{max} $	$COP_{max}$
The JJ device (Fig. 6.1)	$0.735\Delta$ ( $\Delta = 1meV$ ) (Fig. 6.4(a))	0.94 (Fig. 6.4(c))	$0.62\Delta$ (Fig. 6.6(c))	30.61 (Fig. 6.6(d))
Topological Josephson heat engine (Ref. [212])	$2\Delta$ ( $\Delta = 150\mu eV$ ) (Fig. 4(c) of Ref. [212])	0.8 (Figs. 4(b,d) of Ref. [212])	–	20 (Figs. 4(b,d) of Ref. [212])
Josephson heat engine (Ref. [213])	$0.38\Delta$ ( $\Delta = 180eV$ ) (Fig. 14(a) of Ref. [213])	0.5 (Fig. 15(a) of Ref. [213])	–	10 (Fig. 15(a) of Ref. [213])

quantum heat engine and refrigerator can be tuned from engine mode to refrigerator mode via changing the temperatures of left and right reservoirs only. This proposal shows that heat engine to refrigeration mode transition or, for that matter, to Joule or cold pump can



be affected by either the magnetic flux enclosed or by tuning the temperature of reservoirs. It makes the spin flipper doped Josephson junction loop much more versatile as regards possible applications. As a quantum heat engine, the proposed device is much more efficient than previously proposed Josephson quantum heat engines[212, 213]. Further, when operating as a quantum refrigerator, the COP of the proposed device is higher than that seen in Refs. [212, 213]. In Table 6.1, we see that although work done by Josephson heat engine proposed in Ref. [213] is more than ours. However, the efficiency of the Josephson quantum heat engine discussed in this chapter is much larger than those of Josephson heat engines of Refs. [212, 213]. Further, as a Josephson quantum refrigerator, the COP of the proposed device is enormous compared to other Josephson quantum refrigerator proposals.



# Chapter 7

## Conclusion

*“A conclusion is the place where you get tired of thinking.”*

— Arthur Bloch

This thesis deals with studying the effects of spin-flip scattering on Andreev reflection mediated transport in the vicinity of a superconductor. We have investigated the consequences of spin-flip scattering in the vicinity of a metal superconductor junction and Josephson junction.

In chapter 1, we have presented a brief introduction to the three critical phenomena in this thesis: Andreev reflection, spin-flip scattering, and Josephson effect. We have introduced BTK formalism and probed the interplay between Andreev reflection and spin-flip scattering. We have also discussed Andreev bound states, the total Josephson current, and its separation into bound and continuum contributions for a superconductor-normal metal-superconductor junction.

Chapter 2 has studied the formation and properties of Yu-Shiba-Rusinov (YSR) bound states using BTK formalism. We have computed the differential conductance for a normal metal-normal metal-superconductor junction with a spin flipper at the interface between two normal metals and a  $\delta$ -like potential barrier between normal metal and superconductor.

## 7. CONCLUSION

---

A zero-bias conductance peak is seen due to the merger of two YSR bound state energies in the presence of spin-flip scattering. In the same chapter, we have examined the stability of Majorana bound states induced zero-bias conductance peak (ZBCP) seen in a metal-topological superconductor junction to the effects of spin-flip scattering. We see that quantized ZBCP remains stable in the presence of spin-flip scattering for metal- $p$ -wave superconductor junction. However, the quantized ZBCP loses stability when a spin-orbit coupled superconducting wire (SOCSW) replaces the  $p$ -wave superconductor.

In chapter 3, we have studied the emergence of odd frequency equal spin-triplet correlations in a normal metal-spin flipper-superconductor junction due to spin-flip scattering. Using Green's function method, we have analytically computed the even and odd frequency spin-singlet and triplet correlations in both metallic and superconducting regions. We find that due to spin-flip scattering, mixed spin-triplet pairing vanishes, and only spin-singlet and equal-spin-triplet pairings are finite in this setup. The existence of odd frequency equal-spin-triplet correlation tallies well with the characteristic local magnetization density of states and spin-polarized local density of states at the interface. We also compare the obtained results for normal metal-spin flipper-superconductor junction with results from other hybrid junctions, when only spin mixing or both spin mixing and spin-flip scattering are present. When only spin mixing is present, odd frequency equal spin-triplet correlations vanish but odd frequency mixed spin-triplet correlations are finite. When spin mixing and spin-flip scattering occur together, both odd frequency equal spin-triplet correlations and odd frequency mixed spin-triplet correlations are finite. However, only in a Normal metal-Spin flipper-Superconductor setup, finite odd frequency equal spin-triplet correlations are seen along with vanishing odd frequency mixed spin-triplet correlations.

In chapter 4, we have studied the nature of the  $0$  to  $\pi$  Josephson junction transition due to spin-flip scattering. We see that a setup with a spin flipper embedded between two

---

*s*-wave superconductors can transit from a 0 to  $\pi$  Josephson junction by tuning any system parameter like the strength of tunnel contact, the spin or magnetic moment of the spin flipper, or exchange coupling. In the same chapter, we have also studied the anomalous Josephson effect, and the direction-dependent critical current in the ferromagnetic Josephson junction wherein a spin flipper is embedded between two ferromagnetic layers. We show that time reversal and chiral symmetries are broken due to spin-flip scattering and because ferromagnets are misaligned. As a result, an anomalous Josephson current flows in the junction. Further, this setup acts as a phase battery wherein one can store quantized amounts of anomalous phase in the ground state of the junction.

In chapter 5, we have examined the origin of quantum spin torque in a ferromagnetic Josephson junction when magnetization vectors of ferromagnetic layers are aligned parallel or anti-parallel, and a spin flipper is sandwiched between the two ferromagnetic layers. Generally, in the ferromagnetic Josephson junction, an equilibrium spin-transfer torque is seen when magnetization vectors of ferromagnetic layers are misaligned. However, we see that when a spin flipper is embedded between two ferromagnetic layers, a novel quantum spin torque is induced even when magnetization vectors of ferromagnetic layers are aligned parallel or anti-parallel due to spin-flip scattering.

In chapter 6, we have examined the application of a spin-flipper doped Josephson junction in quantum thermodynamics. We see that a 1D Josephson junction loop doped with a spin flipper attached to two thermal reservoirs can operate as a quantum heat engine or quantum refrigerator, a Joule pump, or even as a cold pump with high efficiency and coefficient of performance. Further, we have found that the proposed device can be tuned from engine mode to other operating modes like refrigerator or Joule pump/cold pump via tuning the temperatures of the reservoirs or via the enclosed magnetic flux in the Josephson junction loop.

## 7. CONCLUSION

---

The results of this thesis will hopefully lead to more studies on setups involving spin flippers and other exotic superconductors such as High  $T_c$ , Iron pnictide, etc. These superconductors have nodes in their pairing gap, and the aim would be to exploit these for spintronics applications. Further, studies on odd frequency equal spin-triplet correlations in ferromagnetic Josephson junctions in the presence of spin-flip scattering can be attempted. We have already noticed that a ferromagnetic Josephson junction, with a spin flipper sandwiched in between, generates anomalous Josephson current, which is accompanied by a quantized anomalous phase. One may extend this to find possible relationships between odd frequency equal spin-triplet correlations and quantized anomalous phase. As noticed in chapter 6, spin-flip scattering and Josephson physics have been utilized to design quantum thermodynamic devices; these studies can be extended to ferromagnetic Josephson junction to design spin-based Josephson thermodynamic devices.

# Appendix A

## Analytical expression for Green's functions

In this appendix we present analytical expressions for Green's functions in both normal metal and superconducting regions. These Green's functions are used to calculate induced pairing correlations, LMDOS and SPLDOS in chapter 3.

### A.1 Green's function in normal metal region

Green's function in normal metal is obtained by plugging the wavefunctions from Eq. (3.2) for  $x < 0$  into Eq. (3.4) with  $b_{ij}$  and  $a_{ij}$  found from Eq. (3.3). For electron-electron and electron-hole components of Green's function we get

$$\begin{aligned} [G_{ee}^r]_{\uparrow\uparrow} &= -\frac{i\eta}{2k_e} [b_{11}e^{-ik_e(x+x')} + e^{ik_e|x-x'|}], & [G_{ee}^r]_{\downarrow\downarrow} &= -\frac{i\eta}{2k_e} [b_{22}e^{-ik_e(x+x')} + e^{ik_e|x-x'|}], \\ [G_{ee}^r]_{\uparrow\downarrow} &= -\frac{i\eta}{2k_e} b_{21}e^{-ik_e(x+x')}, & [G_{ee}^r]_{\downarrow\uparrow} &= -\frac{i\eta}{2k_e} b_{12}e^{-ik_e(x+x')}, \\ [G_{eh}^r]_{\uparrow\uparrow} &= -\frac{i\eta}{2k_e} a_{31}e^{-i(k_e x - k_h x')}, & [G_{eh}^r]_{\downarrow\downarrow} &= -\frac{i\eta}{2k_e} a_{42}e^{-i(k_e x - k_h x')}, \\ [G_{eh}^r]_{\uparrow\downarrow} &= -\frac{i\eta}{2k_e} a_{41}e^{-i(k_e x - k_h x')}, & \text{and } [G_{eh}^r]_{\downarrow\uparrow} &= -\frac{i\eta}{2k_e} a_{32}e^{-i(k_e x - k_h x')}. \end{aligned} \tag{A.1}$$

## A. ANALYTICAL EXPRESSION FOR GREEN'S FUNCTIONS

We find that  $b_{11} = b_{22}$ ,  $b_{12} = b_{21}$ ,  $a_{31} = -a_{42} = a_{11}$ ,  $a_{41} = -a_{32} = a_{12}$ . Therefore, we have

$$\begin{aligned} [G_{ee}^r]_{\uparrow\uparrow} &= [G_{ee}^r]_{\downarrow\downarrow} = -\frac{i\eta}{2k_e} [b_{11}e^{-ik_e(x+x')} + e^{ik_e|x-x'|}], \quad [G_{ee}^r]_{\uparrow\downarrow} = [G_{ee}^r]_{\downarrow\uparrow} = -\frac{i\eta}{2k_e} b_{12}e^{-ik_e(x+x')}, \\ [G_{eh}^r]_{\uparrow\uparrow} &= -[G_{eh}^r]_{\downarrow\downarrow} = -\frac{i\eta}{2k_e} a_{11}e^{-i(k_e x - k_h x')}, \quad \text{and} \quad [G_{eh}^r]_{\uparrow\downarrow} = -[G_{eh}^r]_{\downarrow\uparrow} = -\frac{i\eta}{2k_e} a_{12}e^{-i(k_e x - k_h x')}, \end{aligned}$$

where,  $b_{11} = (-f^4 J^4 (u^2 - v^2)^2 - (y_2 y_3 (u^2 - v^2) + J^2 (1 + m')^2 (u^2 - v^2) + y y_3 u^2 + y y_2 v^2 - iJ(1 + m')(u^2 - v^2)(y_2 - y_3 + y - y_1) + (y_2 u^2 + v^2 (y_3 - y) + u^2 y) y_1) (J^2 m'^2 (u^2 - v^2) - y_3 u^2 y + y_3 v^2 y_1 - u^2 y y_1 + v^2 y y_1 - iJm'(u^2 - v^2) (y_3 + y + y_1) + y_2 (y_3 (u^2 - v^2) + iJm'(u^2 - v^2) - v^2 y + u^2 y_1)) - f^2 J^2 (y_3^2 + 2J^2 m' (1 + m') (u^2 - v^2)^2 + y_2^2 - y^2 (u^2 - v^2)^2 + iJ(u^2 - v^2)^2 (y_2 - y_3 - y - 2m' y - y_1) + 2y_3 u^2 (u^2 - v^2) y_1 + (u^2 - v^2)^2 y_1^2 + 2y_2 v^2 (4y_3 u^2 + (u^2 - v^2) y_1))) / D_S$ ,

$$\begin{aligned} b_{12} &= 2ifJy(y_3^2 u^4 + y_2^2 u^2 v^2 + 4y_2 y_3 u^2 v^2 + y_3^2 u^2 v^2 + y_2^2 v^4 + f^2 J^2 (u^2 - v^2)^2 + J^2 m' (1 + m') (u^2 - v^2)^2 \\ &\quad + 2(u^2 - v^2)(y_3 u^2 + y_2 v^2) y_1 + (u^2 - v^2)^2 y_1^2 - iJ(u^2 - v^2)(y_3 u^2 + v^2 (y_2 - y_1) + u^2 y_1)) / D_S, \end{aligned}$$

$$a_{11} = 2fJ(y_2 + y_3)uv\sqrt{y y_1} (J(1 + 2m')(u^2 - v^2) - i(y_2 + y_3 + (u^2 - v^2)(y + y_1))) / D_S,$$

$$\begin{aligned} a_{12} &= 2(y_2 + y_3)uv\sqrt{y y_1} (-J^2 (f^2 - (1 + m')^2) (u^2 - v^2) + y y_3 u^2 - iJ(1 + m') (u^2 - v^2) (y_2 - y_3 + y - y_1) \\ &\quad + y_1 y_3 v^2 + y y_1 (u^2 - v^2) + y_2 (y_3 (u^2 - v^2) + v^2 y + u^2 y_1)) / D_S, \end{aligned}$$

$$y = \sqrt{1 + \frac{\omega}{E_F}}, \quad y_1 = \sqrt{1 - \frac{\omega}{E_F}}, \quad y_2 = \sqrt{1 + \frac{\sqrt{\omega^2 - \Delta^2}}{E_F}}, \quad y_3 = \sqrt{1 - \frac{\sqrt{\omega^2 - \Delta^2}}{E_F}},$$

$$\begin{aligned} D_S &= f^4 J^4 (u^2 - v^2)^2 + (y_2 y_3 (u^2 - v^2) + J^2 (1 + m')^2 (u^2 - v^2) + y y_3 u^2 + y y_2 v^2 - iJ(1 + m')(u^2 - v^2)(y_2 - y_3 \\ &\quad + y - y_1) + (y_2 u^2 + v^2 (y_3 - y) + u^2 y) y_1) (J^2 m'^2 (u^2 - v^2) + y y_3 u^2 + y_1 y_3 v^2 + y y_1 (u^2 - v^2) - iJm'(u^2 - v^2) \\ &\quad (y_3 - y + y_1) + y_2 (y_3 (u^2 - v^2) + iJm'(u^2 - v^2) + v^2 y + u^2 y_1)) + f^2 J^2 (y_3^2 + 2J^2 m' (1 + m') (u^2 - v^2)^2 \\ &\quad + y_2^2 + 2y y_3 u^2 v^2 - 2y y_3 v^4 + u^4 y^2 - 2u^2 v^2 y^2 + v^4 y^2 + iJ(u^2 - v^2)^2 (y_2 - y_3 + y - y_1) + 2y_1 y_3 u^2 (u^2 - v^2) \\ &\quad + (u^2 - v^2)^2 y_1^2 + 2y_2 (4y_3 u^2 v^2 + (u^2 - v^2)(u^2 y + v^2 y_1))). \end{aligned}$$

(A.2)

Spin singlet and spin triplet pairing amplitudes are then calculated using Eq. (3.10) in the main text, resulting in

$$f_0^r(x, x', \omega) = -\frac{i\eta}{2k_e} a_{12} e^{-i(k_e x - k_h x')}, \quad f_1^r(x, x', \omega) = \frac{i\eta}{2k_e} a_{11} e^{-i(k_e x - k_h x')}, \quad f_2^r(x, x', \omega) = 0, \quad \text{and} \quad f_3^r(x, x', \omega) = 0. \quad (\text{A.3})$$



## A.2. Green's function in superconducting region

In absence of spin flip scattering  $b_{12} = a_{11} = 0$ , therefore from Eq. (A.2) we get

$$\begin{aligned} [G_{ee}^r]_{\uparrow\uparrow} = [G_{ee}^r]_{\downarrow\downarrow} &= -\frac{i\eta}{2k_e} [b_{11}e^{-ik_e(x+x')} + e^{ik_e|x-x'|}], \quad [G_{ee}^r]_{\uparrow\downarrow} = [G_{ee}^r]_{\downarrow\uparrow} = 0, \quad [G_{eh}^r]_{\uparrow\uparrow} = -[G_{eh}^r]_{\downarrow\downarrow} = 0, \\ [G_{eh}^r]_{\uparrow\downarrow} &= -[G_{eh}^r]_{\downarrow\uparrow} = -\frac{i\eta}{2k_e} a_{12}e^{-i(k_e x - k_h x')}. \end{aligned} \quad (\text{A.4})$$

wherein amplitudes  $b_{11}$  and  $a_{12}$  for no flip process can be obtained by putting  $f = 0$  in Eq. (A.2). Spin singlet and spin triplet pairing amplitudes in absence of spin flip scattering are obtained from Eq. (3.10) in main text, resulting in

$$f_0^r(x, x', \omega) = -\frac{i\eta}{2k_e} a_{12}e^{-i(k_e x - k_h x')}, \quad f_1^r(x, x', \omega) = 0, \quad f_2^r(x, x', \omega) = 0, \quad \text{and} \quad f_3^r(x, x', \omega) = 0, \quad (\text{A.5})$$

## A.2 Green's function in superconducting region

In superconducting region we use same procedure as for normal metal region and finally get electron-electron and electron-hole components in presence of spin flip scattering as-

$$\begin{aligned} [G_{ee}^r]_{\uparrow\uparrow} = [G_{ee}^r]_{\downarrow\downarrow} &= \frac{\eta}{2i(u^2 - v^2)} \left[ \frac{e^{ik_e^S|x-x'|}u^2 + b_{51}e^{ik_e^S(x+x')}u^2 + a_{81}e^{i(k_e^S x' - k_h^S x)}uv}{k_e^S} \right. \\ &\quad \left. + \frac{a_{81}e^{i(k_e^S x - k_h^S x')}uv + b_{82}e^{-ik_h^S(x+x')}v^2 + v^2e^{-ik_h^S|x-x'|}}{k_h^S} \right], \\ [G_{ee}^r]_{\uparrow\downarrow} = [G_{ee}^r]_{\downarrow\uparrow} &= \frac{\eta}{2i(u^2 - v^2)} \left[ \frac{b_{61}e^{ik_e^S(x+x')}u^2 + a_{62}e^{i(k_e^S x' - k_h^S x)}uv}{k_e^S} - \frac{b_{72}e^{-ik_h^S(x+x')}v^2 - a_{62}e^{i(k_e^S x - k_h^S x')}uv}{k_h^S} \right], \\ [G_{eh}^r]_{\uparrow\uparrow} = -[G_{eh}^r]_{\downarrow\downarrow} &= -\frac{\eta}{2i(u^2 - v^2)} \left[ \frac{b_{61}e^{ik_e^S(x+x')}uv + a_{62}e^{i(k_e^S x' - k_h^S x)}v^2}{k_e^S} + \frac{a_{62}e^{i(k_e^S x - k_h^S x')}u^2 - b_{72}e^{-ik_h^S(x+x')}uv}{k_h^S} \right], \\ [G_{eh}^r]_{\uparrow\downarrow} = -[G_{eh}^r]_{\downarrow\uparrow} &= \frac{\eta}{2i(u^2 - v^2)} \left[ \frac{e^{ik_e^S|x-x'|}uv + b_{51}e^{ik_e^S(x+x')}uv + a_{81}e^{i(k_e^S x' - k_h^S x)}v^2}{k_e^S} \right. \\ &\quad \left. + \frac{a_{81}e^{i(k_e^S x - k_h^S x')}u^2 + b_{82}e^{-ik_h^S(x+x')}uv + e^{-ik_h^S|x-x'|}uv}{k_h^S} \right], \end{aligned}$$

## A. ANALYTICAL EXPRESSION FOR GREEN'S FUNCTIONS

$$\begin{aligned}
\text{where, } b_{51} &= (-f^4 J^4 (u^2 - v^2)^2 - f^2 J^2 (y_3^2 + 2J^2 m'(1 + m')(u^2 - v^2)^2 - y_2^2 + 2yy_3 u^2 v^2 - 2yy_3 v^4 + y^2 (u^2 - v^2)^2 \\
&\quad + 2y_1 y_3 u^2 (u^2 - v^2) + (u^2 - v^2)^2 y_1^2 - iJ(u^2 - v^2)^2 (y_2 + y_3 + 2y_2 m' - y + y_1)) - (y_2 y_3 (u^2 - v^2) \\
&\quad + J^2 (1 + m')^2 (u^2 - v^2) + yy_3 u^2 + yy_2 v^2 - iJ(1 + m')(u^2 - v^2)(y_2 - y_3 + y - y_1) + (y_2 u^2 + v^2 (y_3 - y) \\
&\quad + u^2 y) y_1) (J^2 m'^2 (u^2 - v^2) + yy_3 u^2 + y_1 y_3 v^2 + yy_1 (u^2 - v^2) - iJm'(u^2 - v^2)(y_3 - y + y_1) - y_2 (y_3 (u^2 - v^2) \\
&\quad + iJm'(u^2 - v^2) + v^2 y + u^2 y_1))) / D_S, \\
b_{61} &= 2if' J y_2 (u^2 - v^2) (y_3^2 + f'^2 J^2 + J^2 m'(m' - 1) - 2yy_3 v^2 + v^2 y^2 + 2y_1 y_3 u^2 + u^2 y_1^2 - iJ(y_3 - v^2 y + u^2 y_1)) / D'_S, \\
a_{62} &= -2if' J \sqrt{y_2 y_3} uv (u^2 - v^2) (2f'^2 J^2 - 2y_2 y_3 + 2J^2 m'(m' - 1) + yy_2 - yy_3 + y^2 + iJ(2y_3 (m' - 1) + 2y_2 m' \\
&\quad + y - y_1) - y_2 y_1 + y_1 y_3 + y_1^2) / D'_S, \\
b_{72} &= -2if' J y_3 (u^2 - v^2) (y_2^2 + f'^2 J^2 + J^2 m'(m' - 1) + 2yy_2 u^2 + u^2 y^2 - 2y_1 y_2 v^2 + v^2 y_1^2 + iJ(y_2 + u^2 y - v^2 y_1)) / D'_S, \\
a_{81} &= -2\sqrt{y_2 y_3} uv ((y + y_1)(y_2 y_3 (u^2 - v^2) + J^2 (1 + m')^2 (u^2 - v^2) + yy_3 u^2 + yy_2 v^2 - iJ(1 + m')(u^2 - v^2)(y_2 - y_3 \\
&\quad + y - y_1) + y_1 y_2 u^2 + y_1 y_3 v^2 + yy_1 (u^2 - v^2)) + f^2 J^2 (2y_2 + 2y_3 + (u^2 - v^2)(y + y_1))) / D_S, \\
b_{82} &= (-f^4 J^4 (u^2 - v^2)^2 - (y_2 y_3 (u^2 - v^2) + J^2 (1 + m')^2 (u^2 - v^2) + yy_3 u^2 + yy_2 v^2 - iJ(1 + m')(u^2 - v^2)(y_2 - y_3 \\
&\quad + y - y_1) + (y_2 u^2 + v^2 (y_3 - y) + u^2 y) y_1) (J^2 m'^2 (u^2 - v^2) - yy_3 u^2 + iJm'(u^2 - v^2)(y_3 + y - y_1) - y_1 y_3 v^2 \\
&\quad + yy_1 (u^2 - v^2) + y_2 (iJm'(u^2 - v^2) + y_3 (-u^2 + v^2) + v^2 y + u^2 y_1)) - f^2 J^2 (-y_3^2 + 2J^2 m'(1 + m')(u^2 - v^2)^2 \\
&\quad + y_2^2 + y^2 (u^2 - v^2)^2 + iJ(u^2 - v^2)^2 (y_2 + y_3 + 2y_3 m' + y - y_1) + (u^2 - v^2)^2 y_1^2 + 2y_2 (u^2 - v^2)(u^2 y + v^2 y_1))) / D_S, \\
D'_S &= f^4 J^4 (u^2 - v^2)^2 + (y_2 y_3 (u^2 - v^2) + J^2 m'^2 (u^2 - v^2) + yy_3 u^2 + yy_2 v^2 - iJm'(u^2 - v^2)(y_2 - y_3 \\
&\quad + y - y_1) + (y_2 u^2 + v^2 (y_3 - y) + u^2 y) y_1) (J^2 (m' - 1)^2 (u^2 - v^2) + yy_3 u^2 + y_1 y_3 v^2 + yy_1 (u^2 - v^2) - iJ(m' - 1) \\
&\quad (u^2 - v^2)(y_3 - y + y_1) + y_2 (y_3 (u^2 - v^2) + iJ(m' - 1)(u^2 - v^2) + v^2 y + u^2 y_1)) + f'^2 J^2 (y_3^2 + 2J^2 m'(m' - 1) \\
&\quad (u^2 - v^2)^2 + y_2^2 + 2yy_3 u^2 v^2 - 2yy_3 v^4 + u^4 y^2 - 2u^2 v^2 y^2 + v^4 y^2 + iJ(u^2 - v^2)^2 (y_2 - y_3 + y - y_1) \\
&\quad + 2y_1 y_3 u^2 (u^2 - v^2) + (u^2 - v^2)^2 y_1^2 + 2y_2 (4y_3 u^2 v^2 + (u^2 - v^2)(u^2 y + v^2 y_1))).
\end{aligned} \tag{A.6}$$

From the anomalous electron-hole component of retarded Green's function we get spin singlet and spin triplet pairing amplitudes using Eq. (3.10) as-

$$\begin{aligned}
f_0^r &= \frac{\eta uv}{2i(u^2 - v^2)} \left\{ e^{-\kappa|x-x'|} \left[ \frac{e^{ik_F|x-x'|}}{k_e^S} + \frac{e^{-ik_F|x-x'|}}{k_h^S} \right] + e^{-\kappa(x+x')} \left[ \frac{b_{51} e^{ik_F(x+x')}}{k_e^S} + \frac{b_{82} e^{-ik_F(x+x')}}{k_h^S} \right] \right. \\
&\quad \left. + a_{81} e^{-\kappa(x+x')} \left[ \frac{u e^{ik_F(x-x')}}{v k_h^S} + \frac{v e^{-ik_F(x-x')}}{u k_e^S} \right] \right\}, \\
f_1^r &= \frac{\eta uv}{2i(u^2 - v^2)} \left\{ e^{-\kappa(x+x')} \left[ \frac{b_{61} e^{ik_F(x+x')}}{k_e^S} - \frac{b_{72} e^{-ik_F(x+x')}}{k_h^S} \right] + a_{62} e^{-\kappa(x+x')} \left[ \frac{u e^{ik_F(x-x')}}{v k_h^S} + \frac{v e^{-ik_F(x-x')}}{u k_e^S} \right] \right\}, \\
f_2^r &= 0, \quad f_3^r = 0.
\end{aligned} \tag{A.7}$$

---

## A.2. Green's function in superconducting region

In absence of spin flip scattering  $b_{61} = b_{72} = a_{62} = 0$ , therefore from Eq. (A.6) we obtain

$$\begin{aligned}
 [G_{ee}^r]_{\uparrow\uparrow} &= [G_{ee}^r]_{\downarrow\downarrow} = \frac{\eta}{2i(u^2 - v^2)} \left[ \frac{e^{ik_e^S|x-x'|}u^2 + b_{51}e^{ik_e^S(x+x')}u^2 + a_{81}e^{i(k_e^Sx' - k_h^Sx)}uv}{k_e^S} \right. \\
 &\quad \left. + \frac{a_{81}e^{i(k_e^Sx - k_h^Sx')}uv + b_{82}e^{-ik_h^S(x+x')}v^2 + v^2e^{-ik_h^S|x-x'|}}{k_h^S} \right], \\
 [G_{ee}^r]_{\uparrow\downarrow} &= [G_{ee}^r]_{\downarrow\uparrow} = 0, \quad [G_{eh}^r]_{\uparrow\uparrow} = -[G_{eh}^r]_{\downarrow\downarrow} = 0, \\
 [G_{eh}^r]_{\uparrow\downarrow} &= -[G_{eh}^r]_{\downarrow\uparrow} = \frac{\eta}{2i(u^2 - v^2)} \left[ \frac{e^{ik_e^S|x-x'|}uv + b_{51}e^{ik_e^S(x+x')}uv + a_{81}e^{i(k_e^Sx' - k_h^Sx)}v^2}{k_e^S} \right. \\
 &\quad \left. + \frac{a_{81}e^{i(k_e^Sx - k_h^Sx')}u^2 + b_{82}e^{-ik_h^S(x+x')}uv + e^{-ik_h^S|x-x'|}uv}{k_h^S} \right],
 \end{aligned} \tag{A.8}$$

expressions for  $b_{51}$ ,  $b_{82}$  and  $a_{81}$  in absence of spin flip scattering can be found by putting  $f = 0$  in Eq. (A.6). Finally, the spin singlet and spin triplet pairing amplitudes for no flip process are given as from Eq. (3.10) in main text

$$\begin{aligned}
 f_0^r &= \frac{\eta uv}{2i(u^2 - v^2)} \left\{ e^{-\kappa|x-x'|} \left[ \frac{e^{ik_F|x-x'|}}{k_e^S} + \frac{e^{-ik_F|x-x'|}}{k_h^S} \right] + e^{-\kappa(x+x')} \left[ \frac{b_{51}e^{ik_F(x+x')}}{k_e^S} + \frac{b_{82}e^{-ik_F(x+x')}}{k_h^S} \right] \right. \\
 &\quad \left. + a_{81}e^{-\kappa(x+x')} \left[ \frac{ue^{ik_F(x-x')}}{vk_h^S} + \frac{ve^{-ik_F(x-x')}}{uk_e^S} \right] \right\},
 \end{aligned}$$

while,  $f_1^r = 0$ ,  $f_2^r = 0$ ,  $f_3^r = 0$ .

$$\tag{A.9}$$



# **Appendix B**

## **Analytical expressions for Andreev bound states and anomalous Josephson current**

In this appendix we give the explicit form of  $8 \times 8$  matrix  $M$  and Andreev bound states. Further, we supply spin flip probability ( $f$ ) values of the spin flipper for different spin flipper spin ( $S$ ) and magnetic moment ( $m'$ ) in a tabular format. In addition, we provide explicit form of expression of anomalous Josephson current and show that for no flip case or absence of spin flipper or when magnetizations of Ferromagnet's are aligned, anomalous Josephson current vanishes.

## B.1 Explicit form of Matrix $M$ used in chapter 4

To calculate the bound state contribution of total Josephson current we introduce a  $8 \times 8$  matrix  $M$  in Eq. (4.10) in subsection 4.2.1 of chapter 4 which is given by-

$$M = \begin{pmatrix} M_{11} & M_{12} & M_{13} & M_{14} & M_{15} & M_{16} & M_{17} & M_{18} \\ M_{21} & M_{22} & M_{23} & M_{24} & M_{25} & M_{26} & M_{27} & M_{28} \\ M_{31} & M_{32} & M_{33} & M_{34} & M_{35} & M_{36} & M_{37} & M_{38} \\ M_{41} & M_{42} & M_{43} & M_{44} & M_{45} & M_{46} & M_{47} & M_{48} \\ M_{51} & M_{52} & M_{53} & M_{54} & M_{55} & M_{56} & M_{57} & M_{58} \\ M_{61} & M_{62} & M_{63} & M_{64} & M_{65} & M_{66} & M_{67} & M_{68} \\ M_{71} & M_{72} & M_{73} & M_{74} & M_{75} & M_{76} & M_{77} & M_{78} \\ M_{81} & M_{82} & M_{83} & M_{84} & M_{85} & M_{86} & M_{87} & M_{88} \end{pmatrix}$$

where,

$$\begin{aligned} M_{11} &= (-ie^{ik_{Fa}u} + e^{ik_{Fa}uZ} - e^{2ik_{Fa}uZ}), \quad M_{12} = 0, \quad M_{13} = 0, \quad M_{14} = -v(i e^{ik_{Fa}u} - Z + e^{ik_{Fa}uZ}), \\ M_{15} &= (ie^{ik_{Fa}+i\varphi}u - e^{ik_{Fa}+i\varphi}uZ + e^{2ik_{Fa}+i\varphi}uZ), \quad M_{16} = 0, \quad M_{17} = 0, \\ M_{18} &= (ie^{ik_{Fa}+i\varphi}v + e^{ik_{Fa}+i\varphi}vZ - e^{i\varphi}vZ), \quad M_{21} = 0, \quad M_{22} = (ie^{ik_{Fa}u} - e^{ik_{Fa}uZ} + e^{2ik_{Fa}uZ}), \\ M_{23} &= -v(i e^{ik_{Fa}u} - Z + e^{ik_{Fa}uZ}), \quad M_{24} = 0, \quad M_{25} = 0, \quad M_{26} = (-ie^{ik_{Fa}+i\varphi}u + e^{ik_{Fa}+i\varphi}uZ - e^{2ik_{Fa}+i\varphi}uZ), \\ M_{27} &= (ie^{ik_{Fa}+i\varphi}v + e^{ik_{Fa}+i\varphi}vZ - e^{i\varphi}vZ), \quad M_{28} = 0, \quad M_{31} = 0, \quad M_{32} = (ie^{ik_{Fa}v} - e^{ik_{Fa}vZ} + e^{2ik_{Fa}vZ}), \\ M_{33} &= -u(i e^{ik_{Fa}u} - Z + e^{ik_{Fa}uZ}), \quad M_{34} = 0, \quad M_{35} = 0, \quad M_{36} = (-ie^{ik_{Fa}v} + e^{ik_{Fa}vZ} - e^{2ik_{Fa}vZ}), \\ M_{37} &= (ie^{ik_{Fa}u} - uZ + e^{ik_{Fa}uZ}), \quad M_{38} = 0, \quad M_{41} = (-ie^{ik_{Fa}v} + e^{ik_{Fa}vZ} - e^{2ik_{Fa}vZ}), \quad M_{42} = 0, \\ M_{43} &= 0, \quad M_{44} = -u(i e^{ik_{Fa}u} - Z + e^{ik_{Fa}uZ}), \quad M_{45} = (ie^{ik_{Fa}v} - e^{ik_{Fa}vZ} + e^{2ik_{Fa}vZ}), \quad M_{46} = 0, \\ M_{47} &= 0, \quad M_{48} = (ie^{ik_{Fa}u} - uZ + e^{ik_{Fa}uZ}), \\ M_{51} &= (e^{2ik_{Fa}} Jm'u(i - 2Z) + e^{3ik_{Fa}} (-2i + Jm')uZ + e^{ik_{Fa}} (2i + Jm')u(-i + Z)), \\ M_{52} &= (e^{2ik_{Fa}} fJu(i - 2Z) + e^{3ik_{Fa}} fJuZ + e^{ik_{Fa}} fJu(-i + Z)), \end{aligned}$$

---

B.1. Explicit form of Matrix M used in chapter 4

$$\begin{aligned}
M_{53} &= (-fJvZ - e^{2ik_Fa} fJv(i+Z) + e^{ik_Fa} fJv(i+2Z)), \\
M_{54} &= (2e^{2ik_Fa} v(1-iZ) + (2i+Jm')vZ + e^{2ik_Fa} Jm'v(i+Z) - e^{ik_Fa} Jm'v(i+2Z)), \\
M_{55} &= -2e^{2ik_Fa+i\varphi} u, \quad M_{56} = 0, \quad M_{57} = 0, \quad M_{58} = -2e^{i(k_Fa+\varphi)} v, \\
M_{61} &= (e^{2ik_Fa} fJu(i-2Z) + e^{3ik_Fa} fJuZ + e^{ik_Fa} fJu(-i+Z)), \\
M_{62} &= e^{ik_Fa} u(2 + (1 - e^{ik_Fa})J(1 + m')(i + (-1 + e^{ik_Fa})Z) + 4e^{ik_Fa} Z \sin(k_Fa)), \\
M_{63} &= v((-2i + J(1 + m'))Z + e^{2ik_Fa} (2i + J(1 + m'))(i + Z) - e^{ik_Fa} J(1 + m')(i + 2Z)), \\
M_{64} &= (fJvZ + e^{2ik_Fa} fJv(i+Z) - e^{ik_Fa} fJv(i+2Z)), \quad M_{65} = 0, \quad M_{66} = -2e^{ik_Fa+i(k_Fa+\varphi)} u, \\
M_{67} &= 2e^{i(k_Fa+\varphi)} v, \quad M_{68} = 0, \quad M_{71} = e^{-ik_Fa} (e^{2ik_Fa} fJv(i-2Z) + e^{3ik_Fa} fJvZ + e^{ik_Fa} fJv(-i+Z)), \\
M_{72} &= v((-1 + e^{ik_Fa})J(1 + m')(i + (-1 + e^{ik_Fa})Z) + 2i(i + (-1 + e^{2ik_Fa})Z)), \\
M_{73} &= e^{-ik_Fa} ((2i - J(m' + 1))uZ + e^{2ik_Fa} (-2i - J(m' + 1))u(i + Z) + e^{ik_Fa} J(m' + 1)u(i + 2Z)), \\
M_{74} &= e^{-ik_Fa} (fJuZ + e^{2ik_Fa} fJu(i+Z) - e^{ik_Fa} fJu(i+2Z)), \quad M_{75} = 0, \\
M_{76} &= 2e^{ik_Fa} v, \\
M_{77} &= -2u, \\
M_{78} &= 0, \\
M_{81} &= e^{-ik_Fa} (2e^{ik_Fa} v(1+iZ) + e^{3ik_Fa} (-2i+Jm')vZ + e^{ik_Fa} Jm'v(-i+Z) - e^{2ik_Fa} Jm'v(-i+2Z)), \\
M_{82} &= e^{-ik_Fa} (-e^{2ik_Fa} fJv(i-2Z) - e^{3ik_Fa} fJvZ - e^{ik_Fa} fJv(-i+Z)), \\
M_{83} &= e^{-ik_Fa} (fJuZ + e^{2ik_Fa} fJu(i+Z) - e^{ik_Fa} fJu(i+2Z)), \\
M_{84} &= e^{-ik_Fa} ((2i+Jm')uZ + e^{2ik_Fa} (-2i+Jm')u(i+Z) - e^{ik_Fa} Jm'u(i+2Z)), \\
M_{85} &= -2e^{ik_Fa} v, \\
M_{86} &= 0, \\
M_{87} &= 0, \\
M_{88} &= -2u.
\end{aligned}$$

## B.2 Explicit form of Andreev bound states in chapter 4

In Eq. (4.11) Andreev bound state expression, we introduce the terms  $A(\varphi)$ ,  $B(\varphi)$  and  $C$  in subsection 4.2.1 of chapter 4. The explicit form of  $A(\varphi)$ ,  $B(\varphi)$  and  $C$  is given by

$$\begin{aligned}
 A(\varphi) = & -2e^{3ik_F a}((1+2Z^2)(8(1+2Z^2)^2 + J^4(f^2 + m' + m'^2)^2(1+10(Z^2 + Z^4)) + J^2(3+6m'(1+m') + 8Z^2 \\
 & + 2(f^2 - 8(f^2 + m' + m'^2)Z^2 - 4(-1+2f^2 + 2m'(1+m'))Z^4))) + 2Z^2(1+2Z^2)(16+16J^3(f^2 + m' + m'^2)Z \\
 & - 16Z^2 + 3J^4(f^2 + m' + m'^2)^2(-1+Z^2) + 4J^2(-1+2f^2 + 2m'(1+m'))(-1+Z^2)) \cos(2k_F a) - 2Z^3(16Z(-3+Z^2) \\
 & + J^4(f^2 + m' + m'^2)^2 Z(-3+Z^2) + 4J^2(-1+2f^2 + 2m'(1+m'))Z(-3+Z^2) + 16J(-1+3Z^2) + 4J^3(f^2 + m' \\
 & + m'^2)(-1+3Z^2)) \cos(3k_F a) + 8 \cos(\varphi) + (16Z^2 - J^2(-1+2f^2 - 2m'(1+m'))(1+2Z^2)) \cos(\varphi) + 2Z \cos(k_F a)(8Z \\
 & + 12J(1+2Z^2)^2 + J^2 Z(-3-2f^2 - 6m'(1+m') - 4Z^2 + 8(f^2 + m' + m'^2)Z^2 + 4(-1+2f^2 + 2m'(1+m'))Z^4) \\
 & + 16(Z^3 + Z^5) - 4J^3(f^2 + m' + m'^2)(1+5(Z^2 + Z^4)) - 3J^4(f^2 + m' + m'^2)^2 Z(1+5(Z^2 + Z^4)) + (8Z + J(4 \\
 & + J(-1+2f^2 - 2m'(1+m'))Z)) \cos(\varphi)) + 2Z(-8+12JZ(1+2Z^2)^2 - 16(Z^2 + Z^4) + J^2(3+2f^2 + 6m'(1+m') \\
 & + 4Z^2 - 8(f^2 + m' + m'^2)Z^2 - 4(-1+2f^2 + 2m'(1+m'))Z^4) + 3J^4(f^2 + m' + m'^2)^2(1+5(Z^2 + Z^4)) \\
 & - 4J^3(f^2 + m' + m'^2)Z(1+5(Z^2 + Z^4)) + (-8+J^2(1-2f^2 + 2m'(1+m')) + 4JZ) \cos(\varphi) \sin(k_F a) \\
 & - 4Z^2(1+2Z^2)(-16Z + J^2(-4Z + (f^2 + m' + m'^2)(8Z + J(4+3J(f^2 + m' + m'^2)Z - 4Z^2)))) \sin(2k_F a) \\
 & - 2Z^3(16-48Z^2 + 16JZ(-3+Z^2) + 4J^3(f^2 + m' + m'^2)Z(-3+Z^2) - J^4(f^2 + m' + m'^2)^2(-1+3Z^2) \\
 & - 4J^2(-1+2f^2 + 2m'(1+m'))(-1+3Z^2)) \sin(3k_F a)
 \end{aligned}$$

$$\begin{aligned}
 B(\varphi) = & -2J^2 e^{6ik_F a}(-64f^4 J^2(1+6(Z^2 + Z^4)) - 3(1+2m')^2(32(Z^2 + Z^4) + J^2(1+6(Z^2 + Z^4)))) + 4f^2(-J^2(5 \\
 & + 4m'(1+m'))(1+6(Z^2 + Z^4)) - 16(1+8(Z^2 + Z^4))) + 4J^2 \cos(\varphi) + 16f^2 J^2 \cos(\varphi) - 64f^4 J^2 \cos(\varphi) \\
 & + 16J^2 m' \cos(\varphi) + 16J^2 m'^2 \cos(\varphi) + 128Z^2 \cos(\varphi) + 512f^2 Z^2 \cos(\varphi) + 24J^2 Z^2 \cos(\varphi) + 96f^2 J^2 Z^2 \cos(\varphi) \\
 & - 384f^4 J^2 Z^2 \cos(\varphi) + 512m' Z^2 \cos(\varphi) + 96J^2 m' Z^2 \cos(\varphi) + 512m'^2 Z^2 \cos(\varphi) + 96J^2 m'^2 Z^2 \cos(\varphi) \\
 & + 128Z^4 \cos(\varphi) + 512f^2 Z^4 \cos(\varphi) + 24J^2 Z^4 \cos(\varphi) + 96f^2 J^2 Z^4 \cos(\varphi) - 384f^4 J^2 Z^4 \cos(\varphi) \\
 & + 512m' Z^4 \cos(\varphi) + 96J^2 m' Z^4 \cos(\varphi) + 512m'^2 Z^4 \cos(\varphi) + 96J^2 m'^2 Z^4 \cos(\varphi) - 8JZ(1+2Z^2) \cos(k_F a) \\
 & (-8f^2 - (1+2m')^2 + (1+2m')^2 \cos(\varphi))(-4+JZ+4f^2 JZ + (4+(-1+4f^2)JZ) \cos(\varphi)) + 4Z^2 \cos(2k_F a) \\
 & (-8f^2 - (1+2m')^2 + (1+2m')^2 \cos(\varphi))(16-16JZ-16Z^2 + (1+4f^2)J^2(-1+Z^2) + (16JZ+16(-1+Z^2) \\
 & + (-1+4f^2)J^2(-1+Z^2)) \cos(\varphi) + 64f^2 \cos(2\varphi)J^2 \cos(2\varphi) + 4f^2 J^2 \cos(2\varphi) - 4J^2 m' \cos(2\varphi) \\
 & + 16f^2 J^2 m' \cos(2\varphi) - 4J^2 m'^2 \cos(2\varphi) + 16f^2 J^2 m'^2 \cos(2\varphi) - 32Z^2 \cos(2\varphi) - 6J^2 Z^2 \cos(2\varphi) \\
 & + 24f^2 J^2 Z^2 \cos(2\varphi) - 128m' Z^2 \cos(2\varphi) - 24J^2 m' Z^2 \cos(2\varphi) + 96f^2 J^2 m' Z^2 \cos(2\varphi) - 128m'^2 Z^2 \cos(2\varphi) \\
 & - 24J^2 m'^2 Z^2 \cos(2\varphi) + 96f^2 J^2 m'^2 Z^2 \cos(2\varphi) - 32Z^4 \cos(2\varphi) - 6J^2 Z^4 \cos(2\varphi) + 24f^2 J^2 Z^4 \cos(2\varphi) \\
 & - 128m' Z^4 \cos(2\varphi) - 24J^2 m' Z^4 \cos(2\varphi) + 96f^2 J^2 m' Z^4 \cos(2\varphi) - 128m'^2 Z^4 \cos(2\varphi) - 24J^2 m'^2 Z^4 \cos(2\varphi)
 \end{aligned}$$



### B.3. Table for different values of spin flip probability of spin flipper for different $S$ and $m'$

$$\begin{aligned}
& + 96f^2 J^2 m'^2 Z^4 \cos(2\varphi) + 8JZ(1 + 2Z^2)(-8f^2 - (1 + 2m')^2 + (1 + 2m')^2 \cos(\varphi))(J + 4f^2 J + 4Z + (-J \\
& + 4f^2 J - 4Z) \cos(\varphi)) \sin(k_F a) - 8Z^2(-8f^2 - (1 + 2m')^2 + (1 + 2m')^2 \cos(\varphi))(-16Z + J(-4 + Z(J + 4f^2 J + 4Z)) \\
& + (16Z + J(4 + (-1 + 4f^2)JZ - 4Z^2)) \cos(\varphi)) \sin(2k_F a)
\end{aligned}$$

$$\begin{aligned}
C = e^{3ik_F a} & (-1 - 2Z^2 + 2Z^2 \cos(k_F a) - 2Z \sin(k_F a))(4J^2(1 + 2f^2 + 2m'(1 + m') + 2Z^2 - 4(f^2 + m' + m'^2)Z^2 - 2(-1 + 2f^2 \\
& + 2m'(1 + m'))Z^4) + 16(1 + 6(Z^2 + Z^4)) + J^4(f^2 + m' + m'^2)^2(1 + 6(Z^2 + Z^4)) + 2Z(-2(-4 + J^2(f^2 + m' + m'^2)) \\
& (1 + 2Z^2)(4Z + J(2 + J(f^2 + m' + m'^2)Z)) \cos(k_F a) + Z(4(-1 + Z) + J(J(f^2 + m' + m'^2)(-1 + Z) + 2(1 + Z))) \\
& (4(1 + Z) + J(2 - 2Z + J(f^2 + m' + m'^2)(1 + Z))) \cos(2k_F a) + 2(-4 + J^2(f^2 + m' + m'^2))(4 + J(J(f^2 + m' + m'^2) \\
& - 2Z))(1 + 2Z^2) \sin(k_F a) + 2Z(-4 + J(-J(f^2 + m' + m'^2) + 2Z))(4Z + J(2 + J(f^2 + m' + m'^2)Z)) \sin(2k_F a))
\end{aligned}$$

### B.3 Table for different values of spin flip probability of spin flipper for different $S$ and $m'$

To study the effect of high spin states of spin flipper on the Josephson supercurrent (Eq. (4.14)) in subsection 4.2.6 of chapter 4, we provide spin flip probability ( $f$ ) values of the spin flipper for different  $S$  and  $m'$  in a tabular format.

Table B.1: Spin flip probability ( $f$ ) values of the spin flipper for different  $S$  and  $m'$

$S$	$m'$	$f$	$S$	$m'$	$f$
$\frac{1}{2}$	$-\frac{1}{2}$	1	$\frac{7}{2}$	$-\frac{7}{2}$	$\sqrt{7}$
	$\frac{1}{2}$	0		$-\frac{5}{2}$	$2\sqrt{3}$
$\frac{3}{2}$	$-\frac{3}{2}$	$\sqrt{3}$		$-\frac{3}{2}$	$\sqrt{15}$
	$-\frac{1}{2}$	2		$-\frac{1}{2}$	4
	$\frac{1}{2}$	$\sqrt{3}$		$\frac{1}{2}$	$\sqrt{15}$
	$\frac{3}{2}$	0		$\frac{3}{2}$	$2\sqrt{3}$
$\frac{5}{2}$	$-\frac{5}{2}$	$\sqrt{5}$		$\frac{5}{2}$	$\sqrt{7}$
	$-\frac{3}{2}$	$2\sqrt{2}$		$\frac{7}{2}$	0
	$-\frac{1}{2}$	3			
	$\frac{1}{2}$	$2\sqrt{2}$			
	$\frac{3}{2}$	$\sqrt{5}$			
	$\frac{5}{2}$	0			

B. ANALYTICAL EXPRESSIONS FOR ANDREEV BOUND STATES AND ANOMALOUS JOSEPHSON CURRENT

$S$	$m'$	$f$	$S$	$m'$	$f$
$\frac{9}{2}$	$-\frac{9}{2}$	3	$\frac{15}{2}$	$-\frac{15}{2}$	$\sqrt{15}$
	$-\frac{7}{2}$	4		$-\frac{13}{2}$	$2\sqrt{7}$
	$-\frac{5}{2}$	$\sqrt{21}$		$-\frac{11}{2}$	$\sqrt{39}$
	$-\frac{3}{2}$	$2\sqrt{6}$		$-\frac{9}{2}$	$4\sqrt{3}$
	$-\frac{1}{2}$	5		$-\frac{7}{2}$	$\sqrt{55}$
	$\frac{1}{2}$	$2\sqrt{6}$		$-\frac{5}{2}$	$2\sqrt{15}$
	$\frac{3}{2}$	$\sqrt{21}$		$-\frac{3}{2}$	$3\sqrt{7}$
	$\frac{5}{2}$	4		$-\frac{1}{2}$	8
	$\frac{7}{2}$	3		$\frac{1}{2}$	$3\sqrt{7}$
	$\frac{9}{2}$	0		$\frac{3}{2}$	$2\sqrt{15}$
$\frac{11}{2}$	$-\frac{11}{2}$	$\sqrt{11}$	$\frac{5}{2}$	$\sqrt{55}$	
	$-\frac{9}{2}$	$2\sqrt{5}$	$\frac{7}{2}$	$4\sqrt{3}$	
	$-\frac{7}{2}$	$3\sqrt{3}$	$\frac{9}{2}$	$\sqrt{39}$	
	$-\frac{5}{2}$	$4\sqrt{2}$	$\frac{11}{2}$	$2\sqrt{7}$	
	$-\frac{3}{2}$	$\sqrt{35}$	$\frac{13}{2}$	$\sqrt{15}$	
	$-\frac{1}{2}$	6	$\frac{15}{2}$	0	
	$\frac{1}{2}$	$\sqrt{35}$	$\frac{17}{2}$	$-\frac{17}{2}$	$\sqrt{17}$
	$\frac{3}{2}$	$4\sqrt{2}$		$-\frac{15}{2}$	$4\sqrt{2}$
	$\frac{5}{2}$	$3\sqrt{3}$		$-\frac{13}{2}$	$3\sqrt{5}$
	$\frac{7}{2}$	$2\sqrt{5}$		$-\frac{11}{2}$	$2\sqrt{14}$
$\frac{9}{2}$	$\sqrt{11}$	$-\frac{9}{2}$		$\sqrt{65}$	
$\frac{11}{2}$	0	$-\frac{7}{2}$		$6\sqrt{2}$	
$\frac{13}{2}$	$-\frac{13}{2}$	$\sqrt{13}$		$-\frac{5}{2}$	$\sqrt{77}$
	$-\frac{11}{2}$	$2\sqrt{6}$		$-\frac{3}{2}$	$4\sqrt{5}$
	$-\frac{9}{2}$	$\sqrt{33}$		$-\frac{1}{2}$	9
	$-\frac{7}{2}$	$2\sqrt{10}$		$\frac{1}{2}$	$4\sqrt{5}$
	$-\frac{5}{2}$	$3\sqrt{5}$	$\frac{3}{2}$	$\sqrt{77}$	
	$-\frac{3}{2}$	$4\sqrt{3}$	$\frac{5}{2}$	$6\sqrt{2}$	
	$-\frac{1}{2}$	7	$\frac{7}{2}$	$\sqrt{65}$	
	$\frac{1}{2}$	$4\sqrt{3}$	$\frac{9}{2}$	$2\sqrt{14}$	
	$\frac{3}{2}$	$3\sqrt{5}$	$\frac{11}{2}$	$3\sqrt{5}$	
	$\frac{5}{2}$	$2\sqrt{10}$	$\frac{13}{2}$	$4\sqrt{2}$	
$\frac{7}{2}$	$\sqrt{33}$	$\frac{15}{2}$	$\sqrt{17}$		
$\frac{9}{2}$	$2\sqrt{6}$	$\frac{17}{2}$	0		
$\frac{11}{2}$	$\sqrt{13}$				
$\frac{13}{2}$	0				

## B.4 Explicit form of anomalous Josephson current

The explicit form of  $A_1, A_2, A_3, A_4, A'_1, A'_2, A'_3, A'_4$  in Eq. (4.38) is

$$A_{1(2)} = \Delta_0(T) \sqrt{K - \frac{1}{2}\sqrt{L+M} \pm \frac{1}{2}\sqrt{2L-M - \frac{2N}{\sqrt{L+M}}}},$$

$$A'_{1(2)} = -\frac{1}{2A_{1(2)}} \left( -K' - \frac{L'+M'}{4\sqrt{L+M}} \pm \frac{2L'-M' + \frac{N(L'+M')}{(L+M)^{3/2}} - \frac{2N'}{(L+M)}}{4\sqrt{2L-M - \frac{2N}{\sqrt{L+M}}}} \right),$$

$$A_{3(4)} = \Delta_0(T) \sqrt{K + \frac{1}{2}\sqrt{L+M} \pm \frac{1}{2}\sqrt{2L-M + \frac{2N}{\sqrt{L+M}}}},$$

$$\text{and } A'_{3(4)} = -\frac{1}{2A_{3(4)}} \left( -K' + \frac{L'+M'}{4\sqrt{L+M}} \pm \frac{2L'-M' - \frac{N(L'+M')}{(L+M)^{3/2}} + \frac{2N'}{(L+M)}}{4\sqrt{2L-M + \frac{2N}{\sqrt{L+M}}}} \right),$$

$$\text{where } L = 4T_1^2 - \frac{2}{3}T_2, \quad M = \frac{2^{1/3}X_1}{3(X_2 + \sqrt{X_2^2 - 4X_1^3})} + \frac{(X_2 + \sqrt{X_2^2 - 4X_1^3})^{1/3}}{2^{1/3}3},$$

$$N = 8T_1^3 - 2T_1T_2 + T_3, \quad K = T_1, \quad L' = -8T_1U_1 - \frac{2}{3}U_2,$$

$$M' = \frac{2^{1/3}X'_1}{3(X_2 + \sqrt{X_2^2 - 4X_1^3})^{1/3}} - \frac{2^{1/3}X_1Y_1}{9(X_2 + \sqrt{X_2^2 - 4X_1^3})^{4/3}},$$

$$N' = -192T_1^2U_1 + 16T_2U_1 - 16T_1U_2 + 8U_3, \quad K' = U_1,$$

$$\text{where } X_1 = T_2^2 - 12T_1T_3 - 12T_4,$$

$$X_2 = 2T_2^3 - 36T_1T_2T_3 - 432T_1^2T_4 + 27T_3^2 + 72T_2T_4,$$

$$X'_1 = 2T_2U_2 + 12T_3U_1 - 12T_1U_3,$$

$$Y_1 = Y'_1 + \frac{X_2Y' - 6X_1^2X'_1}{\sqrt{X_2^2 - 4X_1^3}},$$

$$Y'_1 = 6T_2^2U_2 - 36T_1T_3U_2 + 36T_2T_3U_1 + 864T_1T_4U_1 + 54T_3U_3 + 72T_4U_2,$$

## B. ANALYTICAL EXPRESSIONS FOR ANDREEV BOUND STATES AND ANOMALOUS JOSEPHSON CURRENT

---

$$\begin{aligned}
T_1 &= \left( P_1(S, m', f, h, J, k_{Fa}) + P_2(S, m', f, h, J, k_{Fa}) \cos(\theta) + P_3(S, m', f, h, J, k_{Fa}) \cos(2\theta) + P_4(S, m', f, h, J, k_{Fa}) \right. \\
&\quad \left. \cos(3\theta) + P_5(S, m', f, h, J, k_{Fa}) \cos(4\theta) \right) / \left( Q_1(S, m', f, h, J, k_{Fa}) + Q_2(S, m', f, h, J, k_{Fa}) \cos(\theta) + \right. \\
&\quad \left. Q_3(S, m', f, h, J, k_{Fa}) \cos(2\theta) + Q_4(S, m', f, h, J, k_{Fa}) \cos(3\theta) + Q_5(S, m', f, h, J, k_{Fa}) \cos(4\theta) \right), \\
T_2 &= \left( P_6(S, m', f, h, J, k_{Fa}) + P_7(S, m', f, h, J, k_{Fa}) \cos(\theta) + P_8(S, m', f, h, J, k_{Fa}) \cos(2\theta) + P_9(S, m', f, h, J, k_{Fa}) \right. \\
&\quad \left. \cos(3\theta) + P_{10}(S, m', f, h, J, k_{Fa}) \cos(4\theta) \right) / \left( Q_1(S, m', f, h, J, k_{Fa}) + Q_2(S, m', f, h, J, k_{Fa}) \cos(\theta) + \right. \\
&\quad \left. Q_3(S, m', f, h, J, k_{Fa}) \cos(2\theta) + Q_4(S, m', f, h, J, k_{Fa}) \cos(3\theta) + Q_5(S, m', f, h, J, k_{Fa}) \cos(4\theta) \right), \\
T_3 &= \left( P_{11}(S, m', f, h, J, k_{Fa}) + P_{12}(S, m', f, h, J, k_{Fa}) \cos(\theta) + P_{13}(S, m', f, h, J, k_{Fa}) \cos(2\theta) + P_{14}(S, m', f, h, J, k_{Fa}) \right. \\
&\quad \left. \cos(3\theta) + P_{15}(S, m', f, h, J, k_{Fa}) \cos(4\theta) \right) / \left( Q_1(S, m', f, h, J, k_{Fa}) + Q_2(S, m', f, h, J, k_{Fa}) \cos(\theta) + \right. \\
&\quad \left. Q_3(S, m', f, h, J, k_{Fa}) \cos(2\theta) + Q_4(S, m', f, h, J, k_{Fa}) \cos(3\theta) + Q_5(S, m', f, h, J, k_{Fa}) \cos(4\theta) \right), \\
T_4 &= \left( P_{16}(S, m', f, h, J, k_{Fa}) + P_{17}(S, m', f, h, J, k_{Fa}) \cos(\theta) + P_{18}(S, m', f, h, J, k_{Fa}) \cos(2\theta) + P_{19}(S, m', f, h, J, k_{Fa}) \right. \\
&\quad \left. \cos(3\theta) + P_{20}(S, m', f, h, J, k_{Fa}) \cos(4\theta) \right) / \left( Q_1(S, m', f, h, J, k_{Fa}) + Q_2(S, m', f, h, J, k_{Fa}) \cos(\theta) + \right. \\
&\quad \left. Q_3(S, m', f, h, J, k_{Fa}) \cos(2\theta) + Q_4(S, m', f, h, J, k_{Fa}) \cos(3\theta) + Q_5(S, m', f, h, J, k_{Fa}) \cos(4\theta) \right), \\
U_1 &= \left( Jf \sin(\theta) \left( P_{21}(S, m', f, h, J, k_{Fa}) + P_{22}(S, m', f, h, J, k_{Fa}) \cos(\theta) + P_{23}(S, m', f, h, J, k_{Fa}) \cos(2\theta) \right) \right) / \\
&\quad \left( Q_6(S, m', f, h, J, k_{Fa}) + Q_7(S, m', f, h, J, k_{Fa}) \cos(\theta) + Q_8(S, m', f, h, J, k_{Fa}) \cos(2\theta) + Q_9(S, m', f, h, J, k_{Fa}) \right. \\
&\quad \left. \cos(3\theta) + Q_{10}(S, m', f, h, J, k_{Fa}) \cos(4\theta) \right), \\
U_2 &= \left( Jf \sin(\theta) \left( P_{24}(S, m', f, h, J, k_{Fa}) + P_{25}(S, m', f, h, J, k_{Fa}) \cos(\theta) + P_{26}(S, m', f, h, J, k_{Fa}) \cos(2\theta) \right) \right) / \\
&\quad \left( Q_1(S, m', f, h, J, k_{Fa}) + Q_2(S, m', f, h, J, k_{Fa}) \cos(\theta) + Q_3(S, m', f, h, J, k_{Fa}) \cos(2\theta) + Q_4(S, m', f, h, J, k_{Fa}) \right. \\
&\quad \left. \cos(3\theta) + Q_5(S, m', f, h, J, k_{Fa}) \cos(4\theta) \right), \\
U_3 &= \left( Jf \sin(\theta) \left( P_{27}(S, m', f, h, J, k_{Fa}) + P_{28}(S, m', f, h, J, k_{Fa}) \cos(\theta) + P_{29}(S, m', f, h, J, k_{Fa}) \cos(2\theta) \right) \right) / \\
&\quad \left( Q_1(S, m', f, h, J, k_{Fa}) + Q_2(S, m', f, h, J, k_{Fa}) \cos(\theta) + Q_3(S, m', f, h, J, k_{Fa}) \cos(2\theta) + Q_4(S, m', f, h, J, k_{Fa}) \right. \\
&\quad \left. \cos(3\theta) + Q_5(S, m', f, h, J, k_{Fa}) \cos(4\theta) \right).
\end{aligned}$$

Here,  $P_i$  ( $i = 1, 2, \dots, 29$ ) and  $Q_i$  ( $i = 1, 2, \dots, 10$ ) are functions of all parameters like exchange interaction ( $J$ ), magnetization of the Ferromagnets ( $h$ ), spin ( $S$ ) and magnetic moment ( $m'$ ) of spin flipper, phase ( $k_{Fa}$ ) accumulated in ferromagnetic region and spin flip probability of spin flipper ( $f$ ). Since these are large expressions we do not explicitly write them here. From the above expressions for no flip ( $f = 0$ ) or absence of spin flipper ( $J = 0$ ) or  $\theta = 0$  (magnetizations of the Ferromagnets are aligned),  $U_1$ ,  $U_2$ ,  $U_3$  and also  $L'$ ,  $M'$ ,  $N'$  and  $K'$  vanish. Thus, from Eq. (4.38),  $A'_{1(2)} = 0$  and  $A'_{3(4)} = 0$ , implying for no flip case or absence of spin flipper or  $\theta = 0$  anomalous Josephson current vanishes ( $I_{an} = 0$ ).

# Appendix C

## Analytical expression for equilibrium quantum spin torque

In this appendix we provide explicit form of expression of equilibrium quantum spin torque used in subsection 5.3.2 of chapter 5 and show that for no flip case torque vanishes.

### C.1 Explicit form of equilibrium quantum spin torque

The explicit form of  $M_1, M_2, M_3, M_4, M'_1, M'_2, M'_3, M'_4$  in Eq. (5.11) is

$$\begin{aligned} M_{1(2)} &= \Delta_0 \sqrt{D - \frac{1}{2}\sqrt{A+B} \pm \frac{1}{2}\sqrt{2A-B - \frac{2C}{\sqrt{A+B}}}}, \\ M'_{1(2)} &= -\frac{1}{2M_{1(2)}} \left( -D' - \frac{A'+B'}{4\sqrt{A+B}} \pm \frac{2A'-B' + \frac{C(A'+B')}{(A+B)^{3/2}} - \frac{2C'}{(A+B)}}{4\sqrt{2A-B - \frac{2C}{\sqrt{A+B}}}} \right), \\ M_{3(4)} &= \Delta_0 \sqrt{D + \frac{1}{2}\sqrt{A+B} \pm \frac{1}{2}\sqrt{2A-B + \frac{2C}{\sqrt{A+B}}}}, \\ \text{and } M'_{3(4)} &= -\frac{1}{2M_{3(4)}} \left( -D' + \frac{A'+B'}{4\sqrt{A+B}} \pm \frac{2A'-B' - \frac{C(A'+B')}{(A+B)^{3/2}} + \frac{2C'}{(A+B)}}{4\sqrt{2A-B + \frac{2C}{\sqrt{A+B}}}} \right), \end{aligned}$$

$$\text{where } A = 4L_1^2 - \frac{2}{3}L_2,$$

$$B = \frac{2^{1/3}X_1}{3(X_2 + \sqrt{X_2^2 - 4X_1^3})} + \frac{(X_2 + \sqrt{X_2^2 - 4X_1^3})^{1/3}}{2^{1/3}3},$$

$$C = 8L_1^3 - 2L_1L_2 + L_3,$$

$$D = L_1,$$

$$A' = -8L_1K_1 - \frac{2}{3}K_2,$$

$$B' = \frac{2^{1/3}X_1'}{3(X_2 + \sqrt{X_2^2 - 4X_1^3})^{1/3}} - \frac{2^{1/3}X_1Y_1}{9(X_2 + \sqrt{X_2^2 - 4X_1^3})^{4/3}},$$

$$C' = -192L_1^2K_1 + 16L_2K_1 - 16L_1K_2 + 8K_3,$$

$$D' = K_1,$$

$$\text{where } X_1 = L_2^2 - 12L_1L_3 - 12L_4,$$

$$X_2 = 2L_2^3 - 36L_1L_2L_3 - 432L_1^2L_4 + 27L_3^2 + 72L_2L_4,$$

$$X_1' = 2L_2K_2 + 12L_3K_1 - 12L_1K_3,$$

$$Y_1 = Y_1' + \frac{X_2Y_1' - 6X_1^2X_1'}{\sqrt{X_2^2 - 4X_1^3}},$$

$$Y_1' = 6L_2^2K_2 - 36L_1L_3K_2 + 36L_2L_3K_1 + 864L_1L_4K_1 + 54L_3K_3 + 72L_4K_2,$$

$$L_1 = P_1(S, m', f, h, J, k_{Fa}) + P_2(S, m', f, h, J, k_{Fa}) \cos(\varphi),$$

$$L_2 = P_3(S, m', f, h, J, k_{Fa}) \cos(2\varphi) + P_4(S, m', f, h, J, k_{Fa})$$

$$\cos(\varphi) + P_5(S, m', f, h, J, k_{Fa}),$$

$$L_3 = P_6(S, m', f, h, J, k_{Fa}) + P_7(S, m', f, h, J, k_{Fa}) \cos(\varphi)$$

$$+ P_8(S, m', f, h, J, k_{Fa}) \cos(2\varphi) + P_9(S, m', f, h, J, k_{Fa})$$

$$\cos(\varphi) \cos(2\varphi),$$

---

### C.1. Explicit form of equilibrium quantum spin torque

$$\begin{aligned}
L_4 &= P_{10}(S, m', f, h, J, k_{Fa}) + P_{11}(S, m', f, h, J, k_{Fa}) \cos(\varphi) \\
&\quad + P_{12}(S, m', f, h, J, k_{Fa}) \cos(2\varphi) + P_{13}(S, m', f, h, J, k_{Fa}) \\
&\quad \cos(\varphi) \cos(2\varphi) + P_{14}(S, m', f, h, J, k_{Fa}) \cos(4\varphi), \\
K_1 &= f(P_{15}(S, m', f, h, J, k_{Fa}) \sin(\varphi) + P_{16}(S, m', f, h, J, k_{Fa})), \\
K_2 &= f(P_{17}(S, m', f, h, J, k_{Fa}) + P_{18}(S, m', f, h, J, k_{Fa}) \cos(\varphi) \\
&\quad + P_{19}(S, m', f, h, J, k_{Fa}) \sin(\varphi) + P_{20}(S, m', f, h, J, k_{Fa}) \sin(2\varphi)), \\
K_3 &= f(P_{21}(S, m', f, h, J, k_{Fa}) + P_{22}(S, m', f, h, J, k_{Fa}) \cos(\varphi) \\
&\quad + P_{23}(S, m', f, h, J, k_{Fa}) \sin(\varphi) + P_{24}(S, m', f, h, J, k_{Fa}) \\
&\quad \sin(2\varphi) + P_{25}(S, m', f, h, J, k_{Fa}) \sin(\varphi) \cos(2\varphi)).
\end{aligned}$$

Here,  $P_i$  ( $i = 1, 2 \dots 25$ ) are functions of all parameters like exchange interaction ( $J$ ), magnetization of the ferromagnets ( $h$ ), spin ( $S$ ) and magnetic moment ( $m'$ ) of spin flipper, phase ( $k_{Fa}$ ) accumulated in ferromagnetic region and spin flip probability of spin flipper ( $f$ ). Since these are large expressions we do not explicitly write them here. For no flip case the spin flip probability of spin flipper is  $f = 0$ . Thus, from above expressions:  $K_1, K_2, K_3$  and also  $A', B', C'$  and  $D'$  vanish. Therefore, from Eq. (5.11),  $M'_{1(2)} = 0$  and  $M'_{3(4)} = 0$ , implying for no flip case equilibrium quantum spin torque vanishes ( $\tau^{eq} |_{\theta \rightarrow 0} = 0$ ).





# Appendix D

## Mathematica code to calculate pairing amplitudes in metallic region

The Mathematica code described below calculates pairing correlations (Eqs. (3.10)) in normal metal region of a Normal metal-Spin flipper-Superconductor junction as shown in Fig. 3.1 of chapter 3. The time required to run this Mathematica code is less than 5 minutes. Herein, Figs. 3.2 and 3.3 of chapter 3 are generated using the Mathematica program below.

```
J = 1; q = 0.1; y = (1 + q/(EF))^(1/2); y1 = (1 + q/(EF))^(1/2); y3 = (1 - q/(EF))^(1/2); y4 = (1 - q/(EF))^(1/2);
S = 1/2; m1 = -1/2; F2 = Sqrt[(S - m1) * (S + m1 + 1)]; η = 1; kF = 1; EF = 10; ξ = 2;
u = 1/2 * ((1+q)/q)^(1/2) + 1/2 * ((1-q)/q)^(1/2); v = 1/2 * ((1+q)/q)^(1/2) - 1/2 * ((1-q)/q)^(1/2);
qu1 = kF(1 + q/(2EF)); qu2 = kF(1 - q/(2EF)); qd1 = kF(1 + q/(2EF)); qd2 = kF(1 - q/(2EF));
κ = (1 - q^2)^(1/2) * (kF/(2 * EF)); keS = kF + I * κ; khS = kF - I * κ;
kES = (1 + I * ((1-q^2)^(1/2)/EF))^(1/2); kHS = (1 - I * ((1-q^2)^(1/2)/EF))^(1/2);
Clear[α11, α12, α13, α14, α21, α22, α23, α24, α31, α32, α33, α34, α41, α42, α43, α44, β11, β12, β13, β14, β21, β22, β23, β24,
β31, β32, β33, β34, β41, β42, β43, β44];
x1 = 0;
A = ({({1, 0, 0, 0, -u, 0, 0, -v}, {0, 1, 0, 0, 0, -u, v, 0}, {0, 0, 1, 0, 0, v, -u, 0}, {0, 0, 0, 1, -v, 0, 0, -u},
{(y - I * J * m1), -I * J * F2, 0, 0, u * kES, 0, 0, -v * kHS}, {-I * J * F2, (y1 + I * J * (m1 + 1)), 0, 0, 0, u * kES, v * kHS, 0},
{0, 0, (I * J * (m1 + 1) - y3), -I * J * F2, 0, -v * kES, -u * kHS, 0}, {0, 0, -I * J * F2, -(y4 + I * J * m1), v * kES, 0, 0, -u * kHS}));
```

D. MATHEMATICA CODE TO CALCULATE PAIRING AMPLITUDES IN METALLIC REGION

$$B = \begin{pmatrix} -1 \\ 0 \\ 0 \\ 0 \\ y + I * J * m1 \\ I * J * F2 \\ 0 \\ 0 \end{pmatrix}; B1 = \begin{pmatrix} 0 \\ -1 \\ 0 \\ 0 \\ I * J * F2 \\ y1 - I * J * (m1 + 1) \\ 0 \\ 0 \end{pmatrix}; B2 = \begin{pmatrix} 0 \\ 0 \\ -1 \\ 0 \\ 0 \\ 0 \\ -y3 - I * J * (m1 + 1) \\ I * J * F2 \end{pmatrix}; B3 = \begin{pmatrix} 0 \\ 0 \\ 0 \\ -1 \\ 0 \\ 0 \\ I * J * F2 \\ -y4 + I * J * m1 \end{pmatrix};$$

Sol = LinearSolve[A, B]; Sol3 = LinearSolve[A, B3]; Sol1 = LinearSolve[A, B1]; Sol2 = LinearSolve[A, B2];

b11 = Sol[[1, 1]]; b12 = Sol[[2, 1]]; a11 =  $\left(\frac{y^3}{y}\right)^{(1/2)} * \text{Sol}[[3, 1]]$ ; a12 =  $\left(\frac{y^3}{y}\right)^{(1/2)} * \text{Sol}[[4, 1]]$ ;

b21 = Sol1[[1, 1]]; b22 = Sol1[[2, 1]]; a21 =  $\left(\frac{y^3}{y}\right)^{(1/2)} * \text{Sol1}[[3, 1]]$ ; a22 =  $\left(\frac{y^3}{y}\right)^{(1/2)} * \text{Sol1}[[4, 1]]$ ;

b31 =  $\left(\frac{y}{y^3}\right)^{(1/2)} * \text{Sol2}[[1, 1]]$ ; b32 =  $\left(\frac{y}{y^3}\right)^{(1/2)} * \text{Sol2}[[2, 1]]$ ; a31 = Sol2[[3, 1]]; a32 = Sol2[[4, 1]];

b41 =  $\left(\frac{y}{y^3}\right)^{(1/2)} * \text{Sol3}[[1, 1]]$ ; b42 =  $\left(\frac{y}{y^3}\right)^{(1/2)} * \text{Sol3}[[2, 1]]$ ; a41 = Sol3[[3, 1]]; a42 = Sol3[[4, 1]];

b111 = b11; b121 = b12; a111 = a11; a121 = a12; b211 = b21; b221 = b22; a211 = a21; a221 = a22; b311 = b31;

b321 = b32; a311 = a31; a321 = a32; b411 = b41; b421 = b42; a411 = a41; a421 = a42;

A1 = ({u, 0, 0, v, -1, 0, 0, 0}, {0, u, -v, 0, 0, -1, 0, 0}, {0, -v, u, 0, 0, 0, -1, 0}, {v, 0, 0, u, 0, 0, 0, -1},

{u \* kES, 0, 0, -v \* kHS, (y - I \* J \* m1), -I \* J \* F2, 0, 0}, {0, u \* kES, v \* kHS, 0, -I \* J \* F2, (y1 + I \* J \* (m1 + 1)), 0, 0},

{0, -v \* kES, -u \* kHS, 0, 0, 0, -(y3 - I \* J \* (m1 + 1)), -I \* J \* F2}, {v \* kES, 0, 0, -u \* kHS, 0, 0, -I \* J \* F2, -(y4 + I \* J \* m1)});

B4 = ({{-u}, {0}, {0}, {-v}, {u \* kES}, {0}, {0}, {v \* kES}}); B5 = ({{0}, {-u}, {v}, {0}, {0}, {u \* kES}, {-v \* kES}, {0}});

B6 = ({{0}, {v}, {-u}, {0}, {0}, {v \* kHS}, {-u \* kHS}, {0}}); B7 = ({{-v}, {0}, {0}, {-u}, {-v \* kHS}, {0}, {0}, {-u \* kHS}});

Sol4 = LinearSolve[A1, B4]; Sol5 = LinearSolve[A1, B5]; Sol6 = LinearSolve[A1, B6]; Sol7 = LinearSolve[A1, B7];

t51 =  $\left(\frac{y}{kES}\right)^{(1/2)} * \text{Sol4}[[5, 1]]$ ; t52 =  $\left(\frac{y}{kES}\right)^{(1/2)} * \text{Sol4}[[6, 1]]$ ; c51 =  $\left(\frac{y^3}{kES}\right)^{(1/2)} * \text{Sol4}[[7, 1]]$ ;

c52 =  $\left(\frac{y^3}{kES}\right)^{(1/2)} * \text{Sol4}[[8, 1]]$ ; t61 =  $\left(\frac{y}{kES}\right)^{(1/2)} * \text{Sol5}[[5, 1]]$ ; t62 =  $\left(\frac{y}{kES}\right)^{(1/2)} * \text{Sol5}[[6, 1]]$ ;

c61 =  $\left(\frac{y^3}{kES}\right)^{(1/2)} * \text{Sol5}[[7, 1]]$ ; c62 =  $\left(\frac{y^3}{kES}\right)^{(1/2)} * \text{Sol5}[[8, 1]]$ ; t71 =  $\left(\frac{y}{kHS}\right)^{(1/2)} * \text{Sol6}[[5, 1]]$ ;

t72 =  $\left(\frac{y}{kHS}\right)^{(1/2)} * \text{Sol6}[[6, 1]]$ ; c71 =  $\left(\frac{y^3}{kHS}\right)^{(1/2)} * \text{Sol6}[[7, 1]]$ ; c72 =  $\left(\frac{y^3}{kHS}\right)^{(1/2)} * \text{Sol6}[[8, 1]]$ ;

t81 =  $\left(\frac{y}{kHS}\right)^{(1/2)} * \text{Sol7}[[5, 1]]$ ; t82 =  $\left(\frac{y}{kHS}\right)^{(1/2)} * \text{Sol7}[[6, 1]]$ ; c81 =  $\left(\frac{y^3}{kHS}\right)^{(1/2)} * \text{Sol7}[[7, 1]]$ ;

c82 =  $\left(\frac{y^3}{kHS}\right)^{(1/2)} * \text{Sol7}[[8, 1]]$ ; t511 = t51; t521 = t52; c511 = c51; c521 = c52; t611 = t61; t621 = t62; c611 = c61;

c621 = c62; t711 = t71; t721 = t72; c711 = c71; c721 = c72; t811 = t81; t821 = t82;

c811 = c81; c821 = c82;

$$\phi1F = \begin{pmatrix} 1 \\ 0 \\ 0 \\ 0 \end{pmatrix}; \phi2F = \begin{pmatrix} 0 \\ 1 \\ 0 \\ 0 \end{pmatrix}; \phi3F = \begin{pmatrix} 0 \\ 0 \\ 1 \\ 0 \end{pmatrix}; \phi4F = \begin{pmatrix} 0 \\ 0 \\ 0 \\ 1 \end{pmatrix}; \phi11F = \begin{pmatrix} 1 \\ 0 \\ 0 \\ 0 \end{pmatrix}; \phi22F = \begin{pmatrix} 0 \\ 1 \\ 0 \\ 0 \end{pmatrix}; \phi33F = \begin{pmatrix} 0 \\ 0 \\ 1 \\ 0 \end{pmatrix}; \phi44F = \begin{pmatrix} 0 \\ 0 \\ 0 \\ 1 \end{pmatrix};$$

$\psi1[x_] := \phi1F * \text{Exp}[I * qu1 * x] + b11 * \phi1F * \text{Exp}[-I * qu1 * x] + b12 * \phi2F * \text{Exp}[-I * qd1 * x] + a11 * \phi3F * \text{Exp}[I * qu2 * x] + a12 * \phi4F * \text{Exp}[I * qd2 * x]$ ;

$\psi2[x_] := \phi2F * \text{Exp}[I * qd1 * x] + b21 * \phi1F * \text{Exp}[-I * qu1 * x] + b22 * \phi2F * \text{Exp}[-I * qd1 * x] + a21 * \phi3F * \text{Exp}[I * qu2 * x] + a22 * \phi4F * \text{Exp}[I * qd2 * x]$ ;

$\psi3[x_] := \phi3F * \text{Exp}[-I * qu2 * x] + b31 * \phi1F * \text{Exp}[-I * qu1 * x] + b32 * \phi2F * \text{Exp}[-I * qd1 * x] + a31 * \phi3F * \text{Exp}[I * qu2 * x] +$

---

$a32 * \phi4F * \text{Exp}[I * \text{qd2} * x];$   
 $\psi4[x\_]:= \phi4F * \text{Exp}[-I * \text{qd2} * x] + b41 * \phi1F * \text{Exp}[-I * \text{qu1} * x] + b42 * \phi2F * \text{Exp}[-I * \text{qd1} * x] + a41 * \phi3F * \text{Exp}[I * \text{qu2} * x] +$

$a42 * \phi4F * \text{Exp}[I * \text{qd2} * x];$   
 $\psi5[x\_]:= t51 * \phi1F * \text{Exp}[-I * \text{qu1} * x] + t52 * \phi2F * \text{Exp}[-I * \text{qd1} * x] + c51 * \phi3F * \text{Exp}[I * \text{qu2} * x] + c52 * \phi4F * \text{Exp}[I * \text{qd2} * x];$   
 $\psi6[x\_]:= t61 * \phi1F * \text{Exp}[-I * \text{qu1} * x] + t62 * \phi2F * \text{Exp}[-I * \text{qd1} * x] + c61 * \phi3F * \text{Exp}[I * \text{qu2} * x] + c62 * \phi4F * \text{Exp}[I * \text{qd2} * x];$   
 $\psi7[x\_]:= t71 * \phi1F * \text{Exp}[-I * \text{qu1} * x] + t72 * \phi2F * \text{Exp}[-I * \text{qd1} * x] + c71 * \phi3F * \text{Exp}[I * \text{qu2} * x] + c72 * \phi4F * \text{Exp}[I * \text{qd2} * x];$   
 $\psi8[x\_]:= t81 * \phi1F * \text{Exp}[-I * \text{qu1} * x] + t82 * \phi2F * \text{Exp}[-I * \text{qd1} * x] + c81 * \phi3F * \text{Exp}[I * \text{qu2} * x] + c82 * \phi4F * \text{Exp}[I * \text{qd2} * x];$   
 $\psi11[x\_]:= \psi1[x]; \psi22[x\_]:= \psi2[x]; \psi33[x\_]:= \psi3[x]; \psi44[x\_]:= \psi4[x]; \psi55[x\_]:= \psi5[x]; \psi66[x\_]:= \psi6[x];$   
 $\psi77[x\_]:= \psi7[x]; \psi88[x\_]:= \psi8[x];$   
 $\text{Grg}[x\_ , x1\_]:= \psi1[x].(\text{Transpose}[\psi55[x1]] * \alpha11 + \text{Transpose}[\psi66[x1]] * \alpha12 + \text{Transpose}[\psi77[x1]] * \alpha13 + \text{Transpose}[\psi88[x1]] * \alpha14) +$

$\psi2[x].(\text{Transpose}[\psi55[x1]] * \alpha21 + \text{Transpose}[\psi66[x1]] * \alpha22 + \text{Transpose}[\psi77[x1]] * \alpha23 + \text{Transpose}[\psi88[x1]] * \alpha24) +$   
 $\psi3[x].(\text{Transpose}[\psi55[x1]] * \alpha31 + \text{Transpose}[\psi66[x1]] * \alpha32 + \text{Transpose}[\psi77[x1]] * \alpha33 + \text{Transpose}[\psi88[x1]] * \alpha34) +$   
 $\psi4[x].(\text{Transpose}[\psi55[x1]] * \alpha41 + \text{Transpose}[\psi66[x1]] * \alpha42 + \text{Transpose}[\psi77[x1]] * \alpha43 + \text{Transpose}[\psi88[x1]] * \alpha44);$   
 $\text{GrI}[x\_ , x1\_]:= \psi5[x].(\text{Transpose}[\psi11[x1]] * \beta11 + \text{Transpose}[\psi22[x1]] * \beta12 + \text{Transpose}[\psi33[x1]] * \beta13 + \text{Transpose}[\psi44[x1]] * \beta14) +$

$\psi6[x].(\text{Transpose}[\psi11[x1]] * \beta21 + \text{Transpose}[\psi22[x1]] * \beta22 + \text{Transpose}[\psi33[x1]] * \beta23 + \text{Transpose}[\psi44[x1]] * \beta24) +$   
 $\psi7[x].(\text{Transpose}[\psi11[x1]] * \beta31 + \text{Transpose}[\psi22[x1]] * \beta32 + \text{Transpose}[\psi33[x1]] * \beta33 + \text{Transpose}[\psi44[x1]] * \beta34) +$   
 $\psi8[x].(\text{Transpose}[\psi11[x1]] * \beta41 + \text{Transpose}[\psi22[x1]] * \beta42 + \text{Transpose}[\psi33[x1]] * \beta43 + \text{Transpose}[\psi44[x1]] * \beta44);$

$\text{GG} = \text{Grg}[x1, x1] - \text{GrI}[x1, x1];$   
 $\text{GG1} = D[\text{Grg}[x, x1], x] /. x \rightarrow x1;$   
 $\text{GG2} = D[\text{GrI}[x, x1], x] /. x \rightarrow x1;$   
 $\text{GG3} = \text{GG1} - \text{GG2};$   
 $G =$

$(\{ \{ \text{Coefficient}[\text{Collect}[\text{Expand}[\text{GG}[[1, 1]]], \alpha11], \alpha11], \text{Coefficient}[\text{Collect}[\text{Expand}[\text{GG}[[1, 1]]], \alpha12], \alpha12],$   
 $\text{Coefficient}[\text{Collect}[\text{Expand}[\text{GG}[[1, 1]]], \alpha13], \alpha13], \text{Coefficient}[\text{Collect}[\text{Expand}[\text{GG}[[1, 1]]], \alpha14], \alpha14],$   
 $\text{Coefficient}[\text{Collect}[\text{Expand}[\text{GG}[[1, 1]]], \alpha21], \alpha21], \text{Coefficient}[\text{Collect}[\text{Expand}[\text{GG}[[1, 1]]], \alpha22], \alpha22],$   
 $\text{Coefficient}[\text{Collect}[\text{Expand}[\text{GG}[[1, 1]]], \alpha23], \alpha23], \text{Coefficient}[\text{Collect}[\text{Expand}[\text{GG}[[1, 1]]], \alpha24], \alpha24],$   
 $\text{Coefficient}[\text{Collect}[\text{Expand}[\text{GG}[[1, 1]]], \alpha31], \alpha31], \text{Coefficient}[\text{Collect}[\text{Expand}[\text{GG}[[1, 1]]], \alpha32], \alpha32],$   
 $\text{Coefficient}[\text{Collect}[\text{Expand}[\text{GG}[[1, 1]]], \alpha33], \alpha33], \text{Coefficient}[\text{Collect}[\text{Expand}[\text{GG}[[1, 1]]], \alpha34], \alpha34],$   
 $\text{Coefficient}[\text{Collect}[\text{Expand}[\text{GG}[[1, 1]]], \alpha41], \alpha41], \text{Coefficient}[\text{Collect}[\text{Expand}[\text{GG}[[1, 1]]], \alpha42], \alpha42],$   
 $\text{Coefficient}[\text{Collect}[\text{Expand}[\text{GG}[[1, 1]]], \alpha43], \alpha43], \text{Coefficient}[\text{Collect}[\text{Expand}[\text{GG}[[1, 1]]], \alpha44], \alpha44],$   
 $\text{Coefficient}[\text{Collect}[\text{Expand}[\text{GG}[[1, 1]]], \beta11], \beta11], \text{Coefficient}[\text{Collect}[\text{Expand}[\text{GG}[[1, 1]]], \beta12], \beta12],$   
 $\text{Coefficient}[\text{Collect}[\text{Expand}[\text{GG}[[1, 1]]], \beta13], \beta13], \text{Coefficient}[\text{Collect}[\text{Expand}[\text{GG}[[1, 1]]], \beta14], \beta14],$   
 $\text{Coefficient}[\text{Collect}[\text{Expand}[\text{GG}[[1, 1]]], \beta21], \beta21], \text{Coefficient}[\text{Collect}[\text{Expand}[\text{GG}[[1, 1]]], \beta22], \beta22],$



































# Appendix E

## Mathematica code to calculate anomalous Josephson current and anomalous phase

### E.1 Anomalous Josephson current

The Mathematica code mentioned below calculates anomalous Josephson current flowing through the ferromagnetic Josephson junction in the presence of a spin-flipper as shown in Fig. 4.13 of chapter 4. The time required to run this Mathematica code is less than 5 minutes. Herein, Fig. 4.15(a) of chapter 4 is generated using the Mathematica program below.

```
Clear[u, v];
```

```
Z = 0; p = 0.5; y = (1 + p)^(1/2); y1 = (1 - p)^(1/2); s = 1/2; m = 1/2; S = 1/2; m1 = -1/2; kFa = Pi;
```

```
SetSharedVariable[list]
```

E. MATHEMATICA CODE TO CALCULATE ANOMALOUS JOSEPHSON CURRENT AND ANOMALOUS PHASE

---

```

list = {};

ParallelDo[

 $\theta_1 = \text{Pi}/2; \theta_2 = 0; F_1 = \text{Sqrt}[(s + m) * (s - m + 1)]; F_2 = \text{Sqrt}[(S - m_1) * (S + m_1 + 1)];$ 

A =

Det[({{u * Exp[I * kFa/2], 0, 0, v * Exp[-I * kFa/2], -Cos[ $\theta_1/2$ ], -Exp[I * kFa * y/2] * Cos[ $\theta_1/2$ ], -I * Sin[ $\theta_1/2$ ],
-I * Sin[ $\theta_1/2$ ] * Exp[I * kFa * y/2], 0, 0, 0, 0, 0, 0, 0, 0, 0, 0, 0, 0, 0, 0, 0, 0, 0, 0},
{0, u * Exp[I * kFa/2], -v * Exp[-I * kFa/2], 0, -I * Sin[ $\theta_1/2$ ], -I * Sin[ $\theta_1/2$ ] * Exp[I * kFa * y/2], -Cos[ $\theta_1/2$ ],
-Exp[I * kFa * y/2] * Cos[ $\theta_1/2$ ], 0, 0, 0, 0, 0, 0, 0, 0, 0, 0, 0, 0, 0, 0},
{0, -v * Exp[I * kFa/2], u * Exp[-I * kFa/2], 0, 0, 0, 0, -Cos[ $\theta_1/2$ ], -Exp[-I * kFa * y/2] * Cos[ $\theta_1/2$ ], I * Sin[ $\theta_1/2$ ],
I * Sin[ $\theta_1/2$ ] * Exp[-I * kFa * y/2], 0, 0, 0, 0, 0, 0, 0, 0, 0, 0, 0, 0},
{v * Exp[I * kFa/2], 0, 0, u * Exp[-I * kFa/2], 0, 0, 0, 0, I * Sin[ $\theta_1/2$ ], I * Sin[ $\theta_1/2$ ] * Exp[-I * kFa * y/2], -Cos[ $\theta_1/2$ ],
-Exp[-I * kFa * y/2] * Cos[ $\theta_1/2$ ], 0, 0, 0, 0, 0, 0, 0, 0, 0, 0, 0, 0},
{u * Exp[I * kFa/2], 0, 0, -v * Exp[-I * kFa/2], (y + I * 2 * Z) * Cos[ $\theta_1/2$ ], (I * 2 * Z - y) * Cos[ $\theta_1/2$ ] * Exp[I * kFa * y/2],
(I * 2 * Z + y) * I * Sin[ $\theta_1/2$ ], (I * 2 * Z - y) * I * Sin[ $\theta_1/2$ ] * Exp[I * kFa * y/2], 0, 0, 0, 0, 0, 0, 0, 0, 0, 0, 0, 0, 0},
{0, u * Exp[I * kFa/2], v * Exp[-I * kFa/2], 0, (y + I * 2 * Z) * I * Sin[ $\theta_1/2$ ], (I * 2 * Z - y) * I * Sin[ $\theta_1/2$ ] * Exp[I * kFa * y/2],
(I * 2 * Z + y) * Cos[ $\theta_1/2$ ], (I * 2 * Z - y) * Cos[ $\theta_1/2$ ] * Exp[I * kFa * y/2], 0, 0, 0, 0, 0, 0, 0, 0, 0, 0, 0, 0, 0},
{0, -v * Exp[I * kFa/2], -u * Exp[-I * kFa/2], 0, 0, 0, 0, (I * 2 * Z - y) * Cos[ $\theta_1/2$ ], (I * 2 * Z + y) * Exp[-I * kFa * y/2] * Cos[ $\theta_1/2$ ],
(y1 - I * 2 * Z) * I * Sin[ $\theta_1/2$ ], -(y1 + I * 2 * Z) * Exp[-I * kFa * y/2] * I * Sin[ $\theta_1/2$ ], 0, 0, 0, 0, 0, 0, 0, 0, 0, 0, 0, 0},
{v * Exp[I * kFa/2], 0, 0, -u * Exp[-I * kFa/2], 0, 0, 0, 0, -(I * 2 * Z - y) * I * Sin[ $\theta_1/2$ ],
-(I * 2 * Z + y) * Exp[-I * kFa * y/2] * I * Sin[ $\theta_1/2$ ], (I * 2 * Z - y) * Cos[ $\theta_1/2$ ], (I * 2 * Z + y) * Exp[-I * kFa * y/2] * Cos[ $\theta_1/2$ ],
0, 0, 0, 0, 0, 0, 0, 0, 0, 0, 0, 0}, {0, 0, 0, 0, Exp[I * kFa * y/2] * Cos[ $\theta_1/2$ ], Cos[ $\theta_1/2$ ], Exp[I * kFa * y/2] * I * Sin[ $\theta_1/2$ ],
I * Sin[ $\theta_1/2$ ], 0, 0, 0, 0, -Cos[ $\theta_2/2$ ], -Exp[I * kFa * y/2] * Cos[ $\theta_2/2$ ], -I * Sin[ $\theta_2/2$ ], -Exp[I * kFa * y/2] * I * Sin[ $\theta_2/2$ ],
0, 0, 0, 0, 0, 0, 0, 0}, {0, 0, 0, 0, Exp[I * kFa * y/2] * I * Sin[ $\theta_1/2$ ], I * Sin[ $\theta_1/2$ ], Exp[I * kFa * y/2] * Cos[ $\theta_1/2$ ],
Cos[ $\theta_1/2$ ], 0, 0, 0, 0, -I * Sin[ $\theta_2/2$ ], -Exp[I * kFa * y/2] * I * Sin[ $\theta_2/2$ ], -Cos[ $\theta_2/2$ ], -Exp[I * kFa * y/2] * Cos[ $\theta_2/2$ ],

```

## E.1. Anomalous Josephson current

---

$$\begin{aligned}
 &0, 0, 0, 0, 0, 0, 0, 0, \{0, 0, 0, 0, 0, 0, 0, \text{Exp}[-I * kFa * y/2] * \text{Cos}[\theta 1/2], \text{Cos}[\theta 1/2], -\text{Exp}[-I * kFa * y/2] * I * \text{Sin}[\theta 1/2], \\
 & -I * \text{Sin}[\theta 1/2], 0, 0, 0, 0, -\text{Cos}[\theta 2/2], -\text{Exp}[-I * kFa * y/2] * \text{Cos}[\theta 2/2], I * \text{Sin}[\theta 2/2], \text{Exp}[-I * kFa * y/2] * I * \text{Sin}[\theta 2/2], 0, 0, 0, 0\}, \\
 & \\
 &\{0, 0, 0, 0, 0, 0, 0, -\text{Exp}[-I * kFa * y/2] * I * \text{Sin}[\theta 1/2], -I * \text{Sin}[\theta 1/2], \text{Exp}[-I * kFa * y/2] * \text{Cos}[\theta 1/2], \text{Cos}[\theta 1/2], \\
 & 0, 0, 0, 0, I * \text{Sin}[\theta 2/2], \text{Exp}[-I * kFa * y/2] * I * \text{Sin}[\theta 2/2], -\text{Cos}[\theta 2/2], -\text{Exp}[-I * kFa * y/2] * \text{Cos}[\theta 2/2], 0, 0, 0, 0\}, \\
 & \\
 &\{0, 0, 0, 0, (I * 2 * J * m * m1 * \text{Cos}[\theta 1/2] - J * F1 * F2 * \text{Sin}[\theta 1/2] + y * \text{Cos}[\theta 1/2]) * \text{Exp}[I * kFa * y/2], \\
 & (I * 2 * J * m * m1 * \text{Cos}[\theta 1/2] - J * F1 * F2 * \text{Sin}[\theta 1/2] - y * \text{Cos}[\theta 1/2]), \\
 & (-2 * J * (m - 1) * (m1 + 1) * \text{Sin}[\theta 1/2] + I * J * F1 * F2 * \text{Cos}[\theta 1/2] + y1 * I * \text{Sin}[\theta 1/2]) * \text{Exp}[I * kFa * y/2], \\
 & (-2 * J * (m - 1) * (m1 + 1) * \text{Sin}[\theta 1/2] + I * J * F1 * F2 * \text{Cos}[\theta 1/2] - y1 * I * \text{Sin}[\theta 1/2]), 0, 0, 0, 0, -y * \text{Cos}[\theta 2/2], \\
 & y * \text{Exp}[I * kFa * y/2] * \text{Cos}[\theta 2/2], -y1 * I * \text{Sin}[\theta 2/2], y1 * \text{Exp}[I * kFa * y/2] * I * \text{Sin}[\theta 2/2], 0, 0, 0, 0, 0, 0, 0, 0\}, \\
 & \\
 &\{0, 0, 0, 0, (-2 * J * m * m1 * \text{Sin}[\theta 1/2] + I * J * F1 * F2 * \text{Cos}[\theta 1/2] + y * I * \text{Sin}[\theta 1/2]) * \text{Exp}[I * kFa * y/2], \\
 & (-2 * J * m * m1 * \text{Sin}[\theta 1/2] + I * J * F1 * F2 * \text{Cos}[\theta 1/2] - y * I * \text{Sin}[\theta 1/2]), \\
 & (I * 2 * J * (m - 1) * (m1 + 1) * \text{Cos}[\theta 1/2] - J * F1 * F2 * \text{Sin}[\theta 1/2] + y1 * \text{Cos}[\theta 1/2]) * \text{Exp}[I * kFa * y/2], \\
 & (I * 2 * J * (m - 1) * (m1 + 1) * \text{Cos}[\theta 1/2] - J * F1 * F2 * \text{Sin}[\theta 1/2] - y1 * \text{Cos}[\theta 1/2]), 0, 0, 0, 0, -y * I * \text{Sin}[\theta 2/2], \\
 & y * \text{Exp}[I * kFa * y/2] * I * \text{Sin}[\theta 2/2], -y1 * \text{Cos}[\theta 2/2], y1 * \text{Exp}[I * kFa * y/2] * \text{Cos}[\theta 2/2], 0, 0, 0, 0, 0, 0, 0, 0\}, \\
 & \\
 &\{0, 0, 0, 0, 0, 0, 0, 0, (I * 2 * J * (m - 1) * (m1 + 1) * \text{Cos}[\theta 1/2] + J * F1 * F2 * \text{Sin}[\theta 1/2] - y * \text{Cos}[\theta 1/2]) * \text{Exp}[-I * kFa * y/2], \\
 & (I * 2 * J * (m - 1) * (m1 + 1) * \text{Cos}[\theta 1/2] + J * F1 * F2 * \text{Sin}[\theta 1/2] + y * \text{Cos}[\theta 1/2]), \\
 & (2 * J * m * m1 * \text{Sin}[\theta 1/2] + I * J * F1 * F2 * \text{Cos}[\theta 1/2] + y1 * I * \text{Sin}[\theta 1/2]) * \text{Exp}[-I * kFa * y/2], \\
 & (2 * J * m * m1 * \text{Sin}[\theta 1/2] + I * J * F1 * F2 * \text{Cos}[\theta 1/2] - y1 * I * \text{Sin}[\theta 1/2]), 0, 0, 0, 0, y * \text{Cos}[\theta 2/2], \\
 & -y * \text{Exp}[-I * kFa * y/2] * \text{Cos}[\theta 2/2], -y1 * I * \text{Sin}[\theta 2/2], y1 * \text{Exp}[-I * kFa * y/2] * I * \text{Sin}[\theta 2/2], 0, 0, 0, 0\}, \\
 & \\
 &\{0, 0, 0, 0, 0, 0, 0, 0, (2 * J * (m - 1) * (m1 + 1) * \text{Sin}[\theta 1/2] + I * J * F1 * F2 * \text{Cos}[\theta 1/2] + y * I * \text{Sin}[\theta 1/2]) * \text{Exp}[-I * kFa * y/2], \\
 & (2 * J * (m - 1) * (m1 + 1) * \text{Sin}[\theta 1/2] + I * J * F1 * F2 * \text{Cos}[\theta 1/2] - y * I * \text{Sin}[\theta 1/2]), \\
 & (I * 2 * J * m * m1 * \text{Cos}[\theta 1/2] + J * F1 * F2 * \text{Sin}[\theta 1/2] - y1 * \text{Cos}[\theta 1/2]) * \text{Exp}[-I * kFa * y/2], \\
 & (I * 2 * J * m * m1 * \text{Cos}[\theta 1/2] + J * F1 * F2 * \text{Sin}[\theta 1/2] + y1 * \text{Cos}[\theta 1/2]), 0, 0, 0, 0, -y * I * \text{Sin}[\theta 2/2], \\
 & y * \text{Exp}[-I * kFa * y/2] * I * \text{Sin}[\theta 2/2], y1 * \text{Cos}[\theta 2/2], -y1 * \text{Exp}[-I * kFa * y/2] * \text{Cos}[\theta 2/2], 0, 0, 0, 0\},
 \end{aligned}$$

E. MATHEMATICA CODE TO CALCULATE ANOMALOUS JOSEPHSON CURRENT AND ANOMALOUS PHASE

---

```

{0, 0, 0, 0, 0, 0, 0, 0, 0, 0, 0, 0, Exp[I * kFa * y/2] * Cos[θ2/2], Cos[θ2/2], Exp[I * kFa * y1/2] * I * Sin[θ2/2],
I * Sin[θ2/2], 0, 0, 0, 0, -u * Exp[I * φ] * Exp[I * kFa/2], 0, 0, -v * Exp[I * φ] * Exp[-I * kFa/2]},
{0, 0, 0, 0, 0, 0, 0, 0, 0, 0, 0, 0, Exp[I * kFa * y/2] * I * Sin[θ2/2], I * Sin[θ2/2], Exp[I * kFa * y1/2] * Cos[θ2/2],
Cos[θ2/2], 0, 0, 0, 0, -u * Exp[I * φ] * Exp[I * kFa/2], v * Exp[I * φ] * Exp[-I * kFa/2], 0},
{0, 0, 0, 0, 0, 0, 0, 0, 0, 0, 0, 0, 0, 0, 0, 0, 0, 0, Exp[-I * kFa * y/2] * Cos[θ2/2], Cos[θ2/2], -Exp[-I * kFa * y1/2] * I * Sin[θ2/2],
-I * Sin[θ2/2], 0, v * Exp[I * kFa/2], -u * Exp[-I * kFa/2], 0},
{0, 0, 0, 0, 0, 0, 0, 0, 0, 0, 0, 0, 0, 0, 0, 0, -Exp[-I * kFa * y/2] * I * Sin[θ2/2], -I * Sin[θ2/2], Exp[-I * kFa * y1/2] * Cos[θ2/2],
Cos[θ2/2], -v * Exp[I * kFa/2], 0, 0, -u * Exp[-I * kFa/2]},
{0, 0, 0, 0, 0, 0, 0, 0, 0, 0, 0, 0, (I * 2 * Z - y) * Exp[I * kFa * y/2] * Cos[θ2/2], (I * 2 * Z + y) * Cos[θ2/2],
(I * 2 * Z - y1) * Exp[I * kFa * y1/2] * I * Sin[θ2/2], (I * 2 * Z + y1) * I * Sin[θ2/2], 0, 0, 0, 0, u * Exp[I * φ] * Exp[I * kFa/2],
0, 0, -v * Exp[I * φ] * Exp[-I * kFa/2]}, {0, 0, 0, 0, 0, 0, 0, 0, 0, 0, 0, 0, (I * 2 * Z - y) * Exp[I * kFa * y/2] * I * Sin[θ2/2],
(I * 2 * Z + y) * I * Sin[θ2/2], (I * 2 * Z - y1) * Exp[I * kFa * y1/2] * Cos[θ2/2], (I * 2 * Z + y1) * Cos[θ2/2], 0, 0, 0, 0,
u * Exp[I * φ] * Exp[I * kFa/2], v * Exp[I * φ] * Exp[-I * kFa/2], 0},
{0, 0, 0, 0, 0, 0, 0, 0, 0, 0, 0, 0, 0, 0, 0, 0, (I * 2 * Z + y) * Exp[-I * kFa * y/2] * Cos[θ2/2], (I * 2 * Z - y) * Cos[θ2/2],
-(I * 2 * Z + y1) * Exp[-I * kFa * y1/2] * I * Sin[θ2/2], -(I * 2 * Z - y1) * I * Sin[θ2/2], 0, -v * Exp[I * kFa/2], -u * Exp[-I * kFa/2], 0},
{0, 0, 0, 0, 0, 0, 0, 0, 0, 0, 0, 0, 0, 0, 0, 0, 0, 0, -(I * 2 * Z + y) * Exp[-I * kFa * y/2] * I * Sin[θ2/2], -(I * 2 * Z - y) * I * Sin[θ2/2],
(I * 2 * Z + y1) * Exp[-I * kFa * y1/2] * Cos[θ2/2], (I * 2 * Z - y1) * Cos[θ2/2], v * Exp[I * kFa/2], 0, 0, -u * Exp[-I * kFa/2]}];
B = Simplify[A];
B1 = B /. u → ((x + (x2 - 1)(1/2)) / (2 * x))(1/2) /. v → ((x - (x2 - 1)(1/2)) / (2 * x))(1/2);
B2 = Numerator[Chop[Together[B1], 10(-5)]];
B3 = Numerator[B2];
A1 = x /. Solve[B3 == 0, x][[2]];
A2 = x /. Solve[B3 == 0, x][[4]];
a = A1 /. φ → 0;

```

```

b = A2/. $\phi$  → 0;

c = D[A1,  $\phi$ ]/. $\phi$  → 0;

d = D[A2,  $\phi$ ]/. $\phi$  → 0;

T = 7.19 * 0.01;

Tc = 7.19;

k = 1.38 * 10^(-23);

 $\beta$  = 1/(k * T);

 $\Delta$  = 10^(-3) * 1.6 * 10^(-19) * Tanh[1.74 * (Tc/T - 1)^(1/2)];

 $\Pi$  = -2 * Tanh[ $\beta$  * a *  $\Delta$ /2] * c - 2 * Tanh[ $\beta$  * b *  $\Delta$ /2] * d;

list = AppendTo[list, {J,  $\Pi$ }], {J, -4, 4, 0.05}];

list = Sort[list];

ListLinePlot [list, AxesLabel → {Style[J, 25, Bold], Style[" $I_{an}/I_0$ ", 25, Bold]}, PlotStyle → {Blue, Thickness[0.006]},

BaseStyle → {FontSize → 20}, AxesStyle → {Thickness[0.002], Thickness[0.002]}, LabelStyle → Directive[Black],

TicksStyle → Directive[Black, Bold]]

```

## E.2 Anomalous phase

The Mathematica program described below computes anomalous phase which is stored in a ferromagnetic Josephson junction in the presence of a spin-flipper as shown in Fig. 4.13 of chapter 4. The time required to run this Mathematica code is less than 5 minutes. Herein, Fig. 4.18(a) of chapter 4 is generated using the Mathematica code below.

```

Clear[u, v, Z, J, y, y1, p];

Z = 0;

p = 0.5;

y = (1 + p)^(1/2);

y1 = (1 - p)^(1/2);

```

E. MATHEMATICA CODE TO CALCULATE ANOMALOUS JOSEPHSON CURRENT AND ANOMALOUS PHASE

---

```

s = 1/2;
m = 1/2;
S = 1/2;
m1 = -1/2;
kFa = Pi;
SetSharedVariable[list]
list = {};
ParallelDo[{
θ1 = Pi/2;
θ2 = 0;
F1 = Sqrt[(s + m) * (s - m + 1)];
F2 = Sqrt[(S - m1) * (S + m1 + 1)];
A =
Det[({{u * Exp[I * kFa/2], 0, 0, v * Exp[-I * kFa/2], -Cos[θ1/2], -Exp[I * kFa * y/2] * Cos[θ1/2], -I * Sin[θ1/2],
-I * Sin[θ1/2] * Exp[I * kFa * y1/2], 0, 0, 0, 0, 0, 0, 0, 0, 0, 0, 0, 0, 0, 0, 0, 0, 0},
{0, u * Exp[I * kFa/2], -v * Exp[-I * kFa/2], 0, -I * Sin[θ1/2], -I * Sin[θ1/2] * Exp[I * kFa * y/2], -Cos[θ1/2],
-Exp[I * kFa * y1/2] * Cos[θ1/2], 0, 0, 0, 0, 0, 0, 0, 0, 0, 0, 0, 0, 0, 0, 0},
{0, -v * Exp[I * kFa/2], u * Exp[-I * kFa/2], 0, 0, 0, 0, -Cos[θ1/2], -Exp[-I * kFa * y/2] * Cos[θ1/2], I * Sin[θ1/2],
I * Sin[θ1/2] * Exp[-I * kFa * y1/2], 0, 0, 0, 0, 0, 0, 0, 0, 0, 0, 0, 0},
{v * Exp[I * kFa/2], 0, 0, u * Exp[-I * kFa/2], 0, 0, 0, 0, I * Sin[θ1/2], I * Sin[θ1/2] * Exp[-I * kFa * y/2], -Cos[θ1/2],
-Exp[-I * kFa * y1/2] * Cos[θ1/2], 0, 0, 0, 0, 0, 0, 0, 0, 0, 0, 0},
{u * Exp[I * kFa/2], 0, 0, -v * Exp[-I * kFa/2], (y + I * 2 * Z) * Cos[θ1/2], (I * 2 * Z - y) * Cos[θ1/2] * Exp[I * kFa * y/2],
(I * 2 * Z + y1) * I * Sin[θ1/2], (I * 2 * Z - y1) * I * Sin[θ1/2] * Exp[I * kFa * y1/2], 0, 0, 0, 0, 0, 0, 0, 0, 0, 0, 0, 0},
{0, u * Exp[I * kFa/2], v * Exp[-I * kFa/2], 0, (y + I * 2 * Z) * I * Sin[θ1/2], (I * 2 * Z - y) * I * Sin[θ1/2] * Exp[I * kFa * y/2],
(I * 2 * Z + y1) * Cos[θ1/2], (I * 2 * Z - y1) * Cos[θ1/2] * Exp[I * kFa * y1/2], 0, 0, 0, 0, 0, 0, 0, 0, 0, 0, 0, 0},
{0, -v * Exp[I * kFa/2], -u * Exp[-I * kFa/2], 0, 0, 0, 0, (I * 2 * Z - y) * Cos[θ1/2], (I * 2 * Z + y) * Exp[-I * kFa * y/2] * Cos[θ1/2],
(y1 - I * 2 * Z) * I * Sin[θ1/2], -(y1 + I * 2 * Z) * Exp[-I * kFa * y1/2] * I * Sin[θ1/2], 0, 0, 0, 0, 0, 0, 0, 0, 0, 0},
{v * Exp[I * kFa/2], 0, 0, -u * Exp[-I * kFa/2], 0, 0, 0, 0, -(I * 2 * Z - y) * I * Sin[θ1/2],
-(I * 2 * Z + y) * Exp[-I * kFa * y/2] * I * Sin[θ1/2], (I * 2 * Z - y1) * Cos[θ1/2], (I * 2 * Z + y1) * Exp[-I * kFa * y1/2] * Cos[θ1/2],
0, 0, 0, 0, 0, 0, 0, 0, 0, 0}, {0, 0, 0, Exp[I * kFa * y/2] * Cos[θ1/2], Cos[θ1/2], Exp[I * kFa * y1/2] * I * Sin[θ1/2],
I * Sin[θ1/2], 0, 0, 0, 0, -Cos[θ2/2], -Exp[I * kFa * y/2] * Cos[θ2/2], -I * Sin[θ2/2], -Exp[I * kFa * y1/2] * I * Sin[θ2/2],
0, 0, 0, 0, 0, 0, 0}, {0, 0, 0, Exp[I * kFa * y/2] * I * Sin[θ1/2], I * Sin[θ1/2], Exp[I * kFa * y1/2] * Cos[θ1/2],
Cos[θ1/2], 0, 0, 0, 0, -I * Sin[θ2/2], -Exp[I * kFa * y/2] * I * Sin[θ2/2], -Cos[θ2/2], -Exp[I * kFa * y1/2] * Cos[θ2/2],
0, 0, 0, 0, 0, 0, 0}, {0, 0, 0, 0, 0, 0, 0, Exp[-I * kFa * y/2] * Cos[θ1/2], Cos[θ1/2], -Exp[-I * kFa * y1/2] * I * Sin[θ1/2],
-I * Sin[θ1/2], 0, 0, 0, 0, -Cos[θ2/2], -Exp[-I * kFa * y/2] * Cos[θ2/2], I * Sin[θ2/2], Exp[-I * kFa * y1/2] * I * Sin[θ2/2], 0, 0, 0, 0},

```



$$\begin{aligned}
 & \{0, 0, 0, 0, 0, 0, 0, -\text{Exp}[-I * kFa * y/2] * I * \text{Sin}[\theta 1/2], -I * \text{Sin}[\theta 1/2], \text{Exp}[-I * kFa * y 1/2] * \text{Cos}[\theta 1/2], \text{Cos}[\theta 1/2], \\
 & 0, 0, 0, 0, I * \text{Sin}[\theta 2/2], \text{Exp}[-I * kFa * y/2] * I * \text{Sin}[\theta 2/2], -\text{Cos}[\theta 2/2], -\text{Exp}[-I * kFa * y 1/2] * \text{Cos}[\theta 2/2], 0, 0, 0, 0, 0\}, \\
 & \{0, 0, 0, 0, (I * 2 * J * m * m1 * \text{Cos}[\theta 1/2] - J * F1 * F2 * \text{Sin}[\theta 1/2] + y * \text{Cos}[\theta 1/2]) * \text{Exp}[I * kFa * y/2], \\
 & (I * 2 * J * m * m1 * \text{Cos}[\theta 1/2] - J * F1 * F2 * \text{Sin}[\theta 1/2] - y * \text{Cos}[\theta 1/2]), \\
 & (-2 * J * (m - 1) * (m1 + 1) * \text{Sin}[\theta 1/2] + I * J * F1 * F2 * \text{Cos}[\theta 1/2] + y1 * I * \text{Sin}[\theta 1/2]) * \text{Exp}[I * kFa * y 1/2], \\
 & (-2 * J * (m - 1) * (m1 + 1) * \text{Sin}[\theta 1/2] + I * J * F1 * F2 * \text{Cos}[\theta 1/2] - y1 * I * \text{Sin}[\theta 1/2]), 0, 0, 0, 0, -y * \text{Cos}[\theta 2/2], \\
 & y * \text{Exp}[I * kFa * y/2] * \text{Cos}[\theta 2/2], -y1 * I * \text{Sin}[\theta 2/2], y1 * \text{Exp}[I * kFa * y 1/2] * I * \text{Sin}[\theta 2/2], 0, 0, 0, 0, 0, 0, 0\}, \\
 & \{0, 0, 0, 0, (-2 * J * m * m1 * \text{Sin}[\theta 1/2] + I * J * F1 * F2 * \text{Cos}[\theta 1/2] + y * I * \text{Sin}[\theta 1/2]) * \text{Exp}[I * kFa * y/2], \\
 & (-2 * J * m * m1 * \text{Sin}[\theta 1/2] + I * J * F1 * F2 * \text{Cos}[\theta 1/2] - y * I * \text{Sin}[\theta 1/2]), \\
 & (I * 2 * J * (m - 1) * (m1 + 1) * \text{Cos}[\theta 1/2] - J * F1 * F2 * \text{Sin}[\theta 1/2] + y1 * \text{Cos}[\theta 1/2]) * \text{Exp}[I * kFa * y 1/2], \\
 & (I * 2 * J * (m - 1) * (m1 + 1) * \text{Cos}[\theta 1/2] - J * F1 * F2 * \text{Sin}[\theta 1/2] - y1 * \text{Cos}[\theta 1/2]), 0, 0, 0, 0, -y * I * \text{Sin}[\theta 2/2], \\
 & y * \text{Exp}[I * kFa * y/2] * I * \text{Sin}[\theta 2/2], -y1 * \text{Cos}[\theta 2/2], y1 * \text{Exp}[I * kFa * y 1/2] * \text{Cos}[\theta 2/2], 0, 0, 0, 0, 0, 0, 0\}, \\
 & \{0, 0, 0, 0, 0, 0, 0, (I * 2 * J * (m - 1) * (m1 + 1) * \text{Cos}[\theta 1/2] + J * F1 * F2 * \text{Sin}[\theta 1/2] - y * \text{Cos}[\theta 1/2]) * \text{Exp}[-I * kFa * y/2], \\
 & (I * 2 * J * (m - 1) * (m1 + 1) * \text{Cos}[\theta 1/2] + J * F1 * F2 * \text{Sin}[\theta 1/2] + y * \text{Cos}[\theta 1/2]), \\
 & (2 * J * m * m1 * \text{Sin}[\theta 1/2] + I * J * F1 * F2 * \text{Cos}[\theta 1/2] + y1 * I * \text{Sin}[\theta 1/2]) * \text{Exp}[-I * kFa * y 1/2], \\
 & (2 * J * m * m1 * \text{Sin}[\theta 1/2] + I * J * F1 * F2 * \text{Cos}[\theta 1/2] - y1 * I * \text{Sin}[\theta 1/2]), 0, 0, 0, 0, y * \text{Cos}[\theta 2/2], \\
 & -y * \text{Exp}[-I * kFa * y/2] * \text{Cos}[\theta 2/2], -y1 * I * \text{Sin}[\theta 2/2], y1 * \text{Exp}[-I * kFa * y 1/2] * I * \text{Sin}[\theta 2/2], 0, 0, 0, 0, 0\}, \\
 & \{0, 0, 0, 0, 0, 0, 0, (2 * J * (m - 1) * (m1 + 1) * \text{Sin}[\theta 1/2] + I * J * F1 * F2 * \text{Cos}[\theta 1/2] + y * I * \text{Sin}[\theta 1/2]) * \text{Exp}[-I * kFa * y/2], \\
 & (2 * J * (m - 1) * (m1 + 1) * \text{Sin}[\theta 1/2] + I * J * F1 * F2 * \text{Cos}[\theta 1/2] - y * I * \text{Sin}[\theta 1/2]), \\
 & (I * 2 * J * m * m1 * \text{Cos}[\theta 1/2] + J * F1 * F2 * \text{Sin}[\theta 1/2] - y1 * \text{Cos}[\theta 1/2]) * \text{Exp}[-I * kFa * y 1/2], \\
 & (I * 2 * J * m * m1 * \text{Cos}[\theta 1/2] + J * F1 * F2 * \text{Sin}[\theta 1/2] + y1 * \text{Cos}[\theta 1/2]), 0, 0, 0, 0, -y * I * \text{Sin}[\theta 2/2], \\
 & y * \text{Exp}[-I * kFa * y/2] * I * \text{Sin}[\theta 2/2], y1 * \text{Cos}[\theta 2/2], -y1 * \text{Exp}[-I * kFa * y 1/2] * \text{Cos}[\theta 2/2], 0, 0, 0, 0, 0\}, \\
 & \{0, 0, 0, 0, 0, 0, 0, 0, 0, 0, \text{Exp}[I * kFa * y/2] * \text{Cos}[\theta 2/2], \text{Cos}[\theta 2/2], \text{Exp}[I * kFa * y 1/2] * I * \text{Sin}[\theta 2/2], \\
 & I * \text{Sin}[\theta 2/2], 0, 0, 0, 0, -u * \text{Exp}[I * \phi] * \text{Exp}[I * kFa/2], 0, 0, -v * \text{Exp}[I * \phi] * \text{Exp}[-I * kFa/2]\}, \\
 & \{0, 0, 0, 0, 0, 0, 0, 0, 0, 0, \text{Exp}[I * kFa * y/2] * I * \text{Sin}[\theta 2/2], I * \text{Sin}[\theta 2/2], \text{Exp}[I * kFa * y 1/2] * \text{Cos}[\theta 2/2], \\
 & \text{Cos}[\theta 2/2], 0, 0, 0, 0, -u * \text{Exp}[I * \phi] * \text{Exp}[I * kFa/2], v * \text{Exp}[I * \phi] * \text{Exp}[-I * kFa/2], 0\}, \\
 & \{0, 0, 0, 0, 0, 0, 0, 0, 0, 0, 0, 0, 0, 0, \text{Exp}[-I * kFa * y/2] * \text{Cos}[\theta 2/2], \text{Cos}[\theta 2/2], -\text{Exp}[-I * kFa * y 1/2] * I * \text{Sin}[\theta 2/2], \\
 & -I * \text{Sin}[\theta 2/2], 0, v * \text{Exp}[I * kFa/2], -u * \text{Exp}[-I * kFa/2], 0\}, \\
 & \{0, 0, 0, 0, 0, 0, 0, 0, 0, 0, 0, 0, 0, 0, -\text{Exp}[-I * kFa * y/2] * I * \text{Sin}[\theta 2/2], -I * \text{Sin}[\theta 2/2], \text{Exp}[-I * kFa * y 1/2] * \text{Cos}[\theta 2/2], \\
 & \text{Cos}[\theta 2/2], -v * \text{Exp}[I * kFa/2], 0, 0, -u * \text{Exp}[-I * kFa/2]\}, \\
 & \{0, 0, 0, 0, 0, 0, 0, 0, 0, 0, 0, (I * 2 * Z - y) * \text{Exp}[I * kFa * y/2] * \text{Cos}[\theta 2/2], (I * 2 * Z + y) * \text{Cos}[\theta 2/2], \\
 & (I * 2 * Z - y1) * \text{Exp}[I * kFa * y 1/2] * I * \text{Sin}[\theta 2/2], (I * 2 * Z + y1) * I * \text{Sin}[\theta 2/2], 0, 0, 0, 0, u * \text{Exp}[I * \phi] * \text{Exp}[I * kFa/2], \\
 & 0, 0, -v * \text{Exp}[I * \phi] * \text{Exp}[-I * kFa/2]\}, \{0, 0, 0, 0, 0, 0, 0, 0, 0, 0, 0, 0, 0, 0, (I * 2 * Z - y) * \text{Exp}[I * kFa * y/2] * I * \text{Sin}[\theta 2/2], \\
 & (I * 2 * Z + y) * I * \text{Sin}[\theta 2/2], (I * 2 * Z - y1) * \text{Exp}[I * kFa * y 1/2] * \text{Cos}[\theta 2/2], (I * 2 * Z + y1) * \text{Cos}[\theta 2/2], 0, 0, 0, 0, 0, \\
 & u * \text{Exp}[I * \phi] * \text{Exp}[I * kFa/2], v * \text{Exp}[I * \phi] * \text{Exp}[-I * kFa/2], 0\}, \\
 & \{0, 0, 0, 0, 0, 0, 0, 0, 0, 0, 0, 0, 0, 0, (I * 2 * Z + y) * \text{Exp}[-I * kFa * y/2] * \text{Cos}[\theta 2/2], (I * 2 * Z - y) * \text{Cos}[\theta 2/2], \\
 & -(I * 2 * Z + y1) * \text{Exp}[-I * kFa * y 1/2] * I * \text{Sin}[\theta 2/2], -(I * 2 * Z - y1) * I * \text{Sin}[\theta 2/2], 0, -v * \text{Exp}[I * kFa/2], -u * \text{Exp}[-I * kFa/2], 0\},
 \end{aligned}$$



# Bibliography

- [1] J. R. Schrieffer and M. Tinkham, Superconductivity, vol. 71 (American Physical Society, 1999).
- [2] W. Meissner and R. Ochsenfeld, Ein neuer effekt bei eintritt der supraleitfähigkeit, Naturwissenschaften, 21, 787 (1933).
- [3] J. Bardeen, L. N. Cooper, and J. R. Schrieffer, Theory of Superconductivity, Phys. Rev. 108, 1175 (1957).
- [4] P. G. DE GENNES, Boundary Effects in Superconductors, Rev. Mod. Phys. 36, 225 (1964).
- [5] A. I. Buzdin, Proximity effects in superconductor-ferromagnet heterostructures, Rev. Mod. Phys. 77, 935-975 (2005).
- [6] J. Linder and J. W. A Robinson, Superconducting spintronics, Nat. Phys. 11, 307-315 (2015).
- [7] F. S. Bergeret, A. F. Volkov, and K. B. Efetov, Long-Range Proximity Effects in Superconductor-Ferromagnet Structures, Phys. Rev. Lett. 86, 4096 (2001).
- [8] R. S. Keizer et al., A spin triplet supercurrent through the half-metallic ferromagnet CrO<sub>2</sub>, Nature 439, 825-827 (2006).

- [9] G. E. Blonder, M. Tinkham, and T. M. Klapwijk, Transition from metallic to tunneling regimes in superconducting micro- constrictions: Excess current, charge imbalance, and supercurrent conversion, *Phys. Rev. B* 25, 4515 (1982).
- [10] M. J. M. de Jong and C. W. J. Beenakker, Andreev Reflection in Ferromagnet-Superconductor Junctions, *Phys. Rev. Lett.* 74, 1657 (1995).
- [11] P. C. W. G. Vugts, Hybrid ferromagnet-superconductor nano devices created by FEBID and FIBID towards spin polarisation measurements, Master's thesis, Eindhoven University of Technology, 2013.
- [12] Y. Rohanizadegan, Generalization of the BTK Theory to the Case of Finite Quasiparticle Lifetimes, Master's thesis, BROCK UNIVERSITY, 2013.
- [13] O. L. T. de Menezes, J. S. Helman, Spin flip enhancement at resonant transmission, *Am. J. Phys.* 53, 1100 (1985).
- [14] G. Cordourier-Maruri, Y. Omar, R. de Coss, and S. Bose, Graphene-enabled low-control quantum gates between static and mobile spins, *Phys. Rev. B* 89, 075426 (2014).
- [15] D. Kuzmanovski, R. S. Souto, and A. V. Balatsky, Odd-frequency superconductivity near a magnetic impurity in a conventional superconductor, *Phys. Rev. B* 101, 094505 (2020).
- [16] A. V. Balatsky, I. Vekhter, and Jian-Xin Zhu, Impurity-induced states in conventional and unconventional superconductors, *Rev. Mod. Phys.* 78, 373 (2006).
- [17] H. D. Liu, X. X. Yi, Geometric phases in a scattering process, *Phys. Rev. A* 84, 022114 (2011).

- [18] B. D. Josephson, Possible new effects in superconductive tunnelling, *Phys. Lett.* 1, 251 (1962).
- [19] A. A. Golubov, M. Y. Kupriyanov, and E. Il'ichev, The current-phase relation in Josephson junctions, *Rev. Mod. Phys.* 76, 411 (2004).
- [20] L. N. Bulaevskii, V. V. Kuzii, and A. A. Sobyenin, Superconducting system with weak coupling to the current in the ground state, *JETP Lett.* 25, 290 (1977).
- [21] V. V. Ryazanov, V. A. Oboznov, A. Yu. Rusanov, A. V. Veretennikov, A. A. Golubov, and J. Aarts, Coupling of Two Superconductors through a Ferromagnet: Evidence for a  $\pi$  Junction, *Phys. Rev. Lett.* 86, 2427 (2001).
- [22] J. Mooij, T. Orlando, L. Levitov, L. Tian, C. H. Van der Wal, and S. Lloyd, Josephson Persistent-Current Qubit, *Science* 285, 1036 (1999).
- [23] T. Yamashita, K. Tanikawa, S. Takahashi, and S. Maekawa, Superconducting  $\pi$  Qubit with a Ferromagnetic Josephson Junction, *Phys. Rev. Lett.* 95, 097001 (2005).
- [24] G. Annunziata, H. Enoksen, J. Linder, M. Cuoco, C. Noce and A. Sudbø, Josephson effect in S/F/S junctions: Spin bandwidth asymmetry versus Stoner exchange, *Phys. Rev. B* 83, 144520 (2011).
- [25] A. Krichevsky, M. Schechter, Y. Imry, and Y. Levinson, Spectrum and thermodynamic currents in one-dimensional Josephson elements, *Phys. Rev. B* 61, 3723 (2000).
- [26] I. O. Kulik, Macroscopic quantization and the proximity effect in s-n-s junctions, *Sov. Phys. JETP* 30, 944 (1970).
- [27] H. Enoksen, J. Linder, and A. Sudbø, Spin-flip scattering and critical currents in ballistic half-metallic d-wave Josephson junctions, *Phys. Rev. B* 85, 014512 (2012).

- [28] A. Furusaki, H. Takayanagi, and M. Tsukada, Josephson effect of the superconducting quantum point contact, *Phys. Rev. B* 45, 10563 (1992).
- [29] Philip F. Bagwell, Suppression of the Josephson current through a narrow, mesoscopic, semiconductor channel by a single impurity, *Phys. Rev. B* 46, 12573 (1992).
- [30] A. Furusaki and M. Tsukada, Dc Josephson effect and Andreev reflection, *Solid state Commun.* 78, 299 (1991).
- [31] C. Benjamin and J. K. Pachos,  $\pi$  junction qubit in monolayer graphene, *Phys. Rev. B* 79, 155431 (2009).
- [32] S. Pal, C. Benjamin, Yu-Shiba-Rusinov bound states induced by a spin flipper in the vicinity of a *s*-wave superconductor, *Scientific Reports* 8: 11949 (2018).
- [33] S. Pal, C. Benjamin, Stability of Majorana bound states in the presence of spin flip scattering, *Physica E* 126, 114389 (2020).
- [34] S. Pal, C. Benjamin, Exciting odd frequency equal spin-triplet correlations at metal-superconductor interfaces, *Phys. Rev. B* 104, 054519 (2021).
- [35] S. Pal, C. Benjamin, Tuning the  $0 - \pi$  Josephson junction with a magnetic impurity: Role of tunnel contacts, exchange coupling, electron-electron interactions and high spin states, *Scientific Reports* 8: 5208 (2018).
- [36] S. Pal, C. Benjamin, Quantized Josephson phase battery, *EPL (Euro Physics Letters)* 126, 57002 (2019).
- [37] S. Pal, C. Benjamin, Spin flip scattering engendered quantum spin torque in a Josephson junction, *Proc. R. Soc. A* 475: 20180775 (2019).

- [38] S. Pal, C. Benjamin, Josephson quantum spin thermodynamics, arXiv:2105.01726.
- [39] L. Yu, Bound state in superconductors with paramagnetic impurities, *Acta Phys. Sin.* 21, 75 (1965).
- [40] H. Shiba, Classical Spins in Superconductors, *Prog. Theor. Phys.* 40, 435 (1968).
- [41] A. I. Rusinov, Superconductivity near a paramagnetic impurity, *Zh. Eksp. Teor. Fiz. Pisma Red.* 9, 146 (1968).
- [42] A. Yazdani et al., Probing the Local Effects of Magnetic Impurities on Superconductivity, *Science* 275, 1767 (1997).
- [43] K. J. Franke, G. Schulze, & J. I. Pascual, Competition of Superconducting Phenomena and Kondo Screening at the Nanoscale, *Science* 332, 940 (2011).
- [44] M. Ruby et al., Tunneling Processes into Localized Subgap States in Superconductors, *Phys. Rev. Lett.* 115, 087001 (2015).
- [45] M. Ruby et al., End States and Subgap Structure in Proximity-Coupled Chains of Magnetic Adatoms, *Phys. Rev. Lett.* 115, 197204 (2015).
- [46] C. W. J. Beenakker, Search for Majorana Fermions in Superconductors, *Annu. Rev. Con. Mat. Phys.* 4, 113 (2013).
- [47] C. Benjamin, J. K. Pachos, Detecting Majorana bound states *Phys. Rev. B* 81, 085101 (2010).
- [48] R. Pawlak et al., Probing atomic structure and Majorana wavefunctions in monoatomic Fe chains on superconducting Pb surface, *npj Quantum Information* 2, 16035 (2016).

- [49] M. V. Mazziotti, N. Scopign, M. Grilli and S. Caprara, Majorana Fermions in One-Dimensional Structures at  $\text{LaAlO}_3/\text{SrTiO}_3$  Oxide Interfaces, *Condens. Matter.* 3(4) 37 (2018).
- [50] A. Y. Kitaev, Unpaired Majorana fermions in quantum wires, *Phys. Usp.* 44 131 (2001).
- [51] B. Feldman et al., High-resolution studies of the Majorana atomic chain platform, *Nature Phys* 13, 286-291 (2017).
- [52] B. W. Heinrich, J. I. Pascual, K. J. Franke, Single magnetic adsorbates on *s*-wave superconductors, *Prog. Surf. Sci.* 93, 1-19 (2018).
- [53] V. Koerting, B. M. Andersen, K. Flensberg, & J. Paaske, Nonequilibrium transport via spin-induced subgap states in superconductor/quantum dot/normal metal cotunnel junctions, *Phys. Rev. B* 82, 245108 (2010).
- [54] F. Ciccarello, G. M. Palma, M. Zarcone, Y. Omar, V.R. Vieira, Entanglement-induced electron coherence in a mesoscopic ring with two magnetic impurities, *New J. Phys.* 8, 214 (2006).
- [55] S. Pal, C. Benjamin, Characterizing a high spin magnetic impurity via Andreev reflection spectroscopy, *Eur. Phys. J. B* (2018) 91:190.
- [56] Q. Cheng, B. Jin, Quantum transport in normal-metal/ferromagnet/spin-triplet superconductor junctions, *Physica B* 426, 42 (2013).
- [57] S. Kashiwaya et al., Spin current in ferromagnet-insulator-superconductor junctions, *Phys. Rev. B* 60, 3572 (1999).



- [58] A. Costa, J. Fabian, and D. Kochan, Connection between zero-energy Yu-Shiba-Rusinov states and  $0 - \pi$  transitions in magnetic Josephson junctions, *Phys. Rev. B* 98, 134511 (2018).
- [59] D. Persson et al., Spin-polarized currents and noise in normal-metal/superconductor junctions with Yu-Shiba-Rusinov impurities, *Phys. Rev. B* 94, 155424 (2016).
- [60] T. Schäpers, *Superconductor/Semiconductor Junctions (Springer Tracts in Modern Physics Volume 174, 2001)*.
- [61] F. Setiawan, P. M. R. Brydon, J. D. Sau and S. DasSarma, Conductance spectroscopy of topological superconductor wire junctions, *Phys. Rev. B* 91, 214513 (2015).
- [62] J. D. Sau, S. Tewari, R. M. Lutchyn, T. D. Stanescu and S. DasSarma, Non-Abelian quantum order in spin-orbit-coupled semiconductors: Search for topological Majorana particles in solid-state systems, *Phys. Rev. B* 82, 214509 (2010).
- [63] I. C. Fulga, F. Hassler and A. R. Akhmerov, Scattering theory of topological insulators and superconductors, *Phys. Rev. B* 85, 165409 (2012); C. W. J. Beenakker, Random-matrix theory of Majorana fermions and topological superconductors, *Rev. Mod. Phys.* 87, 1037 (2015).
- [64] I. C. Fulga, F. Hassler, A. R. Akhmerov and C. W. J. Beenakker, Scattering formula for the topological quantum number of a disordered multimode wire *Phys. Rev. B* 83, 155429 (2011).
- [65] A. R. Akhmerov, J. P. Dahlhaus, F. Hassler, M. Wimmer and C. W. J. Bennakker, Quantized Conductance at the Majorana Phase Transition in a Disordered Superconducting Wire *Phys. Rev. Lett.* 106, 057001 (2011).

- [66] M. Sigrist and K. Ueda, Phenomenological theory of unconventional superconductivity, *Rev. Mod. Phys.* 63, 239 (1991).
- [67] V. L. Berezinskii, New model of the anisotropic phase of superfluid  $^3\text{He}$ , *Zh. Eksp. Teor. Fiz.* 20, 628 (1974) [*JETP Lett.* 20, 287 (1974)].
- [68] T. R. Kirkpatrick and D. Belitz, Disorder-Induced Triplet Superconductivity, *Phys. Rev. Lett.* 66, 1533 (1991).
- [69] D. Belitz and T. R. Kirkpatrick, Even-parity spin-triplet superconductivity in disordered electronic systems, *Phys. Rev. B* 46, 8393 (1992).
- [70] A. Balatsky and E. Abrahams, New class of singlet superconductors which break the time reversal and parity, *Phys. Rev. B* 45, 13125 (1992).
- [71] Y. Asano and A. Sasaki, Odd-frequency Cooper pairs in two-band superconductors and their magnetic response, *Phys. Rev. B* 92, 224508 (2015).
- [72] L. Komendová, A. V. Balatsky, and A. M. Black-Schaffer, Experimentally observable signatures of odd-frequency pairing in multiband superconductors, *Phys. Rev. B* 92, 094517 (2015).
- [73] L. Komendová and A. M. Black-Schaffer, Odd-Frequency Superconductivity in  $\text{Sr}_2\text{RuO}_4$  Measured by Kerr Rotation, *Phys. Rev. Lett.* 119, 087001 (2017).
- [74] A. M. Black-Schaffer and A. V. Balatsky, Odd-frequency superconducting pairing in multiband superconductors, *Phys. Rev. B* 88, 104514 (2013).
- [75] C. Triola and A. M. Black-Schaffer, Odd-frequency pairing and Kerr effect in the heavy-fermion superconductor  $\text{UPt}_3$ , *Phys. Rev. B* 97, 064505 (2018).

- [76] C. Triola and A. V. Balatsky, Odd-frequency superconductivity in driven systems, *Phys. Rev. B* 94, 094518 (2016).
- [77] C. Triola and A. V. Balatsky, Pair symmetry conversion in driven multiband superconductors, *Phys. Rev. B* 95, 224518 (2017).
- [78] Y. Tanaka, Y. Tanuma, and A. A. Golubov, Odd-frequency pairing in normal-metal/superconductor junctions, *Phys. Rev. B* 76, 054522 (2007).
- [79] Y. Tanaka, A. A. Golubov, S. Kashiwaya, and M. Ueda, Anomalous Josephson Effect between Even- and Odd-Frequency Superconductors, *Phys. Rev. Lett.* 99, 037005 (2007).
- [80] P. Burset, B. Lu, S. Tamura, and Y. Tanaka, Current fluctuations in unconventional superconductor junctions with impurity scattering, *Phys. Rev. B* 95, 224502 (2017).
- [81] A. F. Volkov, F. S. Bergeret, and K. B. Efetov, Odd Triplet Superconductivity in Superconductor-Ferromagnet Multilayered Structures, *Phys. Rev. Lett.* 90, 117006 (2003).
- [82] F. S. Bergeret, A. F. Volkov, and K. B. Efetov, Odd triplet superconductivity and related phenomena in superconductor-ferromagnet structures, *Rev. Mod. Phys.* 77, 1321 (2005).
- [83] Y. V. Fominov, A. F. Volkov, and K. B. Efetov, Josephson effect due to the long-range odd-frequency triplet superconductivity in SFS junctions with Néel domain walls, *Phys. Rev. B* 75, 104509 (2007).

- [84] T. Yokoyama, Y. Tanaka, and A. A. Golubov, Manifestation of the odd-frequency spin-triplet pairing state in diffusive ferromagnet/superconductor junctions, *Phys. Rev. B* 75, 134510 (2007).
- [85] A. M. Black-Schaffer and A. V. Balatsky, Proximity-induced unconventional superconductivity in topological insulators, *Phys. Rev. B* 87, 220506 (2013).
- [86] A. M. Black-Schaffer and A. V. Balatsky, Odd-frequency superconducting pairing in topological insulators, *Phys. Rev. B* 86, 144506 (2012).
- [87] P. Bursset, B. Lu, G. Tkachov, Y. Tanaka, E. M. Hankiewicz, and B. Trauzettel, Superconducting proximity effect in three-dimensional topological insulators in the presence of a magnetic field, *Phys. Rev. B* 92, 205424 (2015).
- [88] J. Cayao and A. M. Black-Schaffer, Odd-frequency superconducting pairing and subgap density of states at the edge of a two-dimensional topological insulator without magnetism, *Phys. Rev. B* 96, 155426 (2017).
- [89] J. Cayao and A. M. Black-Schaffer, Odd-frequency superconducting pairing in junctions with Rashba spin-orbit coupling, *Phys. Rev. B* 98, 075425 (2018).
- [90] I. V. Bobkova and A. M. Bobkov, Quasiclassical theory of magnetoelectric effects in superconducting heterostructures in the presence of spin-orbit coupling, *Phys. Rev. B* 95, 184518 (2017).
- [91] C. R. Reeg and D. L. Maslov, Proximity-induced triplet superconductivity in Rashba materials, *Phys. Rev. B* 92, 134512 (2015).

- [92] A. D. Bernardo, S. Diesch, Y. Gu, J. Linder, G. Divitini, C. Ducati, E. Scheer, M. Blamire, and J. Robinson, Signature of magnetic-dependent gapless odd frequency states at superconductor/ferromagnet interfaces, *Nat. Commun.* 6, 8053 (2015).
- [93] V. T. Petrashov, V. N. Antonov, S. V. Maksimov, and R. S. Shaikhvaldarov, Conductivity of mesoscopic structures with ferromagnetic and superconducting regions, *Pis'ma Zh. Eksp. Teor. Fiz.* 59, 523 (1994) [*JETP Lett.* 59, 551 (1994)].
- [94] J. Linder and A. V. Balatsk, Odd-frequency superconductivity, *Rev. Mod. Phys.* 91, 045005 (2019).
- [95] R.M. Lutchyn, J.D. Sau, S. Das Sarma, Majorana Fermions and a Topological Phase Transition in Semiconductor-Superconductor Heterostructures, *Phys. Rev. Lett.* 105, 077001 (2010).
- [96] L. Fu, C.L. Kane, Josephson current and noise at a superconductor/quantum-spin-Hall-insulator/superconductor junction, *Phys. Rev. B* 79, 161408 (2009).
- [97] L. Fu, C.L. Kane, Superconducting Proximity Effect and Majorana Fermions at the Surface of a Topological Insulator, *Phys. Rev. Lett.* 100, 096407 (2008).
- [98] N. Traverso Ziani, C. Fleckenstein, L. Vigliotti, B. Trauzettel, and M. Sasseti, From fractional solitons to Majorana fermions in a paradigmatic model of topological superconductivity, *Phys. Rev. B* 101, 195303 (2020).
- [99] J. Cayao, C. Triola, and A. M. Black-Schaffer, Odd-frequency superconducting pairing in one-dimensional systems, *Eur. Phys. J. Spec. Top.* 229, 545-575 (2020).
- [100] S.P. Lee, R.M. Lutchyn, J. Maciejko, Odd-frequency superconductivity in a nanowire coupled to Majorana zero modes, *Phys. Rev. B* 95, 184506 (2017).

- [101] S. Tamura, S. Hoshino, Odd-frequency pairs in chiral symmetric systems: Spectral bulk-boundary correspondence and topological criticality, Y. Tanaka, Phys. Rev. B 99, 184512 (2019).
- [102] D. Takagi, S. Tamura, Y. Tanaka, Odd-frequency pairing and proximity effect in Kitaev chain systems including topological critical point, Phys. Rev. B 101, 024509 (2020).
- [103] J. Linder, T. Yokoyama, A. Sudbø, and M. Eschrig, Pairing Symmetry Conversion by Spin-Active Interfaces in Magnetic Normal-Metal-Superconductor Junctions, Phys. Rev. Lett. 102, 107008 (2009); J. Linder, A. Sudbø, T. Yokoyama, R. Grein, and M. Eschrig, Signature of odd-frequency pairing correlations induced by a magnetic interface, Phys. Rev. B 81, 214504 (2010).
- [104] Y. Asano, M. Ozaki, T. Habe, A. A. Golubov, Y. Tanaka, Anomalous surface impedance in a normal-metal/superconductor junction with a spin-active interface, Phys. Rev. B 86, 024510 (2012).
- [105] Flávio L. N. Santos et al., Odd-frequency superconductivity in dilute magnetic superconductors, Phys. Rev. Research 2, 033229 (2020).
- [106] V. Perrin et al., Unveiling Odd-Frequency Pairing around a Magnetic Impurity in a Superconductor, Phys. Rev. Lett. 125, 117003 (2020).
- [107] J. Linder and J. W. A. Robinson, Superconducting spintronics, Nat. Phys. 11, 307-315 (2015).
- [108] M. Eschrig, Spin-polarized supercurrents for spintronics: a review of current progress, Rep. Prog. Phys. 78, 104501 (2015).

- [109] D. Holmes, A. Ripple, & A. M. Manheimer, Energy-efficient superconducting computing-power budgets and requirements, *IEEE Trans. Appl. Supercond.* 23, 1701610-1701610 (2013).
- [110] A. Tsintzis, A. M. Black-Schaffer, and J. Cayao, Odd-frequency superconducting pairing in Kitaev-based junctions, *Phys. Rev. B* 100, 115433 (2019).
- [111] W. L. McMillan, Theory of Superconductor-Normal-Metal Interfaces, *Phys. Rev.* 175, 559 (1968).
- [112] Jun-Feng Liu and K. S. Chan, Anomalous Josephson current through a ferromagnetic trilayer junction, *Phys. Rev. B* 82, 184533 (2010).
- [113] L. Covaci and F. Marsiglio, Proximity effect and Josephson current in clean strong/weak/strong superconducting trilayers, *Phys. Rev. B* 73, 014503 (2006).
- [114] A. M. Black-Schaffer and S. Doniach, Possibility of measuring intrinsic electronic correlations in graphene using a d-wave contact Josephson junction, *Phys. Rev. B* 81, 014517 (2010).
- [115] L. Trifunovic, Z. Popović, and Z. Radović, Josephson effect and spin-triplet pairing correlations in  $SF_1F_2S$  junctions, *Phys. Rev. B* 84, 064511 (2011).
- [116] P. Dutta, K. R. Alves, and A. M. Black-Schaffer, Thermoelectricity carried by proximity-induced odd-frequency pairing in ferromagnet/superconductor junctions, *Phys. Rev. B* 102, 094513.
- [117] H. Meng, J. Wu, X. Wu, M. Ren & Y. Ren, Long-range superharmonic Josephson current and spin-triplet pairing correlations in a junction with ferromagnetic bilayers, *Scientific Reports* 6: 21308 (2016).

- [118] A. K. Feofanov et al., Implementation of superconductor/ferromagnet/ superconductor  $\pi$ -shifters in superconducting digital and quantum circuits, *Nature Physics* 6, 593-597 (2010).
- [119] A. Y. Herr and Q. P. Herr, Josephson magnetic random access memory system and method, US Patent 8, 270, 209 (2012).
- [120] D. S. Holmes, A. L. Ripple & M. A. Manheimer, Energy-efficient superconducting computing-power budgets and requirements, *IEEE Trans. Appl. Supercond.* 23, 1701610 (2013).
- [121] E. C. Gingrich et al., Controllable  $0 - \pi$  Josephson junctions containing a ferromagnetic spin valve, *Nature Physics* 12, 564-567 (2016).
- [122] A. Buzdin and A. E. Koshelev, Periodic alternating  $0$ - and  $\pi$ -junction structures as realization of  $\varphi$ -Josephson junctions, *Phys. Rev. B* 67, 220504(R) (2003).
- [123] A. Buzdin, Direct Coupling Between Magnetism and Superconducting Current in the Josephson  $\varphi_0$  Junction, *Phys. Rev. Lett.* 101, 107005 (2008).
- [124] Y. Tanaka, T. Yokoyama, and N. Nagaosa, Manipulation of the Majorana Fermion, Andreev Reflection, and Josephson Current on Topological Insulators, *Phys. Rev. Lett.* 103, 107002 (2009).
- [125] M. A. Silaev, I. V. Tokatly, and F. S. Bergeret, Anomalous current in diffusive ferromagnetic Josephson junctions, *Phys. Rev. B* 95, 184508 (2017).
- [126] Jun-Feng Liu and K. S. Chan, Anomalous Josephson current through a ferromagnetic trilayer junction, *Phys. Rev. B* 82, 184533 (2010).



- [127] Jun-Feng Liu, K. S. Chan, and J. Wang, Anomalous Josephson Current through a Ferromagnet-Semiconductor Hybrid Structure, *J. Phys. Soc. Jpn.* 80, 124708 (2011).
- [128] G. Campagnano, P. Lucignano, D. Giuliano, and A. Tagliacozzo, Spin-orbit coupling and anomalous Josephson effect in nanowires, *J. Phys.: Condens. Matter* 27 205301 (2015).
- [129] V. Braude, Yu. V. Nazarov, Fully Developed Triplet Proximity Effect, *Phys. Rev. Lett.* 98, 077003 (2007).
- [130] Jun-Feng Liu and K. S. Chan, Relation between symmetry breaking and the anomalous Josephson effect, *Phys. Rev. B* 82, 125305 (2010).
- [131] A. Rasmussen et al., Effects of spin-orbit coupling and spatial symmetries on the Josephson current in SNS junctions, *Phys. Rev. B* 93, 155406 (2016).
- [132] I. V. Krive, L. Y. Gorelik, R. I. Shekhter, and M. Jonson, Chiral symmetry breaking and the Josephson current in a ballistic superconductor-quantum wire-superconductor junction, *Low Temp. Phys.* 30, 398-404 (2004).
- [133] T. Yokoyama, M. Eto, and Y. V. Nazarov, Anomalous Josephson effect induced by spin-orbit interaction and Zeeman effect in semiconductor nanowires, *Phys. Rev. B* 89, 195407 (2014).
- [134] K. N. Nesterov, M. Houzet, and J. S. Meyer, Anomalous Josephson effect in semiconducting nanowires as a signature of the topologically nontrivial phase, *Phys. Rev. B* 93, 174502 (2016).
- [135] Y. Asano, Y. Tanaka, M. Sigrist, and S. Kashiwaya, Josephson current in *s*-wave-superconductor/ $Sr_2RuO_4$  junctions, *Phys. Rev. B* 67, 184505 (2003).

- [136] M. Eschrig and T. Lofwander, Triplet supercurrents in clean and disordered half-metallic ferromagnets, *Nature Physics* 4, 138 (2008).
- [137] F. Konschelle and A. Buzdin, Magnetic Moment Manipulation by a Josephson Current, *Phys. Rev. Lett.* 102, 017001 (2009).
- [138] A. Zazunov, R. Egger, T. Jonckheere, and T. Martin, Anomalous Josephson current through a spin-orbit coupled quantum dot, *Phys. Rev. Lett.* 103, 147004 (2009).
- [139] L. Dell'Anna, A. Zazunov, R. Egger, and T. Martin, Josephson current through a quantum dot with spin-orbit coupling. *Phys. Rev. B* 75, 085305 (2007).
- [140] A. A. Reynoso, G. Usaj, C. A. Balseiro, D. Feinberg, and M. Avignon, Anomalous Josephson Current in Junctions with Spin Polarizing Quantum Point Contacts, *Phys. Rev. Lett.* 101, 107001 (2008).
- [141] A. A. Reynoso, G. Usaj, C. A. Balseiro, D. Feinberg, and M. Avignon, Spin-orbit-induced chirality of Andreev states in Josephson junctions, *Phys. Rev. B* 86, 214519 (2012).
- [142] Bo Lu, Keiji Yada, A. A. Golubov, and Yukio Tanaka, Anomalous Josephson effect in d-wave superconductor junctions on a topological insulator surface, *Phys. Rev. B* 92, 100503(R) (2015).
- [143] S. Kashiwaya and Y. Tanaka, Tunnelling effects on surface bound states in unconventional superconductors, *Reports on Progress in Physics* 63, 1641 (2000).
- [144] R. Grein, M. Eschrig, G. Metalidis, and G. Schön, Spin-Dependent Cooper Pair Phase and Pure Spin Supercurrents in Strongly Polarized Ferromagnets, *Phys. Rev. Lett.* 102, 227005 (2009).

- [145] S. Yip, Josephson current-phase relationships with unconventional superconductors, *Phys. Rev. B* 52, 3087 (1995).
- [146] Y. Tanaka, A. A. Golubov, S. Kashiwaya, and M. Ueda, Anomalous Josephson Effect between Even- and Odd-Frequency Superconductors, *Phys. Rev. Lett.* 99, 037005 (2007).
- [147] D. B. Szombati, et al., Josephson  $\varphi_0$ -junction in nanowire quantum dots, *Nat. Phys.* 12, 568 (2016).
- [148] M. Minutillo et al., Anomalous Josephson Effect in S/SO/F/S heterostructures, *Phys. Rev. B* 98, 144510 (2018).
- [149] V. V. Ryazanov, et al., Coupling of two superconductors through a ferromagnet: Evidence for a  $\pi$ -junction, *Phys. Rev. Lett.* 86, 2427-2430 (2001).
- [150] D. J. Van Harlingen, Phase-sensitive tests of the symmetry of the pairing state in the high-temperature superconductors-evidence for  $d_{x^2-y^2}$  symmetry, *Rev. Mod. Phys.* 67, 515-535 (1995).
- [151] C. Padurariu and Y. V. Nazarov, Theoretical proposal for superconducting spin qubits, *Phys. Rev. B* 81, 144519 (2010).
- [152] E. C. Gingrich, et al., Controllable  $0-\pi$  Josephson junctions containing a ferromagnetic spin valve, *Nature Phys.* 12, 564-567 (2016).
- [153] T. Ortlepp, Ariando, O. Mielke, C. J. M. Verwijs, K. F. K. Foo, H. Rogalla, F. H. Uhlmann, and H. Hilgenkamp, Flip-Flopping Fractional Flux Quanta, *Science* 312, 1495 (2006).

- [154] A. Costa, P. Högl, & J. Fabian, Magnetoanisotropic Josephson effect due to interfacial spin-orbit fields in superconductor/ferromagnet/superconductor junctions, *Phys. Rev. B* 95, 024514 (2017).
- [155] C. W. J. Beenakker, Universal limit of critical-current fluctuations in mesoscopic Josephson junctions, *Phys. Rev. Lett.* 67, 3836 (1991).
- [156] A. Furusaki, H. Takayanagi, & M. Tsukada, Theory of quantum conduction of supercurrent through a constriction, *Phys. Rev. Lett.* 67, 132 (1991).
- [157] M. S. Kalenkov, A. V. Galaktionov, & A. D. Zaikin, Josephson current in ballistic heterostructures with spin-active interfaces, *Phys. Rev. B* 79, 014521 (2009).
- [158] C. Benjamin, T. Jonckheere, A. Zazunov, & T. Martin, Controllable  $\pi$  junction in a Josephson quantum-dot device with molecular spin, *European Physical Journal B* 57 279 (2007).
- [159] L. B. Ioffe et al., Quiet SDS Josephson Junctions for Quantum Computing, *Nature* 398, 679 (1999); A. L. Fauchere, Ph. D thesis, Theoretische Physik, ETH-Zurich, Switzerland (1999).
- [160] E. Il'ichev et al., Degenerate Ground State in a Mesoscopic  $YBa_2Cu_3O_{7-x}$  Grain Boundary Josephson Junction, *Phys. Rev. Lett.* 86, 5369 (2001).
- [161] H. T. Man, T.M. Klapwijk, and A. F. Morpurgo, Transport through a superconductor-interacting normal metal junction: a phenomenological description, arXiv:cond-mat/0504566 (unpublished).

- [162] R. Mélin, C. Benjamin, and T. Martin, Positive cross correlations of noise in superconducting hybrid structures: Roles of interfaces and interactions, *Phys. Rev. B* **77**, 094512 (2008).
- [163] A. O. Govorov, & A. V. Kalameitsev, Optical properties of a semiconductor quantum dot with a single magnetic impurity: photoinduced spin orientation, *Phys. Rev. B* **71**, 035338 (2005).
- [164] A. O. Govorov, Optical probing of the spin state of a single magnetic impurity in a self-assembled quantum dot, *Phys. Rev. B* **70**, 035321 (2004).
- [165] K. Halterman et al., Charge and spin currents in ferromagnetic Josephson junctions, *Phys. Rev. B* **92**, 174516 (2015).
- [166] P. G. de Gennes, *Superconductivity of Metals and Alloys* (Benjamin, New York, 1966).
- [167] P. W. Anderson, & J. M. Rowell, Probable Observation of the Josephson Superconducting Tunneling Effect, *Phys. Rev. Lett.* **10**, 230 (1963).
- [168] M. Colci et al., Anomalous polarization-dependent transport in nanoscale double-barrier superconductor/ferromagnet/superconductor junctions, *Phys. Rev. B* **85**, 180512(R) (2012).
- [169] J. P. Cleuziou, W. Wernsdorfer, V. Bouchiat, T. Ondarçuhu, & M. Monthieux, Carbon nanotube superconducting quantum interference device, *Nature Nanotechnology* **1**, 53-59 (2006).

- [170] Y. Peng, Y. Vinkler-Aviv, P. W. Brouwer, L. I. Glazman, & F. Oppen, Parity Anomaly and Spin Transmutation in Quantum Spin Hall Josephson Junctions, *Phys. Rev. Lett.* 117, 267001 (2016).
- [171] J. C. Slonczewski, Current-Driven Excitation of Magnetic Multilayers, *J. Magn. Magn. Mater.* 159, L1 (1996).
- [172] L. Berger, Emission of Spin Waves by a Magnetic Multilayer Traversed by a Current, *Phys. Rev. B* 54, 9353 (1996).
- [173] J. A. Katine, F. J. Albert, R. A. Buhrman, E. B. Myers, and D. C. Ralph, Current-Driven Magnetization Reversal and Spin-Wave Excitations in Co/Cu/Co Pillars, *Phys. Rev. Lett.* 84, 3149 (2000).
- [174] E. Zhao and J. A. Sauls, Theory of nonequilibrium spin transport and spin-transfer torque in superconducting-ferromagnetic nanostructures, *Phys. Rev. B* 78, 174511 (2008).
- [175] B. Baek et al., Spin-Transfer Torque Switching in Nanopillar Superconducting-Magnetic Hybrid Josephson Junctions, *Phys. Rev. Applied* 3, 011001 (2015).
- [176] M. D. Stiles and A. Zangwill, Anatomy of Spin-Transfer Torque, *Phys. Rev. B* 66, 014407 (2002).
- [177] A. S. Mel'nikov et al., Interference Phenomena and Long-Range Proximity Effect in Clean Superconductor-Ferromagnet Systems, *Phys. Rev. Lett.* 109, 237006 (2012).
- [178] C. Richard et al., Superharmonic Long-Range Triplet Current in a Diffusive Josephson Junction, *Phys. Rev. Lett.* 110, 217004 (2013).

- [179] X. Waintal and P. W. Brouwer, Magnetic exchange interaction induced by a Josephson current, *Phys. Rev. B* 65, 054407 (2002).
- [180] K. Halterman and M. Alidoust, Josephson currents and spin-transfer torques in ballistic SFSFS nanojunctions, *Supercond. Sci. Technol.* 29 (2016) 055007 (11pp).
- [181] S. Zhang, Quantum Spin Torque, *Physics* 10, 135 (2017).
- [182] A. Zholud et al., Spin Transfer due to Quantum Magnetization Fluctuations, *Phys. Rev. Lett.* 119, 257201 (2017).
- [183] E. B. Myers et al., Current-induced switching of domains in magnetic multilayer devices, *Science* 285, 867 (1999).
- [184] M. Tsoi et al., Excitation of a Magnetic Multilayer by an Electric Current. *Phys. Rev. Lett.* 80, 4281 (1998).
- [185] J. Linder, T. Yokoyama and A. Sudbø, Spin-transfer torque and magnetoresistance in superconducting spin valves, *Phys. Rev. B* 79, 224504 (2009).
- [186] Z. P. Niu and D. Y. Xing, Spin-Triplet Pairing States in Ferromagnet/Ferromagnet/*d*-Wave Superconductor Heterojunctions with Noncollinear Magnetizations, *Phys. Rev. Lett.* 98, 057005 (2007).
- [187] M. Alidoust et al., Spin-polarized Josephson current in superconductor/ferromagnet/superconductor junctions with inhomogeneous magnetization, *Phys. Rev. B* 81, 014512 (2010).
- [188] F. Giazotto, T. T. Heikkilä, G. P. Pepe, P. Helistö, A. Luukanen, J. P. Pekola, Ultrasensitive proximity Josephson sensor with kinetic inductance readout, *Appl. Phys. Lett.* 92, 162507 (2008).

- [189] C. Guarcello, A. Braggio, P. Solinas, G. P. Pepe, F. Giazotto, Josephson-Threshold Calorimeter, *Phys. Rev. Applied* 11, 054074 (2019).
- [190] P. Solinas, F. Giazotto, G. P. Pepe, Proximity SQUID Single-Photon Detector via Temperature-to-Voltage Conversion, *Phys. Rev. Applied* 10, 024015 (2018).
- [191] M. Zgirski, M. Foltyn, A. Savin, K. Norowski, M. Meschke, J. Pekola, Nanosecond Thermometry with Josephson Junctions, *Phys. Rev. Applied* 10, 044068 (2018).
- [192] L. B. Wang, O. P. Saira, J. P. Pekola, Fast thermometry with a proximity Josephson junction, *Appl. Phys. Lett.* 112, 013105 (2018).
- [193] F. Giazotto, T. T. Heikkilä, A. Luukanen, A. M. Savin, J. P. Pekola, Opportunities for mesoscopics in thermometry and refrigeration: Physics and applications, *Rev. Mod. Phys.* 78, 217 (2006).
- [194] J. Yang, J. C. Elouard, J. Splettstoesser, B. Sothmann, R. Sánchez, A. N. Jordan, Thermal transistor and thermometer based on Coulomb-coupled conductors, *Phys. Rev. B* 100, 045418 (2019).
- [195] B. Sothmann, F. Giazotto, E. M. Hankiewicz, High-efficiency thermal switch based on topological Josephson junctions, *New J. Phys.* 19, 023056 (2017).
- [196] B. Dutta et al., Thermal Conductance of a Single-Electron Transistor, *Phys. Rev. Lett.* 119, 077701 (2017).
- [197] G. Marchegiani, P. Virtanen, F. Giazotto, and M. Campisi, Self-Oscillating Josephson Quantum Heat Engine, *Phys. Rev. Applied* 6, 054014 (2016).
- [198] F. Vischi, M. Carrega, P. Virtanen, E. Strambini, A. Braggio, F. Giazotto, Thermodynamic cycles in Josephson junctions, *Sci Rep* 9, 3238 (2019).



- [199] B. Karimi and J. P. Pekola, Otto refrigerator based on a superconducting qubit: Classical and quantum performance, *Phys. Rev. B* 94, 184503 (2016).
- [200] M. M. Leivo, J. P. Pekola, D. V. Averin, Efficient Peltier refrigeration by a pair of normal metal/insulator/superconductor junctions, *Appl. Phys. Lett.* 68, 1996 (1996).
- [201] H. Q. Nguyen, J. T. Peltonen, M. Meschke, and J. P. Pekola, Cascade Electronic Refrigerator Using Superconducting Tunnel Junctions, *Phys. Rev. Applied* 6, 054011 (2016).
- [202] P. Solinas, R. Bosisio, and F. Giazotto, Microwave quantum refrigeration based on the Josephson effect, *Phys. Rev. B* 93, 224521 (2016).
- [203] G. Marchegiani, P. Virtanen and F. Giazotto, On-chip cooling by heating with superconducting tunnel junctions, *Europhys. Lett.* 124, 48005 (2018).
- [204] R. Hussein et al., Nonlocal thermoelectricity in a Cooper-pair splitter, *Phys. Rev. B* 99, 075429 (2019).
- [205] G. Marchegiani, A. Braggio, and F. Giazotto, Nonlinear Thermoelectricity with Electron-Hole Symmetric Systems, *Phys. Rev. Lett.* 124, 106801 (2020).
- [206] R. Kosloff, Quantum Thermodynamics: A Dynamical Viewpoint, *Entropy* 15, 2100-2128 (2013).
- [207] R. Kosloff and A. Levy, Quantum heat engines and refrigerators: Continuous devices, *Annu. Rev. Phys. Chem.* 65, 365 (2014).
- [208] F. Giazotto and M. J. Martinez-Perez, The Josephson heat interferometer, *Nature* 492, 401 (2012).

- [209] P. Virtanen, F. Vischi, E. Strambini, M. Carrega, and F. Giazotto, Quasiparticle entropy in superconductor/normal metal/superconductor proximity junctions in the diffusive limit, *Phys. Rev. B* 96, 245311 (2017).
- [210] A. Fornieri et al., Nanoscale phase engineering of thermal transport with a Josephson heat modulator, *Nat. Nanotechnol.* 11, 258 (2016).
- [211] A. Fornieri and F. Giazotto, Towards phase-coherent caloritronics in superconducting circuits, *Nat. Nanotechnol.* 12, 944 (2017).
- [212] B. Scharf et al., Topological Josephson Heat Engine, *Commun Phys* 3, 198 (2020).
- [213] F. Vischi, M. Carrega, A. Braggio, P. Virtanen, and F. Giazotto, Thermodynamics of a Phase-Driven Proximity Josephson Junction, *Entropy* 21, 1005 (2019).
- [214] M. Büttiker and T. M. Klapwijk, Flux sensitivity of a piecewise normal and superconducting metal loop, *Phys. Rev. B* 33, 5114(R) (1986).
- [215] A. Mani, S. Pal and C. Benjamin, Designing a highly efficient graphene quantum spin heat engine, *Sci Rep* 9, 6018 (2019).
- [216] J. P. S. Bizarro, Comment on “Not all counterclockwise thermodynamic cycles are refrigerators” [*Am. J. Phys.* 84, 413-418 (2016)], *Am. J. Phys.* 85, 861-863 (2017).
- [217] I. Sochnikov et al., Nonsinusoidal Current-Phase Relationship in Josephson Junctions from the 3D Topological Insulator HgTe, *Phys. Rev. Lett.* 114, 066801 (2015).
- [218] S. Hart et al., Current-phase relations of InAs nanowire Josephson junctions: From interacting to multimode regimes, *Phys. Rev. B* 100, 064523 (2019).

- [219] I. Sochnikov et al., Direct Measurement of Current-Phase Relations in Superconductor/Topological Insulator/Superconductor Junctions, *Nano Lett.* 13, 3086 (2013).